Vinyl Ether Moieties as a Key Component for Cleavable Poly(ethylene glycol) Copolymers

Dissertation

zur Erlangung des Grades

“Doktor der Naturwissenschaften”

im Promotionsfach Chemie

am Fachbereich Chemie, Pharmazie und Geowissenschaften der

Johannes Gutenberg-Universität Mainz

vorgelegt von

Johannes Ewald

geboren in Zweibrücken

Mainz, Mai 2020

Tag der mündlichen Prüfung 01.07.2020

Die als Dissertation vorgelegte Arbeit wurde im Zeitraum von November 2016 bis Mai 2020 am Institut für Organische Chemie der Johannes Gutenberg-Universität Mainz in der Arbeitsgruppe von [redacted].angefertigt.

Hiermit versichere ich gemäß § 10 Abs. 3d der Promotionsordnung vom 24.07.2007

a) Ich habe die jetzt als Dissertation vorgelegte Arbeit selbst angefertigt und alle benutzten Hilfsmittel (Literatur, Apparaturen, Material) in der Arbeit angegeben.

b) Ich habe oder hatte die jetzt als Dissertation vorgelegte Arbeit nichts als Prüfungsarbeit für eine staatliche oder andere wissenschaftliche Prüfung eingereicht.

c) Ich hatte weder die jetzt als Dissertation vorgelegte Arbeit noch Teile davon bei einer anderen Fakultät bzw. einem anderen Fachbereich als Dissertation eingereicht

_____

Johannes Ewald

Danksagung

TABLE OF CONTENTS

Motivation and Objectives

Aliphatic polyethers area of crucial interest both in academia as well as in industry.[1] Among them, poly(ethylene glycol) (PEG) is the most important representative for biomedical applications, if not the most important polyether in general. Because of its unique properties like excellent water-solubility, low immunogenicity and toxicity, PEG is referred to as the "gold standard" for polymers in biomedical and pharmaceutical applications, to which other contenders are compared to.[2–4] While higher molecular weights are usually referred to as poly(ethylene oxide) (PEO), in the biomedical field, the term PEG is commonly used independent of the molecular weight.[5,6] The importance of PEG in therapeutic applications has been increasing since the last quarter of the 20th century. Especially the rise of protein-based drugs for the therapy of cancer, inflammatory and immune diseases or vaccines and therefore the demand for advanced drug delivery systems for these delicate cargos can be connected to the increasing significance of PEG.[7–9]

Protein and peptide-based drugs suffer chronically from low bioavailability, they are very susceptible to chemical and enzymatic degradation and bear the risk of severe immune reactions. [10–12] As their only applicable administration route is parental, the life-quality of patients is impaired by the necessary frequent injections of these drugs in order to maintain a therapeutically effective blood concentration.[13] These disadvantages can be overcome by the development of advanced delivery systems for these sensitive drugs, such as polymer-protein conjugates or hydrogels as delivery vehicles. Such systems dramatically improve pharmacokinetic profiles and therefore significantly affect the therapeutic outcome and the patient's life-quality by maintaining a more even blood concentration profile and reduction of the injection intervals.[14–16]

This leads to one of the most important and popular biomedical applications for PEG, the so called "PEGylation". This term describes the covalent attachment of PEG chains to proteins, peptides, nanoparticular structures or small molecular drugs. [17–19] For the first time reported by Abuchwski *et al.* in 1977, the PEGylation of bovine serum albumin (BSA) did not result in an immunogenic response to this protein, and the PEGylation of liver catalase improved the circulation time *in vivo* from 12 up to 48 hours.[20,21] These works can be seen as the beginning of a revolution in drug delivery and paved the way for PEGylation as a standard technique in today's academic research and pharmaceutical industry. The commercial success of PEGylated protein drugs started with Adagen© in 1990, and as for 2019, at least sixteen PEG-protein conjugates are currently FDA-approved with another forty one conjugates in clinical trials and pharmaceutical pipelines.[22,14]

Another popular application for PEG can be found in the field of cell culture and tissue engineering in the form of hydrogels as matrices or scaffolds for cell growth.[23–25] As PEG is highly hydrophilic, a broad variety of molecular architectures exist and end group functionalized PEGs and crosslinkers are commercially available, PEG is a popular building block for a large variety of hydrogel systems.

The often-quoted drawback of PEG concerning its low functionality, offering only two chemically addressable termini, is not the striking one in these applications. A more significant challenge lies in its non-degradability. The renal excretion limit refers to linear PEGs in solution of around M_n = 40,000 g mol^{-1}, which limits the molecular weight for safe application of PEG, albeit higher molecular weights have shown to be favourable to enhance pharmacokinetic parameters of PEG-conjugates.[13,26,27,16] This restriction is present in all FDA-approved PEGylated drugs, as they often rely on PEGs with a molecular weight of $M_n \leq$ 40,000 g mol^{-1} to avoid bioaccumulation.[28]

Overcoming this contradiction between the desired high molecular weights and the limited excretion is a main motivation and objective for this work. A large variety of cleavable PEGs is known, but most of them rely on the polyaddition or polycondensation of commercially available, end group-functionalized PEGs. This results *per* se in broad molecular weight distributions and poor control over the molecular weight, which renders these polymers unsuitable for medical application.[29] While some approaches have already been reported to synthesize intrinsically cleavable PEGs, they lack control over the polymer end groups or the distribution of fragments after degradation.[30,31] As PEGs with molecular weights of $M_n \leq 400$ g mol^{-1} were reported to show toxic effects, precise adjustment of the molecular weight and distribution ($Đ$) of the fragments by controlling the number and position of cleavable moieties in the polyether backbone is crucial for degradable PEG architectures for medical or pharmaceutical applications.[29] If PEG is synthesized *via* the anionic ring-opening polymerization (AROP), precise tailoring of molecular weights is possible, while preserving narrow molecular weight distributions.[32] This is a fundamental prerequisite for all pharmaceutical and biomedical applications, as the reproducibility for example of circulation times and immunogenicity of carrier systems is strongly dependent on the molecular weight and its distribution, making $Đ \leq 1.10$ to be considered favourable.[19]

Additionally, beside the improvement of PEG degradation and excretion, the use of cleavable PEGs as functional components in stimuli-responsive drug delivery systems is a targeted application. Especially delicate cargos like protein and peptide-based drugs profit significantly from the delivery by polymeric drug carrier systems.

As lowered pH is a major stimulus for such systems, the pH and reaches values of 6.5 in solid tumours as well as pH 5.0-6.0 in endosomes and (endo)lysosomes, the development of acid-labile PEGs for such applications is a promising approach.[33–35]

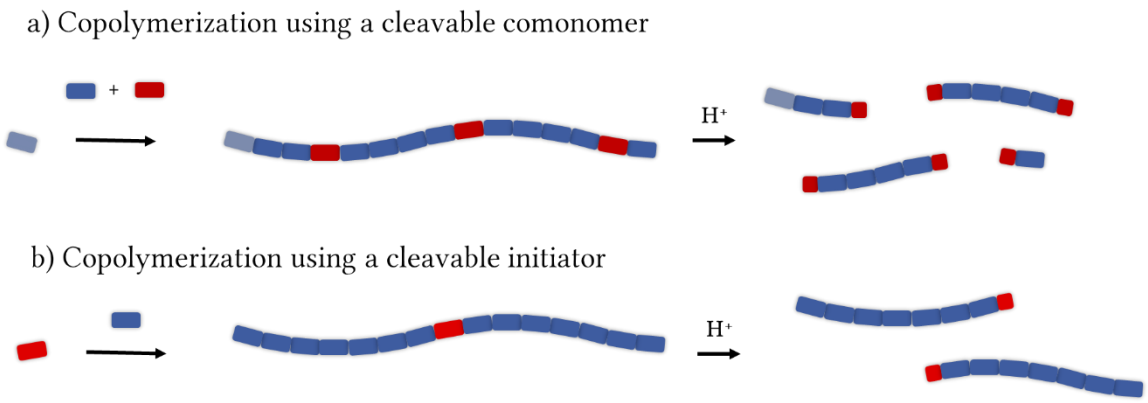

Figure 1: Schematic illustration of different approaches to introduce intrinsic degradability into PEG *via* AROP of epoxide monomers: a) via a degradable comonomer and b) via a degradable initiator, leading to a central predetermined breaking point.

This thesis aims at extending the scope of acid labile vinyl ether-functional PEGs for biomedical applications, while preserving the favourable properties of PEGs obtained *via* the classical AROP technique. Therefore, this work can be divided into two main parts:

(i) Copolymerizaton of EO with EPB to obtain vinyl ether PEGs and their biomedical application

The **chapters 2.1** and **2.2** are based on the principle of copolymerization of ethylene oxide (EO) with 3,4-epoxy-1-butene (EPB) in order to obtain allyl ether functional PEG copolymers (P(EG-*co*-EPB)).

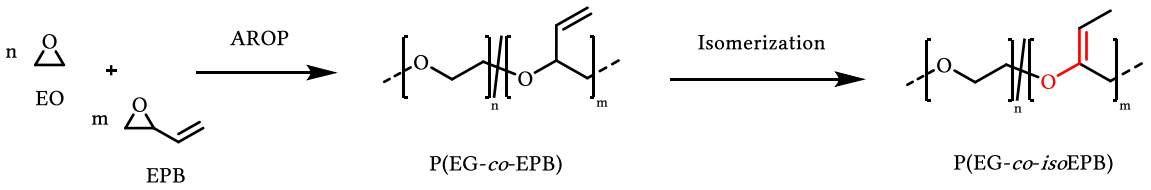

Scheme 1: Copolymerization of EO with EPB to obtain P(EG-*co*-EPB), followed by isomerization to acid labile P(EG-*co*-*iso*EPB). The vinyl ether moiety is highlighted in red.

These polymeric precursors can be isomerized to vinyl ether functional PEGs (P(EG-*co*-*iso*EPB)), which gives access to well-defined, acid labile PEG copolymers with chemically addressable end groups (**Scheme 1** and **Figure 1a**).

In **chapter 2.1**, these materials are analysed regarding their potential for application as building blocks for pH-degradable hydrogels that may serve as stimuli-responsive delivery systems for proteins. The encapsulation and pH-dependent release of fluorescence-labelled ovalbumin (OVA-Alexa488) as a classical model protein was analysed *via* an *online*-UV method. By synthesising macromonomers of different molecular weights with varying molecular ratios of cleavable moieties located in the polyether backbone, the influence of the network density and number of degradable moieties on the release kinetics of the entrapped protein in hydrogel networks was analysed at various physiologically relevant pH values.

Beside the application of these copolymers as macromonomers for degradable hydrogels, their potential for the application as pH dependent cleavable PEGylation agents was analysed in **chapter 2.2**. In a collaboration with the group of Professor Wich (former Institute of Pharmacy and Biochemistry, Johannes Gutenberg-University Mainz) an acid-labile PEGylation agent was synthesized and conjugated to lysozyme. These protein-conjugates were analysed regarding their stability at different pH values and used to form acid-labile protein-based nanoparticles *via* the double-emulsion technique. These nanoparticles were loaded with fluorescent-labelled Oregon-Green™488-dextran (OGD) as a model compound and the release of ODG upon incubation of the nanoparticles at different pH values over time was analysed.

(ii) Alternative routes for vinyl ether PEGs

As vinyl ether PEGs demonstrated their great potential as acid-labile materials for biomedical applications, we aimed at developing further strategies for their synthesis and biomedical application.

Both the number and position of cleavable moieties in the polymer backbone directly determines the molecular weight and the molecular weight distribution of the polymer fragments after degradation. Therefore, not only techniques to precisely tailor

the comonomer ratio and the molecular weight of the polymer are important, but also techniques to control the polymer microstructure. In this regard, **chapter 3.1** demonstrates the development of a strategy to incorporate the cleavable moieties in a random microstructure, based on the statistical copolymerization of EO with EEGE and subsequent post-modification (**Figure 1a**). The resulting fragments after degradation are compared to *in silico* simulated degradations of copolymers of EO and EPB (slight gradient) and epichlorohydrin (strong gradient), respectively.

Besides different copolymerization-based techniques to synthesize vinyl ether-functional PEGs, the use of an initiator with a built-in breaking point that is suitable for the AROP of EO is another important approach.

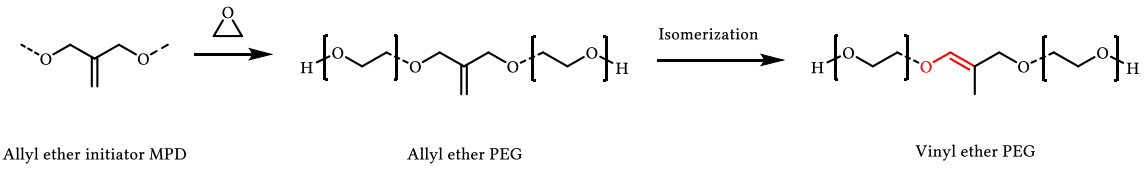

Scheme 2: 2-(methylene)-1,3-propanediol (MPD) as allyl ether synthon for degradable PEG structures. The vinyl ether moiety is highlighted in red.

In **chapter 3.2**, an allyl ether synthon that can be applied as an element of bi- or monofunctional initiators for the AROP of epoxides was developed. This synthon could be synthesized in multigram quantities and routinely worked up *via* distillation. Subsequently, different approaches to isomerize this moiety to obtain a single cleavable vinyl ether moiety in a tuneable position in the polymer backbone were analysed, and these materials were used to synthesize degradable hydrogels (**Scheme 2** and **Figure 1b**).

REFERENCES

(1) Dingels, C.; Schömer, M.; Frey, H. Die vielen Gesichter des Poly(ethylenglykol)s. *Chemie in unserer Zeit* **2011**, *45*, 338–349.

(2) Fruijtier-Pölloth, C. Safety assessment on polyethylene glycols (PEGs) and their derivatives as used in cosmetic products. *Toxicology* **2005**, *214*, 1–38.

(3) P. Garay, R. Immunogenicity of Polyethylene Glycol (PEG). *TOPROCJ* **2011**, *2*, 104–107.

(4) Obermeier, B.; Wurm, F.; Mangold, C.; Frey, H. Multifunctional Poly(ethylene glycol)s. *Angewandte Chemie (International ed. in English)* **2011**, *50*, 7988–7997.

(5) Herzberger, J.; Niederer, K.; Pohlit, H.; Seiwert, J.; Worm, M.; Wurm, F. R.; Frey, H. Polymerization of Ethylene Oxide, Propylene Oxide, and Other Alkylene Oxides: Synthesis, Novel Polymer Architectures, and Bioconjugation. *Chemical reviews* **2016**, *116*, 2170–2243.

(6) Thomas, A.; Müller, S. S.; Frey, H. Beyond poly(ethylene glycol): linear polyglycerol as a multifunctional polyether for biomedical and pharmaceutical applications. *Biomacromolecules* **2014**, *15*, 1935–1954.

(7) Malik, N. N. Drug discovery: past, present and future. *Drug discovery today* **2008**, *13*, 909–912.

(8) Greenwald, R. B.; Choe, Y. H.; McGuire, J.; Conover, C. D. Effective drug delivery by PEGylated drug conjugates. *Advanced Drug Delivery Reviews* **2003**, *55*, 217–250.

(9) Veronese, F. M.; Pasut, G. PEGylation, successful approach to drug delivery. *Drug discovery today* **2005**, *10*, 1451–1458.

(10) Groot, A. S. de; Martin, W. Reducing risk, improving outcomes: bioengineering less immunogenic protein therapeutics. *Clinical immunology (Orlando, Fla.)* **2009**, *131*, 189–201.

(11) Kaliyaperumal, A.; Jing, S. Immunogenicity assessment of therapeutic proteins and peptides. *Current pharmaceutical biotechnology* **2009**, *10*, 352–358.

(12) Manning, M. C.; Chou, D. K.; Murphy, B. M.; Payne, R. W.; Katayama, D. S. Stability of protein pharmaceuticals: an update. *Pharmaceutical research* **2010**, *27*, 544–575.

(13) Caliceti, P. Pharmacokinetic and biodistribution properties of poly(ethylene glycol)–protein conjugates. *Advanced Drug Delivery Reviews* **2003**, *55*, 1261–1277.

(14) Ekladious, I.; Colson, Y. L.; Grinstaff, M. W. Polymer-drug conjugate therapeutics: advances, insights and prospects. *Nature reviews. Drug discovery* **2019**, *18*, 273–294.

(15) Kozlowski, A.; Milton Harris, J. Improvements in protein PEGylation: pegylated interferons for treatment of hepatitis C. *Journal of Controlled Release* **2001**, *72*, 217–224.

(16) Harris, J. M.; Chess, R. B. Effect of pegylation on pharmaceuticals. *Nature reviews. Drug discovery* **2003**, *2*, 214–221.

(17) Duncan, R. The dawning era of polymer therapeutics. *Nature reviews. Drug discovery* **2003**, *2*, 347–360.

(18) Duncan, R.; Vicent, M. J. Polymer therapeutics-prospects for 21st century: the end of the beginning. *Advanced Drug Delivery Reviews* **2013**, *65*, 60–70.

(19) Knop, K.; Hoogenboom, R.; Fischer, D.; Schubert, U. S. Poly(ethylene glycol) in drug delivery: pros and cons as well as potential alternatives. *Angewandte Chemie (International ed. in English)* **2010**, *49*, 6288–6308.

(20) Abuchowski, A.; van Es, T.; Palczuk, N. C.; Davis, F. F. Alteration of immunological properties of bovine serum albumin by covalent attachment of polyethylene glycol. *Journal of Biological Chemistry* **1977**, *252*, 3578–3581.

(21) A Abuchowski; J R McCoy; N C Palczuk; T van Es; F F Davis. Effect of covalent attachment of polyethylene glycol on immunogenicity and circulating life of bovine liver catalase. *J. Biol. Chem.* **1977**, *252*, 3582–3586.

(22) Alconcel, S. N. S.; Baas, A. S.; Maynard, H. D. FDA-approved poly(ethylene glycol)–protein conjugate drugs. *Polym. Chem.* **2011**, *2*, 1442.

(23) Lee, K. Y.; Mooney, D. J. Hydrogels for tissue engineering. *Chemical reviews* **2001**, *101*, 1869–1879.

(24) Drury, J. L.; Mooney, D. J. Hydrogels for tissue engineering: scaffold design variables and applications. *Biomaterials* **2003**, *24*, 4337–4351.

(25) Kamoun, E. A.; Kenawy, E.-R. S.; Chen, X. A review on polymeric hydrogel membranes for wound dressing applications: PVA-based hydrogel dressings. *Journal of advanced research* **2017**, *8*, 217–233.

(26) Markovsky, E.; Baabur-Cohen, H.; Eldar-Boock, A.; Omer, L.; Tiram, G.; Ferber, S.; Ofek, P.; Polyak, D.; Scomparin, A.; Satchi-Fainaro, R. Administration, distribution, metabolism and elimination of polymer therapeutics. *Journal of controlled release : official journal of the Controlled Release Society* **2012**, *161*, 446–460.

(27) Harris, J. M.; Martin, N. E.; Modi, M. Pegylation: a novel process for modifying pharmacokinetics. *Clinical pharmacokinetics* **2001**, *40*, 539–551.

(28) Turecek, P. L.; Bossard, M. J.; Schoetens, F.; Ivens, I. A. PEGylation of Biopharmaceuticals: A Review of Chemistry and Nonclinical Safety Information of Approved Drugs. *Journal of pharmaceutical sciences* **2016**, *105*, 460–475.

(29) Dingels, C.; Frey, H. From Biocompatible to Biodegradable: Poly(Ethylene Glycol)s with Predetermined Breaking Points. In *Hierarchical Macromolecular Structures*: *60 Years after the Staudinger Nobel Prize II*; Percec, V., Ed.; Advances in Polymer Science v.262; Springer International Publishing: Cham, 2013; pp 167–190.

(30) Reid, B.; Tzeng, S.; Warren, A.; Kozielski, K.; Elisseeff, J. Development of a PEG Derivative Containing Hydrolytically Degradable Hemiacetals. *Macromolecules* **2010**, *43*, 9588–9590.

(31) Lundberg, P.; Lee, B. F.; van den Berg, S. A.; Pressly, E. D.; Lee, A.; Hawker, C. J.; Lynd, N. A. Poly(ethylene oxide)-co-(methylene ethylene oxide): A hydrolytically-degradable poly(ethylene oxide) platform. *ACS Macro Lett.* **2012**, *1*, 1240–1243.

(32) Flory, P. J. Molecular Size Distribution in Ethylene Oxide Polymers. *J. Am. Chem. Soc.* **1940**, *62*, 1561–1565.

(33) Manchun, S.; Dass, C. R.; Sriamornsak, P. Targeted therapy for cancer using pH-responsive nanocarrier systems. *Life sciences* **2012**, *90*, 381–387.

(34) Schmaljohann, D. Thermo- and pH-responsive polymers in drug delivery. *Advanced Drug Delivery Reviews* **2006**, *58*, 1655–1670.

(35) Liu, Y.; Wang, W.; Yang, J.; Zhou, C.; Sun, J. pH-sensitive polymeric micelles triggered drug release for extracellular and intracellular drug targeting delivery. *Asian Journal of Pharmaceutical Sciences* **2013**, *8*, 159–167.

SUMMARY

This thesis aims at extending the scope of vinyl ether-functional poly(ethylene glycol) (PEG) as a degradable polymeric material for biomedical applications. PEG is one of the most important polymers in this field and widely used, for example for conjugation to therapeutically active compounds ("PEGylation") or for the formation of hydrogels for cell culture, tissue engineering and drug delivery. A major drawback of PEG for specific applications is its non-degradability, which limits the molecular weight that can be safely applied to around M_n = 40,000 g mol^{-1}, in order to ensure full adequate excretion *via* the kidneys to prevent bioaccumulation. To overcome this drawback, different types of acid labile PEGs with vinyl ether moieties as predetermined breaking points were developed, and their potential for biomedical applications was demonstrated.

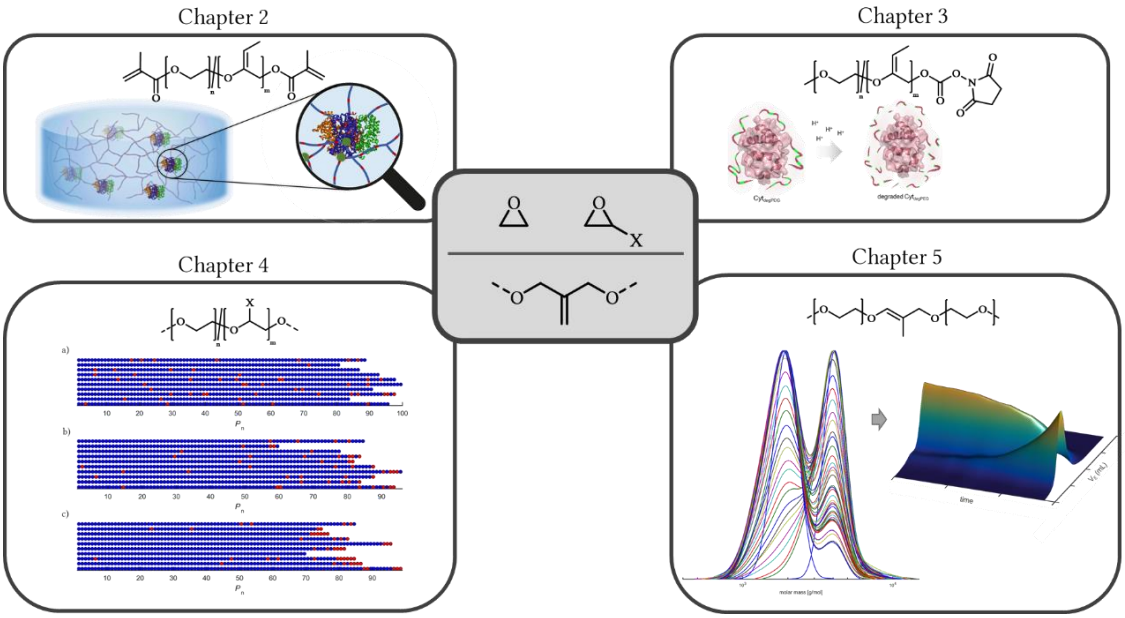

Figure 1: Synopsis of the main topics in this thesis: different approaches and applications for intrinsically degradable PEGs, obtained *via* the AROP of ethylene oxide (EO).

Chapter 1 gives an introduction regarding the significance of PEG in biomedical applications, focusing on the possibilities that are offered by the application of

degradable PEGs and especially acid-labile structures. Beginning with outlining the fundamental properties and the synthesis of PEG in **section 1.1**, the focus shifts towards the benefits of the application of polymeric drug delivery systems and the importance of acid-labile structures for the pH-dependent, stimuli-responsive release of therapeutic active molecules in **section 1.2**. Subsequently, a detailed literature overview, focusing on intrinsically cleavable PEGs. is given in **section 1.3**. The application of PEG for the development of drug delivery systems for protein and peptide-based drugs is highlighted in the **section 1.4.1**. Section **1.4.2** gives an overview over biomedical applications for PEG-based hydrogels in tissue engineering and drug delivery.

Chapter 2.1 demonstrates the application of vinyl ether-containing PEGs as macromonomers for the formation of acid labile hydrogels for the transient immobilization of proteins. For this purpose, EO was copolymerized with 3,4-epoxy-1-butene (EPB) *via* the classical AROP technique using a bifunctional initiator. The resulting allyl ether moieties were subsequently isomerized to acid labile vinyl ether structures. Well-defined copolymers with adjustable molecular weight and tailorable comonomer content were obtained. These polymers were end group-functionalized to radically crosslinkable P(EG-*co*-*iso*EPB) dimethacrylates and used for the formation of hydrogels. During the crosslinking step, a fluorescence-labelled model protein (OVA-Alexa488) was incorporated into the hydrogel matrix. Subsequently, the release of the protein by incubation of the hydrogels in buffer solutions of different pH values (pH 4–6) was analysed *via* an *online* UV measurement technique. Based on these data, the influence of crosslinking density and molecular content of degradable sites in the hydrogel on the protein release kinetics was analysed.

Starting with the same copolymerization technique of EO and EPB, an acid labile PEGylation agent was developed in **chapter 2.2**. By the use of a monofunctional initiator for the AROP of EO with EPB and subsequent isomerization, mP(EG-*co*-*iso*EPB) was synthesized. The hydroxyl polymer end group was activated using NHS-DSC to obtain

mP(EG-*co*-*iso*EPB)-NHS as a PEGylation agent for targeting lysine residues, allowing these copolymers to be conjugated to lysozyme. The conjugates were analysed *via* SDS-PAGE and SEC regarding their degradation in buffer solutions at various pH values (pH 4–6), while demonstrating excellent stability at physiological pH of 7.4. Subsequently, *via* a double emulsion technique the conjugates were used to form protein-based nanoparticles, loaded with Oregon-Green488-dextran (OGD) as a fluorescent-active model compound. The degradation of these nanoparticles under acidic conditions and the release of their payload over time were analysed *via* fluorescence measurements and NTA.

Not only the number, but also the position of the cleavable sites inside a polymer backbone determines the size and dispersity of degradation products. **Chapter 3.1** demonstrates the influence of these parameters and, in addition, presents another synthetic approach to vinyl ether-functional PEGs. To this end, EO was copolymerized with EEGE to P(EG-*co*-EEGE) copolymers with varying molecular weights and comonomer ratios. These copolymers were subsequently modified by post-polymerization reactions to generate vinyl ether-functional P(EG-co-MEO). As the copolymerization of EO with EEGE results in a random copolymer microstructure, these predefined cleavage sites are evenly distributed along the polyether backbone. The resulting distribution of fragments after degradation is compared to *in silico* degraded P(EG-*co*-ECH) and P(EG-*co*-*iso*EPB) copolymers, as examples for strong and slight gradient microstructures.

Chapter 3.2 demonstrates another approach to obtain vinyl ether-functional PEGs, based on the AROP of EO using a novel allyl ether-functional initiator (MBE). This bifunctional initiator was used to synthesize PEGs with a single allyl ether moiety inside the backbone, located symmetrically in the middle of the polymer chain. These well-defined polymers with tailorable molecular weights were isomerized *via* a one-pot approach directly after consumption of EO and additionally *via* a catalytic approach

using Wilkinson's catalyst ($RhCl(PPh_3)_3$). To analyse the kinetics of the degradation of these polymers, an automated SEC-technique was developed, and the half-life time of the vinyl ether moiety at different pH values (pH 4 and pH 5) was determined. The polymers were end group-functionalized with bismethacrylates and radically crosslinked to hydrogels, which were incubated at different pH in buffer solutions (pH 4–6) to analyse their stability and degradation behaviour under acidic conditions. Additionally, the novel allyl ether motif was introduced as an acid labile linker between the end of a PEG chain and an arbitrary residue, demonstrating its potential as a universal synthon in the synthesis for acid labile PEG conjugation.

The appendix of this thesis contains contributions from the author of this thesis to other projects. **Appendix 1** demonstrates a novel approach regarding the synthesis of multihydroxy functional polystyrenes. By the utilization of a simple Grignard reagent, a styrene-derivative bearing two protected hydroxyl functionalities could be synthesized and polymerized, yielding well-defined homopolymers, statistical and block copolymers. The hydroxyl groups could be deprotected and served as macroinitiators for the synthesis of brush copolymers by "grafting from" with L-lactide and EO.

ZUSAMMENFASSUNG

Ziel dieser Arbeit ist den Anwendungsbereich von Vinylether-funktionellem Poly (ethylenglykol) (PEG) als abbaubares Polymermaterial für biomedizinische Anwendungen zu erweitern. PEG ist eines der wichtigsten Polymere auf diesem Gebiet und wird häufig verwendet, beispielsweise zur Konjugation an therapeutisch aktive Moleküle („PEGylierung“) oder zur Bildung von Hydrogelen für Zellkultur, „Tissue Engineering“ und die Verbringung von Wirkstoffen. Ein Nachteil von PEG in manche Anwendungen ist seine Nichtabbaubarkeit, was zur Begrenzung der eingesetzten Molekulargewichte auf etwa M_n = 40,000 g mol^{-1} führt, um eine renale Ausscheidung zu gewährleisten und damit eine Bioakkumulation zu verhindern. Um diesem Nachteil entgegenzuwirken, wurden verschiedene säurelabile PEGs mit Vinylether-Einheiten als vorbestimmte Sollbruchstellen entwickelt und ihr Potenzial für biomedizinische Anwendungen demonstriert.

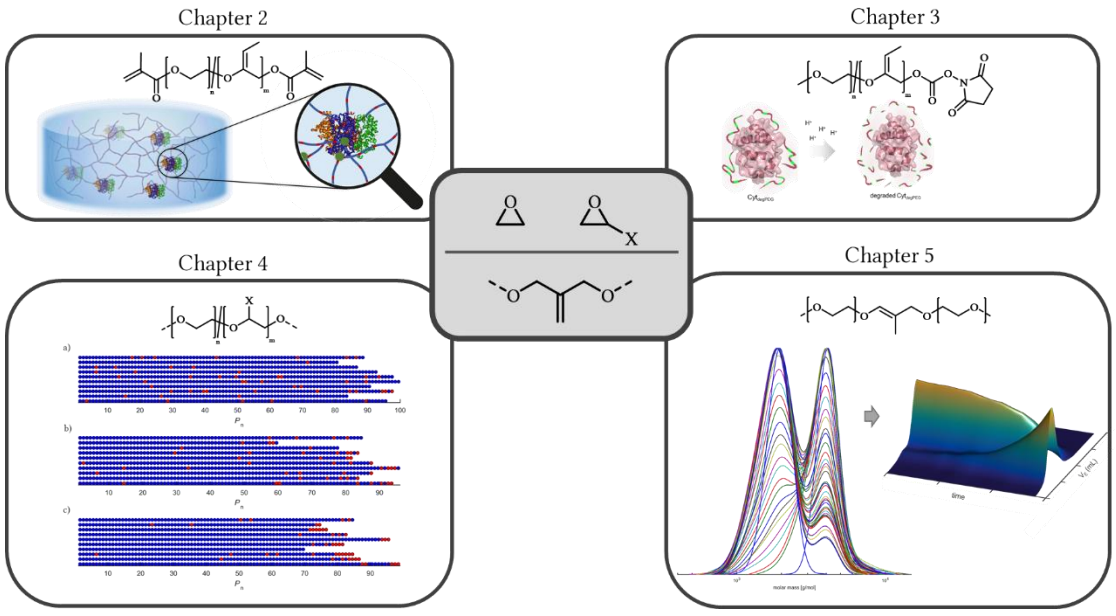

Abbildung 1: Überblick über die Hauptthemen in dieser Arbeit: verschiedene Ansätze zur Synthese und Anwendung von intrinsisch spaltbaren PEGs, hergestellt über die AROP von EO.

Kapitel 1 gibt eine Einführung in die Bedeutung von PEG in biomedizinischen Anwendungen, wobei der Schwerpunkt auf den Möglichkeiten liegt, die die Anwendung abbaubarer PEGs und insbesondere säurelabiler Strukturen bietet. Beginnend mit der Darstellung der grundlegenden Eigenschaften und der Synthese von PEG in **Abschnitt 1.1** verlagert sich der Schwerpunkt auf die Vorteile der Anwendung polymerer Wirkstofftransportsysteme und die Bedeutung säurelabiler Strukturen für die pH-abhängige, Stimuli-responsive Freisetzung therapeutisch aktiver Moleküle in **Abschnitt 1.2**. Anschließend folgt eine detaillierte Literaturübersicht mit Schwerpunkt auf intrinsisch spaltbaren PEGs in **Abschnitt 1.3**. Die Anwendung von PEG zur Entwicklung von Transportsystemen für therapeutisch wirksame Proteine und Peptide wird im **Abschnitt 1.4.1** hervorgehoben. **Abschnitt 1.4.2** gibt einen Überblick über biomedizinische Anwendungen für PEG-basierte Hydrogele im Bereich Tissue Engineering und Wirkstofftransport.

Kapitel 2.1 zeigt die Anwendung von Vinylether-funktionellen PEGs als Makromonomere zur Bildung von säurelabilen Hydrogelen zur temporären Immobilisierung von Proteinen. Zu diesem Zweck wurde EO mit 3,4-Epoxy-1-buten (EPB) mittels klassischer AROP unter Verwendung eines bifunktionellen Initiators copolymerisiert. Die resultierenden Allylether Einheiten wurden anschließend zu säurelabilen Vinylether Strukturen isomerisiert. Es wurden definierte Copolymere mit einstellbarem Molekulargewicht und anpassbarem Gehalt an Comonomer erhalten. Diese Polymere wurden zu radikalisch vernetzbaren P(EG-*co*-*iso*EPB)-Dimethacrylaten endgruppenfunktionalisiert und zur Bildung von Hydrogelen verwendet. Während des Vernetzungsschritts wurde ein fluoreszenzmarkiertes Modellprotein (OVA-Alexa488) in die Hydrogelmatrix eingebaut. Anschließend wurde die Freisetzung des Proteins durch Inkubation der Hydrogele in Pufferlösungen mit unterschiedlichen pH-Werten (pH 4-6) über einen *online*-UV Messaufbau analysiert. Basierend auf diesen Daten wurde der

Einfluss der Vernetzungsdichte und des Gehalts abbaubarer Einheiten im Hydrogel-Netzwerk auf die Kinetik der Proteinfreisetzung analysiert.

Basierend auf der gleichen Copolymerisations-Technik von EO und EPB wurde in **Kapitel 2.2** ein säurelabiles PEGylierung-Reagens entwickelt. Unter Verwendung eines monofunktionellen Initiators für die AROP von EO mit EPB und anschließender Isomerisierung wurde mP(EG-*co*-*iso*EPB) synthetisiert. Die Hydroxyl-Polymerendgruppe wurde durch Umsetzung mit NHS-DSC aktiviert, um mit mP(EG-*co*-*iso*EPB)-NHS einen Aktivester zu erhalten, worüber dieses Copolymere an Lysinreste von Lysozym konjugiert werden konnten. Die Konjugate wurden über SDS-PAGE und GPC hinsichtlich ihres Abbaus in Pufferlösungen bei verschiedenen pH Werten (pH 4–6) analysiert und zeigten gleichzeitig eine ausgezeichnete Stabilität bei einem physiologischen pH-Wert von 7,4. Anschließend wurden diese Konjugate verwendet, um über eine Doppelemulsionstechnik Nanopartikel auf Proteinbasis zu bilden, die mit Oregon-Green488-Dextran (OGD) als fluoreszenzaktive Modellverbindung beladen waren. Der Abbau dieser Nanopartikel und die Freisetzung ihrer Gastmoleküle unter sauren Bedingungen über die Zeit wurden durch Fluoreszenzmessungen und NTA analysiert.

Nicht nur die Anzahl, sondern auch die Position der spaltbaren Stellen innerhalb eines Polymerrückgrates bestimmt die Größe und Dispersität der Abbauprodukte. **Kapitel 3.1** zeigt den Einfluss dieser Parameter und stellt darüber hinaus einen weiteren Syntheseansatz für Vinylether-funktionelle PEGs vor. Zu diesem Zweck wurde EO mit EEGE zu P(EG-*co*-EEGE) Copolymeren mit unterschiedlichen Molekulargewichten und Comonomer-Verhältnissen copolymerisiert. Diese Copolymere wurden anschließend durch polymeranaloge Reaktionen modifiziert, um Vinylether-funktionelles P(EG-co-MEO) zu erhalten. Da die Copolymerisation von EO mit EEGE zu einer zufälligen Copolymer-Mikrostruktur führt, sind diese vordefinierten Spaltstellen gleichmäßig entlang des Polymerrückgrates verteilt. Die resultierende Verteilung der Fragmente

nach dem Abbau wird mit *in silico* abgebauten P(EG-*co*-ECH) und P(EG-*co*-*iso*EPB) Copolymeren verglichen, als Beispiele für starke und leichte Gradienten-Mikrostrukturen.

Kapitel 3.2 zeigt einen anderen Ansatz zur Herstellung von Vinylether-funktionellen PEGs, basierend auf der AROP von EO unter Verwendung eines neuartigen Allylether-funktionellen Initiators (MBE). Dieser bifunktionelle Initiator wurde eingesetzt, um PEGs mit einer einzelnen Allylethereinheit innerhalb des Polymerrückgrates zu synthetisieren, die sich symmetrisch in der Mitte der Polymerkette befindet. Diese wohldefinierten Polymere mit steuerbaren Molekulargewichten wurden direkt nach dem vollständigen Umsatz von EO über einen „one-pot"-Ansatz und zusätzlich über einen katalytische Route unter Verwendung des Wilkinson-Katalysators ($RhCl(PPh_3)_3$) isomerisiert. Um die Kinetik des Abbaus dieser Polymere zu analysieren, wurde eine automatisierter GPC-Versuchsaufbau entwickelt und die Halbwertszeit der Vinylethereinheit bei verschiedenen pH-Werten (pH 4 und pH 5) bestimmt. Die Polymere wurden zu Bismethacrylaten endgruppenfunktionalisiert und radikalisch zu Hydrogelen vernetzt, die bei verschiedenen pH-Werten in Pufferlösungen (pH 4–6) inkubiert wurden, um ihre Stabilität und ihr Abbauverhalten unter sauren Bedingungen zu analysieren. Zusätzlich wurde diese neuartige Allyletherstruktur als säurelabiler Linker zwischen dem Kettenende von PEG und einem beliebigen Rest eingebaut, was ihr Potenzial als universelles Synthon bei der Synthese von säurelabilen PEG-Konjugaten demonstriert.

Der Anhang dieser Arbeit enthält einen Beitrag des Autors dieser Arbeit zu einem weiteren Projekt. **Anhang 1** zeigt einen neuartigen Ansatz zur Synthese von multihydroxy-funktionellen Polystyrolen. Durch die Verwendung eines einfachen Grignard-Reagens konnte ein Styrolderivat mit zwei geschützten Hydroxylfunktionalitäten synthetisiert und polymerisiert werden, wobei genau definierte Homopolymere, statistische Copolymere und Blockcopolymere erhalten

wurden. Die Hydroxylgruppen konnten entschützt werden und als Makroinitiatoren für die Synthese von Bürstencopolymeren durch „grafting from“ mit L-Lactid und EO dienen.

GRAPHICAL ABSTRACT

2 CLEAVABLE PEGS VIA COPOLYMERIZATION OF EO WITH EPB

2.1 Acid-cleavable Poly(ethylene Glycol) Hydrogels Displaying Protein Release at pH 5

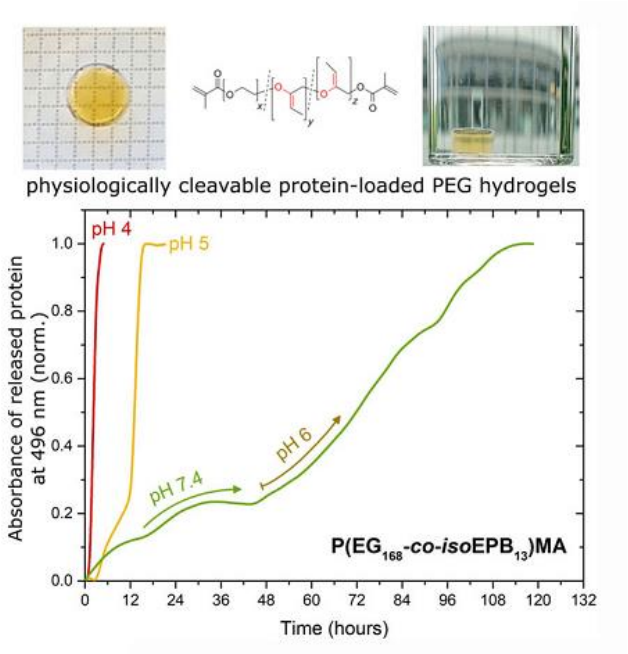

2.2 pH-Responsive Protein Nanoparticles via Conjugation of Degradable PEG to the Surface of Cytochrome c

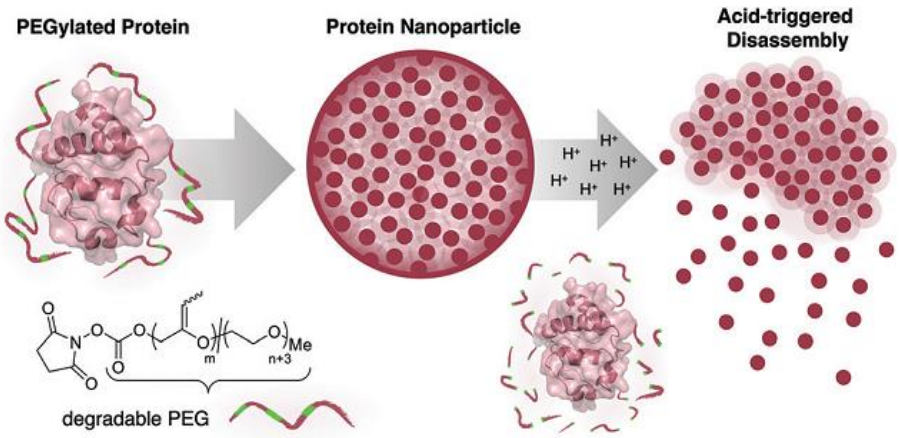

3 ALTERNATIVE ROUTES FOR VINYL ETHER PEGS

3.1 Predefined Cleavage Sites in Degradable Polymers Installed via Statistical Copolymerization: How reactivity ratios determine the Fragment distribution

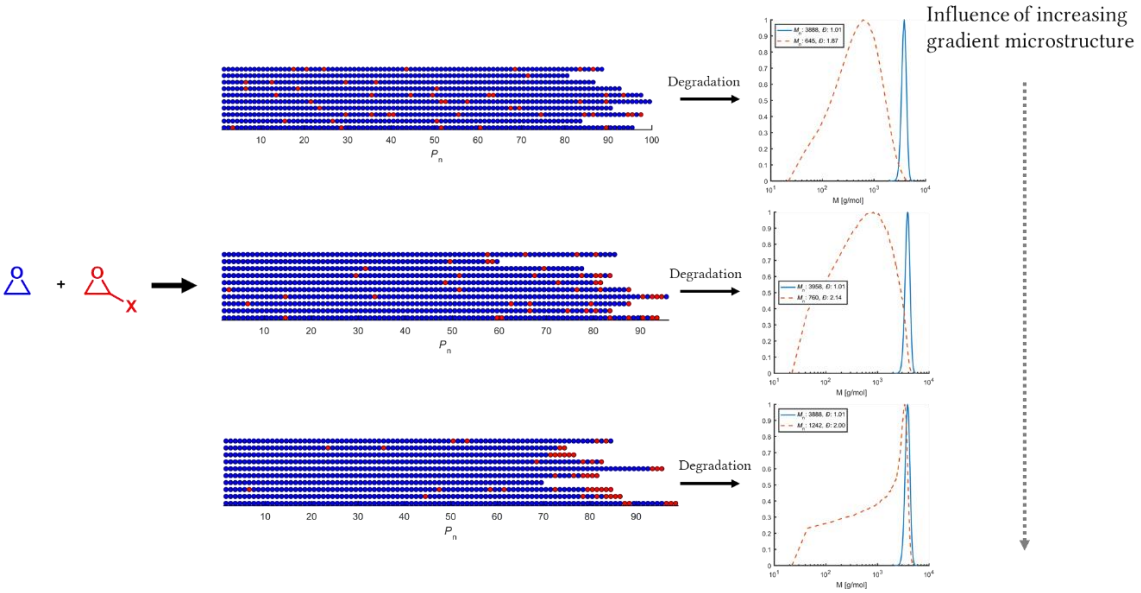

3.2 2,2‘-(2-Methylenepropane-1,3-diyldioxy)bisethanol as a Universal Synthon for Acid-labile Poly(ethylene glycol)

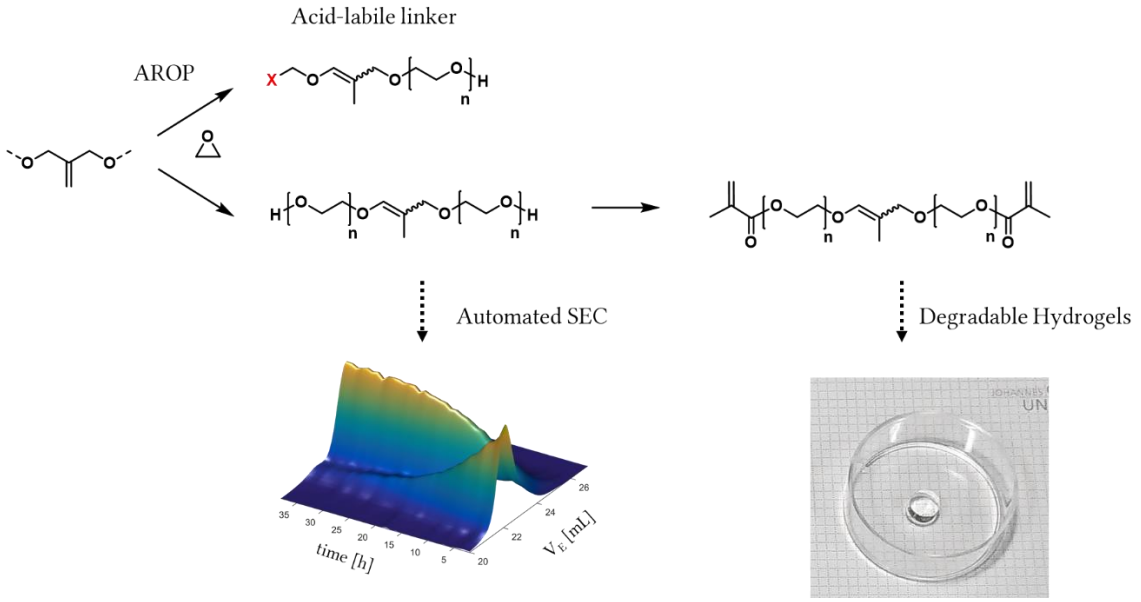

4 APPENDIX

4.1 A non-conventional approach towards multi-hydroxy functional polystyrenes relying on a simple Grignard reagent

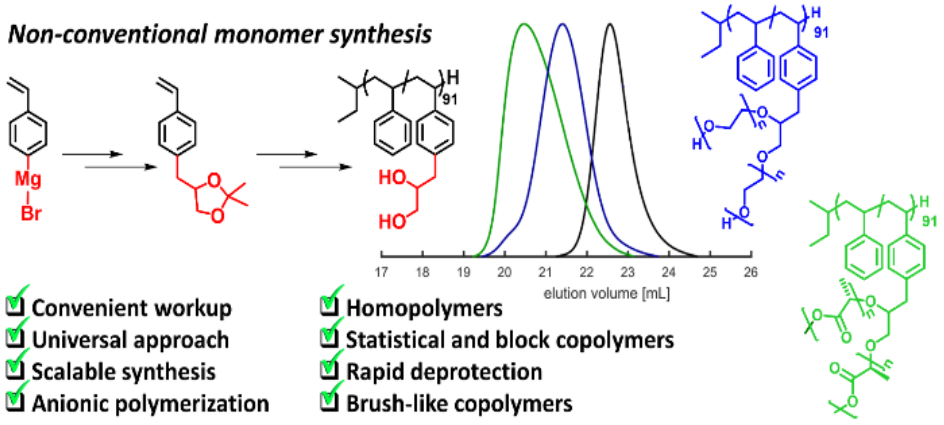

1 Introduction

This chapter will give a comprehensive overview over degradable poly(ethylene glycol) (PEG) in biomedical applications. Starting from the basic properties and synthesis in the first section, the focus will shift towards the general significance of degradable polymers for drug delivery systems in the second section. Subsequently, the third section will cover the chemistry of intrinsically cleavable PEGs. As a last section, selected biomedical applications for degradable PEGs will be presented.

1.1 Aliphatic Polyethers

Aliphatic polyethers are a class of polymers, that are represented by the general formula $(R\text{-}O\text{-}R')_n$. Herein, R and R' represent alkyl groups and n represents the degree of polymerization. The bond angle between the oxygen and the alkyl groups is 112 ° and the bond length between oxygen and carbon atom is 143 nm.[1] These polymers are of great interest in academia as well as in industry.[2]

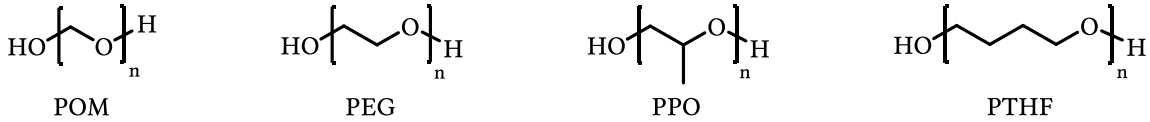

Scheme 1: Overview over the most prominent aliphatic polyethers: poly(acetal) (POM), poly(ethylene glycol) (PEG), poly(propylene oxide) (PPO) and poly(tetrahydrofuran) (PTHF).

Scheme 1 gives an overview over the most prominent and commercially available representatives of the class of aliphatic polyethers. The simplest structure is in fact poly(acetal), also known as poly(oxymethylene) (POM), with only one CH_2 group separating the oxygen atoms in the polymer backbone. By increasing this number, poly(ethylene glycol) (PEG) is reached together with the structurally related poly(propylene oxide) (PPO), which has an additional methyl group attached to the backbone as a side chain. Another prominent representative is poly(tetrahydrofuran) (PTFH), which corresponds to the molecular formula of tetrahydrofuran. For this work,

with no doubts PEG is the most important polymer and will therefore be discussed in detail in the next section.

1.1.1 POLY(ETHYLENE GLYCOL) (PEG)

Although Wurtz reported the polymerization of ethylene oxide (EO) with alkali metal hydroxide or zinc chloride as early as 1863, it took almost 70 years and the famous works of Staudinger and Schweitzer in the 1920s until PEG became commercially available in the 1930s.[3,4]

Depending on the degree of polymerization, the appearance of PEG at room temperature ranges from a colourless oil (~200–500 g mol^{-1}) over a waxy solid (~1,000 g mol^{-1}) to a crystalline solid above approximately 6,000 g mol^{-1}. Higher molecular weight PEGs in the range of 20,000 g mol^{-1} and above are typically referred to as poly(ethylene oxide) (PEO). In the biomedical context, the term PEG is usually used independently from the molecular weight.[5,6] The probably most highlighting characteristic of PEG is its excellent water-solubility, what makes this polymer outstanding among the other aliphatic polyethers, which are usually not water-soluble at room temperature.[7] While low molecular weight PEGs are practically mixable with water in any arbitrary ratio, PEG with a molecular weight of even 35,000 g mol^{-1} is still soluble in 50 wt% solutions with water at room temperature.[8] This feature can be explained by the distance of the oxygen atoms in the polyether backbone, which resembles roughly the distance of oxygen atoms in water. This facilitates the building of hydrogen bonds by the water molecules, leading to solvation.[9] Furthermore, PEG is non-toxic, low immunogenic and chemically almost inert.[10,11] This unique combination of features makes PEG an excellent polymer choice for various biomedical, cosmetic and pharmaceutical applications and justifies its widely known reputation as the gold standard, to which other polymers are compared to.[5,6]

One of the most prominent applications of PEG in the biomedical field is the so called PEGylation, which will be further addressed in **section 1.4.1**. The excellent biocompatibility and water-solubility of PEG makes this polymer also an attractive building block for hydrogels, what will be discussed in **section 1.4.2**. Other prominent applications of PEG can be found in the food industry or in cosmetics. Furthermore, PEG is often used as the hydrophilic component in amphiphilic copolymers, for example in PEG-*b*-PPO-*b*-PEG triblock copolymers, the well-known poloxamers or Pluronics©.[12,13] These low-toxic triblock copolymers are widely used as non-ionic surfactants in personal care products or for medical application.[14,15]

Alongside all unique properties of PEG, two major drawbacks should be mentioned: (i) the chemically inert polyether structure leaves PEG itself not degradable, what will be discussed in more detail in **section 1.2** and **section 1.3**, and (ii) PEG possesses only two chemically addressable functional groups at the chain termini, limiting for example its capacity for drug loading. The latter can be overcome by the copolymerization of EO with functional epoxide monomers. A wide range of possible functionalities can be introduced by this technique, from protected amines over allylic functionalities up to multiple hydroxyl groups and carboxylic acids.[16–18] These polymers usually are referred to as multi-functional PEGs (*mf*PEGs). Furthermore, besides such linear polyether structures, hyper branched or dendrimeric architectures offer a much higher ratio of backbone to end groups.[19]

1.1.2 Anionic Ring-Opening Polymerization (AROP)

Well-defined polymeric materials, exhibiting low dispersity ($Đ$), are a basic prerequisite for all biomedical and pharmaceutical applications. To ensure the reproducibility of crucial parameters like circulation times and immunogenicity of carrier systems, a dispersity of $Đ \leq 1.10$ is considered favourable.[20] To meet this

requirement, PEGs that are applied in these fields are usually synthesized *via* the anionic ring-opening polymerization (AROP) of EO.

In 1940, the remarkable works by Flory gave the theoretical background of the narrow molecular weight distribution and low dispersity of the polymers obtained *via* this technique. Flory demonstrated the living character of this polymerization, what results in a Poisson distribution of the molecular weight for the individual chains.[21]

$$Đ = \frac{M_w}{M_n} = 1 + \left[\frac{X_N}{(1+X_N)^2}\right] \approx 1 + \frac{1}{X_N}$$

As a result of the controlled manner of polymerization, without chain transfer reactions or unwanted termination of the chain end, the dispersity ($Đ$) is only depending on the weight (M_w) and number (M_n) average molecular weight, what connects this value directly to the degree of polymerization (X_N).

The oxyanionic polymerization is not only historically the "classical" technique to polymerize epoxides, it is also the most straightforward approach and is still applied today. Other techniques like coordination polymerization, monomer-activated polymerization (MAROP) or catalytic polymerization were developed and are applied in the industry as well as academia.[22–26]

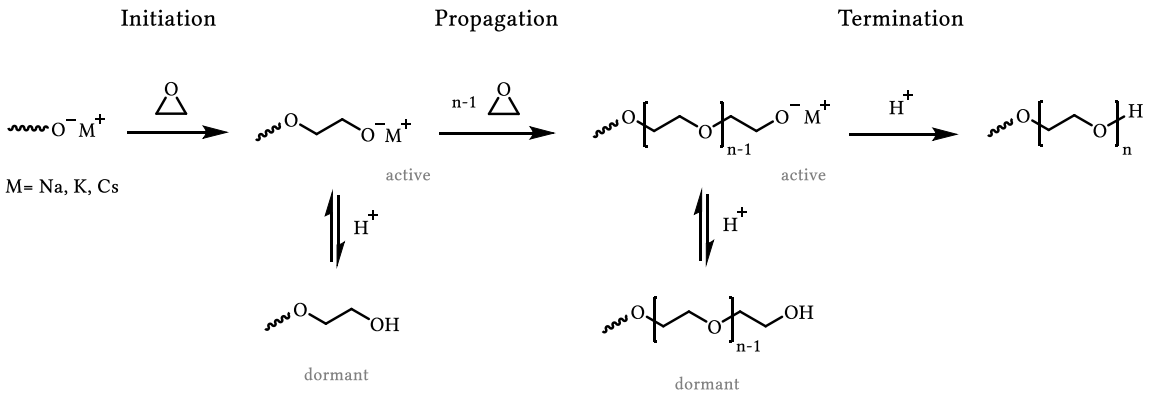

Scheme 2: Mechanism of the AROP of EO using an alkali metal alkoxide as initiator.

The AROP can be initiated by hydroxides, alkoxides, amides, metal alkyls or metal aryls.[27] The reaction mechanism can be described as a nucleophilic attack on the strained epoxide ring, which leads to the ring opening and the addition of a new monomer to the growing chain end (**Scheme 2**). With a value of 114 kJ mol^{-1}, the ring strain for oxiranes is the driving force for the polymerization. Larger rings with lower ring strain like oxolanes (THF, 23 kJ mol^{-1}) cannot be polymerized *via* this technique.[28]

Typically, alkoxide initiators are not quantitatively deprotonated to enhance their solubility and to prevent unwanted aggregation. A quantitative deprotonation is not necessary, as the proton transfer between the active alkoxide and the dormant alcohol species is much faster than the initiation and propagation process. Because of this equilibrium process between dormant and active chain end species, the criteria for a "living" polymerization are not strictly met.[29] To describe this process, the term "degenerative chain transfer" is used. However, as this polymerization technique allows a controlled polymerization with all chains participating in the chain growth, the term "living-like" may be used, referring to the controlled radical polymerization techniques, that also show dormant species and degenerative chain transfer.[25,30]

Despite the reaction temperature, the mainly influencing variables in the classical AROP technique are the choice of solvent and base, especially the corresponding counter ion. As these variables influence the nucleophilicity of the alkoxide initiator and growing chain end, they directly affect the rate of propagation through the active chain end. A chain end which is more separated from the counter ion results in a more active chain end and a faster propagation rate of the polymerization. This is directly influenced by the polarity of the solvent: a more polar solvent leads to a better solvation of the oxygen anion and the alkali metal cation, while an unpolar solvent favours the aggregation of the ions (**Scheme 3**). While bulk (solvent-free) polymerizations may be possible, AROP of EO is often conducted in solution. A solvent must be non-protic to not interfere with the alkoxide initiator and active chain end. Therefore, a wide range of solvents can be

applied, usually *N,N*-dimethylformamide (DMF), *N*-methyl-2-pyrrolidone (NMP), dimethyl sulfoxide (DMSO) or cyclic ethers like tetrahydrofuran (THF) or 1,4-dioxane are used.[31,32] Alkali metal counter ions can be complexed by cryptands or crown ethers. This separates the metal cations effectively from the oxide anions, what facilitates the polymerization by preventing the ions from aggregation, leading to fast propagation rates, or even enables the polymerization of originally non-polymerizable monomers.[33,34]

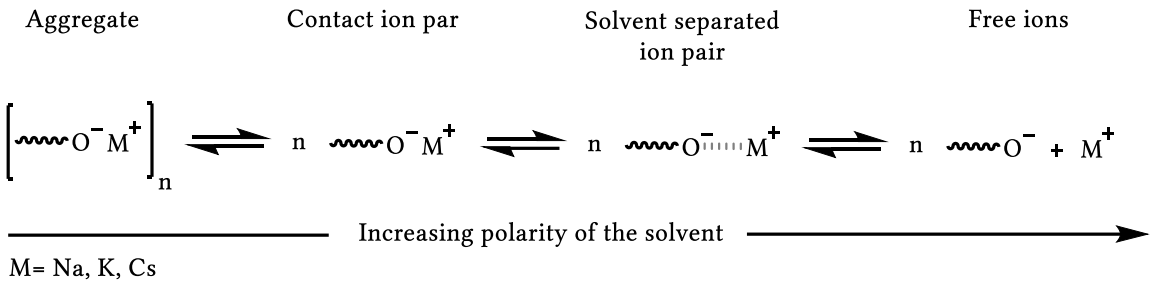

Scheme 3: The effect of solvent polarity on the aggregation of alkali metal alkoxide chain ends during AROP.

Another important factor is the counter ion or its size, respectively. The negatively charged alkoxide chain end, origin from the initiator at the initiation or the growing chain end during the propagation, interacts with the positively charged alkali metal counter ion. Based on Pearson's substantial principle of hard and soft acids and bases (HSAB), an oxygen anion is a "hard base".[35] This predicts the intensity of the interaction with the metal counter ion, serving as the corresponding "acid". A small and therefore "hard" counter ion like lithium prevents any polymerization by a strong aggregation with the oxide anion, while more "soft" and bulkier counter ions like potassium or caesium are used to enable a separation of the ion pair and therefore a propagation of the active chain end. This effect is exploited for the end-capping of butyllithium-initiated carbanionic polymerizations with functional epoxides.[36,37] According to this principle, the propagation rate of alkali metal alkoxide initiated polymerizations of epoxides corresponds with the size of the counter ion: $Na^+ < K^+ < Cs^+$.[38]

The strongly nucleophilic character of the initiator and the growing chain end also limits the range of applicable comonomers and initiators. Using the classical AROP, sensitive functions, possible leaving groups or acidic protons cannot be polymerized.[5,39]

1.2 Polymeric Concepts for pH-Triggered Drug Delivery

This section will briefly discuss the significance of concepts for acid-labile polymers in the context of biomedical applications such as drug delivery or polymer conjugates. While the focus of this dissertation is clearly set on PEG and its close derivatives, the following section is of rather general nature and the discussed concepts and strategies are valid independently from a certain class of polymers. Moreover, they can be, at least, understood as an essential motivation and offer an inspiration to be translated into any arbitrary system.

Beginning in the last quarter of the 20th century, the relevance of polymers in therapeutic applications is continuously increasing. The descriptor "polymer therapeutics" covers a variety of different systems and applications: polymers with an intrinsic therapeutic effect and, far more important, drug delivery systems in the form of polymer-drug conjugates, polymer-protein conjugates as well as polymer-based nanoparticles like nanospheres, micelles and polymersomes or liposomes (**Figure 1**).[20,40-42]

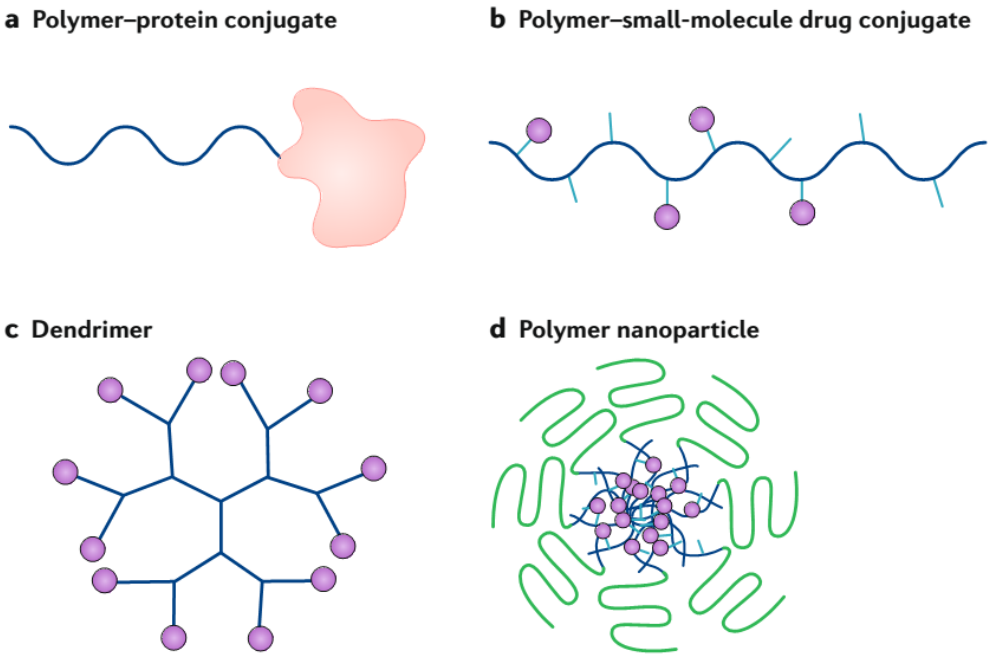

Figure 1: Classes of polymer-drug conjugates on the market or in clinical development. a) and b) water-soluble polymers can be conjugated to proteins or small molecule drugs, c) dendrimeric structures offer a high drug-polymer ratio and d) polymeric nanoparticles, typically as core-shell architectures. (Adapted and modified from Ekladious *et al.*)[42]

While PEG can be considered as the most prominent representative, depending on the desired application and therefore the chemical and physical requirements for the respective materials, various other polymers like poly(methyl methacrylate) (PMMA), poly(lactic acid) (PLA), poly(lactic-*co*-glycolic acid) (PLGA), poly(2-oxazoline)s (POx), polypeptides and a great number of further candidates have been and still are investigated and applied.[43–47]

Firstly mentioned by Paul Ehrlich in the 1910s with his pioneering concept of a "magic bullet", basic drug delivery systems are designed as a barrier between their cargo and their environment, in order to shield the cargo from the surroundings as well as the biological system from the cargo.[48,49] They are applied to improve pharmacokinetic parameters, reduce side-effects and enable targeted drug delivery.[50–52] Obviously, they need to release their therapeutic payload again, a process that can be facilitated with or without the presence of a stimulus.

Basic systems can rely on simple diffusion of the drug from a polymer matrix to the surrounding environment, only driven by chemical potential gradients.[53,54] "Smart" stimuli-responsive systems can release their cargo upon the presence of a specific stimulus, which leads to changes in the carrier environment, structure or chemistry.[54] A wide range of stimuli is possible, from physical influences like temperature, magnetic fields or light over biological stimuli like enzyme activity to chemical stimuli like ion strength, redox gradients and pH changes.[54–58]

For rationally designed polymeric drug delivery systems, acidity is the most important stimulus, since low pH is a characteristic of solid tumour and inflamed tissue and distinct intracellular compartments, which are passed through following cellular uptake.[59] Furthermore, the chemical approaches to exploit this stimulus are well-understood and preparatively realizable in a suitable manner. Tumour cells proliferate at a much higher rate than healthy tissue, leading to an upregulation of glycolysis, what results in an enhancement of the production and accumulation of lactate and protons in these tissues.[60] The extracellular pH of healthy mammal tissue as well as blood is rather strictly maintained at pH 7.4, but can reach pH 6.5 in solid tumours.[56,61] Another important target are intracellular compartments like endosomes and lysosomes. These compartments are part of cellular uptake pathways and can reach pH 5.0–6.0 or even pH 4.0–5.0, respectively.[62] This makes acidity an ideal trigger stimulus for specifically targeting these microenvironments and enhance therapeutic efficacy, what is shown in a variety of polymeric drug delivery systems.[62–66] Techniques to utilize this change in external pH can rely on alterations in configuration, conformation, solubility or volume of the drug delivery systems to release their payload.[67] This is usually realized by polymers which bear ionizable moieties or cleavable bonds.[68] The first group relies on the reversible ionization of weak acids or bases, which alters the swelling behaviour or solubility of the polymer.[68,69] The latter group uses mostly three different approaches or various combinations thereof: one or more chemically labile bonds, that can be

hydrolysed (i) between the polymer and the cargo, (ii) in the polymer backbone and (iii) between hydrophilic and hydrophobic segments of a block or copolymer.[53,58–65,68,70,71] In acidic conditions, the hydrolysis of such an acid-labile bond can lead directly to a release of the conjugated cargo by cleavage of a linker structure (i), destabilizing and degradation (ii) or by altering the solubility of the delivery system (iii), a concept often found for example in liposomes and micelles.[72]

1.3 Cleavable Moieties for Degradable PEGs

Beside the triggered release of therapeutically active molecules from a drug delivery system, the development of degradable polymer structures is driven by a very basic physiological parameter: the kidney excretion limit. While the conjugation with higher molecular weight PEGs has proven to be more favourable in order to prolong the circulation time of the conjugate, the applied polymer must not exceed a molecular weight of approximately 40,000 g mol^{-1}. This limit is set in order to prevent bioaccumulation by ensuring an effective clearance from the bloodstream by the kidney, followed by excretion *via* the urine.[73,74] On the other hand, the molecular weight of the degradation fragments should not be below 400 g mol^{-1}, as such small fragments were reported to show toxic effects.[20,75] PEG may be degraded *in vivo* by reactive oxygen species due to β-scission, but only in long time scales and unspecific.[76] This leads to many different approaches and to a lot of effort, that is undertaken to introduce degradability into the backbone of PEG, preserving its favourable properties while offering access to safely applicable high molecular weight PEGs.

1.3.1 SYNTHETIC APPROACHES FOR INTRINSICALLY CLEAVABLE PEGS

This section focuses especially on the different synthetical approaches to obtain intrinsically cleavable PEGs. To keep a clear structure, PEG-containing block-based structures with degradable linkers, grafted PEGs and PEGs in side-chains or systems with only short ethylene glycol oligomers will not be covered, even though they may show very creative approaches.[77–87]

The various synthetic approaches to introduce acid-labile moieties directly into the backbone of PEG are summarized in **Table 1**. It must be noted that the introduction of these moieties *via* the AROP of EO with a functional comonomer, that leads directly to the acid-labile moiety, may be the most desired approach. This approach would combine the favourable properties of the AROP, such as tailorable molecular weight and comonomer content, narrow molecular weight distribution and well-defined polymer end-groups with a clean and straight forward polymerization technique without the need for possibly toxic reagents like transition metals or other toxic reagents. Nevertheless, this has not been reported yet and the nature of the AROP with its harsh conditions limits the range of functional groups, that can be used to design functional monomers. Because of the nucleophilicity and the strong basic conditions, the range of interesting acid-labile functional groups is limited to acetals, ketals, ortho ester and vinyl or allyl ethers. Another important aspect is the chemical stability of possible monomers, as for example allene oxide or disulfur oxide may have been synthesized, but cannot be used for a copolymerization as they are not stable at relevant temperatures.[88–90]

Table 1: Compilation of cleavable groups, synthesis strategies and respective stimuli reported for PEGs and derivatives. Adapted and extended from Dingels, C.; Frey, H. In *Hierarchical Macromolecular Structures: 60 Years after the Staudinger Nobel Prize II*; Percec, V., Ed.; Springer International Publishing: 2013; Vol. 262, p 167. Copyright 2013 Springer.

Cleavable moiety	Structure	Synthetic approach	Degradation[a]	Ref.
Acetals	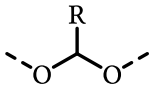	PEG coupling	pH < 7.4	78,91–104b
		Cleavable AROP initiator	pH < 7.4	105
Ketals	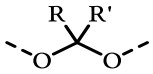	PEG coupling	pH < 7.4	106,107
		Cleavable AROP initiator	pH < 7.4	108–111
Aconitic acid	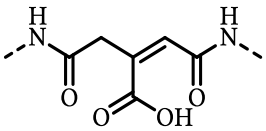	PEG coupling	pH < 7.4	112,113
Azo groups	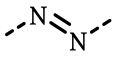	PEG coupling	enzymatic	114,115
Carbonates	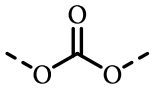	PEG coupling	basic hydrolysis	116–125
Carboxylates	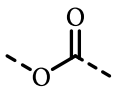	PEG coupling	hydrolytic, enzymatic	91,95,96,114,115,126–149
		Oxidation	hydrolytic, enzymatic	128
		Copolymerization of lactide	hydrolytic, enzymatic	130

Disulfides	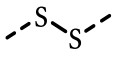	PEG coupling	reductive	133,150–153
Hemi-acetals	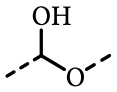	Oxidation	acidic or basic	154
Hydrazones	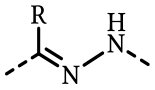	PEG coupling	pH < 7.4	155
Imines/Oxims	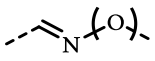	PEG coupling	pH 7.4	156
Maleamic acids	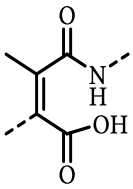	PEG coupling	pH < 7.4	157
o-Nitro benzyl ethers	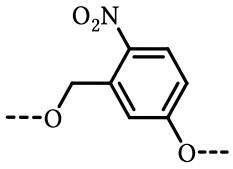	PEG coupling	light	158
Orthoesters	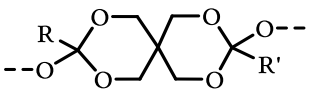	PEG coupling	pH < 7.4	159,160
Peptides	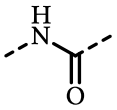	PEG coupling	hydrolytic, enzymatic	120,161–176
Phosphoesters	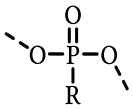	PEG coupling	acidic or basic	177–190
Urethane	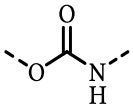	PEG coupling	hydrolytic	191–199
Vinyl ethers	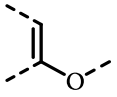	Elimination of P(ECH)	pH < 7.4	200

Copolymerization of EPB	pH < 7.4	[201–203], chap.. 2.1 and 2.2
Cleavable AROP initiator	pH < 7.4	chap.. 3.2
Elimination of glycidyl tosylate	pH < 7.4	chap.. 3.1

[a] Conditions may vary for the same cleavable unit due to different adjacent moieties.
[b] Includes inimers, which result in hyperbranched architectures.

As summarized in **Table 1**, a broad range of different degradable groups with different degradation mechanisms and stimuli was reported. The most important stimulus for the degradation of these PEGs is acidity, followed by enzymatic and unspecific hydrolytic degradation.

Most of these materials were synthesized starting from commercially available PEGs. As a broad variety of end group-functionalized PEGs are available, most of these approaches rely on the coupling of homotelechelic PEGs *via* polyaddition or polycondensation. As a result of these polymerization techniques, the obtained dispersities are rather high ($Đ$ = 1.6-10) and a precise control over the molecular weight is very difficult.[75] The main advantage of such strategies is, beside the rather non-challenging synthesis procedures using inexpensive or easily accessible difunctional PEG educts, that the degradation products are easily tailorable by the molecular weight of the used PEGs. As these strategies do not affect the backbone of the PEGs and only connect PEG chains at their end groups, the degradation products will remain at the same molecular weight than the original PEGs. This is a major advantage, as the control over the molecular weight of the fragments of degraded PEG is an important aspect.

Besides the PEG coupling techniques, there are principally three different synthetic approaches possible to obtain PEGs with intrinsically cleavable polyether backbones:

(i) oxidation of the polymer backbone, (ii) the polymerization of EO using a cleavable initiator and (iii) copolymerization with a degradable comonomer or a respective precursor.

The oxidation of the polyether backbone was firstly reported by Elisseeff and co-workers in 2010.[154] By using Fenton's reagent, they could partially oxidize the polyether to form hemi-acetals, randomly distributed alongside the polymer backbone. Unfortunately, this technique resulted in degradation already during the preparation process and no SEC data of the degradable polymer and its fragments after hydrolysis was provided. Another oxidation-based approach was reported by Liu and Bielawski with the synthesis of poly[(ethylene glycol)-*co*-(glycolic acid)] by oxidation of PEG using ruthenium oxide.[128] This method provided degradable PEGs with various ratios of cleavable moieties and the authors analysed the polymer degradation regarding rates and molecular weight distribution of the resulting fragments. Nevertheless, the formation of different end groups as result of the oxidation of the PEG chain ends limits the possible applications in the biomedical field.

Pohlit *et al.* presented the introduction of a ketal moiety into the PEG backbone *via* the polymerization of EO using a ketal-containing difunctional AROP initiator.[108] They obtained well-defined polymers ($Đ \leq 1.12$) with a molecular weight of up to M_n = 12.800 g mol^{-1} and investigated the hydrolysis kinetics *via* ^{1}H NMR spectroscopy. They reported half-life times of the dimethyl ketal moiety at pH 6.1 with $t_{1/2}$ = 82.4 min for 23 °C and $t_{1/2}$ = 10.4 for 37 °C. A similar approach was reported earlier by Dingels *et al.* with the implementation of an acetal moiety at the hydroxyl-end of mPEG (M_n = 2,000 g mol^{-1}), resulting in an acetal-functional PEG macroinitiator for the AROP of EO.[105] Using this macroinitiator for the synthesis of PEG, they reported a well-defined polymer ($Đ$ = 1.09) with a molecular weight of M_n = 7,500 g mol^{-1}. Acidic hydrolysis of this polymer resulted in two fragments with a molecular weight of M_n = 1,800 g mol^{-1} and M_n = 5,700 g mol^{-1}, as to be expected from the position of the degradable moiety in

the PEG backbone. Degradation kinetics studies of various acetal structures *via* ^{1}H NMR spectroscopy revealed half-life times of $t_{1/2}$ = 62–143 h at pD 4.9 and $t_{1/2}$ = 961 h at pD 5.4, demonstrating a much higher stability with slower hydrolysis than the reported ketal structures.

More recently, Feng and co-workers presented the copolymerization of EO with (L)-lactide using triethylborane as an activator.[130] They obtained poly(ethylene glycol-*co*-lactic acid) with molecular weights of up to M_n = 48,500 g mol^{-1} with moderate to low dispersities ($Đ$ = 1.05–1.28). The fraction of (L)-lactide as degradable moiety ranged between 1.1 and 11 mol% but could not be adjusted in a targeted and controlled fashion. Furthermore, the obtained yields of these polymers were relatively low.

The introduction of degradability into a polyether backbone by the anionic (co)polymerization of a functional epoxide monomer remains a challenge. So far, the incorporation of in-chain acidic cleavable moieties was only reported for few hyperbranched systems. They were synthesized using the AROP of EO with an acetal or ketal-functional comonomer like 1-(glycidyloxy)ethyl ethylene glycol ether (GEGE) (**Figure 2**).[101,109,110]

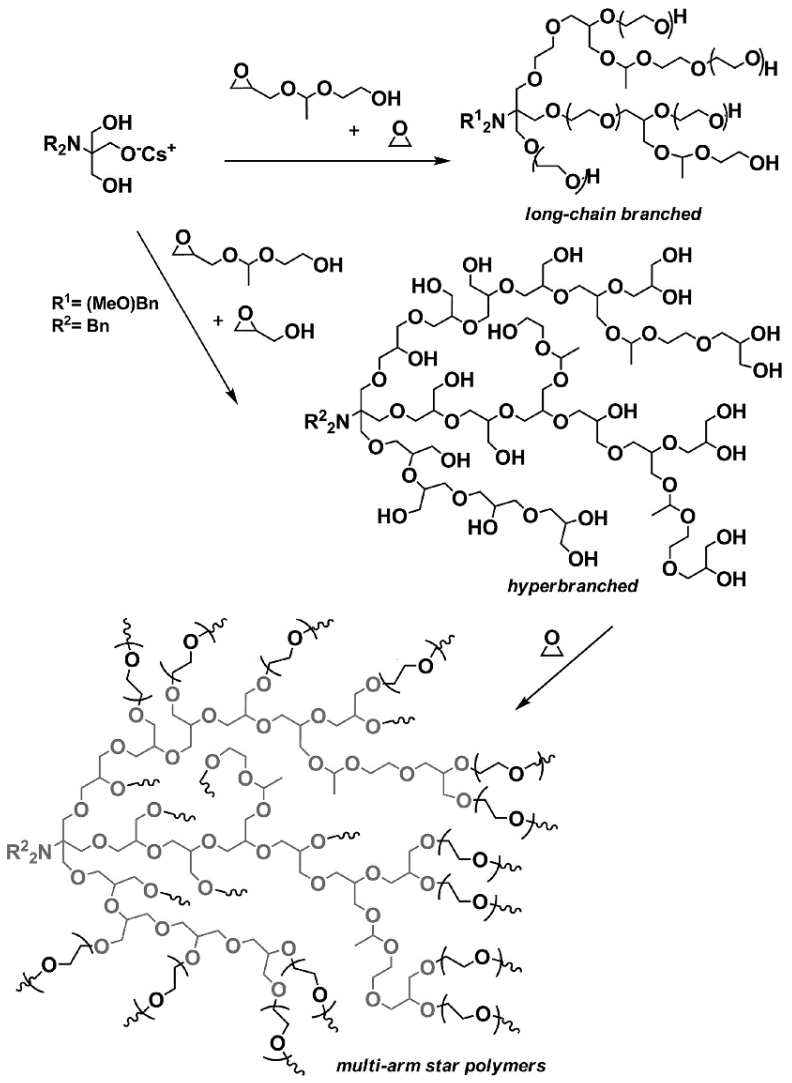

Figure 2: Overview of the different copolymerization routes developed based on the GEGE monomer (from Ref. [101]).

Notably, these concepts remain preserved for branched architectures and cannot be translated into linear structures. During every AROP of epoxide monomers, the polyether backbone is principally formed by the oxirane segment of the monomer. For the formation of hyperbranched architectures, a branching agent in form of a comonomer is added, which contains at least one unprotected hydroxyl group in addition to the epoxide function. This leads to the branching effect, as during the polymerization not only the alkoxide chain end that originates from the last incorporated epoxide, but also the hydroxyl group of the branching comonomer takes part in the propagation process.[204,205] This way, the substituent at the epoxide is directly incorporated into the

growing polyether backbone, additionally to the epoxide segment. As the substituent can be designed to carry a functional spacer (for example an acetal moiety in GEGE, see **Figure 2**) between the epoxide ring and his hydroxyl group, this function will be incorporated into the polyether backbone.

This is fundamentally different to AROP techniques to synthesize linear polymers, where the polyether backbone is formed exclusively by the ring-opening of the epoxide monomers. Possible functional substituents at the epoxide ring do not take part in the propagation of the polymerization and form the polymer side chains and functions attached to the backbone of *mf*PEGs, if present.[5,17]

This explains the challenges for the direct introduction of cleavable moieties into a linear polyether backbone by copolymerization with a functional epoxide. To enable intrinsic cleavability, the respective functionality must be located as a substituent directly at the epoxide ring to enable direct influence on the polyether backbone. Besides this prerequisite, it should not affect the polymerization and withstand the harsh AROP conditions. While such a direct approach has not been reported yet and seems hardly to be possible, only two synthetic approaches have been reported so far to access intrinsically cleavable PEG by copolymerization with an epoxide comonomer. Both synthetic principles rely on a diversion to obtain acid labile vinyl ether PEGs in a two-step procedure.[200,201]

Because of the fundamental significance of the acid-labile vinyl ether moiety for this work, the next section will briefly discuss vinyl ether functional PEGs and strategies for their synthesis in more detail.

1.3.2 VINYL ETHERS AS ACID-LABILE FUNCTIONAL GROUPS IN PEG

Vinyl ethers are no "novel" or revolutionary new functional group in synthetic organic chemistry. From the beginning of the 1960s, vinyl ethers and their precursors, the allyl ethers saw extensive use especially in the carbohydrate chemistry as protective group for hydroxyl groups.[206] The easy formation and cleavage under mild conditions, which is tolerated by many other protective groups, made ally ethers a very common choice for orthogonal synthesis strategies.[207]

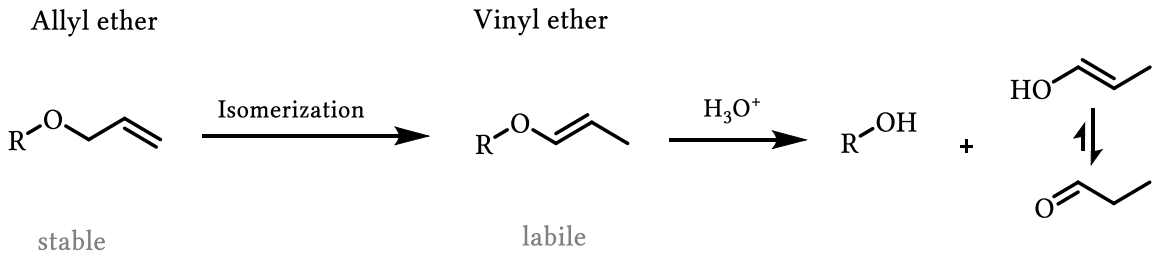

Scheme 4: Transition of the allyl ether group to a vinyl ether and subsequent cleavage.

Scheme 4 illustrates the application of allyl and vinyl ethers for the protection of hydroxyl groups. The allyl ether moiety serves as a stable precursor and can be converted into a vinyl ether moiety by isomerization. Subsequently, the vinyl ether can be cleaved using several different approaches, but usually by acidic hydrolysis or by oxidative methods.[206] The isomerization is a central step in this process and a broad variety of different methods have been investigated. The isomerization of the olefin is often base-catalysed by heating in DMSO with the presence of potassium *tert*-butoxide or by Wilkinson's catalyst ($RhCl(PPh_3)_3$), but various other catalytic systems have been investigated and applied as well.[208–211] More recently, approaches for the one-step cleavage of the allyl ether group became popular.[212–214] Another interesting feature of the allylic group is the protection of thiols and amines, what already found an application in polymer science with the development of the protected amine monomer *N,N*-diallylglycidylamine (DAGA), offering access to amine-functional PEGs.[215–218]

Several reports from Thomson *et al.* showed the application of vinyl ethers as acid-labile linkers in polymeric drug delivery systems. They employed vinyl ethers as acid-labile linkers between hydrophilic PEG and hydrophobic lipid segments and used these materials to form acid-degradable liposomes for drug delivery applications.[81–83,219,220]

As previously mentioned, there are two approaches to utilize this functional group to synthesize intrinsically cleavable PEGs. The first approach was reported by Lundberg *et al.* in 2012.[200] They copolymerized EO with epichlorohydrin (ECH) *via* the monomer-activated ring-opening polymerization technique (MAROP) to obtain poly(ethylene glycol-*co*-epichlorohydrin) (P(EG-*co*-ECH)) and subsequently eliminated the chloride to obtain poly[(ethylene glycol)-*co*-(methylene ethylene oxide)] (P(EG-*co*-MEO)) as a vinyl ether-functional PEG (**Scheme 5**).

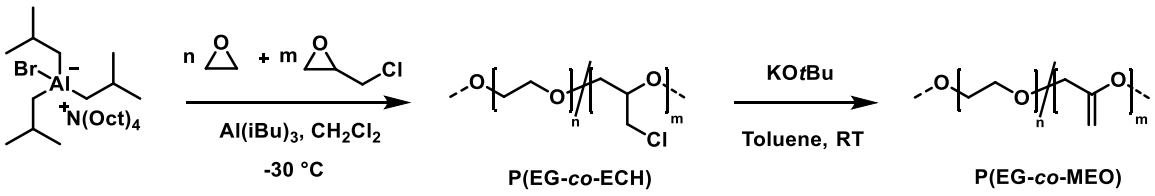

Scheme 5: Synthetic approach to obtain P(EG-*co*-MEO). (Adapted and redrawn from Lundberg *et al.*)[200]

While this was the first report to obtain linear and intrinsically cleavable vinyl ether functional PEG *via* the copolymerization of a functional epoxide, it was obliged to apply the MAROP technique. Alkoxides appearing during the classical AROP would undergo substitution reactions with the chloride of ECH, rendering this technique not applicable with such comonomers. Furthermore, this technique resulted in rather broad molecular weight distributions ($Đ$ = 1.25–1.34) and ill-defined polymer end-groups, limiting the possible use for biomedical application.

Worm *et al.* presented a refined approach, which enables a broad range of biomedical applications for these materials, as the fundamental synthesis strategy relies

on the classical AROP and eliminates the disadvantages given by the MAROP approach.[201] By the copolymerization of EO with 3,4-epoxy-1-butene (EPB), allyl ether-functional PEG copolymers (P(EG-*co*-EPB) were obtained, which were subsequently isomerized to vinyl ether containing PEGs (P(EG-*co*-*iso*EPB) as shown in **Scheme 6**.

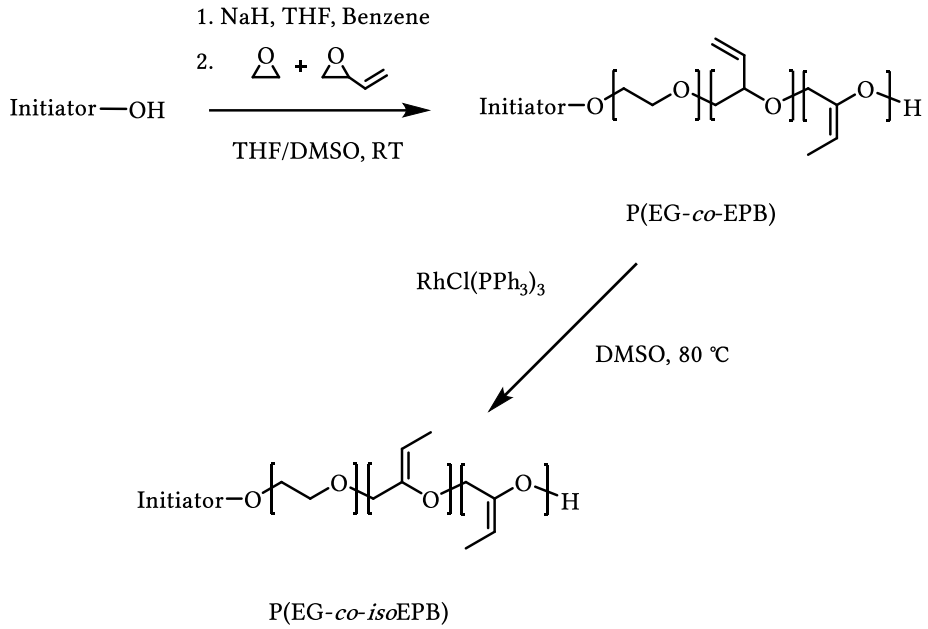

Scheme 6: Synthetic procedure for P(EG-*co*-*iso*EPB) copolymers. (Adapted and redrawn from Worm *et al.*)[201].

This technique enabled the synthesis of well-defined, degradable PEGs ($Đ \leq 1.11$) with molecular weights of up to M_n = 10,000 g mol^{-1} and tailorable content of cleavable moieties inside the polyether backbone (3.4–4.5mol%). Defined and chemically addressable polymer end-groups were obtained, allowing to adopt this concept for a broad variety of biomedical applications (see **chapter 2.1 and 2.2**). Furthermore, they analysed the degradation kinetics of these moieties *via* online ^{1}H NMR spectroscopy, resulting in $t_{1/2}$ = 9–20 h at pD 4.4 and $t_{1/2}$ = 20–34 h at pD 5, ranging between the acidic degradation kinetics of acetals and ketals. As reported by Shin *et al.*, the pH sensitivity can be further fine-tuned by different substitution patterns at the vinyl ether.[82]

1.4 Selected Applications: PEGylation and Hydrogels

This section will discuss some typical applications in the biomedical and therapeutic field for PEG and especially for degradable and stimuli-responsive structures, as presented in the **chapters 1.2 and 1.3**. First the field of polymer-conjugates, especially PEG-conjugates as a subgroup of the already in **chapter 1.2** introduced polymer therapeutics will be discussed, followed by the field of hydrogels as another substantial application for degradable PEG-based materials.

The importance of proteins and peptides as therapeutic molecules is strongly increasing, especially in the therapy of cancer, inflammatory and immune diseases or vaccines.[221] However, the fragile three dimensional structure of proteins is often important for their therapeutic action and needs to be preserved. Generally speaking, protein therapeutics suffer chronically from poor stability due to chemical and enzymatic degradation, unfolding and aggregation and may cause immune reactions.[222–224] Due to the low pH environment of the stomach and the presence of proteolytic enzymes, an oral administration is challenging. Additionally, their large size and hydrophilicity complicates an absorption through biological membranes, what results in a low bioavailability. This makes the parenteral administration to the technique of choice for the application of this class of drugs.[225] Unfortunately, the half-live time of proteins upon injection is very short due to the fast renal clearance and first-pass hepatic metabolism, additionally to the clearance by the immune system, affording frequent injections. Three approaches are under consideration to overcome these pharmacokinetic and pharmacodynamic difficulties: (i) the application of drug-polymer conjugates (as described in the following section), (ii) alternative administration routes like nasal or pulmonal delivery and (iii) the application of injectable or implantable controlled releasable drug delivery systems like liposomes or hydrogels (as will be described in **section 1.4.2**).[226,227]

1.4.1 PEGYLATION AND BIOCONJUGATION

Ringsdorf opened the field of polymer-conjugates as drug delivery systems with his thoughts on a rationale for covalently bound polymer-drug conjugates, based on synthetic polymers.[228,229]

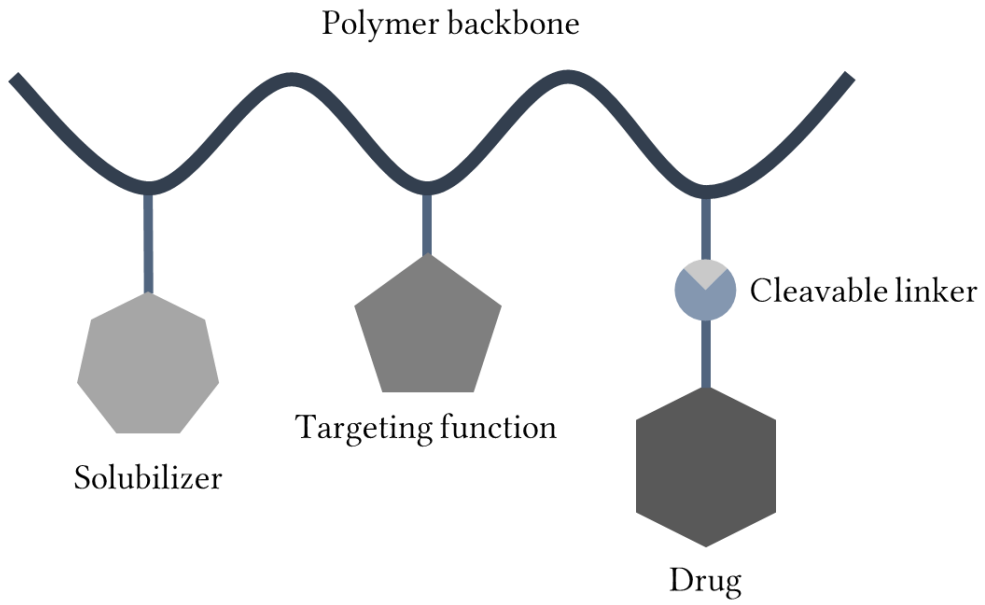

Figure 3: Polymeric drug delivery system as proposed by Ringsdorf.[229]

With his idea of a polymeric carrier system that consists of three functional main components: (i) a solubilizer, (ii) a targeting function and (iii) the drug, conjugated by a degradable linker molecule, with all three components attached to the backbone of a biocompatible polymer, Ringsdorf was far ahead of his time and shaped the foundation of a field, which applies this concept today in a broad variety (**Figure 3**).

Today, we use the term "PEGylation" to refer to the covalent attachment of PEG to surfaces, molecules with a therapeutic effect (small molecules, proteins, peptides), biomolecules or therapeutic vehicles like the broad range of nanoparticles (organic or inorganic particles, micelles, liposomes or polymersomes).[230] As a downright revolution in drug delivery, PEGylation is mostly applied to improve pharmacokinetic parameters like solubility or half-life time of the conjugate, resulting in improved therapeutic

activity.[40,231,232] This is achieved by two major effects: (i) shielding of the conjugate from the immune system and supressing unspecific cellular uptake ("stealth effect") and (ii) increasing of the hydrodynamic radius of the conjugate, preventing a fast clearance from the bloodstream by ultrafiltration and excretion *via* the kidneys.[233,234] For PEG in solution, every ethylene glycol subunit is roughly coordinated by two or three water molecules, resulting in a hydrodynamic radius around five to ten times larger than a protein with the same molecular weight.[235–237] The prolonged half-life time of the conjugate can result in a reduction of the dosage frequency, improving the quality of life and compliance of the patients since these drugs usually need to be injected.[74] Furthermore, PEGylated drugs and proteins show an improved physical and thermal stability and are better protected against enzymatic degradation.[238,239]

The mechanism of the prevention of unspecific cellular uptake of PEG-based conjugates by components of the immune system, the so called stealth effect, was analysed in detail by Wurm and co-workers.[240] They argued that this effect is not depending on the prevention of surface protein binding *per se*, but instead that the formation of a blood plasma protein corona with the abundance of a specific protein (clusterin or also called apolipoprotein J) plays a key role and seems to be responsible for this effect.

The first protein-PEG conjugates were presented by Davis and co-workers in 1977. While maintaining the enzymatic activity of PEGylated liver catalase, they reported an extension of the *in vivo* circulation time from 12 hours up to 48 hours.[241] Furthermore, they demonstrated the non-immunogenicity of PEGylated bovine serum albumin (BSA).[242] Since these pioneering works, PEGylation was further developed to a well-established standard-technique in the modern pharmaceutical industry as well as in academia. The first FDA-approved PEGylated drug to become commercially was Adagen© in 1990, an adenosine deaminase coupled to 11-17 chains of mPEG with a molecular weight of M_n = 5,000 g mol^{-1}.[243] This modification resulted in an increase of

the plasma half-life time from 20 hours to 357 hours, enabling a dosing frequency of once every two weeks instead of two or three doses every week.

These nowadays so-called 1st generation PEG-conjugates were further developed to and mostly replaced by 2nd generation conjugates. While the fist-generation conjugates suffered from difficulties like a mixture of isomers in the prepared conjugate as a result of the modification of multiple lysine residues or crosslinking of the proteins due to diol-contaminated mPEGs, the development aimed to provide better defined and more stable conjugates with more reproducible results.[244,245]

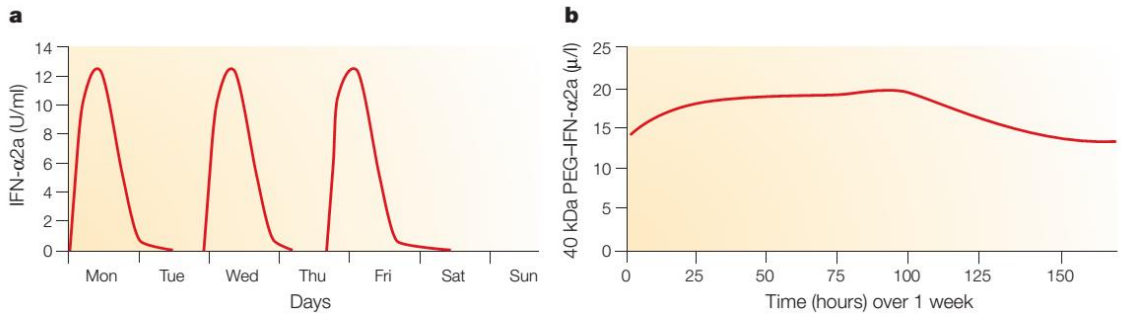

Figure 4: Pharmacokinetic profiles for interferon IFN-α2a and M_n = 40,000 g mol^{-1} polyethylene glycol PEG–IFN-α2a: blood levels upon subcutaneous injection. a) IFN-α2a is injected every other day and b) PEG–IFN-α2a is injected once a week. (Adapted and modified from Harris and Chess).[239]

Characteristic for this improved generation are PEGs with higher molecular weights to create larger conjugates with further improved pharmacokinetic and pharmacodynamic properties. For example, the 2nd generation conjugate Pegasys© (FDA approved in 2002) consists of a branched PEG with M_n = 40,000 g mol^{-1}, conjugated to IFN-α2a. This conjugation extended the half-life from 9 to 77 hours, while providing a nearly constant blood concentration (**Figure 4**).

As for 2019, there are sixteen FDA-approved PEG-protein conjugates available and at least twenty more conjugates in the pipelines of pharmaceutical companies, companied by at least twenty one small molecule conjugates, dendrimers and polymeric nanoparticles in clinical development.[42] To avoid bioaccumulation and enable a safe

application of such conjugates, all FDA-approved PEGylated conjugates employ PEGs with a molecular weight of $M_n \leq 40{,}000$ g mol^{-1}.[246]

Commonly, for the conjugation of larger molecules such as proteins, linear and branched monofunctional PEGs are employed to prevent crosslinking. Small molecule drugs may be conjugated to dendrimeric polymer architectures, enabling much higher drug loading ratios.[162,247] The most common target for PEGylation of therapeutic proteins and peptides are lysine residues due to their large number of amino groups on the accessible surface and their facile modification. Additionally, the thiol group of cysteine is a popular target because of the possibility to use robust Michael-addition chemistry for conjugation.[248] Nevertheless this function may be a difficult choice, as it is often involved in active sites and enzymatic activity of the conjugate may like to be preserved.[249,250] Furthermore, it was demonstrated by Veronese and co-workers, that not only the polymer mass and chemistry of conjugation, but also the shape impair the biological activity of the conjugate, indicating an advantage of branched over linear architectures in preserving enzyme activity.[251] To conjugate PEG to any of these groups, the hydroxyl end group must be activated. Common and commercially available activated PEGylation agents rely on carboxy, various active esters (NHS especially) or maleimide functional end-groups.[252]

Not only the favourable application of higher molecular PEGs to further improve the pharmacokinetic parameters of conjugates, but also the effect, that PEGylation can influence the biological activity and the binding of conjugated proteins to their respective cellular receptor and impairing the recognition of targeting functions, highlights the significance of improved PEGylation agents.[235] To solve these problems, the development of reversible or releasable “rPEGylation” approaches has been promoted since the beginning of the 2000s. Commonly, these approaches focus on the implementation of transient linkers like hydrazone, disulfide, esters or bicine between the polymer and the conjugate. A large number of different systems has been reported

and already extensively reviewed.[253–257] While these approaches still rely on the chemical modification of commercially available PEGs and focus on the linker chemistry, there are only very few reports on intrinsically cleavable PEGs for reversible or transient PEGylation.[5] More recently, Maynard and co-workers presented an original approach for reversible bioconjugation, which relied on the ring-opening metathesis polymerization of a mono-unsaturated crown ether, resulting in an aldehyde-functional PEG-derivative, that was conjugated to lysozyme.[85] Although the successful conjugation and subsequent removal of the polymer was demonstrated, the presented stimulus for degradation in form of depolymerization by Grubbs III was not physiological. So far, the use of tailor-made, intrinsically cleavable PEGs for PEGylation is sparsely reported because of the preparative difficulties of polymerizing PEG in-house and the commercial availability of readily functionalized PEGs, but still offers a wide range of promising possibilities for further developments.

1.4.2 PEG Hydrogels for Biomedical Applications

Three-dimensional cross-linked networks, made of hydrophilic polymers, are commonly referred to as hydrogels.[258] The crosslinking can be conducted by various methods, from mainly physical and reversible methods like molecular entanglement, ionic or hydrophobic interactions or hydrogen bonding to irreversible chemical crosslinking under formation of covalent bonds.[259–261] They are usually characterized by their mechanical stability, mesh size and swelling behaviour.[262]

Depending on their polymeric building blocks or macromonomers and methods of crosslinking, “smart” hydrogels can be designed which respond to a wide array of stimuli like pH, temperature or ionic strength.[259,263] The most important applications for these systems are the delivery of therapeutically active molecules (small molecules as well as macromolecules) and to serve as a scaffold for cell growth in two or three dimensional

cell culture and tissue engineering, beside traditionally serving in wound dressing applications.[264–266] Because of its favourable properties like water-solubility and low toxicity while offering a wide range of molecular weights, architectures and reactive derivatives "off the shelf", PEG is an popular polymer to synthesize such materials. Common techniques apply very robust radical or Michael-type crosslinking strategies that use reactive end groups like acrylate, methacrylate, maleimides, thiols or vinyl sulfones to crosslink PEG macromonomers.[267,268] More recently, the use of "click-chemistry" is getting popular as biorthogonal crosslinking strategy.[269] Generally, the chemical crosslinking step can be classified as a chain-growth or step-growth mechanism or a mixture of both (**Figure 5**).[270] For example popular PEG-bismethacrylate can be crosslinked by radical initiator molecules, resulting in chain polymerization of the methacrylate moieties, leading to the formation of covalently crosslinked high molecular weight chains.

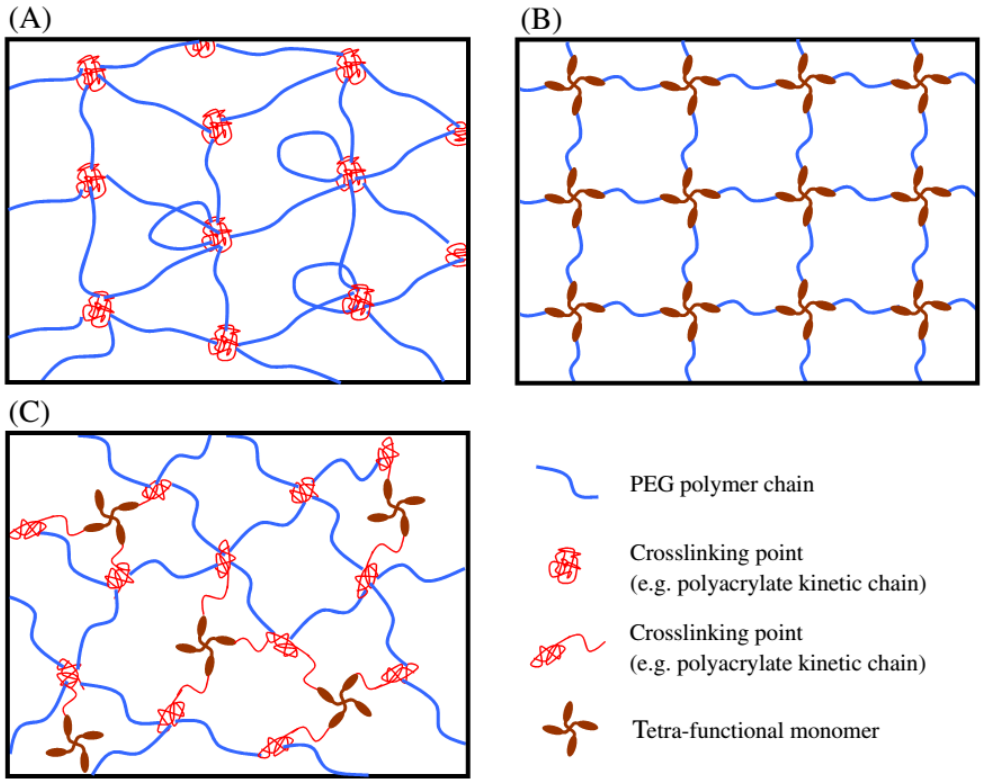

Figure 5: Schematic structures of PEG hydrogels formed *via* (A) chain-growth, (B) step-growth, and (C) mixed-mode step and chain growth polymerization (Components not scale to actual size). (Adapted from Lin and Anseth).[267]

Step growth mechanisms occur by the combination of at least two mutually reactive multifunctional (macro)monomers with an average monomer functionality greater than two.[271] This reaction can be conducted without the use of free-radical initiator molecules and offers a better control over the network formation and crosslinking density, while providing fewer structural network defects and a more uniformly dense crosslinked hydrogel.[272] Furthermore, the use of crosslinkers or functional (macro)monomers allows to precisely introduce additional functionalities into the network, for example stimulus responsive structures like degradable moieties.[273] For example Fisher and co-workers incorporated ketal moieties into the matrix of a PEG hydrogel by radically crosslinking PEG diacrylate with a cyclic ketal-bearing and diacrylate-functional comonomer. This gave access to acid degradable EH-PEG hydrogels with controllable swelling degree and sol fraction.[274] In a follow-up study, the degradable hydrogels were loaded with a therapeutically active protein (BMP-2) to enhance the bone regeneration process in an orbital floor defect in rabbits. A subsequent successful BMP-2-mediated bone growth at the place of the implanted hydrogel demonstrated the ability of this system for local drug delivery *in vivo*.[275]

In vivo tissue is a very dynamic and complex environment, in which cells strongly interact with components of their extracellular surroundings.[276] As tissue engineering and cell culture approaches try to mimic *in vitro* this environment, it is a crucial feature especially for the study of differentiation and tissue evolution to control the physical and chemical properties of the three dimensional hydrogel scaffold in a spatially and temporary controlled manner.[264,277,278] Typically, these polymeric material properties can be changed by controlled degradation of the material under the breaking of chemical bonds. The most commonly applied mechanisms of degradation are hydrolysis and enzymatic cleavage, because the degradation must be facilitated in a manner, which does not greatly impair the vitality of the host cells. Therefore, harsh conditions are not applicable. Ester bonds are frequently used as predetermined breaking points *in vitro*, as

anhydrides are hydrolysed too fast and amides without the presence of a catalyst hydrolyse too slow. Nevertheless, the non-enzymatic ester hydrolysis is still slow and rather uncommon *in vivo*.[277] This facilitated the development of materials which are enzymatically cleaved by natural matrix metalloproteinase (MPP), secreted by the cells themselves.[279–281] For example Hubbell and co-workers presented a hybrid hydrogel system by crosslinking of a tetra-arm vinyl sulfone-functional PEG with a bifunctional cysteine oligopeptide *via* Michael-type addition, incorporating the enzymatic sensitive peptide as linkages into the hydrogel.[282] These approaches enable a remodelling of the scaffold during three dimensional cell migration and invasion, offering an improved model system that behaves closer to natural environments.

Another interesting feature of hydrogels is the option to incorporate therapeutically active molecules into the scaffold. Hydrogels can be used to entrap small molecules, macromolecules or nanoparticle. For example, Zisch *et al.* incorporated vascular endothelial growth factor (VEGF) and a cell adhesive peptide into a PEG-based scaffold to precisely enhance the local angiogenesis *in vivo*, resulting in the remodelling of the hydrogel craft into native, vascularized tissue.[283] Another interesting application for degradable PEG-based hydrogels, which are loaded with therapeutic active substances, is the use for bone mineralization. As reported by Schröder *et al.*, the incorporation of vaterite nanoparticles into a degradable PEG-based scaffold results in a promising biomimetic material, that has the potential to improve the rapid regeneration of bone defects.[284,285] Additionally in the context of bone mineralisation, the group of Gburek reported hydroxyapatite cement composites with addition of non-degradable HEMA or degradable PEG-PLLA dimethacrylate triblock copolymers as a degradable crosslinker in the HEMA matrix, demonstrating five to six times higher toughness values compared to the pure inorganic cement matrix.[286]

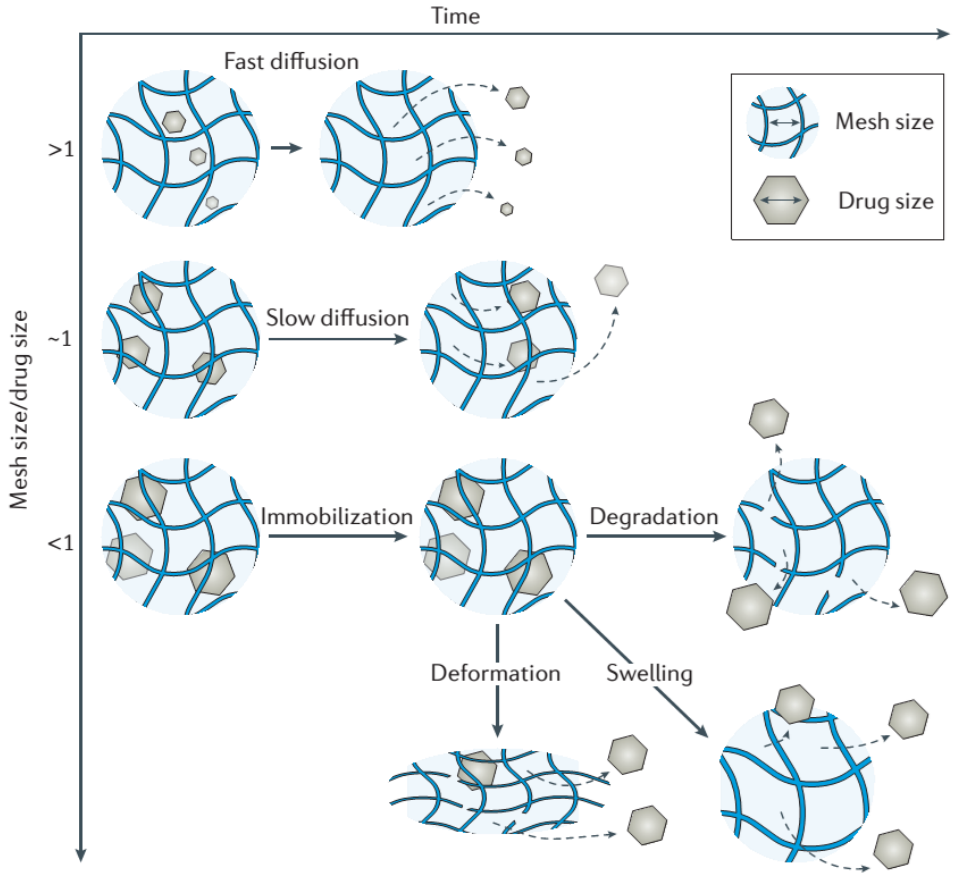

Figure 6: Mesh size mediates drug diffusion. When the size of a drug approaches the mesh size ($r_{mesh}/r_{drug} \approx 1$), drug release is dramatically slowed. When the drug is larger than the mesh size ($r_{mesh}/r_{drug}<1$), drugs are physically entrapped inside the network. To release the originally immobilized drugs, the mesh size can be enlarged through network degradation or swelling, or by applying deformation to disrupt the network. (Adapted and modified from Lee and Mooney).[264]

Beside their applications in tissue engineering and cell culture, hydrogels also play an important role as drug delivery systems, especially for macromolecular drugs like proteins and peptides. The release of therapeutic active molecules from hydrogels depends on multiple factors, such as the crosslinking density of the gel and the molecular characteristics of the drug. In general, these approaches can be categorized into diffusion controlled and degradation or swelling controlled (**Figure 6**).

In the first scenario, the hydrodynamic radius of the host molecule is smaller than the pore size of the hydrogel, making diffusion the driving mechanism for release. In the second case, the hydrodynamic radius of the host molecule is larger than the average

pore size, making swelling or degradation of the hydrogel needed to release the entrapped and immobilized molecule.[225] These approaches rely mainly on the mesh size and the size of the entrapped molecule and are independent from direct or covalent network-drug interactions. In this fashion, the group of Peppas reported a pH sensitive hydrogel system for oral protein delivery. Based on the radical copolymerization of PEG mono-methacrylate (PEGMA) and methacrylic acid (MAA), they synthesized a partial "PEG grafted on PMMA" (P(MAA-g-PEG)) hydrogel structure. This hydrogel system could release entrapped insulin in a pH-dependent way, that relied on the relaxation behaviour of the hydrogel upon deprotonation of the ionic methacrylate acid functions at higher pH values.[287] They used this system as a foundation for various other reports and different payloads, for example the incorporation of doxorubicin-loaded nanoparticles allowed a pH-dependent release of drug-loaded nanoparticles.[288–290]

Especially to precisely deliver drugs or to fine-tune release kinetics, a broad range of linker chemistry can be applied. This covers a wide range of functional groups and stable or stimuli-responsive covalent linkages that can be employed, with most frequently hydrolytic and enzymatic degradable linker systems used.[291,292] For example Schneider *et al.* reported an exciting hydrogel drug delivery system, which relies on injectable PEG hydrogel microspheres with a GLP-1 agonist (exenatide) attached *via* a cleavable β-eliminative linker. This system could enable a weekly or biweekly subcutaneous injection of the drug instead of twice daily dosages. Furthermore, a second linker was incorporated into the hydrogel matrix, to ensure the degradation of the gel after drug release.[293]

The possibility of local injection of hydrogels and thus formation of a locally defined depot is especially of interest in cancer therapy, where the systemic action of the often cytotoxic drugs causes severe side-effects (**Figure 7**).

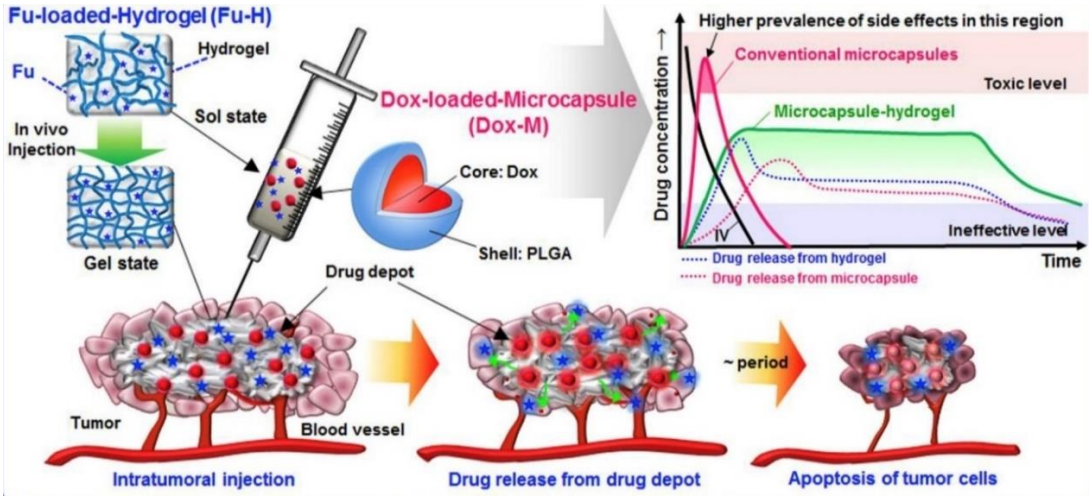

Figure 7: Schematic representation of synergistic tumour suppression *via* intra-tumoral injections of dual-drug depots and controlled release of DOX and FU in the first and second stage. (Adapted and modified from Kim *et al.*)[294]

For example, Kim and co-workers proposed an advanced hydrogel-based dual drug delivery system for the local intra-tumour sustained release of the small molecular drugs doxorubicin (DOX) and 5-fluorouracil (FU) for up to 18 days upon injection.[294] They applied an *in situ* upon injection formed FU-loaded hydrogel, based on mPEG-*b*-(PCL-*ran*-PLLA) or commercially available poloxamers and additionally loaded these hydrogel with DOX-loaded microcapsules. This double-loaded hydrogel served as a local depot for the combined sustained release of DOX and FU. Compared to DOX-loaded microcapsules alone, this hydrogel system demonstrated a prolonged release, while preventing transient high drug concentrations.

Beside the release of entrapped molecules, the design of degradable hydrogels is also favourable to prevent bioaccumulation of these materials after their use for drug delivery, comparable with the efforts to synthesize degradable polymers for conjugation (see previous section).

REFERENCES

(1) Klein, R.; Wurm, F. R. *Macromol. Rapid Commun.* **2015**, *36* (12), 1147–1165. DOI: 10.1002/marc.201500013.

(2) Dingels, C.; Schömer, M.; Frey, H. *Chemie in unserer Zeit* **2011**, *45* (5), 338–349. DOI: 10.1002/ciuz.201100551.

(3) Wurtz, C. A. *Ann. Chim. Phys.* **1863,** No. 69, 317–354.

(4) Staudinger, H.; Schweitzer, O. *Ber. dtsch. Chem. Ges. A/B* **1929**, *62* (8), 2395–2405. DOI: 10.1002/cber.19290620879.

(5) Herzberger, J.; Niederer, K.; Pohlit, H.; Seiwert, J.; Worm, M.; Wurm, F. R.; Frey, H. *Chemical reviews* **2016**, *116* (4), 2170–2243. DOI: 10.1021/acs.chemrev.5b00441.

(6) Thomas, A.; Müller, S. S.; Frey, H. *Biomacromolecules* **2014**, *15* (6), 1935–1954. DOI: 10.1021/bm5002608.

(7) Kadajji, V. G.; Betageri, G. V. *Polymers* **2011**, *3* (4), 1972–2009. DOI: 10.3390/polym3041972.

(8) In *The MAK-collection for occupational health and safety*; Wiley-VCH Verl.: Germany, 1988; pp 248–270.

(9) Kjellander, R.; Florin, E. *J. Chem. Soc., Faraday Trans. 1* **1981**, *77* (9), 2053. DOI: 10.1039/f19817702053.

(10) Fruijtier-Pölloth, C. *Toxicology* **2005**, *214* (1-2), 1–38. DOI: 10.1016/j.tox.2005.06.001.

(11) P. Garay, R. *TOPROCJ* **2011**, *2* (1), 104–107. DOI: 10.2174/2210289201102010104.

(12) Alexandridis, P.; Alan Hatton, T. *Colloids and Surfaces A: Physicochemical and Engineering Aspects* **1995**, *96* (1-2), 1–46. DOI: 10.1016/0927-7757(94)03028-X.

(13) Schmolka, I. R. *J Amer Oil Chem Soc* **1977**, *54* (3), 110–116. DOI: 10.1007/BF02894385.

(14) Arambulo, A. S.; Liu, M.-S.; Rosen, A. L.; Dobben, G.; Long, D. H. *Drug Development Communications* **1974**, *1* (1), 73–87. DOI: 10.3109/03639047409088169.

(15) Batrakova, E. V.; Kabanov, A. V. *Journal of controlled release : official journal of the Controlled Release Society* **2008**, *130* (2), 98–106. DOI: 10.1016/j.jconrel.2008.04.013.

(16) Mangold, C.; Wurm, F.; Frey, H. *Polym. Chem.* **2012**, *3* (7), 1714. DOI: 10.1039/c2py00489e.

(17) Obermeier, B.; Wurm, F.; Mangold, C.; Frey, H. *Angewandte Chemie (International ed. in English)* **2011**, *50* (35), 7988–7997. DOI: 10.1002/anie.201100027.

(18) Linker, O.; Blankenburg, J.; Maciol, K.; Bros, M.; Frey, H. *Macromolecules* **2020.** DOI: 10.1021/acs.macromol.9b02320.

(19) Schömer, M.; Schüll, C.; Frey, H. *J. Polym. Sci. A Polym. Chem.* **2013**, *51* (5), 995–1019. DOI: 10.1002/pola.26496.

(20) Knop, K.; Hoogenboom, R.; Fischer, D.; Schubert, U. S. *Angewandte Chemie (International ed. in English)* **2010**, *49* (36), 6288–6308. DOI: 10.1002/anie.200902672.

(21) Flory, P. J. *J. Am. Chem. Soc.* **1940**, *62* (6), 1561–1565. DOI: 10.1021/ja01863a066.

(22) Aida, T.; Mizuta, R.; Yoshida, Y.; Inoue, S. *Makromol. Chem.* **1981**, *182* (4), 1073–1079. DOI: 10.1002/macp.1981.021820408.

(23) Doytcheva, M.; Dotcheva, D.; Stamenova, R.; Orahovats, A.; Tsvetanov, C.; Leder, J. *J. Appl. Polym. Sci.* **1997**, *64* (12), 2299–2307. DOI: 10.1002/(SICI)1097-4628(19970620)64:12<2299:AID-APP5>3.0.CO;2-G.

(24) Ionescu, M. *Chemistry and technology of polyols for polyurethanes*; Rapra Technology Ltd: Shawbury, U.K, 2005.

(25) Brocas, A.-L.; Mantzaridis, C.; Tunc, D.; Carlotti, S. *Progress in Polymer Science* **2013**, *38* (6), 845–873. DOI: 10.1016/j.progpolymsci.2012.09.007.

(26) Sloop, S. E.; Lerner, M. M.; Stephens, T. S.; Tipton, A. L.; Paull, D. G.; Stenger-Smith, J. D. *J. Appl. Polym. Sci.* **1994**, *53* (12), 1563–1572. DOI: 10.1002/app.1994.070531202.

(27) PENCZEK, S.; CYPRYK, M.; DUDA, A.; KUBISA, P.; SLOMKOWSKI, S. *Progress in Polymer Science* **2007**, *32* (2), 247–282. DOI: 10.1016/j.progpolymsci.2007.01.002.

(28) Sasaki, H. *J. Photopol. Sci. Technol.* **2000**, *13* (1), 119–124. DOI: 10.2494/photopolymer.13.119.

(29) Quirk, R. P.; Lee, B. *Polym. Int.* **1992**, *27* (4), 359–367. DOI: 10.1002/pi.4990270412.

(30) SZWARC, M. *Nature* **1956**, *178* (4543), 1168–1169. DOI: 10.1038/1781168a0.

(31) Solov'yanov, A. A.; Kazanskii, K. S. *Polymer Science U.S.S.R.* **1972**, *14* (5), 1186–1195. DOI: 10.1016/0032-3950(72)90162-1.

(32) *Anionic Polymerization: Principles, Practice, Strength, Consequences and Applications;* Hadjichristidis, N., Hirao, A., Eds., 1st ed. 2015; Springer: Tokyo, 2015.

(33) Blankenburg, J.; Wagner, M.; Frey, H. *Macromolecules* **2017**, *50* (22), 8885–8893. DOI: 10.1021/acs.macromol.7b01324.

(34) Deffieux, A.; Boileau, S. *Polymer* **1977**, *18* (10), 1047–1050. DOI: 10.1016/0032-3861(77)90011-8.

(35) Pearson, R. G. *J. Am. Chem. Soc.* **1963**, *85* (22), 3533–3539. DOI: 10.1021/ja00905a001.

(36) Hsieh, H. L.; Quirk, R. P. *Anionic Polymerization: Principles and Practical Applications*; Plastics Engineering Ser v.34; Chapman and Hall/CRC: Boca Raton, 1996.

(37) Tonhauser, C.; Frey, H. *Macromol. Rapid Commun.* **2010**, *31* (22), 1938–1947. DOI: 10.1002/marc.201000353.

(38) Kazanskii, K. S.; Solovyanov, A. A.; Entelis, S. G. *European Polymer Journal* **1971**, *7* (10), 1421–1433. DOI: 10.1016/0014-3057(71)90036-X.

(39) Jung, P.; Ziegler, A. D.; Blankenburg, J.; Frey, H. *Angewandte Chemie (International ed. in English)* **2019**, *58* (37), 12883–12886. DOI: 10.1002/anie.201904203.

(40) Duncan, R. *Nature reviews. Drug discovery* **2003**, *2* (5), 347–360. DOI: 10.1038/nrd1088.

(41) Duncan, R.; Vicent, M. J. *Advanced Drug Delivery Reviews* **2013**, *65* (1), 60–70. DOI: 10.1016/j.addr.2012.08.012.

(42) Ekladious, I.; Colson, Y. L.; Grinstaff, M. W. *Nature reviews. Drug discovery* **2019**, *18* (4), 273–294. DOI: 10.1038/s41573-018-0005-0.

(43) Wei, Q.; Deng, N.-N.; Guo, J.; Deng, J. *International journal of biomaterials* **2018**, *2018*, 7158621. DOI: 10.1155/2018/7158621.

(44) Ramakrishna, S.; Mayer, J.; Wintermantel, E.; Leong, K. W. *Composites Science and Technology* **2001**, *61* (9), 1189–1224. DOI: 10.1016/S0266-3538(00)00241-4.

(45) Barz, M.; Luxenhofer, R.; Zentel, R.; Vicent, M. J. *Polym. Chem.* **2011**, *2* (9), 1900. DOI: 10.1039/c0py00406e.

(46) Hoang Thi, T. T.; Pilkington, E. H.; Nguyen, D. H.; Lee, J. S.; Park, K. D.; Truong, N. P. *Polymers* **2020**, *12* (2). DOI: 10.3390/polym12020298.

(47) Li, X.; Li, H.; Zhao, Y.; Tang, X.; Ma, S.; Gong, B.; Li, M. *Polym. Chem.* **2015**, *6* (36), 6452–6456. DOI: 10.1039/C5PY00762C.

(48) Strebhardt, K.; Ullrich, A. *Nature reviews. Cancer* **2008**, *8* (6), 473–480. DOI: 10.1038/nrc2394.

(49) Choi, Y. H.; Han, H.-K. *Journal of pharmaceutical investigation* **2018**, *48* (1), 43–60. DOI: 10.1007/s40005-017-0370-4.

(50) Li, M.; Al-Jamal, K. T.; Kostarelos, K.; Reineke, J. *ACS nano* **2010**, *4* (11), 6303–6317. DOI: 10.1021/nn1018818.

(51) Vega-Villa, K. R.; Takemoto, J. K.; Yáñez, J. A.; Remsberg, C. M.; Forrest, M. L.; Davies, N. M. *Advanced Drug Delivery Reviews* **2008**, *60* (8), 929–938. DOI: 10.1016/j.addr.2007.11.007.

(52) *Fundamentals of nanoparticles: Classifications, synthesis methods, properties and characterization;* Barhoum, A., Makhlouf, A. S. H., Eds.; Elsevier: Amsterdam, Netherlands, 2018.

(53) Ding, C.; Li, Z. *Materials science & engineering. C, Materials for biological applications* **2017**, *76*, 1440–1453. DOI: 10.1016/j.msec.2017.03.130.

(54) Lee, J. H.; Yeo, Y. *Chemical Engineering Science* [Online] **2015**, *125*, 75–84. http://www.sciencedirect.com/science/article/pii/S0009250914004710.

(55) Rijcken, C. J. F.; Soga, O.; Hennink, W. E.; van Nostrum, C. F. *Journal of controlled release : official journal of the Controlled Release Society* **2007**, *120* (3), 131–148. DOI: 10.1016/j.jconrel.2007.03.023.

(56) Manchun, S.; Dass, C. R.; Sriamornsak, P. *Life sciences* **2012**, *90* (11-12), 381–387. DOI: 10.1016/j.lfs.2012.01.008.

(57) Said, S. S.; Campbell, S.; Hoare, T. *Chem. Mater.* **2019**, *31* (14), 4971–4989. DOI: 10.1021/acs.chemmater.9b01798.

(58) Hossen, S.; Hossain, M. K.; Basher, M. K.; Mia, M. N. H.; Rahman, M. T.; Uddin, M. J. *Journal of advanced research* **2019**, *15*, 1–18. DOI: 10.1016/j.jare.2018.06.005.

(59) Ganta, S.; Devalapally, H.; Shahiwala, A.; Amiji, M. *Journal of controlled release : official journal of the Controlled Release Society* **2008**, *126* (3), 187–204. DOI: 10.1016/j.jconrel.2007.12.017.

(60) Kamaly, N.; Yameen, B.; Wu, J.; Farokhzad, O. C. *Chemical reviews* **2016**, *116* (4), 2602–2663. DOI: 10.1021/acs.chemrev.5b00346.

(61) Schmaljohann, D. *Advanced Drug Delivery Reviews* **2006**, *58* (15), 1655–1670. DOI: 10.1016/j.addr.2006.09.020.

(62) Liu, Y.; Wang, W.; Yang, J.; Zhou, C.; Sun, J. *Asian Journal of Pharmaceutical Sciences* **2013**, *8* (3), 159–167. DOI: 10.1016/j.ajps.2013.07.021.

(63) Cajot, S.; van Butsele, K.; Paillard, A.; Passirani, C.; Garcion, E.; Benoit, J. P.; Varshney, S. K.; Jérôme, C. *Acta biomaterialia* **2012**, *8* (12), 4215–4223. DOI: 10.1016/j.actbio.2012.08.049.

(64) Chen, W.-L.; Yang, S.-d.; Li, F.; Li, J.-Z.; Yuan, Z.-Q.; Zhu, W.-J.; Liu, Y.; Zhou, X.-F.; Liu, C.; Zhang, X.-N. *International journal of pharmaceutics* **2016**, *511* (2), 728–740. DOI: 10.1016/j.ijpharm.2016.07.060.

(65) Liu, J.; Huang, Y.; Kumar, A.; Tan, A.; Jin, S.; Mozhi, A.; Liang, X.-J. *Biotechnology advances* **2014**, *32* (4), 693–710. DOI: 10.1016/j.biotechadv.2013.11.009.

(66) Pang, X.; Jiang, Y.; Xiao, Q.; Leung, A. W.; Hua, H.; Xu, C. *Journal of controlled release : official journal of the Controlled Release Society* **2016**, *222*, 116–129. DOI: 10.1016/j.jconrel.2015.12.024.

(67) Mura, S.; Nicolas, J.; Couvreur, P. *Nature materials* **2013**, *12* (11), 991–1003. DOI: 10.1038/nmat3776.

(68) Binauld, S.; Stenzel, M. H. *Chemical communications (Cambridge, England)* **2013**, *49* (21), 2082–2102. DOI: 10.1039/c2cc36589h.

(69) Dai, S.; Ravi, P.; Tam, K. C. *Soft Matter* **2008**, *4* (3), 435. DOI: 10.1039/b714741d.

(70) Seidi, F.; Jenjob, R.; Crespy, D. *Chemical reviews* **2018**, *118* (7), 3965–4036. DOI: 10.1021/acs.chemrev.8b00006.

(71) Pushpalatha, R.; Selvamuthukumar, S.; Kilimozhi, D. *Journal of Drug Delivery Science and Technology* **2017**, *39*, 362–371. DOI: 10.1016/j.jddst.2017.04.019.

(72) Kanamala, M.; Wilson, W. R.; Yang, M.; Palmer, B. D.; Wu, Z. *Biomaterials* **2016**, *85*, 152–167. DOI: 10.1016/j.biomaterials.2016.01.061.

(73) Markovsky, E.; Baabur-Cohen, H.; Eldar-Boock, A.; Omer, L.; Tiram, G.; Ferber, S.; Ofek, P.; Polyak, D.; Scomparin, A.; Satchi-Fainaro, R. *Journal of controlled release : official journal of the Controlled Release Society* **2012**, *161* (2), 446–460. DOI: 10.1016/j.jconrel.2011.12.021.

(74) Caliceti, P. *Advanced Drug Delivery Reviews* **2003**, *55* (10), 1261–1277. DOI: 10.1016/S0169-409X(03)00108-X.

(75) Dingels, C.; Frey, H. In *Hierarchical Macromolecular Structures: 60 Years after the Staudinger Nobel Prize II*; Percec, V., Ed.; Advances in Polymer Science v.262; Springer International Publishing: Cham, 2013; pp 167–190.

(76) Ulbricht, J.; Jordan, R.; Luxenhofer, R. *Biomaterials* **2014**, *35* (17), 4848–4861. DOI: 10.1016/j.biomaterials.2014.02.029.

(77) Worm, M.; Kang, B.; Dingels, C.; Wurm, F. R.; Frey, H. *Macromol. Rapid Commun.* **2016**, *37* (9), 775–780. DOI: 10.1002/marc.201600080.

(78) Müller, S. S.; Fritz, T.; Gimnich, M.; Worm, M.; Helm, M.; Frey, H. *Polym. Chem.* **2016**, *7* (40), 6257–6268. DOI: 10.1039/C6PY01308B.

(79) Kanamala, M.; Palmer, B. D.; Wilson, W. R.; Wu, Z. *International journal of pharmaceutics* **2018**, *548* (1), 288–296. DOI: 10.1016/j.ijpharm.2018.07.009.

(80) Li, Z.; Qiu, L.; Chen, Q.; Hao, T.; Qiao, M.; Zhao, H.; Zhang, J.; Hu, H.; Zhao, X.; Chen, D.; Mei, L. *Acta biomaterialia* **2015**, *11*, 137–150. DOI: 10.1016/j.actbio.2014.09.014.

(81) Kim, H.-K.; van den Bossche, J.; Hyun, S.-H.; Thompson, D. H. *Bioconjugate chemistry* **2012**, *23* (10), 2071–2077. DOI: 10.1021/bc300266y.

(82) Shin, J.; Shum, P.; Grey, J.; Fujiwara, S.-i.; Malhotra, G. S.; González-Bonet, A.; Hyun, S.-H.; Moase, E.; Allen, T. M.; Thompson, D. H. *Molecular pharmaceutics* **2012**, *9* (11), 3266–3276. DOI: 10.1021/mp300326z.

(83) Boomer, J. A.; Qualls, M. M.; Inerowicz, H. D.; Haynes, R. H.; Patri, V. S.; Kim, J.-M.; Thompson, D. H. *Bioconjugate chemistry* **2009**, *20* (1), 47–59. DOI: 10.1021/bc800239b.

(84) Chen, D.; Liu, W.; Shen, Y.; Mu, H.; Zhang, Y.; Liang, R.; Wang, A.; Sun, K.; Fu, F. *International journal of nanomedicine* **2011**, *6*, 2053–2061. DOI: 10.2147/IJN.S24344.

(85) Pelegri-O'Day, E. M.; Matsumoto, N. M.; Tamshen, K.; Raftery, E. D.; Lau, U. Y.; Maynard, H. D. *Bioconjugate chemistry* **2018**, *29* (11), 3739–3745. DOI: 10.1021/acs.bioconjchem.8b00635.

(86) Molla, M. R.; Marcinko, T.; Prasad, P.; Deming, D.; Garman, S. C.; Thayumanavan, S. *Biomacromolecules* **2014**, *15* (11), 4046–4053. DOI: 10.1021/bm501091p.

(87) Satoh, K.; Poelma, J. E.; Campos, L. M.; Stahl, B.; Hawker, C. J. *Polym. Chem.* **2012**, *3* (7), 1890–1898. DOI: 10.1039/C1PY00484K.

(88) Lo, W.-J.; Wu, Y.-J.; Lee, Y.-P. *The Journal of Chemical Physics* **2002**, *117* (14), 6655–6661. DOI: 10.1063/1.1506155.

(89) Yoo, H. S.; Lee, E. A.; Park, T. G. *Journal of Controlled Release* **2002**, *82* (1), 17–27. DOI: 10.1016/S0168-3659(02)00088-3.

(90) Lo, W.-J.; Wu, Y.-J.; Lee, Y.-P. *J. Phys. Chem. A* **2003**, *107* (36), 6944–6947. DOI: 10.1021/jp034563j.

(91) Cui, W.; Qi, M.; Li, X.; Huang, S.; Zhou, S.; Weng, J. *International journal of pharmaceutics* **2008**, *361* (1-2), 47–55. DOI: 10.1016/j.ijpharm.2008.05.005.

(92) England, R. M.; Masiá, E.; Giménez, V.; Lucas, R.; Vicent, M. J. *Journal of controlled release : official journal of the Controlled Release Society* **2012**, *164* (3), 314–322. DOI: 10.1016/j.jconrel.2012.08.017.

(93) Gillies, E. R.; Fréchet, J. M. J. *Bioconjugate chemistry* **2005**, *16* (2), 361–368. DOI: 10.1021/bc049851c.

(94) Giménez, V.; James, C.; Armiñán, A.; Schweins, R.; Paul, A.; Vicent, M. J. *Journal of controlled release : official journal of the Controlled Release Society* **2012**, *159* (2), 290–301. DOI: 10.1016/j.jconrel.2011.12.035.

(95) Kaihara, S.; Fisher, J. P.; Matsumura, S. *Macromol. Biosci.* **2009**, *9* (6), 613–621. DOI: 10.1002/mabi.200800308.

(96) Kaihara, S.; Matsumura, S.; Fisher, J. P. *Macromolecules* **2007**, *40* (21), 7625–7632. DOI: 10.1021/ma071297p.

(97) Knorr, V.; Allmendinger, L.; Walker, G. F.; Paintner, F. F.; Wagner, E. *Bioconjugate chemistry* **2007**, *18* (4), 1218–1225. DOI: 10.1021/bc060327a.

(98) Pohlit, H.; Bellinghausen, I.; Schömer, M.; Heydenreich, B.; Saloga, J.; Frey, H. *Biomacromolecules* **2015**, *16* (10), 3103–3111. DOI: 10.1021/acs.biomac.5b00458.

(99) Rickerby, J.; Prabhakar, R.; Ali, M.; Knowles, J.; Brocchini, S. *J. Mater. Chem.* **2005**, *15* (18), 1849. DOI: 10.1039/b414803g.

(100) Tomlinson, R.; Heller, J.; Brocchini, S.; Duncan, R. *Bioconjugate chemistry* **2003**, *14* (6), 1096–1106. DOI: 10.1021/bc030028a.

(101) Tonhauser, C.; Schüll, C.; Dingels, C.; Frey, H. *ACS Macro Lett.* **2012**, *1* (9), 1094–1097. DOI: 10.1021/mz300265z.

(102) Vicent, M. J.; Tomlinson, R.; Brocchini, S.; Duncan, R. *Journal of drug targeting* **2004**, *12* (8), 491–501. DOI: 10.1080/10611860400011885.

(103) Wang, Y.; Morinaga, H.; Sudo, A.; Endo, T. *J. Polym. Sci. A Polym. Chem.* **2011**, *49* (3), 596–602. DOI: 10.1002/pola.24425.

(104) Tomlinson, R.; Klee, M.; Garrett, S.; Heller, J.; Duncan, R.; Brocchini, S. *Macromolecules* **2002**, *35* (2), 473–480. DOI: 10.1021/ma0108867.

(105) Dingels, C.; Müller, S. S.; Steinbach, T.; Tonhauser, C.; Frey, H. *Biomacromolecules* **2013**, *14* (2), 448–459. DOI: 10.1021/bm3016797.

(106) Kim, S.; Linker, O.; Garth, K.; Carter, K. R. *Polymer Degradation and Stability* **2015**, *121*, 303–310. DOI: 10.1016/j.polymdegradstab.2015.09.014.

(107) Ruff, L. E.; Mahmoud, E. A.; Sankaranarayanan, J.; Morachis, J. M.; Katayama, C. D.; Corr, M.; Hedrick, S. M.; Almutairi, A. *Integrative biology : quantitative biosciences from nano to macro* **2013**, *5* (1), 195–203. DOI: 10.1039/c2ib20109g.

(108) Pohlit, H.; Leibig, D.; Frey, H. *Macromolecular bioscience* **2017**, *17* (10). DOI: 10.1002/mabi.201600532.

(109) Shenoi, R. A.; Lai, B. F. L.; Kizhakkedathu, J. N. *Biomacromolecules* **2012**, *13* (10), 3018–3030. DOI: 10.1021/bm300959h.

(110) Feng, X.; Chaikof, E. L.; Absalon, C.; Drummond, C.; Taton, D.; Gnanou, Y. *Macromolecular rapid communications* **2011**, *32* (21), 1722–1728. DOI: 10.1002/marc.201100459.

(111) Shenoi, R. A.; Narayanannair, J. K.; Hamilton, J. L.; Lai, B. F. L.; Horte, S.; Kainthan, R. K.; Varghese, J. P.; Rajeev, K. G.; Manoharan, M.; Kizhakkedathu, J. N. *Journal of the American Chemical Society* **2012**, *134* (36), 14945–14957. DOI: 10.1021/ja305080f.

(112) DuBois Clochard, M.-C.; Rankin, S.; Brocchini, S. *Macromol. Rapid Commun.* **2000**, *21* (12), 853–859. DOI: 10.1002/1521-3927(20000801)21:12<853:AID-MARC853>3.0.CO;2-M.

(113) Hu, F.-Q.; Zhang, Y.-Y.; You, J.; Yuan, H.; Du, Y.-Z. *Molecular pharmaceutics* **2012**, *9* (9), 2469–2478. DOI: 10.1021/mp300002v.

(114) Lai, J.; Tu, K.; Wang, H.; Chen, Z.; Wang, L.-Q. *J. Appl. Polym. Sci.* **2008**, *108* (5), 3305–3312. DOI: 10.1002/app.27741.

(115) Lai, J.; Wang, L.-Q.; Tu, K.; Zhao, C.; Sun, W. *Macromol. Rapid Commun.* **2005**, *26* (19), 1572–1577. DOI: 10.1002/marc.200500550.

(116) Bourke, S. L.; Kohn, J. *Advanced Drug Delivery Reviews* **2003**, *55* (4), 447–466. DOI: 10.1016/S0169-409X(03)00038-3.

(117) Goldberg, E. P. *J. polym. sci., C Polym. symp.* **1963**, *4* (1), 707–730. DOI: 10.1002/polc.5070040153.

(118) Meabe, L.; Sardon, H.; Mecerreyes, D. *European Polymer Journal* **2017**, *95*, 737–745. DOI: 10.1016/j.eurpolymj.2017.06.046.

(119) Sharma, R. I.; Kohn, J.; Moghe, P. V. *Journal of biomedical materials research. Part A* **2004**, *69* (1), 114–123. DOI: 10.1002/jbm.a.20125.

(120) Sousa, A.; Schut, J.; Kohn, J.; Libera, M. *Macromolecules* **2006**, *39* (21), 7306–7312. DOI: 10.1021/ma061286g.

(121) Suzuki, T.; Chihara, H.; Kotaka, T. *Polym J* **1984**, *16* (2), 129–138. DOI: 10.1295/polymj.16.129.

(122) Suzuki, T.; Kotaka, T. *Macromolecules* **1980**, *13* (6), 1495–1501. DOI: 10.1021/ma60078a026.

(123) Suzuki, T.; Kotaka, T. *Polym J* **1983**, *15* (1), 15–23. DOI: 10.1295/polymj.15.15.

(124) Tanisugi, H.; Ohnuma, H.; Kotaka, T. *Polym J* **1984**, *16* (8), 633–640. DOI: 10.1295/polymj.16.633.

(125) Tziampazis, E.; Kohn, J.; Moghe, P. V. *Biomaterials* **2000**, *21* (5), 511–520. DOI: 10.1016/S0142-9612(99)00212-4.

(126) Cai, Q.; Li, X.; Zhu, W. *Macromolecules* **2020**, *53* (6), 2177–2186. DOI: 10.1021/acs.macromol.9b02177.

(127) Chen, Y.; Liu, S.; Zhao, J.; Pahovnik, D.; Žagar, E.; Zhang, G. *ACS Macro Lett.* **2019**, *8* (12), 1582–1587. DOI: 10.1021/acsmacrolett.9b00789.

(128) Di Liu; Bielawski, C. W. *Macromol. Rapid Commun.* **2016**, *37* (19), 1587–1592. DOI: 10.1002/marc.201600336.

(129) Mero, A.; Schiavon, O.; Pasut, G.; Veronese, F. M.; Emilitri, E.; Ferruti, P. *Journal of Bioactive and Compatible Polymers* **2009**, *24* (3), 220–234. DOI: 10.1177/0883911509103783.

(130) Varghese, J. K.; Hadjichristidis, N.; Gnanou, Y.; Feng, X. *Polym. Chem.* **2019**, *10* (27), 3764–3771. DOI: 10.1039/C9PY00605B.

(131) Wang, N.; Dong, A.; Tang, H.; van Kirk, E. A.; Johnson, P. A.; Murdoch, W. J.; Radosz, M.; Shen, Y. *Macromolecular bioscience* **2007**, *7* (11), 1187–1198. DOI: 10.1002/mabi.200700065.

(132) Bhatia, S.; Mohr, A.; Mathur, D.; Parmar, V. S.; Haag, R.; Prasad, A. K. *Biomacromolecules* **2011**, *12* (10), 3487–3498. DOI: 10.1021/bm200647a.

(133) Braunová, A.; Pechar, M.; Laga, R.; Ulbrich, K. *Macromol. Chem. Phys.* **2007**, *208* (24), 2642–2653. DOI: 10.1002/macp.200700315.

(134) Braunová, A.; Pechar, M.; Ulbrich, K. *Collect. Czech. Chem. Commun.* **2004**, *69* (8), 1643–1656. DOI: 10.1135/cccc20041643.

(135) Chen, S.; Wang, Y.; Fan, Y.; Ma, J. *Journal of biomedical materials research. Part A* **2009**, *88* (3), 769–777. DOI: 10.1002/jbm.a.31909.

(136) Dou, S.; Zhang, S.; Klein, R. J.; Runt, J.; Colby, R. H. *Chem. Mater.* **2006**, *18* (18), 4288–4295. DOI: 10.1021/cm0603699.

(137) Hawker, C. J.; Chu, F.; Pomery, P. J.; Hill, D. J. T. *Macromolecules* **1996**, *29* (11), 3831–3838. DOI: 10.1021/ma951909i.

(138) Kumar, R.; Chen, M.-H.; Parmar, V. S.; Samuelson, L. A.; Kumar, J.; Nicolosi, R.; Yoganathan, S.; Watterson, A. C. *Journal of the American Chemical Society* **2004**, *126* (34), 10640–10644. DOI: 10.1021/ja039651w.

(139) Nagahama, K.; Hashizume, M.; Yamamoto, H.; Ouchi, T.; Ohya, Y. *Langmuir : the ACS journal of surfaces and colloids* **2009**, *25* (17), 9734–9740. DOI: 10.1021/la901092x.

(140) Nagata, M.; Hizakae, S. *Macromol. Biosci.* **2003**, *3* (8), 412–419. DOI: 10.1002/mabi.200350011.

(141) Nagata, M.; Hizakae, S. *J. Polym. Sci. A Polym. Chem.* **2003**, *41* (19), 2930–2938. DOI: 10.1002/pola.10884.

(142) Padmaja, T.; Lele, B. S.; Deshpande, M. C.; Kulkarni, M. G. *J. Appl. Polym. Sci.* **2002**, *85* (10), 2108–2118. DOI: 10.1002/app.10777.

(143) Unal, S.; Lin, Q.; Mourey, T. H.; Long, T. E. *Macromolecules* **2005**, *38* (8), 3246–3254. DOI: 10.1021/ma047534v.

(144) Wang, H.-Y.; Zhou, Y.-J.; Wang, Z.; Wang, N.; Li, K.; Yu, X.-Q. *Macromol. Biosci.* **2011**, *11* (5), 595–599. DOI: 10.1002/mabi.201000488.

(145) Wang, N.; Dong, A.; Radosz, M.; Shen, Y. *Journal of biomedical materials research. Part A* **2008**, *84* (1), 148–157. DOI: 10.1002/jbm.a.31466.

(146) Wang, W.; Liu, W.; Tudryn, G. J.; Colby, R. H.; Winey, K. I. *Macromolecules* **2010**, *43* (9), 4223–4229. DOI: 10.1021/ma100379j.

(147) Wang, W.; Tudryn, G. J.; Colby, R. H.; Winey, K. I. *Journal of the American Chemical Society* **2011**, *133* (28), 10826–10831. DOI: 10.1021/ja201405v.

(148) Won, C.-Y.; Chu, C.-C.; Lee, J. D. *Polymer* **1998**, *39* (25), 6677–6681. DOI: 10.1016/S0032-3861(98)00032-9.

(149) Won, C.-Y.; Chu, C.-C.; Lee, J. D. *J. Polym. Sci. A Polym. Chem.* **1998**, *36* (16), 2949–2959. DOI: 10.1002/(SICI)1099-0518(19981130)36:16<2949:AID-POLA13>3.0.CO;2-A.

(150) Etrych, T.; Kovář, L.; Šubr, V.; Braunová, A.; Pechar, M.; Chytil, P.; Říhova, B.; Ulbrich, K. *Journal of Bioactive and Compatible Polymers* **2010**, *25* (1), 5–26. DOI: 10.1177/0883911509353485.

(151) Hernandez-Mireles, T.; Rito-Palomares, M. *J. Chem. Technol. Biotechnol.* **2006**, *81* (6), 997–1002. DOI: 10.1002/jctb.1506.

(152) Lee, J.; Joo, M. K.; Kim, J.; Park, J. S.; Yoon, M.-Y.; Jeong, B. *Journal of biomaterials science. Polymer edition* **2009**, *20* (7-8), 957–965. DOI: 10.1163/156856209X444367.

(153) Lee, Y.; Koo, H.; Jin, G.-w.; Mo, H.; Cho, M. Y.; Park, J.-Y.; Choi, J. S.; Park, J. S. *Biomacromolecules* **2005**, *6* (1), 24–26. DOI: 10.1021/bm049658l.

(154) Reid, B.; Tzeng, S.; Warren, A.; Kozielski, K.; Elisseeff, J. *Macromolecules* **2010**, *43* (23), 9588–9590. DOI: 10.1021/ma1020648.

(155) Qian, Q.; Zhu, L.; Zhu, X.; Sun, M.; Yan, D. *Matter* **2019**, *1* (6), 1618–1630. DOI: 10.1016/j.matt.2019.09.016.

(156) Collins, J.; Xiao, Z.; Connal, L. A. *J. Polym. Sci. A Polym. Chem.* **2017**, *55* (23), 3826–3831. DOI: 10.1002/pola.28856.

(157) Su, S.; Du, F.-S.; Li, Z.-C. *Macromolecules* **2018**, *51* (17), 6571–6579. DOI: 10.1021/acs.macromol.8b01053.

(158) Yamahira, S.; Yamaguchi, S.; Kawahara, M.; Nagamune, T. *Macromol. Biosci.* **2014**, *14* (12), 1670–1676. DOI: 10.1002/mabi.201400312.

(159) Heller, J.; Chang, A. C.; Rood, G.; Grodsky, G. M. *Journal of Controlled Release* **1990**, *13* (2-3), 295–302. DOI: 10.1016/0168-3659(90)90019-P.

(160) Qi, M.; Li, X.; Yang, Y.; Zhou, S. *European journal of pharmaceutics and biopharmaceutics : official journal of Arbeitsgemeinschaft fur Pharmazeutische Verfahrenstechnik e.V* **2008**, *70* (2), 445–452. DOI: 10.1016/j.ejpb.2008.05.003.

(161) Aimetti, A. A.; Machen, A. J.; Anseth, K. S. *Biomaterials* **2009**, *30* (30), 6048–6054. DOI: 10.1016/j.biomaterials.2009.07.043.

(162) Berna, M.; Dalzoppo, D.; Pasut, G.; Manunta, M.; Izzo, L.; Jones, A. T.; Duncan, R.; Veronese, F. M. *Biomacromolecules* **2006**, *7* (1), 146–153. DOI: 10.1021/bm050480s.

(163) d'Acunz, F.; Kohn, J. *Macromolecules* **2002**, *35* (25), 9360–9365. DOI: 10.1021/ma0113879.

(164) d'Acunzo, F.; Le, T.-Q.; Kohn, J. *Macromolecules* **2002**, *35* (25), 9366–9371. DOI: 10.1021/ma0113881.

(165) Huang, S. Y.; Pooyan, S.; Wang, J.; Choudhury, I.; Leibowitz, M. J.; Stein, S. *Bioconjugate chemistry* **1998**, *9* (5), 612–617. DOI: 10.1021/bc980038p.

(166) Pechar, M.; Ulbrich, K.; Subr, V.; Seymour, L. W.; Schacht, E. H. *Bioconjugate chemistry* **2000**, *11* (2), 131–139. DOI: 10.1021/bc990092l.

(167) Pechar, M.; Braunová, A.; Ulbrich, K. *Collect. Czech. Chem. Commun.* **2005**, *70* (3), 327–338. DOI: 10.1135/cccc20050327.

(168) Pechar, M.; Braunová, A.; Ulbrich, K.; Jelínková, M.; Ríhová, B. *Journal of Bioactive and Compatible Polymers* **2005**, *20* (4), 319–341. DOI: 10.1177/0883911505055161.

(169) Pechar, M.; Strohalm, J.; Ulbrich, K. *Collect. Czech. Chem. Commun.* **1995**, *60* (10), 1765–1780. DOI: 10.1135/cccc19951765.

(170) Pechar, M.; Strohalm, J.; Ulbrich, K.; Schacht, E. *Macromol. Chem. Phys.* **1997**, *198* (4), 1009–1020. DOI: 10.1002/macp.1997.021980408.

(171) Pechar, M.; Ulbrich, K.; Jelínková, M.; Říhová, B. *Macromol. Biosci.* **2003**, *3* (7), 364–372. DOI: 10.1002/mabi.200350004.

(172) Ramanathan, S.; Qiu, B.; Pooyan, S.; Zhang, G.; Stein, S.; Leibowitz, M. J.; Sinko, P.J. *Journal of Controlled Release* **2001**, *77* (3), 199–212. DOI: 10.1016/S0168-3659(01)00474-6.

(173) Rao, Z.; Sasaki, M.; Taguchi, T. *Colloids and surfaces. B, Biointerfaces* **2013**, *101*, 223–227. DOI: 10.1016/j.colsurfb.2012.06.033.

(174) Ulbrich, K.; Šubr, V.; Pechar, M.; Strohalm, J.; Jelínková, M.; Říhova, B. *Macromol. Symp.* **2000**, *152* (1), 151–162. DOI: 10.1002/1521-3900(200003)152:1<151:AID-MASY151>3.0.CO;2-I.

(175) Ulbrich, K.; Pechar, M.; Strohalm, J.; Šubr, V.; Říhová, B. *Macromol. Symp.* **1997**, *118* (1), 577–585. DOI: 10.1002/masy.19971180176.

(176) Ulbrich, K.; Strohalm, J.; Kopeček, J. *Makromol. Chem.* **1986**, *187* (5), 1131–1144. DOI: 10.1002/macp.1986.021870510.

(177) Georgieva, R.; Tsevi, R.; Kossev, K.; Kusheva, R.; Balgjiska, M.; Petrova, R.; Tenchova, V.; Gitsov, I.; Troev, K. *Journal of medicinal chemistry* **2002**, *45* (26), 5797–5801. DOI: 10.1021/jm020309o.

(178) Kraicheva, I.; Bogomilova, A.; Tsacheva, I.; Momekov, G.; Momekova, D.; Troev, K. *European journal of medicinal chemistry* **2010**, *45* (12), 6039–6044. DOI: 10.1016/j.ejmech.2010.10.002.

(179) Gitsov, I.; Johnson, F. E. *J. Polym. Sci. A Polym. Chem.* **2008**, *46* (12), 4130–4139. DOI: 10.1002/pola.22759.

(180) Penczek, S.; Pretula, J. *Macromolecules* **1993**, *26* (9), 2228–2233. DOI: 10.1021/ma00061a014.

(181) Pretula, J.; Kaluzynski, K.; Szymanski, R.; Penczek, S. *Macromolecules* **1997**, *30* (26), 8172–8176. DOI: 10.1021/ma970390i.

(182) Pretula, J.; Penczek, S. *Makromol Chem Rapid Commun* **1988,** No. 9, 731–737.

(183) Pretula, J.; Penczek, S. *Makromol. Chem.* **1990**, *191* (3), 671–680. DOI: 10.1002/macp.1990.021910322.

(184) Stanimirov, S.; Vasilev, A.; Haupt, E.; Petkov, I.; Deligeorgiev, T. *Journal of fluorescence* **2009**, *19* (1), 85–95. DOI: 10.1007/s10895-008-0384-4.

(185) Troev, K.; Tsatcheva, I.; Koseva, N.; Georgieva, R.; Gitsov, I. *J. Polym. Sci. A Polym. Chem.* **2007**, *45* (7), 1349–1363. DOI: 10.1002/pola.21906.

(186) Troev KD. *Polyphosphoesters*; Elsevier: Oxford, 2012.

(187) Tzevi, R.; Novakov, P.; Troev, K.; Roundhill, D. M. *J. Polym. Sci. A Polym. Chem.* **1997**, *35* (4), 625–630. DOI: 10.1002/(SICI)1099-0518(199703)35:4<625:AID-POLA4>3.0.CO;2-O.

(188) Tzevi, R.; Todorova, G.; Kossev, K.; Troev, K.; Georgiev, E. M.; Roundhill, D. M. *Makromol. Chem.* **1993**, *194* (12), 3261–3269. DOI: 10.1002/macp.1993.021941205.

(189) Wang, D. *Biomaterials* **2003**, *24* (22), 3969–3980. DOI: 10.1016/S0142-9612(03)00280-1.

(190) Wang, J.; Zhuo, R. *European Polymer Journal* **1999**, *35* (3), 491–497. DOI: 10.1016/S0014-3057(98)00139-6.

(191) Fu, H.; Gao, H.; Wu, G.; Wang, Y.; Fan, Y.; Ma, J. *Soft Matter* **2011**, *7* (7), 3546. DOI: 10.1039/c0sm01350a.

(192) Liu, X.-M.; Quan, L.-d.; Tian, J.; Laquer, F. C.; Ciborowski, P.; Wang, D. *Biomacromolecules* **2010**, *11* (10), 2621–2628. DOI: 10.1021/bm100578c.

(193) Liu, X.-M.; Thakur, A.; Wang, D. *Biomacromolecules* **2007**, *8* (9), 2653–2658. DOI: 10.1021/bm070430i.

(194) Luo, Y.-L.; Nan, Y.-F.; Xu, F.; Chen, Y.-S.; Zhao, P. *Journal of biomaterials science. Polymer edition* **2010**, *21* (8-9), 1143–1172. DOI: 10.1163/092050609X12459333183584.

(195) Nathan, A.; Zalipsky, S.; Ertel, S. I.; Agathos, S. N.; Yarmush, M. L.; Kohn, J. *Bioconjugate chemistry* **1993**, *4* (1), 54–62. DOI: 10.1021/bc00019a008.

(196) Nathan, A.; Bolikal, D.; Vyavahare, N.; Zalipsky, S.; Kohn, J. *Macromolecules* **1992**, *25* (18), 4476–4484. DOI: 10.1021/ma00044a004.

(197) Nathan, A.; Zalipsky, S.; Kohn, J. *Journal of Bioactive and Compatible Polymers* **1994**, *9* (3), 239–251. DOI: 10.1177/088391159400900301.

(198) Sarkar, D.; Lopina, S. T. *Polymer Degradation and Stability* **2007**, *92* (11), 1994–2004. DOI: 10.1016/j.polymdegradstab.2007.08.003.

(199) Sun, X.; Gao, H.; Wu, G.; Wang, Y.; Fan, Y.; Ma, J. *International journal of pharmaceutics* **2011**, *412* (1-2), 52–58. DOI: 10.1016/j.ijpharm.2011.04.007.

(200) Lundberg, P.; Lee, B. F.; van den Berg, S. A.; Pressly, E. D.; Lee, A.; Hawker, C. J.; Lynd, N. A. *ACS Macro Lett.* **2012**, *1* (11), 1240–1243. DOI: 10.1021/mz300477t.

(201) Worm, M.; Leibig, D.; Dingels, C.; Frey, H. *ACS Macro Lett.* **2016**, *5* (12), 1357–1363. DOI: 10.1021/acsmacrolett.6b00735.

(202) Steiert, E.; Ewald, J.; Wagner, A.; Hellmich, U. A.; Frey, H.; Wich, P. R. *Polym. Chem.* **2020**, *11* (2), 551–559. DOI: 10.1039/C9PY01162E.

(203) Ewald, J.; Blankenburg, J.; Worm, M.; Besch, L.; Unger, R. E.; Tremel, W.; Frey, H.; Pohlit, H. *Chemistry (Weinheim an der Bergstrasse, Germany)* **2020**, *26* (13), 2947–2953. DOI: 10.1002/chem.201905310.

(204) Wilms, D.; Schömer, M.; Wurm, F.; Hermanns, M. I.; Kirkpatrick, C. J.; Frey, H. *Macromol. Rapid Commun.* **2010**, *31* (20), 1811–1815. DOI: 10.1002/marc.201000329.

(205) Wilms, D.; Stiriba, S.-E.; Frey, H. *Accounts of chemical research* **2010**, *43* (1), 129–141. DOI: 10.1021/ar900158p.

(206) Wuts, P. G. M.; Greene, T. W. *Greene's protective groups in organic synthesis*, Fifth edition; Wiley: Hoboken, New Jersey, 2014.

(207) Guibé, F. *Tetrahedron* **1997**, *53* (40), 13509–13556. DOI: 10.1016/S0040-4020(97)00524-3.

(208) Cunningham, J.; Gigg, R.; Warren, C. D. *Tetrahedron Letters* **1964**, *5* (19), 1191–1196. DOI: 10.1016/S0040-4039(00)90452-0.

(209) Cadot, C.; Dalko, P. I.; Cossy, J. *Tetrahedron Letters* **2002**, *43* (10), 1839–1841. DOI: 10.1016/S0040-4039(02)00141-7.

(210) Gent, P. A.; Gigg, R. *J. Chem. Soc., Chem. Commun.* **1974,** No. 7, 277. DOI: 10.1039/c39740000277.

(211) Price, C. C.; Snyder, W. H. *J. Am. Chem. Soc.* **1961**, *83* (7), 1773. DOI: 10.1021/ja01468a062.

(212) Atienza, B. J. P.; Truong, N.; Williams, F. J. *Organic letters* **2018**, *20* (20), 6332–6335. DOI: 10.1021/acs.orglett.8b02356.

(213) Kitov, P. I.; Bundle, D. R. *Organic letters* **2001**, *3* (18), 2835–2838. DOI: 10.1021/ol016278t.

(214) Sanz, R.; Martínez, A.; Marcos, C.; Fañanás, F. *Synlett* **2008**, *2008* (13), 1957–1960. DOI: 10.1055/s-2008-1077962.

(215) Reuss, V. S.; Obermeier, B.; Dingels, C.; Frey, H. *Macromolecules* **2012**, *45* (11), 4581–4589. DOI: 10.1021/ma300292m.

(216) Price, C. C.; Snyder, W. H. *J. Org. Chem.* **1962**, *27* (12), 4639–4641. DOI: 10.1021/jo01059a505.

(217) Price, C. C.; Snyder, W. E. *Tetrahedron Letters* **1962**, *3* (2), 69–73. DOI: 10.1016/S0040-4039(00)70488-6.

(218) Tarbell, D. S.; Lovett, W. E. *J. Am. Chem. Soc.* **1956**, *78* (10), 2259–2264. DOI: 10.1021/ja01591a063.

(219) Shin, J.; Shum, P.; Thompson, D. H. *Journal of Controlled Release* **2003**, *91* (1-2), 187–200. DOI: 10.1016/S0168-3659(03)00232-3.

(220) Kim, H.-K.; Thompson, D. H.; Jang, H. S.; Chung, Y. J.; van den Bossche, J. *ACS applied materials & interfaces* **2013**, *5* (12), 5648–5658. DOI: 10.1021/am400977t.

(221) Malik, N. N. *Drug discovery today* **2008**, *13* (21-22), 909–912. DOI: 10.1016/j.drudis.2008.09.007.

(222) Groot, A. S. de; Martin, W. *Clinical immunology (Orlando, Fla.)* **2009**, *131* (2), 189–201. DOI: 10.1016/j.clim.2009.01.009.

(223) Kaliyaperumal, A.; Jing, S. *Current pharmaceutical biotechnology* **2009**, *10* (4), 352–358. DOI: 10.2174/138920109788488860.

(224) Manning, M. C.; Chou, D. K.; Murphy, B. M.; Payne, R. W.; Katayama, D. S. *Pharmaceutical research* **2010**, *27* (4), 544–575. DOI: 10.1007/s11095-009-0045-6.

(225) Vermonden, T.; Censi, R.; Hennink, W. E. *Chemical reviews* **2012**, *112* (5), 2853–2888. DOI: 10.1021/cr200157d.

(226) Antosova, Z.; Mackova, M.; Kral, V.; Macek, T. *Trends in biotechnology* **2009**, *27* (11), 628–635. DOI: 10.1016/j.tibtech.2009.07.009.

(227) Werle, M.; Makhlof, A.; Takeuchi, H. *Recent patents on drug delivery & formulation* **2009**, *3* (2), 94–104. DOI: 10.2174/187221109788452221.

(228) Haag, R.; Kratz, F. *Angewandte Chemie (International ed. in English)* **2006**, *45* (8), 1198–1215. DOI: 10.1002/anie.200502113.

(229) Ringsdorf, H. *J. polym. sci., C Polym. symp.* **1975**, *51* (1), 135–153. DOI: 10.1002/polc.5070510111.

(230) Suk, J. S.; Xu, Q.; Kim, N.; Hanes, J.; Ensign, L. M. *Advanced Drug Delivery Reviews* **2016**, *99* (Pt A), 28–51. DOI: 10.1016/j.addr.2015.09.012.

(231) Duncan, R. *Nature reviews. Cancer* **2006**, *6* (9), 688–701. DOI: 10.1038/nrc1958.

(232) Harris, J. M.; Martin, N. E.; Modi, M. *Clinical pharmacokinetics* **2001**, *40* (7), 539–551. DOI: 10.2165/00003088-200140070-00005.

(233) Pasut, G.; Veronese, F. M. *Isr. J. Chem.* **2010**, *50* (2), 151–159. DOI: 10.1002/ijch.201000019.

(234) Roberts, M. J.; Bentley, M. D.; Harris, J. M. *Advanced Drug Delivery Reviews* **2002**, *54* (4), 459–476. DOI: 10.1016/S0169-409X(02)00022-4.

(235) Kozlowski, A.; Milton Harris, J. *Journal of Controlled Release* **2001**, *72* (1-3), 217–224. DOI: 10.1016/S0168-3659(01)00277-2.

(236) Basu, A.; Yang, K.; Wang, M.; Liu, S.; Chintala, R.; Palm, T.; Zhao, H.; Peng, P.; Wu, D.; Zhang, Z.; Hua, J.; Hsieh, M.-C.; Zhou, J.; Petti, G.; Li, X.; Janjua, A.; Mendez, M.; Liu, J.; Longley, C.; Zhang, Z.; Mehlig, M.; Borowski, V.; Viswanathan, M.; Filpula, D. *Bioconjugate chemistry* **2006**, *17* (3), 618–630. DOI: 10.1021/bc050322y.

(237) Manjula, B. N.; Tsai, A.; Upadhya, R.; Perumalsamy, K.; Smith, P. K.; Malavalli, A.; Vandegriff, K.; Winslow, R. M.; Intaglietta, M.; Prabhakaran, M.; Friedman, J. M.; Acharya, A. S. *Bioconjugate chemistry* **2003**, *14* (2), 464–472. DOI: 10.1021/bc0200733.

(238) Banerjee, S. S.; Aher, N.; Patil, R.; Khandare, J. *Journal of drug delivery* **2012**, *2012*, 103973. DOI: 10.1155/2012/103973.

(239) Harris, J. M.; Chess, R. B. *Nature reviews. Drug discovery* **2003**, *2* (3), 214–221. DOI: 10.1038/nrd1033.

(240) Schöttler, S.; Becker, G.; Winzen, S.; Steinbach, T.; Mohr, K.; Landfester, K.; Mailänder, V.; Wurm, F. R. *Nature nanotechnology* **2016**, *11* (4), 372–377. DOI: 10.1038/nnano.2015.330.

(241) A Abuchowski; J R McCoy; N C Palczuk; T van Es; F F Davis. *J. Biol. Chem.* **1977**, *252* (11), 3582–3586.

(242) Abuchowski, A.; van Es, T.; Palczuk, N. C.; Davis, F. F. *Journal of Biological Chemistry* **1977**, *252* (11), 3578–3581.

(243) Alconcel, S. N. S.; Baas, A. S.; Maynard, H. D. *Polym. Chem.* **2011**, *2* (7), 1442. DOI: 10.1039/c1py00034a.

(244) Dust, J. M.; Fang, Z. H.; Harris, J. M. *Macromolecules* **1990**, *23* (16), 3742–3746. DOI: 10.1021/ma00218a005.

(245) Zalipsky, S. *Advanced Drug Delivery Reviews* **1995**, *16* (2-3), 157–182. DOI: 10.1016/0169-409X(95)00023-Z.

(246) Turecek, P. L.; Bossard, M. J.; Schoetens, F.; Ivens, I. A. *Journal of pharmaceutical sciences* **2016**, *105* (2), 460–475. DOI: 10.1016/j.xphs.2015.11.015.

(247) Pasut, G.; Scaramuzza, S.; Schiavon, O.; Mendichi, R.; Veronese, F. M. *Journal of Bioactive and Compatible Polymers* **2005**, *20* (3), 213–230. DOI: 10.1177/0883911505053377.

(248) Veronese, F. M.; Mero, A. *BioDrugs : clinical immunotherapeutics, biopharmaceuticals and gene therapy* **2008**, *22* (5), 315–329. DOI: 10.2165/00063030-200822050-00004.

(249) Pasut, G.; Veronese, F. M. *Progress in Polymer Science* **2007**, *32* (8-9), 933–961. DOI: 10.1016/j.progpolymsci.2007.05.008.

(250) Parveen, S.; Sahoo, S. K. *Clinical pharmacokinetics* **2006**, *45* (10), 965–988. DOI: 10.2165/00003088-200645100-00002.

(251) Monfardini, C.; Schiavon, O.; Caliceti, P.; Morpurgo, M.; Harris, J. M.; Veronese, F. M. *Bioconjugate chemistry* **1995**, *6* (1), 62–69. DOI: 10.1021/bc00031a006.

(252) Herman, S.; Hooftman, G.; Schacht, E. *Journal of Bioactive and Compatible Polymers* **1995**, *10* (2), 145–187. DOI: 10.1177/088391159501000205.

(253) Filpula, D.; Zhao, H. *Advanced Drug Delivery Reviews* **2008**, *60* (1), 29–49. DOI: 10.1016/j.addr.2007.02.001.

(254) Gong, Y.; Leroux, J.-C.; Gauthier, M. A. *Bioconjugate chemistry* **2015**, *26* (7), 1172–1181. DOI: 10.1021/bc500611k.

(255) Greenwald, R. B.; Choe, Y. H.; McGuire, J.; Conover, C. D. *Advanced Drug Delivery Reviews* **2003**, *55* (2), 217–250. DOI: 10.1016/S0169-409X(02)00180-1.

(256) Pasut, G.; Veronese, F. M. *Journal of controlled release : official journal of the Controlled Release Society* **2012**, *161* (2), 461–472. DOI: 10.1016/j.jconrel.2011.10.037.

(257) Chang, M.; Zhang, F.; Wei, T.; Zuo, T.; Guan, Y.; Lin, G.; Shao, W. *Journal of drug targeting* **2016**, *24* (6), 475–491. DOI: 10.3109/1061186X.2015.1108324.

(258) Koetting, M. C.; Peters, J. T.; Steichen, S. D.; Peppas, N. A. *Materials science & engineering. R, Reports : a review journal* **2015**, *93*, 1–49. DOI: 10.1016/j.mser.2015.04.001.

(259) Akhtar, M. F.; Hanif, M.; Ranjha, N. M. *Saudi pharmaceutical journal : SPJ : the official publication of the Saudi Pharmaceutical Society* **2016**, *24* (5), 554–559. DOI: 10.1016/j.jsps.2015.03.022.

(260) Basu, A.; Kunduru, K. R.; Doppalapudi, S.; Domb, A. J.; Khan, W. *Advanced Drug Delivery Reviews* **2016**, *107*, 192–205. DOI: 10.1016/j.addr.2016.07.004.

(261) Varaprasad, K.; Raghavendra, G. M.; Jayaramudu, T.; Yallapu, M. M.; Sadiku, R. *Materials science & engineering. C, Materials for biological applications* **2017**, *79*, 958–971. DOI: 10.1016/j.msec.2017.05.096.

(262) Onaciu, A.; Munteanu, R. A.; Moldovan, A. I.; Moldovan, C. S.; Berindan-Neagoe, I. *Pharmaceutics* **2019**, *11* (9). DOI: 10.3390/pharmaceutics11090432.

(263) Qiu, Y.; Park, K. *Advanced Drug Delivery Reviews* **2001**, *53* (3), 321–339. DOI: 10.1016/S0169-409X(01)00203-4.

(264) Lee, K. Y.; Mooney, D. J. *Chemical reviews* **2001**, *101* (7), 1869–1879. DOI: 10.1021/cr000108x.

(265) Drury, J. L.; Mooney, D. J. *Biomaterials* **2003**, *24* (24), 4337–4351. DOI: 10.1016/S0142-9612(03)00340-5.

(266) Kamoun, E. A.; Kenawy, E.-R. S.; Chen, X. *Journal of advanced research* **2017**, *8* (3), 217–233. DOI: 10.1016/j.jare.2017.01.005.

(267) Lin, C.-C.; Anseth, K. S. *Pharmaceutical research* **2009**, *26* (3), 631–643. DOI: 10.1007/s11095-008-9801-2.

(268) Kharkar, P. M.; Rehmann, M. S.; Skeens, K. M.; Maverakis, E.; Kloxin, A. M. *ACS biomaterials science & engineering* **2016**, *2* (2), 165–179. DOI: 10.1021/acsbiomaterials.5b00420.

(269) Buwalda, S. J.; Vermonden, T.; Hennink, W. E. *Biomacromolecules* **2017**, *18* (2), 316–330. DOI: 10.1021/acs.biomac.6b01604.

(270) Rydholm, A. E.; Bowman, C. N.; Anseth, K. S. *Biomaterials* **2005**, *26* (22), 4495–4506. DOI: 10.1016/j.biomaterials.2004.11.046.

(271) Odian, G. *Principles of Polymerization (Fourth Edition)*, 4th ed.; Wiley-Interscience: S.l., 2004.

(272) Malkoch, M.; Vestberg, R.; Gupta, N.; Mespouille, L.; Dubois, P.; Mason, A. F.; Hedrick, J. L.; Liao, Q.; Frank, C. W.; Kingsbury, K.; Hawker, C. J. *Chemical communications (Cambridge, England)* **2006,** No. 26, 2774–2776. DOI: 10.1039/b603438a.

(273) Zhang, X.; Malhotra, S.; Molina, M.; Haag, R. *Chemical Society reviews* **2015**, *44* (7), 1948–1973. DOI: 10.1039/c4cs00341a.

(274) Kaihara, S.; Matsumura, S.; Fisher, J. P. *European journal of pharmaceutics and biopharmaceutics : official journal of Arbeitsgemeinschaft fur Pharmazeutische Verfahrenstechnik e.V* **2008**, *68* (1), 67–73. DOI: 10.1016/j.ejpb.2007.05.019.

(275) Betz, M. W.; Caccamese, J. F.; Coletti, D. P.; Sauk, J. J.; Fisher, J. P. *Journal of biomedical materials research. Part A* **2009**, *90* (3), 819–829. DOI: 10.1002/jbm.a.32131.

(276) Kharkar, P. M.; Kiick, K. L.; Kloxin, A. M. *Chemical Society reviews* **2013**, *42* (17), 7335–7372. DOI: 10.1039/c3cs60040h.

(277) Lutolf, M. P.; Hubbell, J. A. *Nature biotechnology* **2005**, *23* (1), 47–55. DOI: 10.1038/nbt1055.

(278) Bryant, S. J.; Anseth, K. S. *Journal of biomedical materials research. Part A* **2003**, *64* (1), 70–79. DOI: 10.1002/jbm.a.10319.

(279) West, J. L.; Hubbell, J. A. *Macromolecules* **1999**, *32* (1), 241–244. DOI: 10.1021/ma981296k.

(280) Chen, G.; Taghavi, S.; Marecak, D.; Amsden, B. G. *Macromol. Mater. Eng.* **2018**, *303* (1), 1700162. DOI: 10.1002/mame.201700162.

(281) Stevens, K. R.; Miller, J. S.; Blakely, B. L.; Chen, C. S.; Bhatia, S. N. *Journal of biomedical materials research. Part A* **2015**, *103* (10), 3331–3338. DOI: 10.1002/jbm.a.35478.

(282) Lutolf, M. P.; Hubbell, J. A. *Biomacromolecules* **2003**, *4* (3), 713–722. DOI: 10.1021/bm025744e.

(283) Zisch, A. H.; Lutolf, M. P.; Ehrbar, M.; Raeber, G. P.; Rizzi, S. C.; Davies, N.; Schmökel, H.; Bezuidenhout, D.; Djonov, V.; Zilla, P.; Hubbell, J. A. *FASEB journal : official publication of the Federation of American Societies for Experimental Biology* **2003**, *17* (15), 2260–2262. DOI: 10.1096/fj.02-1041fje.

(284) Schröder, R.; Pohlit, H.; Schüler, T.; Panthöfer, M.; Unger, R. E.; Frey, H.; Tremel, W. *J. Mater. Chem. B* **2015**, *3* (35), 7079–7089. DOI: 10.1039/C5TB01032B.

(285) Schröder, R.; Besch, L.; Pohlit, H.; Panthöfer, M.; Roth, W.; Frey, H.; Tremel, W.; Unger, R. E. *Journal of tissue engineering and regenerative medicine* **2018**, *12* (7), 1754–1768. DOI: 10.1002/term.2703.

(286) Rödel, M.; Teßmar, J.; Groll, J.; Gbureck, U. *Materials (Basel, Switzerland)* **2018**, *12* (1). DOI: 10.3390/ma12010053.

(287) Kim, B.; Peppas, N. A. *Biomedical Microdevices* **2003**, *5* (4), 333–341. DOI: 10.1023/A:1027313931273.

(288) Schoener, C. A.; Hutson, H. N.; Peppas, N. A. *Journal of biomedical materials research. Part A* **2013**, *101* (8), 2229–2236. DOI: 10.1002/jbm.a.34532.

(289) Sharpe, L. A.; Daily, A. M.; Horava, S. D.; Peppas, N. A. *Expert opinion on drug delivery* **2014**, *11* (6), 901–915. DOI: 10.1517/17425247.2014.902047.

(290) Puranik, A. S.; Pao, L. P.; White, V. M.; Peppas, N. A. *European journal of pharmaceutics and biopharmaceutics : official journal of Arbeitsgemeinschaft fur Pharmazeutische Verfahrenstechnik e.V* **2016**, *108*, 196–213. DOI: 10.1016/j.ejpb.2016.09.007.

(291) Li, J.; Mooney, D. J. *Nature reviews. Materials* **2016**, *1* (12). DOI: 10.1038/natrevmats.2016.71.

(292) Kolate, A.; Baradia, D.; Patil, S.; Vhora, I.; Kore, G.; Misra, A. *Journal of controlled release : official journal of the Controlled Release Society* **2014**, *192*, 67–81. DOI: 10.1016/j.jconrel.2014.06.046.

(293) Schneider, E. L.; Henise, J.; Reid, R.; Ashley, G. W.; Santi, D. V. *Bioconjugate chemistry* **2016**, *27* (5), 1210–1215. DOI: 10.1021/acs.bioconjchem.5b00690.

(294) Kim, D. Y.; Kwon, D. Y.; Kwon, J. S.; Park, J. H.; Park, S. H.; Oh, H. J.; Kim, J. H.; Min, B. H.; Park, K.; Kim, M. S. *Biomaterials* **2016**, *85*, 232–245. DOI: 10.1016/j.biomaterials.2016.02.001.

2 Cleavable PEGs via copolymerization of EO with EPB

2.1 Acid-cleavable Poly(ethylene Glycol) Hydrogels Displaying Protein Release at pH 5

Johannes Ewald,[a] Jan Blankenburg,[a],[b] Matthias Worm,[a] Laura Besch,[c] Ronald E. Unger,[d] Wolfgang Tremel,[c] Holger Frey,[a] Hannah Pohlit*[a],[e]*

[a] Institute of Organic Chemistry, Johannes Gutenberg-University, Duesbergweg 10-14, 55128 Mainz, Germany

[b] Graduate School Materials Science in Mainz, Staudinger Weg 9, 55128 Mainz, Germany

[c] Institute of Inorganic Chemistry and Analytical Chemistry, Johannes Gutenberg-University, Duesbergweg 10-14, 55128 Mainz, Germany

[d] Institute of Pathology, Johannes Gutenberg University Mainz, Obere Zahlbacher Straße 63, 55101 Mainz, Germany

[e] Engineering Sciences Department, Science for Life Laboratory, Uppsala University, Lägerhyddsvägen 1, 75121 Uppsala, Sweden

Published in Chemistry, A European Journal (Doi: 10.1002/chem.201905310)

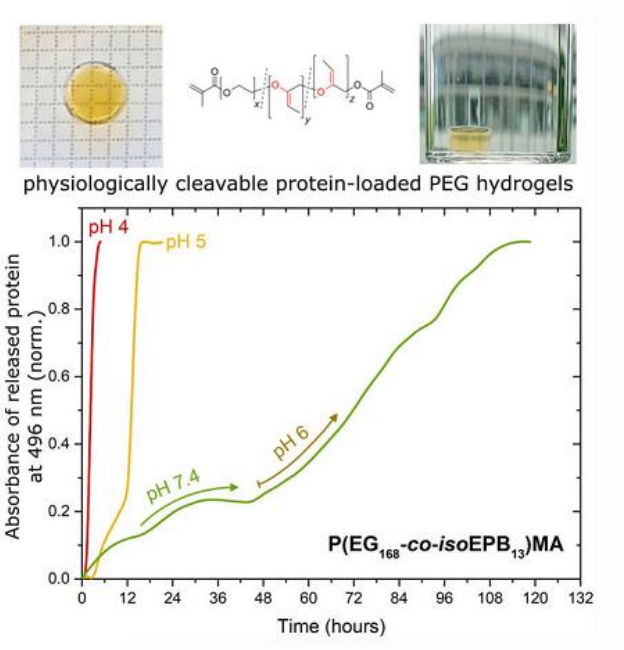

2.1.1 ABSTRACT

PEG is the gold standard polymer for pharmaceutical applications, however it lacks degradability. Degradation under physiologically relevant pH as present in endolysosomes, cancerous and inflammatory tissues is crucial for many areas. We present the anionic ring-opening copolymerization of ethylene oxide with 3,4-epoxy-1-butene (EPB) and its subsequent modification to yield acid-degradable vinyl ether groups as well as methacrylate (MA) units, enabling radical cross-linking. Copolymers with different molar ratios of EPB, molecular weights (Mn) up to 10,000 g mol^{-1} and narrow dispersities (Đ<1.05) are generated. Both the P(EG-co-isoEPB)MA copolymer and the hydrogels, showed pH-dependent, rapid hydrolysis at pH 5 - 6) and long-term storage stability at neutral pH (pH 7.4). By designing the degree of polymerization and content of degradable vinyl ether groups, the release time of an entrapped protein OVA-Alexa488 can be tailored from a few hours to several days (pH 5: 13 h < t1/2 < 51 h).

2.1.2 INTRODUCTION

Poly(ethylene glycol) (PEG) is a biocompatible, water-soluble polymer used for cosmetics, pharmaceutics and medical applications.[1] Due to its low immunogenicity, antigenicity and toxicity, the bioconjugation of protein drugs with PEG (known as "PEGylation") is the established gold standard employed to modify therapeutic molecules like peptides, proteins or aptamers.[2] Furthermore, PEG is used extensively as a hydrogel scaffold for the controlled release of biomolecules[3] or cells[4] in regenerative medicine.[5] The PEG delivery vehicles take advantage of the versatility of the PEG chemistry that allows for a tailored design of the required hydrogel properties. While mechanical[6] and biological properties[7] as well as hydrogel porosity[8] can be optimized independently, adjusting degradability without altering the aforementioned properties remains a challenge. In general, PEG hydrogels lack degradability under physiological conditions within relevant time spans. Hydrogels derived from traditional diacrylated PEG (PEGDA) are hydrolysed slowly and unspecifically *in vivo,* which renders them unsuitable for long-term storage as well as for implantable applications.[9] Therefore, the use of nondegradable PEG molecules larger than 30 kDa for medical applications is limited as these cannot be excreted by the kidney due to the kidney-threshold and may accumulate in the tissue.[10] However, the use of hydrogels composed of high molecular weight PEG chains would result in larger average pore size and greater swellability of the gel, which is thought to be favourable for the release of larger therapeutic molecules depending solely on diffusion[11] like antibodies. This approach can be advantageous when considering a constant diffusive release. On the other hand, acid-triggered controlled release combined with advanced storage stability is typical for hydrogels from shorter, degradable PEG chains eliminating unspecific drug release depending solely on diffusion. This may open a new range of applications for the use of PEG hydrogels for *in vivo* applications, e.g. degradable injectable hydrogels, micro- or

nanosized delivery vehicles, wound-healing hydrogel patches, and directed drug delivery for tumour treatment.

In this context, considerable efforts have been devoted to synthesize intrinsically cleavable PEGs that respond to environmental stimuli.[1, 12] Polymer cleavability in acidic environment as found intracellularly inside the endolysosome,[13] in inflamed tissue,[11a, 14] tumor tissue,[15] or vaginal tissue[16] can be achieved by inserting acid-labile moieties.[17] Various innovative approaches for introduction of acid-degradable functional groups into a polyether backbone were reported. These strategies include step-growth polymerization, oxidation, or copolymerization with epichlorohydrin or lactide, or by introducing acetals,[18] ketals,[19] hydrazones,[20] cis-acetonitic acids,[21] maleamic acid derivatives,[22] imines,[23] β-thiopropionates,[24] or esters[25]. However, these strategies generate either polydisperse materials or polymers with ill-defined end-groups.[26] The availability of nearly monodisperse, high molecular weight PEGs with acid-labile vinyl ether degradation sites has the potential to open up a vast range of applications using PEG hydrogels *in vivo*. Here, we present well-defined PEG building blocks with cross-linkable end groups that degrade at physiologically relevant pH in practicable time scales, while preserving long-term storage stability. Furthermore, we demonstrate that the size of the non-toxic degradation products can be tailored by customizing the number of degradable vinyl ether units per polymer chain.

2.1.3 RESULTS AND DISCUSSION

2.1.3.1 SYNTHESIS

Recently, we established the synthesis of multi allyl ether-functional PEG by anionic ring-opening copolymerization of ethylene oxide (EO) and 3,4-epoxy-1-butene (EPB).[27] Copolymerization of EPB and EO was performed in a DMSO/THF mixture at room temperature using sodium hydride as a base (see **Scheme 1**).

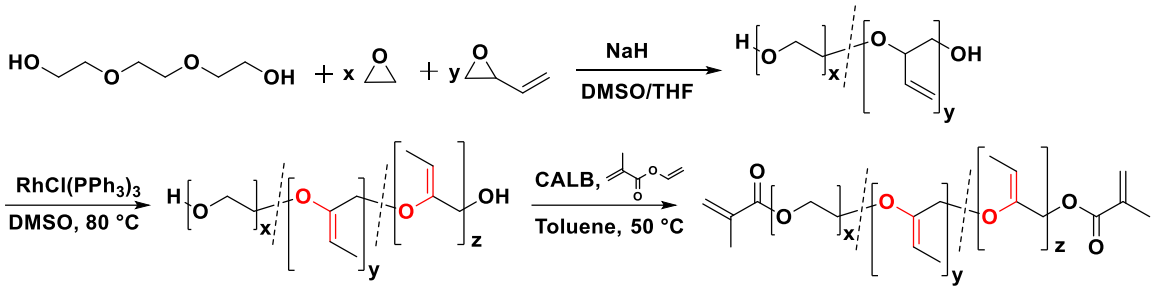

Scheme 1: Copolymerization of EO and EPB as well as post-polymerization isomerization and methacrylate derivatization.

We use triethylene glycol as a bifunctional initiator resulting in well-defined P(EG-*co*-EPB) copolymers ($Đ$ = 1.03–1.05) with adjustable EPB content (5-10 mol%) and molecular weight (5,000-10,000 g mol^{-1}, see **Table 1**). Isomerization of the allyl moieties with Wilkinson's catalyst ($RhCl(PPh_3)_3$) results in vinyl ethers (*iso*EPB) that exhibit fast hydrolysis in slightly acidic conditions, while being long-term stable under neutral conditions.[27] In the final step, methacrylate units are attached to the degradable polymers using an enzyme-catalysed, mild esterification reaction. The latter simple modification enables radical crosslinking of the PEG copolymer building block to degradable hydrogels that are suitable for drug delivery and controlled release.

2.1.3.2 CHARACTERIZATION

All synthesized copolymers were characterized by ^{1}H NMR, size exclusion chromatography (SEC) and mass spectrometry (MALDI-ToF). Exemplarily, the data of P(EG_{168}-*co*-EPB_{13}) and its derivatives are discussed in the main text. Extensive analytical data of the other polymers can be found in the Supporting Information. Molecular weights were calculated from ^{1}H NMR spectra by comparing the signals of the ethylene oxide polymer backbone with the signal of the hydroxyl units. The percentage of EPB incorporation was calculated by comparing the integrals of the allyl NMR signals at 5.84 ppm and 5.74 ppm (EPB) or the vinyl NMR signal at 4.78 ppm (*iso*EPB) with the signal of the two hydroxyl end-groups at 4.6 ppm.

Table 1: Molecular characteristics of P(EG-*co*-EPB) copolymers and of post-polymerization modified copolymers.

					after isomerisation				after methacrylation				after hydrolysis			
sample	M_n[a] g/mol	mol% EPB	M_n[b] g/mol	$Đ$	M_n[a] g/mol	mol% EPB	M_n[b] g/mol	$Đ$	M_n[a] g/mol	mol% EPB	M_n[b] g/mol	$Đ$	M_n[b] g/mol	$Đ$	$t_{1/2}$ at pH 4[a]	$t_{1/2}$ at pH 5[a]
p(EG_{112}-*co*-EPB_5)	5150	5	3730	1.03	5280	5	3720	1.03	5280	5	3700	1.03	880	1.75	4.5 h	51 h
p(EG_{202}-*co*-EPB_9)	9310	5	6950	1.03	9540	5	6730	1.04	9540	4	6690	1.03	830	1.85	3.6 h	15 h
p(EG_{113}-*co*-EPB_9)	5410	10	3620	1.03	5620	8	3580	1.05	5640	8	3600	1.05	670	1.55	2.3 h	14 h
p(EG_{168}-*co*-EPB_{13})	7970	9	6420	1.03	8280	8	6360	1.03	8280	7	6190	1.04	900	1.94	2.3 h	13 h

[a]NMR [400 MHz, DMSO-d_6]; mol% EPB: Content of EPB calculated from ^{1}H NMR; [b]SEC (DMF, PEG standards, RI signal); $Đ = M_w/M_n$: Dispersity of polymer samples (SEC); $t_{1/2}$ = half life time of hydrolysis reaction.

Isomerization with Wilkinson's catalyst resulted in the disappearance of the EPB signals between 6.0 and 5.2 ppm and the appearance of the vinyl ether signals at 4.8-4.5 ppm (compare **Figure S19**). SEC underestimates the actual molecular weights because of the different hydrodynamic volume of the copolymer that is compared to the PEG standard used for SEC calibration. All SEC traces showed monomodal molecular weight distributions, and molecular weights did not change significantly upon post-polymerization functionalization. A typical ^{1}H NMR spectra of P(EG-*co*-*iso*EPB)MA is given in **Figure 1a**. SEC traces of P(EG_{168}-*co*-EPB_{13}) copolymer and its derivatives are presented in **Figure 1b**. MALDI-ToF was performed to confirm that all polymers were initiated from triethylene glycol and to confirm copolymerization of EPB and EO (**Figure S5** + **S11**).

To comprehend the monomer sequence distribution during anionic ring-opening copolymerization, on-line ^{1}H NMR measurements – a technique that has been proven extremely useful to monitor polymerization reactions *in situ*[28] – has been employed during copolymerization of EPB and EO. The reactivity ratios were determined by fitting the *in situ* data to the ideal copolymerization model to be $r_{EPB} = 0.35$ and $r_{EO} = 2.8$ (**Figure S33**).[29]

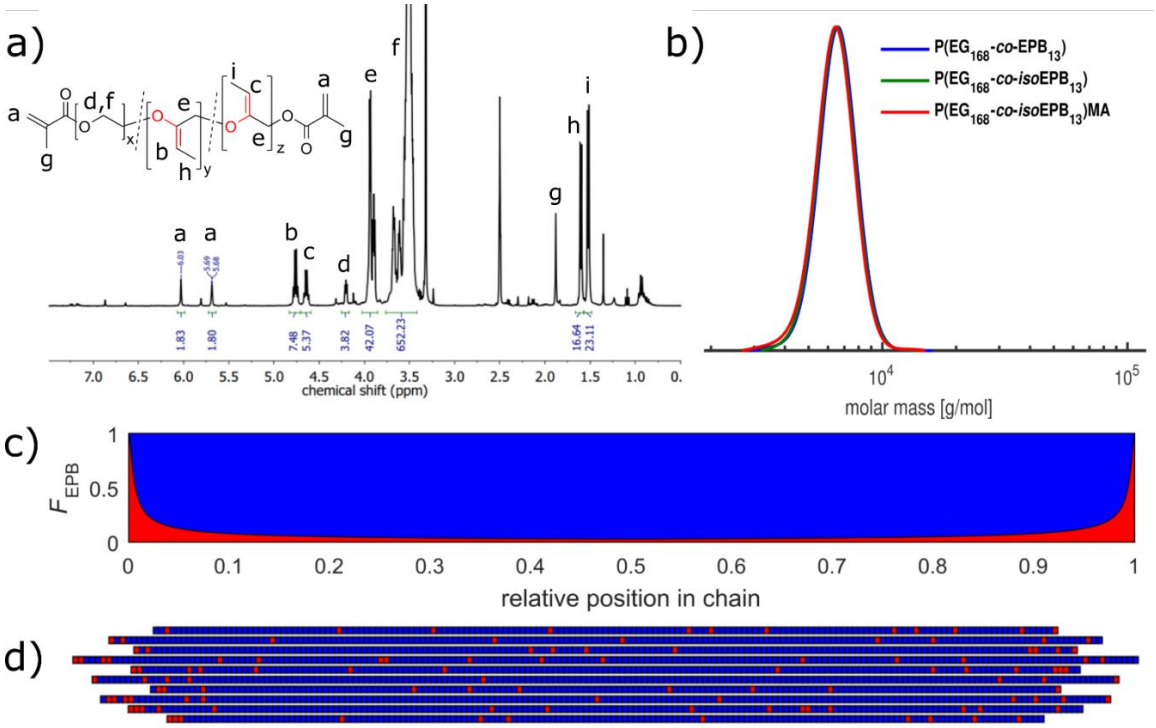

Figure 1: Polymer analytics of representative copolymer P(EG_{168}-*co*-EPB_{13}) a) ^{1}H NMR spectrum (400 MHz, DMSO-d_6); b) SEC traces (DMF, PEG standards, RI signal) of synthesized copolymer and after subsequent post polymerization reactions; c) Gradient of EPB units along the copolymer chain polymerized from bifunctional initiator based on the determined reactivity ratios, blue: ethylene oxide, red: EPB; d) Sample of ten individual copolymer chains obtained by Monte Carlo simulation performed for the polymer composition P(EG_{168}-*co*-EPB_{13}) started from triethylene glycol and is based on the determined reactivity ratios.

To comprehend the monomer sequence distribution during anionic ring-opening copolymerization, on-line ^{1}H NMR measurements – a technique that has been proven extremely useful to monitor polymerization reactions *in situ*[28] – has been employed during copolymerization of EPB and EO. The reactivity ratios were determined by fitting the *in situ* data to the ideal copolymerization model to be r_{EPB} = 0.35 and r_{EO} = 2.8 (**Figure S33**).[29]

The results were confirmed by classical aliquot taking at determined points of time from the bulk polymerization reaction. Based on these reactivity ratios the average microstructure was depicted for a copolymer started by a bifunctional initiator with the same composition as P(EG_{168}-*co*-EPB_{13}), see **Figure 1c**. Individual copolymer chains

obtained by a Monte Carlo simulation carried out for the composition of P(EG_{168}-*co*-EPB_{13}), based on the determined reactivity ratios and living polymerization behavior are displayed in **Figure 1d**. Incorporation of EPB moieties results in a gradient microstructure with higher ratio of EPB at the termini of the polymer chains and lower EPB content near the bifunctional initiator.

To investigate the biocompatibility of the polymer to cells, *in vitro* cell studies with MG 63 and primary HUVEC cells were conducted. A solution of 50 – 500 µg/mL P(EG_{92}-*co*-*iso*EPB_6) was added to the cell culture and vitality staining with Calcein-AM was performed after 24 h, 72 h and 7 days. For MG-63 cells, no difference compared to the untreated control cells was detected upon incubation of 500 µg/mL P(EG_{92}-*co*-*iso*EPB_6) after 7 days of culture. However, for primary HUVEC cells, only for the highest concentration of 500 µg/mL tested, P(EG_{92}-*co*-*iso*EPB_6) showed diminished cell survival after 72 h of cell culture. For 100 µg/mL, no difference compared to the untreated control cells was observed.

2.1.3.3 MACROMONOMER DEGRADATION

The vinyl ether units within the P(EG-*co*-*iso*EPB)MA polymer backbone are susceptible to hydrolysis upon acidification (see **Figure 2a**, bottom). These macromonomers break down completely upon incubation with dilute HCl overnight. Subsequently, base was added to adjust the pH above 3, and degradation fragments were analysed by SEC (representative elution trace is displayed in **Figure 2a** top). Half-life degradation times for hydrolysis were determined with ^{1}H NMR as described previously[27] (**Table 1**). The EPB content was tailored to give degradation products of 670 – 900 g mol^{-1}, which allows for renal excretion. The degradation behaviour can be predicted by the Monte Carlo simulation shown in **Figure S26**. In the simulated degradation of P(EG_{168}-*co*-EPB_{13}) the PEG-fragments show a very similar size distribution as obtained experimentally.

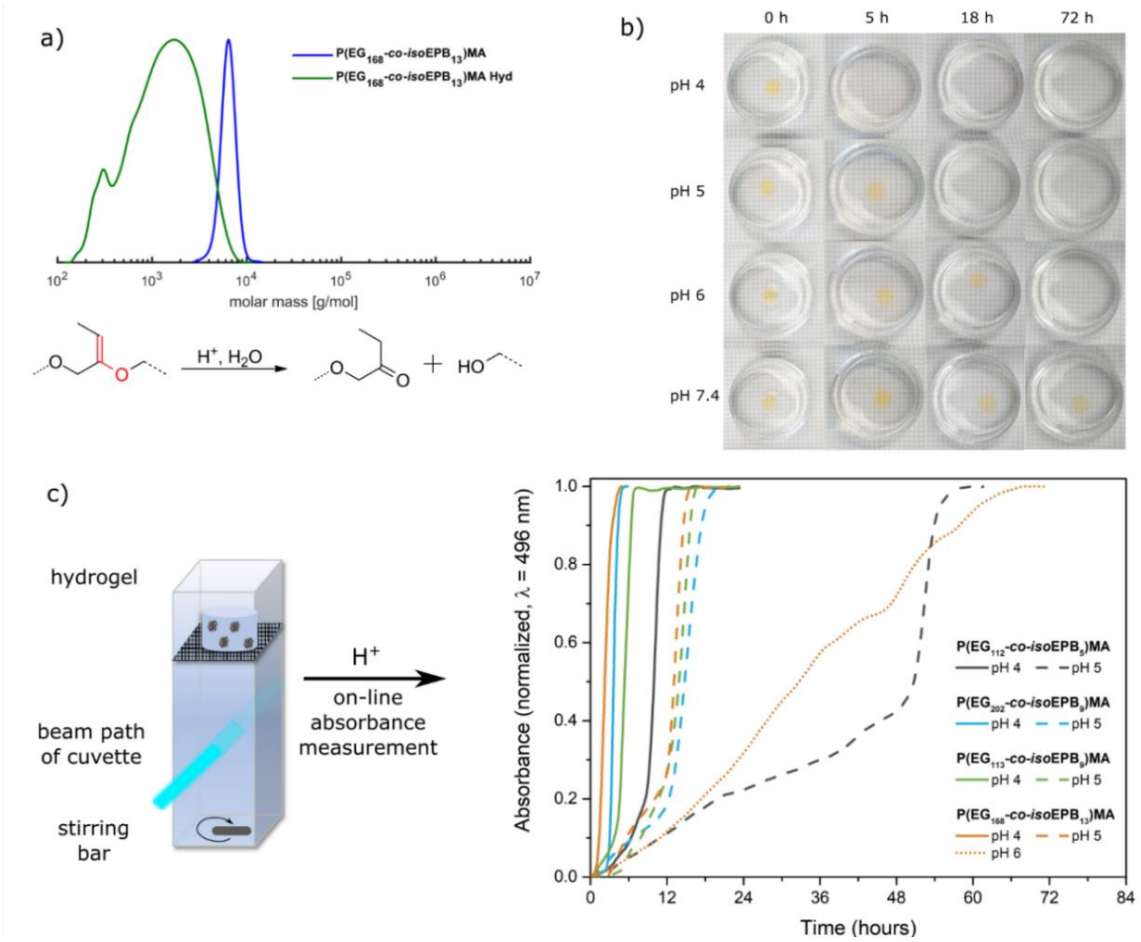

Figure 2: Hydrogel degradation and protein release a) SEC traces (DMF, PEG standards, RI signal) of P(EG$_{168}$-*co*-EPB$_{13}$)MA before and after hydrolysis. Bottom: Reaction scheme of hydrolysis of vinyl ether moieties in copolymer chain at acidic pH; b) photographs of the degradation of OVA-Alexa488 loaded hydrogels from P(EG$_{168}$-*co*-*iso*EPB$_{13}$)MA incubated at different pH over 72 h at room temperature. c) (left) scheme of experimental setup for on-line absorbance measurements of OVA-Alexa488 release kinetics from hydrogel composed of P(EG$_{168}$-*co*-*iso*EPB$_{13}$)MA in cuvette at different pH values; (right) on-line absorbance measurements of OVA-Alexa488 release kinetics from hydrogels prepared from copolymers with different molecular weight and different EPB content (pH 4 and pH 5).

2.1.3.4 HYDROGEL SYNTHESIS, DEGRADATION AND PROTEIN RELEASE

To obtain a hydrogel, 10 wt% P(EG-*co*-*iso*EPB)MA solutions were mixed with 2-hydroxy-4′-(2-hydroxyethoxy)-2-methylpropiophenone (photoinitiator in ethanolic solution (1:10)) and cross-linked for 15 min, using a 365 nm UV lamp and a 96 well plate at pH 7.4. Employing this composition results in transparent hydrogels with defined edges that hold the shape of the mold well. Furthermore, the hydrogel's good mechanical

stability allows for easy handling with tweezers. To help monitoring the hydrogel degradation during macroscopic degradation studies with the unaided eye, the gel was loaded with the dye labelled model protein OVA-Alexa488. This results in transparent yellowish gels (**Fig. 2b**). Hydrogel disks from copolymer P(EG_{168}-*co*-*iso*EPB_{13})MA were incubated in a phosphate-citrate buffer at pH 4, 5 or 6 or phosphate buffer at pH 7.4 as a control (compare **Figure 2b**). The plastic Petri dishes containing the buffer solution and hydrogel were incubated at room temperature. The control hydrogel at pH 7.4 remained unchanged for periods exceeding 5 days, whereas the hydrogel incubated at pH 4 disintegrated within 5 hours, the hydrogel at pH 5 within 18 hours and the hydrogel at pH 6 within 72 hours. These results demonstrate that 10 wt% hydrogels comprising the synthesized P(EG_{168}-*co*-*iso*EPB_{13})MA macromonomer degraded quickly under physiological conditions of pH 5-6, as found in the endolysosome or inflamed tissue while being storage stable in neutral solutions for several months (data not shown). Note that the proton diffusion occurs on much shorter time scales than the observed degradation and OVA-Alexa 488 release of the hydrogels. This proves that the polymer hydrolysis is location-independent and takes place in the entire gel simultaneously (see **Figure S38**). This shows that hydrogels can be perfused with small molecules for possible application as bioreactor when enzymatically active proteins are encapsulated in the hydrogel. Further, the protein release from a 10 wt% P(EG-*co*-*iso*EPB)MA hydrogel was investigated using absorbance measurements at 496 nm in a disposable PMMA cuvette. To ensure that the change in absorbance measured arose exclusively from the released protein and not from the protein encapsulated in the hydrogel, a cuvette with an incubation chamber for the hydrogel with spatial separation from the absorbance beam path was designed (see **Figure 2c**, left and **S34**). The acidified buffer solution was stirred constantly with a magnetic stir bar, while the absorbance was measured every 5 minutes until the absorbance signal remained constant. Incubation of the hydrogel in more acidic buffer solution resulted in faster degradation (see **Figure 2c**), whereas incubation at

neutral pH did not lead to significant release over the same period of time. We normalized the absorbance values of hydrogels prepared from different macromonomers and degraded at different pH, since the absorbance of OVA-Alexa488 differs with pH. Three trends can be observed: (i) The lower the pH, the faster hydrogel degradation and consequently protein release take place. (ii) In addition, with increasing content of degradable vinyl ether units in the macromonomers, the degradation rate increases. (iii) The highest degradation rate was observed for the hydrogel composed of the largest macromonomer with high EPB molar content. On the other hand, the lowest degradation rates are observed for the smallest macromonomer with low EPB content under otherwise similar conditions.

These findings can be rationalized by considering network density, which determines protein diffusion. As shown in **Figure 2c**, the protein release rate from the networks increases once a few *iso*EPB units are cleaved. In case of slow release of OVA-Alexa488, the absence of an initial burst release is observed. When the protein-loaded hydrogels are incubated first at neutral pH (pH 7.4), the protein release reaches a plateau once the surface-adsorbed protein is released (see **Figure S28** + **S35**). Subsequent transfer of the hydrogel into a slightly more acidic solution (pH 6) results in continued protein release. Similar behaviour is visible for the network obtained from the smallest copolymer P(EG_{112}-*co*-*iso*EPB_5) incubated at pH 5, where the densely cross-linked hydrogel in the beginning only allows surface-adsorbed OVA-Alexa488 to be washed out.

After a certain time, a critical amount of *iso*EPB units is cleaved to open up larger pores for OVA-Alexa488 to diffuse out of the hydrogel. This trend can be observed both at pH 4 and at pH 5. The half-life hydrolysis time at pH 4 ranges from 2.3 to 4.5 hours and at pH 5 from 13 to 51 hours, depending on the copolymer employed (see **Table 1**). The P(EG_{168}-*co*-*iso*EPB_{13})MA macromonomer ($t_{1/2}$ (pH 5) = 13 h) is superior to previously published PEG-acetal macromonomers that required much longer time for

degradation at physiological relevant pH values ($t_{1/2}$ (pH 5) = 48 h)[30]. Likewise, it outperforms ketal-PEG macromonomers that degrade very quickly at acidic pH, but are not stable in neutral solutions, impeding storage for prolonged periods.[31]

The degradation behaviour of a hydrogel consisting of the copolymer P(EG_{168}-*co*-*iso*EPB_{13}) is investigated by straightforward incubation at different pH values as well as by on-line absorbance release kinetics of entrapped OVA-Alexa488 (**Figure 2b** and **2c**). Timescales of the hydrogel degradation behaviour obtained by the two different methods are in good correlation, confirming these results.

In general, significant protein release (OVA-Alexa488, 45 kDa) from a non-degradable hydrogel of 10 wt% PEG with molecular weights of approximately 6000 Da does not occur.[32] This together with the fact that we cannot see a significant protein release of the hydrogel based on the largest macromonomer at pH 7.4 (compare **Figure S27**), but a remarkable release at pH 4, 5 and 6 evidences that the protein release from the hydrogels depends solely upon acid stimuli and is not due to diffusion.

2.1.4 CONCLUSIONS

In summary, we have developed a novel acid-degradable PEG hydrogel for pH-controlled degradation and protein release. Anionic ring-opening copolymerization of ethylene oxide and 3,4-epoxy-1-butene (EPB) allows for the precise adjustment of molecular weights and determines the amount of degradable units within the polyether chains in the network. The reaction yields well-defined P(EG-*co*-EPB) copolymers with molecular weights from 5000 to 10000 g mol^{-1} (dispersities $Đ$ below 1.05) and high or low EPB content. Mild enzymatic conditions have been employed to obtain cross-linkable and degradable P(EG-*co*-*iso*EPB) methacrylate macromonomers. The highly water-soluble macromonomers readily degrade at physiologically relevant pH (pH 5-6) present in endolysosomes, inflammatory and cancerous tissue while being stable for

several weeks in solution at neutral pH (pH 7.4). Hydrogels prepared from the novel macromonomers degrade macroscopically within 5 hours (pH 4), 18 hours (pH 5) or 72 hours (pH 6). The release of an encapsulated protein OVA-Alexa488 was monitored using a custom-designed release setup for on-line absorbance measurements and lasted between 13 hours for the hydrogel from the largest macromonomer with high EPB content to 51 hours for the hydrogel from the smallest macromonomer with low EPB content at pH 5. As expected, the hydrogels release the protein faster in more acidic buffer (pH 4, 2.3–4.5 hours) compared to less acidic conditions (pH 5, 13 - 51 hours). In neutral pH, no significant protein release can be detected.

The presented synthetic strategy paves the way for a new type of PEG hydrogel that combines the outstanding properties of PEG as a hydrogel constituent (e.g. biocompatibility, water-solubility and low immunogenicity) with degradation at physiologically relevant pH. To the best of our knowledge, long-term storage stability at pH 7.4 in combination with degradation at pH 6 reflects a uniquely precise pH sensitivity. In that respect, the concept also offers great potential for degradable PEG hydrogel nanocarriers.[30]

2.1.5 ACKNOWLEDGEMENTS

J. B. acknowledges a fellowship through the Excellence Initiative (DFG/ GSC 266) in the context of the graduate school MAINZ “Materials Science in Mainz”. J.E. is grateful for an associate fellowship at the Mainz Research School of Translational Biomedicine (TransMed). The authors gratefully acknowledge the support of this research by Dr. Elena Berger-Nicoletti and Monika Schmelzer who provided valuable polymer characterization.

2.1.6 EXPERIMENTAL SECTION

Polymerization of P(EG-*co*-EPB): The procedure is exemplarily described for the synthesis of copolymer P(EG_{168}-*co*-EPB_{13}). It was carried out similarly for all P(EG-*co*-EPB) copolymers presented in this paper. Sodium hydride (7 mg, 0.31 mmol) was transferred into a dry Schlenk flask and a solution of triethylene glycol (117 mg, 0.778 mmol) in benzene (6 mL) was added. The solution was stirred under slightly reduced pressure at 60 °C for 30 min keeping the stopcock closed. Moisture was removed by azeotropic distillation of benzene and subsequent drying at 60 °C in high vacuum for 16 h. After cooling to RT, dry THF (4 mL) was cryo-transferred into the Schlenk flask to dissolve the initiator. EPB (1.44 mL, 17.9 mmol, stirred over CaH_2 for 30 min and freshly distilled prior to use) and dry DMSO (7 mL) were injected into the Schlenk flask via syringe at −80 °C. Ethylene oxide (5 mL, 0.11 mol) was cryo-transferred via a graduated ampule, and the polymerization was proceeded at RT for 7 days and was subsequently quenched with methanol (2 mL). After dialysis against methanol for 24 h (MWCO 1000 Da), the polymer was dried in vacuo. (Yield: 80 %) ^{1}H NMR (400 MHz, DMSO-d6): δ [ppm] 5.72 (ddd, 15.6H, $^3J_{AB}$ = 17.2 Hz, $^3J_{AB}$ = 10.5 Hz, $^3J_{AB}$ = 6.7 Hz, -C*H*=CH_2), 5.26 (m, 32.4H, $^3J_{AB}$ = 17.2 Hz, $^3J_{AB}$ = 2.1 Hz, $^3J_{AB}$ = 1.1 Hz, -CH=H*H*), 4.76 (q, 0.92H, *J* = 6.7 Hz, C=C*H*-CH_3 (*E* isomer)), 4.57 (bs, 2H, O*H*), 3.96–3.87 (m, 19.48H, C*H*O-CH=CH_2, OCH_2-C=CH-CH_3 and CH_2O-C=CH-CH_3), 3.71–3.35 (m, 732H, CH_2O), 1.52 (d, 3.05H, *J* = 6.7 Hz, C=CH-CH_3 (*E* isomer)).

Isomerization of P(EG-*co*-EPB) to P(EG-*co-iso*EPB): The procedure is exemplarily described for the synthesis of copolymer P(EG_{168}-*co-iso*EPB_{13}). The procedure was used accordingly for all P(EG-*co-iso*EPB) copolymers presented in this paper. In a Schlenk tube, P(EG_{168}-*co*-EPB_{13}) (800 mg, 0.10 mmol) was dissolved in DMSO and subjected to two freeze-pump-thaw cycles. Under argon atmosphere, $RhCl(PPh_3)_3$ (25 mg, 0.0275 mmol) was added and the solution was thoroughly degassed via two additional

freeze-pump-thaw cycles. The light orange solution was stirred at 80 °C for one day and was twice precipitated in acetone/diethyl ether (1:1). The purified copolymer was obtained after drying in vacuum. (Yield: 94 %) Isomerized copolymers were routinely stored in a refrigerator at 4 °C. ^{1}H NMR (400 MHz, DMSO-d6): δ [ppm] 4.77 (q, 7.46H, *J* = 6.7 Hz, C=C*H*-CH$_3$ (*E* isomer)), 4.65 (q, 5.28H, *J* = 6.7 Hz, C=C*H*-CH$_3$ (*E* isomer)), 4.57 (bs, 1.48H, O*H*), 3.99–3.88 (m, 42.02H, OC*H*$_2$-C=CH-CH$_3$ and C*H*$_2$O-C=CH-CH$_3$), 3.71–3.35 (m, 655H, C*H*$_2$O), 1.61 (d, 16.7H, *J* = 6.7 Hz, C=CH-C*H*$_3$ (Z isomer)), 1.52 (d, 23H, *J* = 6.7 Hz, C=CH-C*H*$_3$ (*E* isomer)).

Methacrylation of P(EG-*co*-*iso*EPB) to P(EG-*co*-*iso*EPB)MA: The procedure is exemplarily described for the synthesis of copolymer P(EG$_{168}$-*co*-*iso*EPB$_{13}$)MA. The procedure was used accordingly for all P(EG-*co*-*iso*EPB)MA copolymers presented in this paper. In a Schlenk tube, P(EG$_{168}$-*co*-*iso*EPB$_{13}$) (400 mg, 0.05 mmol) was dissolved in toluene and CALB (30 mg) and vinyl methacrylate (60 µL, 0.50 mmol) were added. After stirring for 24 hours at 40 °C, the mixture was filtered, concentrated in vacuum and precipitated twice in diethyl ether. BHT was added as a stabilizer to prevent unwanted crosslinking and the polymer was dried in vacuum. (Yield 85%) ^{1}H NMR (400 MHz, DMSO-d6): δ [ppm] 6.04 (s, 1.89H, *H*$_2$C=CCH$_3$-C=O), 5.70 (s, 1.83H, *H*$_2$C=CCH$_3$-C=O)4.77 (q, 7.26H, *J* = 6.7 Hz, C=C*H*-CH$_3$ (*E* isomer)), 4.65 (q, 5.09H, *J* = 6.7 Hz, C=C*H*-CH$_3$ (*E* isomer)), 3.99–3.88 (m, 40.75H, OC*H*$_2$-C=CH-CH$_3$ and C*H*$_2$O-C=CH-CH$_3$), 3.71–3.35 (m, 655H, C*H*$_2$O), 1.88 (s, 5.99H, H$_2$C=CC*H*$_3$-C=O) 1.61 (d, 16.7H, *J* = 6.7 Hz, C=CH-C*H*$_3$ (*Z* isomer)), 1.52 (d, 23H, *J* = 6.7 Hz, C=CH-C*H*$_3$ (*E* isomer)). ^{13}C NMR (100.6 MHz, DMSO-d6): δ [ppm] 152.40 (1C, OCH$_2$-*C*=CH-CH$_3$ (*Z*-Isomer)) 150.62 (1C, OCH$_2$-C=C*H*-CH$_3$ (*E* isomer)), 135.81 (1C, CO-*C*=CH$_2$CH$_3$), 125.81 (1C, CO-C=*C*H$_2$CH$_3$), 106.35 (1C, C=*C*H-CH$_3$ (*E* isomer)), 96.13 (1C, C=*C*H-CH$_3$ (*Z* isomer)), 73.21-67.29 (48C, *C*H2O), 63.77 (1C, *C*O-C=CH$_2$CH$_3$), 17.97 (CO-C=CH$_2$*C*H$_3$), 11.34 (1C, C=C-CH$_3$ (*Z* isomer)) 9.95 (1C, C=CH-*C*H$_3$ (*E* isomer)).

2.1.7 REFERENCES

[1] J. Herzberger, K. Niederer, H. Pohlit, J. Seiwert, M. Worm, F. R. Wurm, H. Frey, *Chem Rev* **2016**, *116*, 2170-2243.

[2] K. Knop, R. Hoogenboom, D. Fischer, U. S. Schubert, *Angew Chem Int Ed Engl* **2010**, *49*, 6288-6308.

[3] a) C. C. Lin, K. S. Anseth, *Pharm Res* **2009**, *26*, 631-643; b) T. Vermonden, R. Censi, W. E. Hennink, *Chem Rev* **2012**, *112*, 2853-2888.

[4] C. R. Nuttelman, M. A. Rice, A. E. Rydholm, C. N. Salinas, D. N. Shah, K. S. Anseth, *Prog Polym Sci* **2008**, *33*, 167-179.

[5] B. V. Slaughter, S. S. Khurshid, O. Z. Fisher, A. Khademhosseini, N. A. Peppas, *Adv Mater* **2009**, *21*, 3307-3329.

[6] B. D. Polizzotti, B. D. Fairbanks, K. S. Anseth, *Biomacromolecules* **2008**, *9*, 1084-1087.

[7] J. Zhu, *Biomaterials* **2010**, *31*, 4639-4656.

[8] a) E. G. Gacasan, R. M. Sehnert, D. A. Ehrhardt, M. A. Grunlan, *Macromolecular Materials and Engineering* **2017**, *302*; b) A. Sannino, P. A. Netti, M. Madaghiele, V. Coccoli, A. Luciani, A. Maffezzoli, L. Nicolais, *J Biomed Mater Res A* **2006**, *79*, 229-236.

[9] M. B. Browning, S. N. Cereceres, P. T. Luong, E. M. Cosgriff-Hernandez, *J Biomed Mater Res A* **2014**, *102*, 4244-4251.

[10] a) P. Caliceti, *Advanced Drug Delivery Reviews* **2003**, *55*, 1261-1277; b) E. Markovsky, H. Baabur-Cohen, A. Eldar-Boock, L. Omer, G. Tiram, S. Ferber, P. Ofek, D. Polyak, A. Scomparin, R. Satchi-Fainaro, *J Control Release* **2012**, *161*, 446-460.

[11] a) X. Yu, Q. Pan, Z. Zheng, Y. Chen, Y. Chen, S. Weng, L. Huang, *RSC Advances* **2018**, *8*, 37424-37432; b) A. Bertz, S. Wohl-Bruhn, S. Miethe, B. Tiersch, J. Koetz, M. Hust, H. Bunjes, H. Menzel, *J Biotechnol* **2013**, *163*, 243-249; c) G. M. Cruise, D. S. Scharp, J. A. Hubbell, *Biomaterials* **1998**, *19*, 1287-1294.

[12] a) S. J. Buwalda, T. Vermonden, W. E. Hennink, *Biomacromolecules* **2017**, *18*, 316-330; b) S. Deshayes, A. M. Kasko, *Journal of Polymer Science Part A: Polymer Chemistry* **2013**, *51*, 3531-3566.

[13] a) N. Demaurex, *Physiology* **2002**, *17*, 1-5; b) H. Sun, T. L. Andresen, R. V. Benjaminsen, K. Almdal, *Journal of Biomedical Nanotechnology* **2009**, *5*, 676-682; c) A. Asokan, M. J. Cho, *Journal of Pharmaceutical Sciences* **2002**, *91*, 903-913.

[14] S. Guragain, B. P. Bastakoti, V. Malgras, K. Nakashima, Y. Yamauchi, *Chemistry* **2015**, *21*, 13164-13174.

[15] a) P. Vaupel, F. Kallinowski, P. Okunieff, *Cancer Research* **1989**, *49*, 6449-6465; b) N. R. Patel, B. S. Pattni, A. H. Abouzeid, V. P. Torchilin, *Adv Drug Deliv Rev* **2013**, *65*, 1748-1762; c) E. S. Lee, Z. Gao, Y. H. Bae, *J Control Release* **2008**, *132*, 164-170.

[16] a) X. Sun, H. Qiu, Y. Jin, *Int J Pharm* **2017**, *525*, 175-182; b) E. L. Larkin, L. Long, N. Isham, K. Borroto-Esoda, S. Barat, D. Angulo, S. Wring, M. Ghannoum, *Antimicrob Agents Chemother* **2019**, *63*.

[17] P. Gupta, K. Vermani, S. Garg, *Drug Discovery Today* **2002**, *7*, 569-579.

[18] a) R. Tomlinson, J. Heller, S. Brocchini, R. Duncan, *Bioconjugate Chemistry* **2003**, *14*, 1096-1106; b) E. R. Gillies, J. M. J. Fréchet, *Bioconjugate Chemistry* **2005**, *16*, 361-368.

[19] a) S. Kim, O. Linker, K. Garth, K. R. Carter, *Polymer Degradation and Stability* **2015**, *121*, 303-310; b) L. E. Ruff, E. A. Mahmoud, J. Sankaranarayanan, J. M. Morachis, C. D. Katayama, M. Corr, S. M. Hedrick, A. Almutairi, *Integr Biol (Camb)* **2013**, *5*, 195-203.

[20] a) Y. Bae, S. Fukushima, A. Harada, K. Kataoka, *Angew Chem Int Ed Engl* **2003**, *42*, 4640-4643; b) D. Chen, W. Liu, Y. Shen, H. Mu, Y. Zhang, R. Liang, A. Wang, K. Sun, F. Fu, *Int J Nanomedicine* **2011**, *6*, 2053-2061.

[21] a) J. Liu, Y. Huang, A. Kumar, A. Tan, S. Jin, A. Mozhi, X. J. Liang, *Biotechnol Adv* **2014**, *32*, 693-710; b) F.-Q. Hu, Y.-Y. Zhang, J. You, H. Yuan, Y.-Z. Du, *Molecular Pharmaceutics* **2012**, *9*, 2469-2478.

[22] S. Su, F.-S. Du, Z.-C. Li, *Macromolecules* **2018**, *51*, 6571-6579.

[23] E. Fleige, K. Achazi, K. Schaletzki, T. Triemer, R. Haag, *J Control Release* **2014**, *185*, 99-108.

[24] M. R. Molla, T. Marcinko, P. Prasad, D. Deming, S. C. Garman, S. Thayumanavan, *Biomacromolecules* **2014**, *15*, 4046-4053.

[25] a) C. Wang, Q. Ge, D. Ting, D. Nguyen, H. R. Shen, J. Chen, H. N. Eisen, J. Heller, R. Langer, D. Putnam, *Nat Mater* **2004**, *3*, 190-196; b) J. Heller, A. C. Chang, G. Rood, G. M. Grodsky, *Journal of Controlled Release* **1990**, *13*, 295-302; c) D. Koylu, K. R. Carter, *Macromolecules* **2009**, *42*, 8655-8660; d) J. K. Varghese, N. Hadjichristidis, Y. Gnanou, X. Feng, *Polymer Chemistry* **2019**.

[26] a) D. Liu, C. W. Bielawski, *Macromol Rapid Commun* **2016**, *37*, 1587-1592; b) P. Lundberg, B. F. Lee, S. A. van den Berg, E. D. Pressly, A. Lee, C. J. Hawker, N. A. Lynd, *ACS Macro Lett* **2012**, *1*, 1240-1243.

[27] M. Worm, D. Leibig, C. Dingels, H. Frey, *Acs Macro Letters* **2016**, *5*, 1357-1363.

[28] a) M. R. Aguilar, A. Gallardo, M. d. M. Fernández, J. S. Román, *Macromolecules* **2002**, *35*, 2036-2041; b) A. Natalello, M. Werre, A. Alkan, H. Frey, *Macromolecules* **2013**, *46*, 8467-8471; c) J. Herzberger, K. Fischer, D. Leibig, M. Bros, R. Thiermann, H. Frey, *Journal of the American Chemical Society* **2016**, *138*, 9212-9223.

[29] J. Blankenburg, E. Kersten, K. Maciol, M. Wagner, S. Zarbakhsh, H. Frey, *Polymer Chemistry* **2019**, *10*, 2863-2871.

[30] H. Pohlit, I. Bellinghausen, M. Schömer, B. Heydenreich, J. Saloga, H. Frey, *Biomacromolecules* **2015**, *16*, 3103-3111.

[31] H. Pohlit, D. Leibig, H. Frey, *Macromolecular Bioscience* **2017**, *17*.

[32] a) E. Merrill, K. Dennison, C. Sung, *Biomaterials* **1993**, *14*, 1117-1126; b) L. M. Weber, C. G. Lopez, K. S. Anseth, *J Biomed Mater Res A* **2009**, *90*, 720-729.

2.1.8 SUPPORTING INFORMATION

Materials and methods

Chemicals:

Sodium hydride (NaH), Triethylene glycol (TEG), Benzophenone, *trans*-2-[3-(4-*tert*-Butylphenyl)-2-methyl-2-propenylidene]malononitrile (DCTB), Calcium hydride (CaH_2), Potassium triflate, toluene, dichloromethane, benzene, tetrahydrofuran (THF), lipase B from Candida antarctica immobilized on Immobead 150 (CALB), diethyl ether, 2-hydroxy-4′-(2-hydroxyethoxy)-2-methylpropiophenone, citric acid, and disodium hydrogen phosphate were purchased from Sigma Aldrich. Ethylene oxide (EO) was purchased from Air Liquide. THF used for anionic ring-opening polymerization (AROP) was dried with sodium prior to use and stored over sodium/benzophenone. LiBr, and dimethyl sulfoxide (DMSO) were purchased from Acros. Sodium bicarbonate, calcium chloride, ethanol, isopropanol, OVA-Alexa488 and sterile water were purchased from Fisher Scientific. Vinyl methacrylate was purchased from Tokyo Chemical Industry (TCI). Phosphate buffered saline (PBS) buffer was obtained from gibco life technologies. Epoxy butadiene (EPB) was purchased from Alfa Aesar. Spectra/PORTM dialysis membranes regenerated cellulose (RC) tubing molecular weight cut-off (MWCO) 1000 Da were purchased from Spectrum labs. DMSO-d6 was purchased from Deutero GmbH and sodium dihydrogenphosphate and disodium hydrogenphosphate from Merck. All chemicals were used as received without further purification unless stated otherwise. 96 well plates for hydrogel synthesis and disposable petri dishes with lid were purchased from Greiner, Frickenhausen, Germany.

Analytical instrumentation: ^{1}H NMR spectra were measured using a Bruker AMX400 spectrometer (256 Scans, and B-ACS 60 auto sampler) at 296 K. ^{1}H NMR kinetic spectra were recorded at 400 MHz on a Bruker Advance III HD 400 (5 mm broad band fluorine observation (BBFO)-SmartProbe with z-gradient and Automated tuning

and matching (ATM)). 2D NMR and ^{13}C NMR spectra were measured on a Bruker Avance II 400 (100.5 MHz, 5 mm BBO probe, and B-ACS 60 auto sampler) at 296 K. All spectra were processed with MestReNova v10.0.1 software and referenced internally to residual proton signals of the deuterated solvent. Calculations of reactivity rations were performed in OriginPro 2016GGPC.

Size exclusion chromatography (SEC) data were obtained using Agilent 1100 Series equipped with PSS HEMA-columns (106/104/102 Å porosity) using DMF with 1 g/L LiBr as an eluent and RI detection. Polydispersity indices (Đ = Mw/Mn) were determined with monodisperse linear PEG standards from Polymer Standard Service GmbH (PSS). The molecular weight of the copolymers was obtained from ^{1}H NMR via end group analysis. MALDI-ToF analysis was performed using an rapifleXTM MALDI-TOF/TOF equipped with a 10 kHz scanning Smartbeam 3D Laser (Nd:YAG at 355 nm) and 10 bit 5 GHZ Digitizer. Analysis was performed in reflectormode positive. DCTB was used as matrix and dichloromethane as solvent for all samples.

^{1}H NMR Kinetics: NaH (1 mg, 0.06 mmol) and and *N,N*-Dibenzylethanolamine (9 mg, 0.04 mmol) were placed in a flame-dried Schlenk tube and 5 mL benzene was added. This mixture was stirred at 60 °C for 30 min and subsequently dried under vacuum overnight. The initiator was dissolved in 364 µL DMSO-d6, transferred under argon atmosphere to a flame-dried Norell S-500- S4 VT-7 NMR tube and EPB (26 µL, 0.3 mmol, stirred over CaH_2 for 30 min and freshly distilled prior to use) was added via a syringe. After cooling in an acetone/liquid nitrogen bath, 150 µL THF was cryotransferred via a graduated ampule, followed by EO (130 µL, 2.86 mmol). The tube was sealed with a Teflon stop-cork and shaken vigorously after warming up to room temperature to ensure homogenization of the solution. In total 9 spectra were recorded over 97 h. The copolymer P(EG-*co*-EPB) isolated from the NMR tube had an average number molecular weight of Mn = 3960 g/mol and a PDI of 1.17 (Figure S37).

SEC Hydrolysis Studies

Aliquots (15 mg) of the P(EG-*co*-*iso*EPB)MA copolymers were dissolved in 100 µL DCM, subsequently one drop of 10 vol% HCl in MeOH was added and the mixture was incubated over night at room temperature (25 °C). After 16 h, $NaHCO_3$ was added until the pH was above 3 and this solution was analysed by measuring size exclusion chromatography (DMF, PEG standards, RI detector).

Hydrogel synthesis

The hydrogel synthesis was performed as previously described.[1] Briefly, 10 wt% polymer solutions of P(EG-*co*-*iso*EPB)MA in PBS were prepared. The photoinitiator 2-hydroxy-4′-(2-hydroxyethoxy)-2-methylpropiophenone (2 µL per 100 µL polymer solution, prediluted 1:10 in ethanol) was added to the polymer solution and for protein encapsulation, 10 µL OVA-Alexa488 in PBS (10 mg/mL) was added to the solution and carefully mixed. 150 µL of this mixture were transferred into a 96-well plate and carefully overlayered with 150 µL isopropanol prior to UV polymerization at 365 nm for 15 min. Once cured, the hydrogels could be transferred into petri dishes or UV cuvettes with buffer solution. Two stock solutions for the phosphate-citrate buffer solution were prepared, stock A with 10×10^{-3} M citric acid monohydrate and stock B with 200×10^{-3} M Na_2HPO_4 in sterile water. Subsequently, the stock solutions were mixed and pH controlled with a pH electrode until desired pH was reached. The hydrogels were incubated tor at room temperature for several days.

Degradation cuvette

The cross-linked hydrogel was transferred into the hydrogel chamber in the top of a disposable PMMA cuvette (BrandTech Scientific, for experimental setup, compare Figure S34). Absorbance at 496 nm was measured at 25 °C every 5 minutes until absorbance signal remained constant.

Hydrogen ion diffusivity study

Hydrogels were prepared as descried above, except that 450 µL hydrogel precursor solution was pipetted into a 48-well plate. Subsequent to crosslinking, the hydrogel was incubated in 0.05 mg/mL of methyl red in PBS. To observe pH shifts within the hydrogel, the gel was placed in a citrate/phosphate buffer solution at pH 4. The expected colour change is from yellow at neutral pH to red at acidic pH (see Figure S38).

Biocompatibility

Cell biocompatibility was evaluated with the human osteoblast cell line MG-63 (ATCC® CRL-1427®, LGC Promochem) and human umbilical vein endothelial cells [HUVEC]. HUVEC were isolated from human umbilical cord obtained from the Department of Gynecology, University Medical Center of the Johannes Gutenberg University. The study was performed in agreement with the Declaration of Helsinki and approved by local ethics committee (Landesärztekammer Rheinland-Pfalz, Mainz, Germany). Informed consent was obtained from each patient. Cells were seeded at 50.000 MG-63 and 80.000 HUVEC cells per well in a sterile 24-well cell culture plate (Greiner bio-one Cellstar®) and cultivated for 24h in a humidified atmosphere (at 37°C and 5% CO_2) before exposure to various concentrations of P(EG-*co*-*iso*EPB). MG-63 cells were cultivated in DMEM (Dulbecco's Modified Eagle Medium, high glucose; Sigma-Aldrich) supplemented with 10% fetal bovine serum [FBS] (Sigma Aldrich), 2mM Glutamax I (Gibco® Thermo Fisher Scientific), and 100 U/ 100 µg/mL Penicillin/Streptomycin (Gibco Thermo Fisher Scientific). HUVEC cells were cultured in medium M199 (Sigma Aldrich) supplemented with 20% FBS (Sigma Aldrich), 2 mM Glutamax I (Gibco Thermo Fisher Scientific), 100 U/ 100 µg/mL Penicillin/Streptomycin (Gibco Thermo Fisher Scientific), 25 µg/mL endothelial growth factor supplement (ECGS; Becton Dickinson and Company), and 25 µg/mL heparin sodium salt (Sigma Aldrich). The cell culture plates for HUVEC culture were coated with gelatine (0.2%

Sigma Aldrich) prior to cell seeding. P(EG-*co*-*iso*EPB) was added in concentrations of 50 µg/mL, 100 µg/mL and 500 µg/mL and incubated for 24 h and 72 h as well as 7 days. Identical cells not exposed to P(EG-*co*-*iso*EPB) were used as control. The cell culture medium was replaced prior to examining cells by fluorescence microscopy. Viable cells were identified by their green fluorescence after staining with Calcein-AM (Calcein acetoxymethyl ester, ThermoFisher Scientific). The experiments with HUVEC were carried out with three different donors and passage 3 of each donor. Studies with MG-63 were performed as triple determinations with three different passages.

Analytical data

P(EG$_{112}$-*co*-EPB$_5$) –and derivatives

2D NMR analysis of P(EG-*co*-EPB) and P(EG-*co-iso*EPB) can be found in our previous publication.[2]

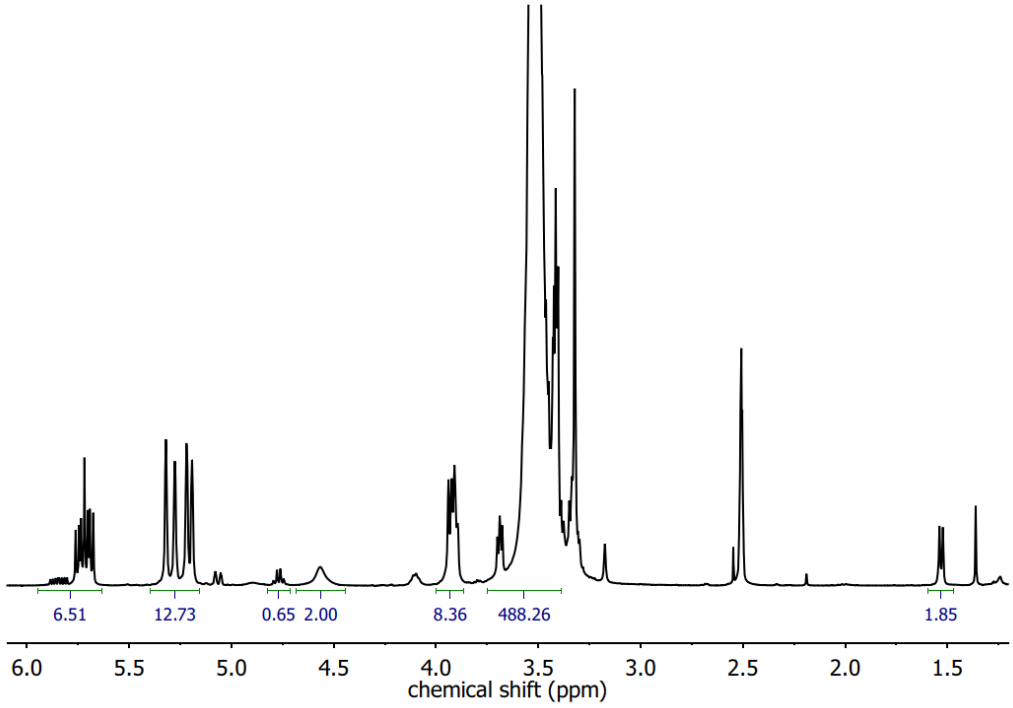

Figure S1: ^{1}H NMR spectrum (400 MHz, DMSO-d$_6$) of P(EG$_{112}$-*co*-EPB$_5$).

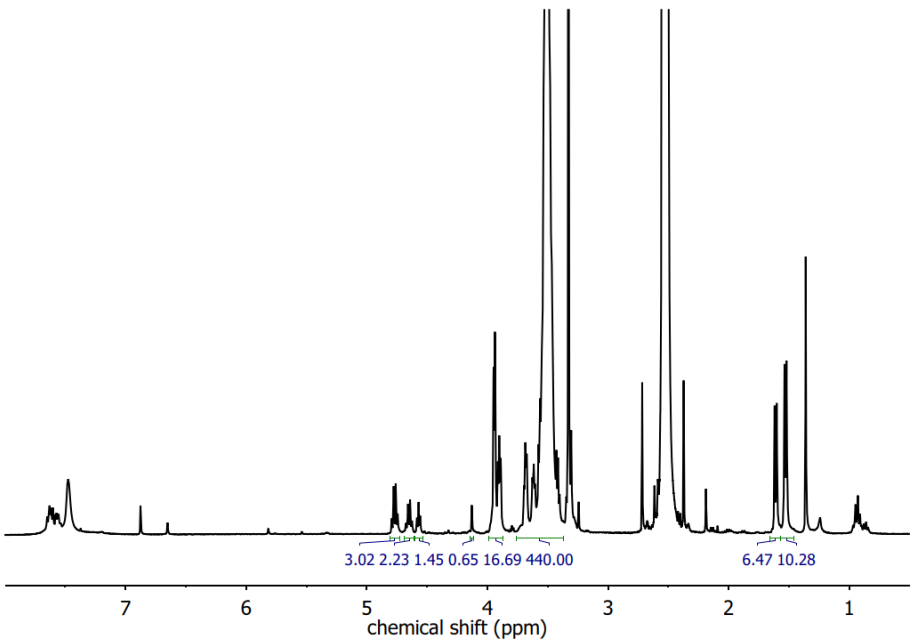

Figure S2: ^{1}H NMR spectrum (400 MHz, DMSO-d$_6$) of P(EG$_{112}$-*co-iso*EPB$_5$).

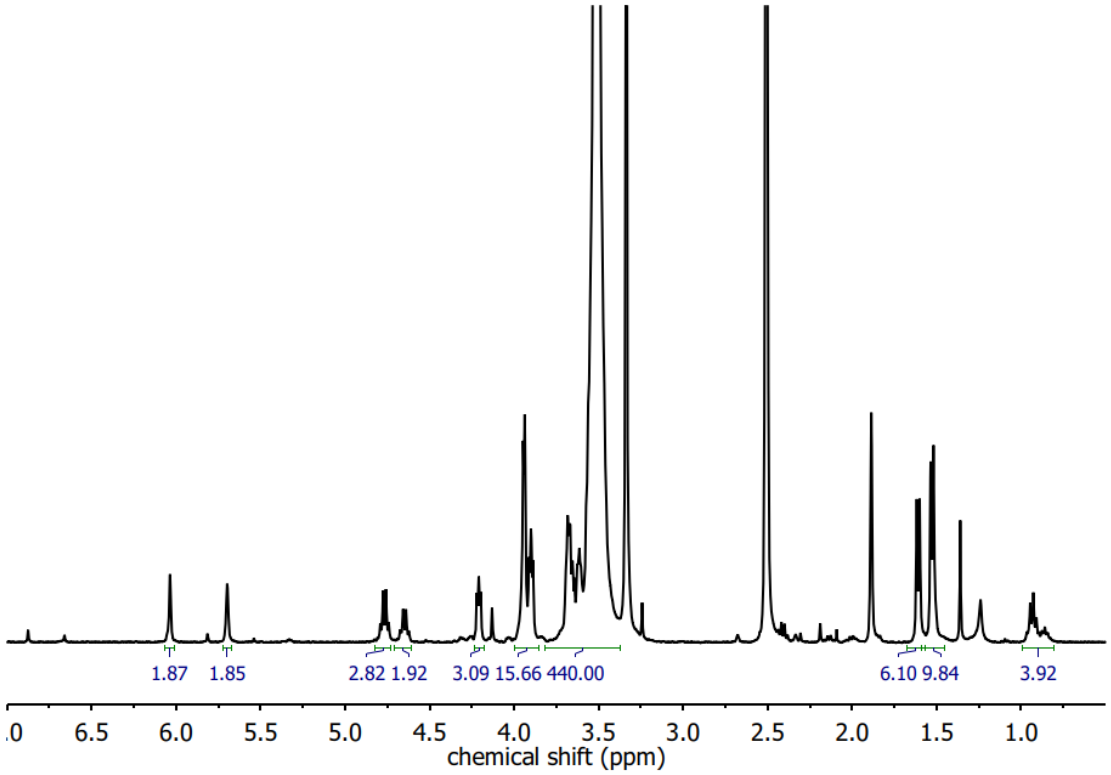

Figure S3: ^{1}H NMR spectrum (400 MHz, DMSO-d$_6$) of P(EG$_{112}$-*co*-*iso*EPB$_5$)MA.

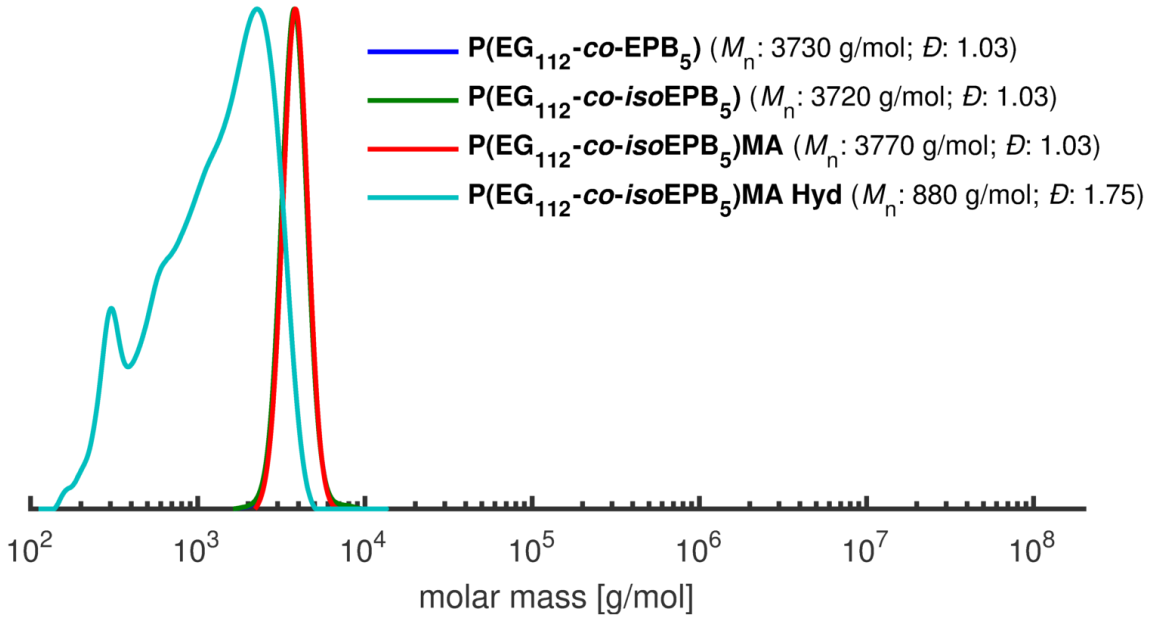

Figure S4 (color online): SEC traces (DMF, PEG standards, RI signal) of P(EG$_{112}$-*co*-EPB$_5$), P(EG$_{112}$-*co*-*iso*EPB$_5$) and P(EG$_{112}$-*co*-*iso*EPB$_5$)MA as well as degradation fragments after hydrolysis.

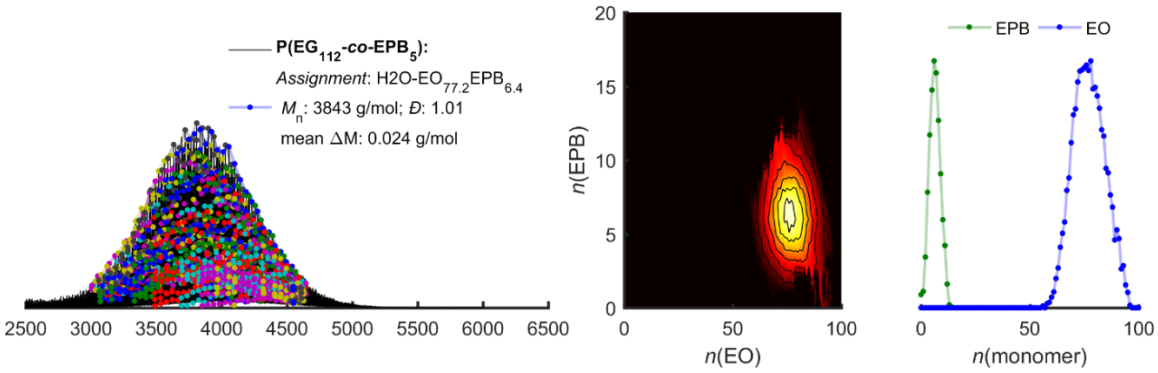

Figure S5 (color online): MALDI-ToF-MS of P(EG$_{112}$-*co*-EPB$_5$) with sodium as counter ion.

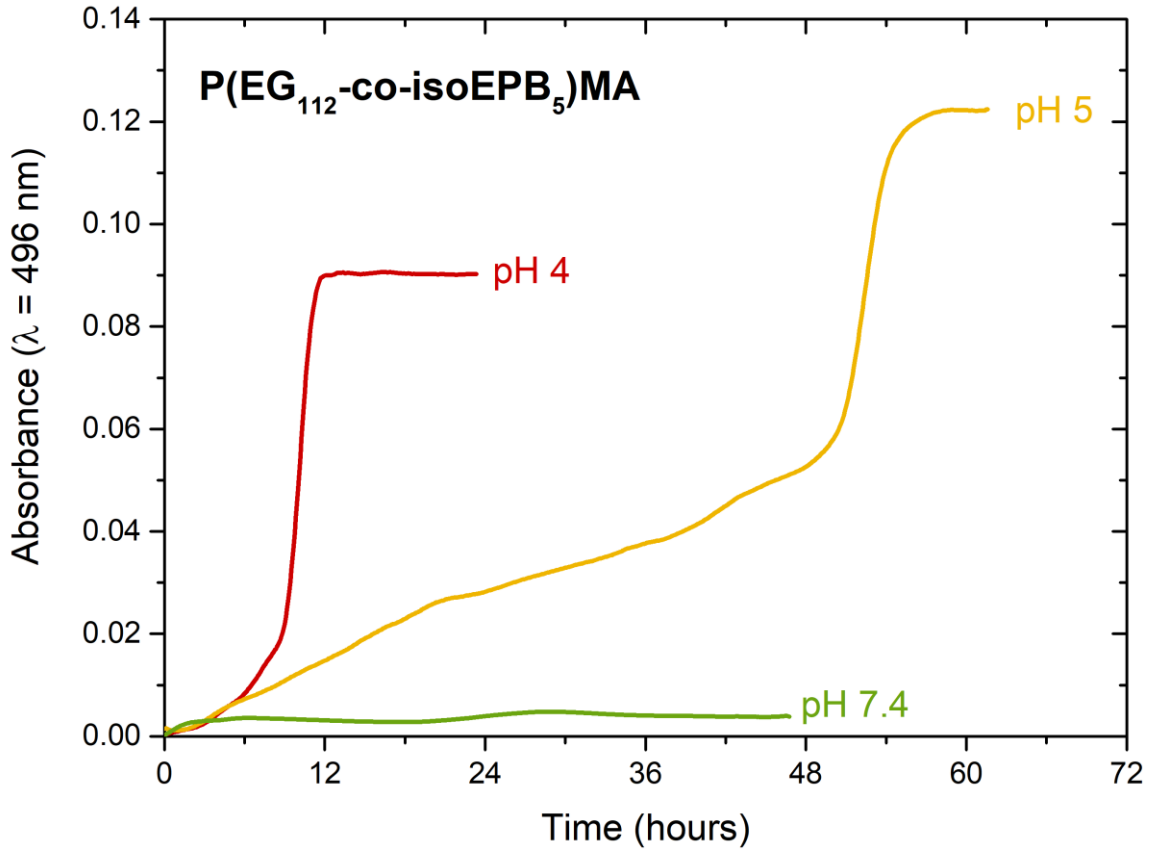

Figure S6: On-line absorbance measurement of OVA-Alexa488 release kinetics from hydrogels prepared from copolymer P(EG$_{112}$-*co*-*iso*EPB$_5$)MA at different pH values.

P(EG$_{202}$-*co*-EPB$_9$) and derivatives

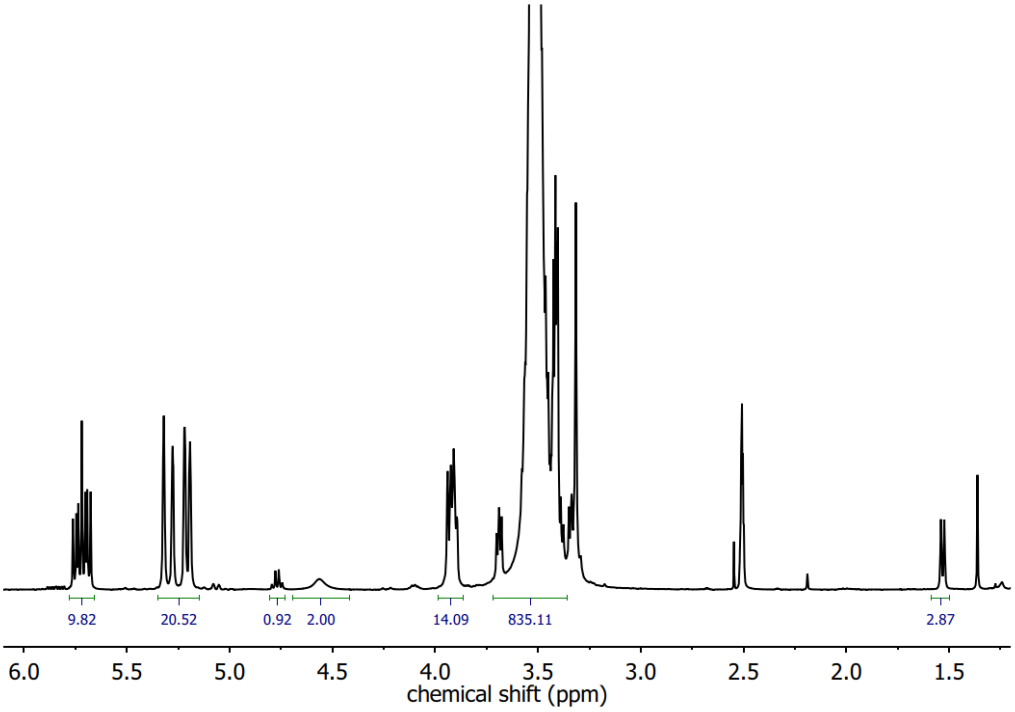

Figure S7: ^{1}H NMR spectrum (400 MHz, DMSO-d$_6$) of P(EG$_{202}$-*co*-EPB$_9$).

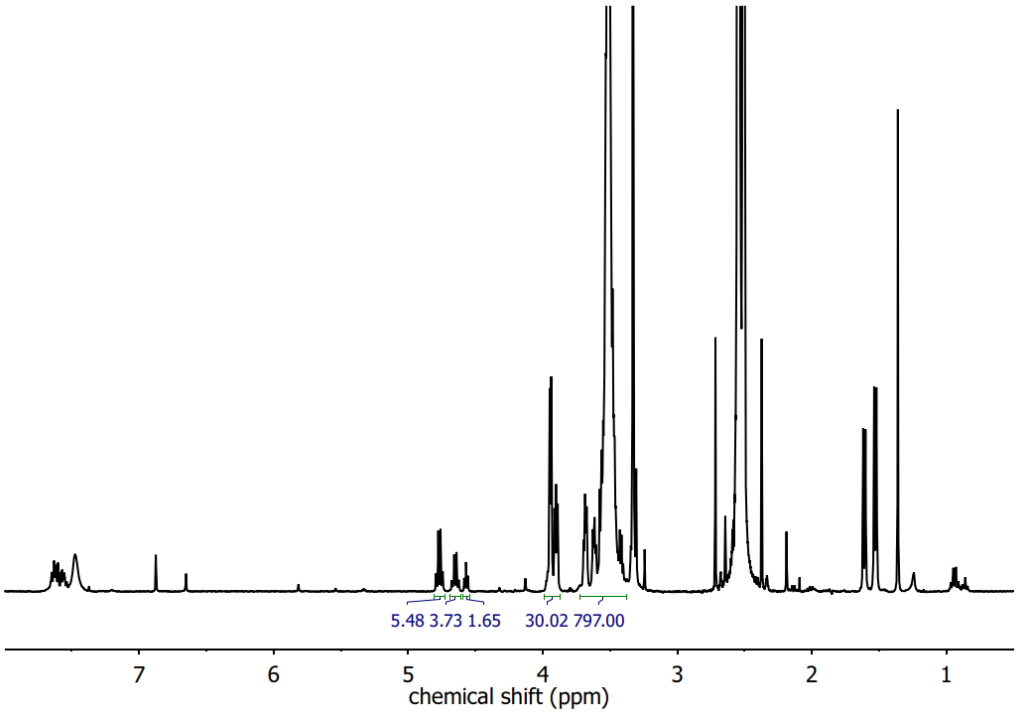

Figure S8: ^{1}H NMR spectrum (400 MHz, DMSO-d$_6$) of P(EG$_{202}$-*co*-*iso*EPB$_9$).

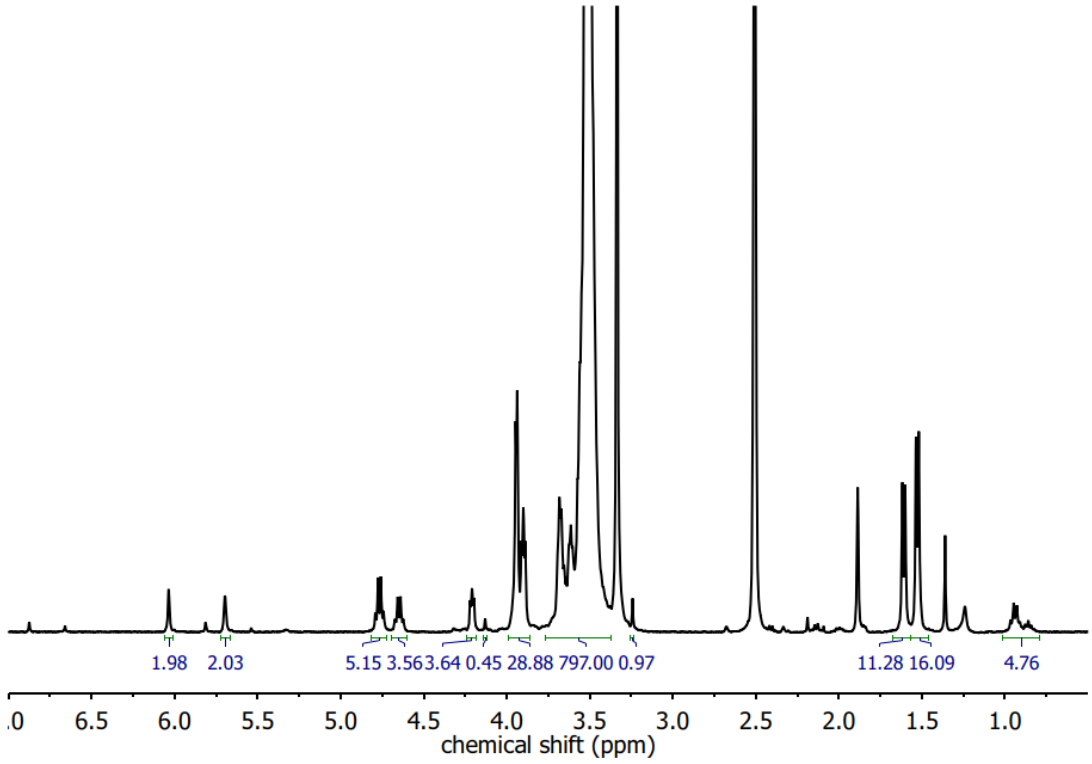

Figure S9: ^{1}H NMR spectrum (400 MHz, DMSO-d$_6$) of P(EG$_{202}$-*co*-isoEPB$_9$)MA.

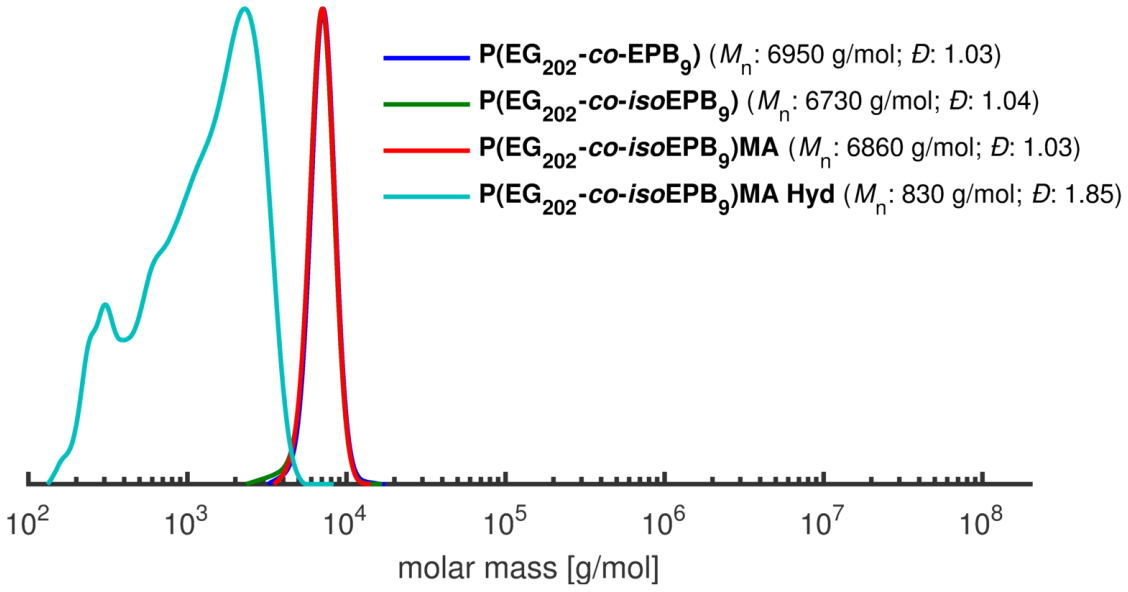

Figure S10 (color online): SEC traces (DMF, PEG standards, RI signal) of P(EG$_{202}$-*co*-EPB$_9$), P(EG$_{202}$-*co*-*iso*EPB$_9$) and P(EG$_{202}$-*co*-*iso*EPB$_9$)MA as well as degradation fragments after hydrolysis.

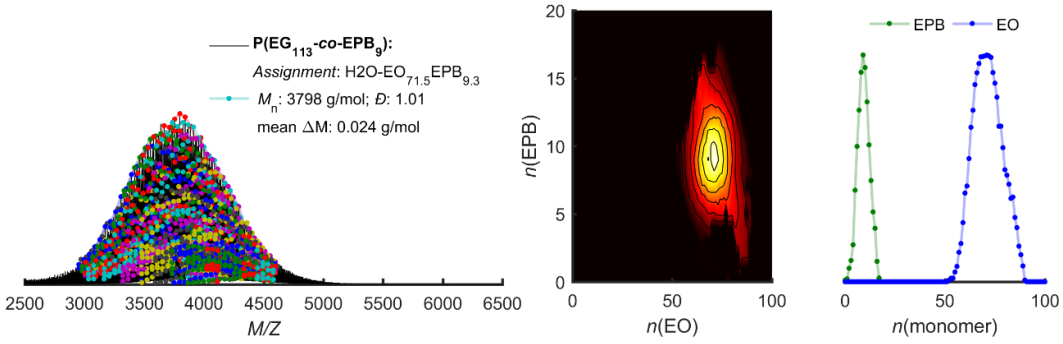

Figure S11 (color online): MALDI-ToF-MS of P(EG$_{202}$-*co*-EPB$_9$) with sodium as counter ion.

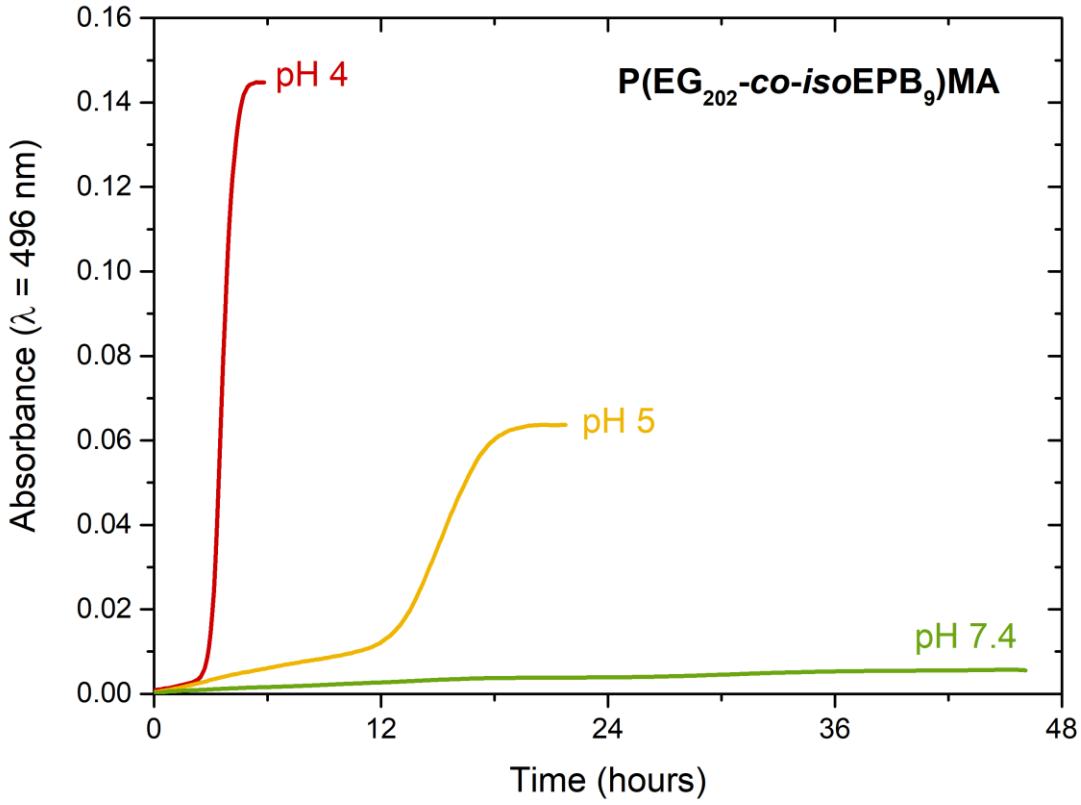

Figure S12: On-line absorbance measurement of OVA-Alexa488 release kinetics from hydrogels prepared from copolymer P(EG$_{202}$-*co*-*iso*EPB$_9$) at different pH values.

P(EG$_{105}$-*co*-EPB$_{11}$) and derivatives

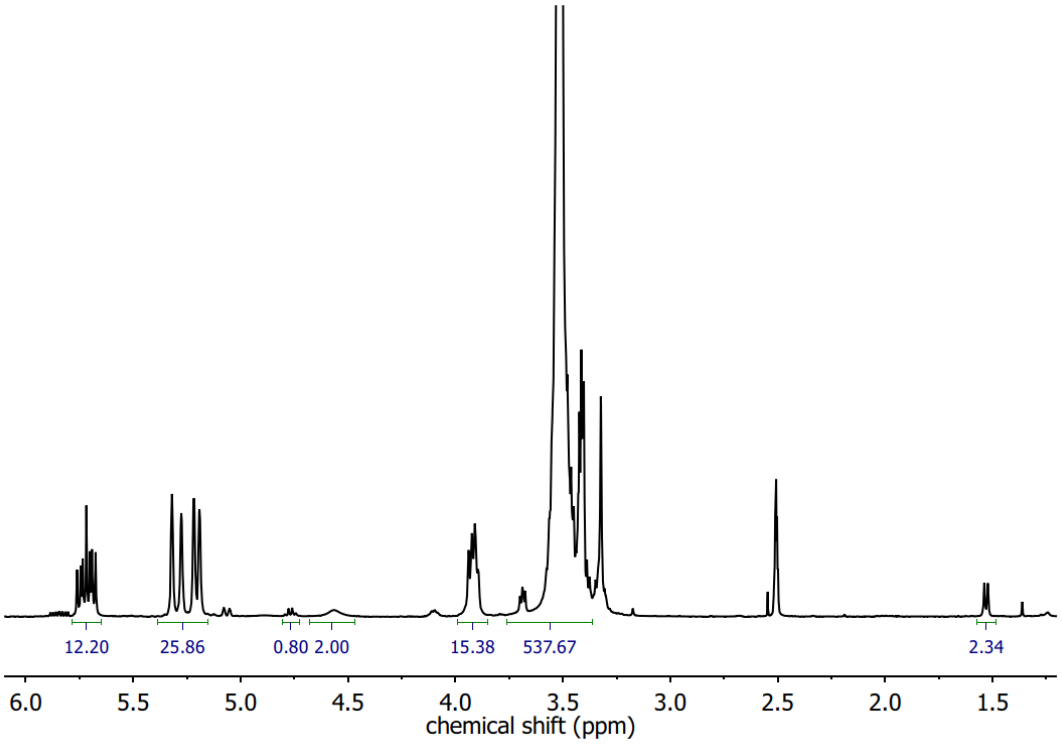

Figure S13: ^{1}H NMR spectrum (400 MHz, DMSO-d$_6$) of P(EG$_{113}$-*co*-EPB$_9$).

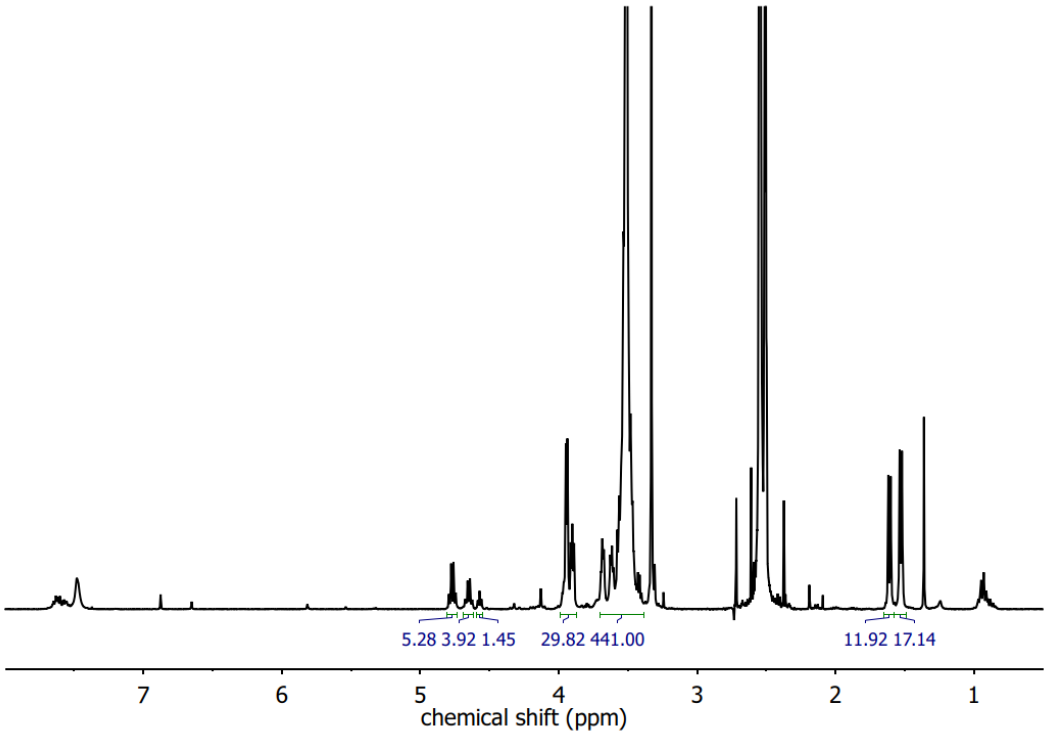

Figure S14: ^{1}H NMR spectrum (400 MHz, DMSO-d$_6$) of P(EG$_{113}$-*co*-isoEPB$_9$).

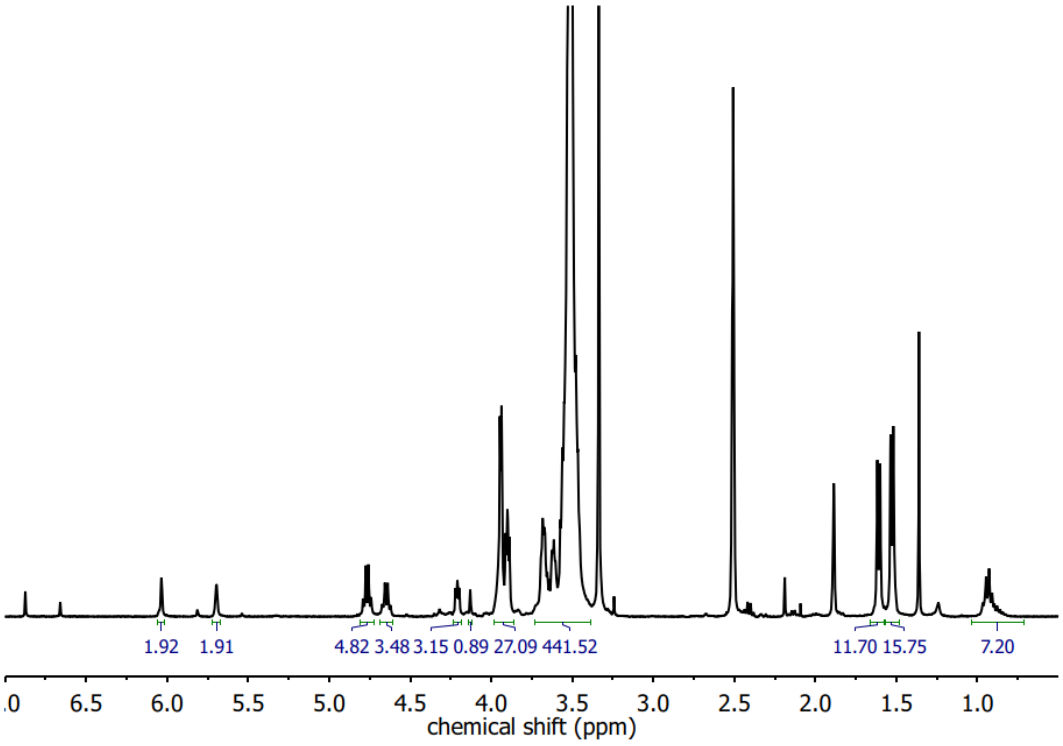

Figure S15: ^{1}H NMR spectrum (400 MHz, DMSO-d_6) of P(EG$_{113}$-*co*-*iso*EPB$_9$)MA.

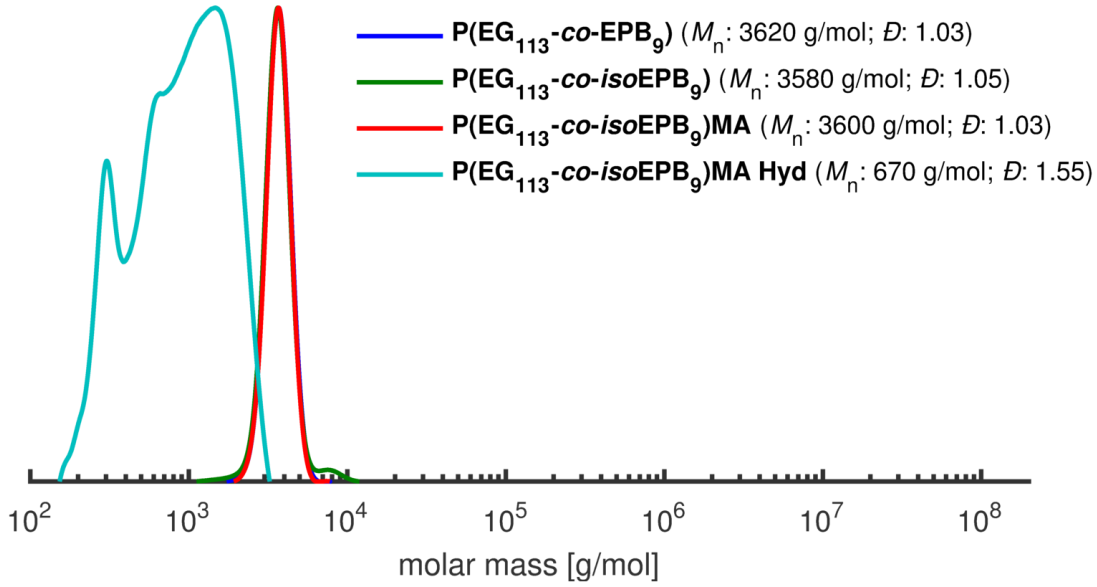

Figure S16 (color online): SEC traces (DMF, PEG standards, RI signal) of P(EG$_{113}$-*co*-EPB$_9$), P(EG$_{113}$-*co*-*iso*EPB$_9$) and P(EG$_{113}$-*co*-*iso*EPB$_9$)MA as well as degradation fragments after hydrolysis.

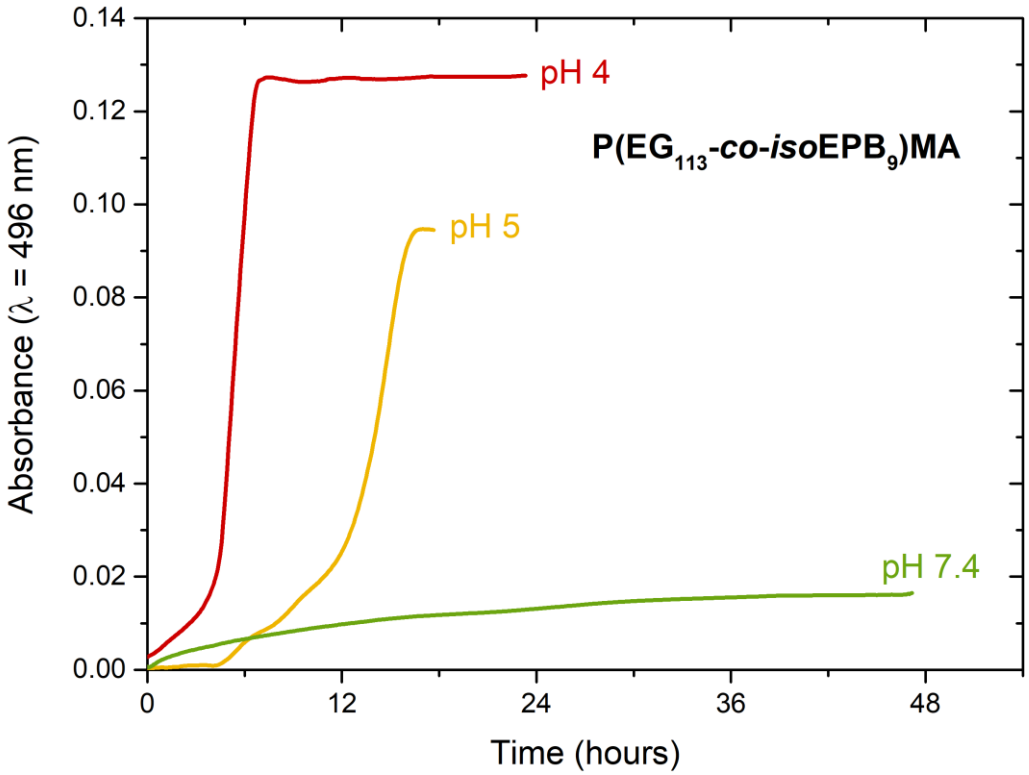

Figure S17: On-line absorbance measurement of OVA-Alexa488 release kinetics from hydrogels prepared from copolymer P(EG$_{113}$-*co*-*iso*EPB$_9$)MA at different pH values.

P(EG_{168}-*co*-EPB_{13}) and derivatives

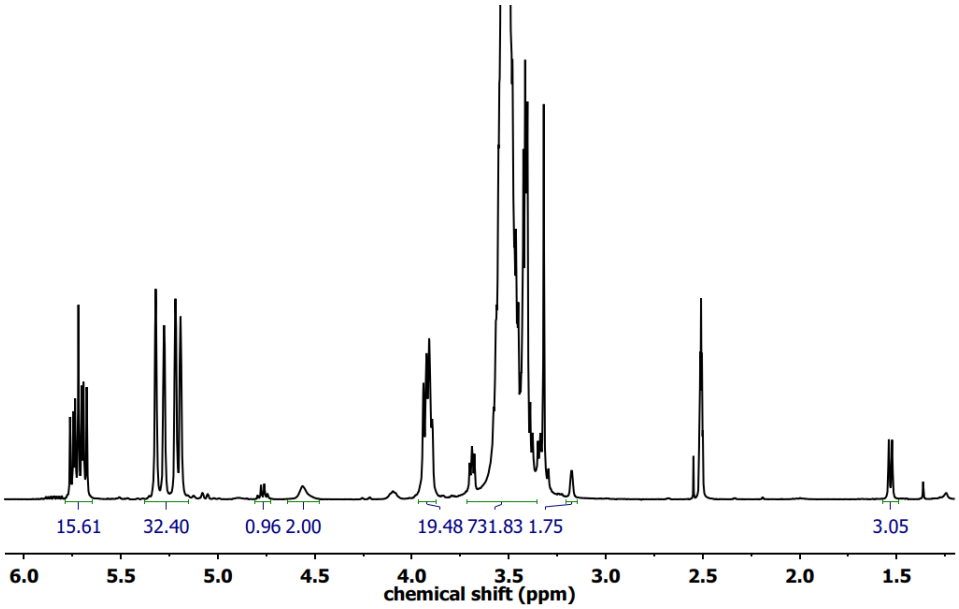

Figure S18: ^{1}H NMR spectrum (400 MHz, DMSO-d_6) of P(EG_{168}-*co*-EPB_{13}).

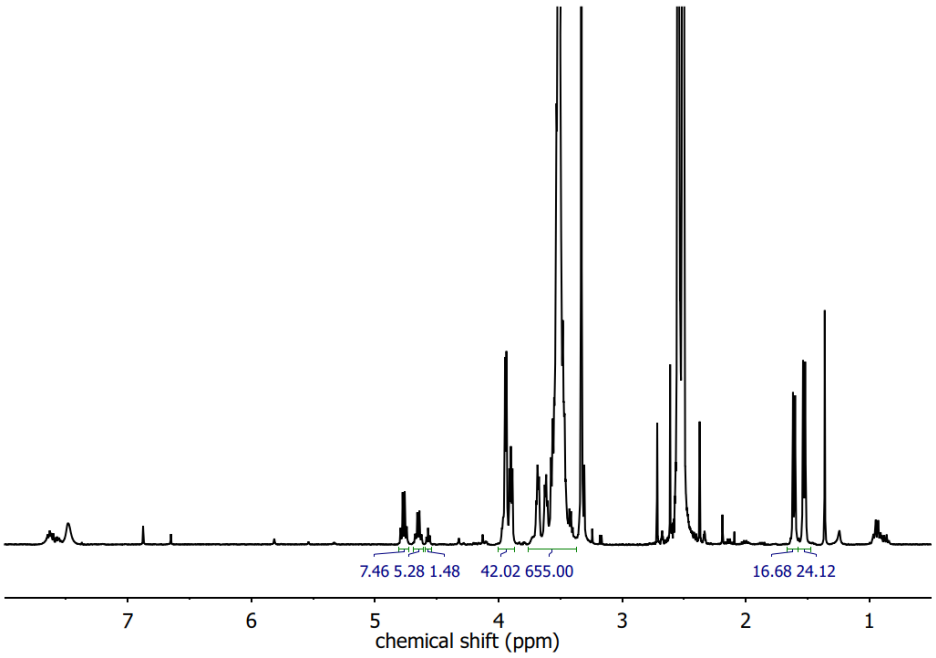

Figure S19: ^{1}H NMR spectrum (400 MHz, DMSO-d_6) of P(EG_{168}-*co*-*iso*EPB_{13}).

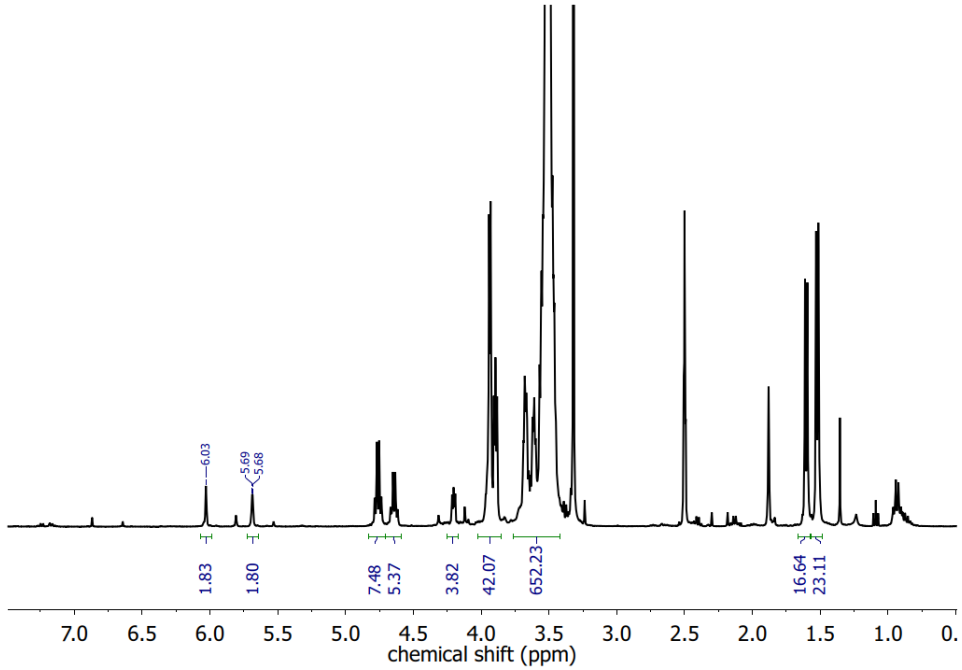

Figure S20: ^{1}H NMR spectrum (400 MHz, DMSO-d_6) of P(EG$_{168}$-*co*-*iso*EPB$_{13}$)MA.

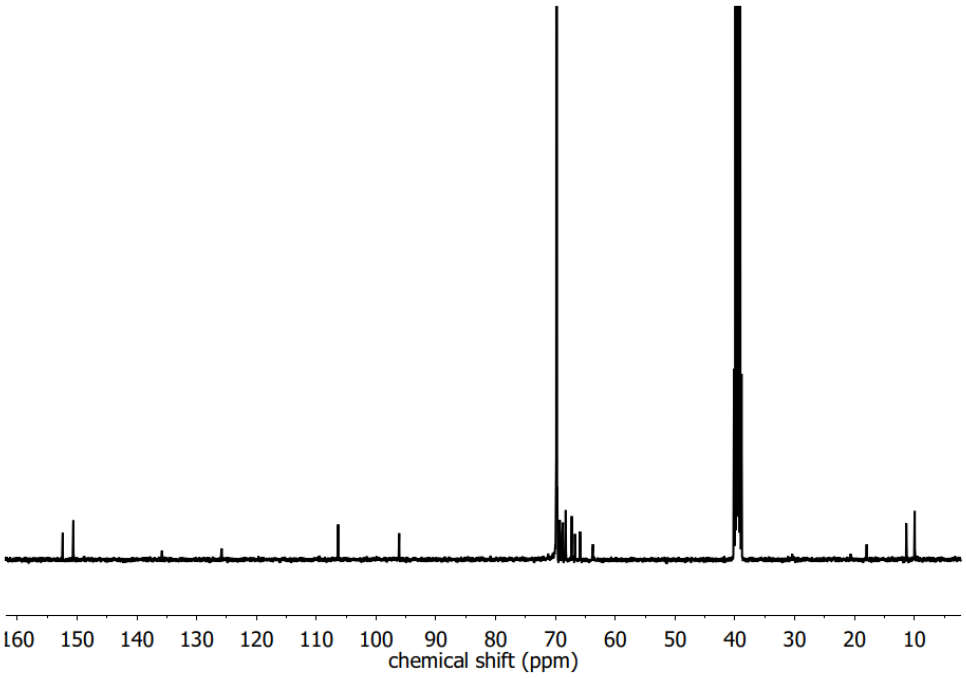

Figure S21: ^{13}C NMR spectrum (400 MHz, DMSO-d_6) of P(EG$_{168}$-*co*-*iso*EPB$_{13}$)MA.

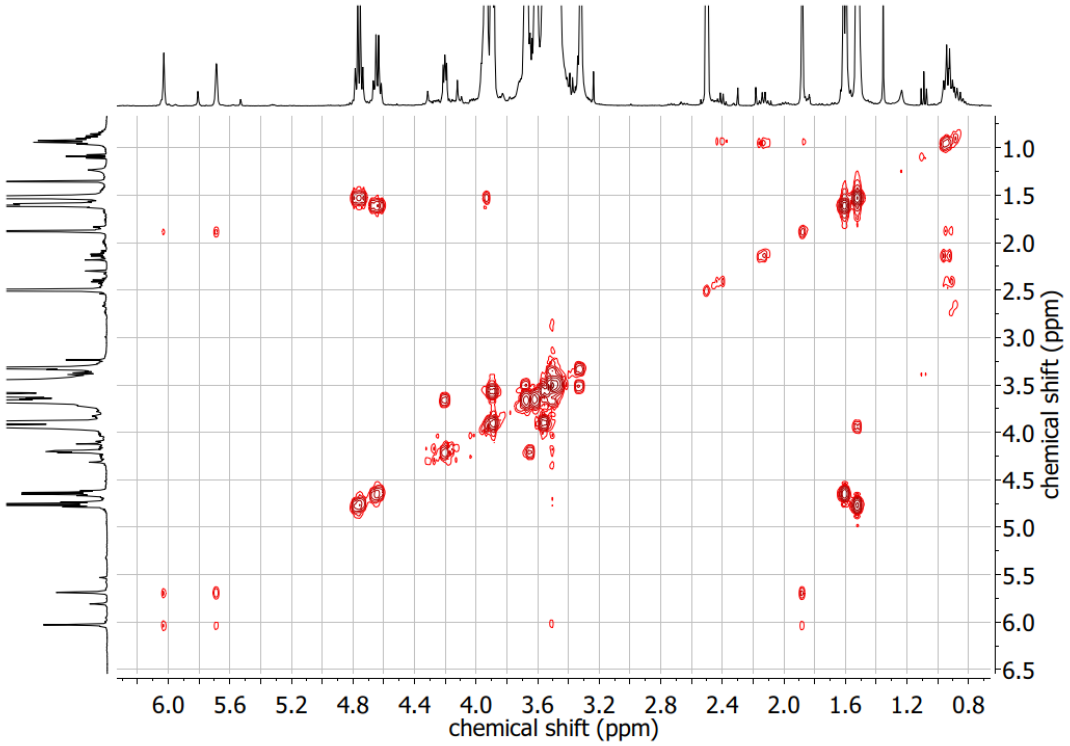

Figure S22: COSY NMR spectrum (400 MHz, DMSO-d_6) of P(EG_{168}-*co*-*iso*EPB_{13})MA.

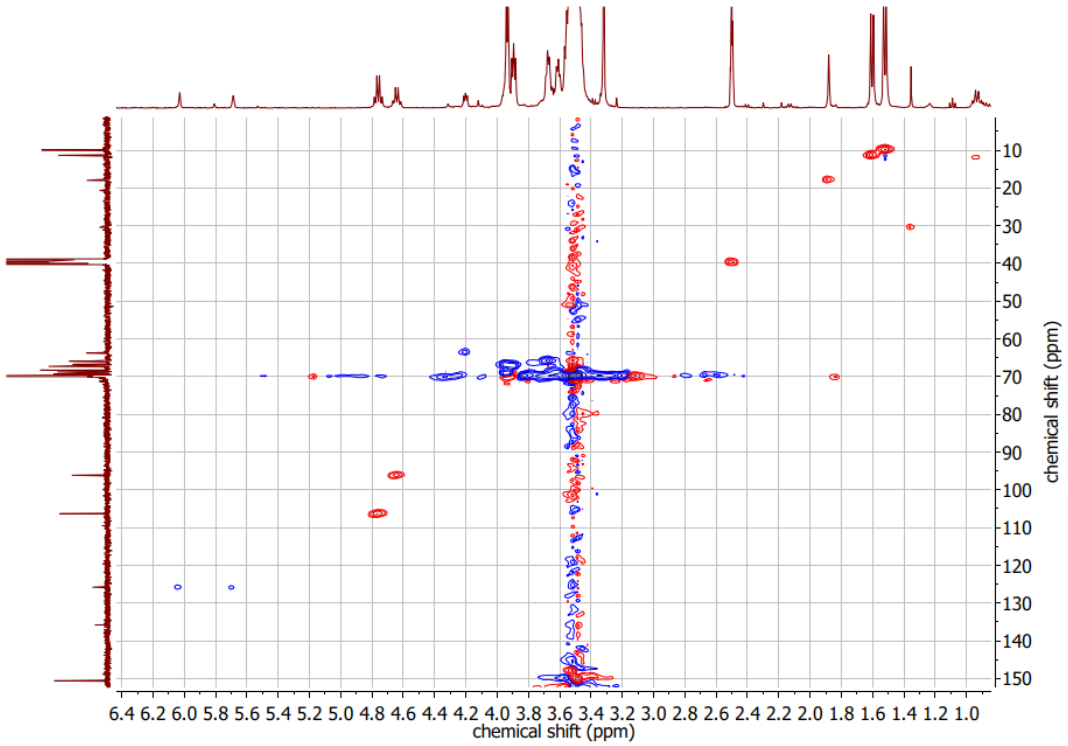

Figure S23 (color online): HSQC NMR spectrum (100.6 MHz, DMSO-d_6) of P(EG_{168}-*co*-*iso*EPB_{13})MA.

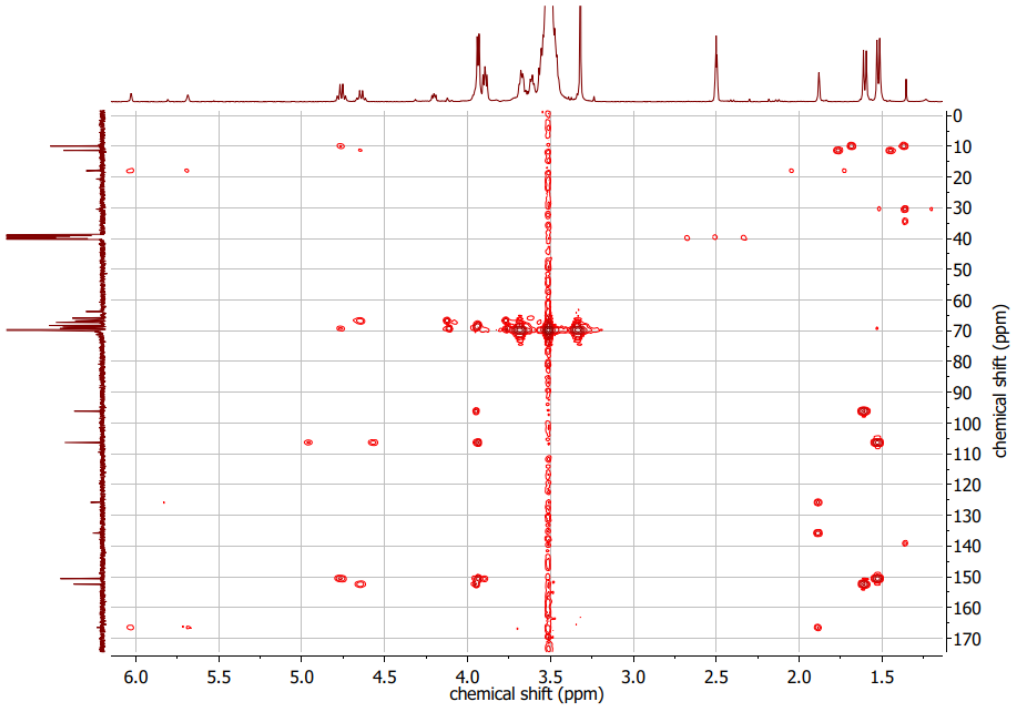

Figure S24: HMBC NMR spectrum (100.6 MHz, DMSO-d_6) of P(EG$_{168}$-*co*-*iso*EPB$_{13}$)MA.

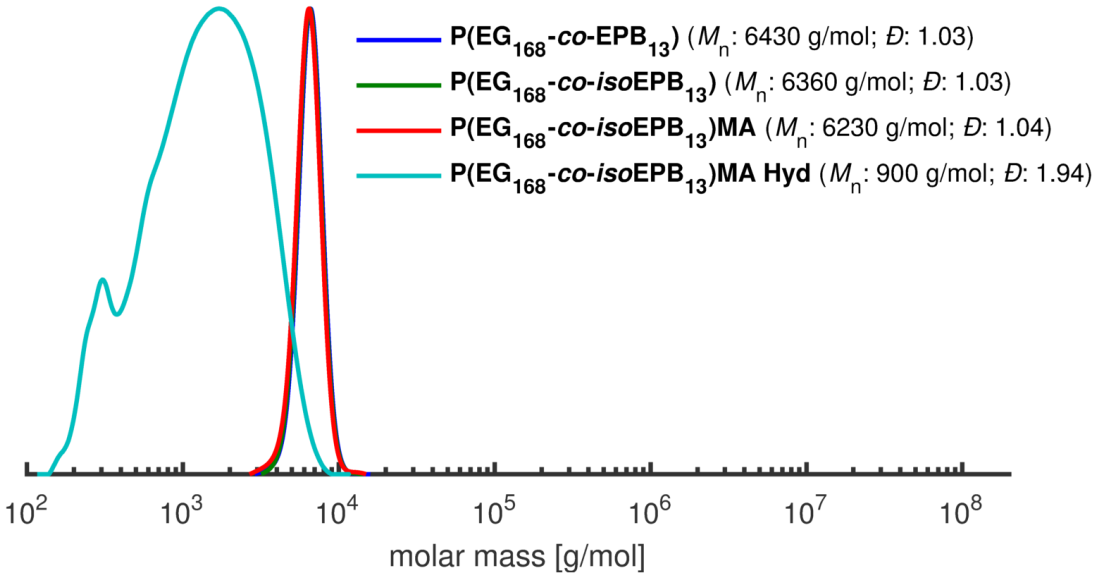

Figure S25 (color online): SEC traces (DMF, PEG standards, RI signal) of P(EG$_{168}$-*co*-EPB$_{13}$), P(EG$_{168}$-*co*-*iso*EPB$_{13}$) and P(EG$_{168}$-*co*-*iso*EPB$_{13}$)MA as well as degradation fragments after hydrolysis.

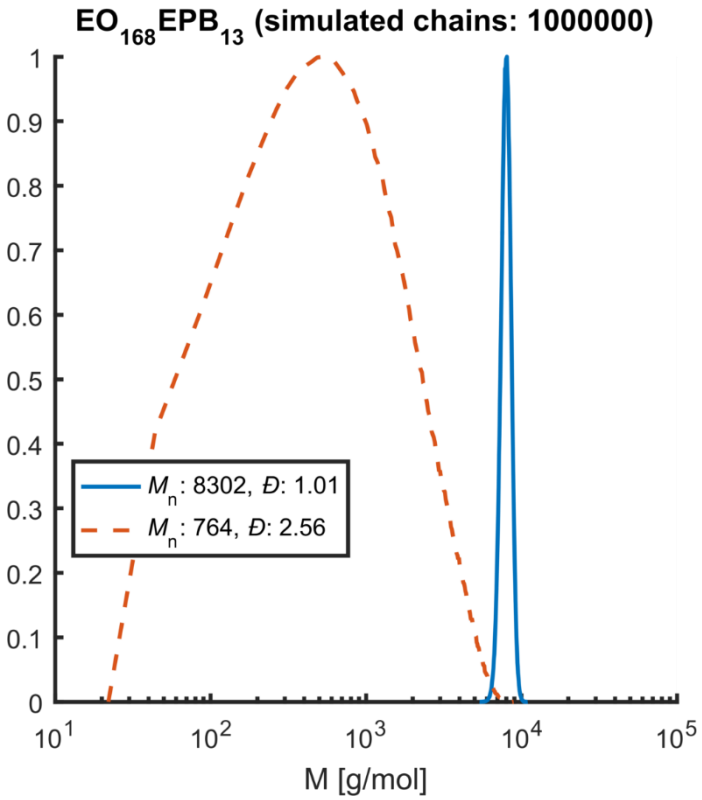

Figure S26: Monte Carlo simulation of the degradation fragments of P(EG$_{168}$-co-EPB$_{13}$). The PEG-fragments show a similar size distribution to the experimentally obtained values.

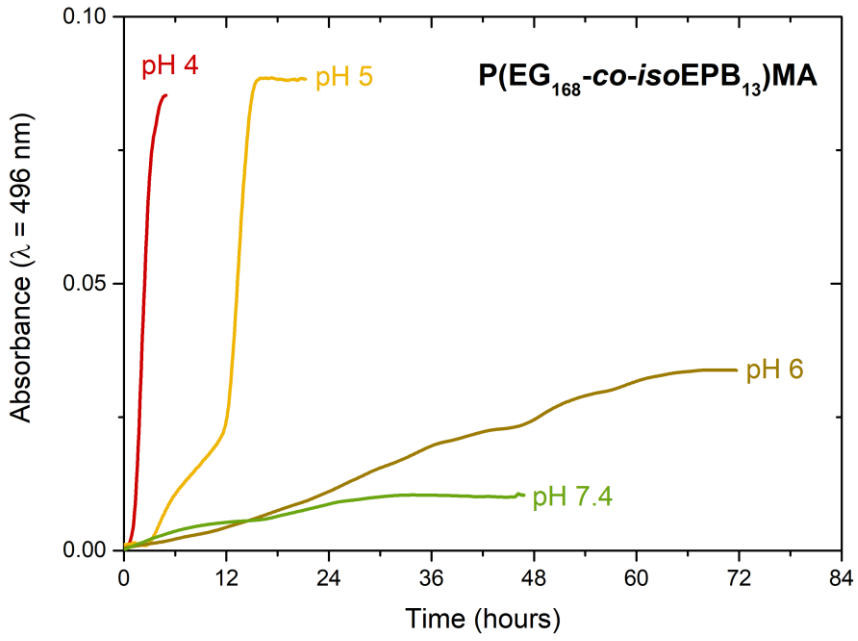

Figure S27: On-line absorbance measurement of OVA-Alexa488 release kinetics from hydrogels prepared from copolymer P(EG$_{168}$-*co-iso*EPB$_{13}$)MA at different pH values.

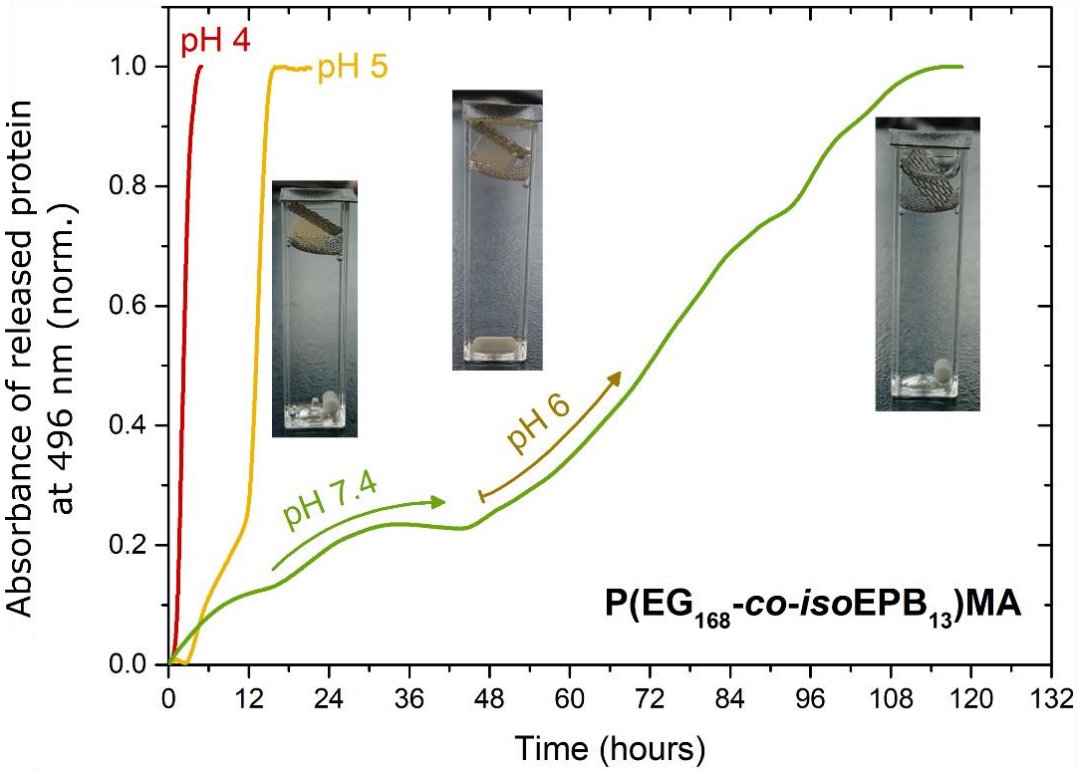

Figure S28 (color online): On-line absorbance measurement of OVA-Alexa488 release kinetics from hydrogels prepared from copolymer P(EG_{168}-*co*-*iso*EPB_{13})MA after pH switch; At first, the hydrogel was incubated at 48 h at pH 7.4 where no significant release of protein can be observed and subsequently, the pH was lowered to 6 where essential protein release takes place.

Comparison between copolymers

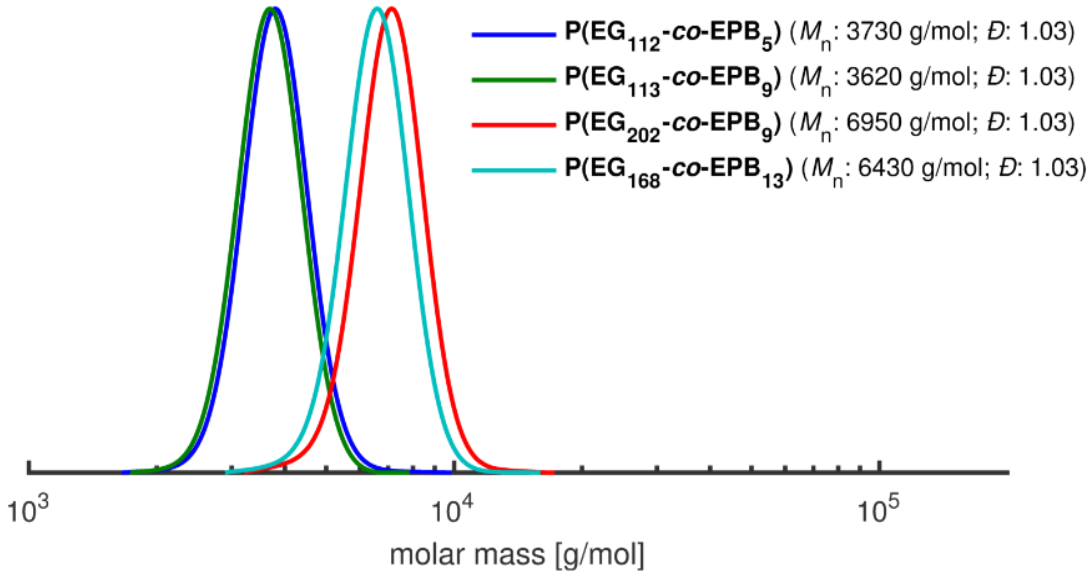

Figure S29 (color online): SEC traces (DMF, PEG standards, RI signal) of P(EG_{112}-*co*-EPB_5), P(EG_{202}-*co*-EPB_9), P(EG_{119}-*co*-EPB_9) and P(EG_{168}-*co*-EPB_{13}).

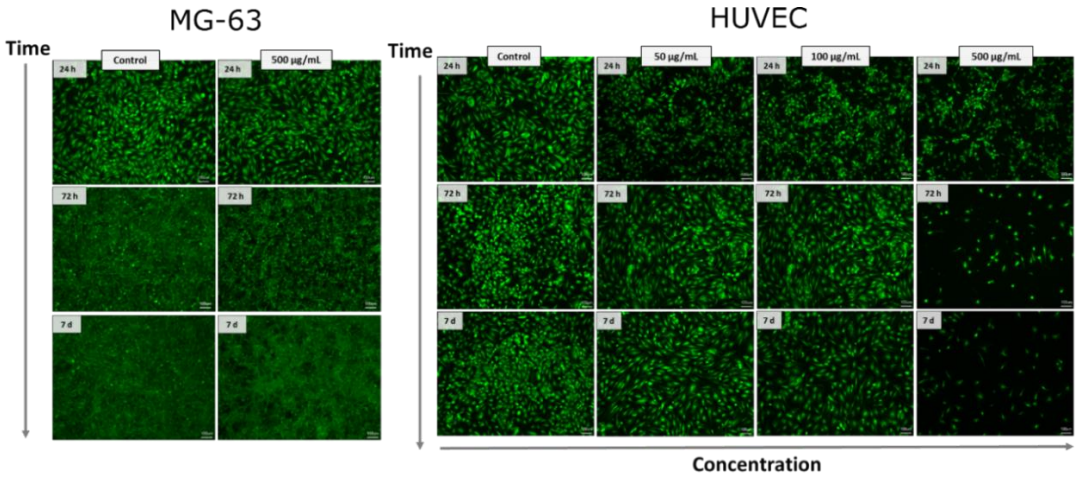

Figure S30 (color online): left: Incubation of MG-63 cells with a concentration of 500 µg/mL P(EG-*co*-*iso*EPB) for 7 days. Staining of vital cells with calcein-AM. Right: Incubation of primary HUVEC cells with different concentrations of P(EG-*co*-isoEPB) for up to 7 days. Staining of vital cells using calcein-AM.

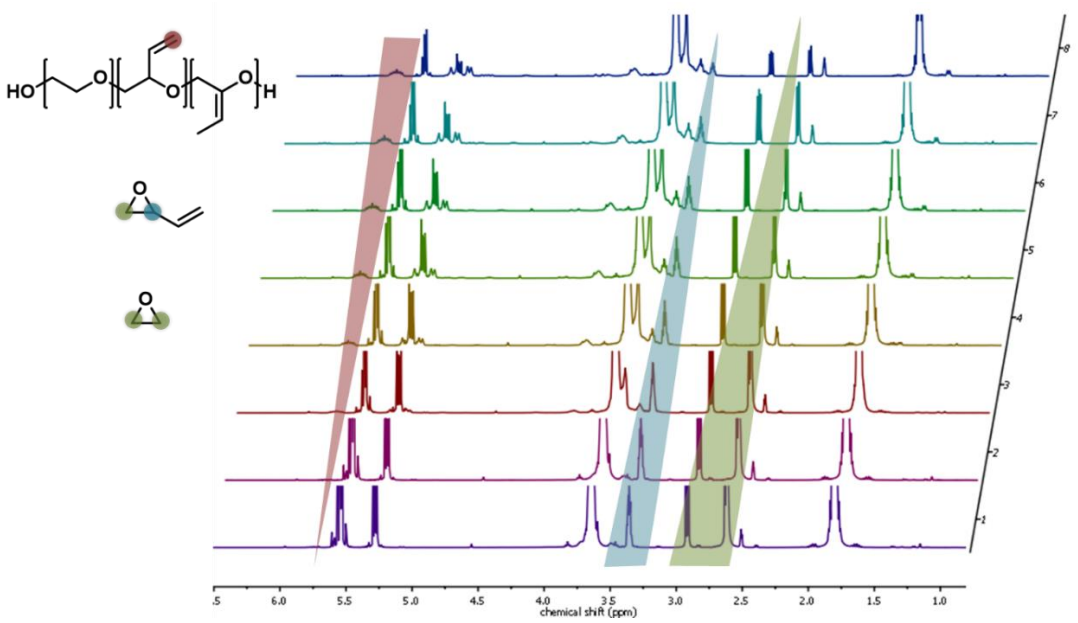

Figure S31 (color online): ^{1}H NMR spectra overlay showing the consumption of EPB (characteristic signals highlighted in blue and green) and EO (epoxide signals highlighted in green) monomers and the formation of P(EG-*co*-EPB) (vinyl signals highlighted in red).

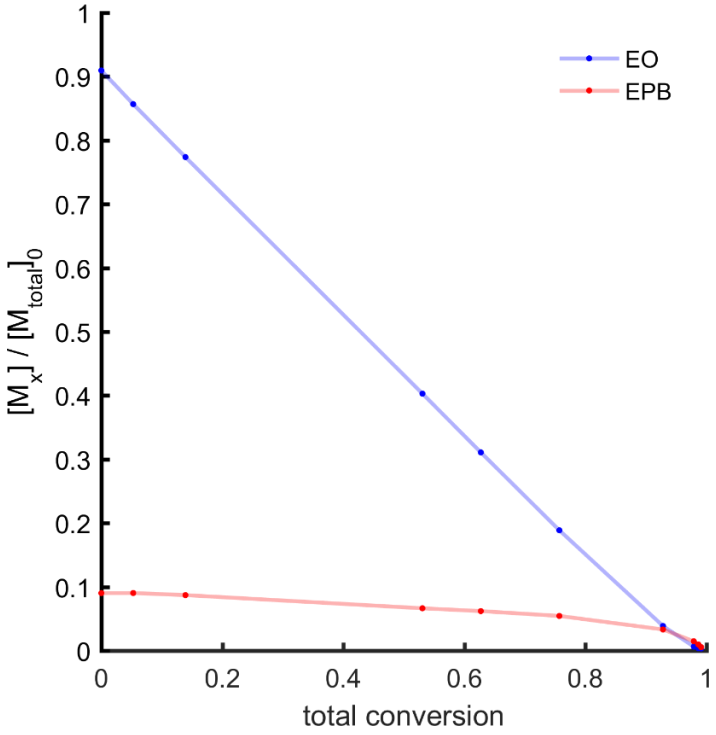

Figure S32: Comonomer concentration versus total conversion in the copolymerization experiment.

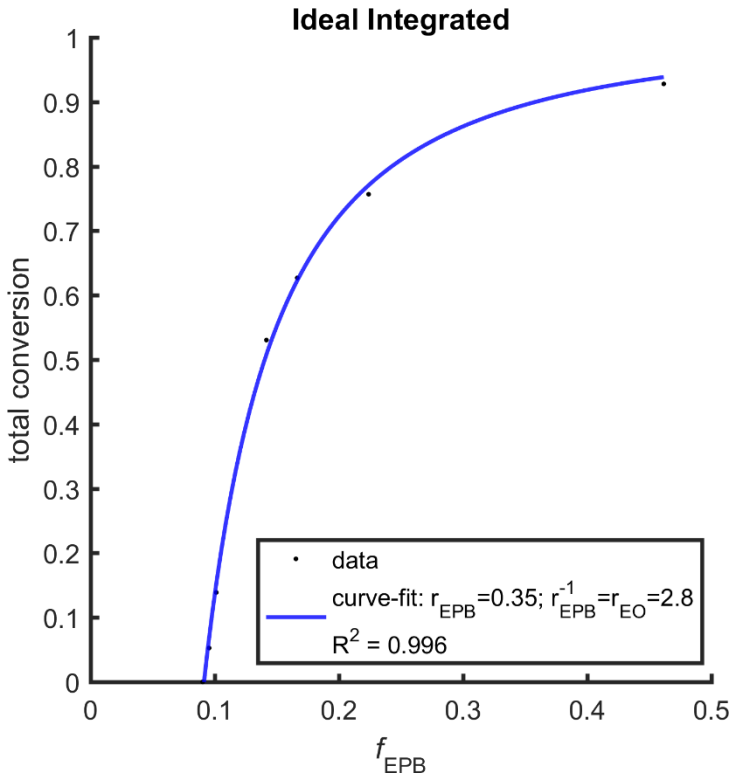

Figure S33: Ideal Integrated fit for the determination of reactivity ratios.[3]

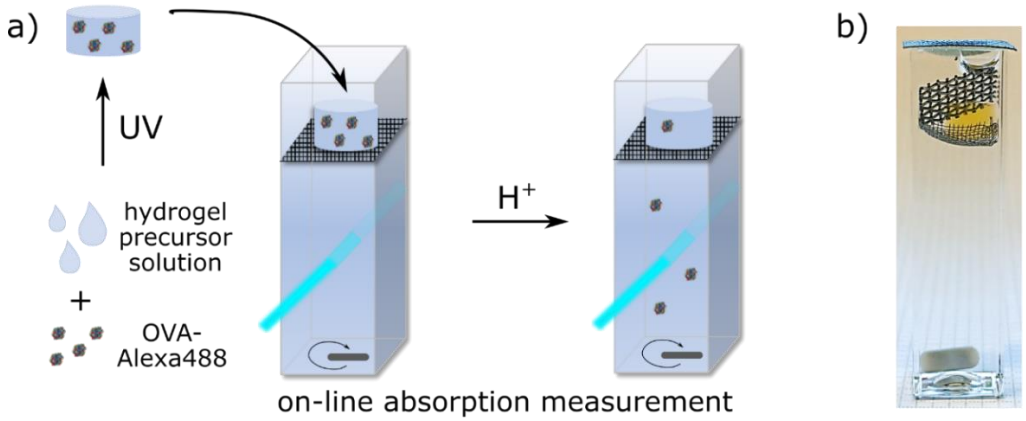

Figure S34: a) schematic of on-line absorbance measurement of OVA-Alexa488 release from hydrogel within a cuvette with stirring bar and separated hydrogel chamber. B) photograph of setup.

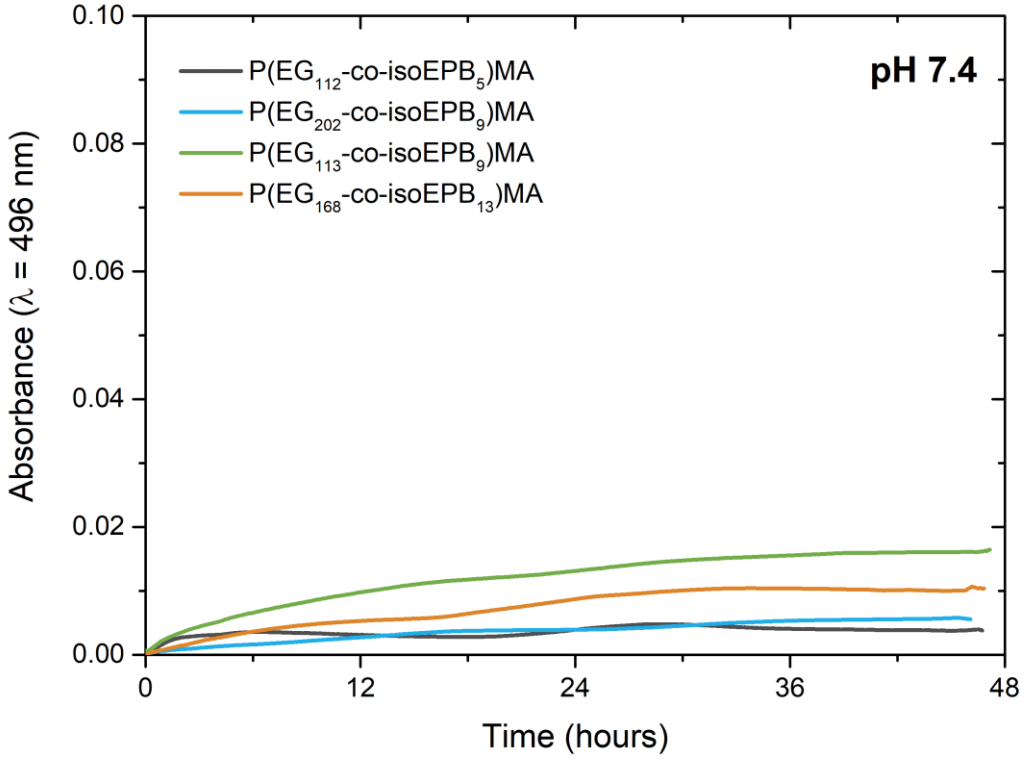

Figure S35 (color online): On-line absorbance measurement of controls. OVA-Alexa488 release kinetics from hydrogels prepared from copolymer P(EG_{168}-*co*-*iso*EPB_{13})MA at neutral pH, degradation of an empty hydrogel.

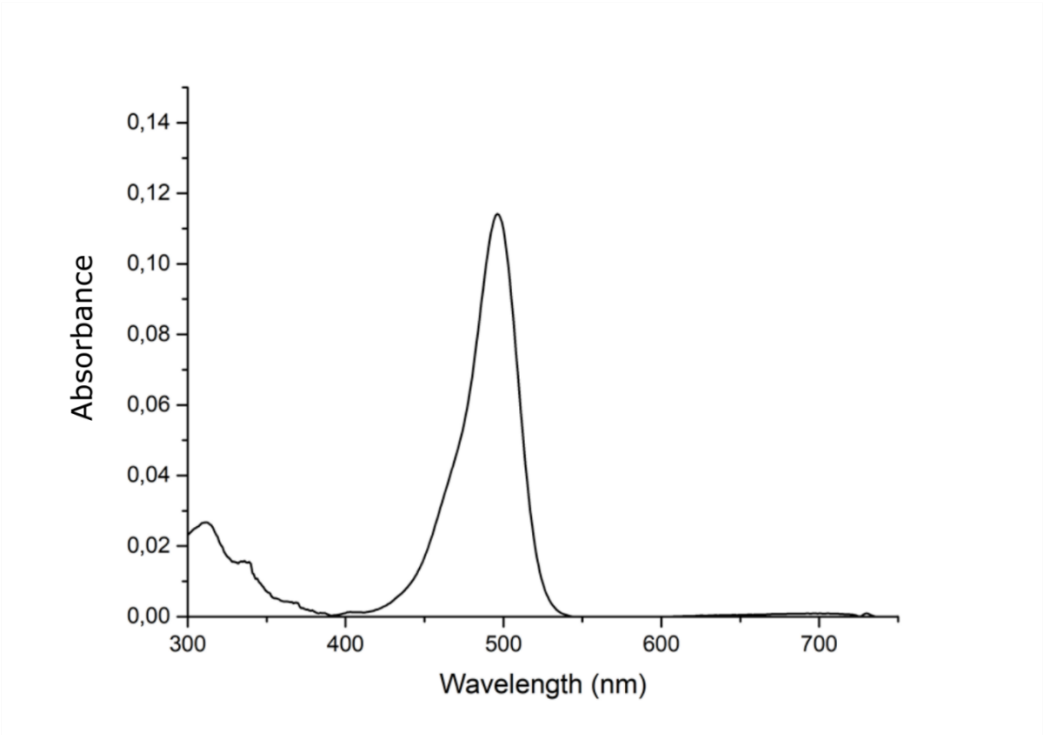

Figure S36: Absorption of a solution of OVA-Alexa488 in PBS.

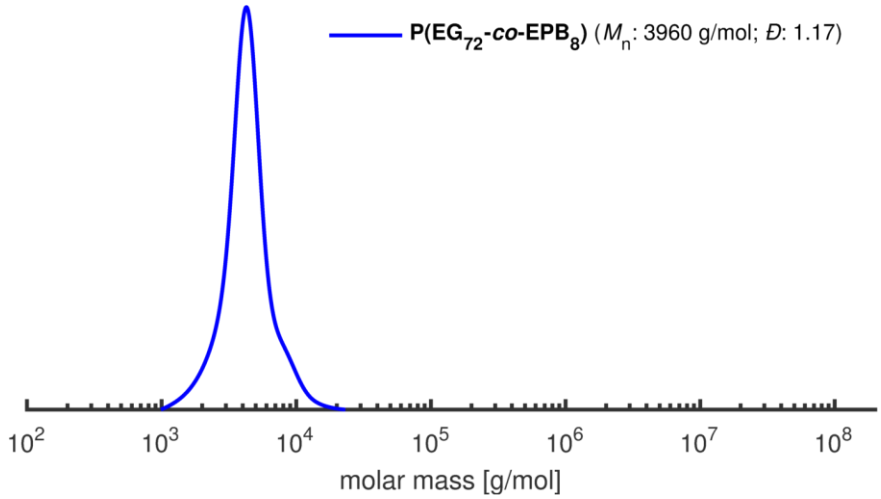

Figure S37: SEC traces (DMF, PEG standards, RI signal) of P(EG_{72}-*co*-EPB_8) as obtained after on-line ^{1}H NMR measurements for copolymerization kinetics studies of EO and EPB in a Norell S-500- S4 VT-7 NMR tube.

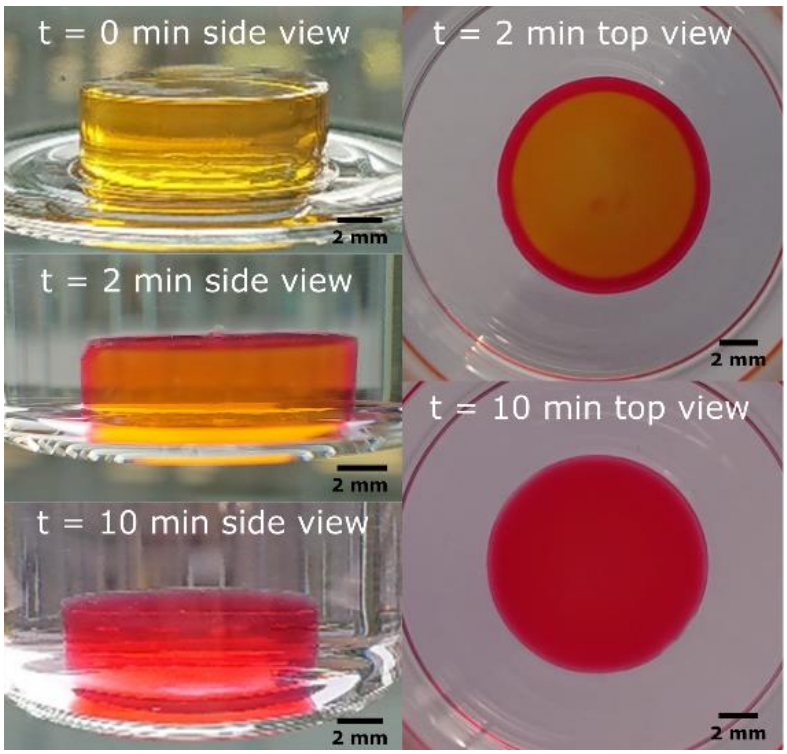

Figure S38: A hydrogel soaked in a 0.05 mg/mL methyl red in PBS solution (pH 7.4) after 2 and 10 min of incubation in citrate phosphate buffer pH 4. The diffusion of hydronium ions is monitored by the pH indicator color change from yellow at neutral pH to red at acidic pH. The diffusion occurs from the periphery to the centre of the hydrogel, as shown in the photograph taken after t = 2 min. The diffusion rate is estimated to be 0.005 mm^2/s and is in agreement with the diffusion rate through a PEG-DA hydrogel reported by Kim et al. (0.01 mm^2/s)[4]

REFERENCES

[33] R. Schröder, H. Pohlit, T. Schüler, M. Panthöfer, R. E. Unger, H. Frey, W. Tremel, *Journal of Materials Chemistry B* **2015**, *3*, 7079-7089.

[34] Y. T. Kim, K. Castro, N. Bhattacharjee, A. Folch, *Micromachines (Basel)* **2018**, *9*.

[1] R. Schröder, H. Pohlit, T. Schüler, M. Panthöfer, R. E. Unger, H. Frey, W. Tremel, *Journal of Materials Chemistry B* **2015**, *3*, 7079-7089.

[2] M. Worm, D. Leibig, C. Dingels, H. Frey, *Acs Macro Letters* **2016**, *5*, 1357-1363.

[3] J. Blankenburg, E. Kersten, K. Maciol, M. Wagner, S. Zarbakhsh, H. Frey, *Polymer Chemistry* **2019**, *10*, 2863-2871.

[4] Y. T. Kim, K. Castro, N. Bhattacharjee, A. Folch, *Micromachines (Basel)* **2018**, *9*.

2.2 pH-Responsive Protein Nanoparticles via Conjugation of Degradable PEG to the Surface of Cytochrome c

Elena Steiert,[a†] Johannes Ewald,[b†] Annika Wagner,[a] Ute A. Hellmich,[a] Holger Frey[b] and Peter R. Wich[a,c,d]*

[a]Institute of Pharmacy und Biochemistry, Johannes Gutenberg-University Mainz, 55128 Mainz, Germany.

[b]Institute of Organic Chemistry, Johannes Gutenberg-University Mainz, 55128 Mainz, Germany.

[c]Australian Centre for NanoMedicine, University of New South Wales, Sydney, NSW 2052, Australia

[d] School of Chemical Engineering, University of New South Wales, Sydney, NSW 2052, Australia.

†E.S. and J.E. contributed equally to this work.

Published in Polymer Chemistry (DOI: 10.1039/C9PY01162E)

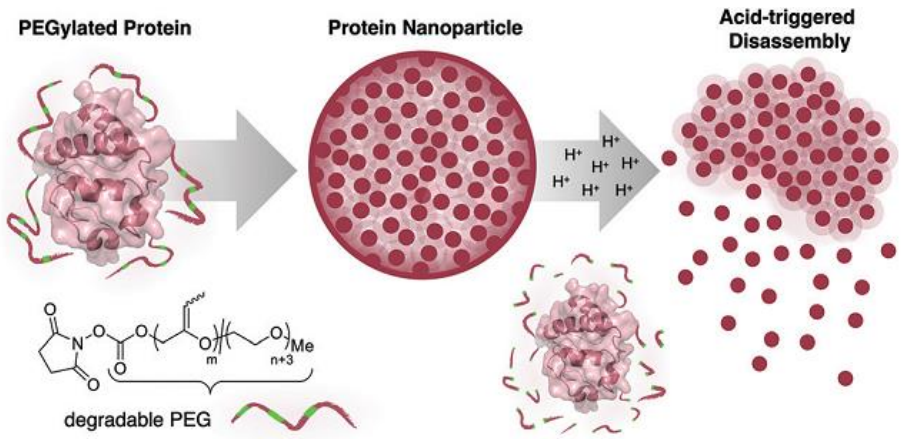

2.2.1 ABSTRACT

Proteins represent a versatile biopolymer material for the preparation of nanoparticles. For drug delivery applications an acid-triggered disassembly and payload release is preferred. Herein, we present a protein nanoparticle system based on cytochrome *c*, which is surface-modified with acid-degradable polyethylene glycol (PEGylation). pH-sensitivity was obtained through vinyl ether moieties distributed in the polyether backbone. When PEGylated, cytochrome *c* shows a different solubility behaviour in organic solvents, which allows for particle preparation using an emulsion-based solvent evaporation method. The resulting particles are stable under physiological conditions but degrade at acidic pH values. Fluorescence-labelled dextran was successfully encapsulated as hydrophilic model payload in these degradable nanoparticles and a release under acidic conditions was observed.

2.2.2 INTRODUCTION

Polyethylene glycol (PEG) is the current gold standard for the protective surface modification of proteins. More than forty years ago it was discovered that the conjugation of proteins with PEG ("PEGylation") leads to better immunogenic properties and increased circulation half-life compared to the unmodified protein.[1, 2] Several protein-polymer conjugates are FDA approved, which highlights the importance of these systems in therapeutic applications.[3] In addition to the reduced immunogenicity and improved pharmacokinetic properties, protein-PEG conjugates show enhanced stability and solubility in biologically relevant environments.[4-6] However, concerns were raised due to the lack of degradability which can cause accumulation in human tissue when higher molecular weight PEGs are used.[7] PEGylation has also been shown to impair the catalytic activity of enzyme conjugates.[8] For these reasons, increased efforts are made to develop PEG alternatives and degradable analogs.[7, 9, 10]

So far, most approaches focus on the use of degradable linkers between protein and polymer, e.g. via hydrazine[11], azidomethyl-methylmaleic anhydride[12] or disulfide[13] linkages, where the protein-polymer bond can be cleaved under acidic or reductive conditions. There are only a few protein-polymer conjugates which make use of a degradable polymer backbone. Acetals[14] or poly(phosphates)[15] in the polymer backbone can result in polymer degradation under acidic or hydrolytic conditions. A recent work by Pelegri-O'Day *et al.* demonstrated the use of a degradable PEG analogue for reversible PEGylation of lysozyme. However, this approach requires a non-physiological Grubbs III catalyst for the degradation by depolymerisation of the polymer.[16]

A very promising cleavable moiety for degradable PEG are vinyl ethers, as they combine a fast hydrolysis rate at physiologically relevant acidic ranges of pH 4-5 with excellent stability at pH 7.4.[17] This structure has first been implemented in PEG by Hawker *et al.* via copolymerization of ethylene oxide (EO) and epichlorohydrin (ECH),

followed by subsequent elimination of chloride.[18] However, these materials still show rather high dispersity and no defined end groups as a result of their triethylaluminium-catalysed polymerization. Furthermore, as recently published by Danner *et al.*, these copolymers show a strong reactivity difference between EO and ECH, which results in a pronounced monomer gradient and consequently an uneven distribution of the predetermined cleaving sites along the backbone and therefore considerable dispersity of the hydrolysed product.[19] The Frey group recently reported another approach to vinyl ether containing PEG.[17] Classic anionic ring opening copolymerization (AROP) of EO and 3,4-epoxy-1-butene (EPB) to obtain P(EG-*co*-EPB), followed by isomerization of allylic ether moieties to vinyl ethers (P(EG-*co*-*iso*EPB)) proved to be the method of choice to combine low polydispersity, well-defined end groups, tailorable molecular weight and adjustable content of cleavable moieties in the polyether backbone. This material may serve as a promising substitute for PEG for various therapeutic and biomedical applications in the future, as it expands the favourable properties of well-known and well-established PEG with degradability at physiologically relevant pH values on reasonable timescales.

In this work we apply this material to prepare a new type of degradable protein-PEG conjugate that can be formulated into acid-responsive nanoparticles. The general concept of preparing nanoparticles based on protein-polymer conjugates has attracted considerable interest in recent years.[20, 21] For example, we reported a protein-based nanoparticle system using highly PEGylated lysozyme (LYZ) for the delivery of anticancer drugs. The LYZ-PEG conjugate is soluble in dichloromethane (DCM) and at the same time, the protein structure is preserved and protected. Nanoparticles are prepared using a mild emulsion-based method that allows the encapsulation of hydrophilic and hydrophobic payloads.[22-24] While the particles are capable of releasing their payload via passive diffusion, a triggered release would be preferred. For this purpose, the introduction of stimuli-responsiveness is desired, in order for the drug

delivery system to release their payload in a controlled manner.[25] For example, De Geest *et al.* developed a pH-sensitive polymer-protein (BSA) conjugate that self-assembles into nanoparticles. The polymer chains include dioxolane groups that can switch under acidic conditions from a hydrophobic form to hydrophilic diol groups. This results in the loss of the self-assembly behaviour of this system and the disassembly of the particles.[26] A drawback of the system is the permanent linkage of the polymers to the protein and the highly acidic conditions (pH 1) required for particle degradation that are, with the exception of the gastrointestinal tract, not accessible in a biological system.

Wang *et al.* developed a multi-stimuli responsive nanoparticle system consisting of hydrazine-modified BSA proteins that were conjugated with aldehyde-functionalized thermo-responsive copolymers. The resulting hydrazone bond between the protein and polymer is acid-sensitive. After the temperature-induced self-assembly of the protein-polymer conjugate above its lower critical solution temperature (LCST) the particles needed further stabilisation by crosslinking the BSA using cysteamine. The resulting disulfide bonds between the proteins introduced sensitivity under reductive conditions. Apart from an elaborate multistep synthesis to obtain the final particles, another disadvantage of this system is that the particles do not disassemble in acidic conditions alone. For complete particle degradation, both acidic and reductive microenvironments have to be present at the same time.[27]

In this work, we present a novel class of pH-sensitive protein nanoparticles using an intrinsic degradable PEG copolymer. In straightforward synthesis steps, we prepare a particle system that is stable without crosslinking and can degrade and disassemble at physiologically relevant acidic pH values. For this, an active ester of fully degradable vinyl ether PEGs was synthesized and conjugated to the surface of cytochrome *c* (Cyt). This new type of protein-polymer conjugate (Cyt_{degPEG}) is soluble in organic solvents and particles can be formed with mild emulsion techniques.

2.2.3 RESULTS AND DISCUSSION

2.2.3.1 SYNTHESIS OF MP(EG$_{81}$-*CO*-*ISO*EPB$_6$)-NHS

For the synthesis of the acid degradable PEG copolymer, triethylene glycol monomethyl ether was chosen as a monofunctional initiator due to its convenient structure, which readily enables determination of molecular weight and comonomer content by NMR integration. The precursor molecule, the allyl ether containing PEG copolymer mP(EG$_{81}$-*co*-EPB$_6$) was synthesised by AROP of EO and EPB based on a procedure recently reported by Worm *et al.* (**Figure 1**).[17]

The resulting allylic ether moieties distributed at the polymer backbone were isomerized quantitively to acid-labile vinyl ethers to obtain mP(EG$_{81}$-*co*-*iso*EPB$_6$), while the structure and integrity of the copolymer chain was retained (**Figure 2b**). To target nucleophilic lysine residues at the surface of cytochrome *c*, the hydroxyl end group of mP(EG$_{81}$-*co*-*iso*EPB$_6$) was reacted with *N,N'*-disuccinimidyl carbonate (NHS-DSC) to obtain the activated carbonate ester.

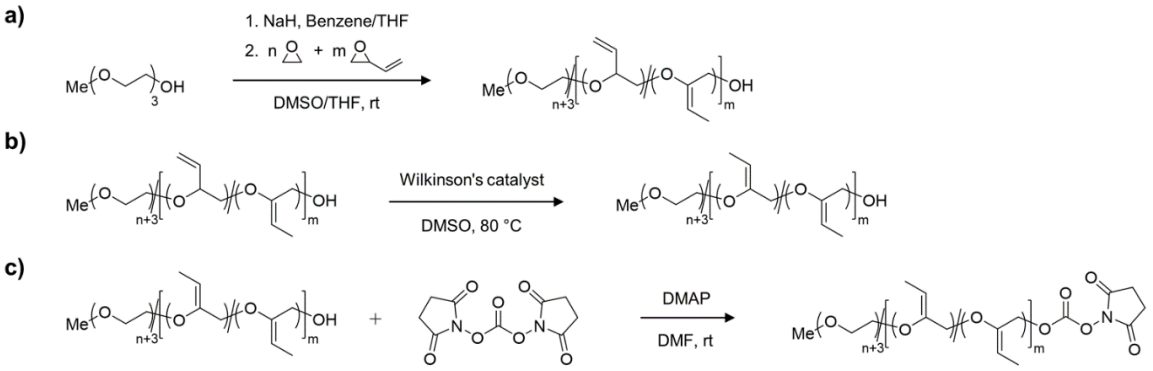

Figure 1: Synthesis route to obtain mP(EG$_{81}$-*co*-*iso*EPB$_6$)-NHS; a) Copolymerization of EO and EPB to obtain mP(EG$_{81}$-*co*-EPB$_6$); b) Isomerization of mP(EG$_{81}$-*co*-EPB$_6$) to mP(EG$_{81}$-*co*-*iso*EPB$_6$); c) Activation of hydroxyl group to NHS active ester m(P(EG$_{81}$-*co*-*iso*EPB$_6$)-NHS) using NHS-DSC.

A molecular weight of M_n=4000 g/mol with 12mol% EPB was targeted. ^{1}H-NMR integration of the allylic moieties (between 6.0 and 4.5 ppm), the ether backbone

(between 4.0 and 3.3 ppm) and the methyl ether end group (3.24 ppm), confirmed this molecular weight (see ESI **Figure S1**).

An incorporation 7mol% of EPB was found, which is lower than targeted but still more than sufficient to guarantee the degradation of the polymer chain (**Figure 2a**). Interestingly, already during the copolymerization a small amount of vinyl ether moieties (around 10% of total allylic units) was formed, as can be seen by NMR. Quantitative isomerization was confirmed by the absence of distinct allylic signals in ^{1}H-NMR spectrum and appearance of vinyl ether signals (4.8 – 4.6 ppm) as reported previously after this step as well.[17]

Table 1: Molecular characteristics of mP(EG_{81}-*co-iso*EPB_6).

Sample	$M_{n,\,NMR}$ g/mol	$M_{n,\,SEC}$ g/mol	$M_{n,\,MALDI}$ g/mol	$Đ_{SEC}$	mol% EPB
mP(EG_{81}-*co-iso*EPB_6)	3815	3380	3620	1.04	7

SEC: DMF, RI Detector, PEG standards.

Figure 2b shows the molecular weight distribution of mP(EG81-co-EPB6) at all stages referred to in this work. Analysis by SEC after polymerization shows a well-defined copolymer with very narrow weight distribution (Đ = 1.03–1.04) and a molecular weight of Mn=3380 g/mol. It should be noted that SEC underestimates the molecular weight of these copolymers, as the hydrodynamic radius of PEG copolymers differs from that of PEG standards. During the post-polymerization steps, the molecular weight distribution remained low (Đ = 1.03-1.04), indicating that no unwanted cleavage or crosslinking of the polymer occurred.

The successful copolymerization was also confirmed by MALDI-ToF, resulting in distinct intervals of 44 g/mol for EG and 70 g/mol for EPB units between the signals as well as a monomodal distribution with Mn=3620 g/mol (**Figure 2c**).

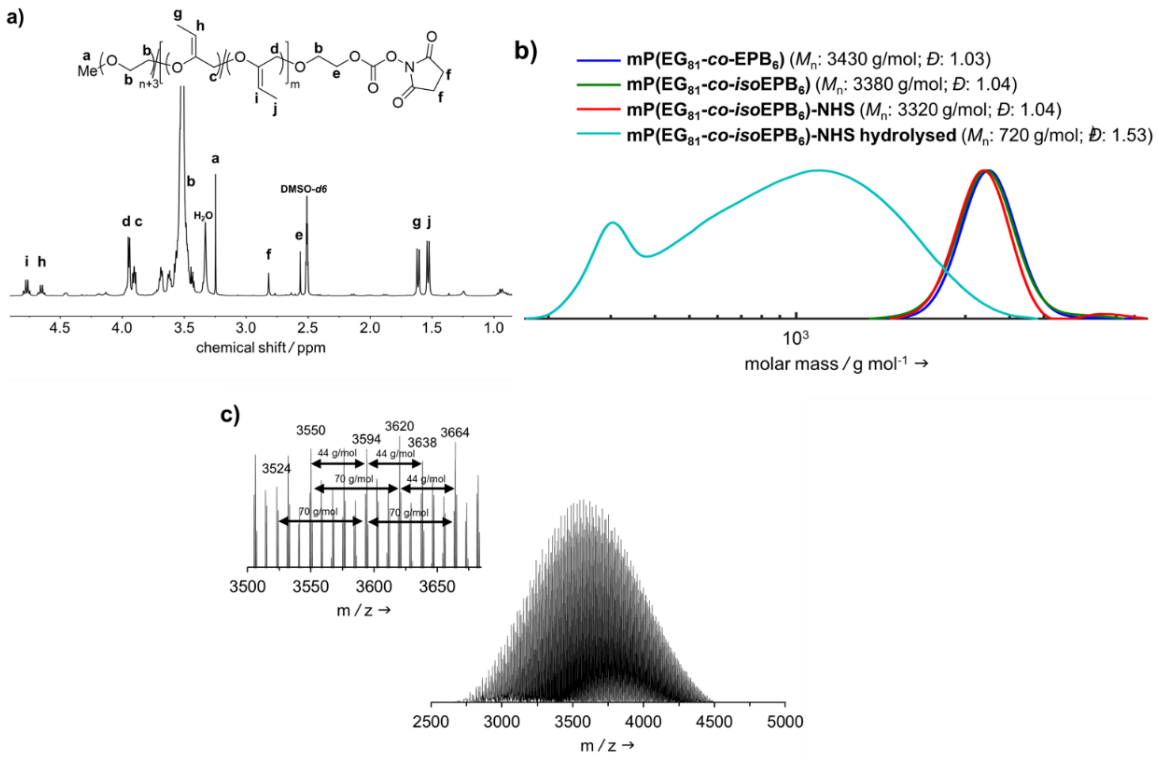

Figure 2: a) ^{1}H-NMR spectrum (400 MHZ, DMSO-*d6*) of mP(EG$_{81}$-*co*-*iso*EPB$_6$)-NHS; b) SEC analysis of mP(EG$_{81}$-*co*-EPB$_6$) copolymers at different stages referred to in this work. (eluent: DMF, RI detector, PEG standard); c) MALDI-ToF analysis of mP(EG$_{81}$-*co*-*iso*EPB$_6$).

The degree of functionalization to NHS ester reached 37%. Most post-functionalization approaches for PEGylating agents targeting lysine residues usually involve the use of carboxylic acids, carboxylic anhydrides or acyl chlorides to form an ester or amide bond between the polymer and a linker to the reactive group used for PEGylation. As this would include the occurrence of acidic protons (which is not favourable in the case of an acid-labile polymer), we decided to use NHS-DSC as the most convenient way to form an activated carbonate ester for targeting of lysine residues. While this reaction did not result in quantitative functionalization of the polymer, this could easily be overcome by increasing the amount of polymer per protein during PEGylation. Importantly, the non-functionalized PEG chains do not interfere with the protein PEGylation and the procedure additionally includes a washing step for the removal of excess PEG.

In an acidic environment, the vinyl ether moieties in the polymer backbone are cleaved by a two-step mechanism: initially, a hydronium ion is transferred to the substrate, followed by the addition of water to form a hemiacetal, which then decomposes.[28] The fast rate of hydrolysis of this type of copolymer has already been reported by ^{1}H-NMR *in situ* kinetics in our previous work.[17] The result of the hydrolysis of the copolymer is demonstrated by SEC (**Figure 2b**). After incubation of mP(EG_{81}-*co*-*iso*EPB_6) under acidic conditions, the molecular weight shifted from M_n=3320 g/mol to M_n=720 g/mol, while the molecular weight distribution increased to $Đ$ = 1.53.

2.2.3.2 PROTEIN MODIFICATION

The activated, degradable PEG was coupled to cytochrome *c* (Cyt) as a model protein, due to the relatively high amount of addressable nucleophilic amine groups at the surface (19x) compared to its small size (12.4 kDa). Furthermore, since Cyt is part of the apoptotic system,[29] catalytically active nanoparticles based on this enzyme could be used as future therapeutic nanomaterials. This may be of particular interest e.g. for cancer treatment. Upon attachment of a sufficient number of polymer chains to the protein surface, the special characteristic of PEG, to have a broad solubility in a variety of solvents, is transferred to the underlying protein. This renders the protein-polymer conjugate soluble in dichloromethane and further allowing for nanoparticle formation using a solvent evaporation method.[23, 24]

The cytochrome *c* modification takes place in buffered aqueous solution with a 17-fold excess of mP(EG_{81}-*co*-*iso*EPB_6)-NHS per protein (which corresponds to 6.3 equivalents of NHS- functionalized polymer per protein) (**Figure 3a**).

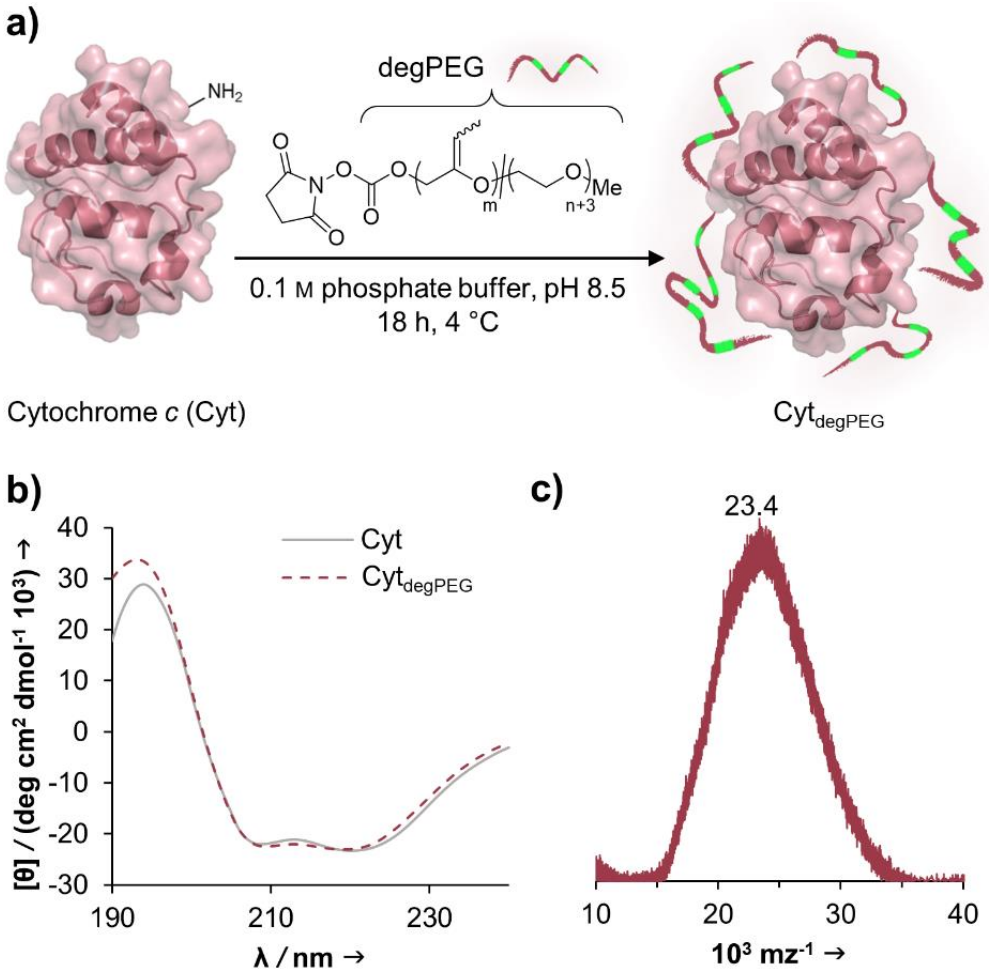

Figure 3: a) Cyt modification with mP(EG_{81}-*co*-*iso*EPB_6)-NHS. The wavy line in the polymer sidechain represents both possible isomerization products. The attachment point of the polymer to the protein is the activated carbonate ester. The resulting in Cyt_{degPEG} is a schematic illustration and does not reflect the final amount and the actual attachment point of polymer chains; b) CD spectra of native Cyt (solid line) and Cyt_{degPEG} (dotted line); d) MALDI-ToF of Cyt_{degPEG}.

After overnight reaction, the resulting Cyt-polymer conjugate (Cyt_{degPEG}) was purified by SEC. The extent of conjugation was qualitatively analysed by SDS-PAGE, which shows a broad band extending from around 23 to 170 kDa (**Figure 4b** and ESI section 2.1). This is a known behaviour of PEGylated protein conjugates, which is commonly explained by interactions between PEG and SDS.[30] Most importantly, the SDS-PAGE confirmed that all proteins were modified. Additional MALDI-ToF MS characterization shows a molecular weight increase from 12.4 to 23 kDa upon PEGylation (**Figure 3c**). This indicates that on average 3 polymer chains per protein

molecule were successfully attached to the protein surface. We preformed circular dichroism (CD) spectroscopy to assess whether the modification of Cyt leads to protein structural changes. Only minor alterations (< 2%) in the secondary structure elements between modified and unmodified Cyt can be seen (**Figure 3b**, ESI **Table S1**). We further analysed the catalytic activity of the Cyt-PEG conjugate compared to the native enzyme using an ABTS assay. Importantly, PEGylation does not affect Cyt_{degPEG} activity, as the modified protein retained 91±5% activity compared to native Cyt (see ESI section 2.3). Together, CD spectroscopy and the enzymatic activity assay confirm that neither protein structure nor activity is majorly affected by PEGylation.

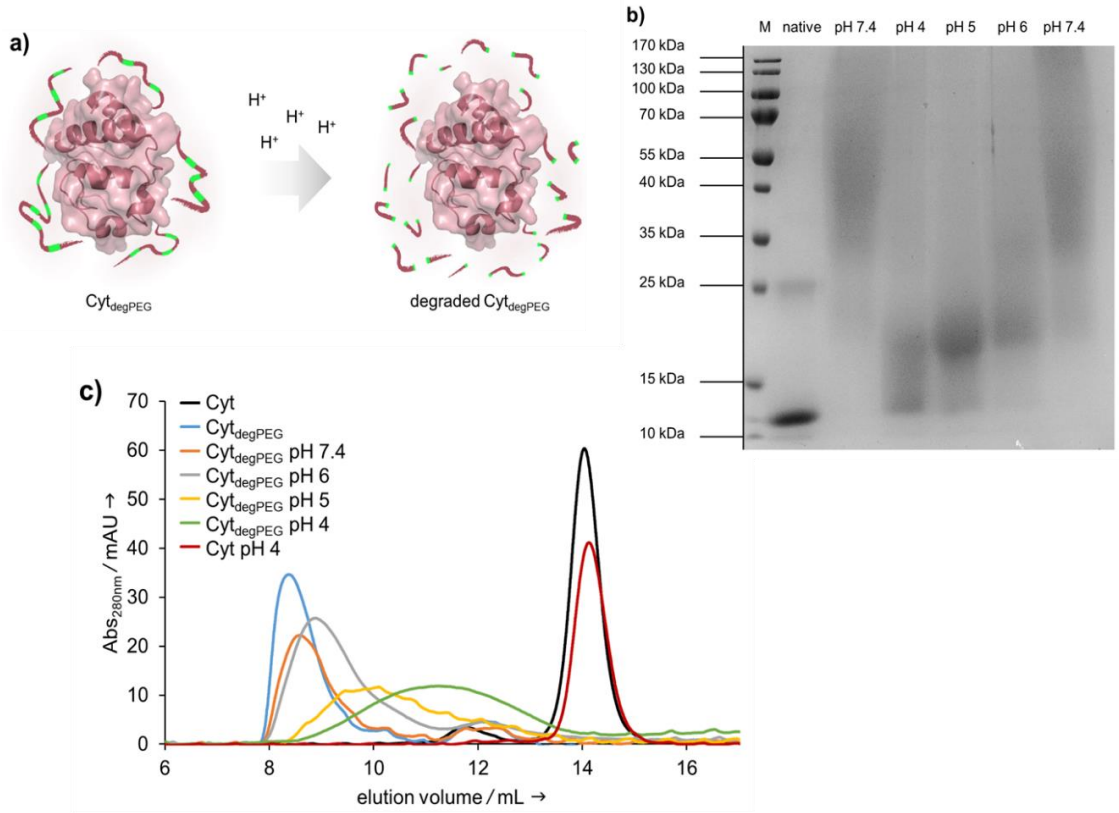

Figure 4: a) Degradation of the vinyl ether moieties in the polyether backbone of Cyt_{degPEG} under acidic conditions; b) SDS-PAGE (15%) of Cyt (native) and Cyt_{degPEG} (left pH 7.4 lane) which were freshly dissolved in *dd*-H_2O. Cyt_{degPEG} was incubated at various pH values at 37 °C for 24 h and subsequently analysed through SDS-PAGE (pH 4, pH 5, pH 6 and pH 7.4); c) SEC analysis of freshly dissolved Cyt and Cyt_{degPEG} (black and blue curves) compared to Cyt_{degPEG} incubated at various pH values at 37 °C for 24 h. Native Cyt shows no change in elution volume when freshly dissolved or incubated at pH 4 for 24 h (black and red curves).

After the successful modification of Cyt, we investigated degradability of the attached PEG polymer (**Figure 4a**). For this, the Cyt_{degPEG} conjugate was dissolved in different acidic buffers, incubated at 37 °C for 24 h and characterised via SDS-PAGE. The incubation at pH 4 leads to nearly complete degradation of the polymer linked to the protein surface, as demonstrated by the down-shifted band on the gel, almost back to the same running height as the non-modified enzyme (**Figure 4b**). As expected, the increase in pH led to slightly reduced extents of PEG degradation. Nonetheless, even mildly acidic conditions at pH 6 were sufficient to induce a noticeable gel shift and thus PEG degradation. The Cyt-polymer conjugate is stable at neutral conditions (pH 7.4) during the incubation time of 24 h, there is no shift recognizable between freshly dissolved and incubated Cyt_{degPEG} in the SDS-PAGE (**Figure 4b**, left and right pH 7.4 lane). Efficient, pH-dependent PEG cleavage was further confirmed by SEC, where consecutively later elution volumes with samples incubated at increasing acidity are observed (**Figure 4c**).

2.2.3.3 NANOPARTICLE PREPARATION, DEGRADATION AND PAYLOAD RELEASE

For the nanoparticle preparation, we adapted a solvent evaporation method described previously.[22] Briefly, the surface modification of Cyt results in a solubility switch and allows the dissolution of Cyt_{degPEG} in dichloromethane. For the emulsion preparation, this solution was covered with an aqueous phase containing Oregon-Green™488-dextran (OGD) as a fluorescent model compound to test the loading efficiency and later the release under acidic conditions. After a first sonication step, additional PBS (pH 7.4) was added, and a second sonication step was carried out, resulting in an w/o/w emulsion. This entraps the hydrophilic payload OGD in the inner water droplet, which is surrounded by the DCM layer that contains the Cyt_{degPEG} particle material.

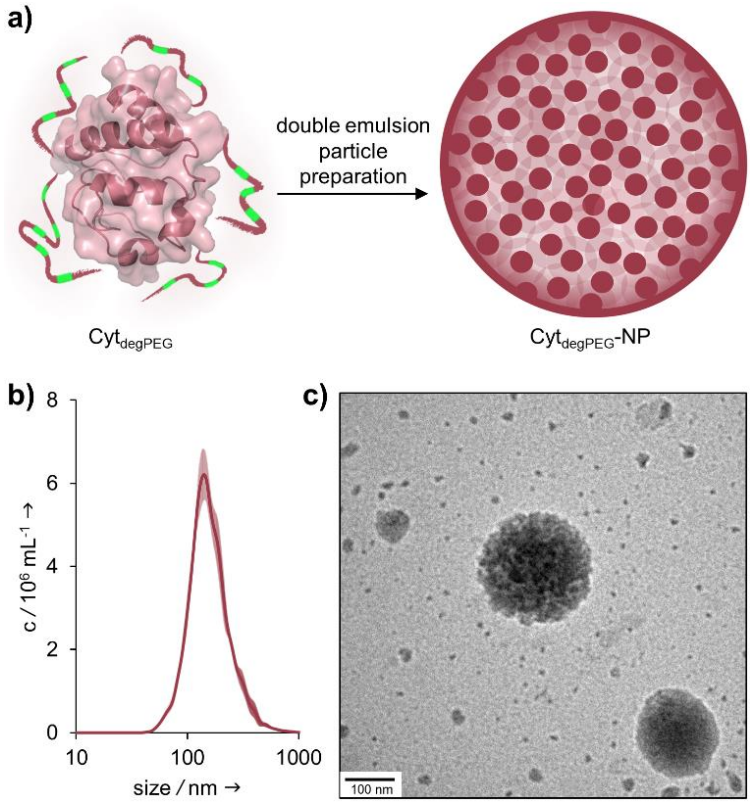

Figure 5: a) Schematic representation of Cyt$_{degPEG}$-NP preparation; b) NTA measurements of Cytd$_{egPEG}$-NP show a size around 140 nm; c) TEM image of Cytd$_{egPEG}$-NP.

Subsequent evaporation of the organic solvent leads to the formation of a particle suspension (Cyt$_{degPEG}$-NP) where the dehydrated PEGylated material forms a tight and stable network (ESI, **Figure S10**).

Free OGD was removed by dialysis. After purification, we determined an encapsulation efficiency of 50 % compared to the initial OGD feed (see ESI). The encapsulated OGD concentration was 2.41 μM (0.04 mol OGD per 1 mol particle material). This corresponds to a loading content of 1.72 wt% of OGD compared to the total weight of the nanoparticle material (see ESI section 3.1).

Nanoparticle tracking analysis (NTA) showed an average diameter of 140 nm for the particles, which was confirmed by transmission electron microscopy (TEM) measurements (**Figure 5b** and **5c**). The surface charge of the nanoparticles was analysed by ζ-potential measurements, showing nearly neutral Cyt$_{degPEG}$-NPs (-2 mV, see ESI

section 3.3). This is most likely a result of the PEGylation, which shields remaining amino acids on the surface of the individual enzymes.

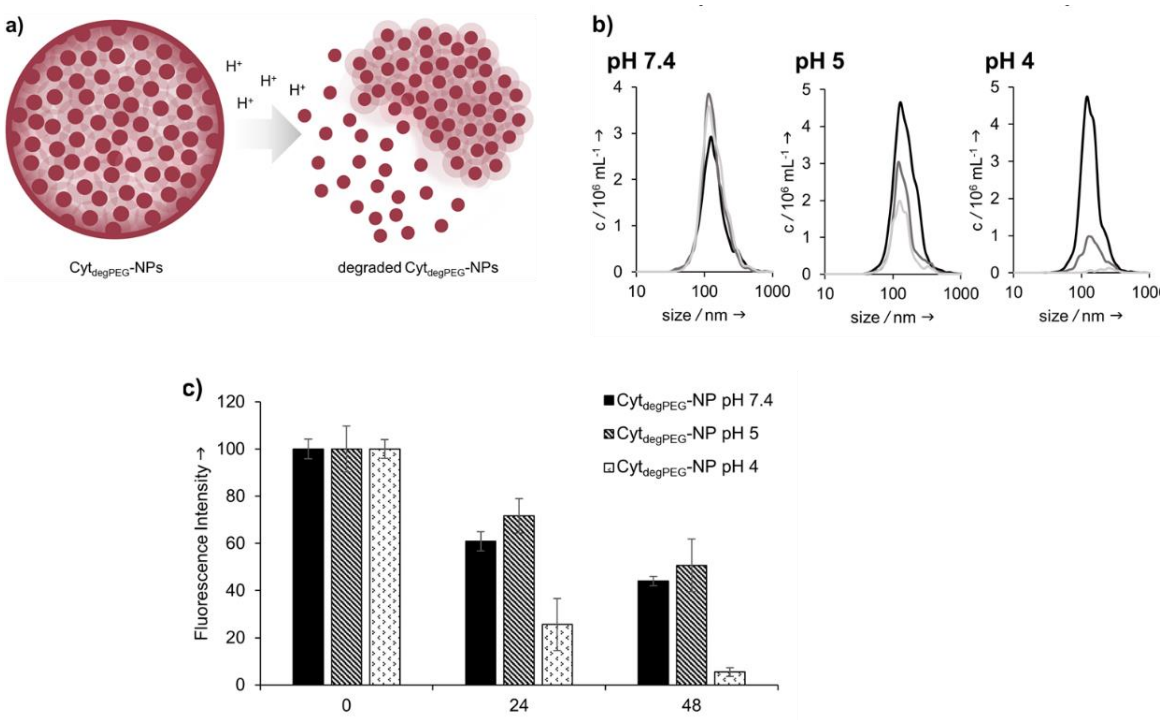

Figure 6: a) Cyt$_{degPEG}$-NP disassembly under acidic conditions; b) NTA and c) fluorescence measurements of Cyt$_{degPEG}$-NP degradation and OGD release over time. Purified particle suspensions were mixed with different buffers and dialysed against corresponding buffers. b) Particle size measurements (NTA curves) at pH 7.4, pH 5 and pH 4 at different time points of the dialysis experiment. (black curves: measurements directly after mixing the nanoparticles suspensions (0 h); grey curves: after 24 h; light grey curves: after 48 h); c) Fluorescence measurement of the nanoparticle suspension at different time points of the dialysis experiment and under various pH conditions. The lower the bars, the more fluorescent payload was released due to the disassembly of the particle system.

Our particles are designed to be stable at neutral pH values but should degrade in an acidic environment due to the intrinsic cleavability of the vinyl ether moieties of the PEG conjugates. This results in the cleavage of the majority of the PEG material with only very small non-degradable PEG segments remaining on the surface of the protein. With this, the protein regains its native hydrophilic solubility, and the individual hydrophobic protein assemblies are broken up, i.e. the overall particle complex falls apart (**Figure 6a**).

We monitored the particle degradation in a dialysis experiment. For this purpose, nanoparticle suspensions were mixed with different buffers (pH 4, 5 and pH 7.4) and dialysed against corresponding buffers at 37 °C. Particle degradation and OGD release was analysed over time with NTA (**Figure 6b**) and fluorescence measurements (**Figure 6c**).

Nanoparticles incubated in neutral buffer are stable over a period of 48 h, as can be seen in the concentration of particles over time in NTA measurements (**Figure 6b**). At pH 5 the concentration of particles decreased by 50% after 48 h, and at pH 4 almost no particles are visible at the end of the experiment.

Looking at the OGD release over time, it can be seen in the fluorescence measurements (**Figure 6c**) that both at pH 7.4 and pH 5 some of the payload is released. This is most likely due to passive diffusion, which is common for hydrophilic payloads, as reported previously.[22] However, at pH 4, a clear difference in fluorescence intensity can be seen at 24 and 48 h, due to the full disassembly of the particles and the active OGD release.

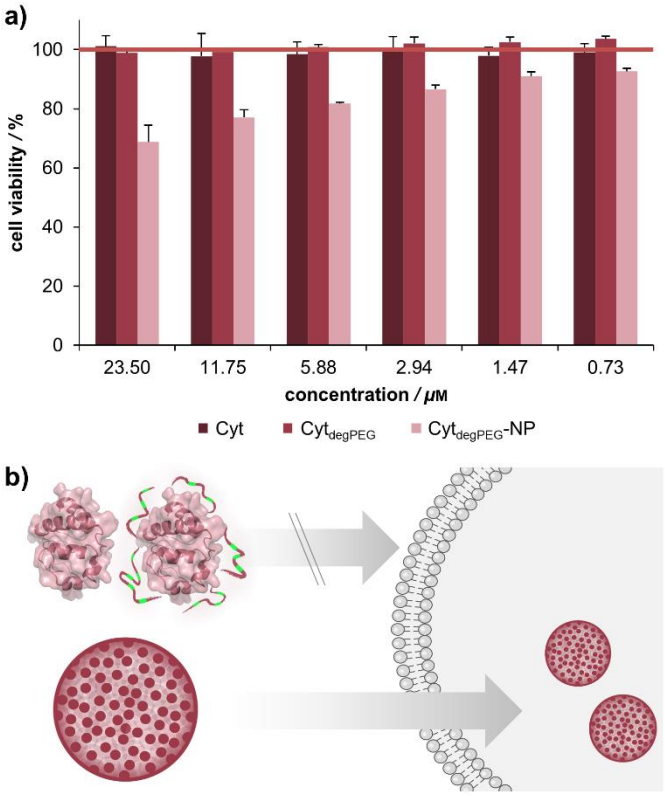

Figure 7: a) Results of cell viability tests using HeLa cells after incubation with native Cyt (dark red), Cyt$_{degPEG}$ (red) and Cyt$_{degPEG}$-NP (light red) in concentrations ranging from 0.73—23.50 μM incubated for 48 h. b) MTT results indicate that native Cyt and Cyt$_{degPEG}$ show no membrane permeability, unlike Cyt$_{degPEG}$-NPs which can be taken up by cells, most likely by endocytic pathways.

For biological applications, the effect of our nanoparticles on human cells needs to be determined. We thus analysed the toxicity of the Cyt$_{degPEG}$ material and the nanoparticles on HeLa cells (**Figure 7a** and ESI section 3.5). The cells were incubated with native Cyt, Cyt$_{degPEG}$ and Cyt$_{degPEG}$-NPs. Native Cyt and the Cyt$_{degPEG}$ material show no toxicity (**Figure 7a**). It has been previously reported,that native Cyt cannot cross the cell membrane.[31] The result of the MTT-assay indicates that this is also the case for Cyt$_{degPEG}$. In contrast, Cyt$_{degPEG}$-NPs are most likely taken up by cells by an endosomal pathway which results in a lower cell survival with increasing material concentrations. This can be explained by the high amount of Cyt in the cytosol of the cells where it can perform its native function. Physiologically, Cyt is part of the intrinsic apoptotic pathway in the cytosol since it binds the protease-activating factor-1 (APAF1) which is

part of the apoptosome.[29] Therefore, our results indicate that the PEG-conjugates are also cleaved *in vitro*, and the unobstructed enzymes might initiate to some extent apoptosis. Future experiments will focus on the detailed analysis of the particle uptake, protein pathways and the remaining enzymatic activity.

2.2.4 CONCLUSIONS

We introduce a degradable PEG copolymer that shows intrinsic acid-degradability and can be used for the PEGylation of proteins. The degradability is achieved by the incorporation of vinyl ether moieties into the backbone of PEG. These groups are acid-cleavable at physiologically relevant pH values. Relying on this degradable polyether structure, we developed a new class of pH-responsive protein nanoparticles using surface-modified cytochrome *c*. The PEGylation renders our model protein soluble in organic solvents while preserving its activity and secondary structure. This approach should in principle be feasible for any protein of choice. Using a mild emulsion-based method we successfully prepared nanoparticles that are stable at pH 7.4 but can degrade and disassemble at mildly acidic conditions, as can be found in endolysosomal compartments, tumour environments or inflamed tissue.

Introducing responsiveness into these protein nanoparticles not only allows for a triggered release of therapeutic payloads, but also almost completely recovers the initial protein starting material. The first *in vitro* results indicate that the underlying enzymatic activity of the particle system might be as important as the payload itself. Hence, for future nanomedicine applications, we envision a combined utilization of drug delivery and material activity.

2.2.5 EXPERIMENTAL

Copolymerization of mP(EG$_{81}$-*co*-EPB$_6$). In a flame dried Schlenk flask, sodium hydride (15 mg, 0.62 mmol) and triethylene glycol monomethyl ether (253 mg, 1.54 mmol) were dissolved in benzene (5 mL) and dry THF (5 mL), stirred under slightly reduced pressure at 60 °C for 30 min and subsequently dried in high vacuum for 16 h. The resulting initiator was dissolved in dry DMSO (7 mL) and dry THF (3 mL, stored over sodium). To this solution, ethylene oxide (5 mL, 110 mmol) was cryo-transferred using a graduated ampule. EPB (1.21 mL, 18.5 mmol, dried over CaH and freshly distilled) was added via syringe and the polymerization was carried out for 5 days at room temperature. After quenching (3 mL Methanol), dialysis was performed against methanol for 24 h (MWCO 1000 Da) and the polymer dried in high vacuum. (Yield 70%) 1H NMR (400 MHz, $DMSO_{d6}$) δ [ppm] 5.72 (ddd, 5.51H, $^3J_{AB}$ = 17.2 Hz, $^3J_{AB}$ = - 10.5 Hz, $^3J_{AB}$ = 6.7 Hz, -C*H*=CH_2), 5.26 (m, 11.41H, $^3J_{AB}$ = 17.2 Hz, $^3J_{AB}$ = 2.1 Hz, $^3J_{AB}$ = 1.1 Hz, -CH=H*H*), 4.76 (q, 0.44H, *J* = 6.7 Hz, C=C*H*-CH_3 (*E* isomer)), 4.57 (bs, 0.77H, O*H*), 3.96–3.87 (m, 7.38H, C*H*O-CH=CH_2, OCH_2-C=CH-CH_3 and CH_2O-C=CH-CH_3), 3.71–3.35 (m, 336H, CH_2O), 3.24 (s, 3H, O-CH_3), 1.52 (d, 1.35H, *J* = 6.7 Hz, C=CH-CH_3 (*E* isomer)).

Isomerization of mP(EG$_{81}$-*co*-*iso*EPB$_6$). mP(EG$_{81}$-*co*-EPB$_6$) (500 mg) was dissolved in DMSO (0.5 mL) and degassed by 3 freeze-pump-thaw cycles. $RhCl(PPh_3)_3$ (20 mg, 0.022 mmol) and BHT (3 mg) were added under argon atmosphere and the resulting solution was stirred at 80 °C for 24 h. Subsequently, the polymer was twice precipitated in acetone/diethylether (50/50 vol%) and dried in high vacuum. (Yield 90%) ^{1}H NMR (400 MHz, $DMSO_{d6}$): δ [ppm] 4.77 (q, 2.47H, *J* = 6.7 Hz, C=C*H*-CH_3 (*E* isomer)), 4.65 (q, 1.84H, *J* = 6.7 Hz, C=C*H*-CH_3 (*E* isomer)), 4.57 (bs, 0.45H, O*H*), 3.99–3.88 (m, 14H, C*H*O-CH=CH_2, OCH_2-C=CH-CH_3 and CH_2O-C=CH-CH_3), 3.71–3.35 (m, 314H, CH_2O), 3.24 (s, 3H, O-CH_3), 1.61 (d, 5.56H, *J* = 6.7 Hz, C=CH-CH_3 (Z isomer)), 1.52 (d, 7.46H, *J* = 6.7 Hz, C=CH-CH_3 (*E* isomer)).

Functionalization to mP(EG$_{81}$-*co*-*iso*EPB$_6$)-NHS. To a solution of mP(EG$_{81}$-*co*-*iso*EPB$_6$) (300 mg, 0.075 mmol) in dioxane (2 mL) *N,N´*-hydroxysuccinimide carbonate (192 mg, 0.75 mmol, dissolved in 2 mL DMF) and DMAP (92 mg, 0.75 mmol, dissolved in 2 mL DMF) were slowly added via syringe. The resulting solution was stirred for 24 h at room temperature and subsequently precipitated three times in acetone/diethylether (50/50vol%). The obtained polymer was dried in high vacuum and stored routinely in a refrigerator at -20 °C. (Yield 85%) ^{1}H NMR (400 MHz, DMSO$_{d6}$): δ [ppm] 4.77 (q, 2.40H, J = 6.7 Hz, C=C*H*-CH$_3$ (*E* isomer)), 4.65 (q, 1.78H, J = 6.7 Hz, C=C*H*-CH$_3$ (*Z* isomer)), 3.99–3.88 (m, 14H, C*H*O-CH=CH$_2$, OC*H*$_2$-C=CH-CH$_3$ and C*H*$_2$O-C=CH-CH$_3$), 3.71–3.35 (m, 317H, C*H*$_2$O), 3.24 (s, 3H, O-C*H*$_3$), 2.82 (s, 1.47h, -CO-C*H*$_2$-C*H*$_2$-CO-)1.61 (d, 5.53H, J = 6.7 Hz, C=CH-C*H*$_3$ (Z isomer)), 1.52 (d, 7.45H, J = 6.7 Hz, C=CH-C*H*$_3$ (*E* isomer)).

PEGylation of Cytochrome c. 5 mg horse heart cytochrome c (0.4 µmol) and 27.42 mg mP(EG81-co-isoEPB6)-NHS (6.9 µmol, 37% functionalized) were dissolved in 1 mL 0.1 m phosphate buffer pH 8.5 and stirred overnight at 4 °C. The mixture was purified by column chromatography (Sephadex® G-75 medium, Sigma Aldrich, buffer: dd-H2O). After collecting the first fraction yielding the product, the modified protein was concentrated with Amicon® Ultra 4 centrifugal filter membranes (regenerated cellulose, MWCO 10 kDa, 7500 x g, 10 min., 4 °C, Merck Millipore). The product was lyophilized (ALPHA 1-2 LD plus).

Activity of PEGylated Enzyme. The enzymatic activity of native Cyt, Cyt$_{degPEG}$ and Cyt$_{degPEG}$-NPs were analysed using an 2,2´-azinobis-(2-ethylbenzthiazoline-6-sulfonate (ABTS)-assay. 10 mm phosphate buffer pH 7.4 was used as working buffer. 100 μL of ABTS solution (2 mm) were mixed with 50 μL of samples (native Cyt or Cyt$_{degPEG}$, 22.6 μm) in a 96-well-microplate (flat bottom). The reaction was initiated by adding 50 μL of an H_2O_2 solution (2 mm in *dd*-H_2O). Subsequently, the change in absorption at 405 nm was measured for 3 minutes (Infinite® 200 PRO (Tecan) plate reader). The absorption

of the background (100 μL ABTS with 50 μL sample, but instead of H_2O_2 solution only 50 μL *dd*-H_2O) was subtracted from each measurement (see ESI section 2.3).

Analysis of Cyt_{degPEG} Degradation by SDS-PAGE. Cyt_{degPEG} was dissolved in 0.1 m sodium acetate buffer pH 4 or pH 5 or 0.1 m phosphate buffer pH 6 or pH 7.4 in concentrations of 8 mg/mL. These samples were incubated for 24 h at 37 °C and shaken with 1000 rpm. Native Cyt (1 mg/mL) and Cyt_{degPEG} (8 mg/mL) was freshly dissolved in *dd*-H_2O. 15 μL of the protein-solutions were denaturized by adding 5 μL of Roti®-Load 1 (Carl Roth) and heated in a boiling water bath for 15 min. The different samples were analysed with a 15% polyacrylamide gel (see ESI section 2.1).

Analysis of Cyt_{degPEG} Degradation by SEC. Cyt_{degPEG} was dissolved in a concentration of 150 μm in 0.1 m sodium acetate buffer (pH 4, pH 5) or in 0.1 m phosphate buffer (pH 6, pH 7.4). Similarly, native Cyt (150 μm) was dissolved in 0.1 m sodium acetate buffer pH 4 as control. These samples were incubated for 24 h at 37 °C and shaken at 1000 rpm. For comparison, native Cyt (150 μm) and Cyt_{degPEG} (150 μm) were freshly dissolved in *dd*-H_2O and measured directly. 150 μL of the protein-solutions were analysed with size exclusion chromatography. The SEC runs were performed on a 24 mL high-resolution size exclusion column (Superdex™ 75 10/300 GE Healthcare Bio-Sciences AB) at 4 °C with a flow rate of 0.8 mL in PBS pH 7.4.

Nanoparticle Preparation by Double Emulsion. Cyt_{degPEG} (2.75 mg) was dissolved in 0.4 mL DCM. After adding 50 μL Oregon-Green™488-dextran (OGD) solution (10 kDa dextran, 2 mg/mL in PBS pH 7.4), the two phases were sonicated on ice for 15 s. To the resulting emulsion 2 mL of ice-cold PBS buffer (pH 7.4) was added and treated again with ultrasonic pulses for 30 s. The DCM of the w/o/w emulsion was evaporated by stirring at RT overnight, resulting in an opaque nanoparticle suspension.

Nanoparticle Degradation and OGD Release. The degradation of Cyt_{degPEG}-NP and the release of OGD under acidic conditions was analysed using a dialysis experiment. OGD-loaded Cyt_{degPEG}-NP were freshly prepared and purified by dialysis (Float-a-Lyzer®G2 Dialysis Device, MWCO 100 kDa, Spectrum Labs) for 4 h to remove not encapsulated OGD. The particles were then mixed in a 1:1 ratio with either 0.1 m sodium acetate buffer pH 4, 0.1 m sodium acetate buffer pH 5 or PBS pH 7.4 as control. 100 µL of these mixtures were dialysed (Xpress Micro Dialyzer MD100, MWCO 140 kDa, Serva) against the corresponding buffer mix (1:1 mix of 0.1 m sodium acetate buffer pH 4 and PBS pH 7.4, 0.1 m sodium acetate buffer pH 5 and PBS pH 7.4 or PBS pH 7.4 alone) at 37°C. The particle degradation and OGD release were analysed by NTA size measurements (see ESI section 3.2) and a fluorescence readout (Ex: 490 nm, Em: 527 nm; Infinite® 200 PRO (Tecan) plate reader) over a period of 48 h. The data for the 0-hour value was measured directly after mixing of the nanoparticle suspension with the appropriate buffer.

2.2.6 ACKNOWLEDGEMENTS

We thank Prof. Dr. P. Besenius, Prof. Dr. T. Efferth and Prof. Dr. P. Langguth (all JGU Mainz, Germany), for the kind permission to use some of their analytical equipment. We also thank Dr. E. Berger-Nicoletti for the help with the MALDI-ToF measurements.

2.2.7 REFERENCES

1. A. Abuchowski, J. R. McCoy, N. C. Palczuk, T. van Es and F. F. Davis, *J. Biol. Chem.*, 1977, **252**, 3582-3586.

2. A. Abuchowski, T. Van Es, N. Palczuk and F. Davis, *J. Biol. Chem.*, 1977, **252**, 3578-3581.

3. S. N. S. Alconcel, A. S. Baas and H. D. Maynard, *Polym. Chem.*, 2011, **2**, 1442-1448.

4. P. Caliceti and F. M. Veronese, *Adv. Drug Delivery Rev.*, 2003, **55**, 1261-1277.

5. M. J. Roberts, M. D. Bentley and J. M. Harris, *Adv. Drug Delivery Rev.*, 2012, **64**, 116-127.

6. T. A. Wright, R. C. Page and D. Konkolewicz, *Polym. Chem.*, 2019, **10**, 434-454.

7. K. Knop, R. Hoogenboom, D. Fischer and U. S. Schubert, *Angew. Chem., Int. Ed.*, 2010, **49**, 6288-6308.

8. J. A. Rodríguez-Martínez, I. Rivera-Rivera, R. J. Solá and K. Griebenow, *Biotechnol. Lett.*, 2009, **31**, 883-887.

9. Y. Qi and A. Chilkoti, *Curr. Opin. Chem. Biol.*, 2015, **28**, 181-193.

10. M. Barz, R. Luxenhofer, R. Zentel and M. J. Vicent, *Polym. Chem.*, 2011, **2**, 1900-1918.

11. A. Grotzky, Y. Manaka, T. Kojima and P. Walde, *Biomacromolecules*, 2011, **12**, 134-144.

12. K. Maier and E. Wagner, *J. Am. Chem. Soc.*, 2012, **134**, 10169-10173.

13. C. G. Decker and H. D. Maynard, *Eur. Polym. J.*, 2015, **65**, 305-312.

14. A. Yurkovetskiy, S. Choi, A. Hiller, M. Yin, C. McCusker, S. Syed, A. J. Fischman and M. I. Papisov, *Biomacromolecules*, 2005, **6**, 2648-2658.

15. T. Steinbach, G. Becker, A. Spiegel, T. Figueiredo, D. Russo and F. R. Wurm, *Macromol. Biosci.*, 2017, **17**.

16. E. M. Pelegri-O'Day, N. M. Matsumoto, K. Tamshen, E. D. Raftery, U. Y. Lau and H. D. Maynard, *Bioconjugate Chem.*, 2018, **29**, 3739-3745.

17. M. Worm, D. Leibig, C. Dingels and H. Frey, *ACS Macro Lett.*, 2016, **5**, 1357-1363.

18. P. Lundberg, B. F. Lee, S. A. van den Berg, E. D. Pressly, A. Lee, C. J. Hawker and N. A. Lynd, *ACS Macro Lett.*, 2012, **1**, 1240-1243.

19. A.-K. Danner, D. Leibig, L.-M. Vogt and H. Frey, *Chin. J. Polym. Sci.*, 2019, DOI: 10.1007/s10118-019-2296-y.

20. C. Boyer, X. Huang, M. R. Whittaker, V. Bulmus and T. P. Davis, *Soft Matter*, 2011, **7**, 1599-1614.

21. K. DeFrates, T. Markiewicz, P. Gallo, A. Rack, A. Weyhmiller, B. Jarmusik and X. Hu, *International Journal of Molecular Sciences*, 2018, **19**.

22. E. Steiert, L. Radi, M. Fach and P. R. Wich, *Macromol. Rapid Commun.*, 2018, **39**, 1800186.

23. M. Fach, L. Radi and P. R. Wich, *J. Am. Chem. Soc.*, 2016, **138**, 14820-14823.

24. L. Radi, M. Fach, M. Montigny, E. Berger-Nicoletti, W. Tremel and P. R. Wich, *MedChemComm*, 2016, **7**, 1738-1744.

25. S. Ganta, H. Devalapally, A. Shahiwala and M. Amiji, *J. Controlled Release*, 2008, **126**, 187-204.

26. N. Vanparijs, R. De Coen, D. Laplace, B. Louage, S. Maji, L. Lybaert, R. Hoogenboom and B. G. De Geest, *Chem. Commun.*, 2015, **51**, 13972-13975.

27. L. Wang, L. Liu, B. Dong, H. Zhao, M. Zhang, W. Chen and Y. Hong, *Acta Biomaterialia*, 2017, **54**, 259-270.

28. A. J. Kresge, D. S. Sagatys and H. L. Chen, *J. Am. Chem. Soc.*, 1977, **99**, 7228-7233.

29. Y.-L. P. Ow, D. R. Green, Z. Hao and T. W. Mak, *Nature Reviews Molecular Cell Biology*, 2008, **9**, 532.

30. C. Y. Zheng, G. Ma and Z. Su, *Electrophoresis*, 2007, **28**, 2801-2807.

31. I. I. Slowing, B. G. Trewyn and V. S. Y. Lin, *J. Am. Chem. Soc.*, 2007, **129**, 8845-8849.

2.2.8 SUPPORTING INFORMATION

Materials

Cytochrome *c* from horse heart [EC 232.700.9] was purchased from SERVA Electrophoresis GmbH, Germany. Sodium hydride (NaH), Triethylene glycol monomethyl ether (mTEG), Benzophenone, *trans*-2-[3-(4-*tert*-Butylphenyl)-2-methyl-2-propenylidene]malononitrile (DCTB), Calcium hydride (CaH_2), dioxane, dimethylformamide (DMF), dichloromethane, benzene, tetrahydrofuran (THF), methanol, *N,N´*-Disuccinimidyl carbonate (NHS-DSC), coomassie brilliant blue G, thiazolyl blue tetrazolium bromide (MTT), Dulbecco's modified eagle medium (DMEM) GlutaMAX™, phosphate buffered saline (PBS), hydrogen peroxide solution 30 % were purchased from Sigma-Aldrich, St. Louis. Ethylene oxide (EO) was purchased by Air Liquide, Germany. Dimethyl sulfoxide (DMSO) was purchased from Acros, Germany. Ammonium persulfate (APS), Roti®-Load 1, Rotiphorese® Gel 30 were purchased from Carl Roth, Germany. Tetramethylethylenediamine (TEMED) was purchased from VWR, Germany. 2,2´-azinobis-(2-ethylbenzthiazoline-6-sulfonate (ABTS) and Epoxy butadiene (EPB) were purchased from Alfa Aesar, Germany. The PageRuler Prestained Protein Ladder for SDS-PAGE and Oregon-Green™ 488 dextran (10 kDa) were purchased from Thermo Scientific, Germany. Fetal calf serum (FCS), glutamine, phosphate buffered saline (PBS, for cell culture), pyruvate and penicillin/streptomycin were purchased from Invitrogen. Spectra/PORTM dialysis membranes regenerated cellulose (RC) tubing molecular weight cut-off (MWCO) 1000 Da were purchased from Spectrum Labs. DMSO-d6 was purchased from Deutero GmbH, Germany. All chemicals were used as received without further purification unless stated otherwise. All used organic solvents were purchased from different suppliers and distilled once prior use.

Analytical Instrumentation

^{1}H NMR and spectra were measured using a Bruker AMX400 spectrometer (256 Scans, and B-ACS 60 auto sampler) at 296 K. 2D NMR and ^{13}C NMR spectra were measured on a Bruker Avance II 400 (100.5 MHz, 5 mm BBO probe, and B-ACS 60 auto sampler) at 296 K. All spectra were processed with MestReNova v12 software and referenced internally to residual proton signals of the deuterated solvent. Size exclusion chromatography (SEC) data were obtained using Agilent 1100 Series equipped with PSS HEMA-columns (106/104/102 Å porosity) using DMF with 1 g/L LiBr as an eluent and RI detection. Polydispersity indices (Đ = Mw/Mn) were determined with monodisperse linear PEG standards from Polymer Standard Service GmbH (PSS). MALDI-ToF analysis was performed using an rapifleXTM MALDI-TOF/TOF equipped with a 10 kHz scanning Smartbeam 3D Laser (Nd:YAG at 355 nm) and 10 bit 5 GHZ Digitizer. Analysis was performed in reflectormode positive for polymer and in linear mode positive for protein and protein-PEG conjugates. DCTB was used as matrix and dichloromethane as solvent for polymer samples and sinapic acid as matrix and CH_3CN/H_2O 1/1 as solvent was used for protein and protein-PEG conjugates.

Polymer Synthesis

2D NMR spectra of P(EG-*co*-EPB) and P(EG-*co-iso*EPB) were already reported in a previous publication.[1]

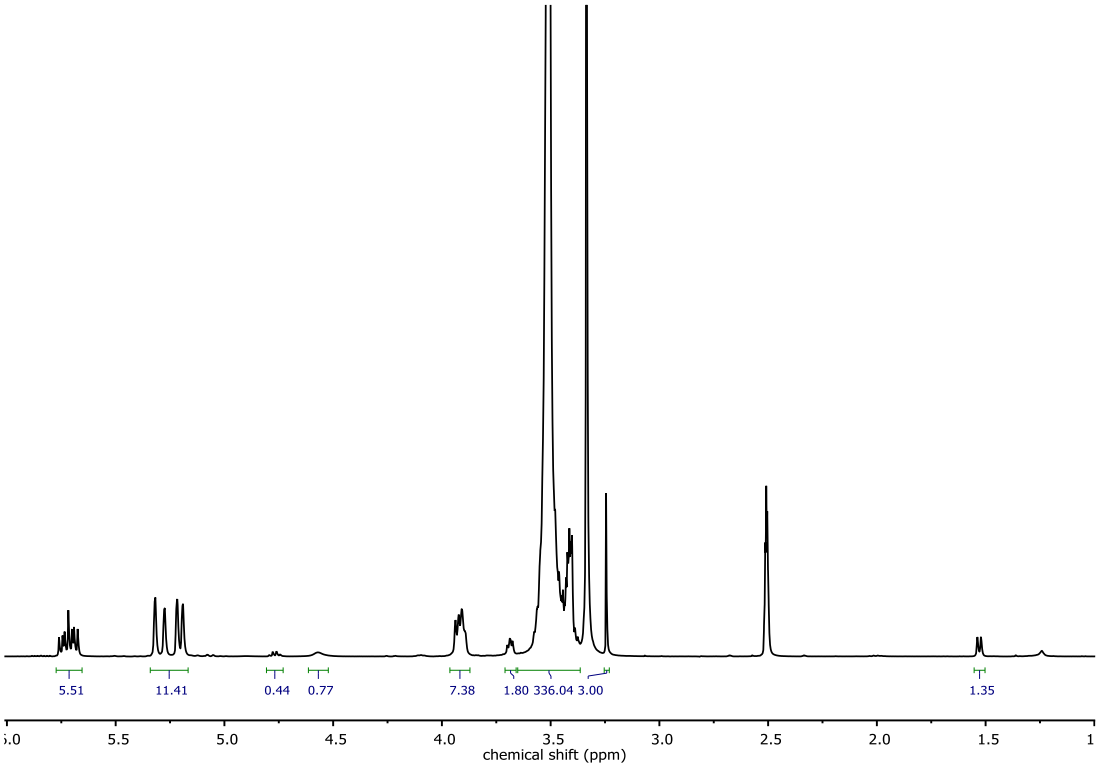

Figure S1: ^{1}H NMR spectrum (400 MHz, DMSO-d_6) of mP(EG$_{81}$-*co*-EPB$_6$).

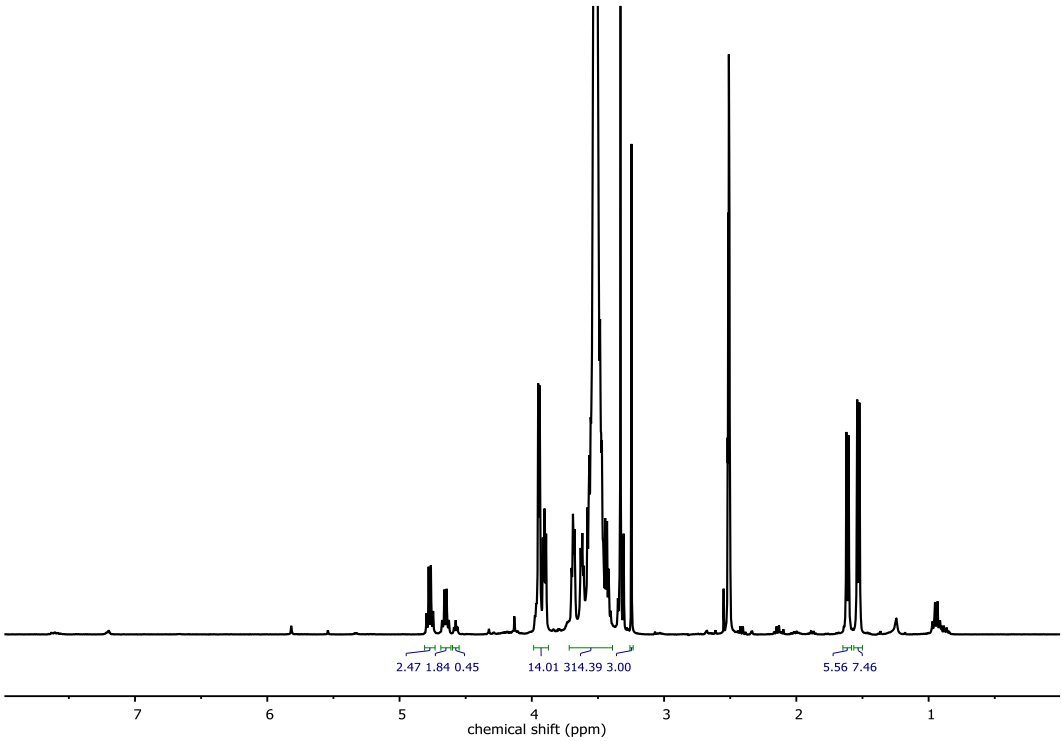

Figure S2: ^{1}H NMR spectrum (400 MHz, DMSO-d_6) of mP(EG$_{81}$-*co-iso*EPB$_6$).

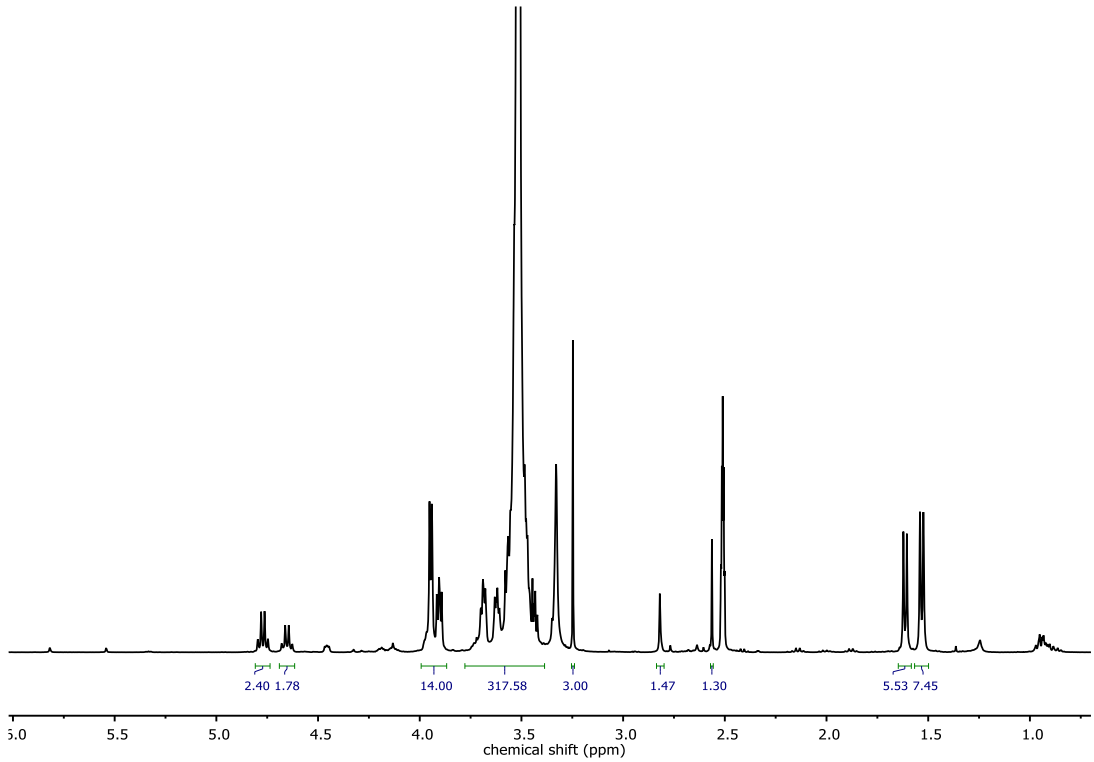

Figure S3: ^{1}H NMR spectrum (400 MHz, DMSO-d_6) of mP(EG$_{81}$-*co*-*iso*EPB$_6$)-NHS.

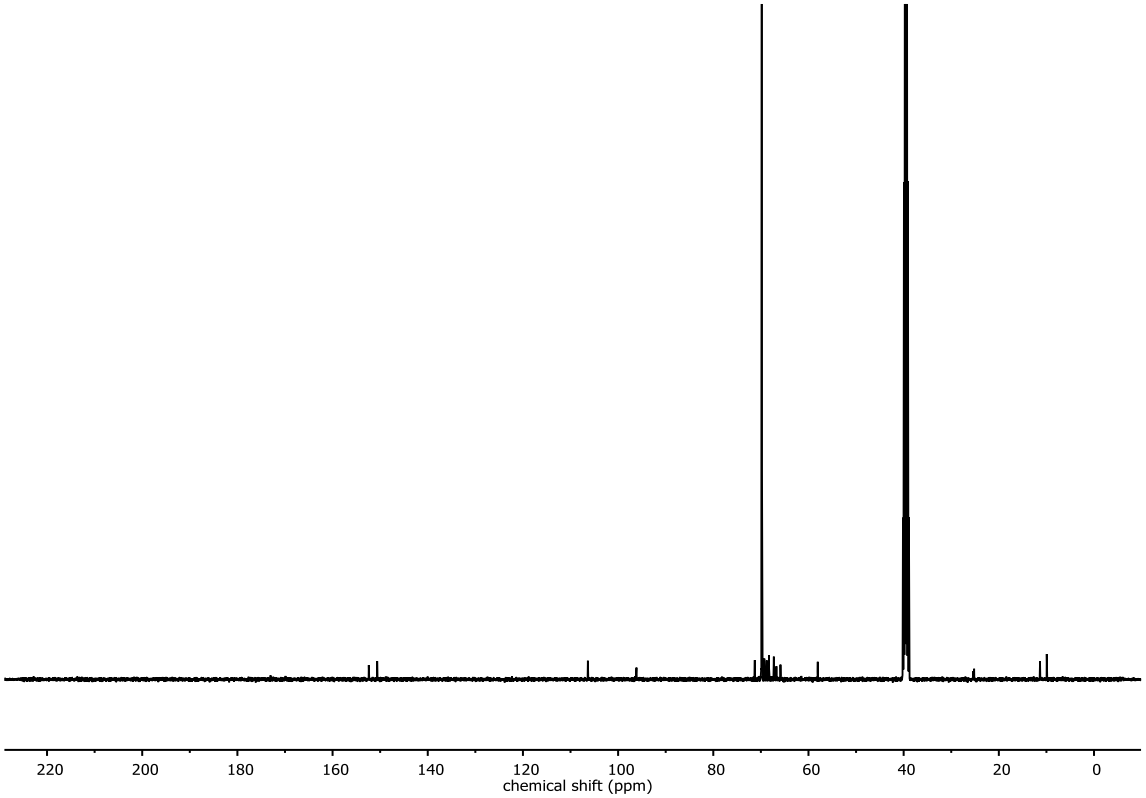

Figure S4: ^{13}C NMR spectrum (400 MHz, DMSO-d_6) of mP(EG$_{81}$-*co*-*iso*EPB$_6$)-NHS.

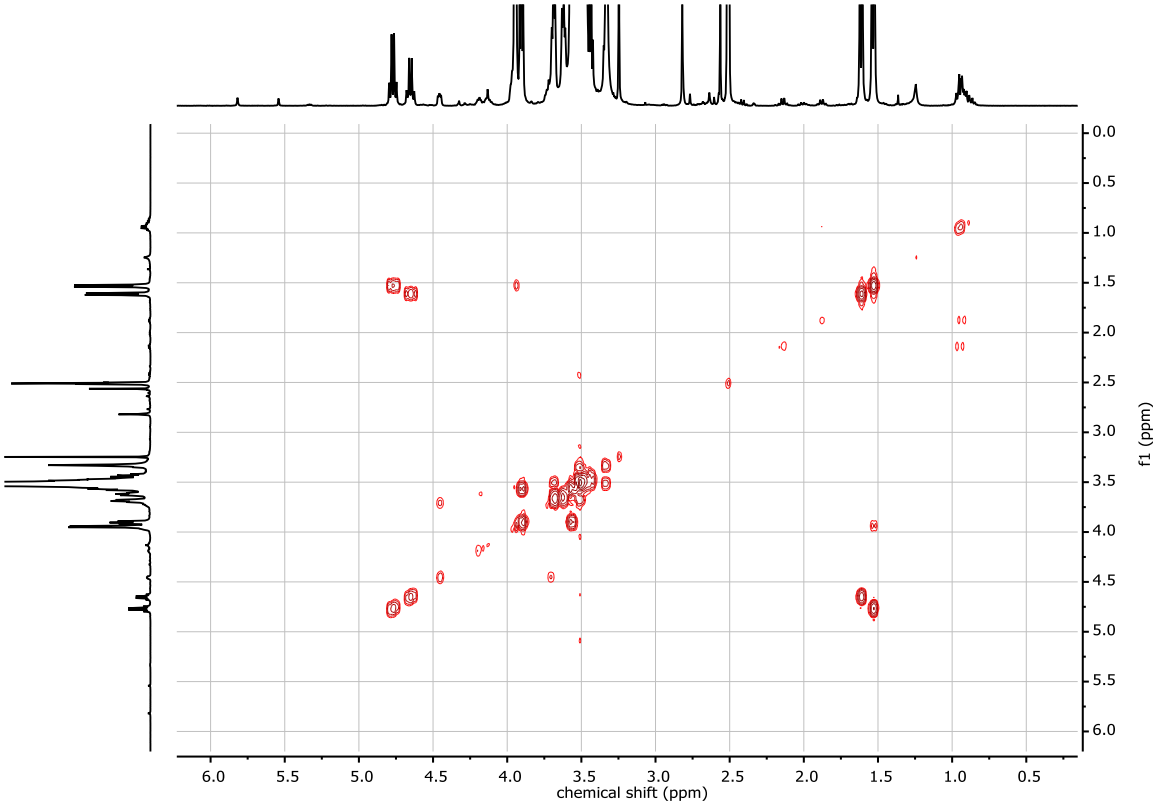

Figure S5: COSY NMR spectrum (400 MHz, DMSO-d_6) of mP(EG_{81}-*co*-*iso*EPB_6)-NHS.

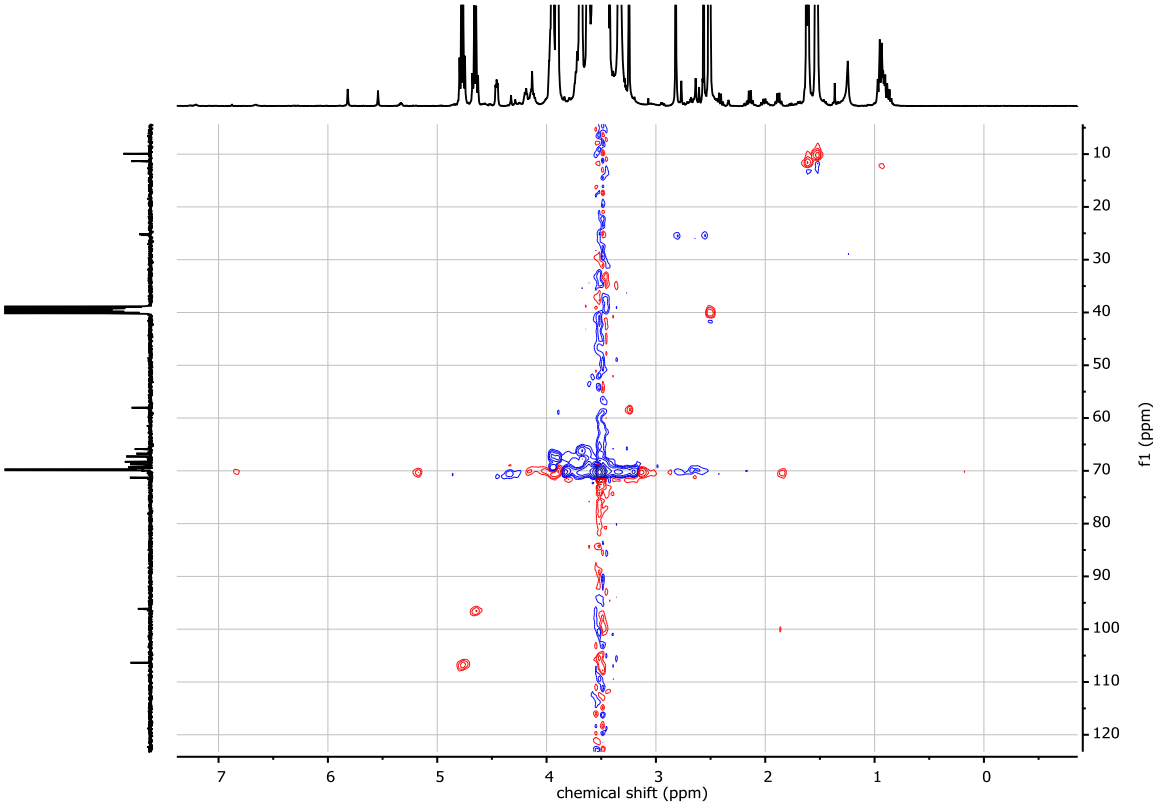

Figure S6: HSQC NMR spectrum (400 MHz, DMSO-d_6) of mP(EG_{81}-*co*-*iso*EPB_6)-NHS.

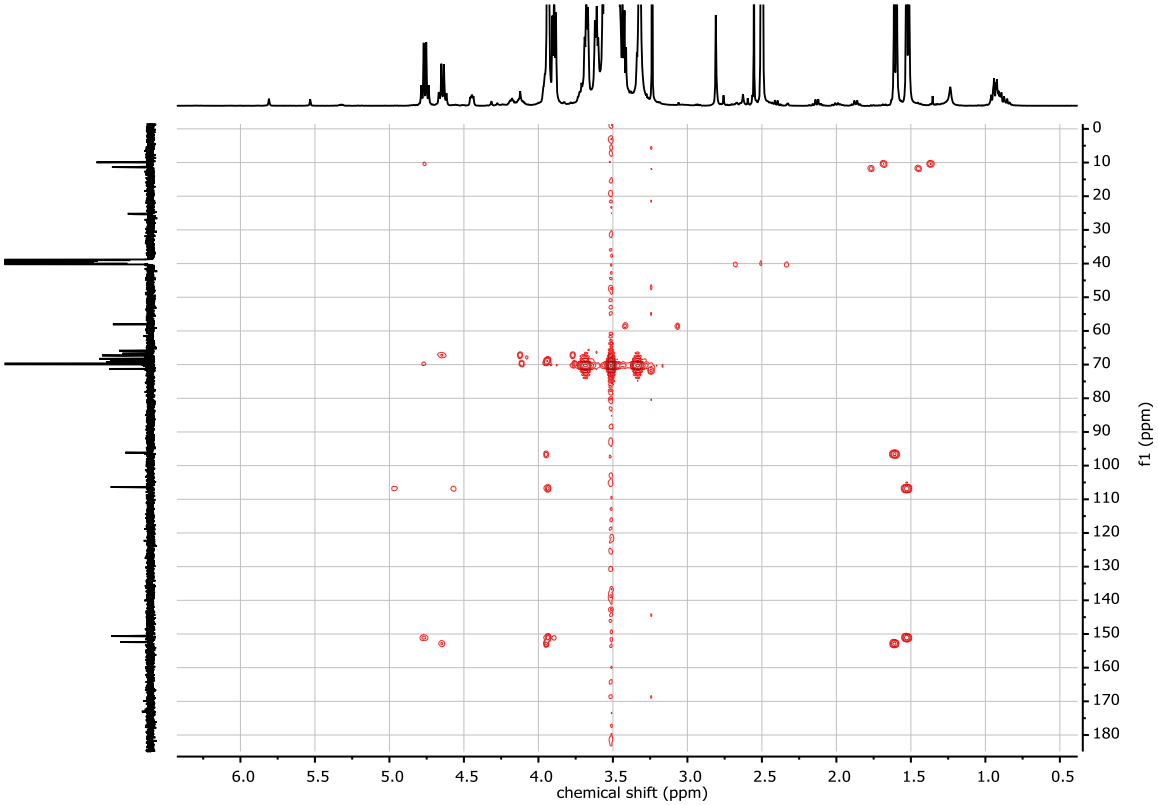

Figure S7: HMBC NMR spectrum (400 MHz, DMSO-d_6) of mP(EG_{81}-*co*-*iso*EPB_6)-NHS

.

Protein Modification and Analysis

SDS-PAGE

The protein analysis by SDS-PAGE was performed like described elsewhere.[2] A 15% polyacrylamide gel (Rotiphorese® 30 gel mix) with a thickness of 0.75 mm (T Spacer, Hoefer, USA) was prepared. Native cytochrome *c* (1 mg/mL) and Cyt_{degPEG} (8 mg/mL) were dissolved in water. Denaturation of 15 µL of the protein solutions were achieved by adding 5 µL of Roti®-Load 1 (Carl Roth) and heating in a boiling water bath for 15 min. These 20 µL mixtures were loaded into separated pockets of the gel and 5 µL of Pre-Stained Protein Ladder (10-170 kDa) was used as marker. After gel running at 90 V for 60 min, and 60 min at 200 V, the gel was stained with Coomassie Brilliant Blue G. The SDS-PAGE was imaged with FUSION PULSE TS (Vilber Lourmat Deutschland GmbH) and processed with the 'Image Master' assistant™ Software (camera filter 2).

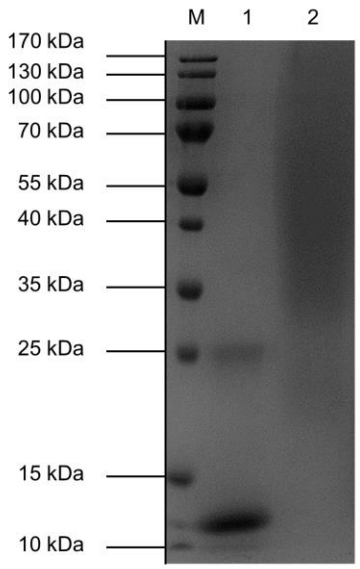

Figure S8: SDS-PAGE (15%) of cytochrome *c* (lane 1) and PEGylated cytochrome *c* (lane 2). Pre-Stained Protein ladder (10–170 kDa) was used as marker. 120 µg of the modified protein and 15 µg of the native cytochrome *c* were analyzed.

Circular Dichroism (CD)

Jasco J-815 Circular Dichroism spectrometer was used for CD measurements. These measurements were carried out in quartz cells with a path length of 1 mm and recorded at 20 °C using the Spectra Manager 2.08.04 software. Native cytochrome *c* and Cyt_{degPEG} were analyzed with concentrations of 0.1 mg/mL in 10 mm potassium phosphate/50 mm Na_2SO_4 pH 7 buffer. All data points were collected with a resolution of 0.1 nm and measurements were performed in triplets. The spectrum of the buffer was subtracted as background from each measurement. Secondary structure was determined with DichroWeb[3, 4] using the analysis program CONTIN (reference set 7[5]). The detailed comparison of secondary structure is in Table S2

Table S2: Calculated secondary structure elements for native Cyt and Cyt_{degPEG} (in %) by DichroWeb using CONTIN.

	Cyt	Cyt_{degPEG}
α-helix	64.4	63.1
β-sheet	3.9	2.5
turns	14.1	14.7
unordered	17.7	19.8

Enzymatic Activity

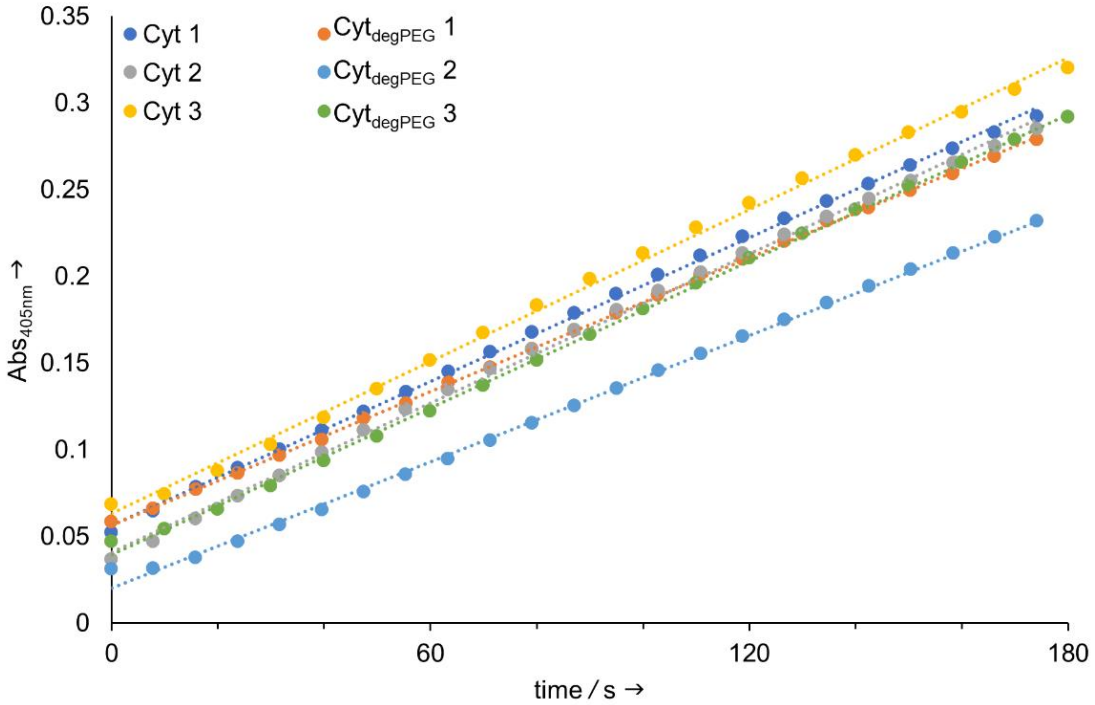

Figure S9: Results of the enzymatic activity assay of native Cyt compared to Cyt$_{degPEG}$ in three individual measurements. The dark blue, grey and yellow straights show the enzymatic activity of native lysozyme and the orange, light blue and green straight of Cyt$_{degPEG}$.

Table S3: Slopes of absorbance change at 405 nm over time of individual measurements. Through the mean of the three individual Cyt$_{degPEG}$ measurements we obtained 91.4±5.0 % of the initial enzymatic activity.

	slope · 10^{-3}	slope / %
Cyt 1	1.3827	100
Cyt$_{degPEG}$ 1	1.2852	92.95
Cyt 2	1.4332	100
Cyt$_{degPEG}$ 2	1.2147	84.75
Cyt 3	1.4615	100
Cyt$_{degPEG}$ 3	1.4119	96.61

Nanoparticle Preparation

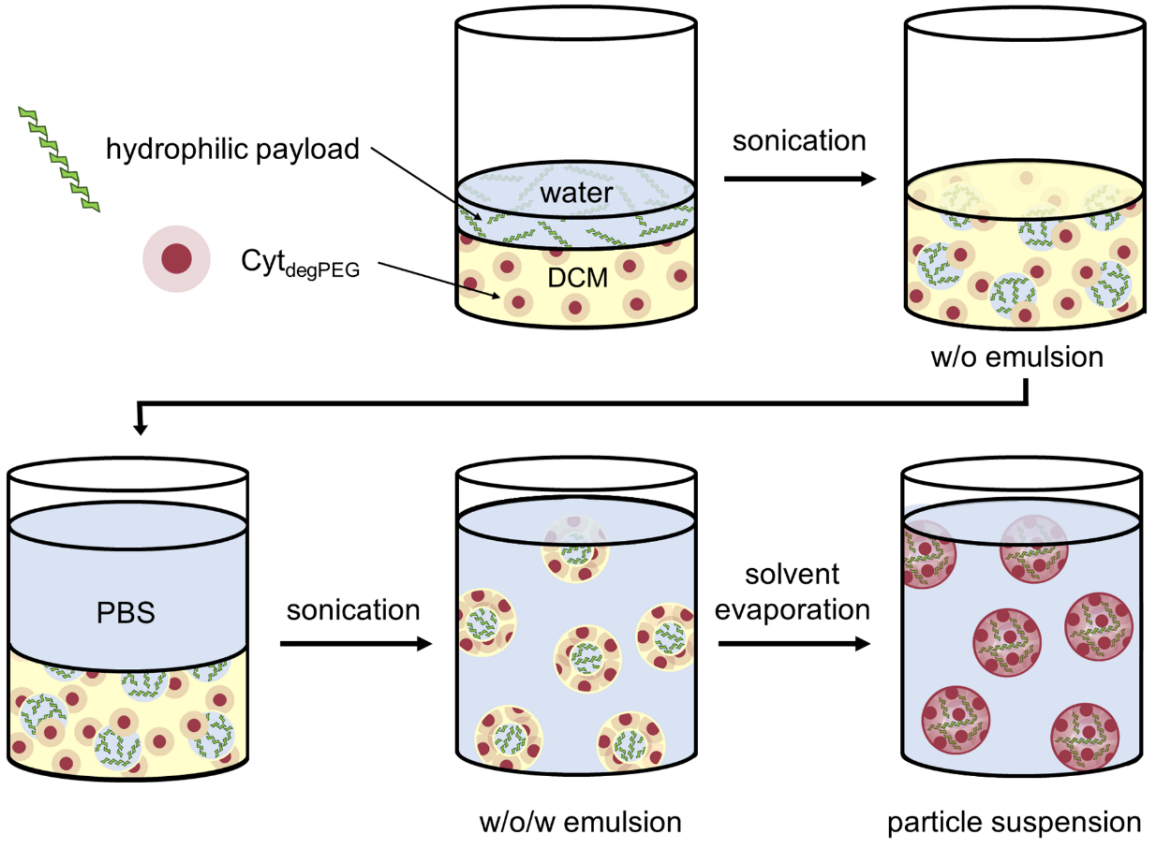

Figure S130: Nanoparticle preparation by double emulsion. Cyt$_{degPEG}$ is dissolved in DCM, covered with a small amount of water, containing the hydrophilic payload OGD. After sonication a w/o emulsion is obtained. Further addition of an aqueous phase and a second ultrasonic treatment results in a w/o/w emulsion. After DCM removal a stable nanoparticle suspension is obtained.

OGD Loading in Nanoparticles

After purification of the nanoparticle suspensions (Cyt$_{degPEG}$-NP) by dialysis (Float-a-Lyzer®G2 Dialysis Device, MWCO 100 kDa, Spectrum Labs) for 4 hours, the OGD content of the particles was determined by measuring the fluorescence (ex. 490 nm, em. 527 nm) of the particle suspension in comparison to an OGD standard in triplets of 100 μL using an Infinite® 200 PRO (Tecan) plate reader. The fluorescence of the background (PBS pH 7.4) was subtracted from each measurement.

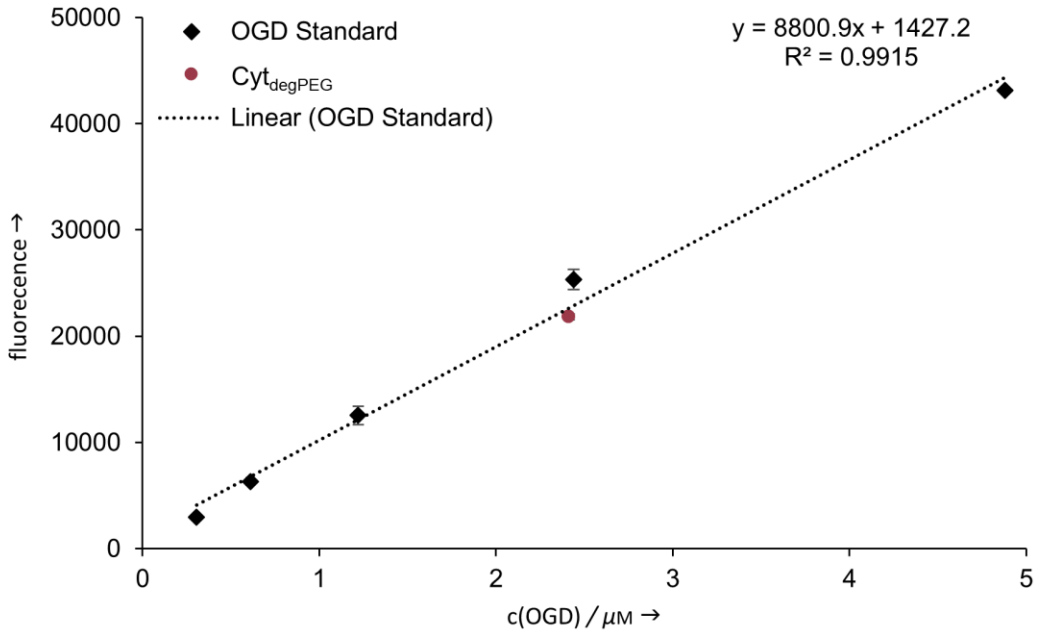

Figure S11: Determination of encapsulated OGD in CytdegPEG-NP (red dot) using OGD as standard (black squares). The amount of encapsulated OGD was determined to be 2.41±0.16 µm (24.13 µg/mL). The concentration of the particle material (CytdegPEG) is assumed to be the initial concentration which was used for the particle preparation (58.76 µm, 2.75 mg/mL). This results in a loading ratio of 0.04 mol OGD per 1 mol particle material (CytdegPEG).

The encapsulation efficiency (EE) and the loading content (LC) were calculated with equations S1 and S2.

$$\text{EE (mol\%)} = \frac{n_{OGD,encapsulated}}{n_{OGD,feed}} \cdot 100\% \qquad \text{(eq. S1)}$$

$$\text{LC (wt\%)} = \frac{m_{OGD,encapsulated}}{m_{OGD,encapsulated} + m_{CytdegPEG}} \cdot 100\% \qquad \text{(eq. S2)}$$

The encapsulated OGD was calculated with $n_{(OGD,encapsulated)}$ of 4.83 ± 0.32 nmol. The initial amount of $n_{(OGD,feed)}$ of the unpurified Cyt_{degPEG}-NP suspension was 9.76 nmol. This results in an encapsulation efficiency of 49.46 ± 3.23%.

The loading content (LC) was calculated with $m_{(OGD,encapsulated)}$ of 48.26 ± 3.15 µg ($n_{(OGD,encapsulated)}$ = 4.83 ± 0.32 nmol, $M_{(OGD,encapsulated)}$ = 10000 g/mol) and $m_{(CytdegPEG)}$ of 2.75 mg ($n_{(CytdegPEG)}$ = 117.52 nmol, $M_{(CytdegPEG)}$ = 23400 g/mol), which results in a loading content of 1.72 ± 0.11%.

Nanoparticle Tracking Analysis (NTA)

Nanoparticle Tracking Analysis (NTA) was performed on a NanoSight LM 14 equipped with a green laser (532 nm) and a marlin charged coupled device (CCD) camera. Samples were diluted (1:25) in appropriate buffers and loaded into the measurement cell. Movements of particles in the samples were recorded as videos for 30 seconds at 25 °C. The videos were analyzed with the NanoSight NTA 3.1 software showing the mean values of three individual measurements.

Zeta-Potential

ζ-potential measurements were performed with a Zetasizer Nano ZS instrument (Malvern). Three measurements with automatic measurement duration (between 10 and 100 runs) were performed. The refractive index (RI) of the dispersant (preset: water) was set to 1.330 and the viscosity to 0.8872 cP. The RI of the particles was set to 1.45 with a dielectric constant of 78.5. Cyt_{degPEG}-NPs were analyzed in a clear disposable folded capillary cell at 25 °C. The results are summarized in Table S4.

Table S4: ζ-potential measurement of Cyt_{degPEG} nanoparticles. Nanoparticles show a slightly negative ζ-potential due to the PEGylation of the surface amines on the proteins.

sample	ζ-potential (mV)
Cyt_{degPEG}-NP	-1.98 ± 0.21

Transmission Electron Microscopy (TEM)

Cyt_{degPEG}-NPs were drop-casted on a 300-mesh copper carbon grid from Plano GmbH for TEM measurements (5 μL). The image acquisition was done with a transmission electron microscope Tecnai T12 (FEI, acceleration voltage: 120 kV, electron source: LaB6 BIO-TWIN cathode) equipped with a 4K CCD camera (Tietz).

Toxicity of Protein Material and Nanoparticles (MTT-Assay)

HeLa cell lines were grown in Dulbecco's Modified Eagle Medium (DMEM) supplemented with 10% (v/v) fetal calf serum (FCS), 1% pyruvate and 1% penicillin/streptomycin. Cell incubations were performed in a humidified incubator at 37 °C with 5% CO_2 atmosphere. All used buffers were either autoclaved, sterile filtered or already sterile when supplied and were preheated to 37 °C. Cells were grown in 75 cm^2 or 25 cm^2 standard cell culture flasks.

Cells were seeded in 96 well plates with a density of $1.5 \cdot 10^4$ cells per well. After cell attachment overnight, the cell culture media was removed and 100 μL of different dilutions of the samples were added as triplets to the well plate. For this, native Cyt, Cyt_{degPEG} and Cyt_{degPEG}-NP were diluted with culture media to concentrations of 23.50–0.73 μm. After an incubation time of 48 h (37 °C, 5% CO2) a solution of 3-(4,5-dimethyl-2-thiazolyl)-2,5-diphenyl-2H-tetrazolium bromide (MTT) in medium (40 μL, 3.0 mg/mL) was added to each well and incubated for additional 30 min. After removal of the medium a mixture of DMSO (200 μL/well) and 0.1 m glycine buffer (25 μL/well, pH 10) was added. 50 μL of each well of this purple DMSO solution was added to fresh clear-bottom 96-well assay plate (Greiner Bio-One) containing a mixture of glycine buffer (17 μL/well, pH 10) and DMSO (133 μL/well). With an Infinite® 200 PRO (Tecan) plate reader the absorbance at 570 nm and 690 nm (background) were measured and the background was subtracted. The cell viability of sample treated cells were compared to untreated cells.

Further Literature

[1] M. Worm, D. Leibig, C. Dingels and H. Frey, *ACS Macro Lett.*, 2016, **5**, 1357-1363.

[2] U. K. Laemmli, *Nature* 1970, **227**, 680.

[3] L. Whitmore, B. A. Wallace, *Nucleic Acids Res.* 2004, **32**, W668.

[4] L. Whitmore, B. A. Wallace, *Biopolymers* 2008, **89**, 392.

[5] N. Sreerama, R. W. Woody, *Anal. Biochem.* 2000, **287**, 252.

3 Alternative routes to vinyl ether PEGs

3.1 Predefined Cleavage Sites in Degradable Polymers Installed via Statistical Copolymerization: How reactivity ratios determine the Fragment distribution

Johannes Ewald,[1,2] Jan Blankenburg,[1,3] Holger Frey[1,]*

[1]Department of Chemistry, Johannes Gutenberg University, Duesbergweg 10-14, 55128 Mainz, Germany

[2]TransMed Mainz Research School of Translational Biomedicine

[3]Graduate School Materials Science in Mainz, Staudinger Weg 9, 55128 Mainz, Germany

to be submitted

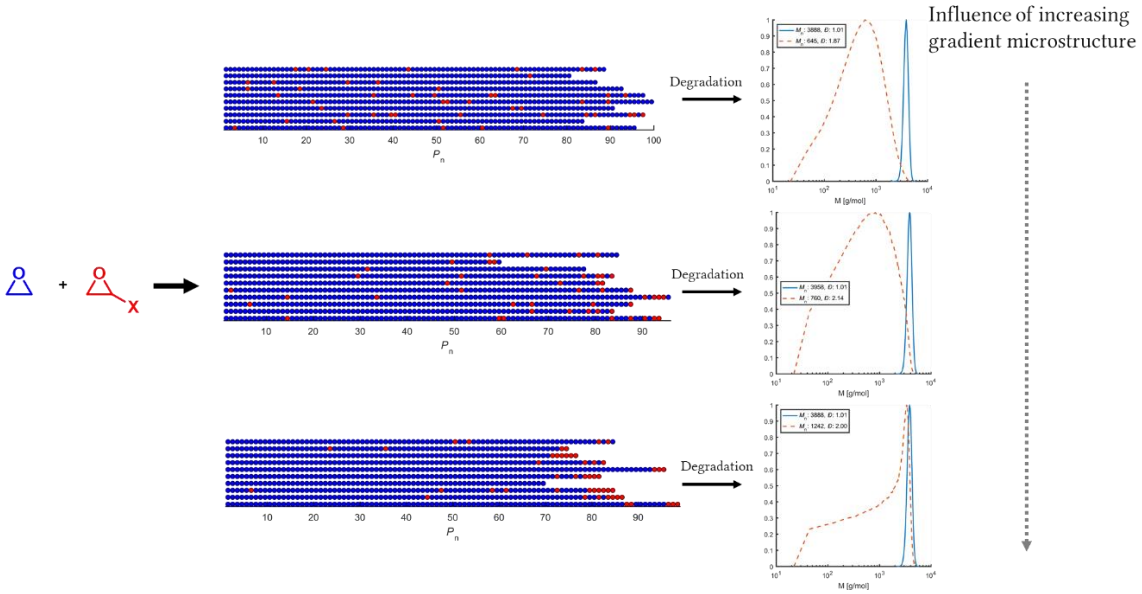

3.1.1 ABSTRACT

We present a novel approach to acid labile, vinyl ether functional poly(ethylene glycol) (PEG). By classical anionic ring-opening (co)polymerization (AROP) of ethylene oxide (EO) with ethoxyethyl glycidyl ether (EEGE) and subsequent post-polymerization modification, methylene ethylene oxide (MEO) moieties at the polyether backbone (P(EG-*co*-MEO)) were obtained. The copolymers were hydrolytically degraded and the influence of the comonomer fraction and their distribution on the size and dispersity of the fragments was analysed *via* SEC. Copolymers with molecular weights of approximately M_n = 4,000 g mol^{-1} and M_n = 8,000 g mol^{-1}, 6 mol% and 11 mol% EEGE content and low dispersities ($Đ \leq 1.12$) were obtained, subsequently modified and hydrolysed. The size of the fragments was found to range between M_n = 560 g mol^{-1} and M_n = 930 g mol^{-1} (depending on the comonomer content), with moderate dispersities of $Đ$ = 1.54 – 1.67. Using a Monte Carlo simulation, (i) ideally random, (ii) slightly tapered and (iii) strongly gradient copolymer microstructures were simulated, based on parameters from several experimental copolymerization examples. These copolymers were degraded *"in silico"* and the size of the resulting fragments was analysed, showing a loss of control of the fragment size distribution with increasing gradient of the microstructure.

3.1.2 INTRODUCTION

The cleavage and programmed degradation of polymer chains can be a crucial feature for various biomedical applications. For example, polymer-based drug delivery systems or hydrogels as scaffolds for tissue engineering require cleavage of the polymer chains to release entrapped therapeutic molecules or to ensure degradation of temporary scaffold structures.[1] Although poly(ethylene glycol) (PEG) is commonly known as the "gold standard" of polyethers in biomedical applications and has already seen extensive use for decades, the chemically inert backbone lacks degradability under physiological conditions, thus the polymers have to be excreted through the kidneys when applied in the body.

While the non-degradability can be overcome by the synthesis of degradable PEGs, an important and usually undervalued aspect is the size of PEG fragments after degradation. Nevertheless, this is highly relevant, as PEGs with a molecular weight of M_n < 400 g mol^{-1} were reported to exhibit toxic effects.[2] This molecular weight limit is of particular importance for safe application of degradable PEGs. Most applications rely on PEG chains that exceed this lower limit, however this limit is especially relevant for PEG fragments after degradation.[3] This highlights the significance of techniques to introduce cleavable moieties in a defined and tailorable fashion to minimize possible toxic effects. Controlling the fraction and position of predefined cleavage sites alongside the polymer backbone is of crucial relevance, as microstructure, i.e. gradient vs. random directly affects the size of the polymer fragments formed.

Among the numerous approaches to introduce cleavage sites into the polyether backbone of PEG that have been developed so far, vinyl ethers are the most promising functional group to achieve this particular goal. As reported by our group, intrinsically cleavable vinyl ether containing PEGs combine fast hydrolysis kinetics already at pH 5 with excellent stability at pH 7.4 as well as under dry conditions for storage.[4,5] Adequate

stability is an essential characteristic not only for long-term storage, handling and application-specific chemical modification of these materials. It is also substantial to prevent undesired and preliminary cleavage of the polymer backbone during the designated application, as long as the specific stimulus is absent (e.g. on the way to the targeted tissue or cellular compartment). On the other hand, fast hydrolysis kinetics is required to ensure degradation within a reasonable timeframe in the place of action, triggered by a specific stimulus. This unique combination of superb stability and fast hydrolysis kinetics with physiologically relevant pH values as a trigger mechanism renders vinyl ether containing PEGs promising candidates for various biomedical applications.

The general principle of introducing vinyl ethery moieties into the backbone of PEG was initially demonstrated by Lynd et al. in 2012.[4] The copolymerization of ethylene oxide (EO) with epichlorohydrin (ECH) *via* monomer-activated anionic ring-opening polymerization and subsequent elimination of the chloride was performed to obtain poly[(ethylene glycol)-*co*-(methylene ethylene oxide)] (P(EG-*co*-MEO)) with acid-labile vinyl ether sites distributed in the polyether chain. However, these copolymers exhibit a rather broad molecular weight distribution ($Đ$ = 1.25 – 1.34) and ill-defined end groups as a result of the monomer-activated polymerization technique. As recently shown by Danner *et al.,* this copolymerization also results in a strong gradient copolymer microstructure (r_{EO} = 9.2, r_{ECH} = 0.1), giving a non-random distribution of cleavage sites along the polymer backbone as well as a broad molecular weight distribution of the fragments formed after cleavage.[6]

Another promising leaving group-containing epoxide monomer besides ECH is glycidyl tosylate (GlyTs), which was recently copolymerized by our group *via* monomer-activated anionic ring-opening polymerization.[7] The obtained series of copolymers with EO or propylene oxide (PO) P(EG-*co*-GlyTs) and P(PO-*co*-GlyTs) were

utilized in various post-polymerization modifications by nucleophilic substitution of the excellent tosylate leaving groups. The monomer-activated copolymerization of EO and GlyTs results in rather high dispersities ($Đ$ = 1.50 – 1.70) and a slight gradient copolymer microstructure as well (r_{EO} = 2.2, r_{GlyTs} = 0.45), as was demonstrated by SEC and *in situ* NMR kinetics studies.

Both ECH and GlyTs copolymers with EO have to be synthesized *via* monomer-activated technique.[8] They share the same disadvantages that are characteristic for this polymerization technique, as mentioned above. The copolymerization of EO with ECH or GlyTs *via* conventional anionic ring-opening (co)polymerization (AROP) is not possible because of the highly nucleophilic nature of the alkoxide initiator and the active chain end, which would result in a nucleophilic substitution of the chloride or tosylate, respectively. The established AROP of EO and 3,4-epoxy-1-butene (EPB) followed by subsequent isomerization of the allyl ether moieties to vinyl ethers is another suitable pathway to install vinyl ether containing PEG copolymers.[5] These materials have already been demonstrated to possess promising potential for biomedical applications, e.g. for degradable PEG hydrogels.[9,10] However, this copolymerization also results in a weak gradient copolymer microstructure (r_{EO} = 2.8, r_{EPB} = 0.35).

To the best of our knowledge, no approach has been reported so far that combines the favourable properties of polyether copolymers obtained *via* classical AROP, such as tailorable molecular weight and comonomer content, low dispersity and well-defined polymer end groups, with randomly distributed predefined vinyl ether cleavage sites in the polyether backbone.

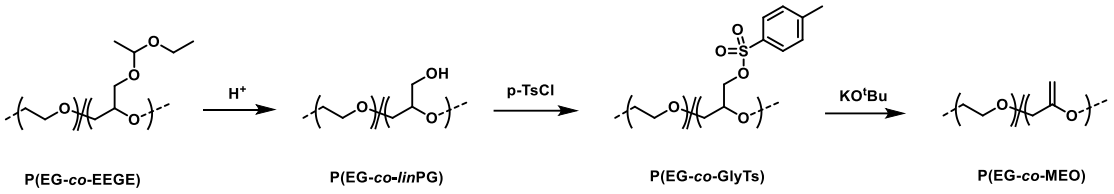

Scheme 1: Copolymerization of EEGE and subsequent tosylation and elimination as a route to introduce vinyl ether moieties into the backbone of PEG.

In this work we present a novel approach to vinyl ether containing PEGs that relies on the established AROP. The post-polymerization modification of P(EG-*co*-EEGE), a random copolymer (r_{EO} = 1.05, r_{EEGE} = 0.94) that is accessible *via* conventional AROP, gives access to P(EG-*co*-GlyTs) with a random copolymer microstructure and after subsequent elimination leads to vinyl ether containing P(EG-*co*-MEO) (**Scheme 1**).[11] By cleavage of the acetal protecting groups of P(EG-*co*-EEGE) and transformation of the hydroxyl groups of the resulting linear polyglycerol copolymer P(EG-*co*-*lin*PG) to excellent leaving groups like tosylates, vinyl ether moieties can be generated *via* simple elimination. Using this approach, we obtained a series of copolymers with narrow molecular weight distributions ($Đ \leq 1.12$) and targeted molecular weights in the range of M_n = 4,000 g mol^{-1} to M_n = 8,000 g mol^{-1} with a comonomer content of 6 mol% and 10 mol%, respectively. These copolymers were subsequently modified to vinyl ether containing PEGs, while maintaining the low dispersity. Additionally, we investigated in an experimental study the influence of the comonomer content on the fragment size and dispersity after degradation. These values were compared to different copolymer microstructures that were degraded in an *"in silico"* simulation.

3.1.3 RESULTS AND DISCUSSION

3.1.3.1 SYNTHESIS AND DEGRADATION OF P(EG-*co*-MEO) COPOLYMERS

All copolymers were synthesized *via* classical AROP in THF and subsequently transformed by common post-polymerization reactions as shown in **Scheme 1** and **2.** The copolymerization of EO with EEGE and deprotection of the copolymer was initially described by Mangold *et al.* in 2010.[12] To demonstrate the versatility of this approach and the control over molecular weight and comonomer content, a series of copolymers was synthesized according to the first step presented in **Scheme 2**.

3.1.3.1.1 Polymer Synthesis and Characterization

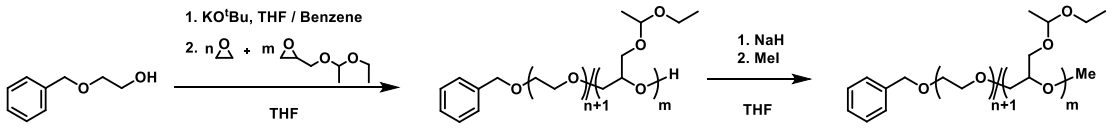

Scheme 2: Copolymerization of P(EG-*co*-EEGE) and methylation of the terminal hydroxyl group.

To prevent undesired side reactions at the chain end of the polymers, the terminal hydroxyl group of all samples was transformed to a chemically inert methoxy group *via* methylation. The key characterization data for these polymers is summarized in **Table 1**.

2-(Benzyloxy)ethanol was used as an initiator to allow for the determination of the molecular weight and comonomer content *via* ^{1}H NMR spectroscopy. A series of copolymers with molar fractions between 6 mol% and 11 mol% and molecular weights slightly exceeding M_n = 4,000 g mol^{-1} and M_n = 8,000 g mol^{-1} were obtained, as determined *via* ^{1}H NMR spectroscopy (**Figure S1–4**).

Table 1: Characterization data for P(EG-*co*-EEGE) copolymers.

	EEGE^{theo} / mol%	EEGE^{a} / mol%	M_n^{theo} / g mol^{-1}	M_n^{a} / g mol^{-1}	M_n^{b} / g mol^{-1}	$Đ^{b}$ = M_w / M_n
P(EG$_{82}$-*co*-EEGE$_5$)	5	6	4,000	4,290	3,390	1.08
P(EG$_{152}$-*co*-EEGE$_{10}$)	5	6	8,000	8,210	5,820	1.12
P(EG$_{76}$-*co*-EEGE$_8$)	10	9	4,000	4,500	3,460	1.07
P(EG$_{129}$-*co*-EEGE$_{17}$)	10	11	8,000	8,110	5,790	1.10

[a]Determined *via* ^{1}H NMR spectroscopy, [b]determined *via* SEC (RI detector, DMF, PEG standards)

These results are in good agreement with the targeted values for the molar content of EEGE of 5 mol% and 10 mol% and the targeted molecular weights of M_n = 4,000 g mol^{-1} and M_n = 8,000 g mol^{-1}, respectively.

The molecular weights determined *via* SEC in DMF using PEG standards show a significant deviation from the targeted values, an effect that can be explained by the different hydrodynamic radii of the copolymers compared to the PEG standards. Copolymers with narrow molecular weight distributions and low dispersities ($Đ \leq 1.12$) were obtained, as is shown in **Figure S25**. Detailed NMR and SEC data can be found in the Supporting Information.

3.1.3.1.2 Post-Polymerization Reactions and Degradation

After blocking the terminal ω-hydroxyl group, linear polyglycerol copolymers P(EG-*co*-*lin*PG) were obtained after subsequent cleavage of the acetal protecting group of EEGE. Quantitative cleavage of the acetal protecting groups was confirmed *via* ^{1}H NMR spectroscopy, as no characteristic acetal signals (4.66 ppm) and methyl proton signals belonging to the ethoxyethyl groups (1.10 ppm) were found anymore

(**Figure S5-8**). The deprotection was carried out in a very convenient way by stirring the copolymer solution in DCM/MeOH 1:1 (v/v) over an ion exchange resin and subsequent removal of the ion exchange resin by filtration. These results are in full accordance with literature.[12]

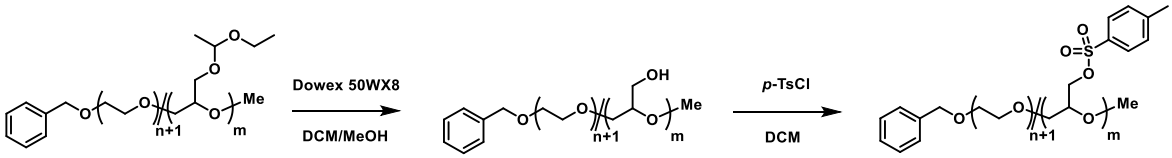

Scheme 3: Cleavage of the acetal protecting groups of P(EG-*co*-EEGE) and subsequent tosylation of P(EG-*co*-*lin*PG).

The hydroxyl groups were converted into tosylate groups by the straightforward reaction with *p*-toluenesulfonyl chloride (*p*-TsCl) in DCM (**Scheme 3**), resulting in the corresponding P(EG-*co*-GlyTs) copolymers. To prevent undesired side reactions, the polymers were purified and analysed after every step during the post-polymerization modification.

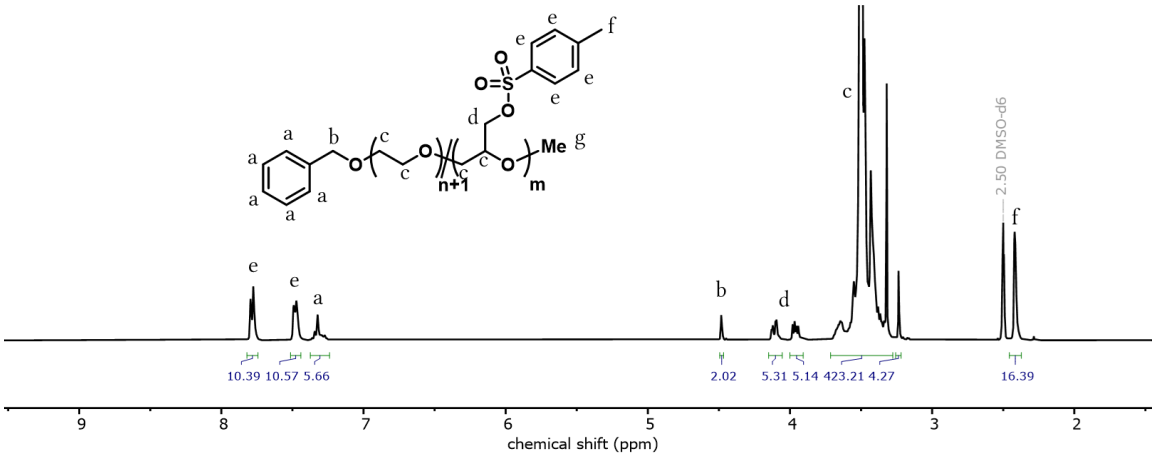

Figure 1: ^{1}H NMR spectrum (400 MHz, DMSO-d_6) of P(EG$_{82}$-*co*-GlyTs$_5$).

Figure 1 demonstrates for the P(EG$_{82}$-*co*-GlyTs$_5$) copolymer that the *lin*PG moieties were quantitatively transformed into glycidyl tosylates, as determined from ^{1}H NMR spectroscopy. The integration of the new aromatic signals at 7.78 ppm and 7.42 ppm as well as the new signals at 4.10 ppm and 3.98 ppm, characteristic for glycidyl tosylates, is congruent with the expected values. Dialysis was necessary for the purification of the copolymers, as sufficient separation from the excess of *p*-toluenesulfonyl chloride was

not possible by precipitation – neither using pure cold diethyl ether nor a mixture of acetone/diethyl ether 1:1 (v/v) as a non-solvent.

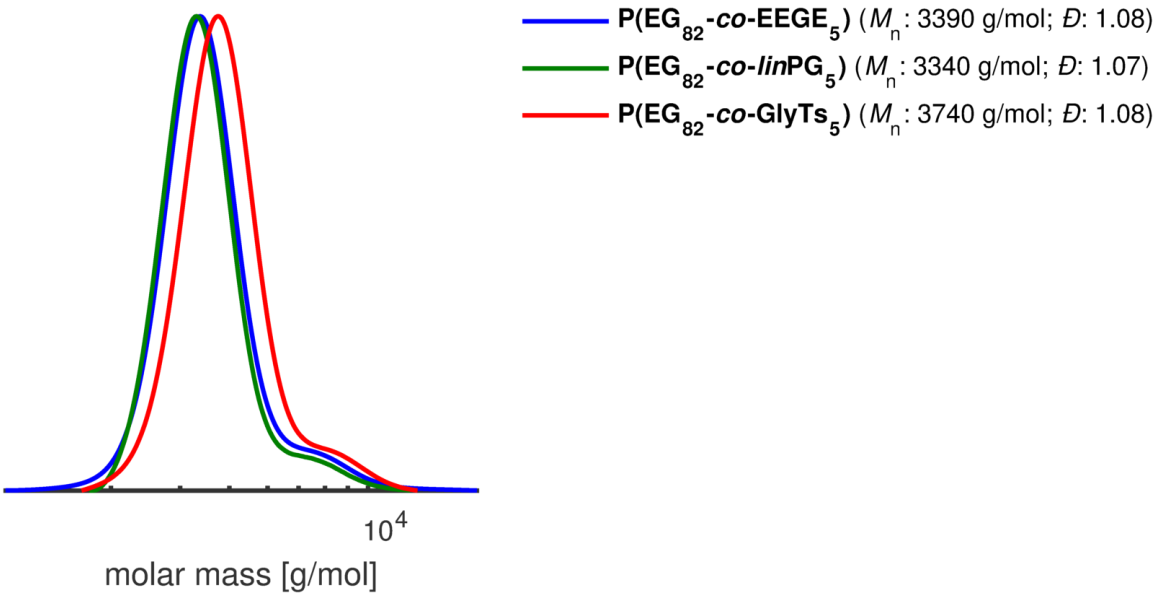

Figure 2: SEC traces (RI detector, solvent DMF, PEG standards) of P(EG$_{82}$-*co*-EEGE$_5$), P(EG$_{82}$-*co*-linPG$_5$) and P(EG$_{82}$-*co*-GlyTs$_5$) copolymers.

The SEC traces of P(EG$_{82}$-*co*-EEGE$_5$) before and after cleavage of the acetal groups and after subsequent tosylation are shown in **Figure 2**. There is no significant difference between the acetal-protected and deprotected form of the copolymers (blue and green lines). After tosylation, the average molecular weight increases significantly (red line), due to the addition of the relatively bulky tosylate groups to the copolymer backbone. As SEC only refers to hydrodynamic radii, the effect of increasing molecular weight upon tosylation could only be qualitatively illustrated, but not quantitatively analysed.

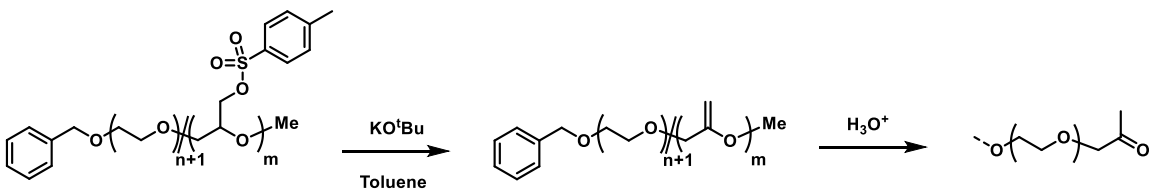

Scheme 4: Elimination of P(EG-*co*-GlyTs) to obtain P(EG-*co*-MEO) and subsequent hydrolysis of the vinyl ether moieties.

The final transformation of P(EG-*co*-GlyTs) to P(EG-*co*-MEO) is shown in **Scheme 4**. It can be monitored by ^{1}H NMR spectroscopy, as demonstrated for

P(EG$_{82}$-*co*-MEO$_5$) in **Figure 3**. After the elimination step, no other aromatic proton signals can be found, except for the signals assigned to the benzyl group of the initiator.

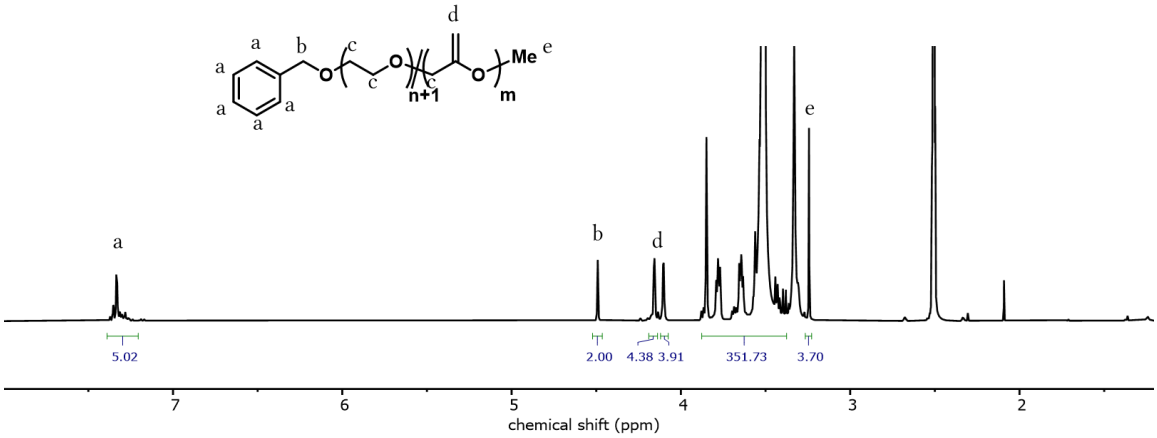

Figure 3: ^{1}H NMR spectrum (400 MHz, DMSO-d_6) of P(EG$_{82}$-*co*-MEO$_5$).

Instead, very distinctive signals for vinyl ethers appear at a chemical shift of 4.16 ppm and 4.11 ppm. The integral of these signals and the absence of characteristic aromatic proton signals support quantitative transformation of the glycidyl tosylate moieties into vinyl ethers and the successful separation from the resulting potassium tosylate salt.

As shown in **Figure 4** for P(EG$_{82}$-*co*-GlyTs$_5$), the SEC traces of the copolymers after the elimination reaction show no unwanted preliminary cleavage of the copolymers.

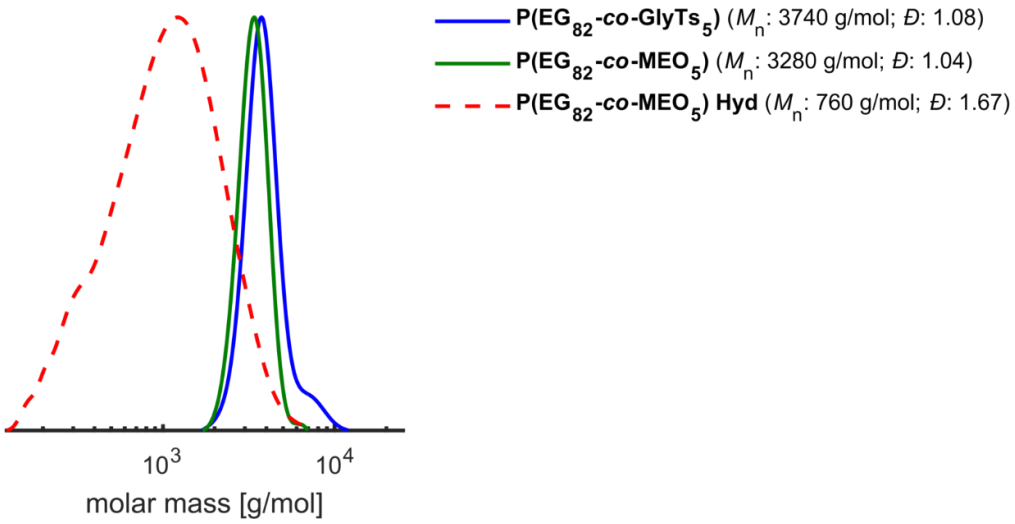

Figure 4: SEC traces (RI detector, solvent DMF, PEG standards) of P(EG$_{82}$-*co*-GlyTs$_5$) and P(EG$_{82}$-*co*-MEO$_5$) copolymers and P(EG$_{82}$-*co*-MEO$_5$) after hydrolysis.

Incubation at acidic conditions of the vinyl ether containing polyethers results in hydrolytic degradation of these materials. To analyse the influence of the number of cleavage sites on the size distribution of the copolymer fragments after hydrolysis, the SEC data of all copolymers before and after hydrolytic degradation was investigated. To achieve full cleavage, 15 mg of the polymer was dissolved in 200 µL DCM and treated with 100 µL 10% HCl in MeOH for two hours. Two major trends can be observed (**Figure 5** and **Table 2**): (i) the higher the content of cleavage sites in the polymer backbone, the smaller the fragments are after cleavage. This can be observed both for the average molecular weights as well as for the maxima of the fragment molecular weight distributions. (ii) The molecular weight of the copolymer does not have a significant influence, the comonomer content (EEGE) determines the size of the fragments.

Table 2: Characterization data for P(EG-*co*-MEO) copolymers before and after hydrolytic degradation.

	before degradation			after degradation		
	MEO[a] / mol%	M_n[b] / g mol^{-1}	$Đ$[b] = M_w / M_n	M_n[b] / g mol^{-1}	$Đ$[b] = M_w / M_n	M_n[b] (Max.) / g mol^{-1}
P(EG$_{82}$-*co*-EEGE$_5$)	6	3,390	1.08	760	1.67	1,220
P(EG$_{152}$-*co*-EEGE$_{10}$)	6	5,820	1.12	930	1.65	1,340
P(EG$_{76}$-*co*-EEGE$_8$)	9	3,460	1.07	620	1.61	940
P(EG$_{129}$-*co*-EEGE$_{17}$)	11	5,790	1.10	560	1.54	770

[a]Determined *via* ^{1}H NMR spectroscopy, [b]determined *via* SEC (RI detector, DMF, PEG standards).

For example, P(EG$_{82}$-*co*-EEGE$_5$) exhibits an average molecular weight of M_n = 3,390 g mol^{-1} (SEC), which decreases to M_n = 760 g mol^{-1} after degradation. The maximum of the distribution drops from M_n = 3,280 g mol^{-1} to M_n = 1,220 g mol^{-1}. This

trend can also be observed for P(EG$_{152}$-*co*-EEGE$_{10}$), sharing the same fraction of cleavage sites at a higher molecular weight of the original copolymer. By increasing the fractional content of comonomer and therefore the number of cleavage sites distributed along the copolymer backbone, the average molecular weight distributions and their maxima after hydrolysis shift significantly, as shown for P(EG$_{76}$-*co*-EEGE$_{8}$) and P(EG$_{129}$-*co*-EEGE$_{17}$). Again, similar EEGE content results in a similar size distribution of the fragments, regardless the varying original molecular weight of the copolymer before hydrolysis.

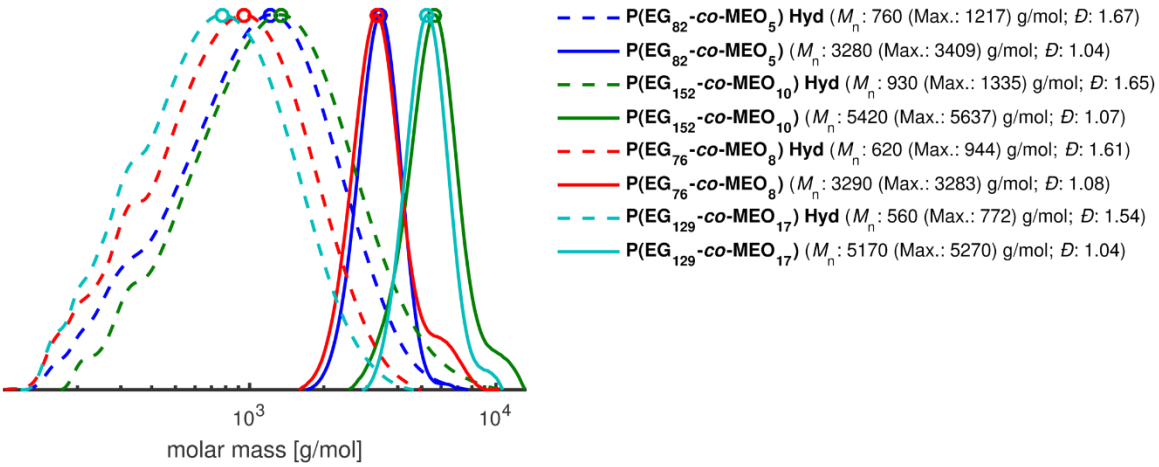

Figure 5: SEC traces (RI detector, solvent DMF, PEG standards) of P(EG-*co*-MEO) copolymers before (solid lines) and after hydrolysis (dashed lines).

From this comparison, we demonstrate that effective control over the fragment size distribution can be achieved by adjusting the EEGE content. The fragment size distribution is independent of the original molecular weight of the copolymer, as expected. Furthermore, moderate dispersity was obtained for the fragment distribution, with $Đ$ = 1.54 – 1.67.

Overall, these results validate the successful synthesis and degradation of vinyl ether containing P(EG-*co*-MEO) copolymers, obtained *via* a convenient post-polymerization elimination strategy. This new approach offers control over the size of the polymer fragments after degradation with moderate dispersities, while preserving

the desired advantages of polymers synthesized by classical AROP, avoiding limitations inherent to the monomer-activated technique.

3.1.3.2 COMPARISON OF DIFFERENT STATISTICAL INCORPORATION PATTERNS OF CLEAVAGE SITES

In cases in which the cleavable moieties are introduced by copolymerization of EO with a comonomer that introduces the cleavable moiety, the distribution of comonomers and (therefore cleavage sites) along the polymer backbone is predefined by the statistics of the respective copolymerization. This ties the copolymerization parameters directly to the molecular weight and dispersity of the polymer fragments after degradation. For each particular pair of comonomers with known copolymerization parameters, Monte Carlo simulation of the copolymer microstructure and therefore the distribution of cleavage sites alongside the polymer backbone is possible. The Monte Carlo simulation was performed assuming perfect living anionic polymerization conditions and for full conversion, according to the procedure recently described by Blankenburg *et al.*[13] Subsequently, this data can be used to determine the molecular weight and molecular weight distribution of the fragments after simulated degradation of the copolymers. To assess the effect of different copolymer microstructures on the fragment size and size distribution, we use this *"in silico"* approach to simulate the outcome for three exemplary copolymerizations, that cover the range from (a) ideally random (AROP of EO and EEGE, this work; r_{EO} = 1.05, r_{EEGE} = 0.94) over (b) slight gradient (EO with EPB; r_{EO} = 2.8, r_{EPB} = 0.35) to (c) strong gradient (EO with ECH, r_{EO} = 9.2, r_{ECH} = 0.1) microstructures. The reactivity ratios can be translated to the distribution of cleavage sites.[11,9,6]

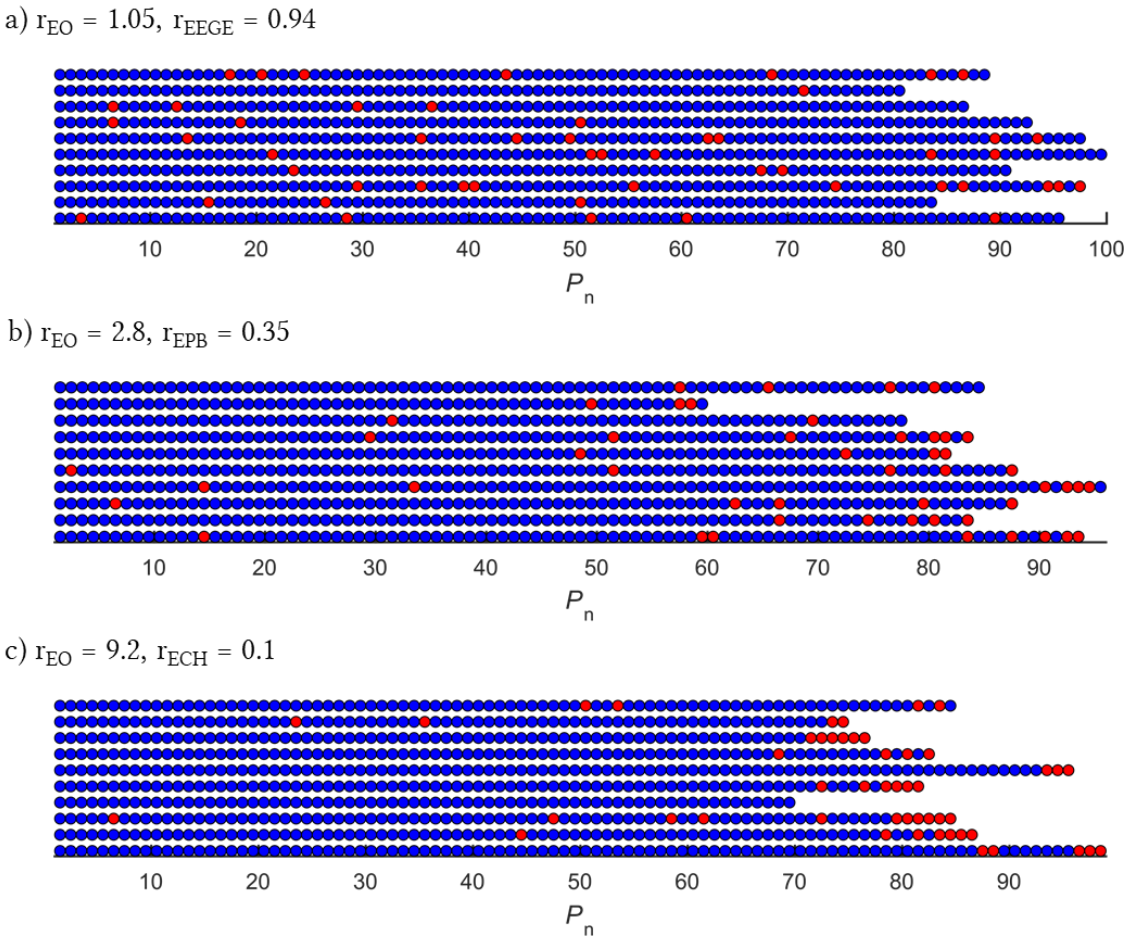

Figure 6: Sample of ten individual copolymer chains obtained by a Monte Carlo simulation performed for the polymer composition a) P(EG$_{82}$-*co*-MEO$_5$), b) P(EG$_{82}$-*co*-EPB$_5$) and c) P(EG$_{82}$-*co*-ECH$_5$).

Figure 6 illustrates the position of the degradable moieties (red) in the polymer backbone, as calculated *via* a Monte Carlo simulation for each of the copolymer microstructures mentioned above. A copolymer composition of P(EG$_{82}$-*co*-X$_5$), was chosen to compare the simulated data to experimental results presented in this work. The different copolymer microstructures are evident in the simulated copolymer chains. While the copolymer P(EG$_{82}$-*co*-EEGE$_5$) shows an even distribution of both comonomers (blue: EG, red: EEGE) in its polymer backbone, the slight gradient microstructure of P(EG$_{82}$-*co*-EPB$_5$) is already clearly visible. The EPB (red) units accumulate towards the end of the polymer chains compared to the sample above. This behaviour is even more pronounced in the third example, P(EG$_{82}$-*co*-ECH$_5$). The accumulation of ECH (red) units at the end of the polymer chain reflects the strong gradient microstructure.

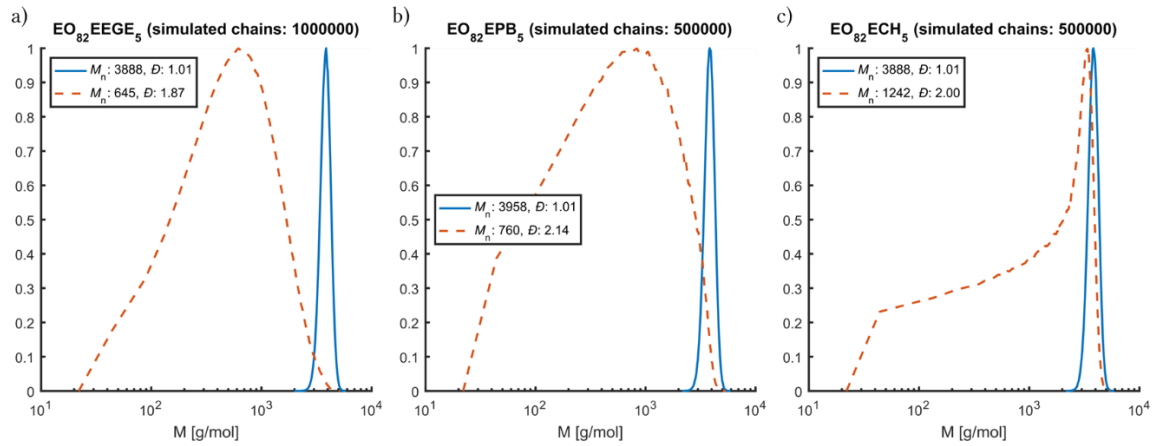

Figure 7: Calculated hydrolysis data for a) P(EG$_{82}$-*co*-MEO$_5$), b) P(EG$_{82}$-*co*-EPB$_5$) and c) P(EG$_{82}$-*co*-ECH$_5$).

The Monte Carlo simulation was then used to calculate the molecular weight distribution of the copolymer fragments after simulated cleavage at the predefined cleavage sites (**Figure 7**). The *"in silico"* degradation of the copolymer P(EG$_{82}$-*co*-MEO$_5$) can be compared to experimental data presented in this work. The simulation resulted in a molecular weight of M_n = 650 g mol^{-1} with a moderate dispersity of $Đ$ = 1.87, which is close to the experimental results of M_n = 760 g mol^{-1} and $Đ$ = 1.67. As calculated for the copolymers P(EG$_{82}$-*co*-EPB$_5$) and P(EG$_{82}$-*co*-ECH$_5$), the increasing gradient microstructure leads to increasingly ill-defined fragments with molecular weight distributions of M_n = 760 g mol^{-1} and M_n = 1,240 g mol^{-1}, exhibiting high dispersities of $Đ$ = 2.14 and $Đ$ = 2.00, respectively.

Overall, this data shows clearly the influence of the copolymer microstructure on the copolymer fragments after degradation. Evenly distributed cleavage sites are a key requirement, since they result in rather defined fragments with tailorable size, while gradient microstructures result in broader molecular weight distributions of fragments, indicating a loss of control over the fragment size and dispersity.

3.1.4 CONCLUSION

In summary, we have developed a novel synthesis route to obtain vinyl ether PEGs. This route capitalizes on the reactivity ratios of (co)polymers of EO and glycidyl ethers obtained *via* classical AROP with evenly distributed predefined cleavage sites along the copolymer backbone and low overall dispersity. As smaller PEGs are associated with toxic effects, tailoring and fine-tuning the size and dispersity of PEG fragments is important for biomedical use of cleavable PEGs.

The copolymerization of EO with EEGE *via* classical AROP permits precise adjustment of molecular weights and comonomer composition of the resulting P(EG-*co*-EEGE) copolymers. This reaction resulted in well-defined copolymers ($Đ \leq 1.12$) with molecular weights of approximately M_n = 4,000 g mol^{-1} and M_n = 8,000 g mol^{-1} and 6 mol% and 11 mol% EEGE content. These copolymers were subsequently converted to vinyl ether containing P(EG-*co*-MEO) by a series of common post-polymerization reactions. SEC measurements after hydrolysis of theses acid-labile copolymer showed that the dispersity of the fragments was moderate ($Đ = 1.67 - 1.54$) and the size could be adjusted by the comonomer fraction (M_n = 560 – 930 g mol^{-1}). Furthermore, an *"in silico"* approach *via* a Monte Carlo simulation showed that an increasing gradient copolymer microstructure leads to increasingly ill-defined fragments with high dispersity. Thus, disparate reactivity ratios result in a loss of control over fragment size and size distribution. The conclusions of this work are general in their nature and can be universally applied to degradable copolymers obtained by copolymerization of monomers containing labile moieties, i.e. predefined cleavage sites.

3.1.5 EXPERIMENTAL

As an example, all procedures are described for P(EG_{82}-*co*-$EEGE_5$) and were accordingly adopted for all copolymers presented in this work[12].

Synthesis of P(EG_{82}-*co*-$EEGE_5$). In a flame dried Schlenk flask, potassium *tert*-butoxide (66 mg, 0.59 mmol) and 2-(benzyloxy)ethanol were dissolved in benzene (5 mL) and dry THF (5 mL), stirred under slightly reduced pressure at 60 °C for 30 min and subsequently dried in high vacuum for 16 hours. The resulting initiator salt was dissolved in 20 mL of dry THF and ethylene oxide (5 mL, 0.11 mol) was cryo-transferred *via* a graduated ampule. The copolymerization was carried out at 60 °C until full conversion was achieved (reaction control *via* ^{1}H NMR) and terminated using 2 mL of methanol. After purification *via* dialysis against methanol for 24 hours (MWCO 1000 Da), the purified copolymer was dried in vacuum for at least 24 hours. (Yield: 80 %). ^{1}H NMR (400 MHz, DMSO-d_6): δ [ppm] 7.38–7.25 (m, 4.78H, Bz), 4.66 (m, 4.97H, H_3C-*CH*O_2), 4.49 (s, 2H, Bz-C*H*2-O), 3.70–3.40 (m, 360H, CH_2O), 1.18 (d, 14.3H, CH_3-CHO_2), 1.10 (t, 14.4H, CH_3-CH_2).

Methylation of P(EG_{82}-*co*-$EEGE_5$). To a solution of P(EG_{82}-*co*-$EEGE_5$) (3.00 g, 0.75 mmol) in dry THF (5 mL), sodium hydride (99 mg, 4.13 mmol) was added and the mixture was stirred at room temperature for 30 minutes. Methyl iodide (233 µL, 3.75 mmol) was added and the reaction was carried out at room temperature for 24 hours. Remaining methyl iodide was quenched by the addition of triethyl amine and the copolymer was purified by dialysis against methanol for 24 hours (MWCO 1000 Da). The copolymer was obtained after drying in vacuum. (Yield: 80%) ^{1}H NMR (400 MHz, DMSO-d_6): δ [ppm] 7.38–7.25 (m, 5H, Bz), 4.66 (m, 4.94H, H_3C-*CH*O_2), 4.49 (s, 1.99H, Bz-C*H*2-O), 3.70–3.40 (m, 387H, CH_2O), 3.24 (s, 3.56H, CH_3-OCH_2), 1.18 (d, 14.8H, CH_3-CHO_2), 1.10 (t, 15zH, CH_3-CH_2).

Synthesis of P(EG$_{82}$-*co*-*lin*PG$_5$). P(EG$_{82}$-*co*-EEGE$_5$) was dissolved in methanol/dichloromethane 1:1 (v/v) and stirred over Dowex 50WX8 at room temperature for 24 hours. The ion exchange resin was removed by filtration and the copolymer was obtained by removal of the solvent and subsequently drying at high vacuum. (Yield: 95%) ^{1}H NMR (400 MHz, DMSO-d_6): δ [ppm] 7.38–7.25 (m, 5H, Bz), 4.49 (s, 2.08H, Bz-C*H*$_2$-O), 3.70–3.40 (m, 391H, C*H*$_2$O), 3.24 (s, 4.09H, C*H*$_3$-OCH$_2$).

Synthesis of P(EG$_{82}$-*co*-GlyTs$_5$). The methylated P(EG$_{82}$-*co*-*lin*PG$_5$) (1.50 g, 0.38 mmol) was dissolved in 5 mL of dry DCM. To this solution, *p*-toluenesulfonyl chloride (1.03 g, 6 mmol), triethyl amine (832 µL, 6 mmol) and DMAP (14 mg, 0.11 mmol) were slowly added under stirring and the reaction was conducted at room temperature for 24 hours. After dialysis against methanol for 24 hours (MWCO 1000 Da), the purified copolymer was obtained after drying under high vacuum. ^{1}H NMR (400 MHz, DMSO-d_6): δ [ppm] 7.81–7.75 (m, 7.78H, Ts), 7.63–7.58 (m, 1.23H Ts), 7.51–7.39 (m, 9.91H, Ts) 7.38–7.25 (m, 5H, Bz), 7.14–7.10 (m, 0.61H, Ts) 4.49 (s, 1.65H, Bz-C*H*$_2$-O), 4.14–4.08 (m, 3.92H, TsO-C*H*$_2$-CH), 3.99–3.94 (m, 3.76H, TsO-C*H*$_2$-CH), 3.70–3.40 (m, 359H, C*H*$_2$O), 3.24 (s, 2.86H, C*H*$_3$-OCH$_2$), 2.45–2.38 (2s, 13.9H, OTs-C*H*$_3$).

Synthesis of P(EG$_{82}$-*co*-MEO$_5$). To a solution of P(EG$_{82}$-*co*-GlyTs$_5$) (245 mg, 0.06mmol) in dry toluene (1 mL), potassium *tert*-butoxide (75 mg, 0.6 mmol) was added and the mixture was stirred at room temperature for 24 hours. After washing three times with water, the copolymer was precipitated in cold diethyl ether and dried under high vacuum. (Yield: 60 %) ^{1}H NMR (400 MHz, DMSO-d_6): δ [ppm] 7.38–7.25 (m, 5.02H, Bz), 4.49 (s, 2H, Bz-C*H*$_2$-O), 4.16 (s, 4.38H, C*H*$_2$-C), 4.11 (s, 3.91H, C*H*$_2$-C), 3.88–3.38 (m, 352H, C*H*$_2$O), 3.24 (s, 3.70H, C*H*$_3$-OCH$_2$).

Hydrolysis of P(EG$_{82}$-*co*-MEO$_5$). 15 mg of P(EG$_{82}$-*co*-MEO$_5$) was dissolved in DCM (200 µL) and treated with 100 µL of 10% HCl in methanol. After incubation for 2 hours,

the solution was neutralized by the addition of $NaHCO_3$ and the molecular weight distribution of the fragments was analysed by SEC.

3.1.6 REFERENCES

(1) Schröder, R.; Besch, L.; Pohlit, H.; Panthöfer, M.; Roth, W.; Frey, H.; Tremel, W.; Unger, R. E. Particles of vaterite, a metastable CaCO3 polymorph, exhibit high biocompatibility for human osteoblasts and endothelial cells and may serve as a biomaterial for rapid bone regeneration. *Journal of tissue engineering and regenerative medicine* **2018**, *12*, 1754–1768.

(2) Knop, K.; Hoogenboom, R.; Fischer, D.; Schubert, U. S. Poly(ethylene glycol) in drug delivery: pros and cons as well as potential alternatives. *Angewandte Chemie (International ed. in English)* **2010**, *49*, 6288–6308.

(3) Herzberger, J.; Niederer, K.; Pohlit, H.; Seiwert, J.; Worm, M.; Wurm, F. R.; Frey, H. Polymerization of Ethylene Oxide, Propylene Oxide, and Other Alkylene Oxides: Synthesis, Novel Polymer Architectures, and Bioconjugation. *Chemical reviews* **2016**, *116*, 2170–2243.

(4) Lundberg, P.; Lee, B. F.; van den Berg, S. A.; Pressly, E. D.; Lee, A.; Hawker, C. J.; Lynd, N. A. Poly(ethylene oxide)-co-(methylene ethylene oxide): A hydrolytically-degradable poly(ethylene oxide) platform. *ACS macro letters* **2012**, *1*, 1240–1243.

(5) Worm, M.; Leibig, D.; Dingels, C.; Frey, H. Cleavable Polyethylene Glycol: 3,4-Epoxy-1-butene as a Comonomer to Establish Degradability at Physiologically Relevant pH. *ACS Macro Lett.* **2016**, *5*, 1357–1363.

(6) Danner, A.-K.; Leibig, D.; Vogt, L.-M.; Frey, H. Monomer-activated Copolymerization of Ethylene Oxide and Epichlorohydrin: In Situ Kinetics Evidences Tapered Block Copolymer Formation. *Chin J Polym Sci* **2019**, *37*, 912–918.

(7) Jung, P.; Ziegler, A. D.; Blankenburg, J.; Frey, H. Glycidyl Tosylate: Polymerization of a "Non-Polymerizable" Monomer permits Universal Post-Functionalization of Polyethers. *Angewandte Chemie (International ed. in English)* **2019**, *58*, 12883–12886.

(8) Billouard, C.; Carlotti, S.; Desbois, P.; Deffieux, A. "Controlled" High-Speed Anionic Polymerization of Propylene Oxide Initiated by Alkali Metal Alkoxide/Trialkylaluminum Systems. *Macromolecules* **2004**, *37*, 4038–4043.

(9) Ewald, J.; Blankenburg, J.; Worm, M.; Besch, L.; Unger, R. E.; Tremel, W.; Frey, H.; Pohlit, H. Acid-Cleavable Poly(ethylene glycol) Hydrogels Displaying Protein Release at pH 5. *Chemistry (Weinheim an der Bergstrasse, Germany)* **2020**, *26*, 2947–2953.

(10) Steiert, E.; Ewald, J.; Wagner, A.; Hellmich, U. A.; Frey, H.; Wich, P. R. pH-Responsive protein nanoparticles via conjugation of degradable PEG to the surface of cytochrome c. *Polym. Chem.* **2020**, *11*, 551–559.

(11) Herzberger, J.; Leibig, D.; Liermann, J. C.; Frey, H. Conventional Oxyanionic versus Monomer-Activated Anionic Copolymerization of Ethylene Oxide with Glycidyl Ethers: Striking Differences in Reactivity Ratios. *ACS Macro Lett.* **2016**, *5*, 1206–1211.

(12) Mangold, C.; Wurm, F.; Obermeier, B.; Frey, H. Hetero-Multifunctional Poly(ethylene glycol) Copolymers with Multiple Hydroxyl Groups and a Single Terminal Functionality. *Macromolecular rapid communications* **2010**, *31*, 258–264.

(13) Blankenburg, J.; Kersten, E.; Maciol, K.; Wagner, M.; Zarbakhsh, S.; Frey, H. The poly(propylene oxide- co -ethylene oxide) gradient is controlled by the polymerization method: determination of reactivity ratios by direct comparison of different copolymerization models. *Polym. Chem.* **2019**, *10*, 2863–2871.

3.1.7 SUPPORTING INFORMATION

Chemicals and Analytical Instrumentation

All chemicals, solvents and materials were purchased from standard commercial suppliers (Acros, Sigma-Aldrich, Fisher Scientific Alfa Aesar, TCI). Ethylene oxide (EO) was purchased from Air Liquide. DMSO-d_6 was purchased from Deutero GmbH. All chemicals were used as received without further purification unless stated otherwise.

^{1}H NMR spectra were measured using a Bruker AMX400 spectrometer (256 Scans, and B-ACS 60 auto sampler) at 296 K. ^{1}H NMR kinetic spectra were recorded at 400 MHz on a Bruker Advance III HD 400 (5 mm broad band fluorine observation (BBFO)-SmartProbe with z-gradient and Automated tuning and matching (ATM)). 2D NMR and ^{13}C NMR spectra were measured on a Bruker Avance II 400 (100.5 MHz, 5 mm BBO probe, and B-ACS 60 auto sampler) at 296 K. All spectra were processed with MestReNova v10.0.1 software and referenced internally to residual proton signals of the deuterated solvent.

Size exclusion chromatography (SEC) data were obtained using Agilent 1100 Series equipped with PSS HEMA-columns (106/104/102 Å porosity) using DMF with 1 g/L LiBr as an eluent and RI detection. Polydispersity indices (Đ = Mw/Mn) were determined with monodisperse linear PEG standards from Polymer Standard Service GmbH (PSS).

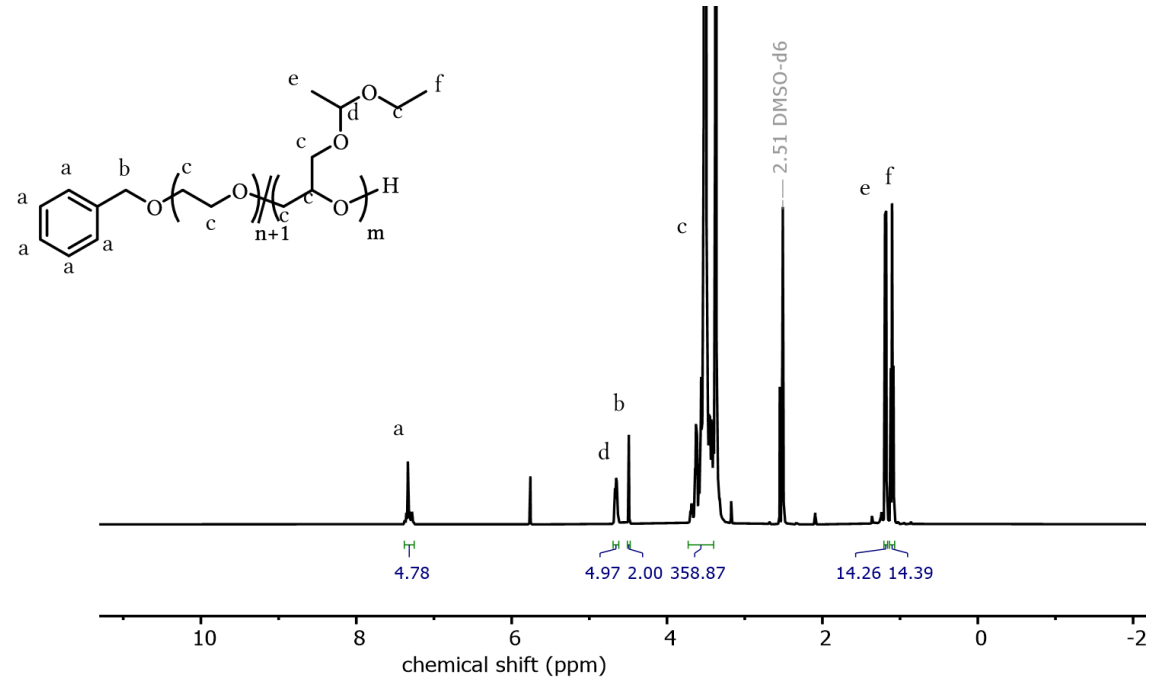

Figure S1: ^{1}H NMR spectrum (400 MHz, DMSO-d_6) of P(EG$_{82}$-*co*-EEGE$_5$).

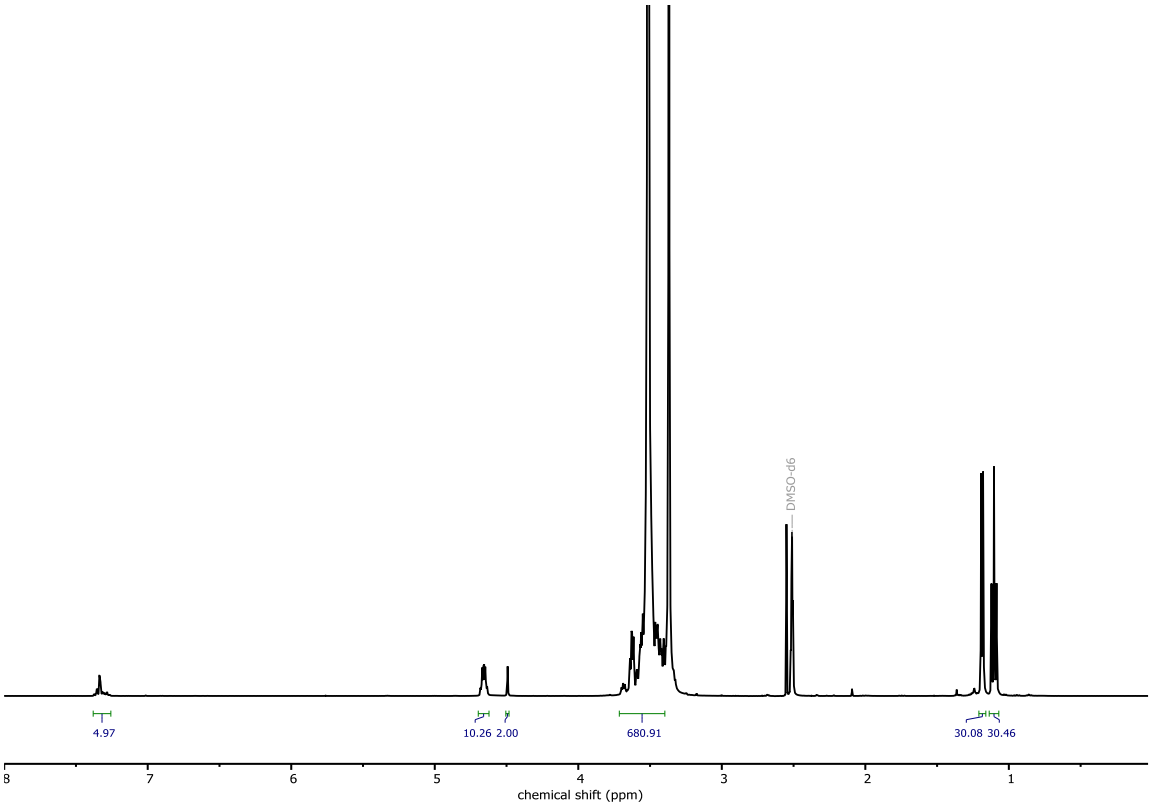

Figure S2: ^{1}H NMR spectrum (400 MHz, DMSO-d_6) of P(EG$_{152}$-*co*-EEGE$_{10}$).

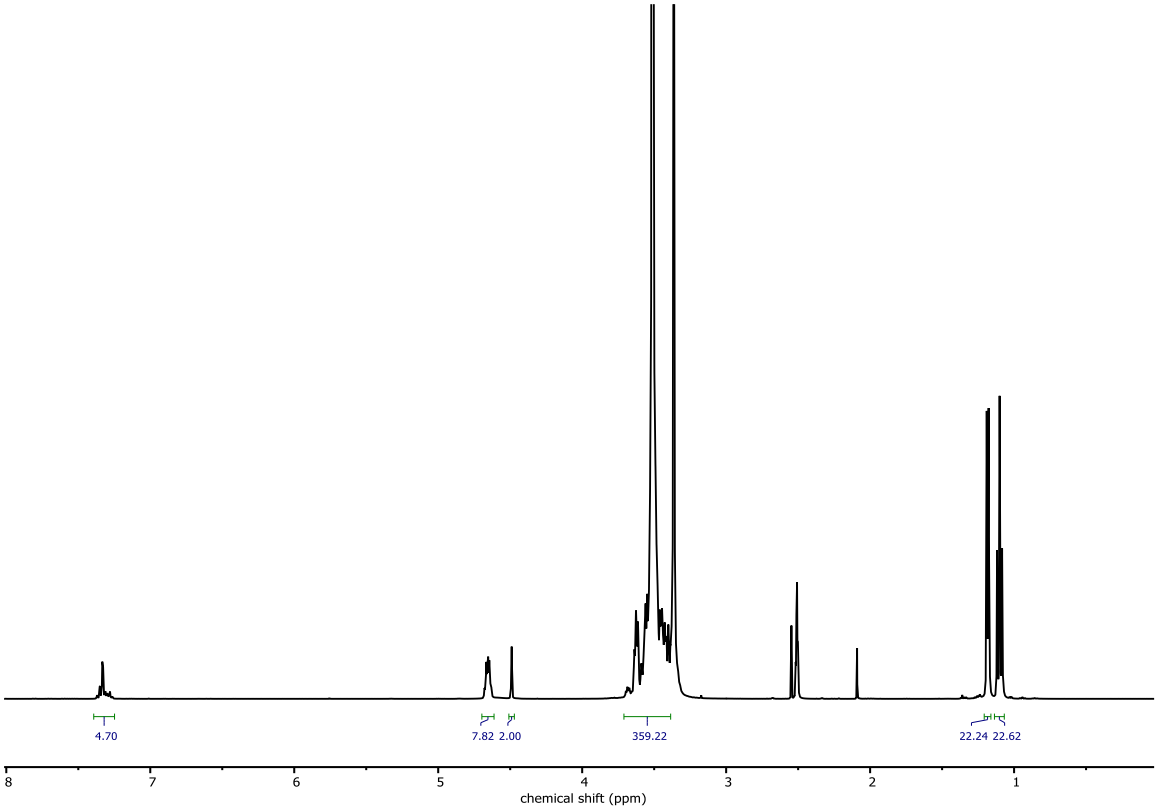

Figure S3: ^{1}H NMR spectrum (400 MHz, DMSO-d_6) of P(EG$_{76}$-*co*-EEGE$_{8}$).

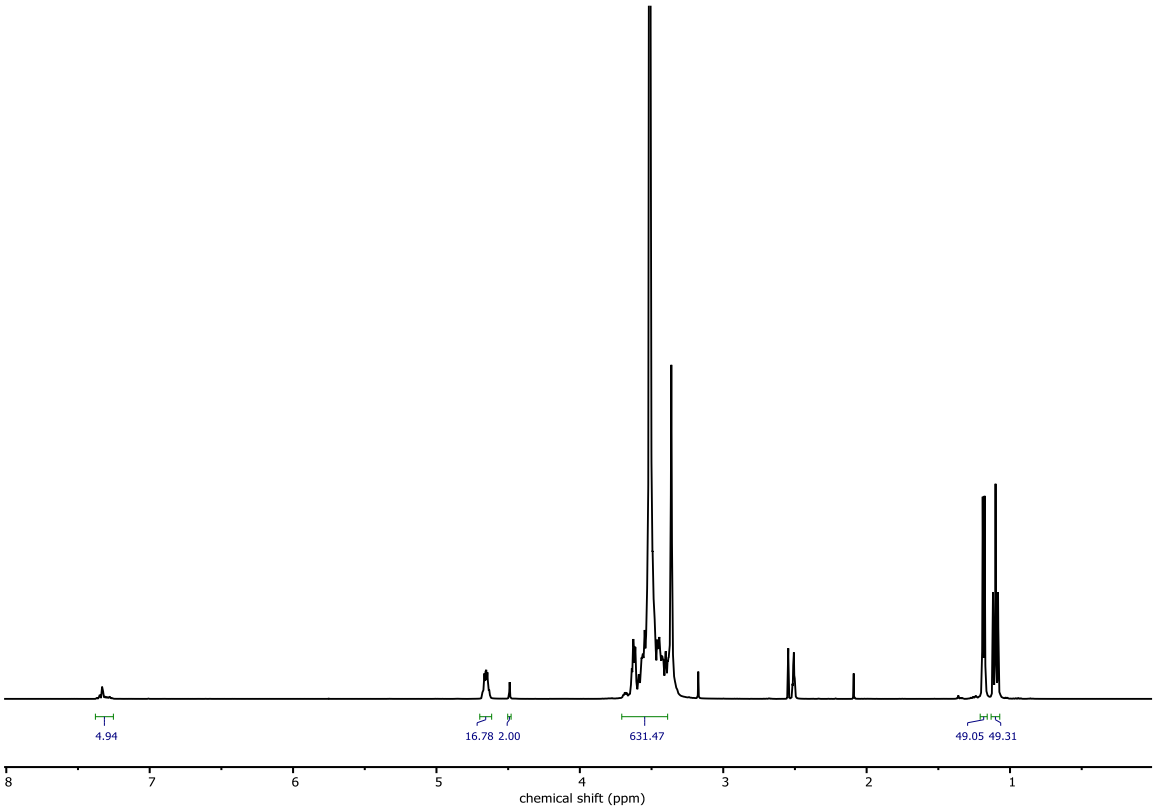

Figure S4: ^{1}H NMR spectrum (400 MHz, DMSO-d_6) of P(EG$_{129}$-*co*-EEGE$_{17}$).

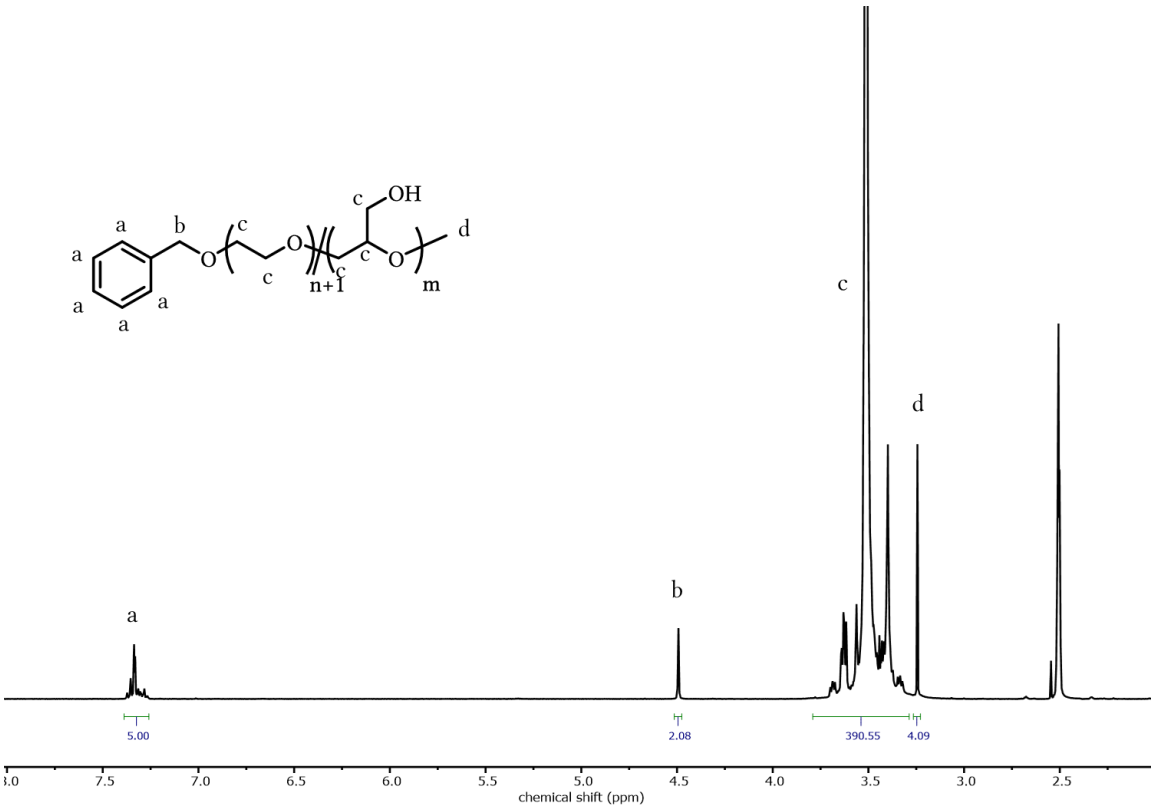

Figure S5: ^{1}H NMR spectrum (400 MHz, DMSO-*d*$_6$) of P(EG$_{82}$-*co*-*lin*PG$_5$) after methylation.

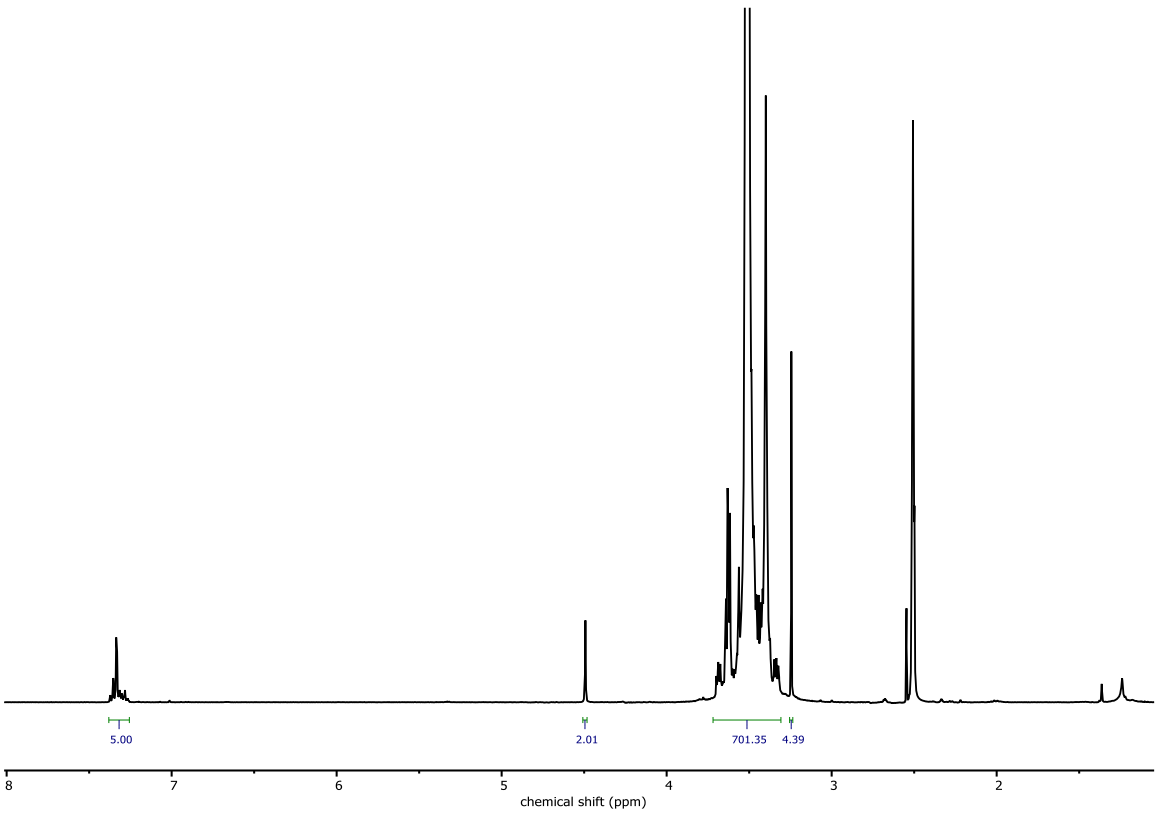

Figure S6: ^{1}H NMR spectrum (400 MHz, DMSO-*d*$_6$) of P(EG$_{152}$-*co*-*lin*PG$_{10}$) after methylation.

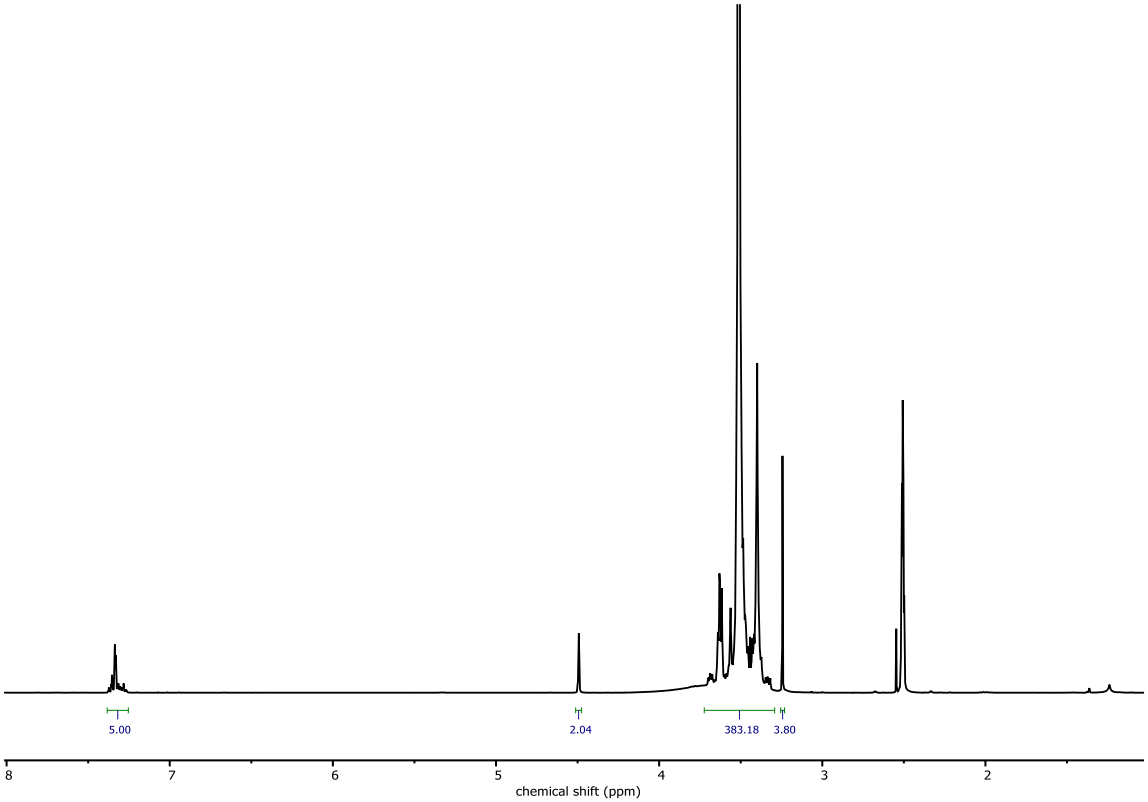

Figure S7: ^{1}H NMR spectrum (400 MHz, DMSO-d_6) of P(EG$_{76}$-*co*-*lin*PG$_8$) after methylation.

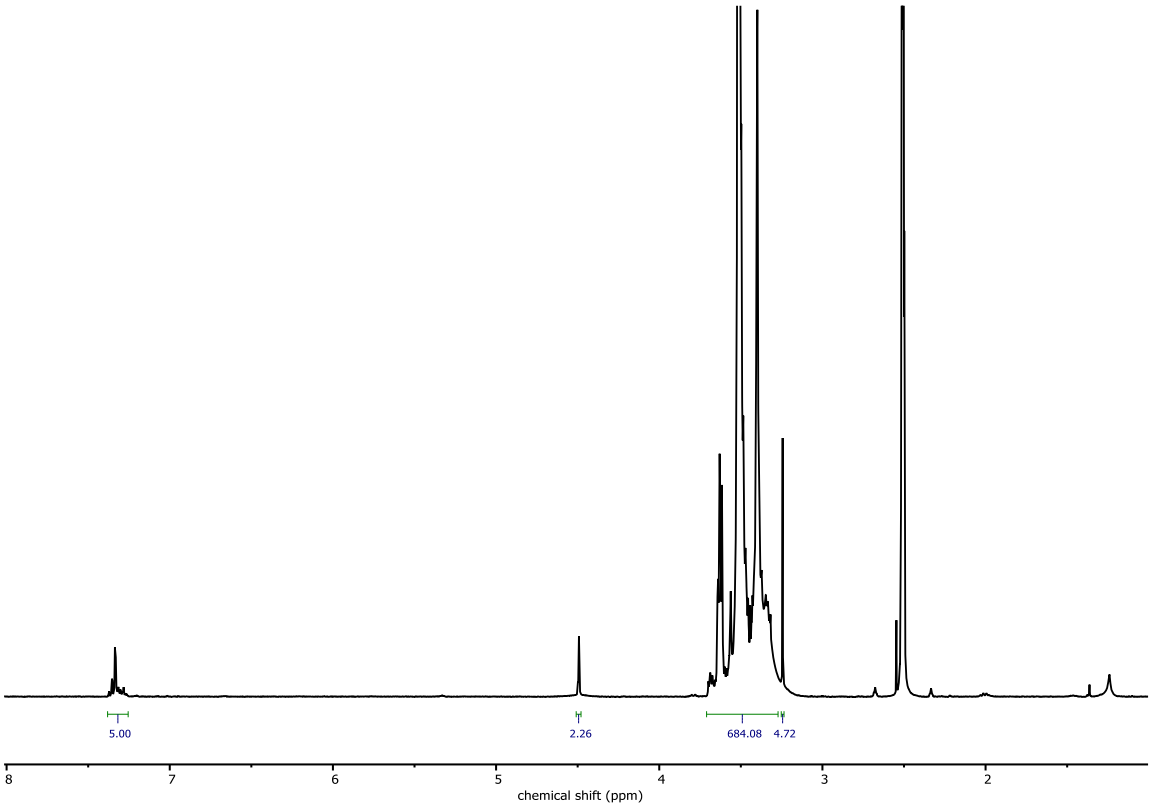

Figure S8: ^{1}H NMR spectrum (400 MHz, DMSO-d_6) of P(EG$_{129}$-*co*-*lin*PG$_{17}$) after methylation.

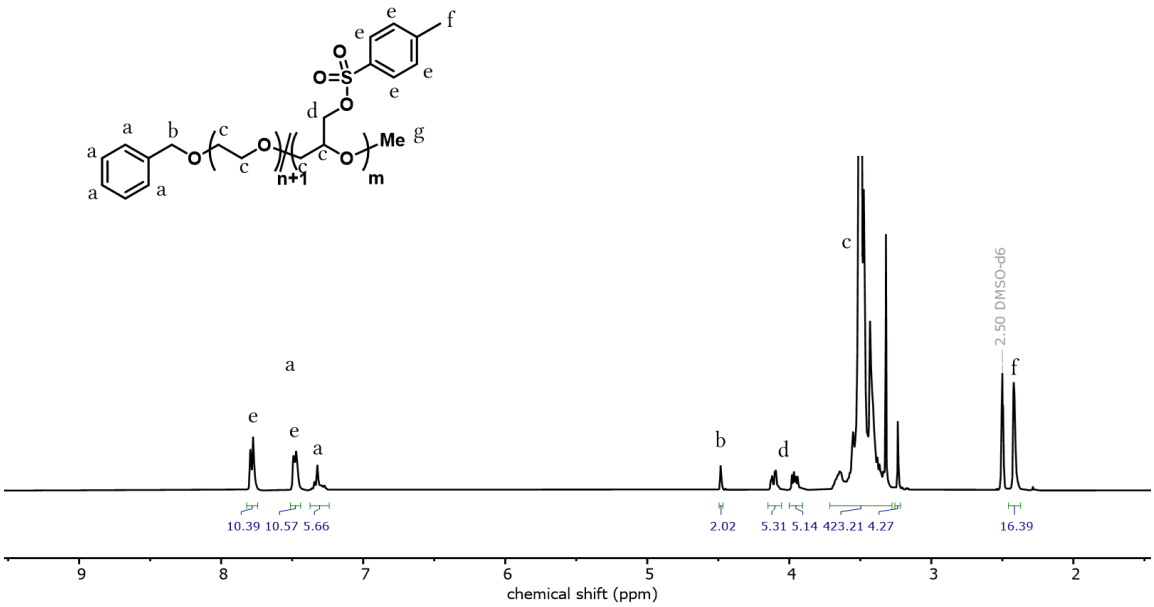

Figure S9: ^{1}H NMR spectrum (400 MHz, DMSO-d_6) of P(EG$_{82}$-*co*-GlyTs$_5$).

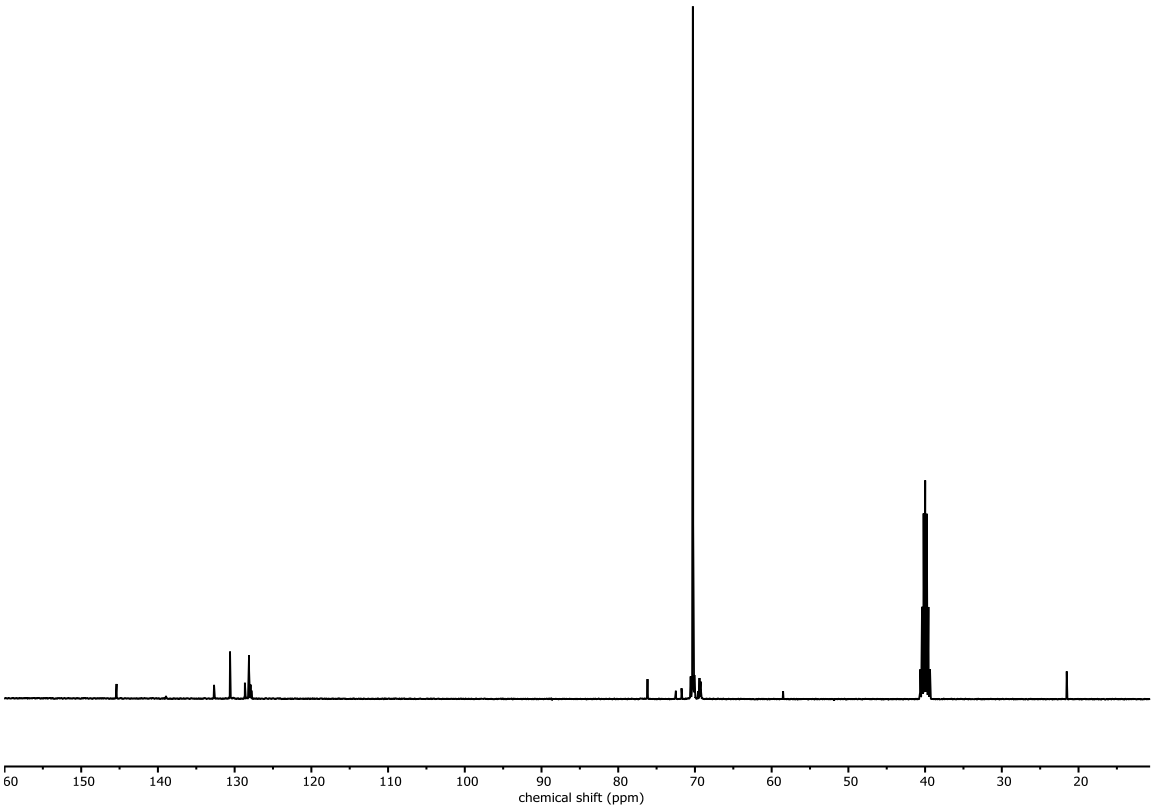

Figure S10: ^{13}C NMR spectrum (100 MHz, DMSO-d_6) of P(EG$_{82}$-*co*-GlyTs$_5$).

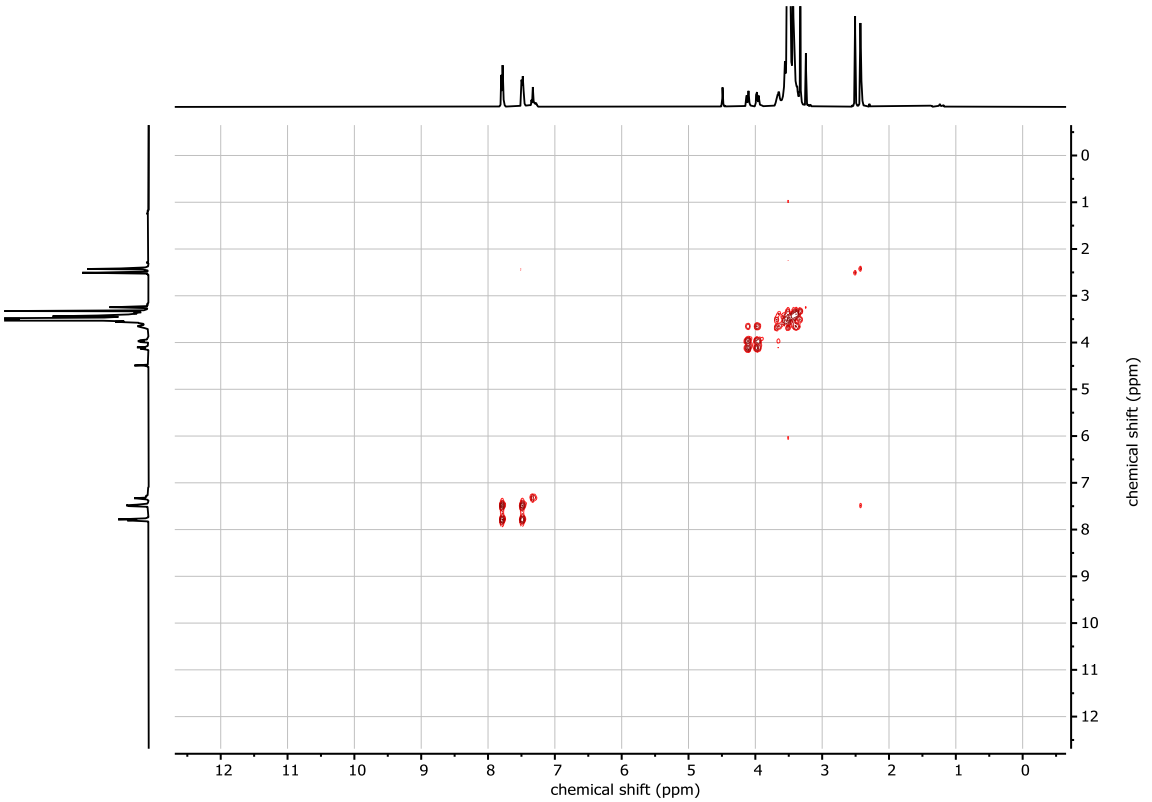

Figure S11: ^{1}H,^{1}H COSY NMR spectrum (400 MHz, DMSO-d_6) of P(EG$_{82}$-*co*-GlyTs$_5$).

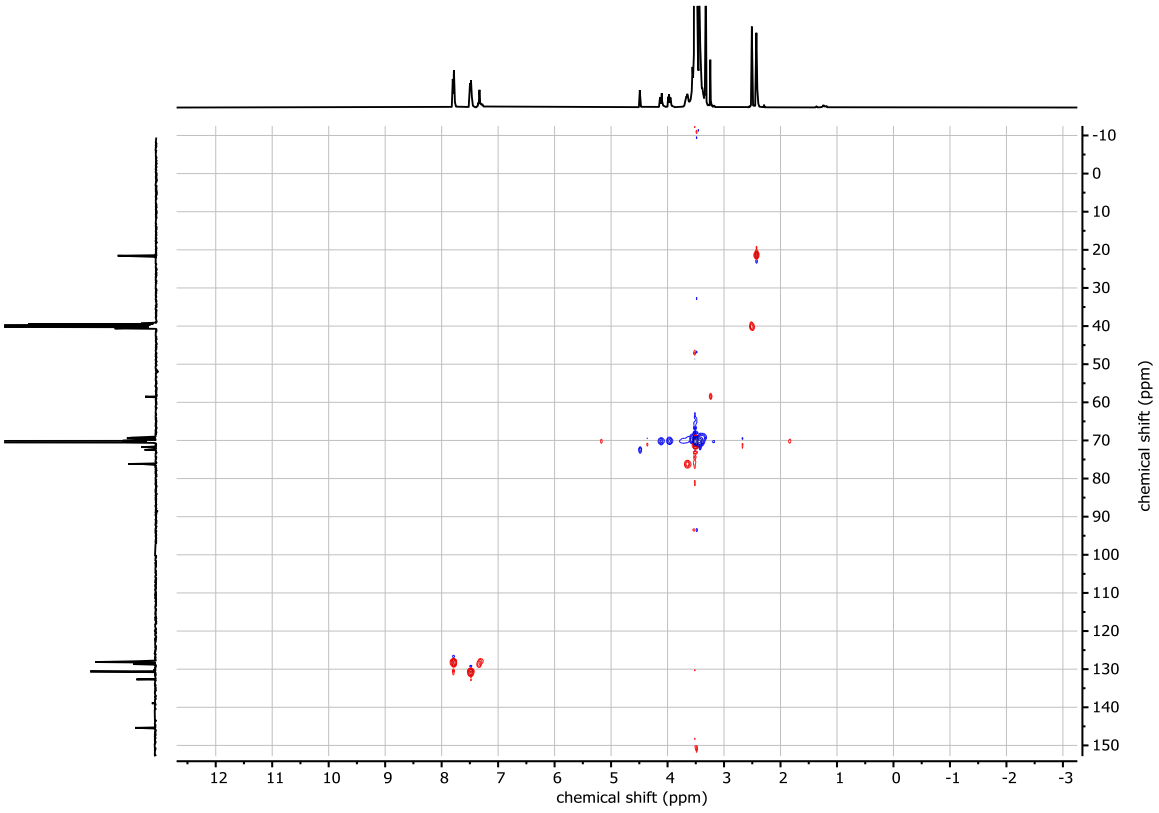

Figure S12: ^{1}H,^{13}C HSQC NMR spectrum (400 / 100 MHz, DMSO-d_6) of P(EG$_{82}$-*co*-GlyTs$_5$).

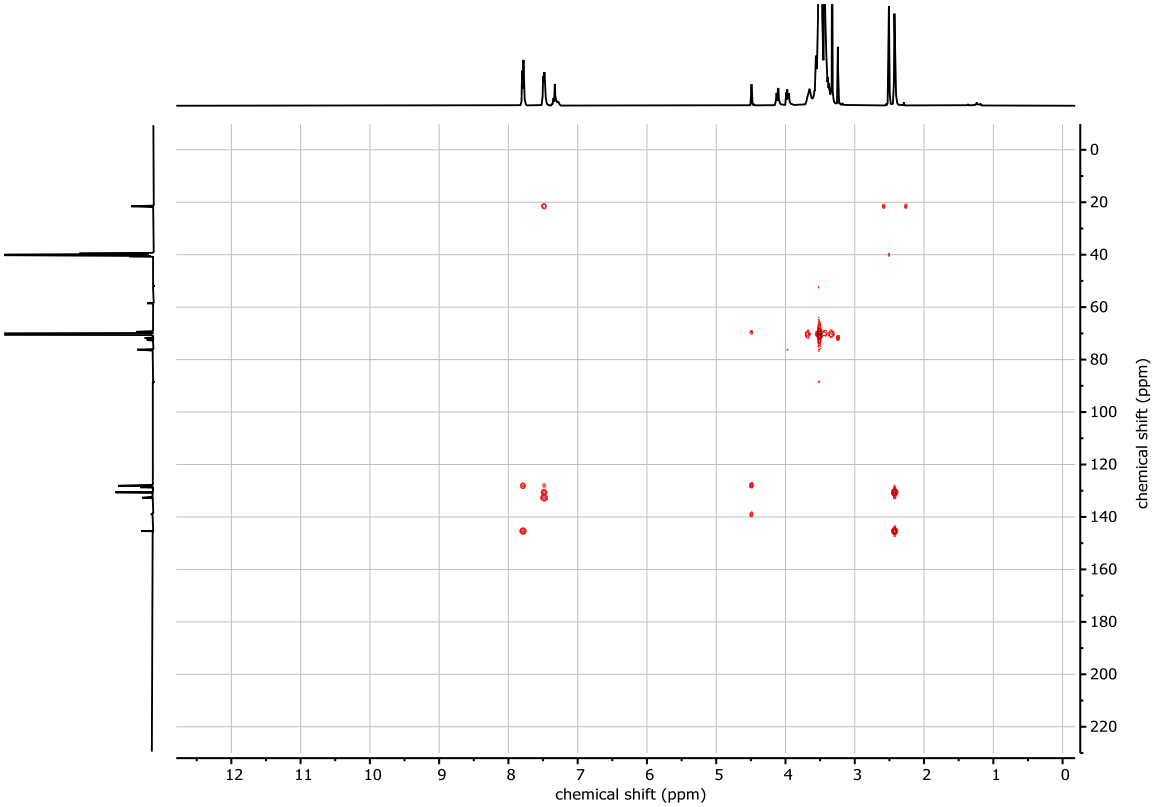

Figure S13: $^{1}H,^{13}C$ HMBC NMR spectrum (400 / 100 MHz, DMSO-d_6) of P(EG_{82}-*co*-$GlyTs_5$).

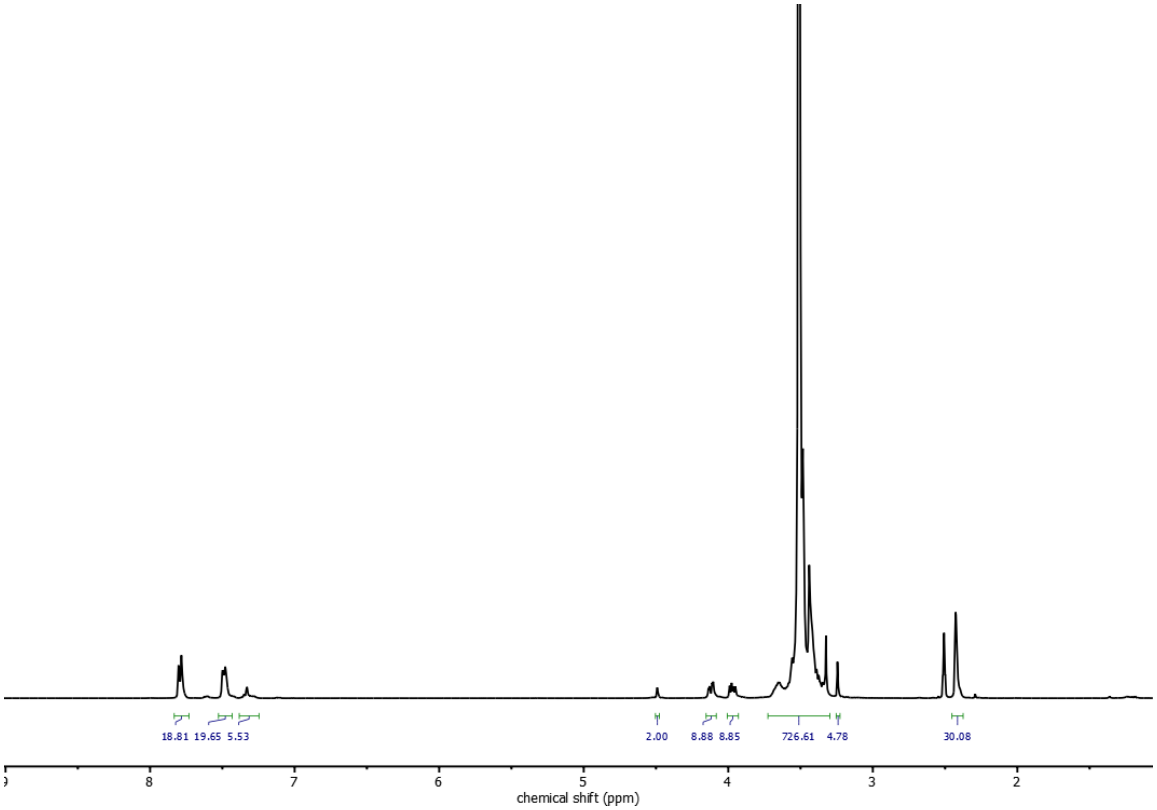

Figure S14: ^{1}H NMR spectrum (400 MHz, DMSO-d_6) of P(EG_{152}-*co*-$GlyTs_{10}$).

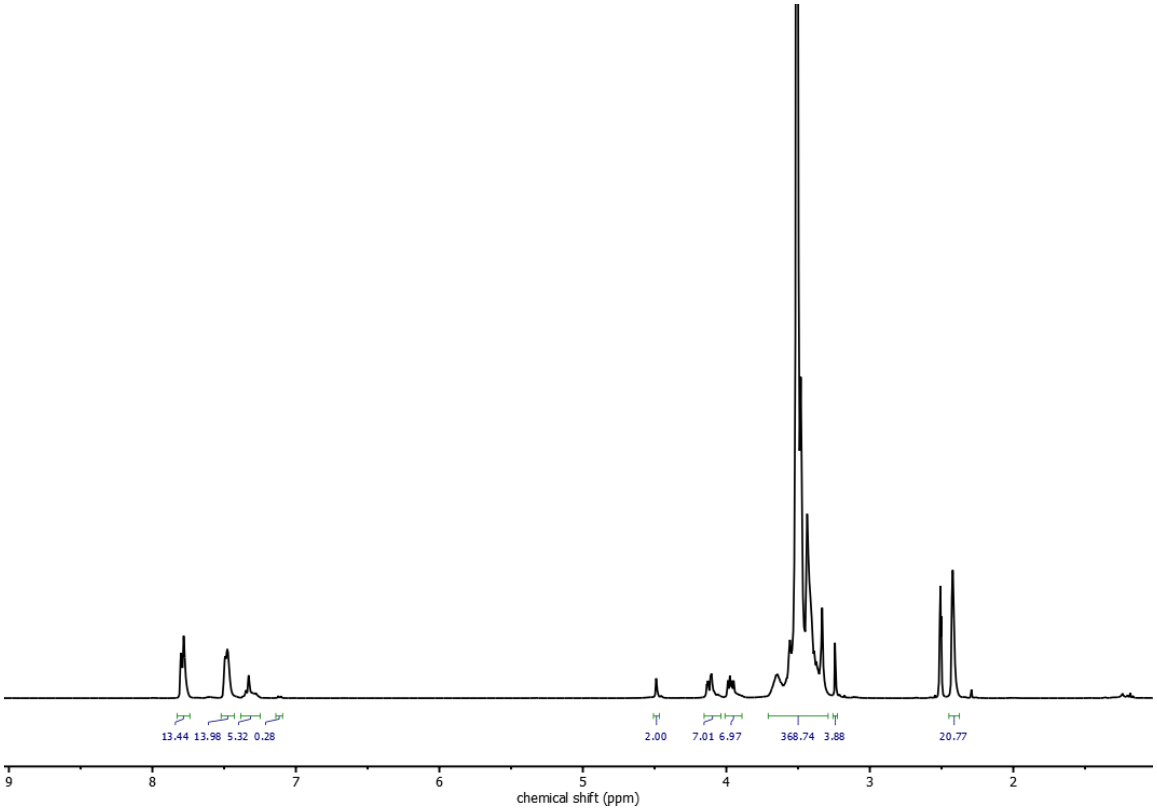

Figure S15: ^{1}H NMR spectrum (400 MHz, DMSO-d_6) of P(EG$_{76}$-*co*-GlyTs$_{8}$).

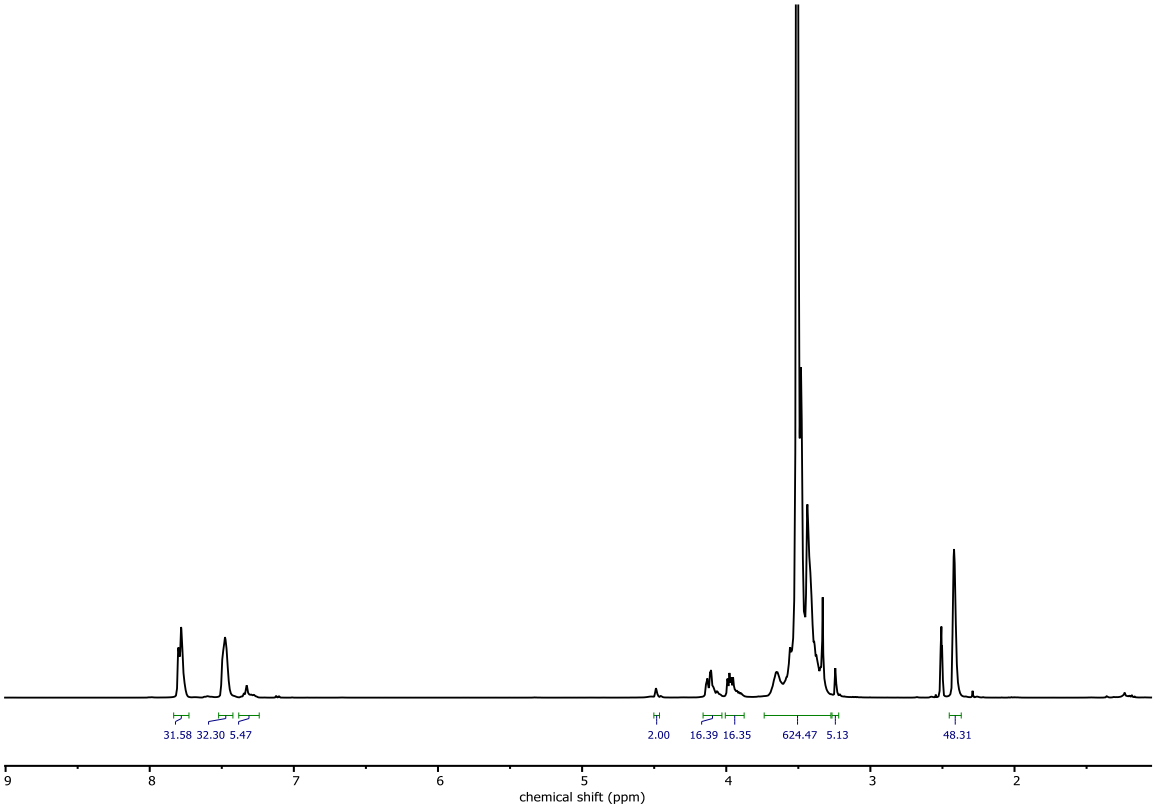

Figure S16: ^{1}H NMR spectrum (400 MHz, DMSO-d_6) of P(EG$_{129}$-*co*-GlyTs$_{17}$).

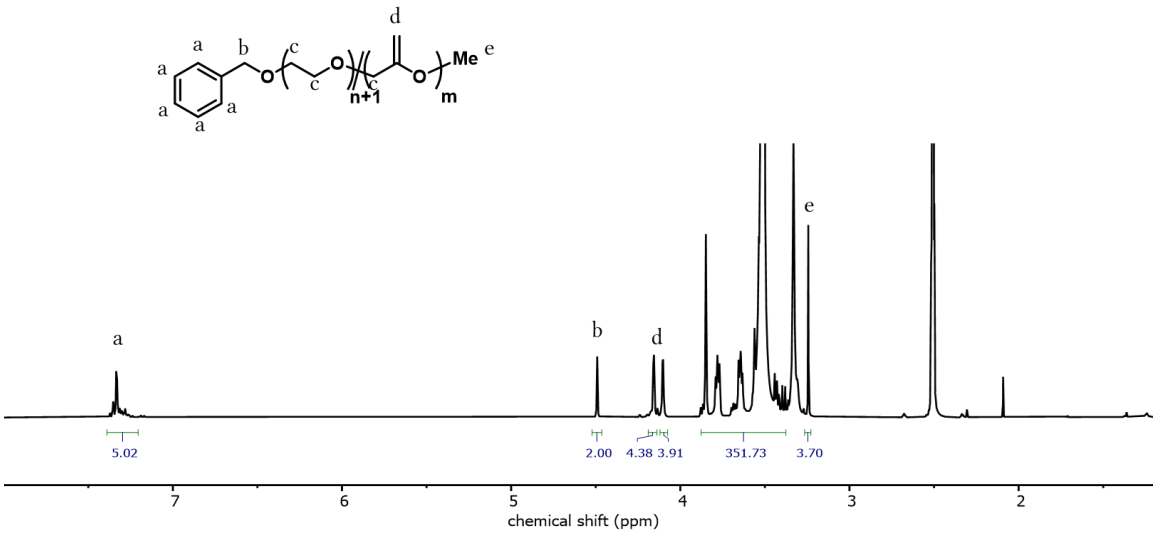

Figure S17: ^{1}H NMR spectrum (400 MHz, DMSO-d_6) of P(EG$_{82}$-*co*-MEO$_5$).

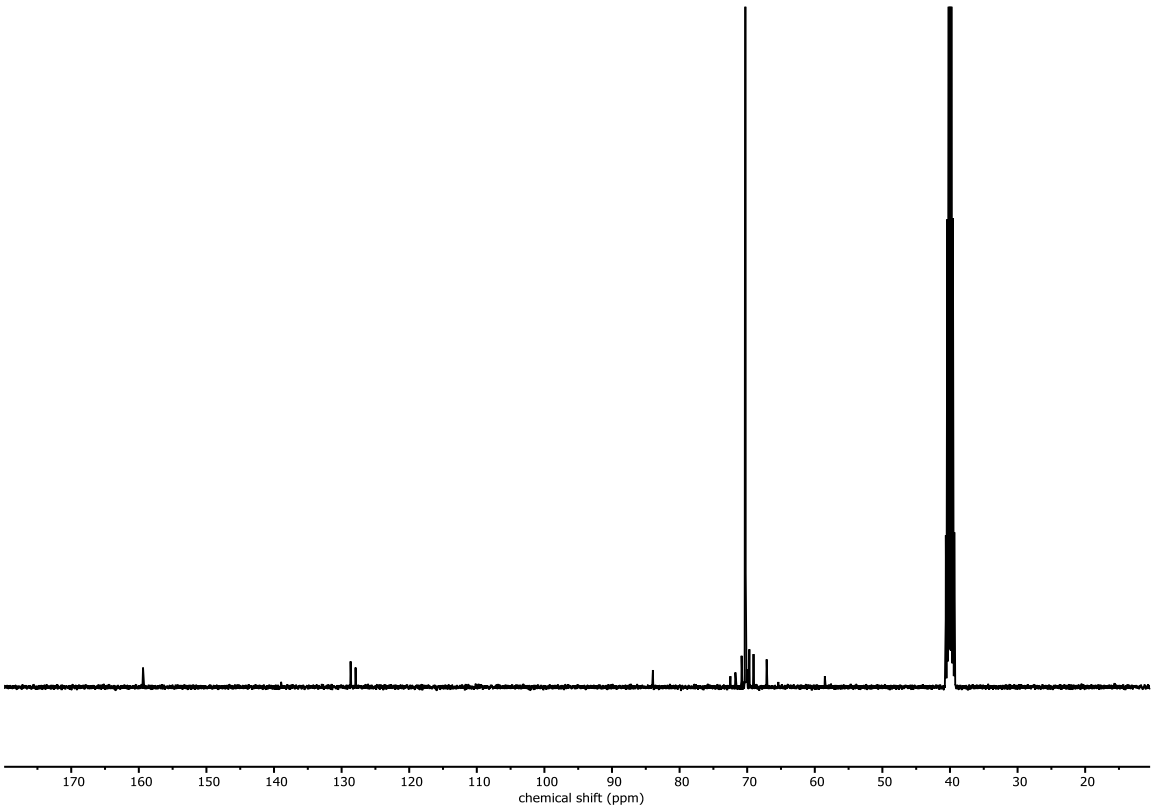

Figure S18: ^{13}C NMR spectrum (400 MHz, DMSO-d_6) of P(EG$_{82}$-*co*-MEO$_5$).

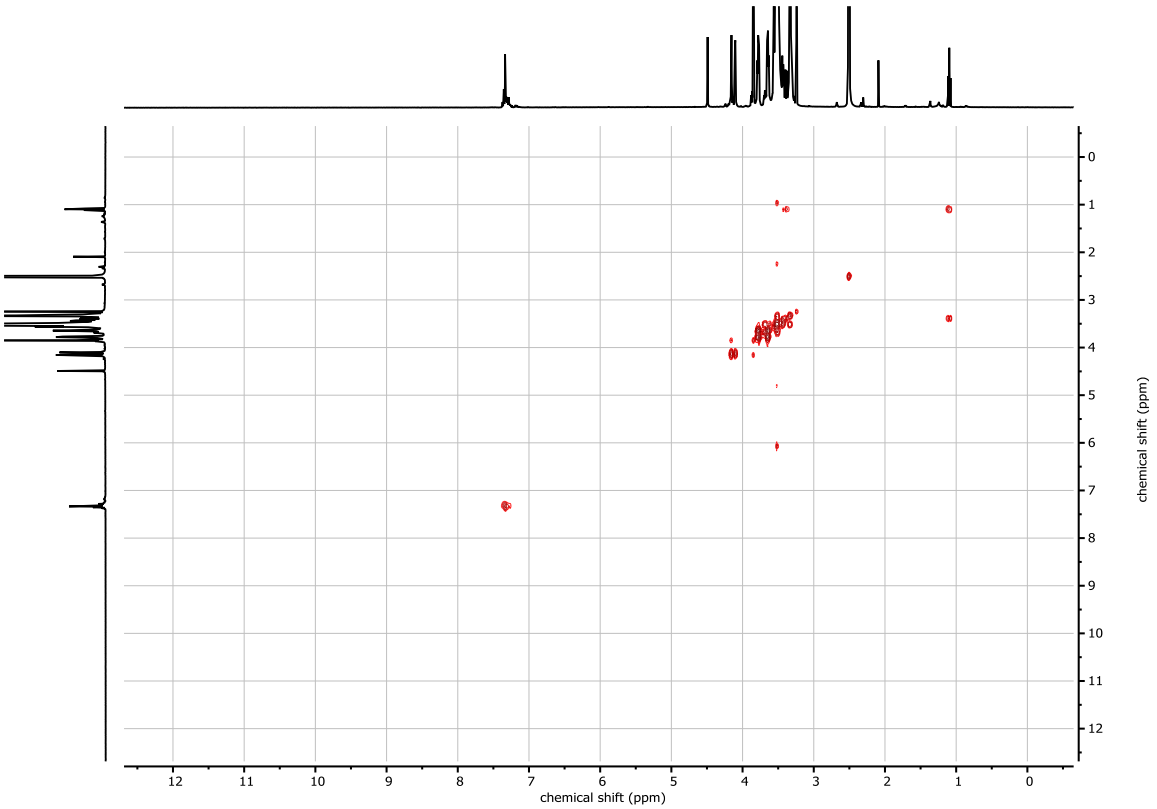

Figure S19: ^{1}H,^{1}H COSY NMR spectrum (400 MHz, DMSO-d_6) of P(EG$_{82}$-*co*-MEO$_5$).

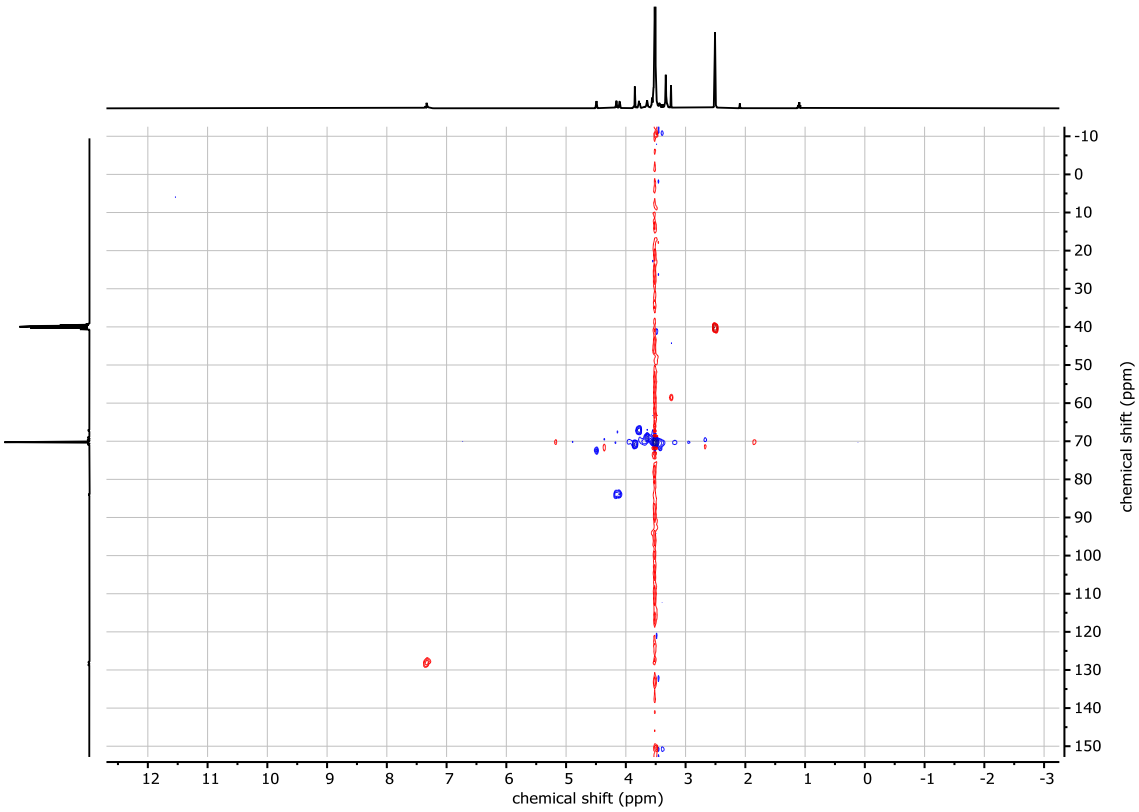

Figure S20: ^{1}H,^{13}C HSQC NMR spectrum (400 / 100 MHz, DMSO-d_6) of P(EG$_{82}$-*co*-MEO$_5$).

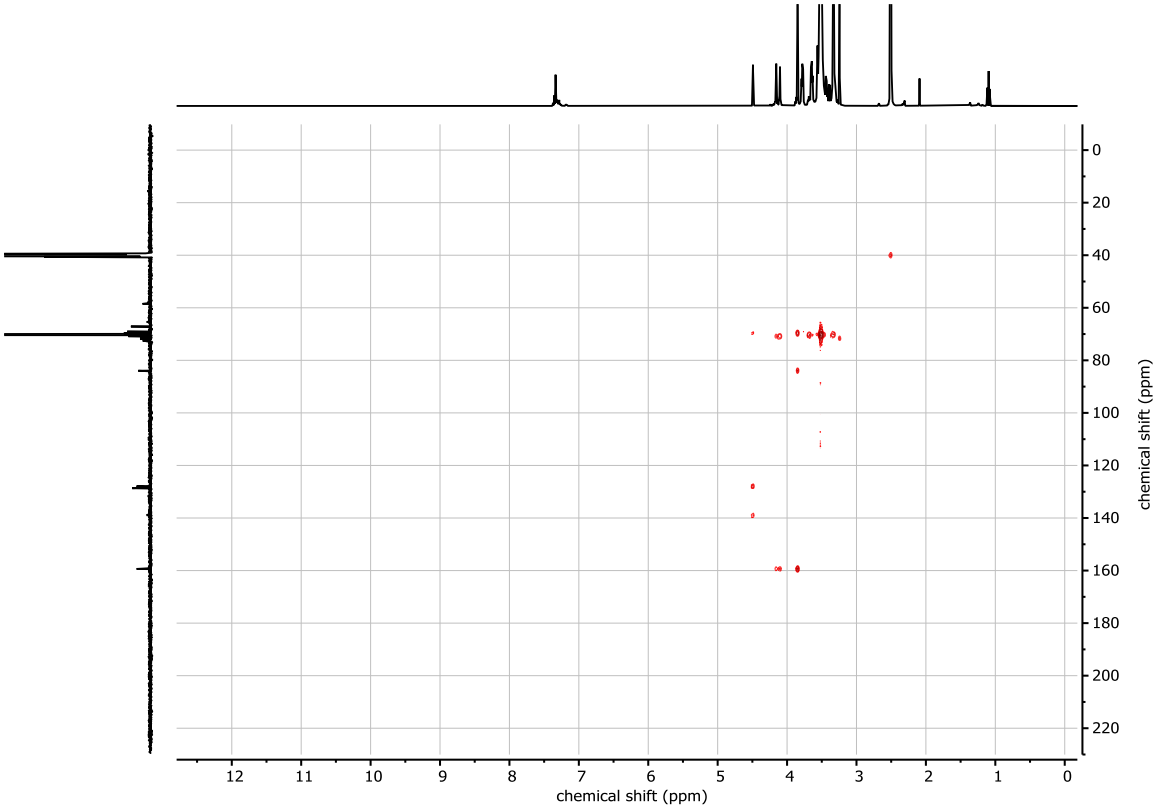

Figure S21: $^{1}H,^{13}C$ HMBC NMR spectrum (400 / 100 MHz, DMSO-d_6) of P(EG$_{82}$-*co*-MEO$_5$).

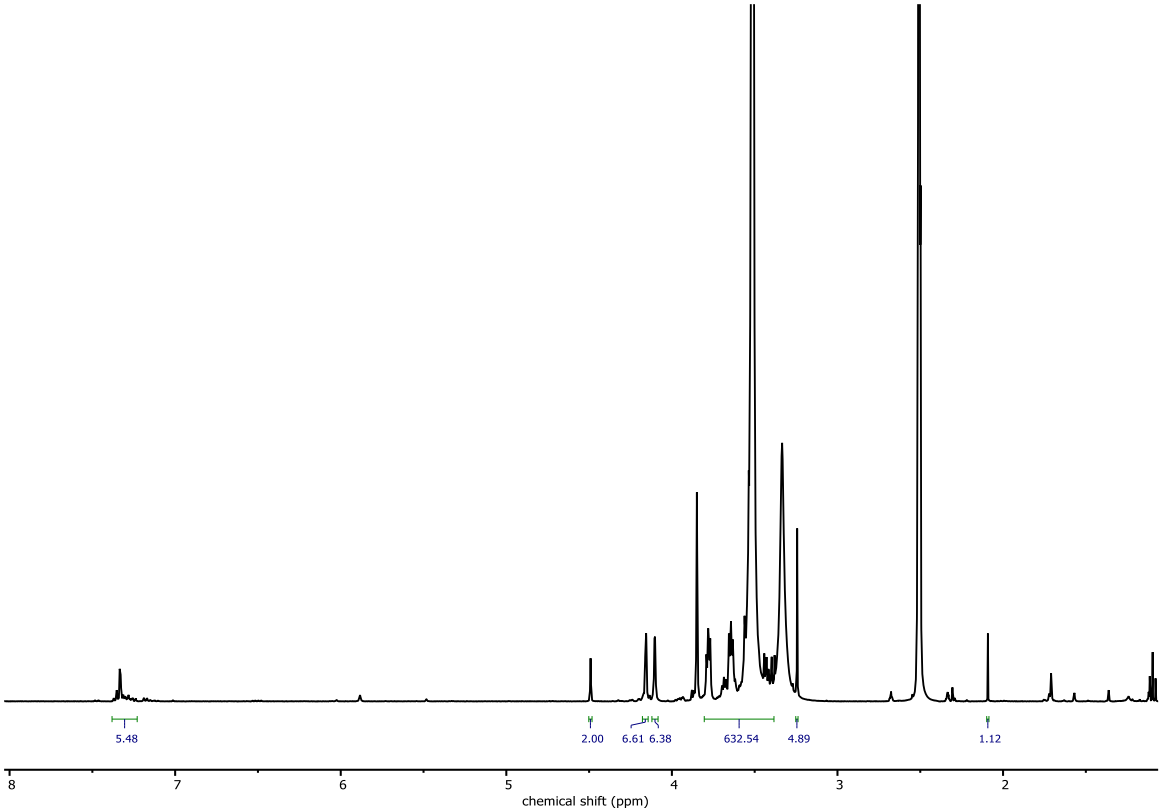

Figure S22: ^{1}H NMR spectrum (400 MHz, DMSO-d_6) of P(EG$_{152}$-*co*-MEO$_{10}$).

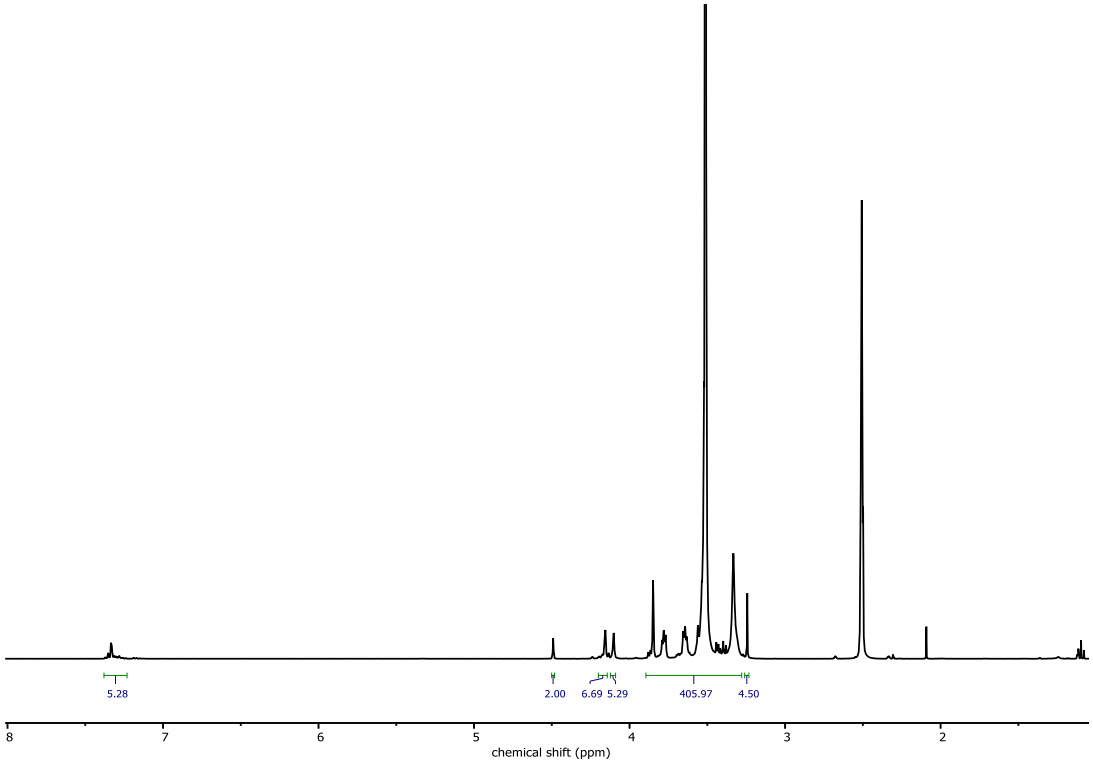

Figure S23: ^{1}H NMR spectrum (400 MHz, DMSO-d_6) of P(EG$_{76}$-*co*-MEO$_8$).

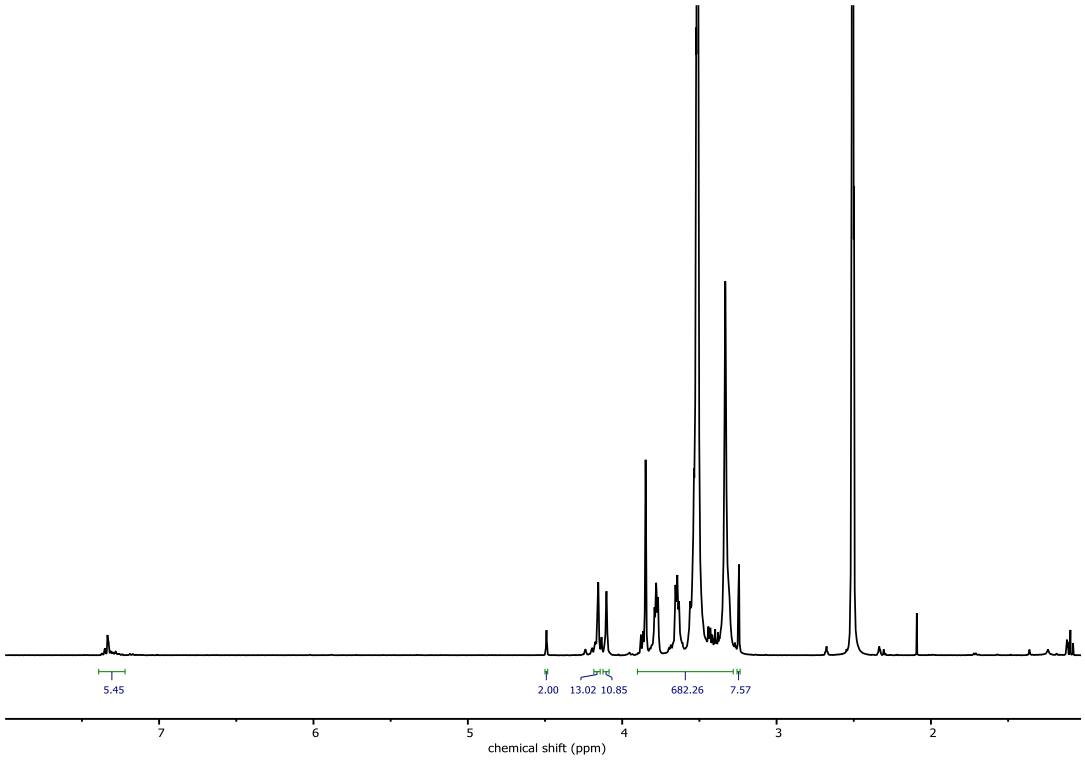

Figure S24: ^{1}H NMR spectrum (400 MHz, DMSO-d_6) of P(EG$_{129}$-*co*-MEO$_{17}$).

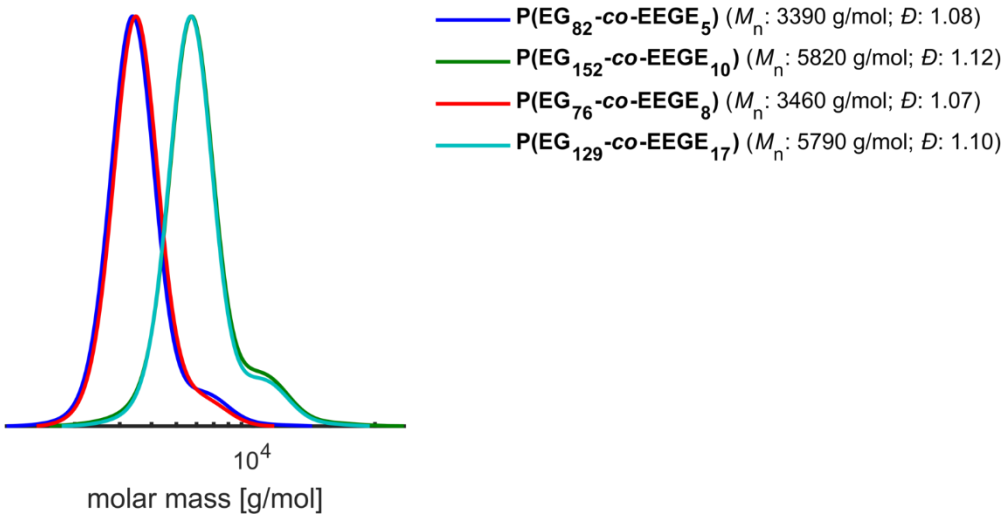

Figure S25: SEC traces (RI detector, solvent DMF, PEG standards) of the series of P(EG-*co*-EEGE) copolymers.

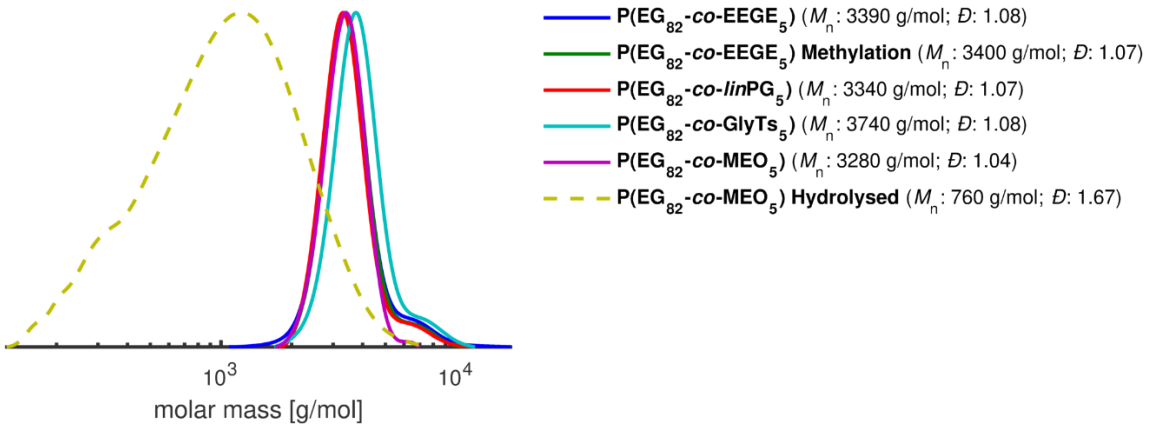

Figure S26: SEC traces (RI detector, solvent DMF, PEG standards) of $P(EG_{82}$-*co*-$EEGE_5)$ copolymers at all stages of post-polymerization modifications.

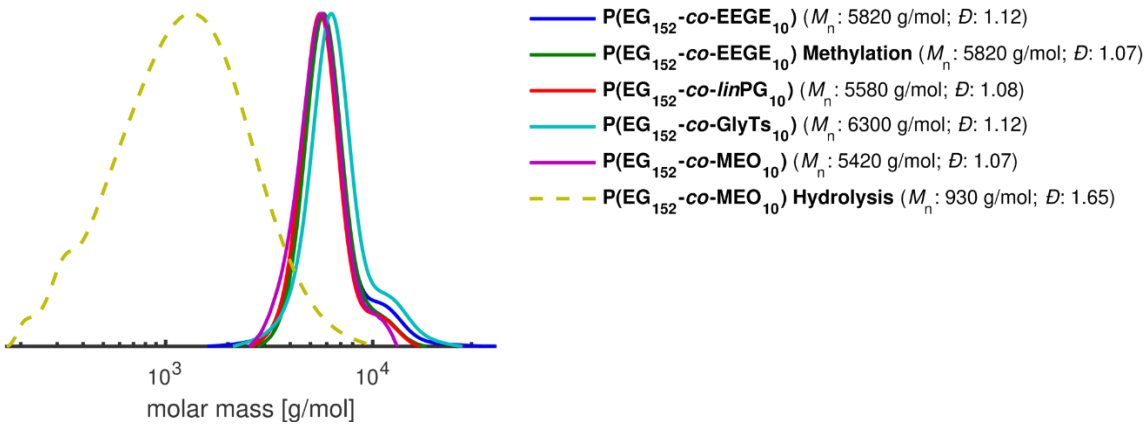

Figure S27: SEC traces (RI detector, solvent DMF, PEG standards) of $P(EG_{152}\text{-}co\text{-}EEGE_{10})$ copolymers at all stages of post-polymerization modifications.

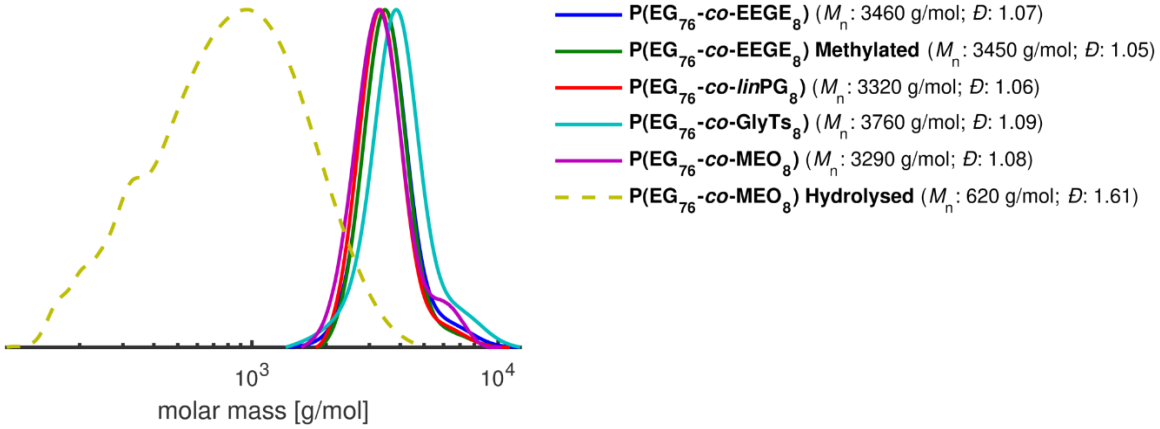

Figure S28: SEC traces (RI detector, solvent DMF, PEG standards) of $P(EG_{76}\text{-}co\text{-}EEGE_{8})$ copolymers at all stages of post-polymerization modifications.

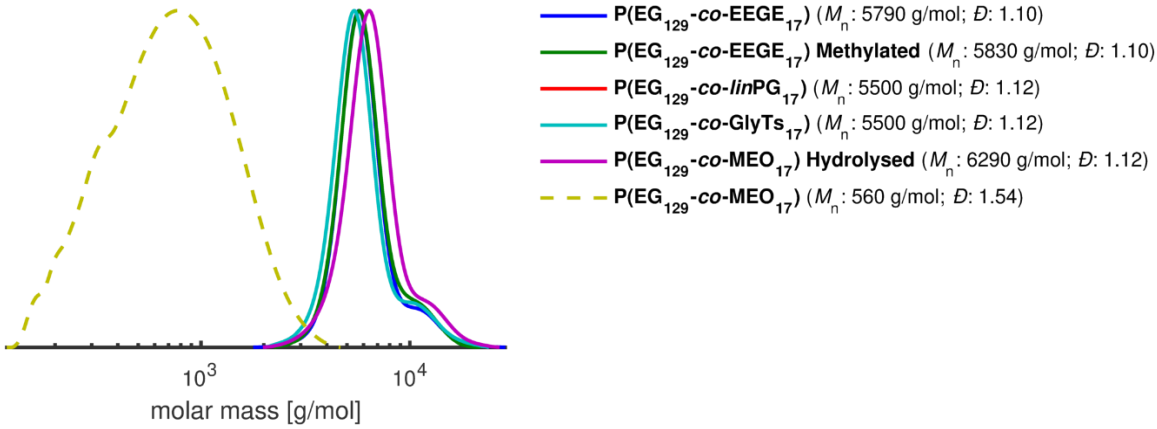

Figure S29: SEC traces (RI detector, solvent DMF, PEG standards) of $P(EG_{129}\text{-}co\text{-}EEGE_{17})$ copolymers at all stages of post-polymerization modifications.

3.2 2,2‘-(2-Methylenepropane-1,3-diyldioxy)bisethanol as a Universal Synthon for Acid-labile Poly(ethylene glycol)

Johannes Ewald,[1,2] Jan Blankenburg,[1,3] Holger Frey[1,]*

[1]Department of Chemistry, Johannes Gutenberg University, Duesbergweg 10-14, 55128 Mainz, Germany

[2]TransMed Mainz Research School of Translational Biomedicine

[3]Graduate School Materials Science in Mainz, Staudinger Weg 9, 55128 Mainz, Germany

to be submitted

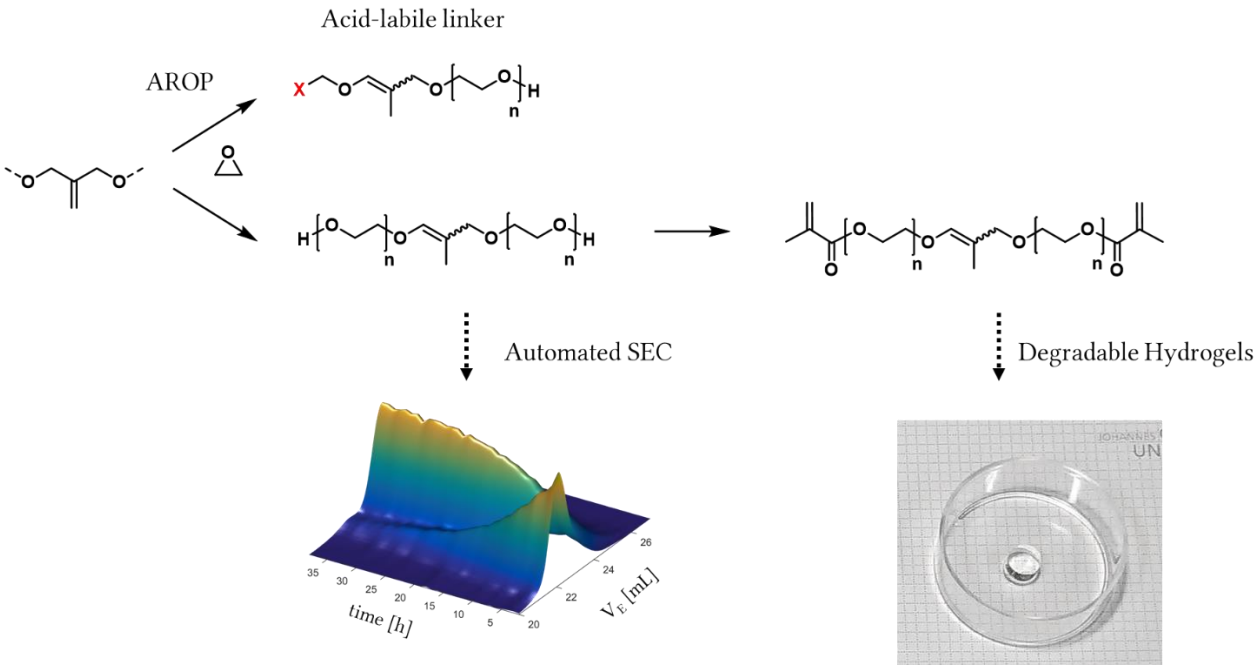

3.2.1 ABSTRACT

We present a method to implement a single vinyl ether moiety at a predefined position in the backbone of poly(ethylene glycol) (PEG). Based on 2-(methylene)-1,3-propanediol (MPD) as an allyl ether lead structure, two novel initiators for the anionic ring-opening polymerization (AROP) of epoxides were developed: (i) bifunctional 2,2‘-(2-methylenepropane-1,3-diyldioxy)bisethanol (MBE), which results in well-defined symmetrical cleavable polyethers and (ii) monofunctional 2-((benzyloxy)methyl)prop-2-en-1-ol (BMP) to demonstrate the applicability of linking this allyl ether motif to any arbitrary residue. In general, the allyl ether function serves as a stable precursor and can be isomerized to an acid-labile vinyl ether moiety *via* various techniques. The monofunctional BMP-initiated PEGs (M_n = 3,150 g mol^{-1} and M_n = 6,430 g mol^{-1} with $Đ$ = 1.04) were isomerized and the linker structure could be hydrolysed with an efficiency of 92%, releasing the attached benzyl group from the polymer. The MBE-initiated polymerizations resulted in well-defined PEGs ($Đ \leq 1.04$) with molecular weights ranging from M_n = 2,000 g mol^{-1} up to M_n = 12,000 g mol^{-1}. These polymers were isomerized by two different approaches (*directly* and *catalytically,* using Wilkinson’s catalyst). The resulting vinyl ether structures could be cleaved under hydrolytic conditions. Using an automated SEC technique, the cleavage was monitored, and the half-life time of the vinyl ether functions was determined for pH 4 ($t_{1/2}$ = 13 h) and pH 5 ($t_{1/2}$ = 31 h). Furthermore, the polymer was transformed into a bismethacrylate and used to form crosslinked acid-labile hydrogels. Subsequently, these materials were analysed regarding their swelling ratio and their degradation in acidic media. Despite excellent stability at pH 7.4 for more than four weeks, the hydrogels fully degraded at pH 4 within four days and at pH 5 within 8 days, demonstrating degradation at physiologically relevant pH in reasonable time scales. MBE and BMP are highly promising for biomedical applications, like the formation of degradable hydrogels or reversible/transient PEGylation or conjugation of drugs.

3.2.2 INTRODUCTION

Polymeric materials are widely used in numerous biomedical and therapeutic applications. One of the most prominent representatives of this class of materials is poly(ethylene glycol) (PEG) due to his extraordinary properties as water solubility and low toxicity.[1,2] This highly biocompatible polyether is widely considered as the "gold standard" of polymers for biomedical applications. It is employed to alter the pharmacokinetic parameters of drug-polymer conjugates, to improve solubility or for temporary scaffolds for tissue engineering.[3–5] The major drawback of PEG for such applications is its non-degradability under physiological conditions, resulting from the chemically inert polyether structure. This also limits the typically employed molecular weights to around M_n = 40,000 g mol^{-1}, in order to ensure effective clearance from the bloodstream and a safe excretion *via* the kidney.[4] However, as the blood circulation times of PEGylated drugs directly correlate with the molecular weight of the PEGylation agent, the use of high molecular weight PEGs might be favourable.[6,7] In this context, degradable PEGs are becoming a vibrant field of research.

To circumvent the risk of bioaccumulation, various approaches for the implementation of predetermined cleavage sites into the polyether backbone of PEG have been developed. Mostly, acetal and ketal groups as well as ester functionalities are used to synthesize degradable PEGs.[8–14] Nevertheless, usually these approaches rely on polyaddition or polycondensation of telechelic PEG precursors, resulting in polymers with large dispersity. Recently, vinyl ethers have come into the focus of research as promising acid-labile moieties. [15–20]

Our group has contributed several recent works concerning the introduction of vinyl ether moieties into the polyether backbone of PEG, capitalizing on the copolymerization of ethylene oxide (EO) with 3,4-epoxy-1-butene (EPB), followed by isomerization of the allyl ether moieties to vinyl ethers.[17,18,16] However, while these

materials have already shown their potential for biomedical applications like the formation of degradable hydrogels or reversible PEGylation, the synthesis is demanding, and the distribution of a number of cleavable moieties along the polyether backbone may be undesired for some applications. Although these polymers can be prepared in a well-defined manner, the fragments formed after acidic cleavage exhibit a broadened molecular weight distribution due to the distribution of labile sites in the chains. Depending on the proposed application of these polymers, a single cleavable moiety located in the polyether backbone may be favourable. This would enable a narrow molecular weight distribution of both the polymers and the fragments after cleavage. In this work we describe a cleavable initiator structure that can be used to create mono- or difunctional PEG structures with a predefined, acid labile vinyl ether moiety.

3.2.3 RESULTS AND DISCUSSION

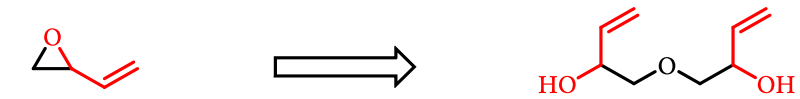

Monomer: EPB Initiator: OBB

Scheme 1: Allyl ether (red) pattern as found in the monomer EPB and the initiator OBB.

We will first consider the design of a suitable initiator containing the allyl ether moiety from an organic synthesis perspective. Full control over the location of the cleavable vinyl ether moiety in the polyether backbone can be achieved by translation of the already established allyl ether structure known from the monomer (EPB) into an initiator, suitable for AROP (**Scheme 1**). Based on this consideration, the bifunctional initiator OBB (1,1'-oxybis(but-3-en-2-ol)) was synthesized and its potential as an initiator for the AROP of EO was evaluated (data not shown).

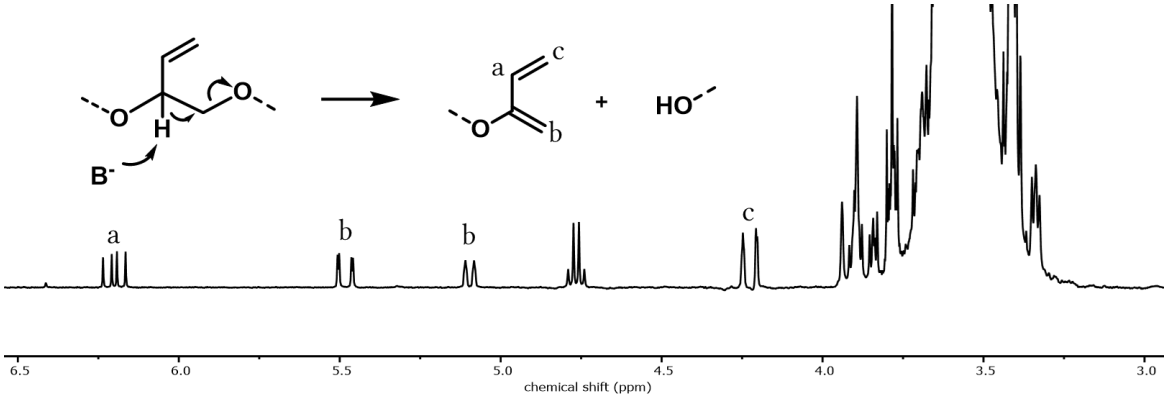

Figure 1: β-Elimination as a side reaction during polymerization of EO using OBB as initiator.

However, depending on temperature, solvent and especially base and counter-ion, β-elimination is a common side-reaction for this type of allyl ether structures. This is shown in **Figure 1**, which displays the ^{1}H NMR spectrum during an OBB-initiated polymerization of EO, using potassium *tert*-butoxide (KOtBu) for partial deprotonation. As OBB and P(EG-*co*-EPB) copolymers share basically the same allyl ether motif, this side reaction will occur during the copolymerization of EO with EPB as well.

To solve this problem, we developed a novel class of allyl ether containing initiators, starting from 2-(methylene)-1,3-propanediol (MPD) as a lead structure. The most interesting and striking feature of this lead structure is the absence of protons in β-position, preventing β-elimination as a side reaction. This enables polyether synthesis from epoxide monomers *via* classical AROP in DMSO using potassium *tert*-butoxide as a deprotonation agent, and the isomerization of allyl ethers to vinyl ethers can be conducted in a convenient on-step reaction *directly* after polymerization, without the need for preceding isolation and purification of the polymers. The isomerization of allyl ethers to vinyl ethers was investigated from a fundamental perspective in the early 1960s by Price and Snyder as well as by Prosser.[21,22] They reported this rearrangement to be greatly facilitated by base-catalysis with the presence of potassium in a polar and aprotic solvent such as DMSO, which closely resembles our polymerization conditions.

Therefore, according to the literature, we only had to rise the temperature to 80 °C to conduct the isomerization in a one-batch approach.

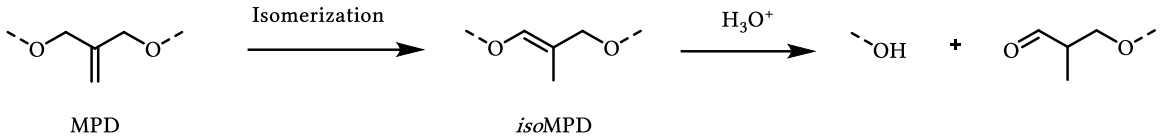

Scheme 2: Isomerization and hydrolysis of MPD-derived substructures.

This leads to two approaches for the implementation of a single allyl ether function in a tuneable position in the polyether backbone: (i) symmetrically in the center of a polymer chain, using a bifunctional initiator, or (ii) at the chain end of a polymer chain, between any arbitrary residue and the terminal hydroxyl group of a monofunctional initiator (**Scheme 2**).

3.2.3.1 INITIATOR SYNTHESIS: BIFUNCTIONAL MBE

While MPD is commercially available, it was found to be not perfectly suitable as an initiator for AROP, as the low molecular weight (88.11 g mol^{-1}) bears the risk of evaporation during the drying process in high vacuum at elevated temperature prior to polymerization and also results in low solubility of the initiator salt. This renders control of the molecular weights difficult. Nevertheless, as first exploratory experiments showed promising results, we decided to implement the allyl ether motif of MPD as a lead structure for further development of an improved AROP initiator and aimed at avoiding these disadvantages.

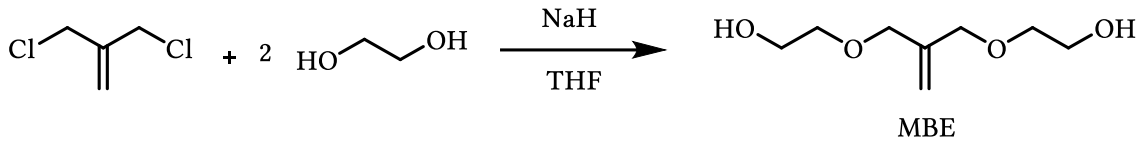

Scheme 3: Synthesis of MBE as a bifunctional initiator for AROP.

Based on all above considerations, 2,2‘-(2-methylenepropane-1,3-diyldioxy)bisethanol (MBE) was synthesized *via* a convenient one-step reaction by

nucleophilic substitution of 2-chloromethyl-3-chloroprop-1-ene with ethylene glycol (**Scheme 3**), basically resulting in the addition of two ethylene glycol spacers at the terminal hydroxyl groups of MPD. This compound can be synthesized on multi gram-scale and can be purified *via* distillation, offering access to large quantities with excellent purity at low costs. The detailed NMR analysis of this compound can be found in the supporting information

3.2.3.2 POLYMER SYNTHESIS BASED ON MBE, CHARACTERIZATION AND DEGRADATION

All polymers presented in this work were synthesized *via* the "classical" anionic ring-opening polymerization (AROP) of ethylene oxide (EO), which is also used to generate FDA-approved PEGs. To demonstrate the excellent control over the molecular weights and the option of different approaches for isomerization, two series of polymers (Samples 1a–d and 2a–d) were synthesized using MBE as an initiator. Isomerization of the ally ether precursors was conducted *via* two techniques (**Scheme 4**.): (i) *directly via* a one-batch approach after polymerization without termination, exploiting the base-catalysed isomerization with potassium in DMSO (Samples 1a-d) and (ii) *catalytically*, after termination and purification of the polymers, using Wilkinson's catalyst (Samples 2a-d).

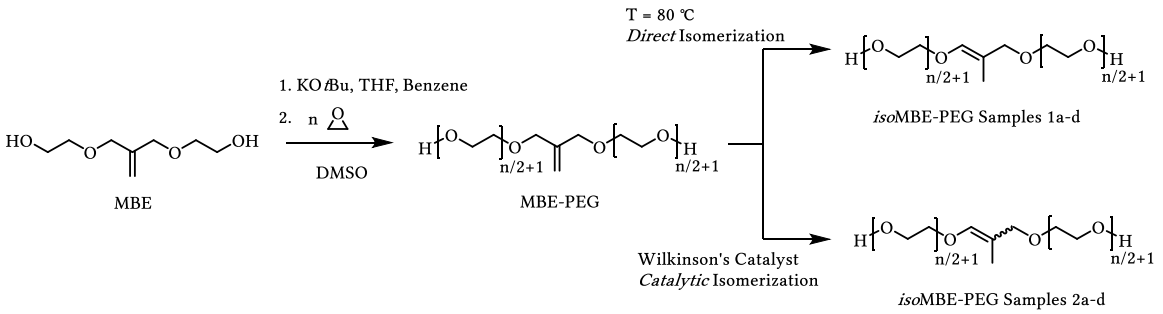

Scheme 4: Synthesis of MBE-PEGs using MBE as an initiator and isomerization using a *direct* and a *catalytic* approach, respectively to obtain *iso*MBE-PEGs.

Table 1 shows the key characterization data for all polymers that were obtained using MBE as a bifunctional initiator. Molecular weights of M_n = 2,000 g mol^{-1} up to M_n = 12,000 g mol^{-1} were targeted, and the obtained values are in good agreement with the targeted values. The molecular weight was determined *via* ^{1}H NMR spectroscopy as well as *via* SEC using PEG standards (**Figure 2** and **Figure 3**). By using the allylic protons at 5.12 ppm as a reference, molecular weights of these polymers could be determined by integration of the polyether backbone signals (between 3.80 ppm and 3.30 ppm).

Table 1: Comprehensive characterization data for MBE initiated polymers and their fragments after acidic cleavage

		before cleavage				*after* cleavage	
Sample	Composition	M_n^{theo} / g mol^{-1}	M_n^a / g mol^{-1}	M_n^b / g mol^{-1}	$Đ^b$ = M_w / M_n	M_n^b / g mol^{-1}	$Đ^b$ = M_w / M_n
1a	MBE-PEG$_{47}$	2,000	2,070	1,930	1.04	950	1.06
1b	MBE-PEG$_{107}$	4,000	4,710	3,990	1.03	1,890	1.04
1c	MBE-PEG$_{217}$	8,000	9,550	8,270	1.03	3,720	1.04
1d	MBE-PEG$_{311}$	12,000	13,700	12,710	1.04	5,840	1.03
2a	MBE-PEG$_{51}$	2,000	2,230	1,940	1.04	1,050	1.06
2b	MBE-PEG$_{99}$	4,000	4,350	3,690	1.03	1,880	1.03
2c	MBE-PEG$_{176}$	8,000	7,740	6,230	1.04	3,120	1.03
2d	MBE-PEG$_{294}$	12,000	12,920	9,970	1.04	5,010	1.03

[a]Determined *via* ^{1}H NMR spectroscopy, [b]determined *via* SEC (RI, DMF, PEG standards).

^{1}H NMR appears to slightly overestimate the obtained molecular weights, but follows the SEC trend, considering the given limitations and inaccuracies of this method for higher molecular weights. The polymers exhibit low dispersities ($Đ \leq 1.04$) (**Figure 2**), as expect for AROP.

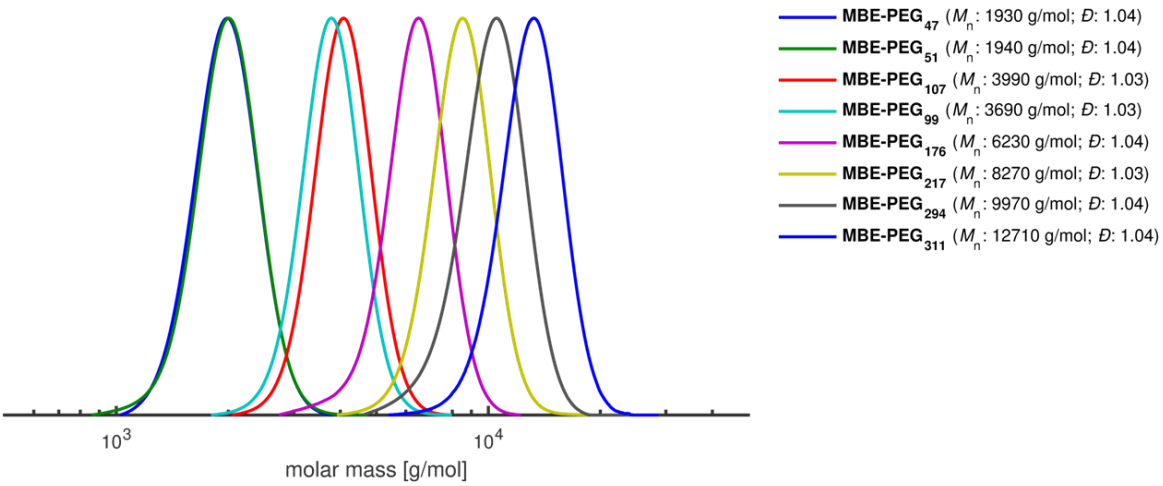

Figure 2: SEC traces (RI detector, solvent DMF, PEG standards) of the series 1a–d of MBE-PEG and *iso*MBE-PEG polymers, isomerized *via direct* isomerization.

The polymer samples 1a–d were isomerized in a very simple and convenient way, only by raising the temperature to 80 °C after full conversion of EO, since base-catalysed isomerization of allyl ethers in DMSO in the presence of potassium is a well-known reaction.[21,22] It should be pointed out that the polymer was not terminated before this isomerization step.

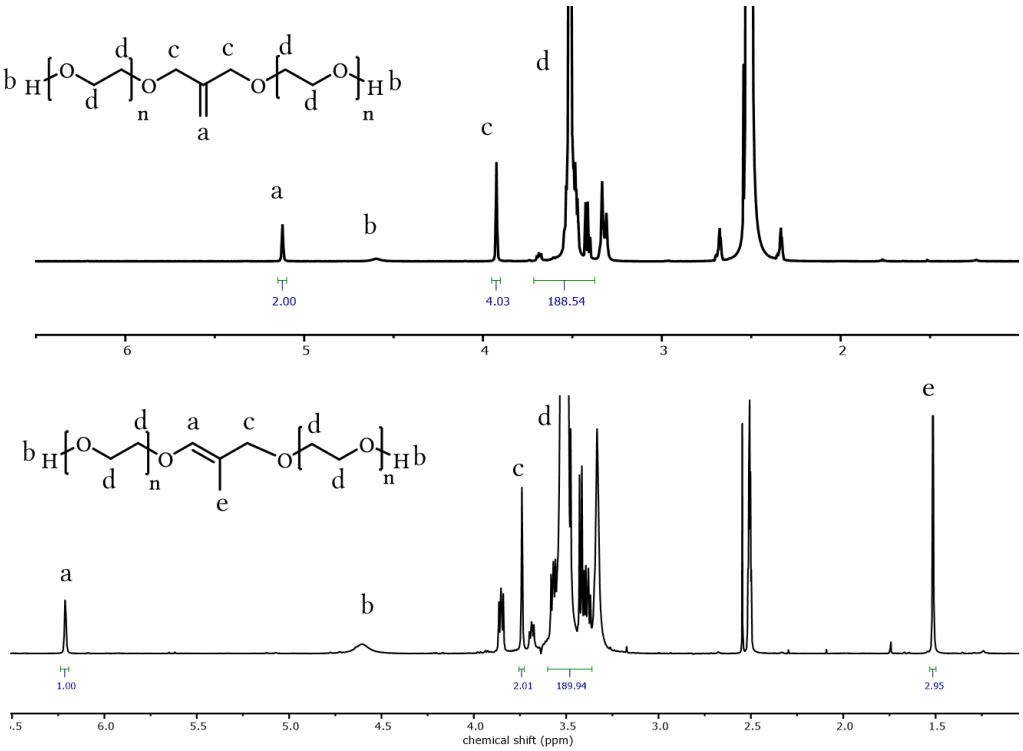

Figure 3: ^{1}H NMR spectrum (400 MHz, DMSO-d_6) of MBE-PEG$_{47}$ (top) and *iso*MBE-PEG$_{47}$ (bottom), shown after *direct* thermal isomerization.

Figure 3 shows exemplarily the ^{1}H NMR spectrum of the polymer MBE-PEG$_{47}$ before and after *direct* isomerization. The ^{1}H NMR spectroscopic data indicate quantitative transformation of the allyl ether moiety to a vinyl ether moiety. The characteristic allylic proton signal at 5.12 ppm (two protons) have vanished, and a single distinctive signal at 6.22 ppm (one proton) appeared. Integration of these signals indicates full conversion and is congruent with the supposed structure. This *direct* or *thermal* approach of isomerization, using the base-catalysis with potassium in DMSO, results in a quantitative formation of only one isomer (*E*), as already reported in the literature. [21-25]

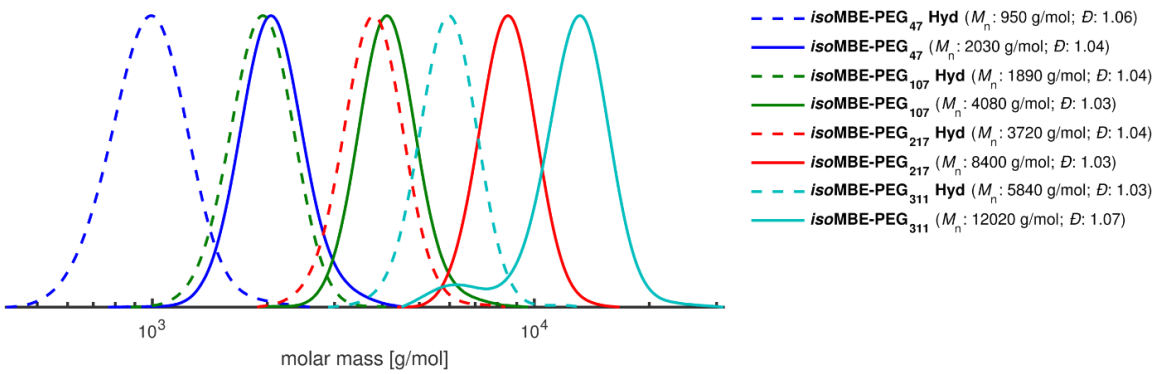

Figure 4: SEC traces (RI detector, solvent DMF, PEG standards) of the series 1a–d of *iso*MBE-PEGs with vinyl ether moieties. Solid lines show *iso*MBE-PEG polymers before and dashed lines *iso*MBE-PEG polymers after hydrolysis.

Subsequently, to study degradation of the isomerized *iso*MBE-PEG polymers, they were hydrolysed by treating a solution of 15 mg polymer in 200 µL DCM with one drop of 10% HCl in MeOH, to ensure complete degradation. The solution was neutralized and the fragments were analysed *via* SEC (**Figure 4**). As expected from using a bifunctional initiator for AROP, the fragments exhibit just half of the molecular weight of their precursor polymers. As an example, the molecular weight of sample 1a (*iso*MBE-PEG$_{47}$) was found to decrease from M_n = 2,030 g mol^{-1} to M_n = 950 g mol^{-1}, preserving the expected low dispersity of the fragment. This evidences that the vinyl ether moiety is located in the centre of the polyether backbone, and both active chain ends propagate at

the same rate, resulting in two well-defined ($Đ \leq 1.06$) polyether chains with the same molecular weight, as is expected from polymerization statistics.

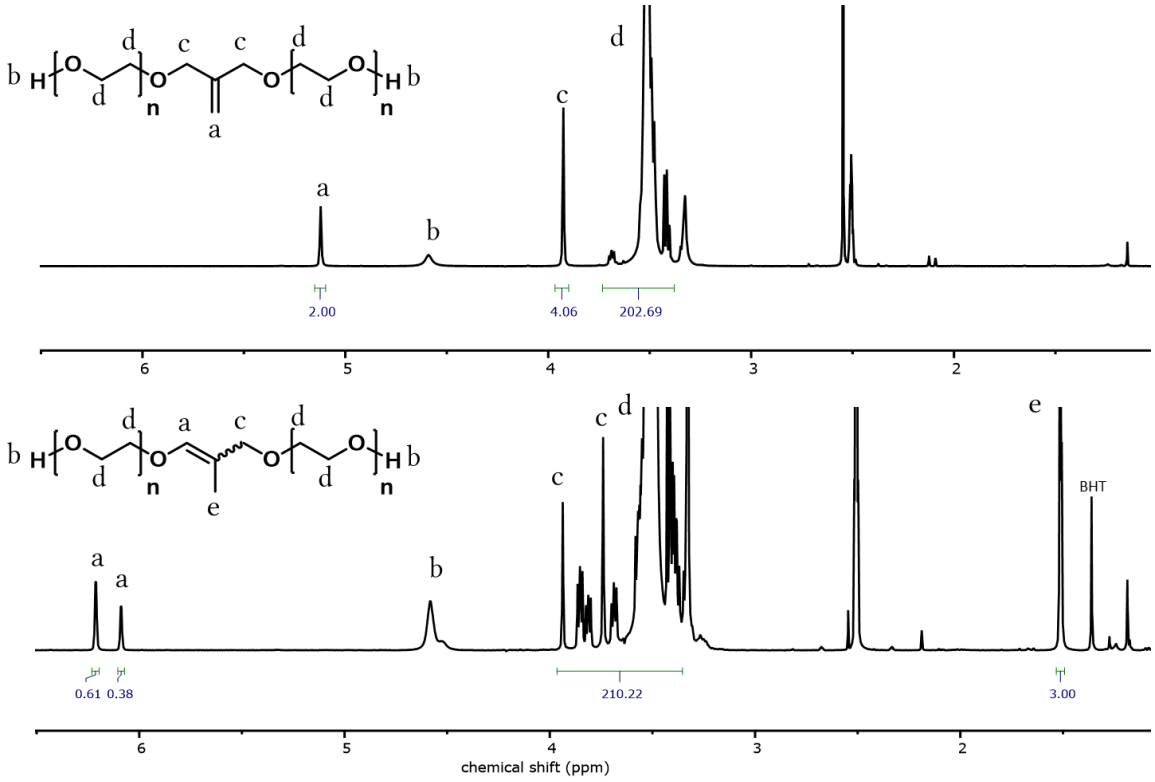

Figure 5: ^{1}H NMR spectrum (400 MHz, DMSO-d_6) of MBE-PEG$_{51}$ (top) and *iso*MBE-PEG$_{51}$ (bottom), after isomerization *via* Wilkinson's catalyst.

As the *thermal* isomerization approach might not be tolerated by functional groups of possible multifunctional copolymers or the allyl ether precursor needs to be stable during further post-polymerization reactions before the activation of the acid labile moiety, we additionally analysed the isomerization *via* Wilkinson's catalyst after the work-up of the polymers.

Figure 5 shows as an example the ^{1}H NMR spectrum of the polymer sample 2a (MBE-PEG$_{51}$) before and after isomerization using Wilkinson's catalyst. As shown before in **Figure 3**, the proton signal of the allyl ether moiety is clearly visible at a chemical shift of 5.12 ppm. In this case, two distinctive signals for vinyl ether moieties appear at 6.22 ppm and 6.09 ppm, indicating the formation of a mixture of (*E*) and (*Z*) isomers. The ratio between these two signals (~ 2/3 (*E*) isomer) is in good agreement

with the already reported selectivity of the Wilkinson's catalyst to form preferably the (*E*) isomer.[26,27,17] For the hydrolysis of these isomers, no significant difference expected, as shown before.[17]

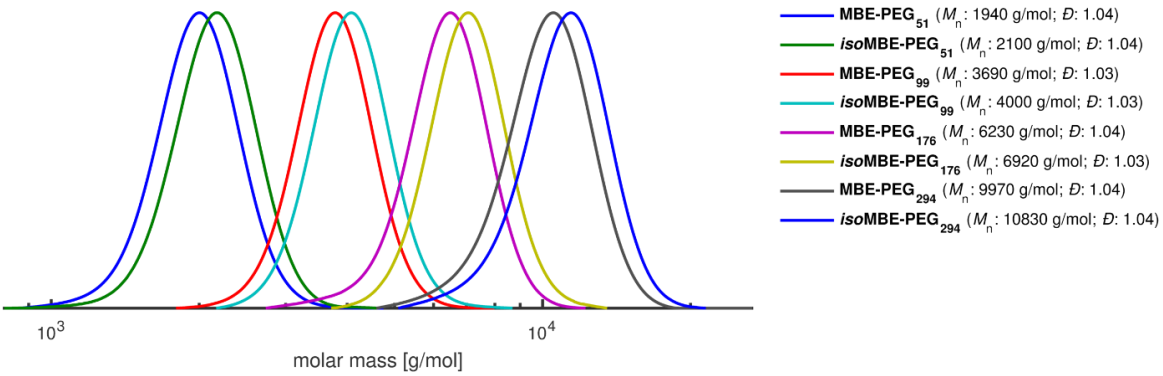

Figure 6: SEC traces (RI detector, solvent DMF, PEG standards) of the series 2a–d of *iso*MBE-PEG polymers isomerized *via* Wilkinson's catalyst.

As the only difference between the MBE-PEG series 1a–d and 2a–d is the technique of isomerization and as a result the partial configuration of one single bond, it is surprising to see a clear difference in hydrodynamic radii after isomerization, manifest in SEC (**Figure 6**). Series 1a–d was *directly* isomerized, yielding only the (*E*) isomer and shows no significant difference between the SEC traces of MBE-PEG and *iso*MBE-PEG (**Figure 2**). In the SEC traces for the series 2a–d, a distinctive shift towards higher molecular weight for the isomerized polymer is visible (**Figure 6**). Compared to the non-isomerized form, an increase of approximately 10% in molecular weight was observed. This indicates a significant effect of the obtained mixture of (*E*) and (*Z*) isomers formed upon isomerization using Wilkinson's catalyst (**Figure 5**). In case of the *direct* approach of thermal isomerization used in the series 1a–d, resulting only in the (*Z*) isomer, this behaviour could not be observed. Previously reported vinyl ether containing PEGs did not show such a distinct variation of hydrodynamic radii after isomerization.[18,16,17] It must be noted that in these cases the vinyl ether moieties were partially oriented in the side chain of the polyether, and in the case of MBE-PEGs, the vinyl ether moiety is located *inside* the backbone. This directly affects the orientation of the following bond

between the quaternary and secondary carbon atom inside the polymer backbone. We assume, that this chain configuration of the (*Z*) isomer results in a higher hydrodynamic radius, albeit this effect should be further investigated.

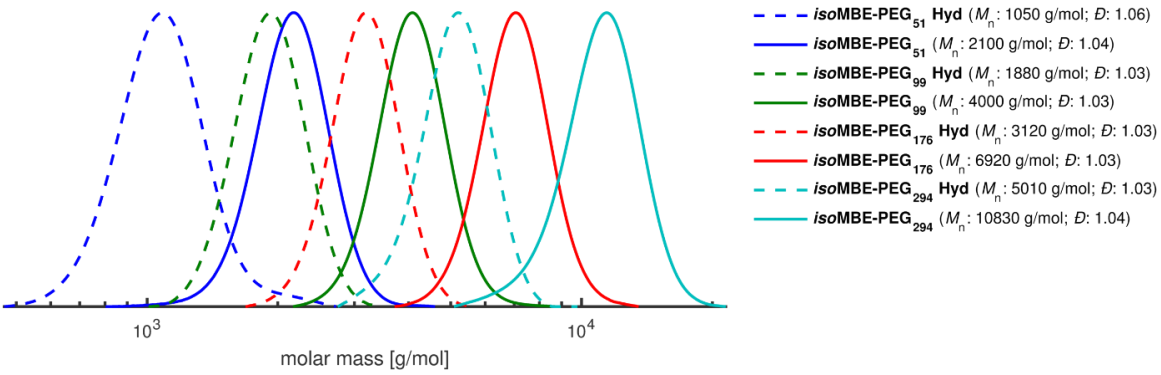

Figure 7: SEC traces (RI detector, solvent DMF, PEG standards) of the series 2a–d of *iso*MBE-PEGs. Solid lines show *iso*MBE-PEG polymers before and dashed lines *iso*MBE-PEG polymers after hydrolysis (in the respective same colour).

The polymer series 2a–d was hydrolysed in the same manner, and the resulting fragments analysed *via* SEC (**Figure 7**). They show the same fragmentation behaviour as the polymers from the series 1a–d: exemplary for polymer 2a (*iso*MBE-PEG$_{51}$), the molecular weight decreases from M_n = 2,100 g mol^{-1} to M_n = 1,050 g mol^{-1} due to slicing the polyether backbone into two halves of the same size. The difference in hydrolysis rate of vinyl ether (*E*) and (*Z*) isomers was already analysed *via in situ* ^{1}H NMR kinetic studies elsewhere for polymers with multiple vinyl ether units obtained via copolymerization.[17] Therefore, we do not focus on this topic here.

3.2.3.3 MBE: SEC KINETICS DEGRADATION STUDY

To investigate the time-dependency of the degradation of the vinyl ether PEGs with a central cleavage site, we developed a method to conduct an automated SEC measurement. By drastically decreasing the injection volume, using a higher concentrated polymer solution and employing customized solvent and waste reservoirs, we could consecutively analyse the same polymer solution from one single SEC vial up to 60 times. This setup gave us the opportunity to follow the degradation of an acid labile

polymer in pH buffer solution *via* SEC, without having to rely on inconvenient techniques like taking aliquots at defined time stamps by hand or using multiple aliquots in different vials to take the samples from.

As the cleavage site is centred in the middle of the polymer chain, only two well-defined fragments are formed during the degradation process (as already demonstrated in **section 3.2.3.2**). This allows to fit the experimental data using a deconvolution method by the addition of two gaussian functions, one function for each polymer distribution.[28]

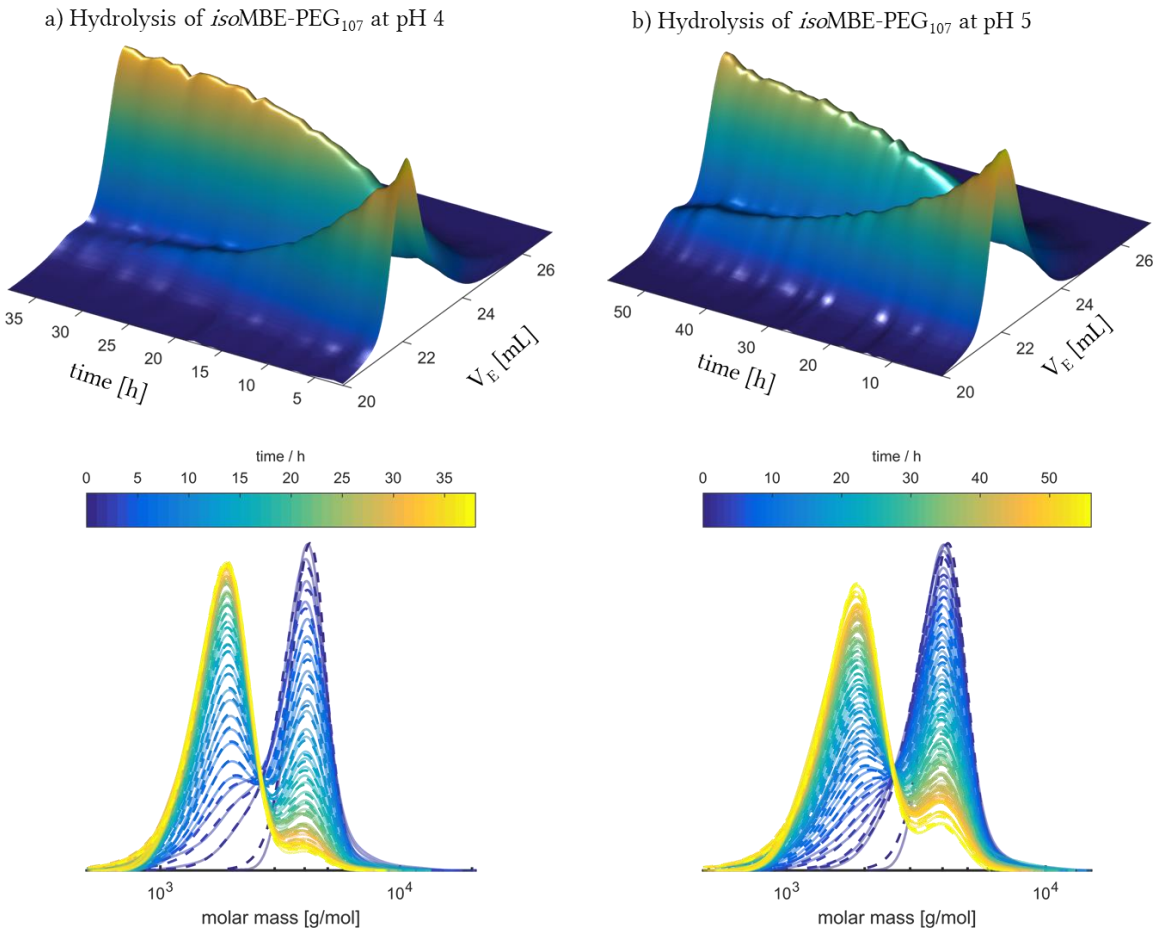

Figure 8: Top: SEC (RI detector, solvent DMF, PEG standards) data of the hydrolytic degradation of *iso*MBE-PEG$_{107}$. Bottom: SEC traces (RI detector, solvent DMF, PEG standards) of *iso*MBE-PEG$_{107}$ during incubation in a) pH 4 buffer solution for 39 hours and b) pH 5 buffer solution for 56 hours at room temperature. Each line represents the SEC curve after every 60 minutes (solid lines: experimental data, dashed lined: fitted data).

Figure 8 shows the superimposed SEC data obtained *via* this method for the incubation of sample 1b (*iso*MBE-PEG$_{107}$) at a) pH 4 and b) pH 5. Each line represents the SEC data of the incubated polymer for every 60 minutes (starting with the unhydrolyzed polymer, dark blue line). For example, as shown in a), the hydrolytic degradation can be followed by the emerging of a second mode at M_n = 1,890 g mol^{-1}, while simultaneously the distribution of the original polymer at M_n = 3,990 g mol^{-1} vanishes.

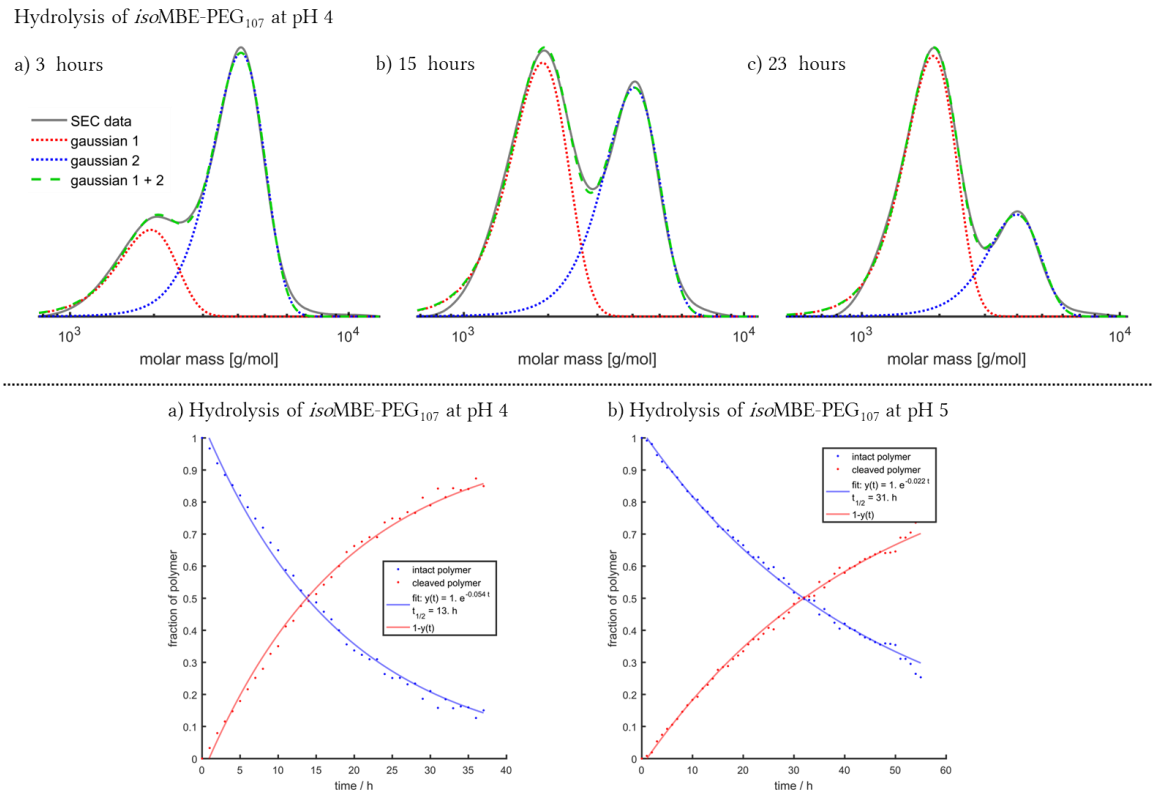

Figure 9: Top: Examples for the addition of two gaussian functions, used to fit the SEC data from the degradation of *iso*MBE-PEG$_{107}$ at pH 4. Bottom: Calculation of the half-life times of *iso*MBE-PEG$_{107}$ during incubation at a) pH 4 and b) pH 5, using these gaussian fits.

The ratio of the area of the two gaussians was used to determine the ratios of intact and cleaved polymers. These ratios were plotted vs. time and fitted to first order kinetics (exponential decay) (**Figure 9**). Based on these fits, the half-life of the cleavage could be calculated. This calculation resulted in $t_{1/2}$ = 13 h at pH 4 and $t_{1/2}$ = 31 h at pH 5, which

aligns well with the data for cleavage of similar vinyl ethers (Worm *et al.*, *via* online ^{1}H NMR, $t_{1/2}$ = 9-20 h at pD 4.4 and $t_{1/2}$ = 20–34 h at pD 5).

3.2.3.1 INITIATOR SYNTHESIS: MONOFUNCTIONAL BMP

The novel allyl ether structure can be connected to any functional group and thereby gives access to an acid-labile linker between the end of a PEG chain and the respective group. 2-((Benzyloxy)methyl)prop-2-en-1-ol (BMP) was chosen as a model compound to demonstrate the versality of the allyl ether structure at the end of the polymer chain *via* a monofunctional initiator.

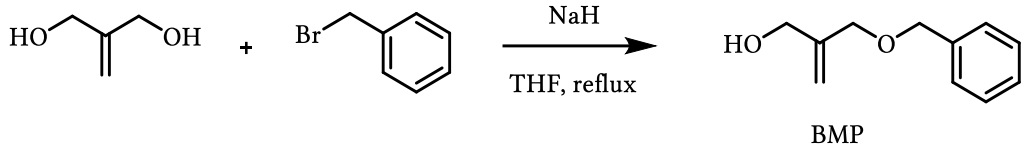

Scheme 5: Synthesis of MBP as a monofunctional initiator for AROP.

BMP can be synthesized in a very straightforward procedure, and a wide range of other functional initiators is accessible using this route. The resulting structure resembles closely the well-established AROP initiator 2-(benzyloxy)ethanol. The aromatic protons allow to determine the molecular weight *via* ^{1}H NMR spectroscopy (**Scheme 5**). Furthermore, the hydrolysis of this residue can be conveniently followed *via* ^{1}H NMR spectroscopy as well. For extensive NMR studies of this compound, see the supporting information.

3.2.3.2 BMP: POLYMER SYNTHESIS, CHARACTERIZATION AND CLEAVAGE

As a proof of concept to demonstrate the universal attachment of the allyl ether moiety at the end of a PEG chain, two polymers were synthesized *via* classical AROP of EO, using BMP as an initiator (**Scheme 6**).

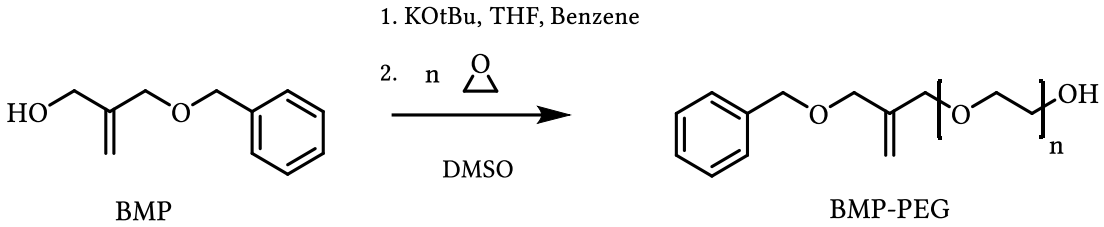

Scheme 6: Polymerization of EO using BMP as an initiator.

Table 2 shows the key characterization data for the BMP initiated polymers. The aromatic protons at a chemical shift of 7.33 ppm were used to determine the molecular weight *via* ^{1}H NMR spectroscopy (**Figure 11**).

Table 2: Characterization data for BMP initiated polymers.

Sample	Name	M_n^{theo} / g mol^{-1}	M_n^a / g mol^{-1}	M_n^b / g mol^{-1}	$Đ^b$ = M_w / M_n
3a	BMP-PEG$_{72}$	3,000	3,150	3,070	1.04
3b	BMP-PEG$_{142}$	6,000	6,430	7,140	1.04

[a]Determined *via* ^{1}H NMR spectroscopy, [b]determined *via* SEC (RI, DMF, PEG standards).

With M_n = 3,150 g mol^{-1} and M_n = 6,430 g mol^{-1} (determined *via* SEC) and M_n = 2,970 g mol^{-1} and M_n = 5,730 g mol^{-1}, determined *via* ^{1}H NMR spectroscopy, the obtained molecular weights are in good agreement with the targeted molecular weights of M_n = 3,000 g mol^{-1} and M_n = 6,000 g mol^{-1}, respectively. With $Đ$ = 1.04, narrow molecular weight distributions were obtained (**Figure 10** and **Figure 11**).

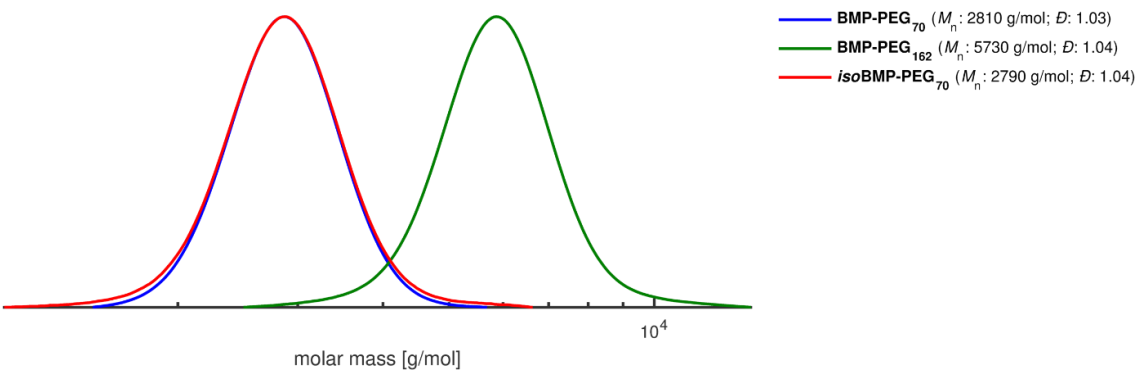

Figure 10: SEC traces (RI detector, solvent DMF, PEG standards) of BMP initiated polymers.

After polymerization, these polymers were *directly* isomerized, as already reported for MBE PEGs. This one-step reaction allows for the synthesis of a polyether that is connected to a functional group *via* an acid-labile vinyl ether linker. Instead of the benzyl group, any other desired AROP-stable group can be attached, for example lipids or cholesterol to form degradable micelles or lipophilic anchoring structures.[29]

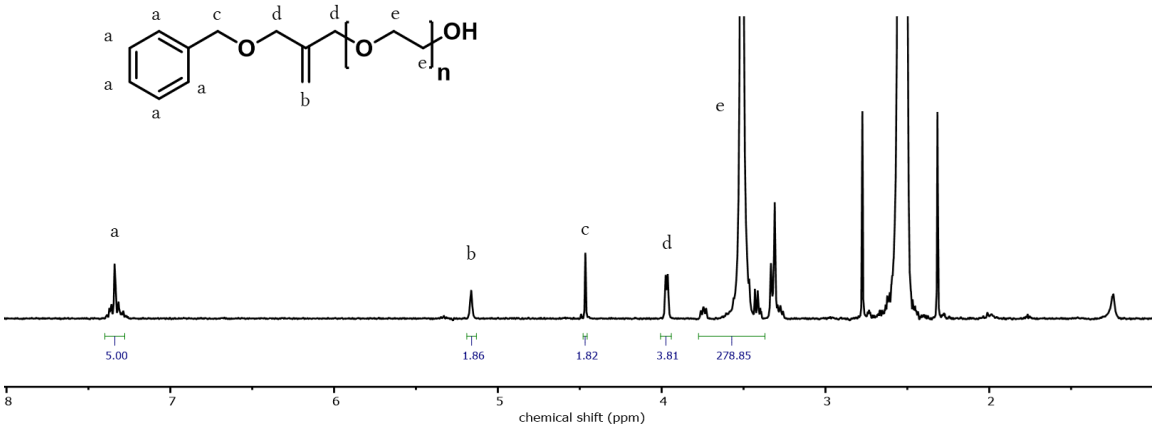

Figure 11: ^{1}H NMR spectrum (400 MHz, DMSO-d_6) of BMP-PEG$_{70}$ after polymerization.

Isomerization was analysed *via* ^{1}H NMR spectroscopy and revealed the characteristic disappearance of the allyl ether proton signals at 5.13 ppm and the appearance of two distinct vinyl ether signals at 6.29 ppm and 6.24 ppm (as exemplified for *iso*BMP-PEG$_{70}$ in **Figure 12**).

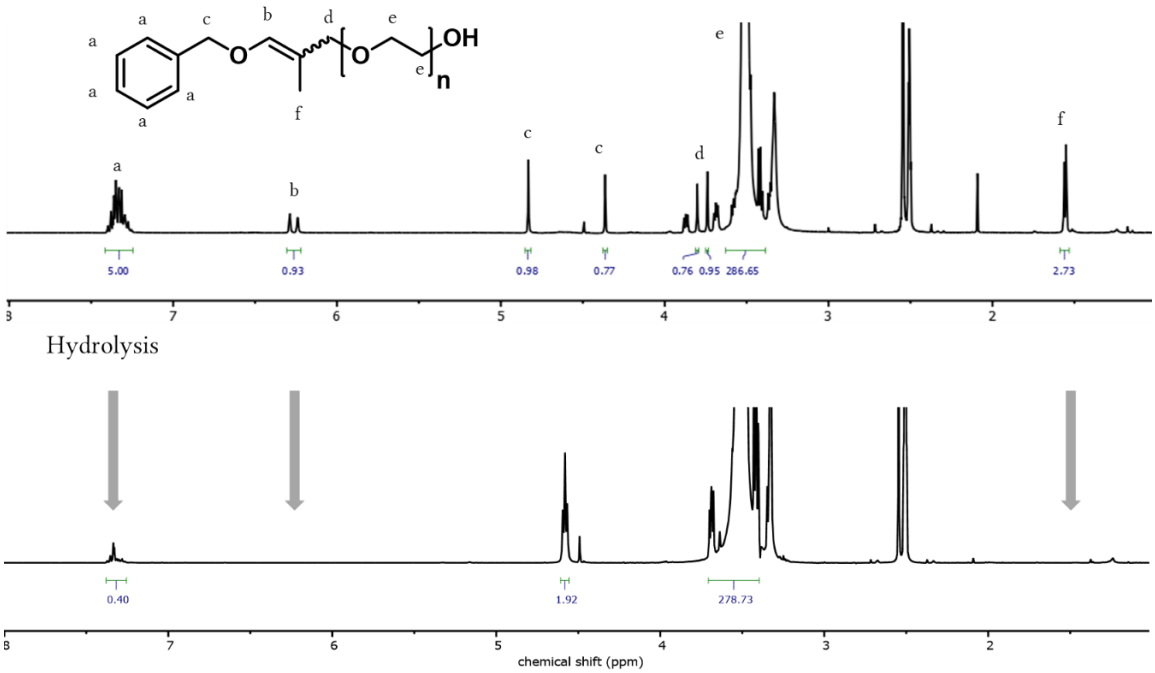

Figure 12: ^{1}H NMR spectrum (400 MHz, DMSO-d_6) of *iso*BMP-PEG$_{70}$ and *iso*BMP-PEG$_{70}$ after hydrolysis of benzyl group.

Interestingly, in contrast to the *direct* isomerization of MBE-PEGs, the thermal isomerization of BMP-PEGs leads to two vinyl ether signals, indicating the formation of a mixture of isomers. This should be further investigated.

Hydrolysis of *iso*BMP-PEG$_{70}$ was performed by stirring the polymer over ion exchange resin for 24 hours, followed by precipitation of the polymer into diethyl ether. As shown for the polymer *iso*BMP-PEG$_{70}$ in **Figure 12**, this leads to an almost quantitative removal of the benzyl group. No reliable signals for referencing remained after the hydrolysis of the benzyl group, so the polyether backbone signals in the ^{1}H NMR spectrum were used for referencing. However, it could be shown that the distinct vinyl ether signals (6.29 ppm and 6.24 ppm) quantitatively disappeared. The integration of the residual aromatic protons (7.33 ppm) shows that only 8% are left, indicating nearly complete removal of this group.

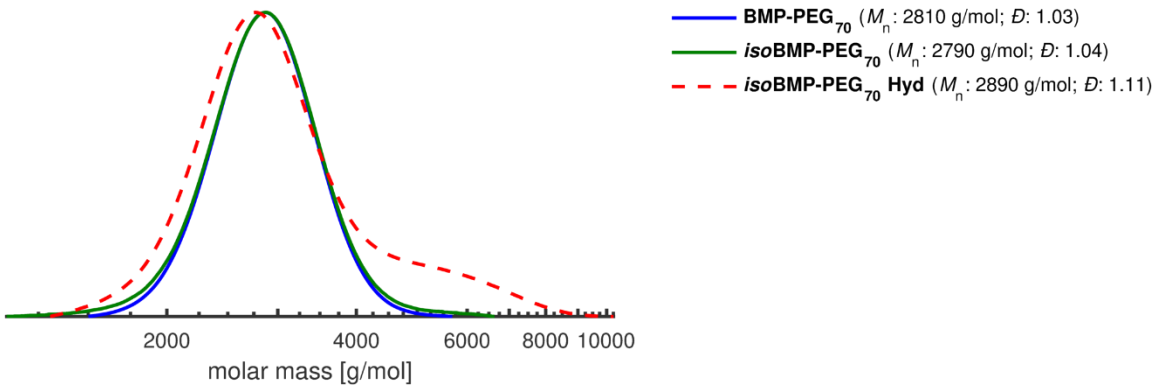

Figure 13: SEC traces (RI detector, solvent DMF, PEG standards) of BMP-PEG$_{70}$ before and after direct isomerization (solid lines) and after hydrolysis of the benzyl group (dashed line).

Figure 13 shows the SEC analysis of BMP-PEG$_{70}$ before and after *direct* isomerization (blue and green lines) and after hydrolysis of the benzyl group (red dashed line). While the SEC traces of BMP-PEG$_{70}$ before and after isomerization are in almost perfect superposition with equally low dispersities ($Đ \leq 1.04$), the trace after hydrolysis shows a slightly higher dispersity ($Đ = 1.11$) and a shoulder at approximately M_n = 6,000 g mol^{-1}, around the twofold molecular weight of the analysed polymer. This, and the remaining 8% benzyl groups after hydrolysis, while no vinyl ether species proton signals were present anymore, could be a hint for a side reaction, leading to dimerization of the polymer chains and will be further investigated.

3.2.3.3 HYDROGEL SYNTHESIS, CHARACTERIZATION AND DEGRADATION

Methacrylation using an enzyme-mediated transesterification by *Candida antarctica* lipase B (CALB) has been proven to be a robust, convenient and effective technique to activate PEGs for radical crosslinking in aqueous media in order to form hydrogels (**Scheme 7**).[13]

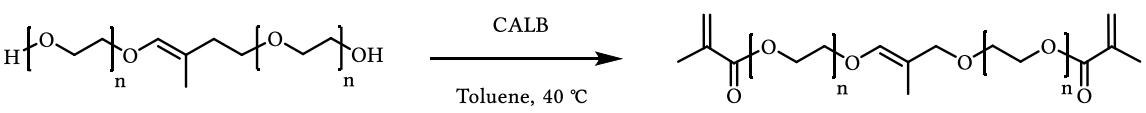

Directly Isomerized Samples 1a-d

*iso*MBE-PEG-DMA

Scheme 7: Methacrylation of *iso*MBE-PEGs to obtain *iso*MBE-PEG-DMA.

In order to form acid-labile hydrogels, the polymer end groups of the *directly* isomerized samples 1a–d (*iso*MBE-PEGs) were methacrylated. **Figure 14** shows exemplary the ^{1}H NMR spectrum of *iso*MBE-PEG$_{47}$ dimethacrylate (DMA). After methacrylation, two distinct proton signals appear at a chemical shift of 6.04 ppm and 5.70 ppm. The integration of these signals, compared to the vinyl ether proton signal at 6.22 ppm, indicates almost quantitative methacrylation (98%).

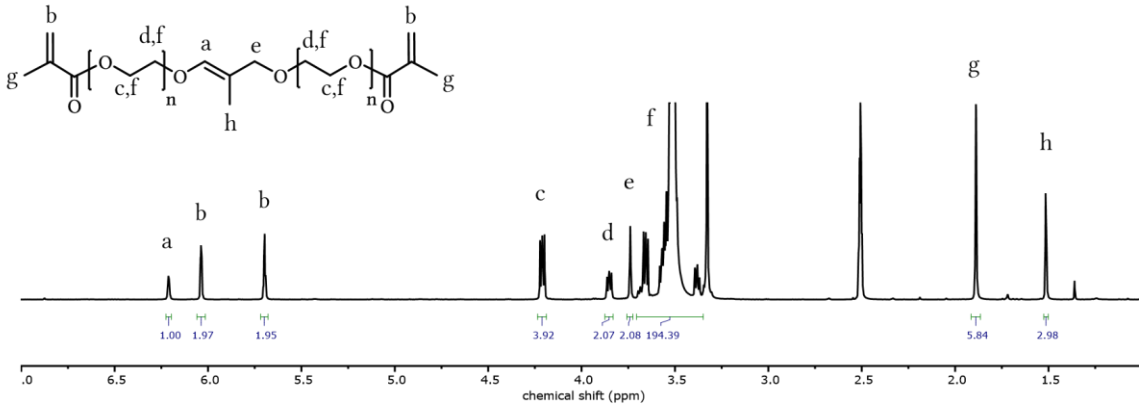

Figure 14: ^{1}H NMR spectrum (400 MHz, DMSO-d_6) of *iso*MBE-PEG$_{47}$-DMA.

The methacrylated macromonomers obtained from the polymer series 1a–d were used to form hydrogels by radical crosslinking. The obtained hydrogels were clear, robust with well-defined edges and allowed for facile handling using tweezers, while preserving their shape. **Figure 15** shows photographs of these gels at different states during their synthesis and analysis of their swelling behaviour.

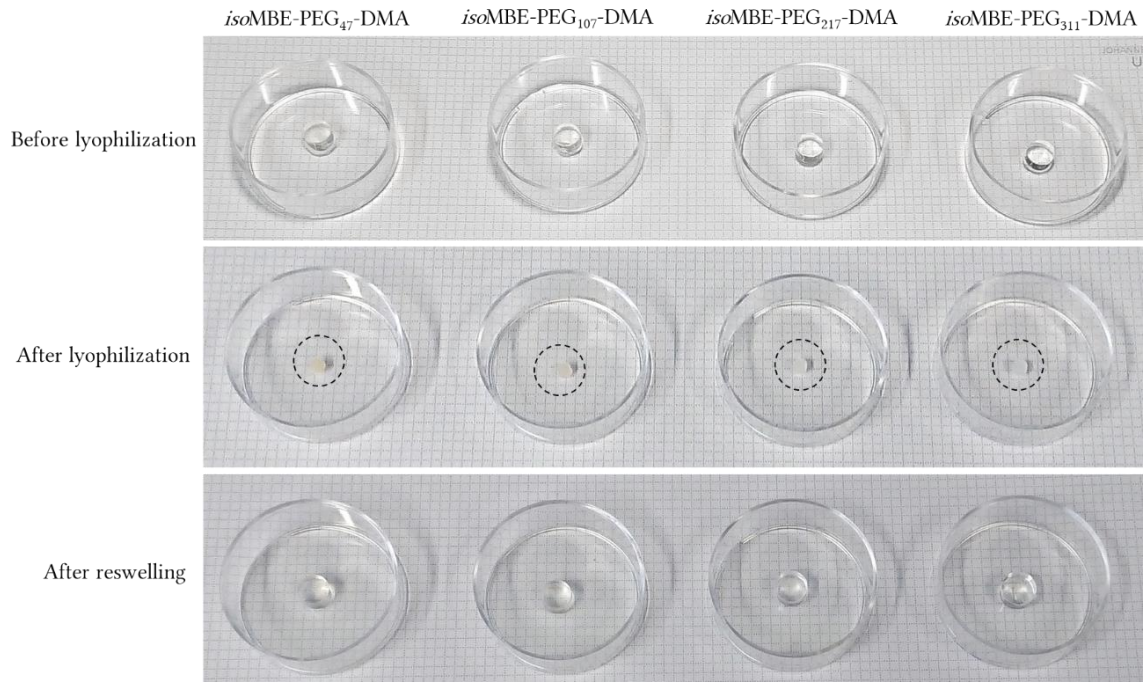

Figure 15: Photographs of *iso*MBE-PEG-DMA hydrogels before and after lyophilization and after reswelling by incubation in PBS buffer for 3 days.

After their synthesis, the hydrogels were incubated in PBS buffer for 24 hours to extract any not incorporated macromonomer. Subsequently, the hydrogels were lyophilized to analyse their swelling behaviour and to investigate if they can be stored in a dried state. After lyophilization, the weight of all dried hydrogel samples was determined to be 15 mg, representing exactly the weight of the used amount of *iso*MBE-PEG macromonomer. They were then placed back into a PBS buffer solution and allowed to reach a swelling equilibrium by incubating them for 3 days.

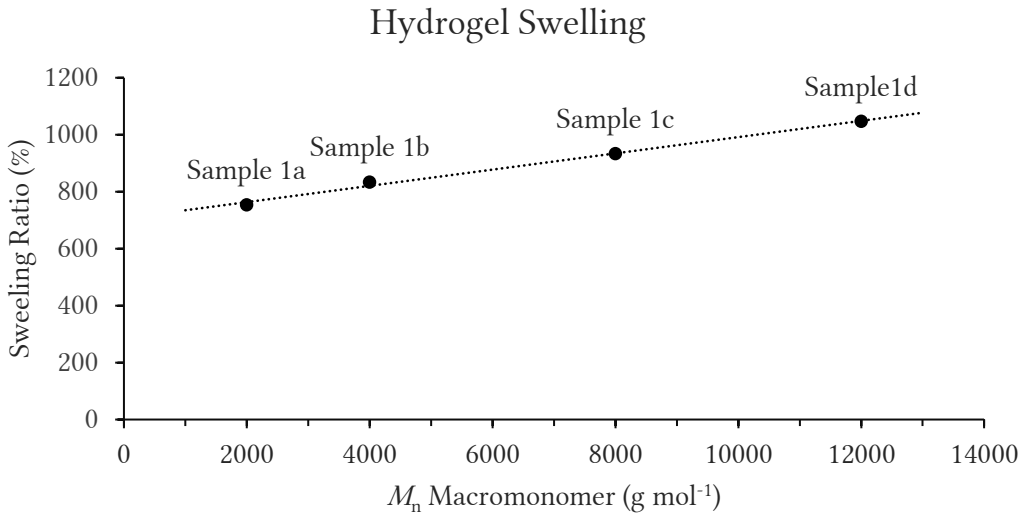

Figure 16: Swelling behaviour of *iso*MBE-PEG-DMA hydrogels depending on the molecular weight of the used macromonomer.

The swelling ratio of these hydrogels was then calculated by the equation

$$\text{Swelling ratio} = \frac{W_s - W_d}{W_d}$$

wherein W_s is the weight of the swollen hydrogel and W_d is the weight of the dried hydrogel. As shown in **Figure 16**, there is a clear trend in the swelling ratio depending on the molecular weight of the used *iso*MBE-PEG-DMA macromonomer: the higher the molecular weight, the higher the swelling ratio of the resulting hydrogels. This is in line with the equilibrium swelling theory, which links the crosslinking density (and therefore the molecular weight of the macromonomer used to form the hydrogel) to the swelling ratio. Briefly, because of their tighter structure, higher densely crosslinked hydrogels swell less than the same hydrogels with a lower crosslinking ratio.[30]

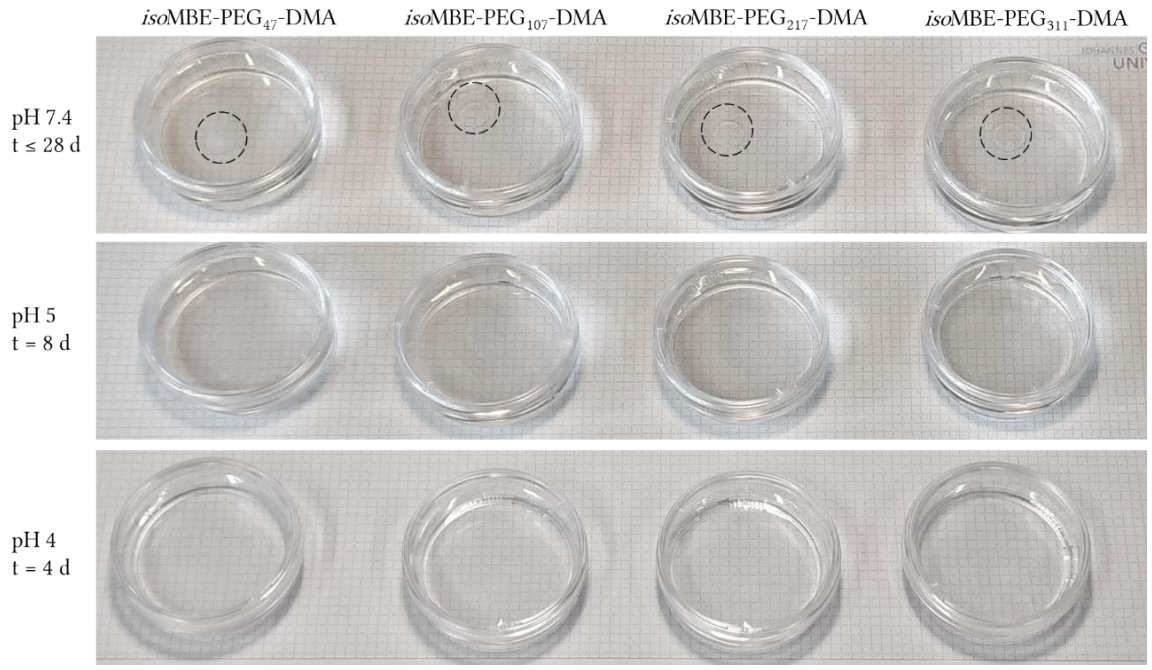

Figure 17: Photographs during incubation of *iso*MBE-PEG-DMA hydrogels at different pH buffer solutions at room temperature over a period of up to 28 days. Timestamps indicate the time until complete disintegration of the hydrogels.

Furthermore, hydrogels prepared from the *iso*MBE-PEG-DMA macromonomers were incubated at different pH values to investigate their stability in acidic conditions as well as in neutral media (PBS) (**Figure 17**). Upon incubation in pH 4 buffer solution, the hydrogels were fully disintegrated after four days. At pH 5, it took eight days until complete degradation. Interestingly, there was no significant difference in stability between the hydrogels obtained from *iso*MBE-PEG-DMA macromonomers with different molecular weights. The hydrogels that were incubated at pH 7.4 were stable for the whole time of observation, that is for more than four weeks.

3.2.4 CONCLUSION

Overall, we synthesized a bifunctional allyl ether initiator with a predefined cleavage site for the AROP of EO and obtained two series of PEG samples (Samples 1a–d and 2a–d), ranging from M_n = 2,000 g mol^{-1} up to M_n = 12,000 g mol^{-1}, with monomodal, narrow molecular weight distributions ($Đ \leq 1.04$). Both series of allyl ether

containing polymers were isomerized to vinyl ether containing PEGs, series 1a–d was *directly* isomerized, resulting purely in the (*E*) isomer, series 2a–d was isomerized using Wilkinson's catalyst, resulting in a mixture of (*E*) and (*Z*) isomers. Subsequently, both series of polymers were hydrolysed, showing a bisection of their molecular weight as a result of the bifunctional initiator. Using an automated SEC approach and the fitting of two gaussian functions, the kinetics of the hydrolysis of polymer series 1a-d was analysed, resulting in in $t_{1/2}$ = 13 h at pH 4 and $t_{1/2}$ = 31 h at pH 5

After their *direct* thermal isomerization, polymers from the series 1a–d were methacrylated and hydrogels were formed from these macromonomers *via* radical crosslinking. These hydrogels were analysed regarding their swelling ratio and stability at various pH values. They exhibit a direct proportional dependency between the molecular weight of the used macromonomer and their swelling ratio. While these hydrogels remain stable at pH 7.4 for over four weeks, they were fully disintegrated in four days at pH 4 and eight days at pH 5.

Furthermore, based on the same lead structure a monofunctional AROP initiator was synthesized, which contains a benzyl group that is well-traceable *via* ^{1}H NMR, linked by an allyl ether moiety. This initiator was used for the polymerization of EO. The obtained molecular weights of the polymers were in good agreement with the targeted values of M_n = 3,000 g mol^{-1} and Mn = 6,000 g mol^{-1} and narrow molecular weight distributions ($Đ$ = 1.04) were obtained. After *direct* isomerization of the allyl ether moiety to a vinyl ether moiety, the benzyl group could be cleaved from the polymer with an efficiency of 92%.

This new synthon gives access to degradable structures for a wide array of possible applications, from intrinsically cleavable PEGs with narrow distributed fragments over the application as an acid-labile linker for example between hydrophilic and

hydrophobic segments of amphiphilic copolymers up to the application as degradable diol-component i.e. in polyesters.

3.2.5 EXPERIMENTAL

Synthesis of 2,2'-(2-Methylenepropane-1,3-diyldioxy)bisethanol (MBE): Ethylene glycol (200 mL) was slowly added under argon atmosphere to a suspension of sodium hydride (10.1 g, 0.42 mol) in dry THF (200 mL). The resulting mixture was stirred at room temperature for 30 minutes. Subsequently, 3-chloro-2-(chloromethyl)prop-1-ene (25 g, 0.20 mol) was added slowly and the mixture was refluxed for 24 hours. THF and excess of ethylene glycol were removed under reduced pressure and the residue was treated with ethanol (150 mL). After filtration of the solid and evaporation of the ethanol, the product was obtained by distillation (B.p. = 140 °C / $1x10^{-3}$ mbar) as a colourless oil (yield: 14.1 g, 40%).^{1}H NMR (400 MHz, DMSO-d_6): δ [ppm] 5.13 (s, 2H, H_2C=C), 4.60 (t, 2H, CH_2OH), 3.93 (s, 4H, H_2C=(C-C$H_2O)_2$), 3.53 (q, 4H, CH_2O), 3.37 (q, 4H, CH_2O).

Synthesis of 2-((Benzyloxy)methyl)prop-2-en-1-ol (BMP): Sodium hydride (0.90 g, 42.6 mmol) was added under agon atmosphere to a solution of 2-methylenepropane-1,3-diol (3.00 g, 34.1 mmol) in dry THF (70 mL) and the resulting mixture was stirred at room temperature for 30 minutes. Benzyl bromide (7.28 g, 42.6 mmol) was added slowly and the mixture was stirred at room temperature for 4 hours. The reaction was quenched be addition of a saturated NH_4Cl solution and the mixture was extracted with ethyl acetate. The combined organic layers were dried over $MgSO_4$, concentrated under reduced pressure and the product was obtained *via* flash chromatography on silica gel (ethyl acetate / cyclohexane 1:1) as a colourless oil (yield: 0.512 g, 49%). ^{1}H NMR (400 MHz, DMSO-d_6): δ [ppm] 7.33 (m, 5H, Ar), 5.13 (m, 1H, H_2C=C), 5.077 (m, 1H, H_2C=C), 4.46 (s, 2H, Ar-CH_2), 3.97 (d, 4H, H_2C=(C-C$H_2O)_2$).

Polymerization of Ethylene oxide: The procedure is described exemplary for the polymer MBE-PEG$_{47}$. All polymerizations were conducted according to the SOP described in the following. In a flame dried Schlenk flask, potassium *tert*-butoxide (90 mg, 0.80 mmol) and MBE (469 mg, 2.66 mmol) were dissolved in benzene (5 mL) and dry THF (5 mL), stirred under slightly reduced pressure at 60 °C for 30 minutes and subsequently dried in high vacuum for 16 hours. The resulting initiator salt was dissolved in 15 mL of dry DMSO and ethylene oxide (5 mL, 0.11 mol) was cryo-transferred *via* a graduated ampule. The polymerization was carried out at room temperature until full conversion was achieved (reaction control *via* ^{1}H NMR). If the isomerization should be conducted *via* Wilkinson's catalyst (RhCl(PPh$_3$)$_3$), the polymerization was terminated by addition of 2 mL methanol and the allyl moiety containing polymer was further purified – if a *direct* isomerization was conducted, please read below. After purification *via* dialysis against methanol for 24 hours (MWCO 1000 Da), the purified copolymer was dried in vacuum (yield: 60%). ^{1}H NMR (400 MHz, DMSO-d_6): δ [ppm] 5.12 (s, 2H, H_2C=C), 3.93 (s, 4H, H$_2$C=(C-CH_2O)$_2$), 3.70–3.40 (m, 189H, CH_2O).

***Direct* Isomerization:** The procedure is described exemplary for the polymer *iso*MBE-PEG$_{47}$. All *direct* isomerizations were conducted according to the SOP described in the following. After full consumption of EO (reaction control *via* ^{1}H NMR), a heating bath was placed under the flask and the isomerization was carried out at 80 °C for approximately 24 hours (again reaction control *via* ^{1}H NMR). After full isomerization, the heating bath was removed and (after cooling down to room temperature) the polymer was purified *via* dialysis against methanol for 24 hours (MWCO 1000 Da) and dried in vacuum (yield: 60%). ^{1}H NMR (400 MHz, DMSO-d_6): δ [ppm] 6.22 (s, 1H, C=CH-O (*E* isomer)), 3.86 (m, 2H, C-CH_2O), 3.70–3.40 (m, 189H, CH_2O), 1.51 (d, 3H, CH_3-C).

Isomerization *via* Wilkinson's Catalyst: The procedure is described exemplary for the polymer *iso*MBE-PEG$_{51}$. All isomerizations *via* Wilkinson's catalyst were conducted according to the SOP described in the following. 200 mg of polymer were dissolved in a

Schlenk tube in DMSO and the solution was degassed *via* two freeze-pump-thaw cycles. Under an argon atmosphere, $RhCl(PPh_3)_3$ (25 mg, 0.028 mmol) was added and the solution was stirred at 80 °C for approximately 24 hours (reaction control *via* ^1H NMR). The polymer was precipitated in acetone/diethyl ether (1:1 v/v) and dried in vacuum (yield: 90%). ^1H NMR (400 MHz, DMSO-d_6): δ [ppm] 6.22 (s, 0.61H, C=C*H*-O (*E* isomer)), 6.09 (s, 0.38H, C=C*H*-O (*Z* isomer)), 3.70–3.40 (m, 189H, CH_2O), 1.51 (dd, 3H, CH_3-C (E and Z isomer)).

Methacrylation: The procedure is described exemplary for the polymer *iso*MBE-PEG_{47}-DMA. All methacrylations were conducted according to the SOP described in the following. 200 mg of polymer (0.1 mmol) was dissolved in a Schlenk tube in toluene and CALB (50 mg), vinyl methacrylate (120 µL, 1 mmol) and a few milligrams of BHT were added. After stirring at 40 °C for 48 hours, the mixture was filtered, concentrated *via* a rotary evaporator and precipitated in diethyl ether. BHT was added and the polymer was dried in vacuum (yield: 80%). ^1H NMR (400 MHz, DMSO-d6): δ [ppm] 6.22 (s, 1H, C=C*H*-O (*E* isomer) 6.04 (s, 1.97H, H_2C=CCH_3-C=O), 5.70 (s, 1.95H, H_2C=CCH_3-C=O), 4.19–4.23 (m, 3.92H, CH_2O-MA), 3.85 (m, 2H, C-CH_2-O), 3.88–3.36 (m, 194H, CH_2O), 1.89 (s, 6H, H_2C=CCH_3-C=O) 1.51 (d, C=CH-CH_3 (*E* isomer)).

SEC Hydrolysis Studies: 15 mg of polymer were dissolved in 100 µL of DCM and treated with 100 µL of 10 vol% HCl in methanol. The mixture was incubated at room temperature for 12 hours, neutralized by addition of $NaHCO_3$ and analysed by SEC (DMF, PEG standards, RI detector).

SEC Hydrolysis Kinetic Studies: 20 mg of polymer were pre-dissolved in 50 µL of DMF and this solution was transferred into a SEC vial. Right before the start of the fist injection of the experiment, the vial was filled with pH buffer solution (approximately 1.50 mL), mixed well and placed into the autosampler. Every 60 minutes, 20 µL of this solution were injected and the results were analysed. The intern toluene standard was

set by injecting 20 µL of a solution of 10 mg of polymer in 1.50 mL of DMF with a drop of toluene before the SEC kinetics experiment.

Hydrogel Synthesis: The hydrogels were synthesized as previously described.[5] Briefly, a 10 wt% solution of the polymer in 150 µL of PBS was prepared. To this solution, 2.50 µL of a solution of 2-hydroxy-4′-(2-hydroxyethoxy)-2-methylpropio-phenone, prediluted in 1:10 in ethanol, was added and the solutions carefully mixed. This mixture was transferred into a 96-well plate and overlayered with 150 µL of isopropanol. After UV polymerization at 365 nm for 15 minutes, the hydrogels could be transferred into petri dished for incubation at different pH values.

Hydrogel Lyophilization and Swelling: For lyophilization, the hydrogels were placed in a petri dish and covered with aluminium foil. Freeze-drying was carried out at -78 °C / 10^{-3} mbar for 48 hours. For swelling experiments, the gels were placed into a PBS solution and allowed to swell at room temperature for 72 hours. To determine their mass, their surface was carefully dried using a Kimtech wipe and the gels were placed on a laboratory scale.

Hydrolysis of BMP-PEGs: For cleavage of the BMP-PEGs, 100 mg of polymer was dissolved in 5 mL of methanol/dichloromethane 1:1 (v/v) and stirred over Dowex 50WX8 at room temperature for 24 hours. The ion exchange resin was removed by filtration and the polymer was recovered by removal of the solvent, precipitation in diethyl ether and subsequently drying at high vacuum.

3.2.6 REFERENCES

(1) Dingels, C.; Schömer, M.; Frey, H. Die vielen Gesichter des Poly(ethylenglykol)s. *Chemie in unserer Zeit* **2011**, *45*, 338–349.

(2) Herzberger, J.; Niederer, K.; Pohlit, H.; Seiwert, J.; Worm, M.; Wurm, F. R.; Frey, H. Polymerization of Ethylene Oxide, Propylene Oxide, and Other Alkylene Oxides: Synthesis, Novel Polymer Architectures, and Bioconjugation. *Chemical Reviews* **2016**, *116*, 2170–2243.

(3) Peppas, N. Hydrogels in pharmaceutical formulations. *European Journal of Pharmaceutics and Biopharmaceutics* **2000**, *50*, 27–46.

(4) Pasut, G.; Veronese, F. M. Polymer–drug conjugation, recent achievements and general strategies. *Progress in Polymer Science* **2007**, *32*, 933–961.

(5) Schröder, R.; Pohlit, H.; Schüler, T.; Panthöfer, M.; Unger, R. E.; Frey, H.; Tremel, W. Transformation of vaterite nanoparticles to hydroxycarbonate apatite in a hydrogel scaffold: relevance to bone formation. *Journal of materials chemistry. B* **2015**, *3*, 7079–7089.

(6) Yamaoka, T.; Tabata, Y.; Ikada, Y. Distribution and tissue uptake of poly(ethylene glycol) with different molecular weights after intravenous administration to mice. *Journal of pharmaceutical sciences* **1994**, *83*, 601–606.

(7) Caliceti, P. Pharmacokinetic and biodistribution properties of poly(ethylene glycol)–protein conjugates. *Advanced Drug Delivery Reviews* **2003**, *55*, 1261–1277.

(8) Gillies, E. R.; Fréchet, J. M. J. pH-Responsive copolymer assemblies for controlled release of doxorubicin. *Bioconjugate chemistry* **2005**, *16*, 361–368.

(9) Kaihara, S.; Matsumura, S.; Fisher, J. P. Synthesis and Properties of Poly[poly(ethylene glycol)- co -cyclic acetal] Based Hydrogels. *Macromolecules* **2007**, *40*, 7625–7632.

(10) Varghese, J. K.; Hadjichristidis, N.; Gnanou, Y.; Feng, X. Degradable poly(ethylene oxide) through metal-free copolymerization of ethylene oxide with l -lactide. *Polymer Chemistry* **2019**, *10*, 3764–3771.

(11) Di Liu; Bielawski, C. W. Synthesis of Degradable Poly(Ethylene Glycol)-co-(Glycolic Acid) via the Post-Polymerization Oxyfunctionalization of Poly(Ethylene Glycol). *Macromolecular Rapid Communications* **2016**, *37*, 1587–1592.

(12) Kim, S.; Linker, O.; Garth, K.; Carter, K. R. Degradation kinetics of acid-sensitive hydrogels. *Polymer Degradation and Stability* **2015**, *121*, 303–310.

(13) Pohlit, H.; Leibig, D.; Frey, H. Poly(Ethylene Glycol) Dimethacrylates with Cleavable Ketal Sites: Precursors for Cleavable PEG-Hydrogels. *Macromolecular bioscience* **2017**, *17*.

(14) Shenoi, R. A.; Lai, B. F. L.; Kizhakkedathu, J. N. Synthesis, characterization, and biocompatibility of biodegradable hyperbranched polyglycerols from acid-cleavable ketal group functionalized initiators. *Biomacromolecules* **2012**, *13*, 3018–3030.

(15) Lundberg, P.; Lee, B. F.; van den Berg, S. A.; Pressly, E. D.; Lee, A.; Hawker, C. J.; Lynd, N. A. Poly(ethylene oxide)-co-(methylene ethylene oxide): A hydrolytically-degradable poly(ethylene oxide) platform. *ACS Macro Lett.* **2012**, *1*, 1240–1243.

(16) Steiert, E.; Ewald, J.; Wagner, A.; Hellmich, U. A.; Frey, H.; Wich, P. R. pH-Responsive protein nanoparticles via conjugation of degradable PEG to the surface of cytochrome c. *Polym. Chem.* **2020**, *11*, 551–559.

(17) Worm, M.; Leibig, D.; Dingels, C.; Frey, H. Cleavable Polyethylene Glycol: 3,4-Epoxy-1-butene as a Comonomer to Establish Degradability at Physiologically Relevant pH. *ACS Macro Lett.* **2016**, *5*, 1357–1363.

(18) Ewald, J.; Blankenburg, J.; Worm, M.; Besch, L.; Unger, R. E.; Tremel, W.; Frey, H.; Pohlit, H. Acid-Cleavable Poly(ethylene glycol) Hydrogels Displaying Protein Release at pH 5. *Chemistry (Weinheim an der Bergstrasse, Germany)* **2020**, *26*, 2947–2953.

(19) Shin, J.; Shum, P.; Grey, J.; Fujiwara, S.-i.; Malhotra, G. S.; González-Bonet, A.; Hyun, S.-H.; Moase, E.; Allen, T. M.; Thompson, D. H. Acid-labile mPEG-vinyl ether-1,2-dioleylglycerol lipids with tunable pH sensitivity: synthesis and structural effects on hydrolysis rates, DOPE liposome release performance, and pharmacokinetics. *Molecular pharmaceutics* **2012**, *9*, 3266–3276.

(20) Boomer, J. A.; Qualls, M. M.; Inerowicz, H. D.; Haynes, R. H.; Patri, V. S.; Kim, J.-M.; Thompson, D. H. Cytoplasmic delivery of liposomal contents mediated by an acid-labile cholesterol-vinyl ether-PEG conjugate. *Bioconjugate chemistry* **2009**, *20*, 47–59.

(21) Price, C. C.; Snyder, W. H. Solvent effects in the base-catalyzed isomerization of ally to propenyl ethers. *J. Am. Chem. Soc.* **1961**, *83*, 1773.

(22) Prosser, T. J. The Rearrangement of Allyl Ethers to Propenyl Ethers. *J. Am. Chem. Soc.* **1961**, *83*, 1701–1704.

(23) Guibé, F. Allylic protecting groups and their use in a complex environment part I: Allylic protection of alcohols. *Tetrahedron* **1997**, *53*, 13509–13556.

(24) Sageot, O.; Monteux, D.; Langlois, Y.; Riche, C.; Chiaroni, A. Preparation and use of chiral (Z)-enol ethers in asymmetric bradsher cycloaddition. *Tetrahedron Letters* **1996**, *37*, 7019–7022.

(25) Taskinen, E. Relative thermodynamic stabilities of isomeric alkyl allyl and alkyl (Z)-propenyl ethers. *Tetrahedron* **1993**, *49*, 11389–11394.

(26) Boons, G.-J.; Burton, A.; Isles, S. A new procedure for the isomerisation of substituted and unsubstituted allyl ethers of carbohydrates. *Chemical Communications [Online]* **1996,** No. 2, 141.

(27) Boons, G.-J.; Isles, S. Vinyl Glycosides in Oligosaccharide Synthesis. 2. The Use of Allyl and Vinyl Glycosides in Oligosaccharide Synthesis. *The Journal of organic chemistry* **1996**, *61*, 4262–4271.

(28) Beres, J. J. Curve Fitting of GPC Chromatograms of Polymer Mixtures Used as Raw Materials. *IFAC Proceedings Volumes [Online]* **1987**, *20*, 229–233. http://www.sciencedirect.com/science/article/pii/S1474667017555901.

(29) Dingels, C.; Müller, S. S.; Steinbach, T.; Tonhauser, C.; Frey, H. Universal concept for the implementation of a single cleavable unit at tunable position in functional poly(ethylene glycol)s. *Biomacromolecules* **2013**, *14*, 448–459.

(30) Flory, P. J.; Rehner, J. Statistical Mechanics of Cross-Linked Polymer Networks II. Swelling. *The Journal of Chemical Physics* **1943**, *11*, 521–526.

3.2.7 SUPPORTING INFORMATION

Terminology

Anionic ring-opening polymerization	AROP
2-((benzyloxy)methyl)prop-2-en-1-ol	BMP
DMA	Dimethacrylate
2,2‘-(2-methylenepropane-1,3-diyldioxy)bisethanol	MBE
2-(methylene)-1,3-propanediol	MPD
1,1'-oxybis(but-3-en-2-ol)	OBB
Poly(ethylene glycol)	PEG

Chemicals and Analytical Instrumentation

All chemicals, solvents and materials were purchased from standard commercial suppliers (Acros, Sigma-Aldrich, Fisher Scientific Alfa Aesar, TCI). Ethylene oxide (EO) was purchased from Air Liquide. DMSO-d_6 was purchased from Deutero GmbH. All chemicals were used as received without further purification unless stated otherwise. 96 well plates for hydrogel synthesis and disposable petri dishes with lid were purchased from Greiner, Frickenhausen, Germany.

^{1}H NMR spectra were measured using a Bruker AMX400 spectrometer (256 Scans, and B-ACS 60 auto sampler) at 296 K. ^{1}H NMR kinetic spectra were recorded at 400 MHz on a Bruker Advance III HD 400 (5 mm broad band fluorine observation (BBFO)-SmartProbe with z-gradient and Automated tuning and matching (ATM)). 2D NMR and ^{13}C NMR spectra were measured on a Bruker Avance II 400 (100.5 MHz, 5 mm BBO probe, and B-ACS 60 auto sampler) at 296 K. All spectra were processed with

MestReNova v10.0.1 software and referenced internally to residual proton signals of the deuterated solvent.

Size exclusion chromatography (SEC) data were obtained using Agilent 1100 Series equipped with PSS HEMA-columns (106/104/102 Å porosity) using DMF with 1 g/L LiBr as an eluent and RI detection. Polydispersity indices (Đ = Mw/Mn) were determined with monodisperse linear PEG standards from Polymer Standard Service GmbH (PSS).

Analytical Data

Initiators

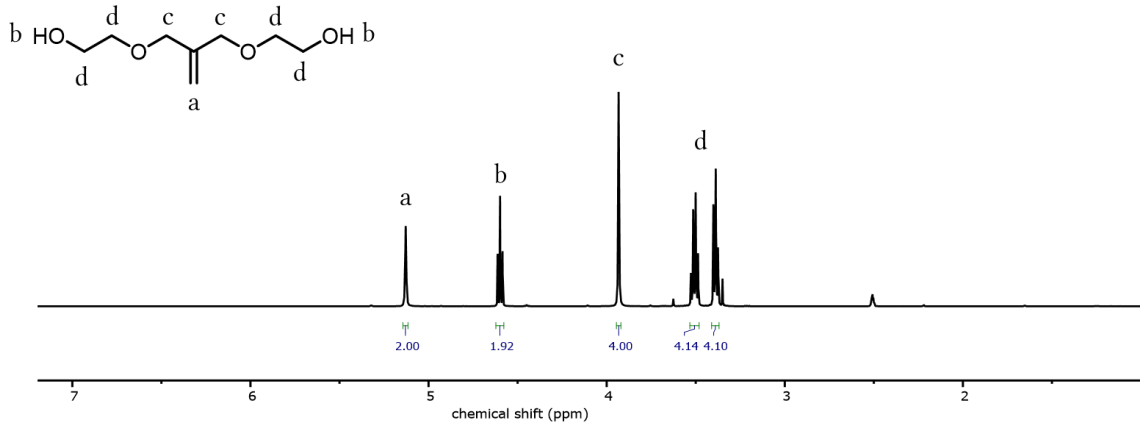

Figure S1: ^{1}H NMR spectrum (400 MHz, DMSO-d_6) of 2,2‘-(2-methylenepropane-1,3-diyldioxy)bisethanol (MBE).

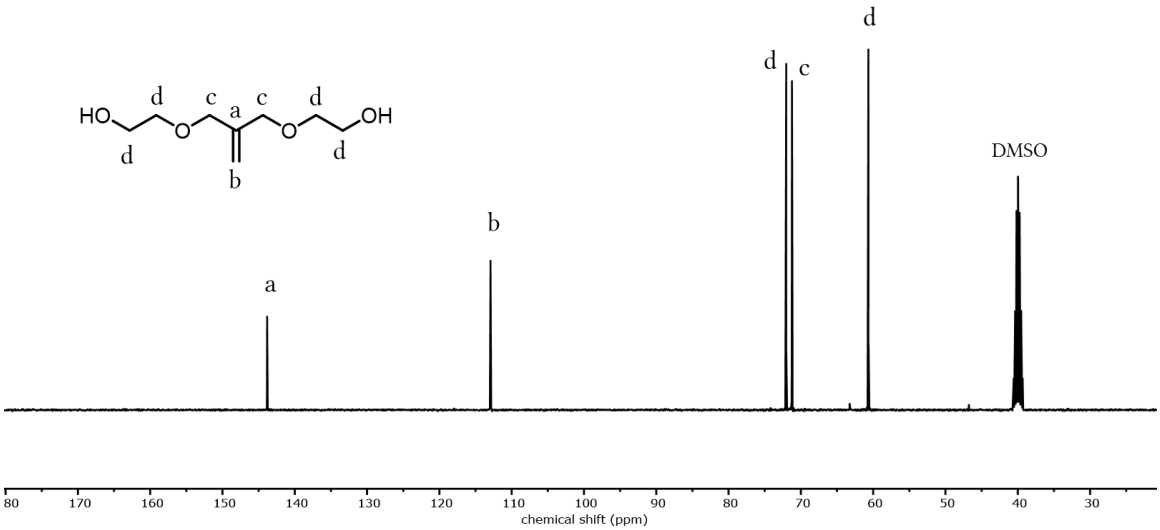

Figure S2: ^{13}C NMR spectrum (100 MHz, DMSO-d_6) of 2,2‘-(2-methylenepropane-1,3-diyldioxy)bisethanol (MBE).

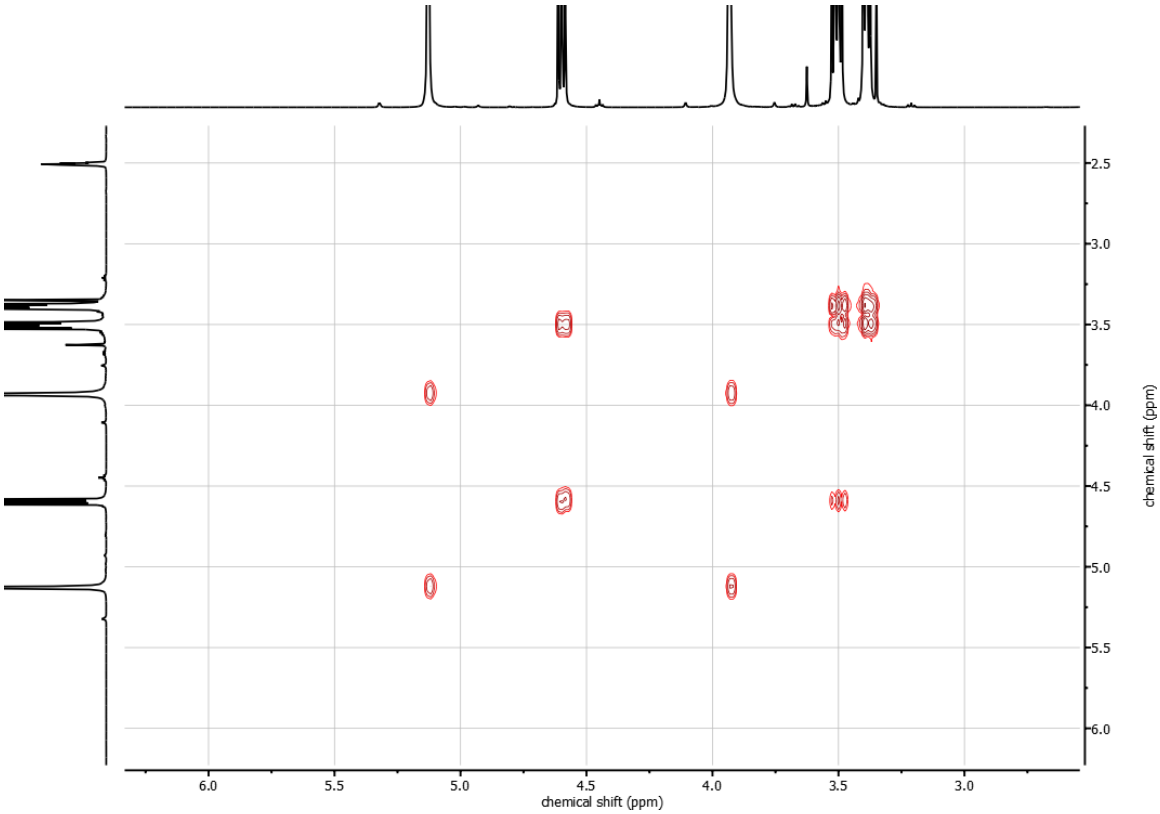

Figure S3: $^{1}H,^{1}H$ COSY NMR spectrum (400 MHz, DMSO-d_6) of 2,2‘-(2-methylenepropane-1,3-diyldioxy)bisethanol (MBE).

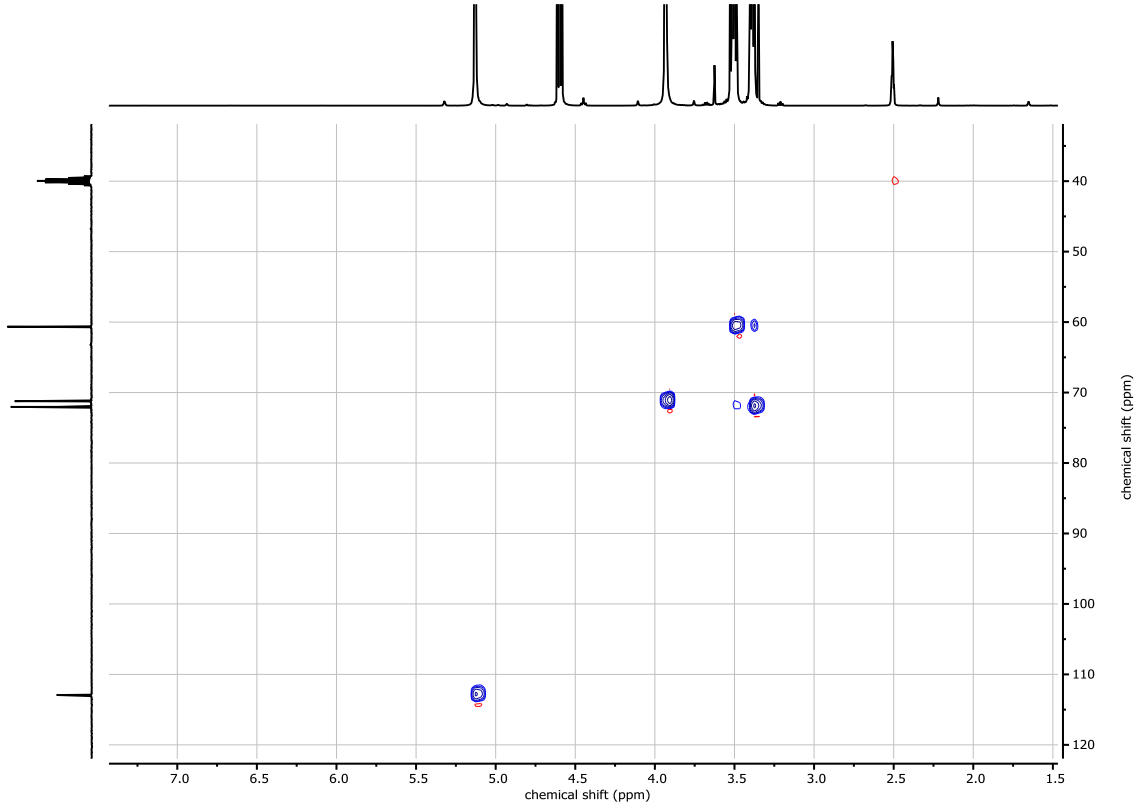

Figure S4: $^{1}H,^{13}C$ HSQC NMR spectrum (400 / 100 MHz, DMSO-d_6) of 2,2‘-(2-methylenepropane-1,3-diyldioxy)bisethanol (MBE).

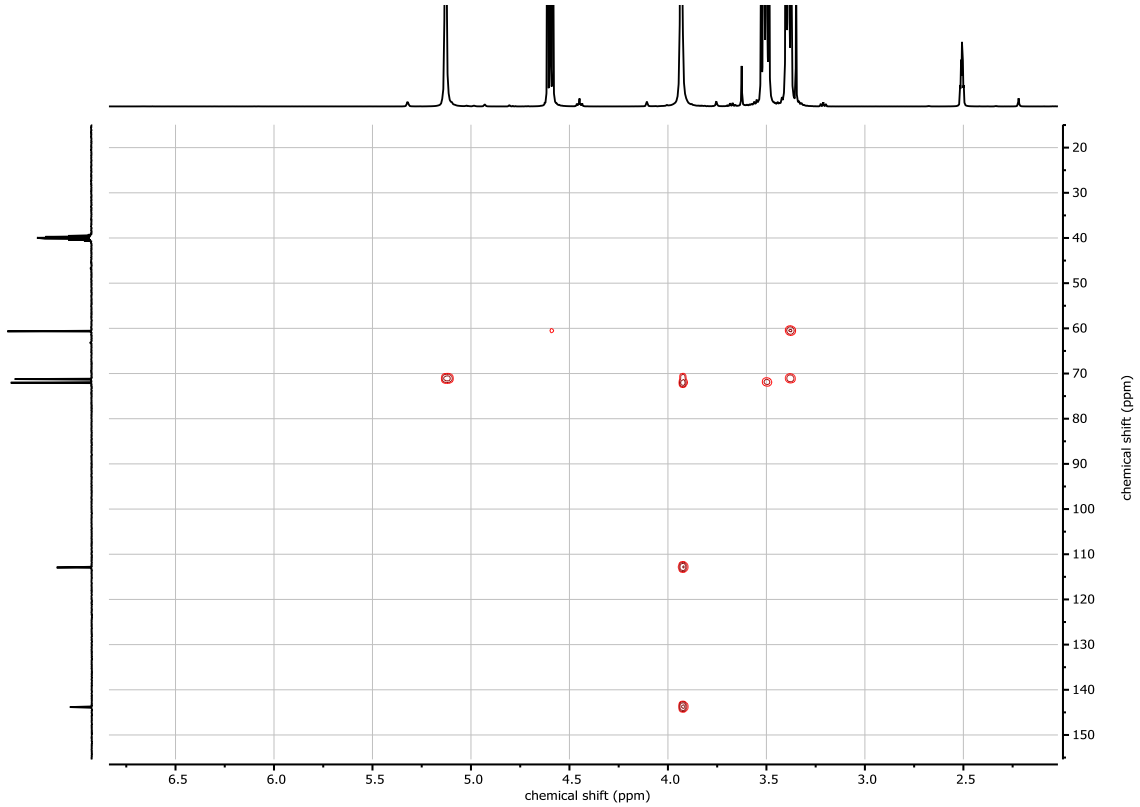

Figure S5: $^{1}H,^{13}C$ HMBC NMR spectrum (400 / 100 MHz, DMSO-d_6) of 2,2‘-(2-methylenepropane-1,3-diyldioxy)bisethanol (MBE)

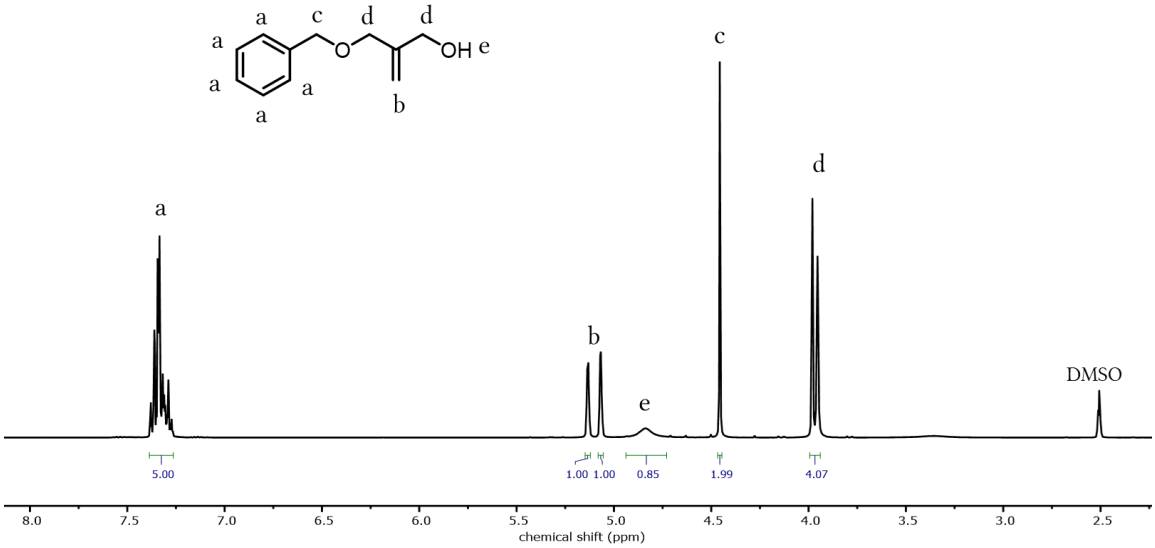

Figure S6: ^{1}H NMR spectrum (400 MHz, DMSO-d_6) of 2-((Benzyloxy)methyl)prop-2-en-1-ol (BMP).

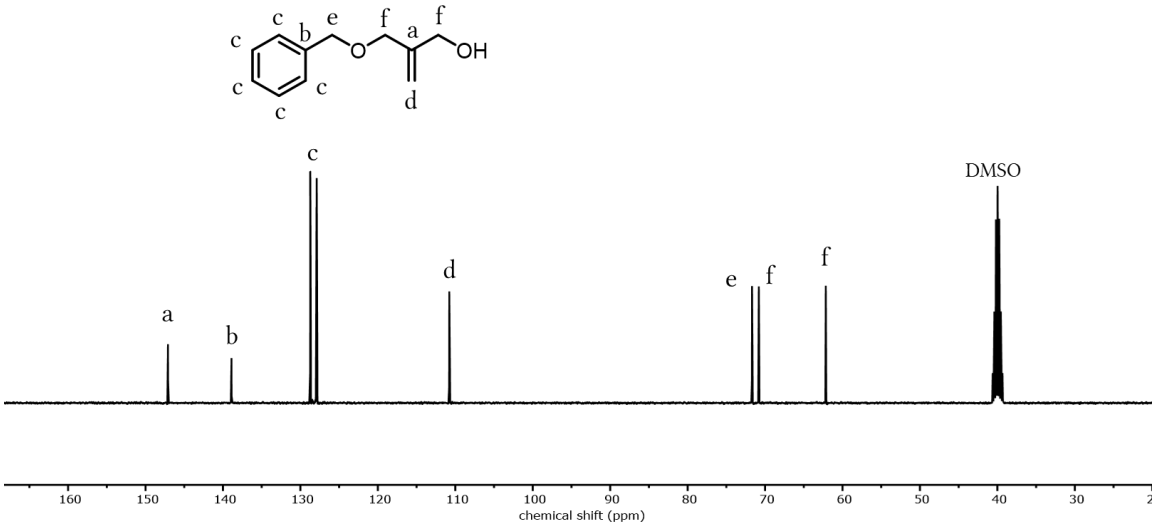

Figure S7: ^{13}C NMR spectrum (100 MHz, DMSO-d_6) of 2-((Benzyloxy)methyl)prop-2-en-1-ol (BMP).

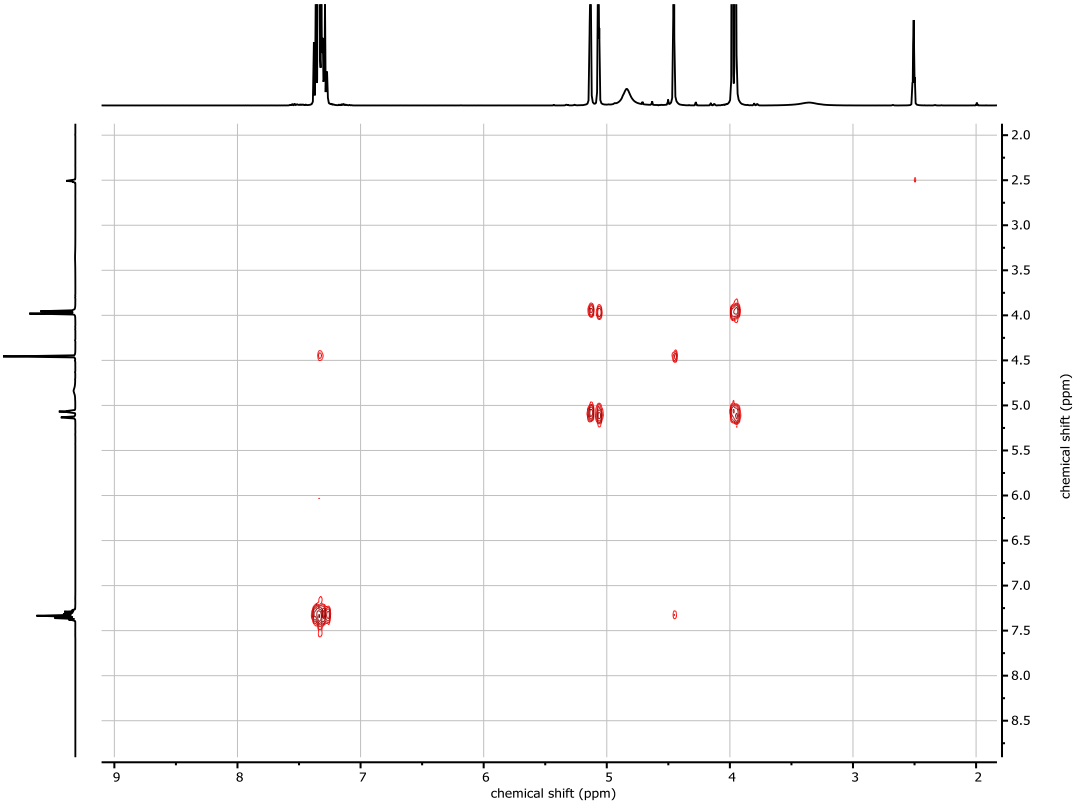

Figure S8: $^{1}H,^{1}H$ COSY NMR spectrum (400 MHz, DMSO-d_6) of 2-((Benzyloxy)methyl)prop-2-en-1-ol (BMP).

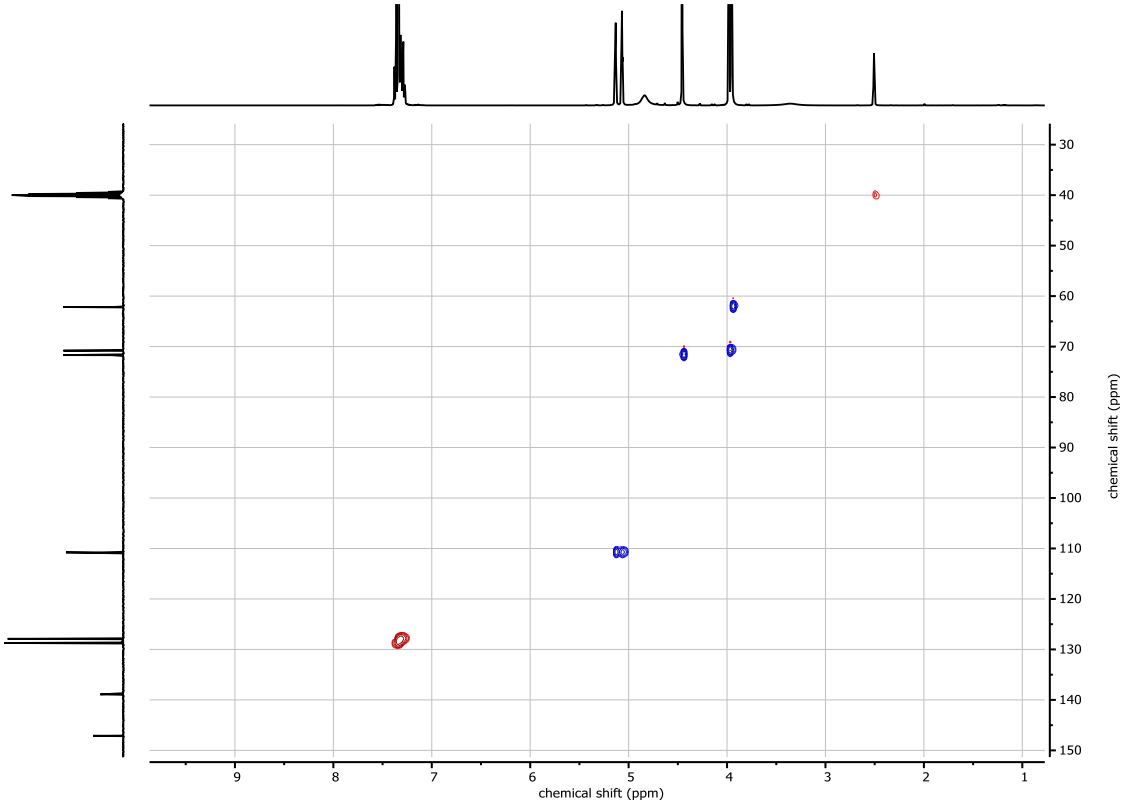

Figure S9: $^{1}H,^{13}C$ HSQC NMR spectrum (400 / 100 MHz, DMSO-d_6) of 2-((Benzyloxy)methyl)prop-2-en-1-ol (BMP).

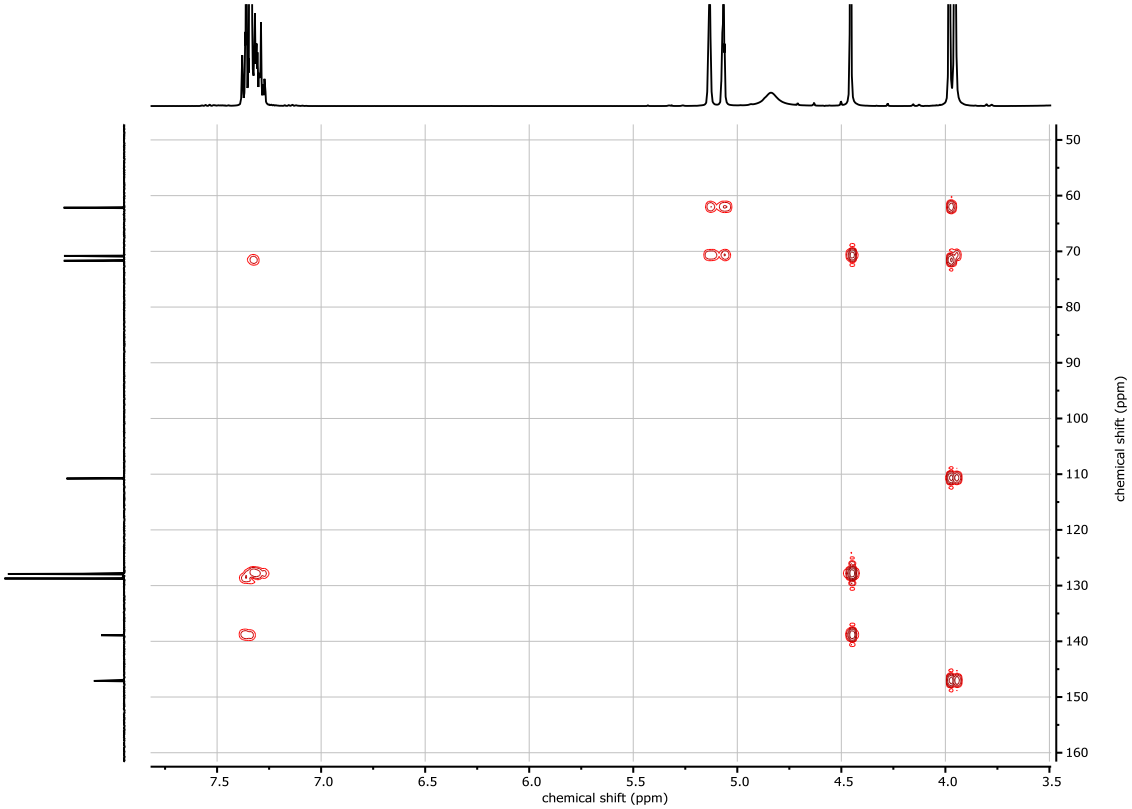

Figure S10: $^{1}H,^{13}C$ HMBC NMR spectrum (400 / 100 MHz, DMSO-d_6) of 2-((Benzyloxy)methyl)prop-2-en-1-ol (BMP).

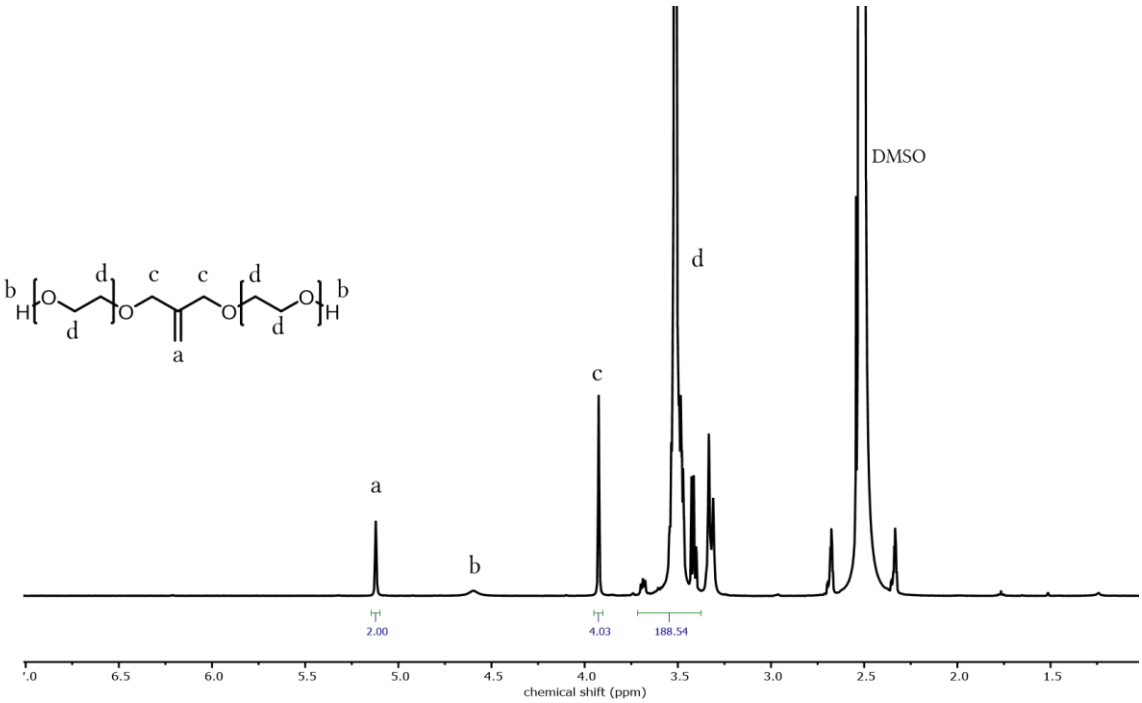

Figure S11. ^{1}H NMR spectrum (400 MHz, DMSO-d_6) of MBE-PEG$_{47}$.

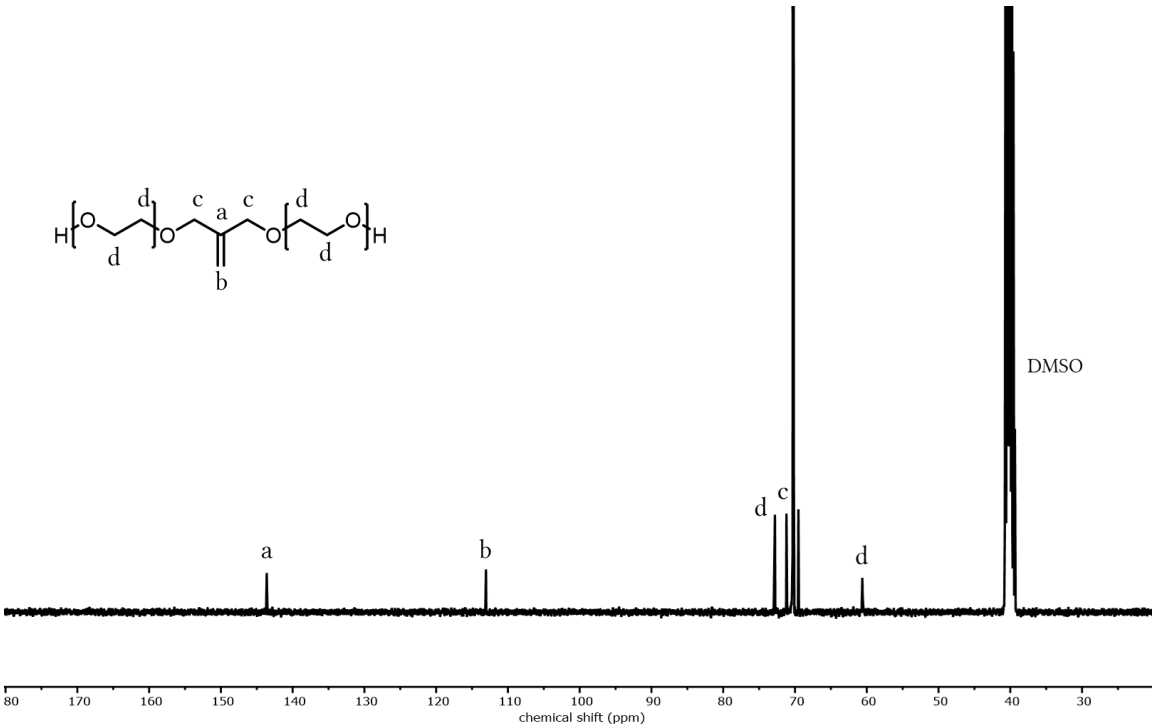

Figure S12: ^{13}C NMR spectrum (100 MHz, DMSO-d_6) of MBE-PEG$_{47}$.

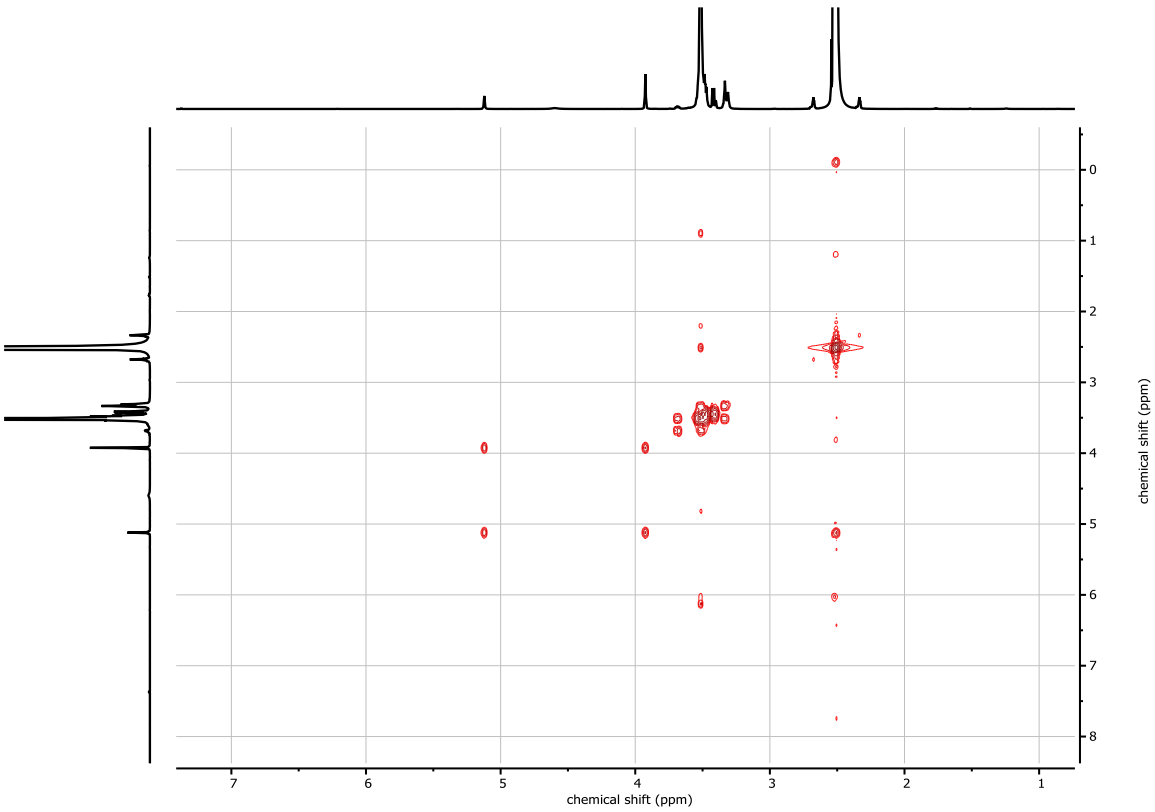

Figure S13: $^{1}H,^{1}H$ COSY NMR spectrum (400 MHz, DMSO-d_6) of MBE-PEG$_{47}$.

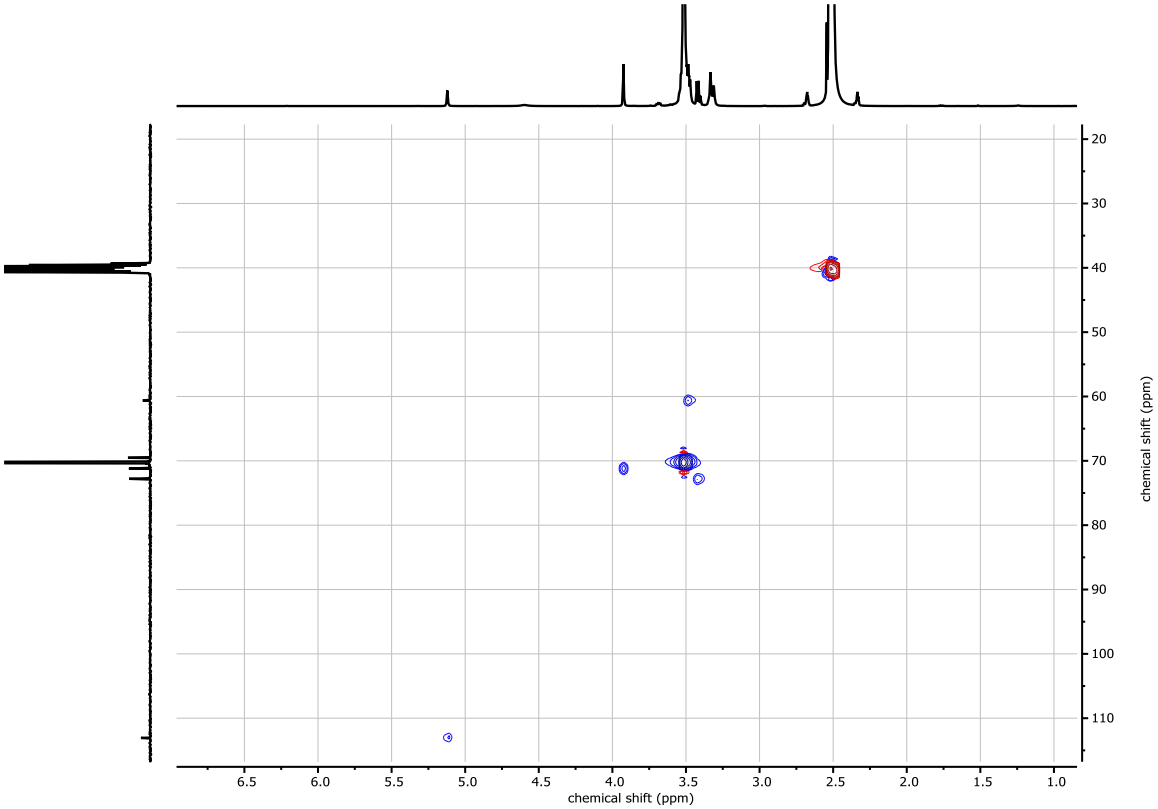

Figure S14: $^{1}H,^{13}C$ HSQC NMR spectrum (400 / 100 MHz, DMSO-d_6) of MBE-PEG$_{47}$.

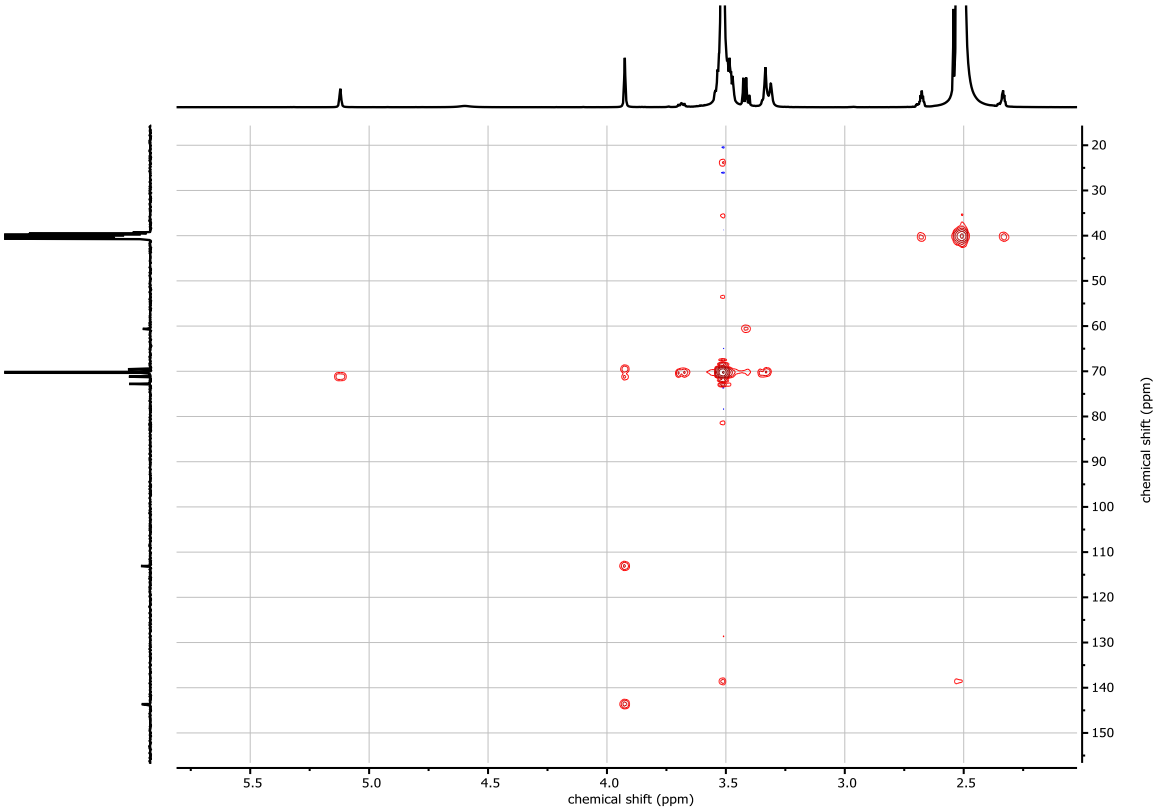

Figure S15: $^{1}H,^{13}C$ HMBC NMR spectrum (400 / 100 MHz, DMSO-d_6) of MBE-PEG$_{47}$.

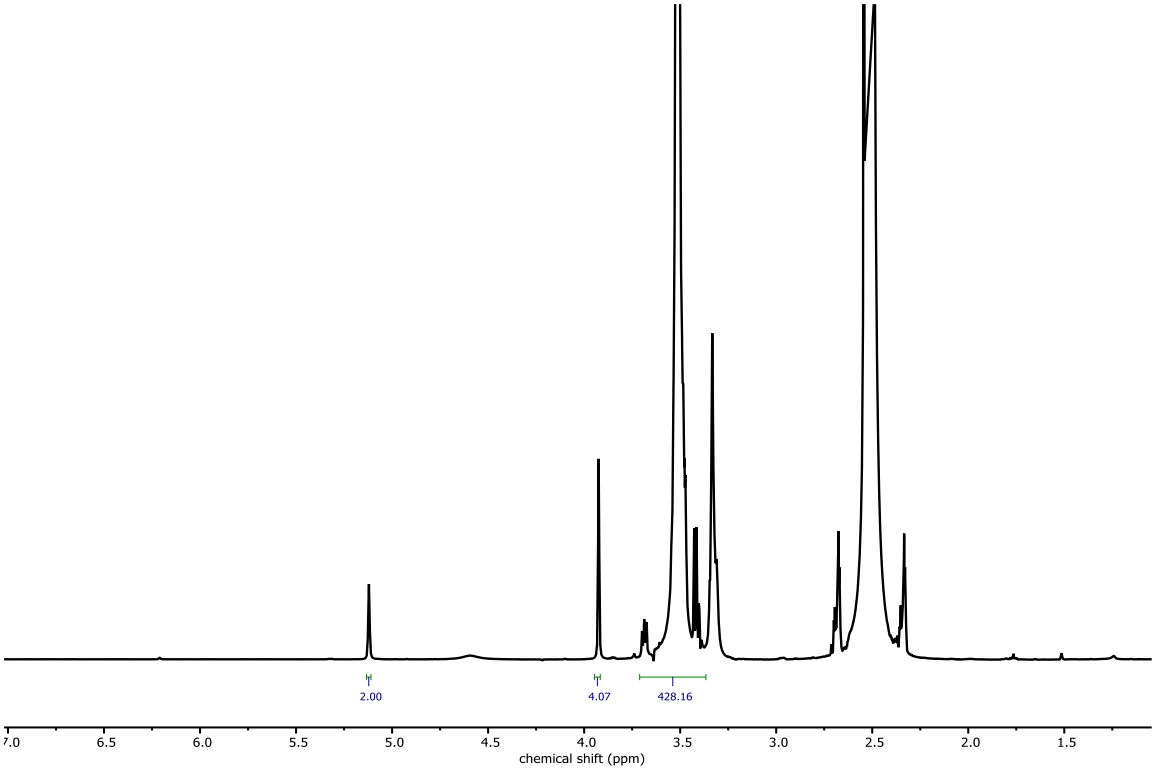

Figure S16: ^{1}H NMR spectrum (400 MHz, DMSO-d_6) of MBE-PEG$_{107}$.

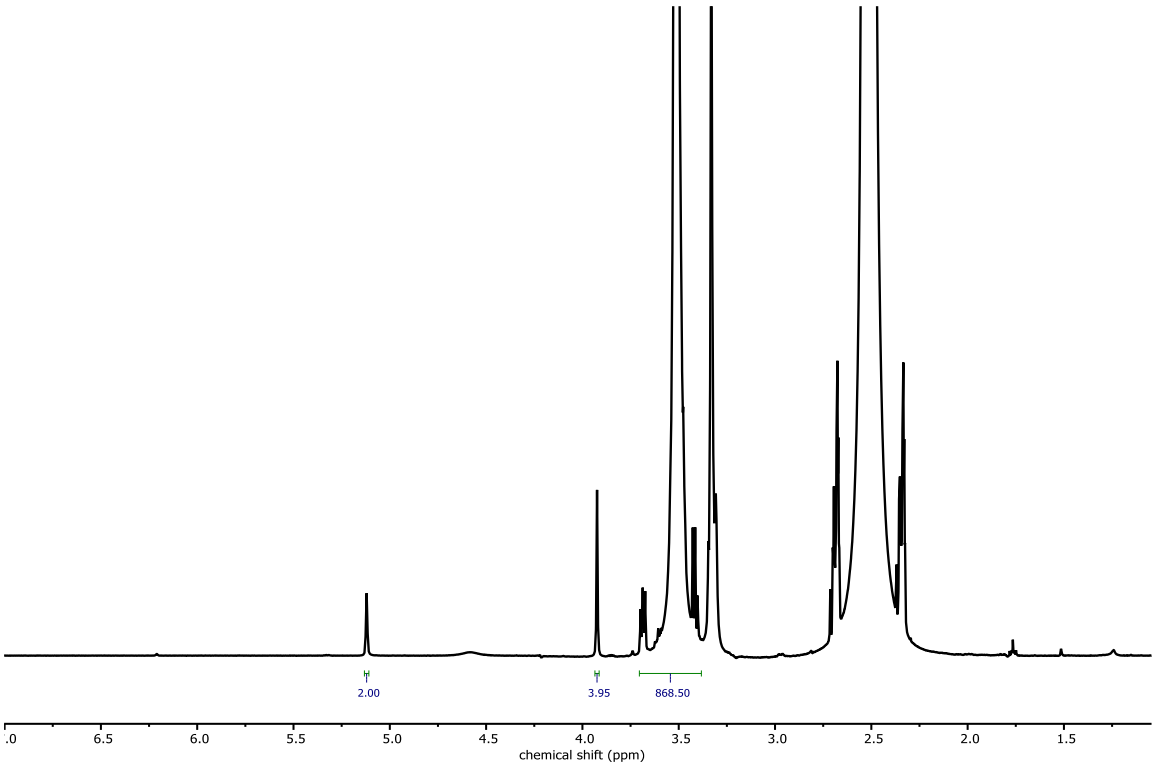

Figure S17: ^{1}H NMR spectrum (400 MHz, DMSO-d_6) of MBE-PEG$_{217}$.

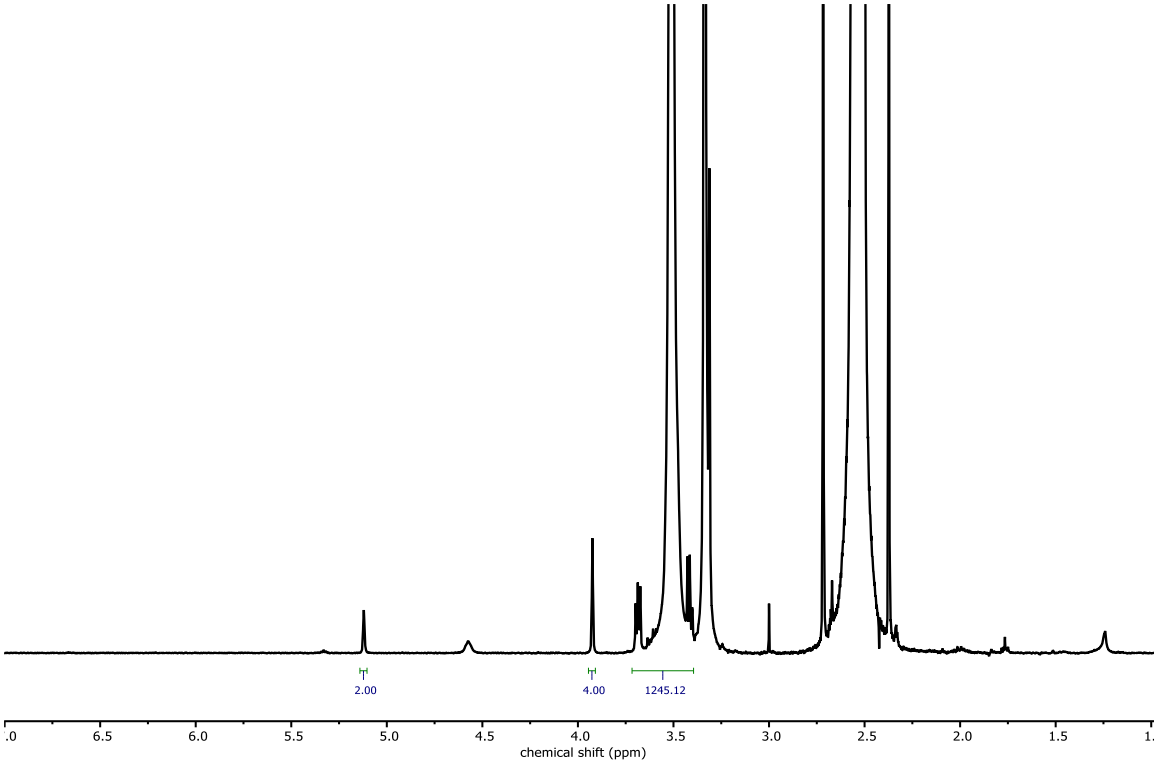

Figure S18: ^{1}H NMR spectrum (400 MHz, DMSO-d_6) of MBE-PEG$_{311}$.

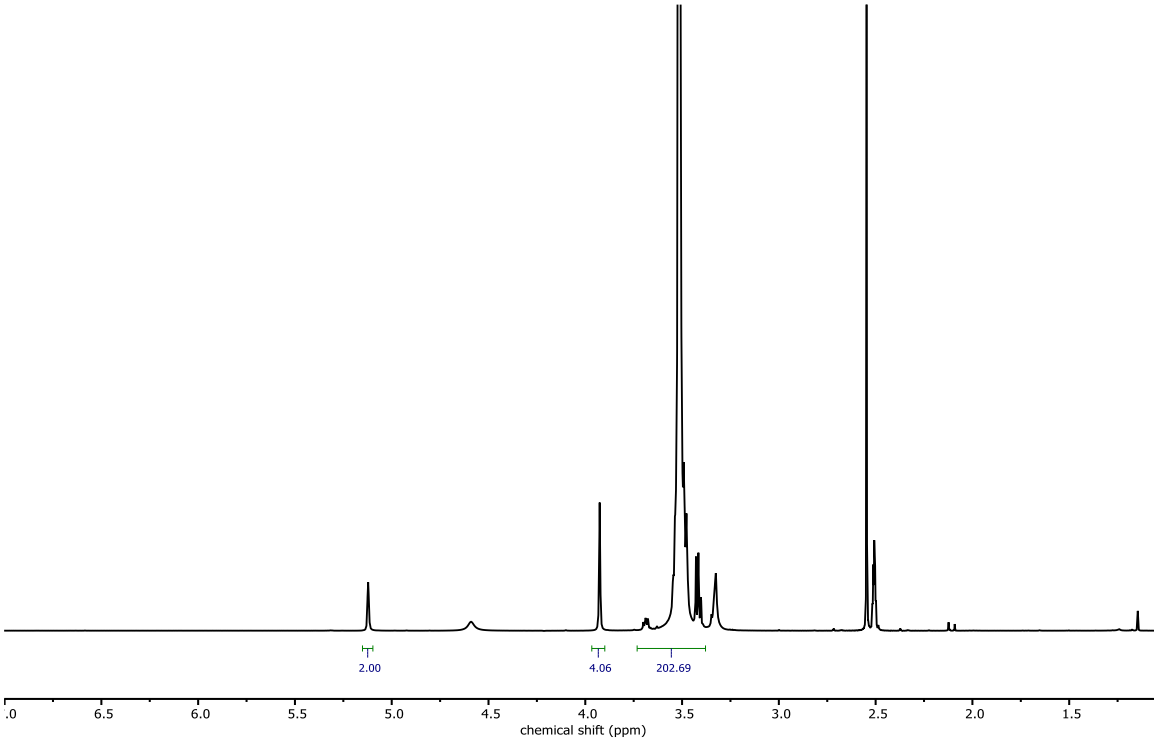

Figure S19: ^{1}H NMR spectrum (400 MHz, DMSO-d_6) of MBE-PEG$_{51}$.

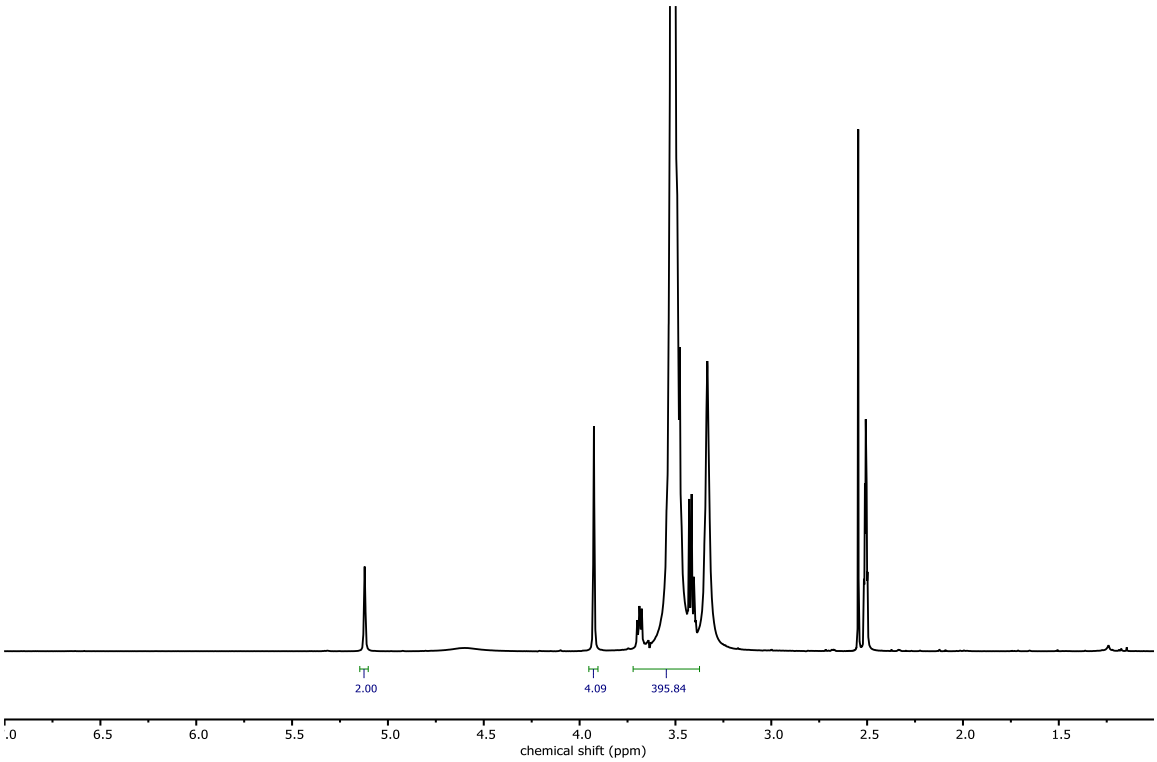

Figure S20: ^{1}H NMR spectrum (400 MHz, DMSO-d_6) of MBE-PEG$_{99}$.

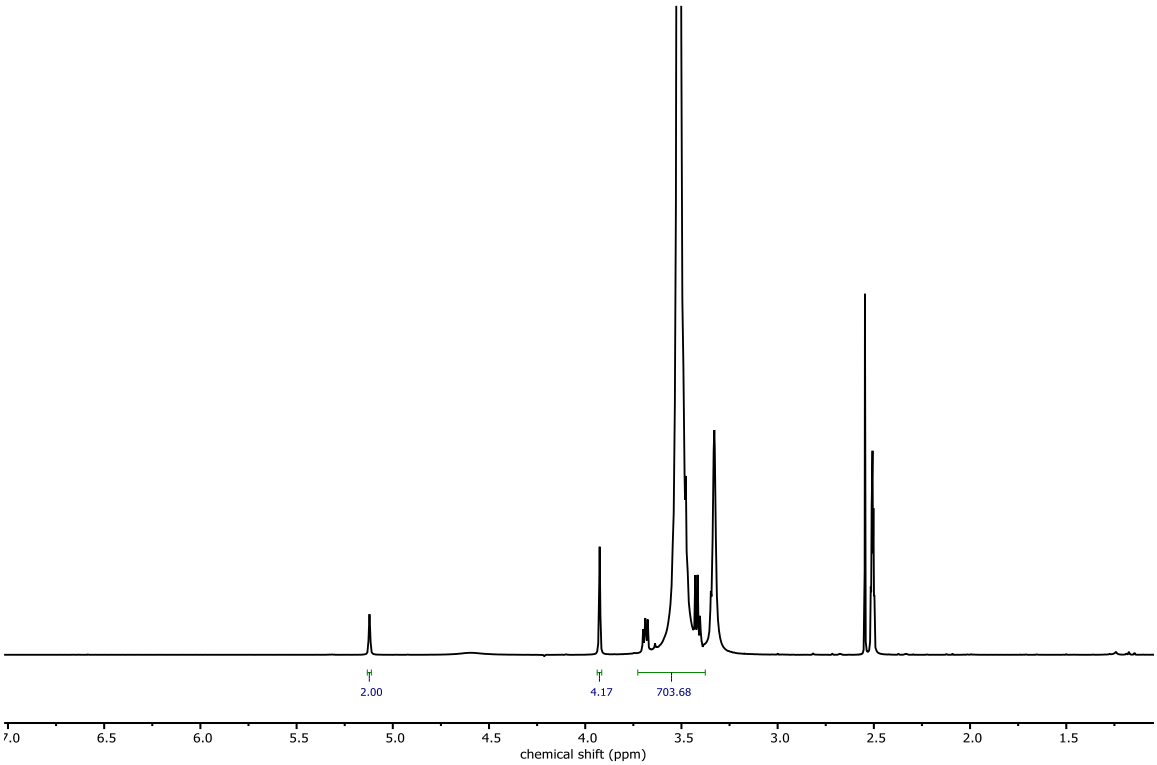

Figure S21: ^{1}H NMR spectrum (400 MHz, DMSO-d_6) of MBE-PEG$_{176}$.

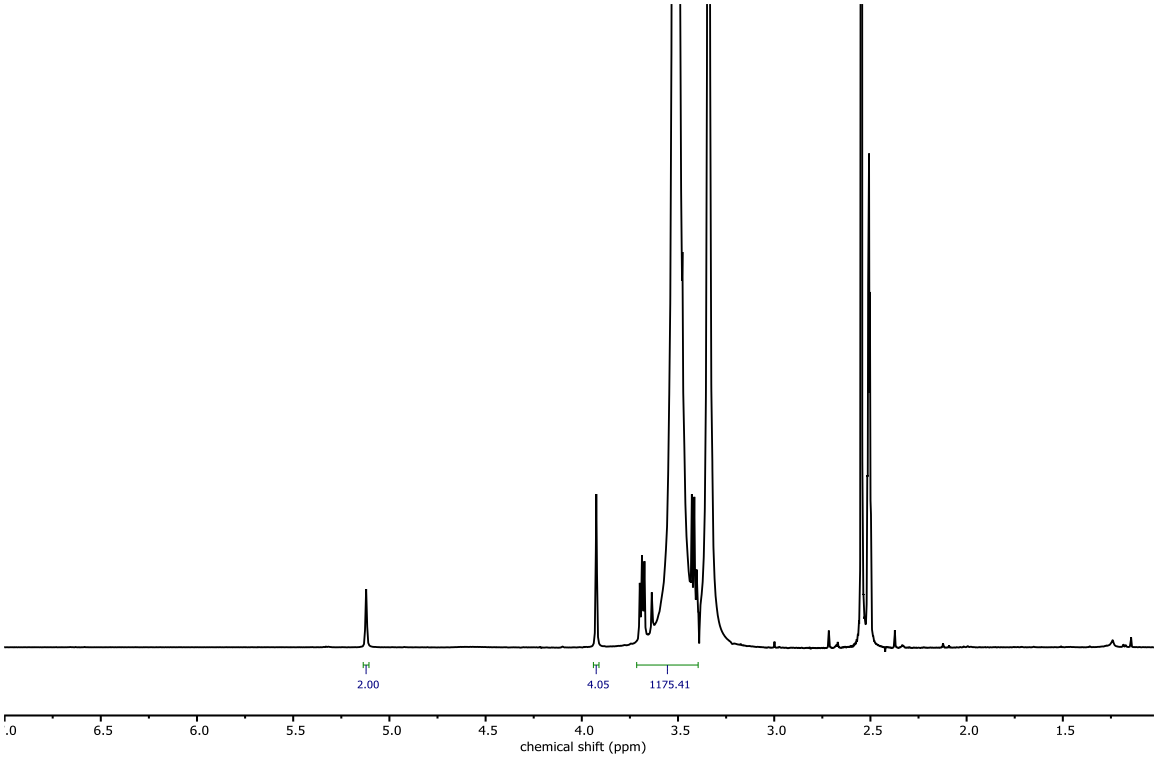

Figure S22: ^{1}H NMR spectrum (400 MHz, DMSO-d_6) of MBE-PEG$_{294}$.

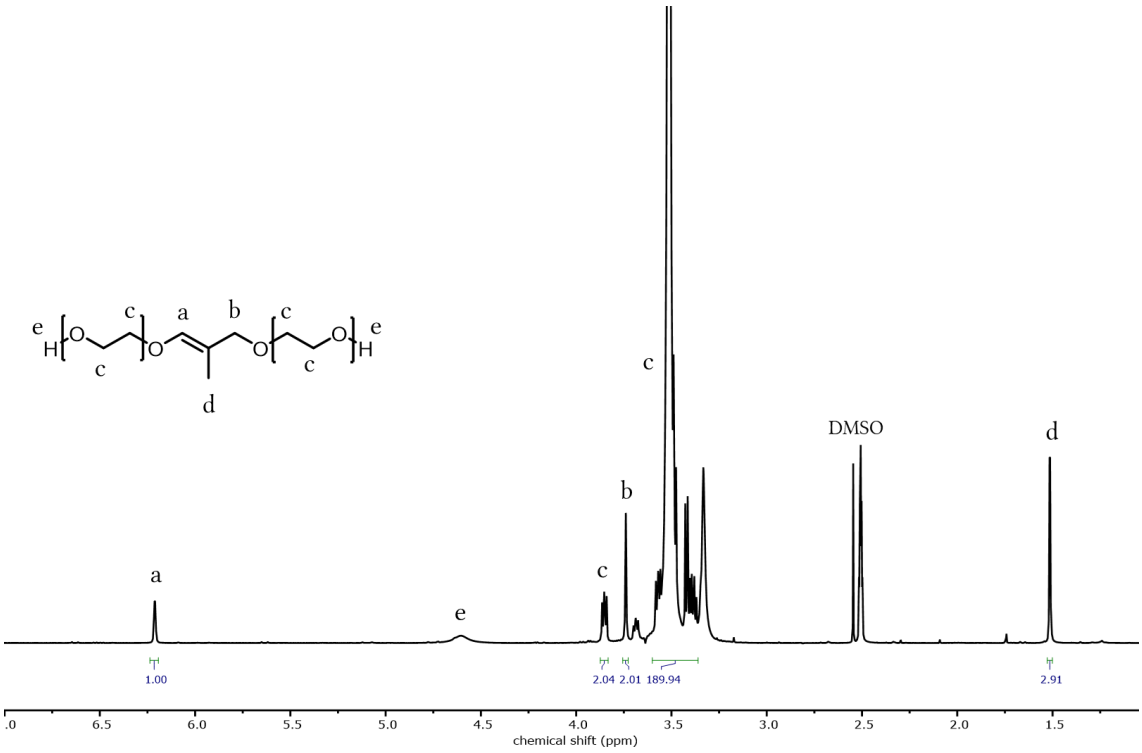

Figure S23: ^{1}H NMR spectrum (400 MHz, DMSO-d_6) of *iso*MBE-PEG$_{47}$.

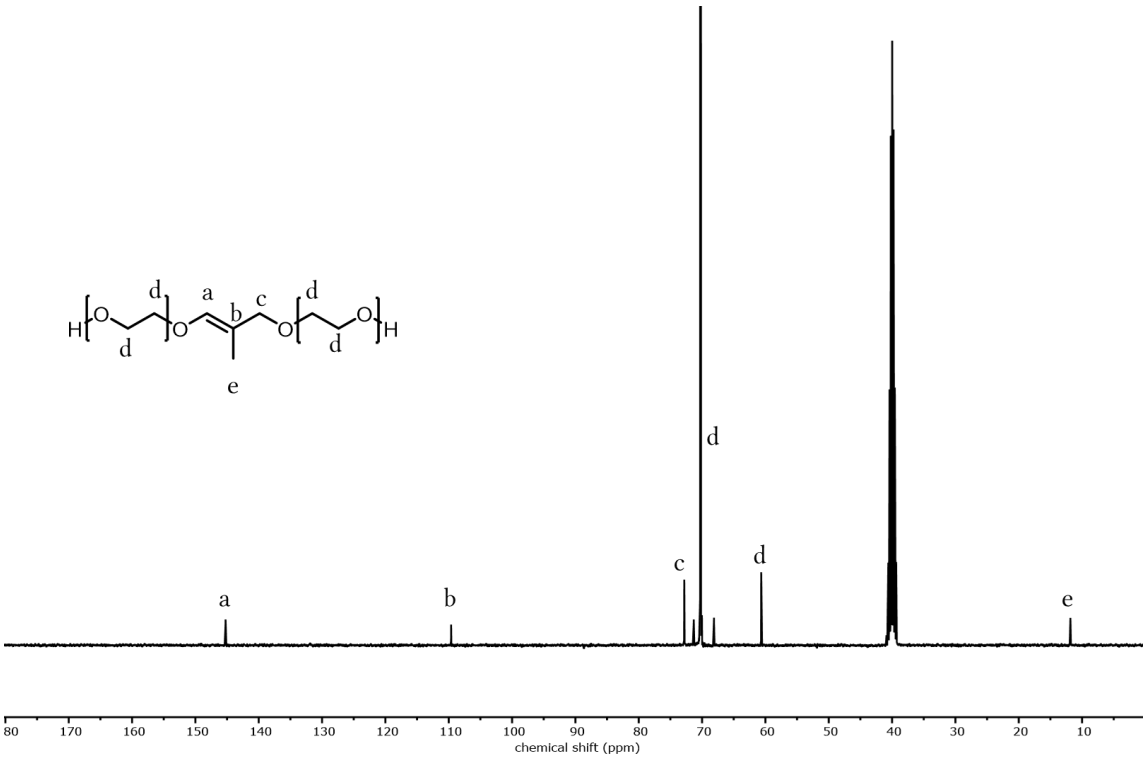

Figure S24: ^{13}C NMR spectrum (100 MHz, DMSO-d_6) of *iso*MBE-PEG$_{47}$.

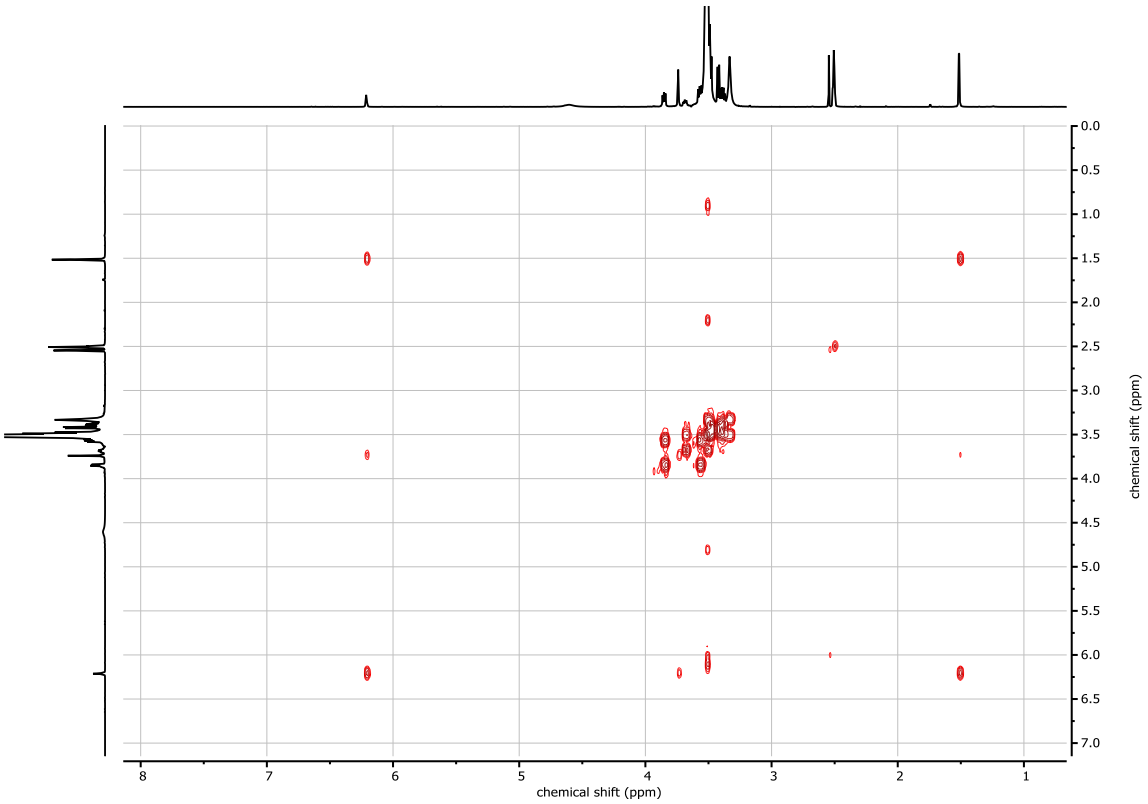

Figure S25: $^{1}H,^{1}H$ COSY NMR spectrum (400 MHz, DMSO-d_6) of *iso*MBE-PEG$_{47}$.

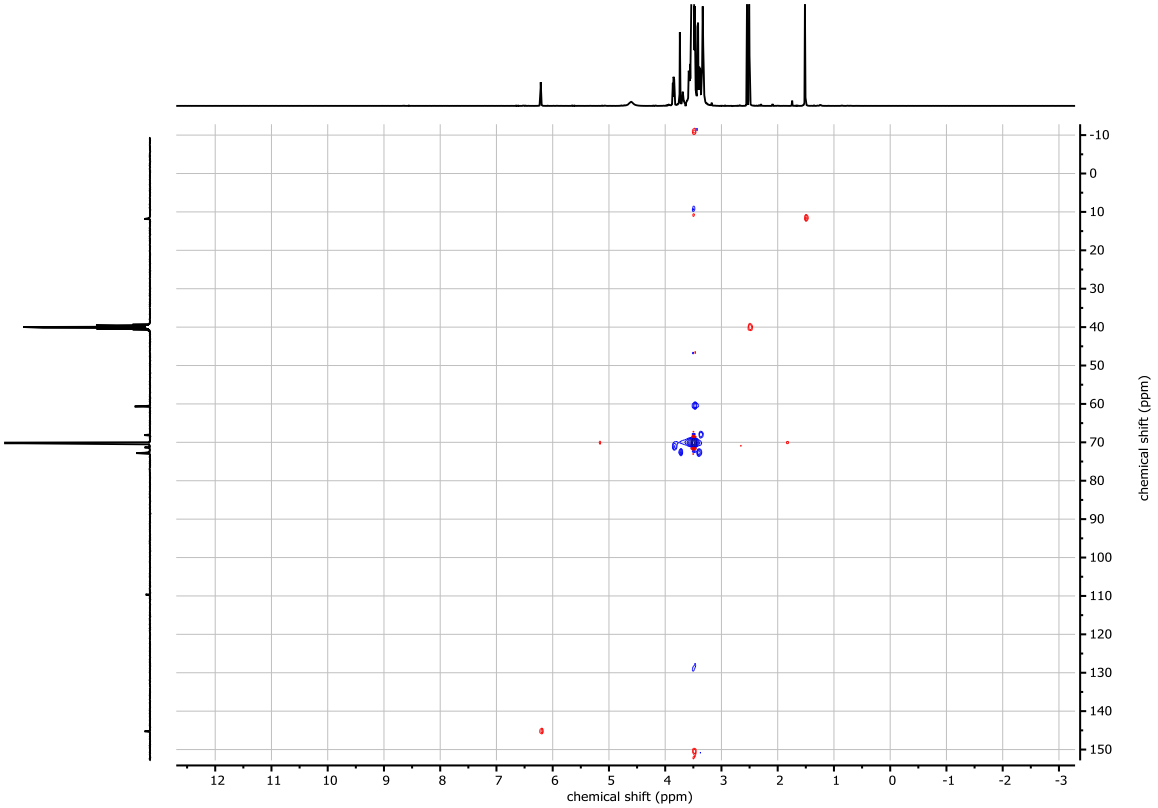

Figure S26: $^{1}H,^{13}C$ HSQC NMR spectrum (400 / 100 MHz, DMSO-d_6) of *iso*MBE-PEG$_{47}$.

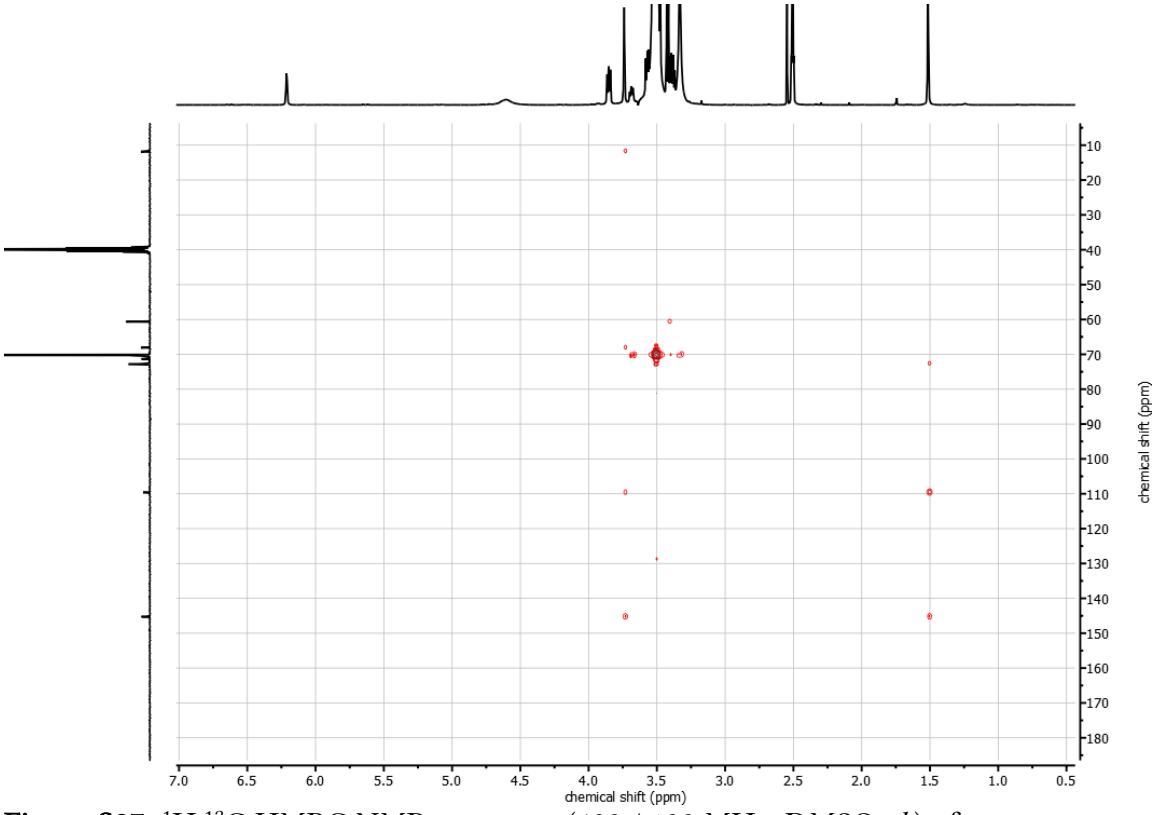

Figure S27: $^{1}H,^{13}C$ HMBC NMR spectrum (400 / 100 MHz, DMSO-d_6) of *iso*MBE-PEG$_{47}$.

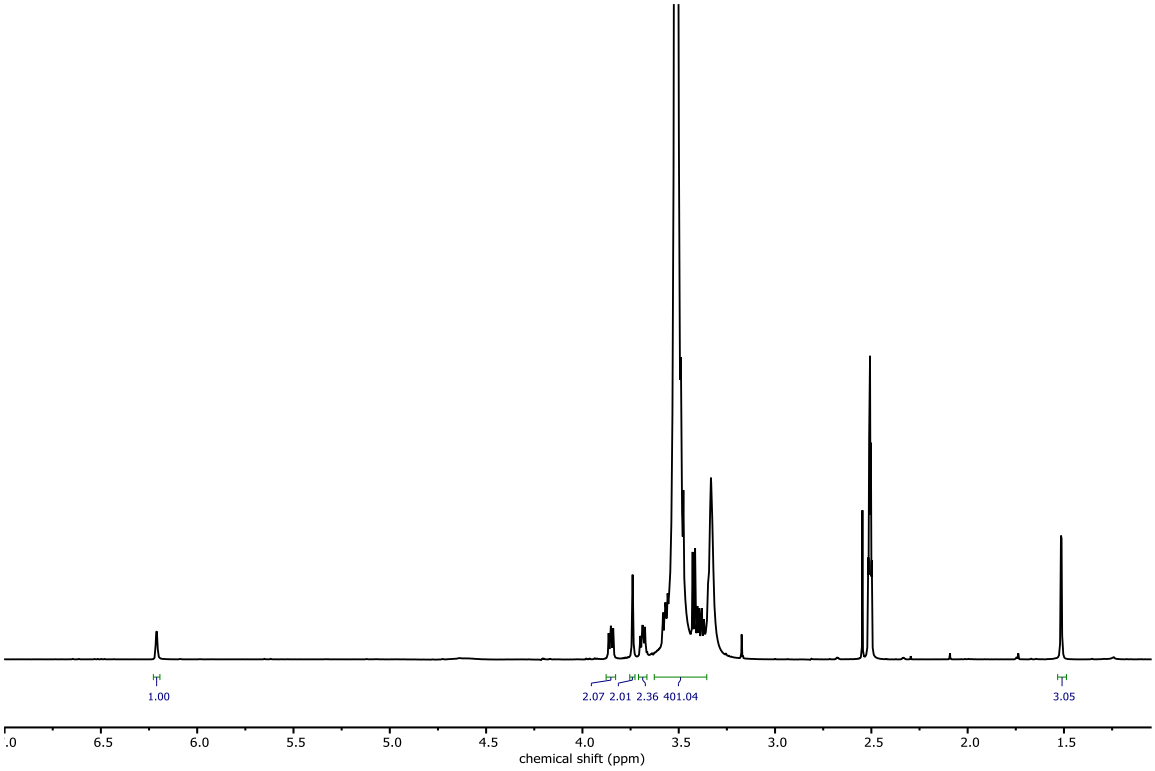

Figure S28: ^{1}H NMR spectrum (400 MHz, DMSO-d_6) of *iso*MBE-PEG$_{107}$.

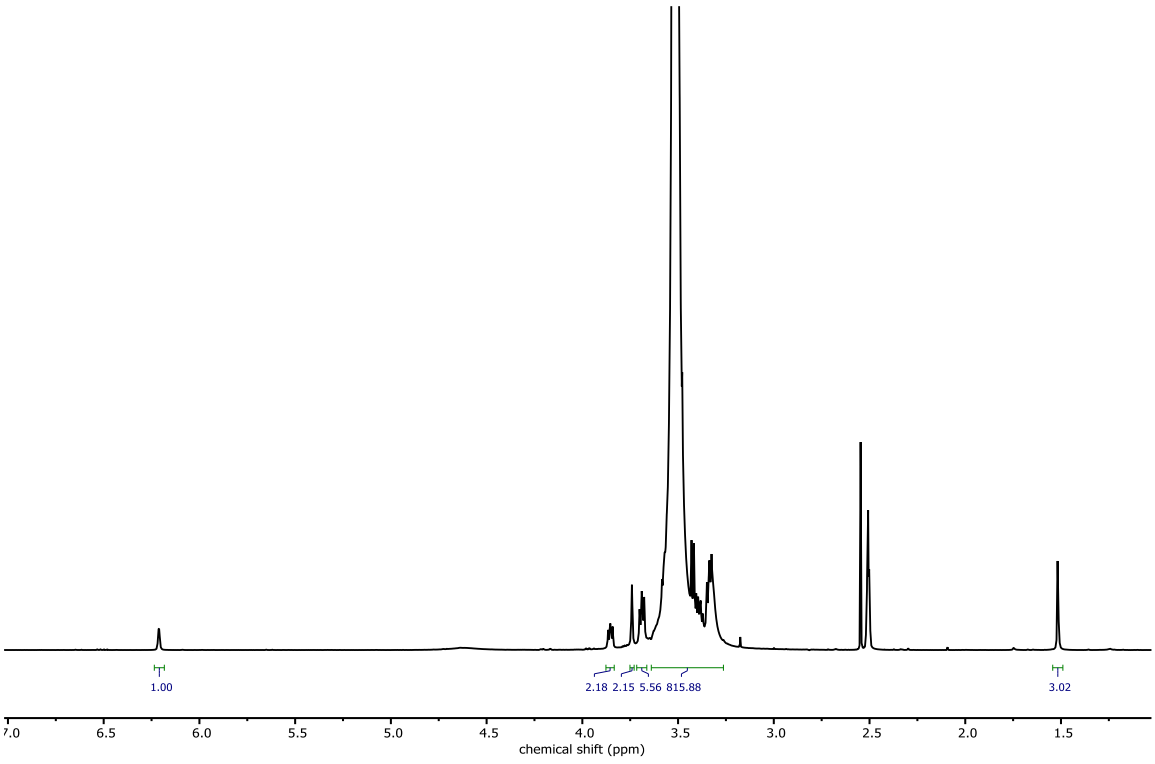

Figure S29: ^{1}H NMR spectrum (400 MHz, DMSO-d_6) of *iso*MBE-PEG$_{217}$.

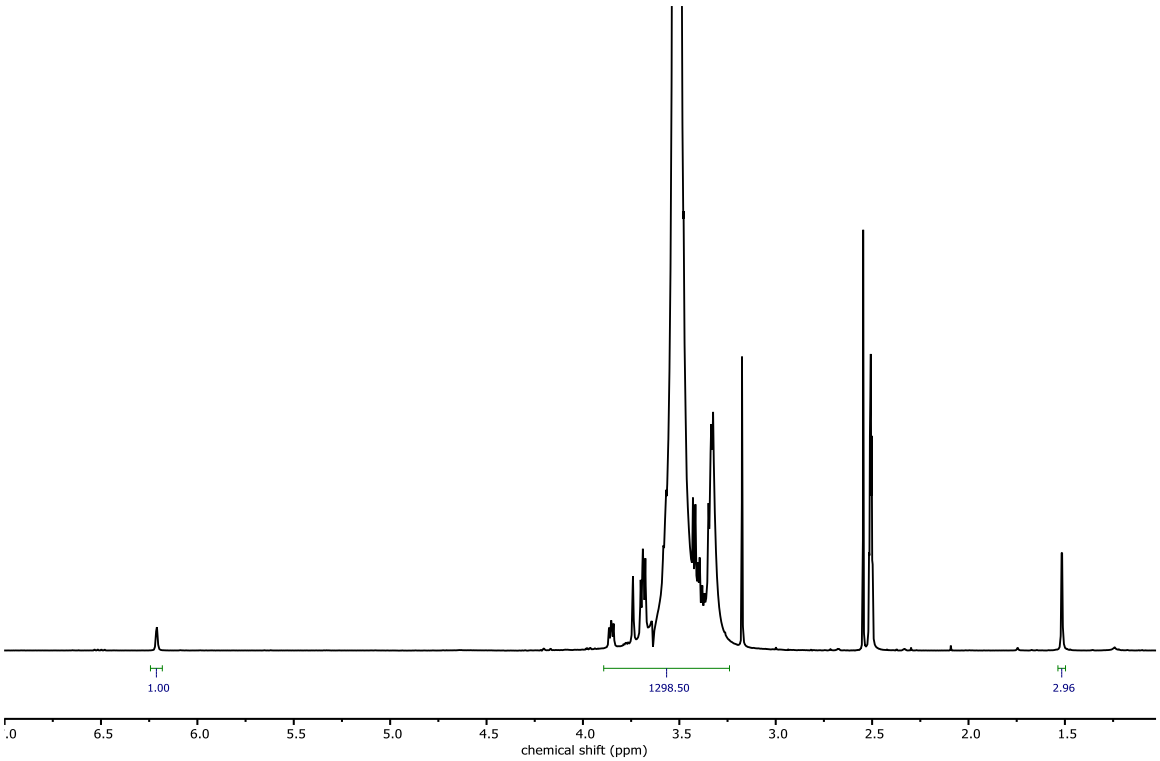

Figure S30: ^{1}H NMR spectrum (400 MHz, DMSO-d_6) of *iso*MBE-PEG$_{311}$.

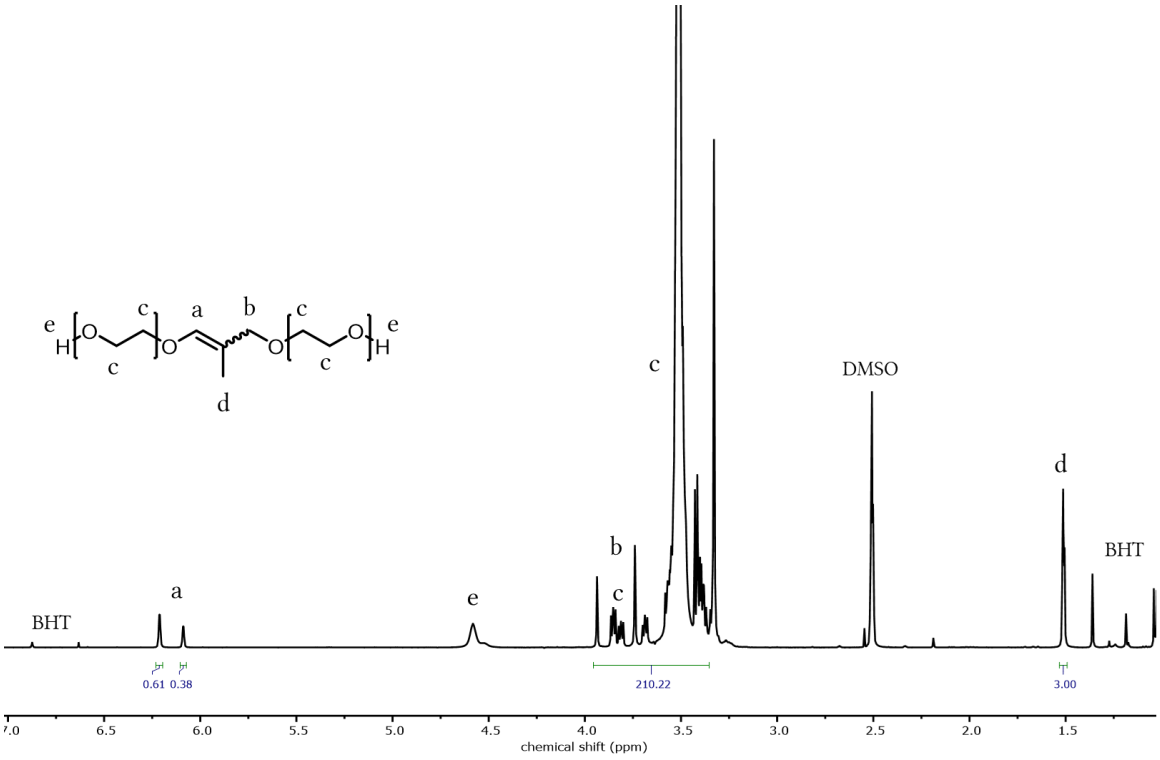

Figure S31: ^{1}H NMR spectrum (400 MHz, DMSO-d_6) of *iso*MBE-PEG$_{51}$.

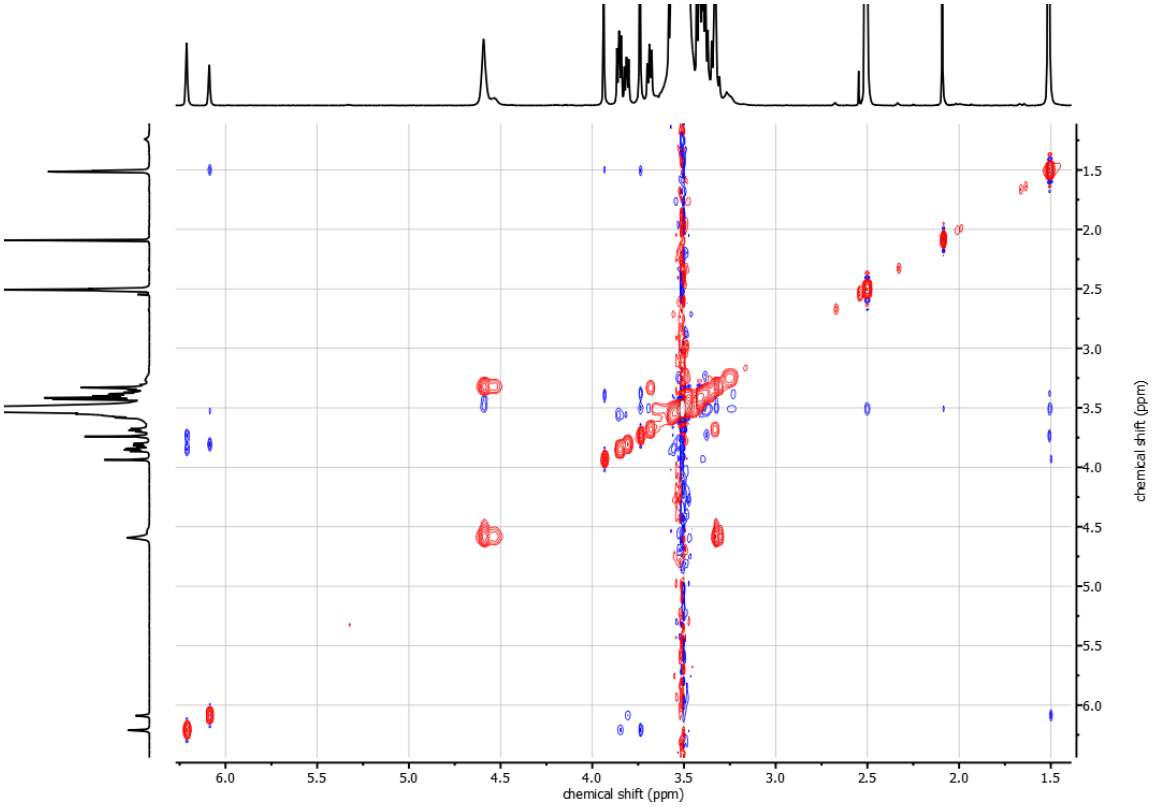

Figure S32: ^{1}H,^{1}H NOESY NMR spectrum (400 MHz, DMSO-d_6) of *iso*MBE-PEG$_{51}$.

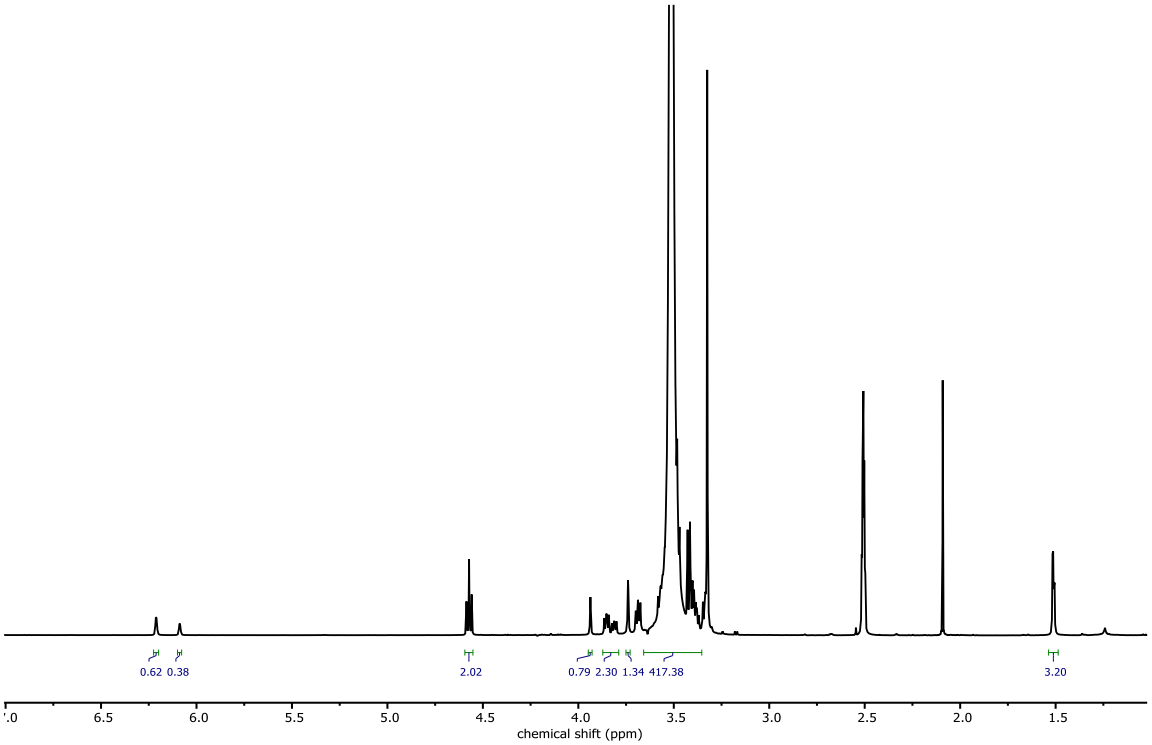

Figure S33: ^{1}H NMR spectrum (400 MHz, DMSO-d_6) of *iso*MBE-PEG$_{99}$.

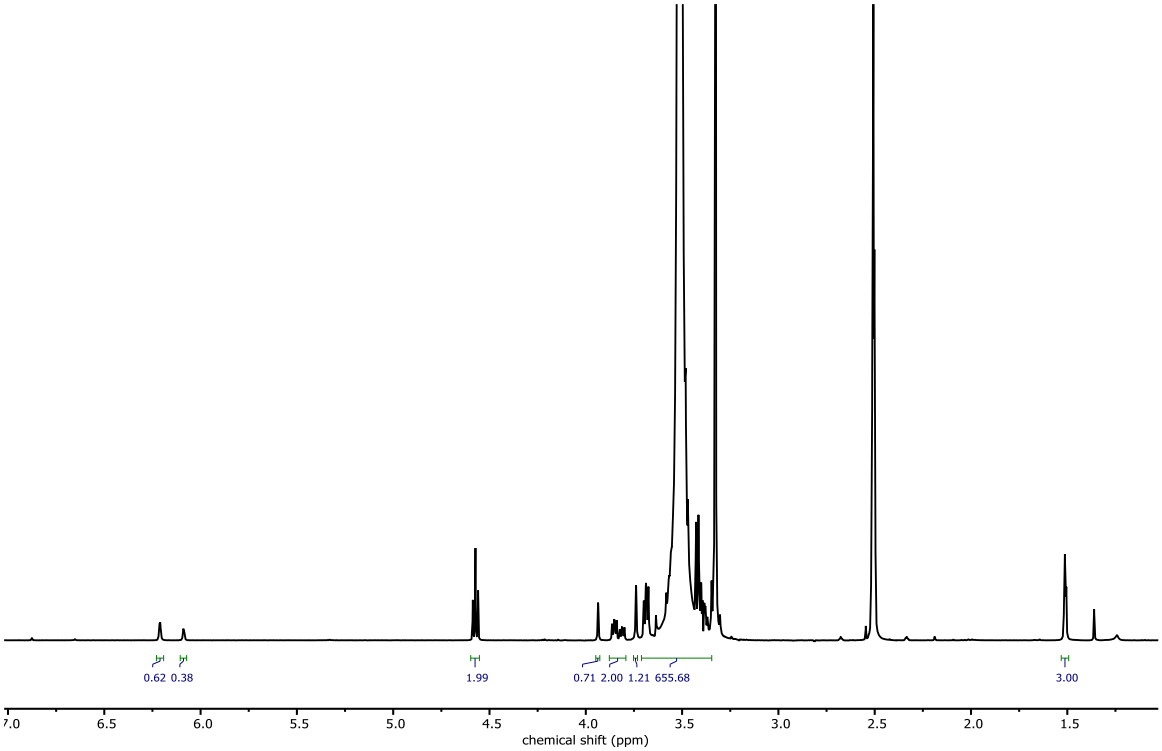

Figure S34: ^{1}H NMR spectrum (400 MHz, DMSO-d_6) of *iso*MBE-PEG$_{176}$.

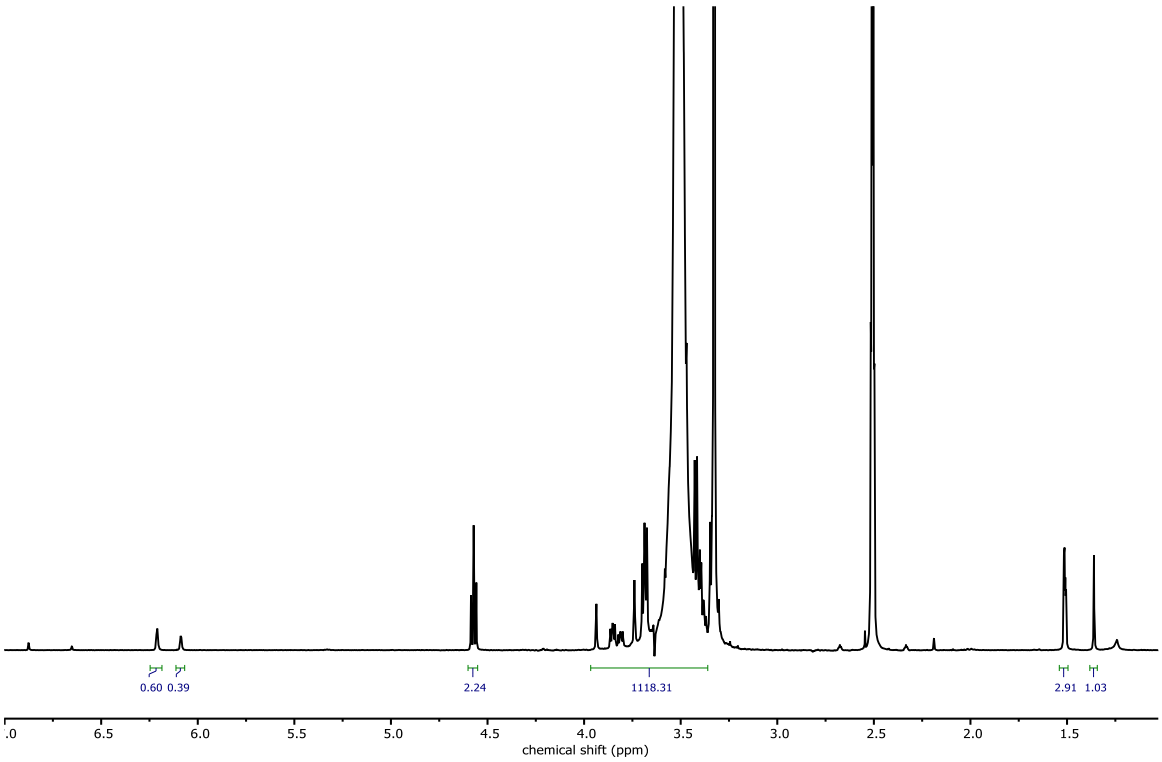

Figure S35: ^{1}H NMR spectrum (400 MHz, DMSO-d_6) of *iso*MBE-PEG$_{294}$.

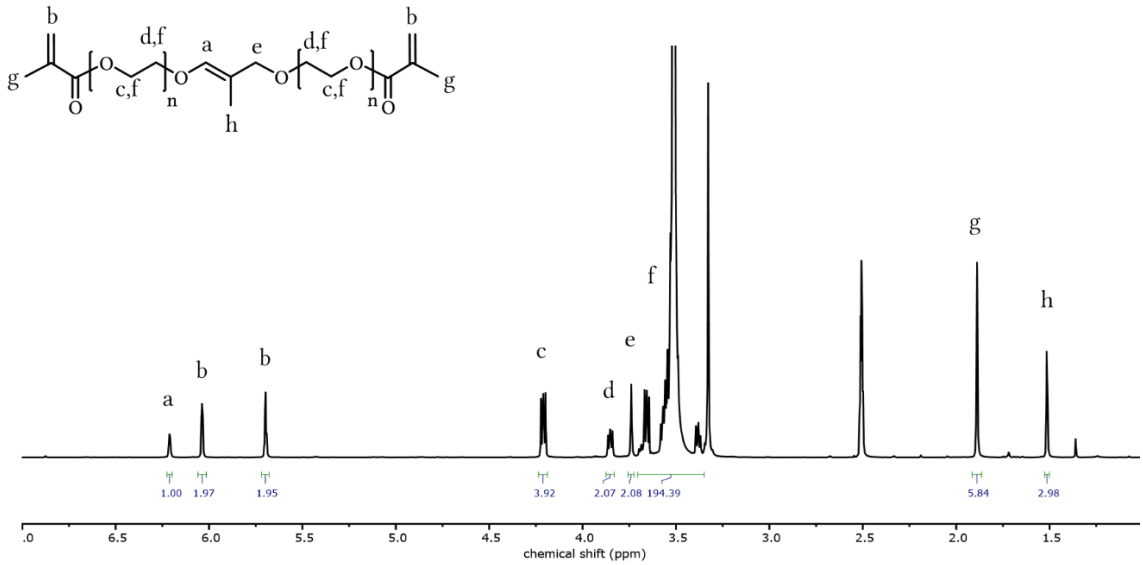

Figure S36: ^{1}H NMR spectrum (400 MHz, DMSO-d_6) of *iso*MBE-PEG$_{47}$-DMA.

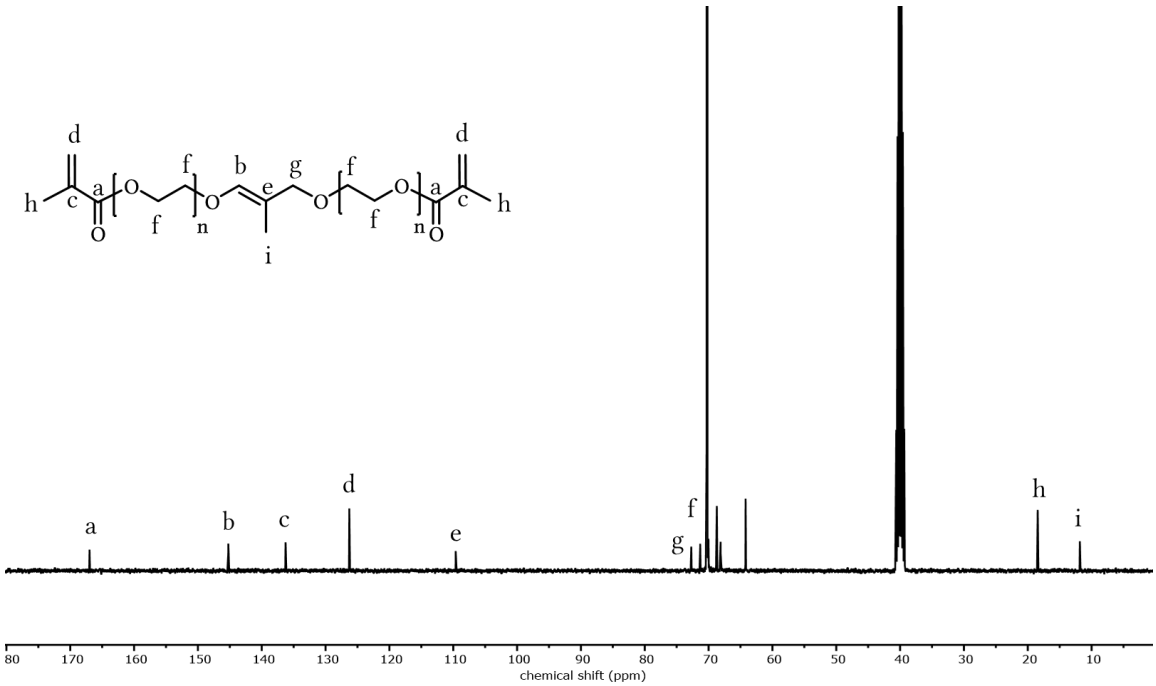

Figure S37: ^{13}C NMR spectrum (100 MHz, DMSO-d_6) of *iso*MBE-PEG$_{47}$-DMA.

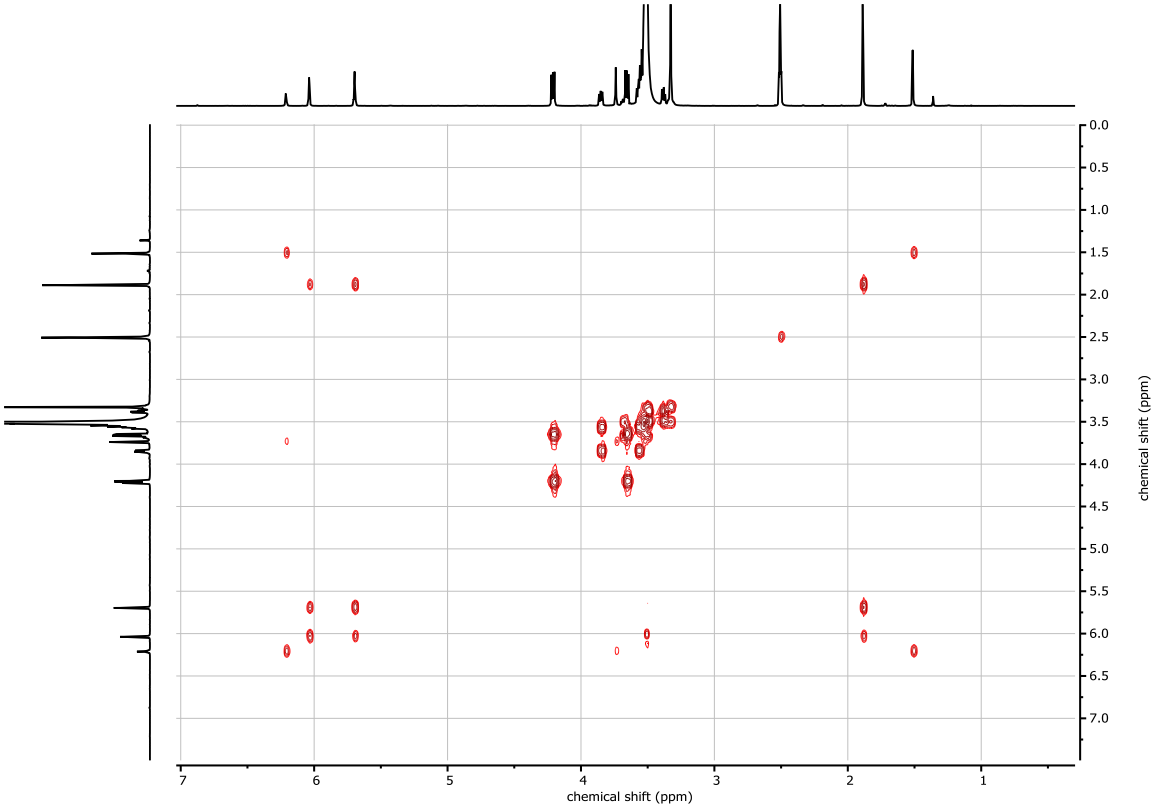

Figure S38: ^{1}H,^{1}H COSY NMR spectrum (400 MHz, DMSO-d_6) of *iso*MBE-PEG$_{47}$-DMA.

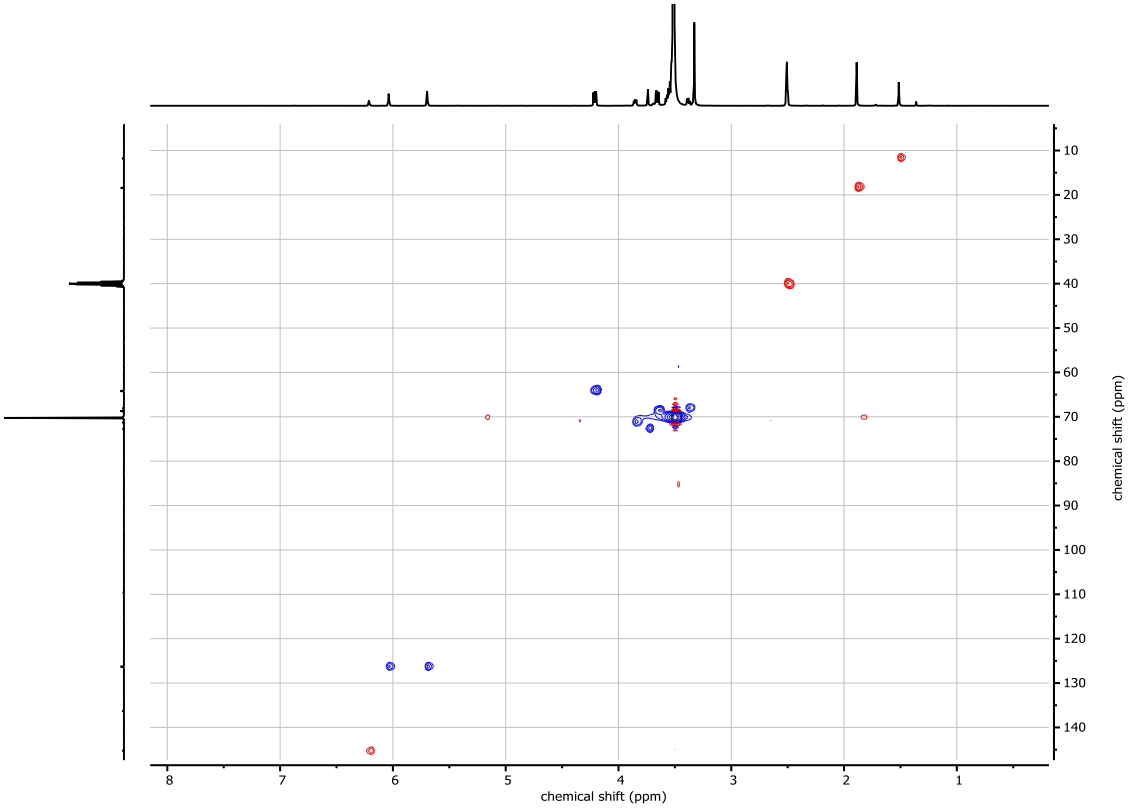

Figure S39: ^{1}H,^{13}C HSQC NMR spectrum (400 / 100 MHz, DMSO-d_6) of *iso*MBE-PEG$_{47}$-DMA.

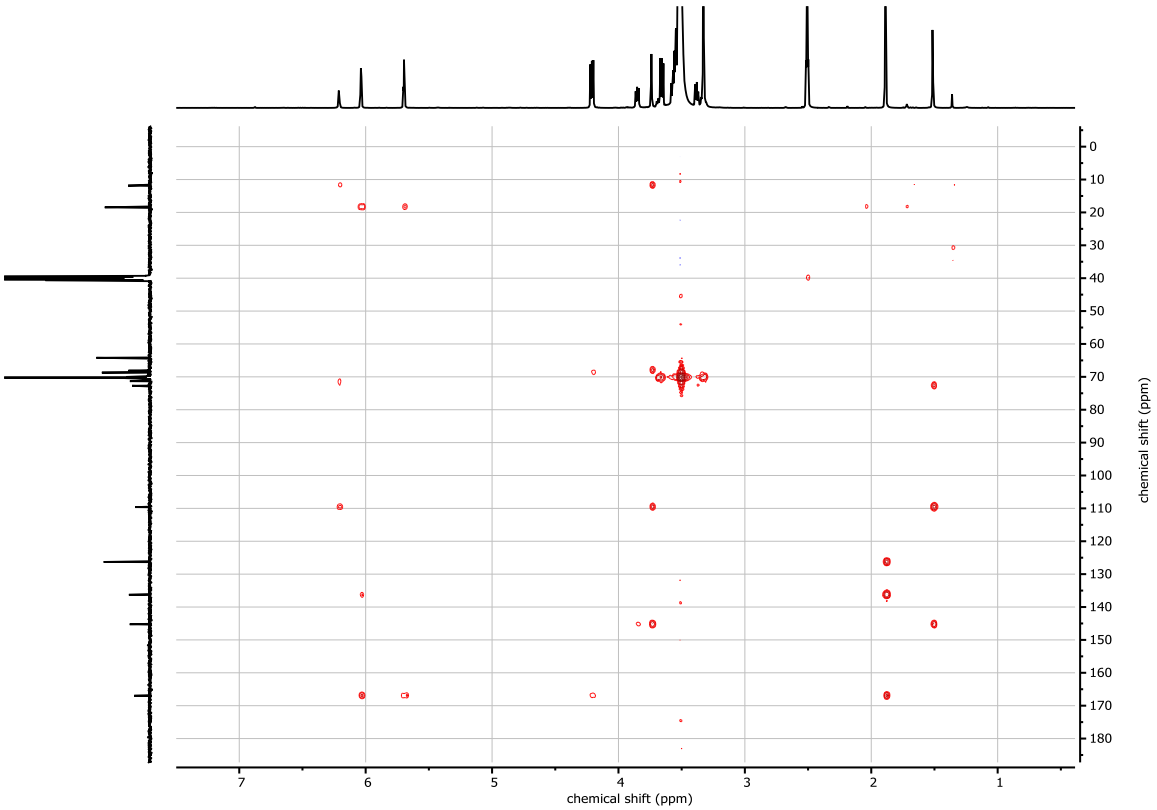

Figure S40: $^{1}H,^{13}C$ HMBC NMR spectrum (400 / 100 MHz, DMSO-d_6) of *iso*MBE-PEG$_{47}$-DMA.

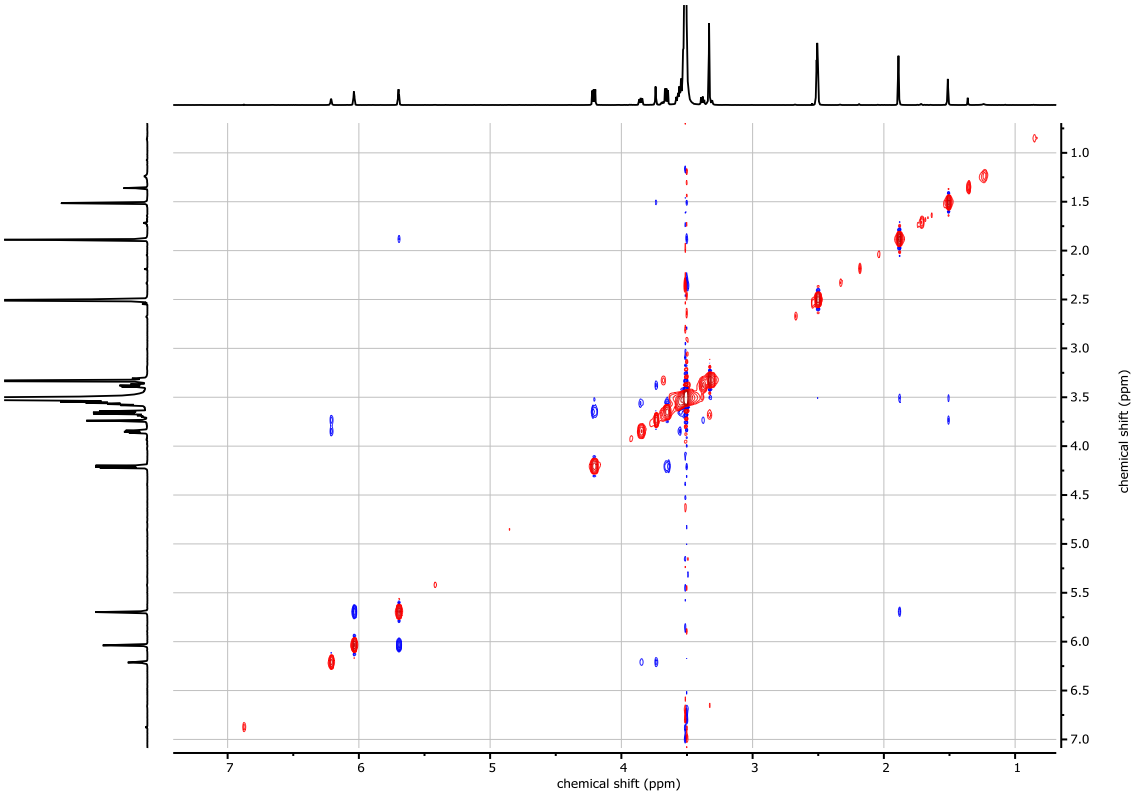

Figure S41: $^{1}H,^{1}H$ NOESY NMR spectrum (400 MHz, DMSO-d_6) of *iso*MBE-PEG$_{47}$-DMA.

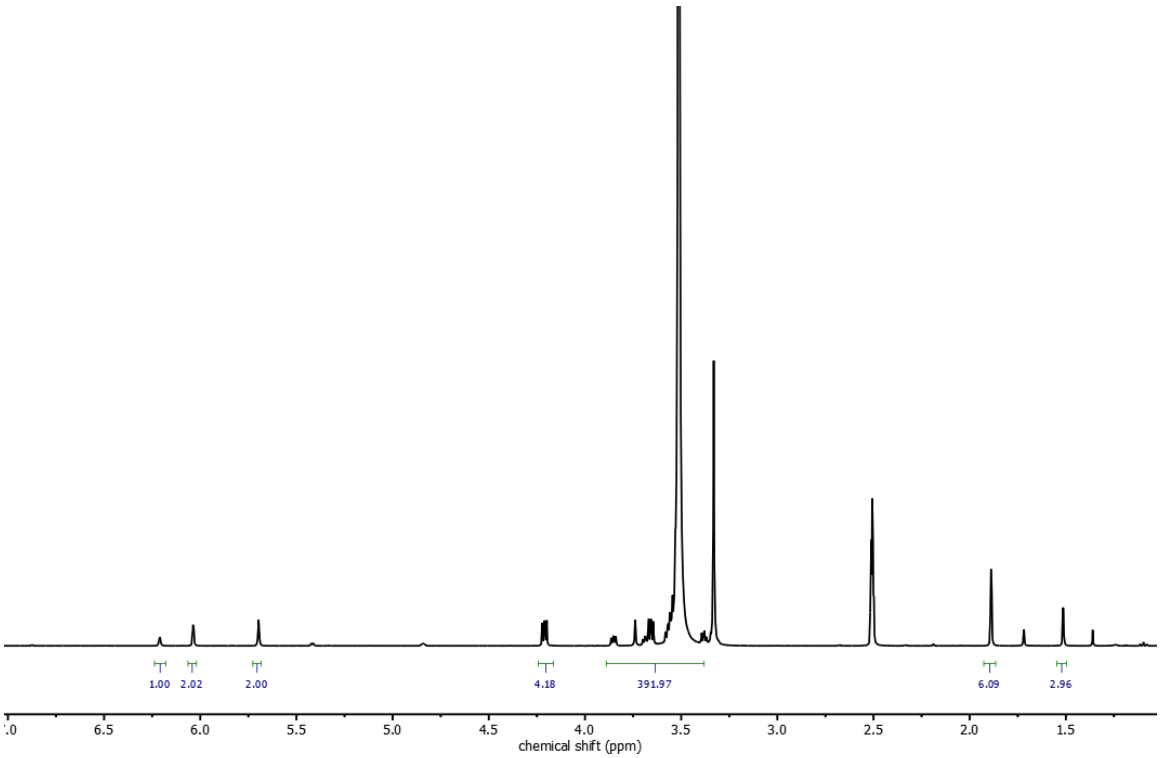

Figure S42: ^{1}H NMR spectrum (400 MHz, DMSO-d_6) of *iso*MBE-PEG$_{107}$-DMA.

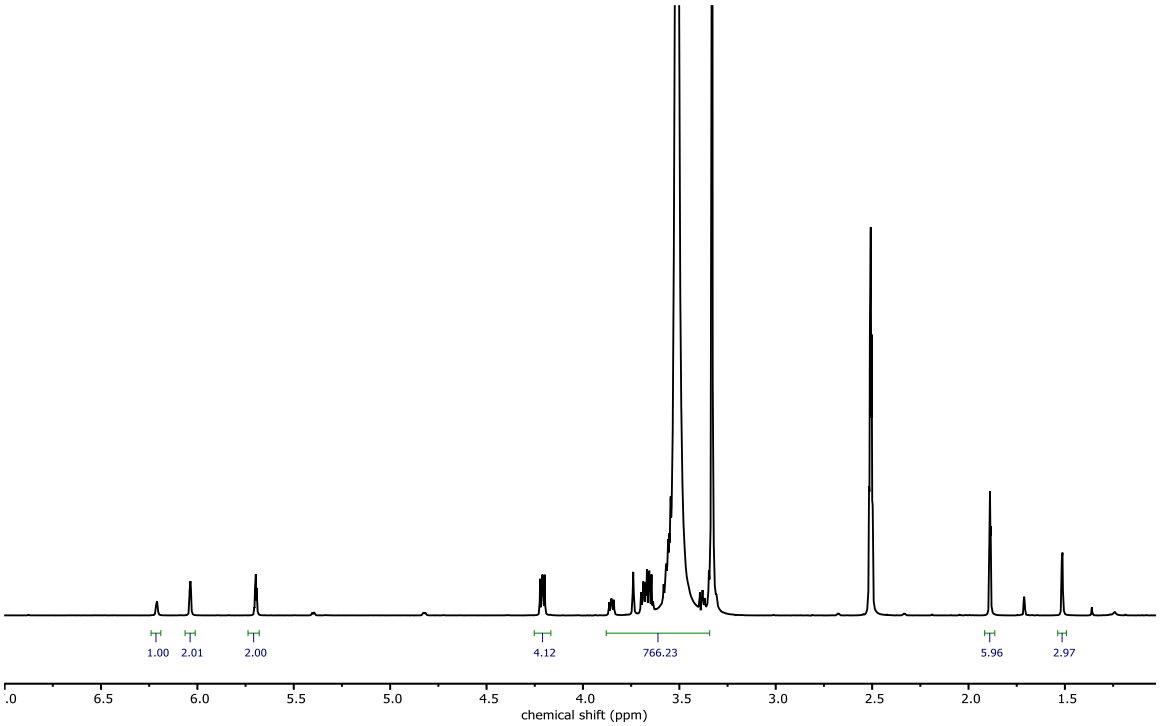

Figure S43: ^{1}H NMR spectrum (400 MHz, DMSO-d_6) of *iso*MBE-PEG$_{217}$-DMA.

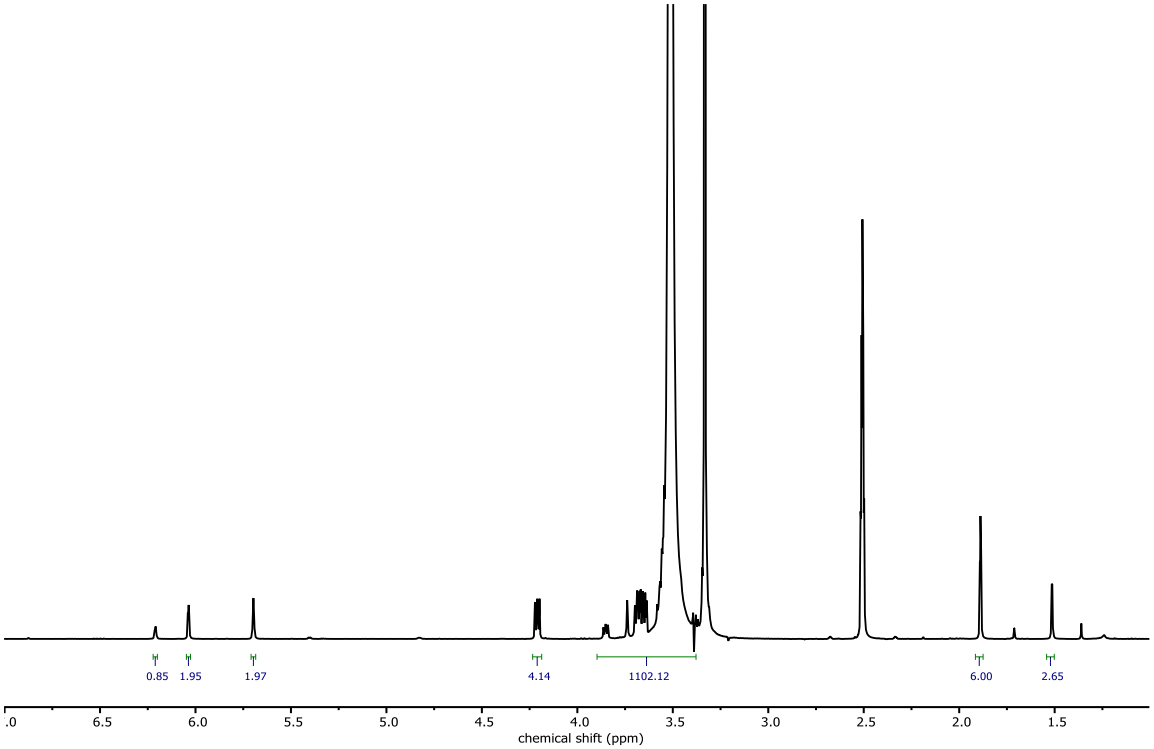

Figure S44: ^{1}H NMR spectrum (400 MHz, DMSO-d_6) of *iso*MBE-PEG$_{311}$-DMA.

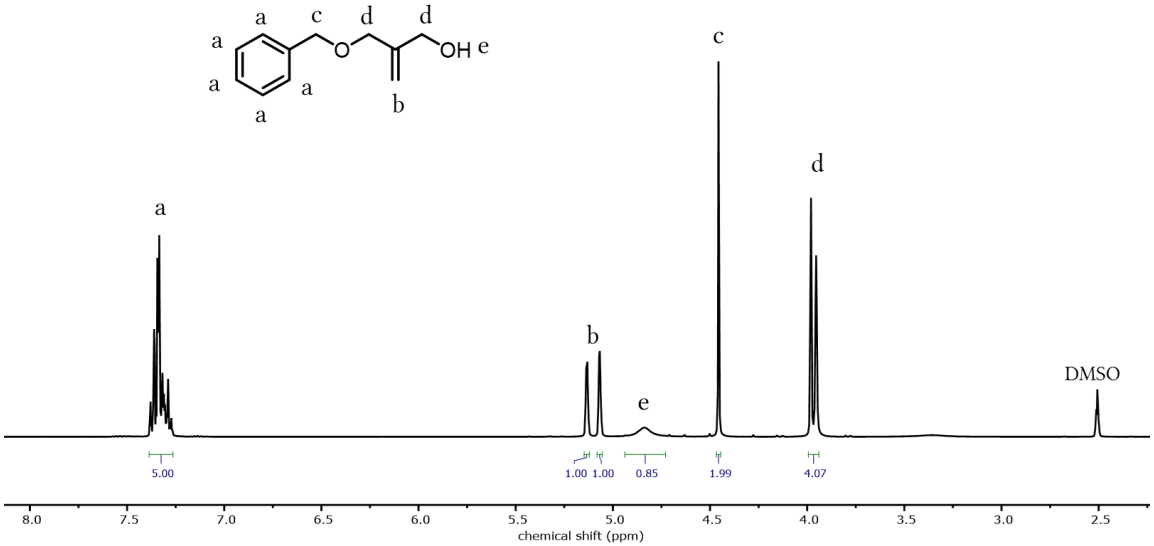

Figure S45: ^{1}H NMR spectrum (400 MHz, DMSO-d_6) of BMP.

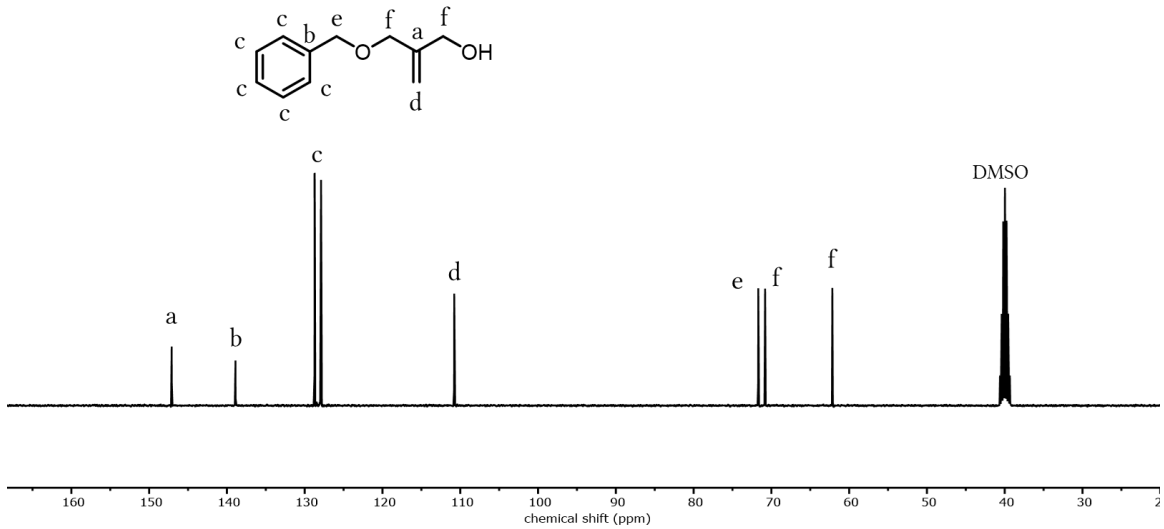

Figure S46: ^{13}C NMR spectrum (100 MHz, DMSO-d_6) of BMP.

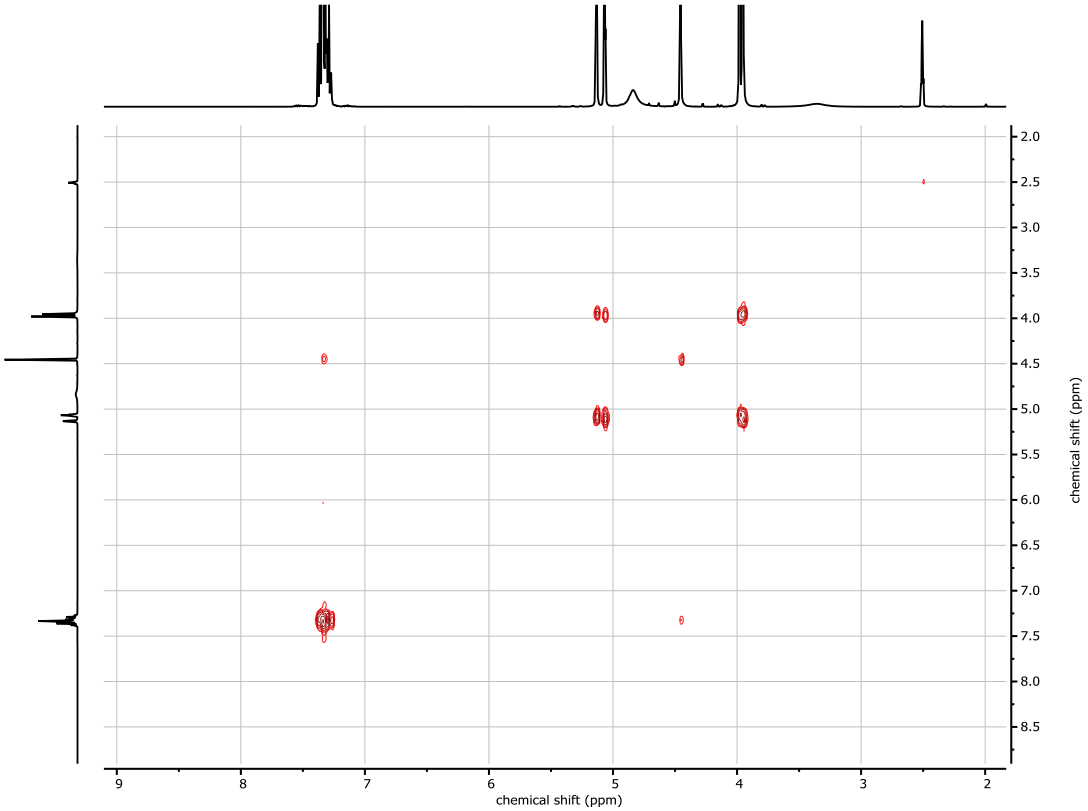

Figure S47: ^{1}H,^{1}H COSY NMR spectrum (400 MHz, DMSO-d_6) of BMP.

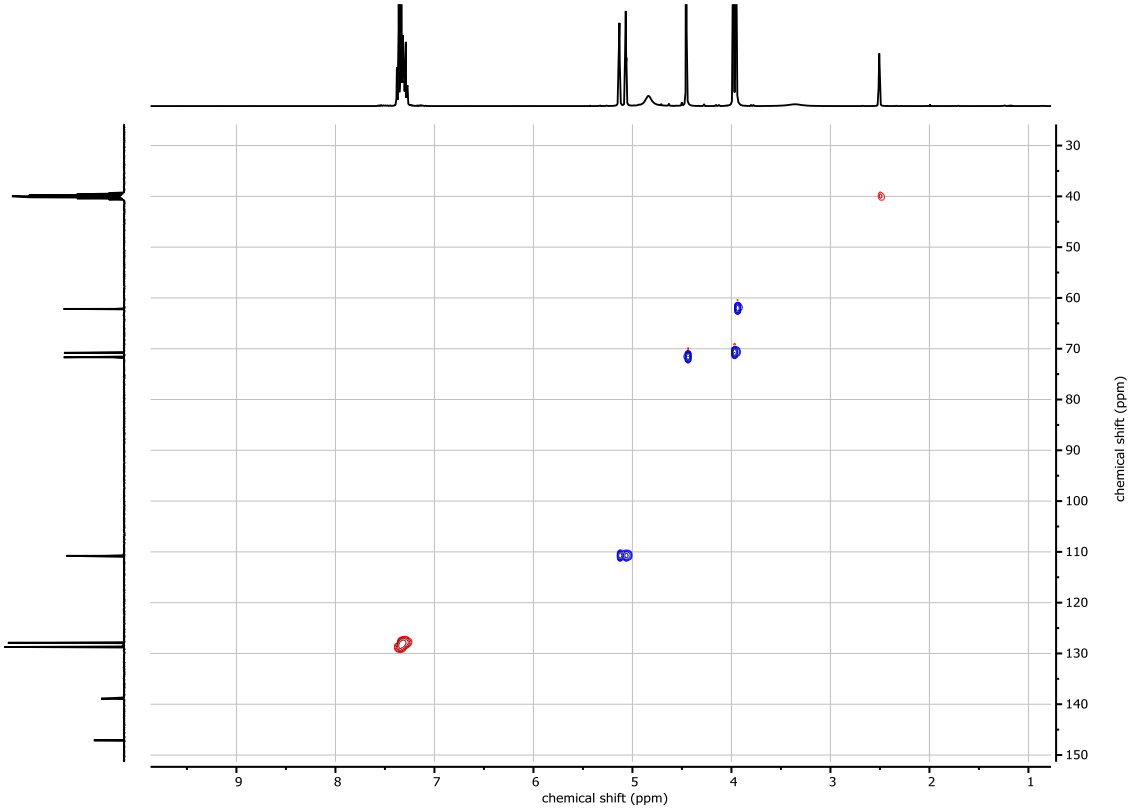

Figure S48: $^{1}H,^{13}C$ HSQC NMR spectrum (400 / 100 MHz, DMSO-d_6) of BMP.

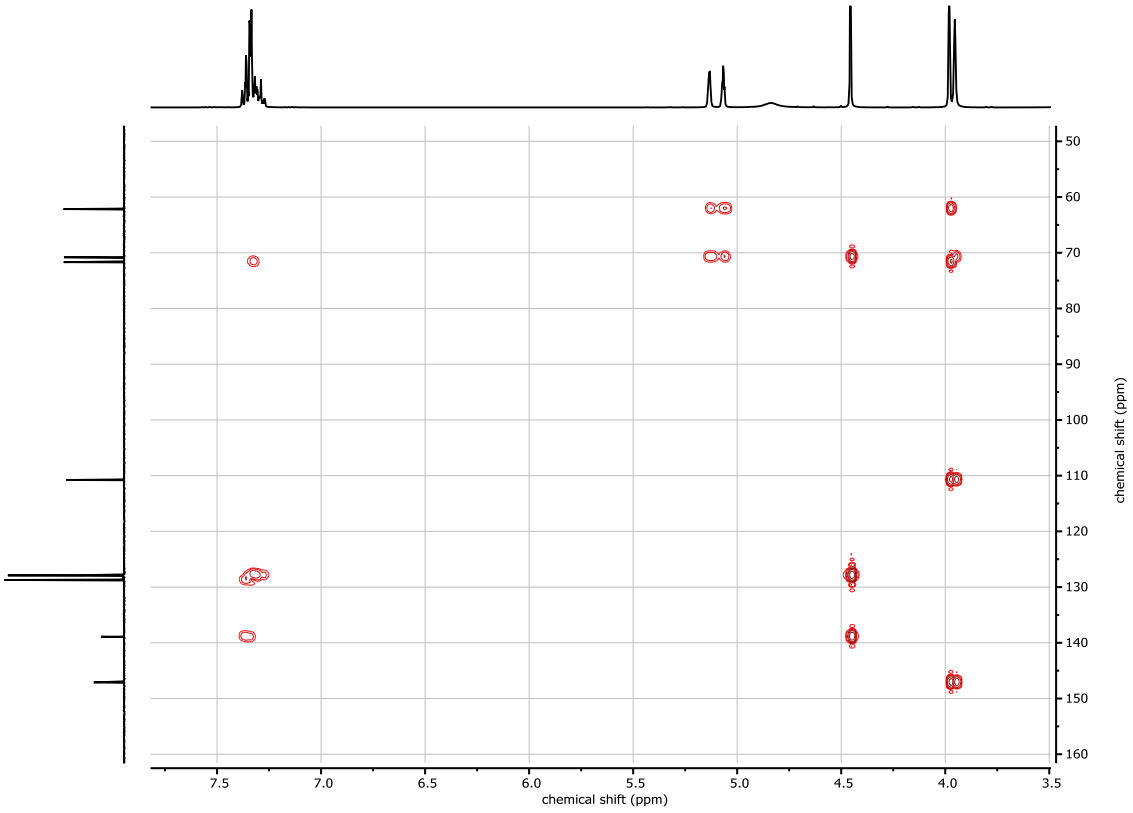

Figure S49: $^{1}H,^{13}C$ HMBC NMR spectrum (400 / 100 MHz, DMSO-d_6) of BMP.

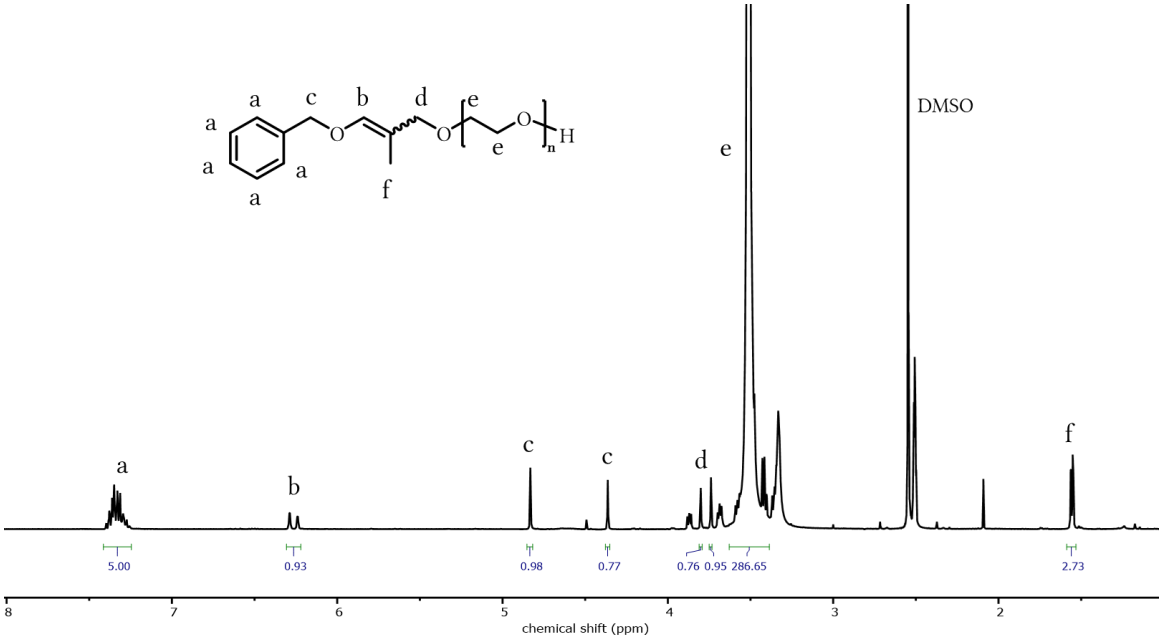

Figure S50: ^{1}H NMR spectrum (400 MHz, DMSO-d_6) of *iso*BMP-PEG$_{70}$.

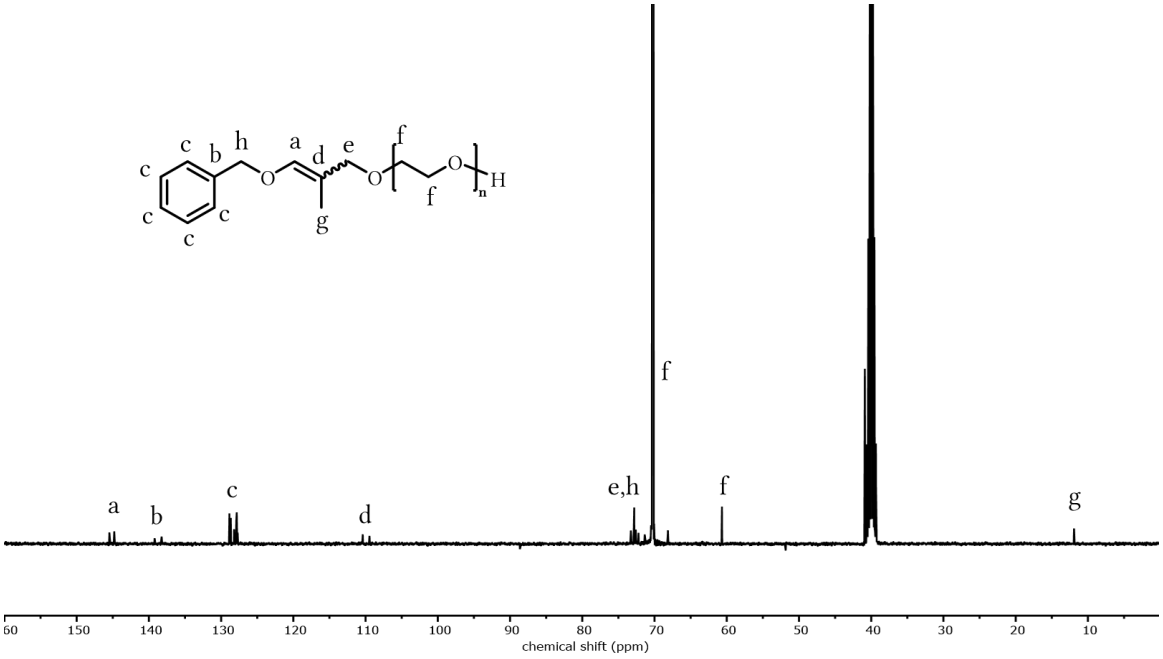

Figure S51: ^{13}C NMR spectrum (100 MHz, DMSO-d_6) of *iso*BMP-PEG$_{70}$.

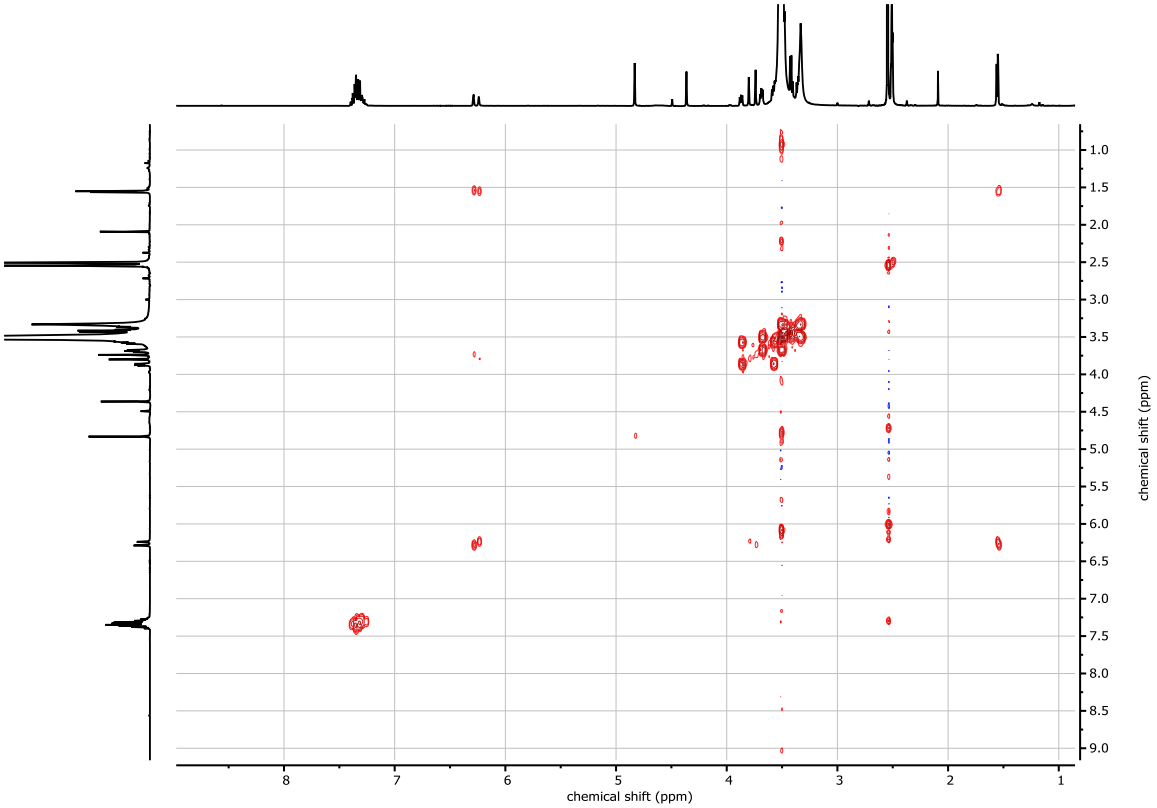

Figure S52: ^{1}H,^{1}H COSY NMR spectrum (400 MHz, DMSO-d_6) of *iso*BMP-PEG$_{70}$.

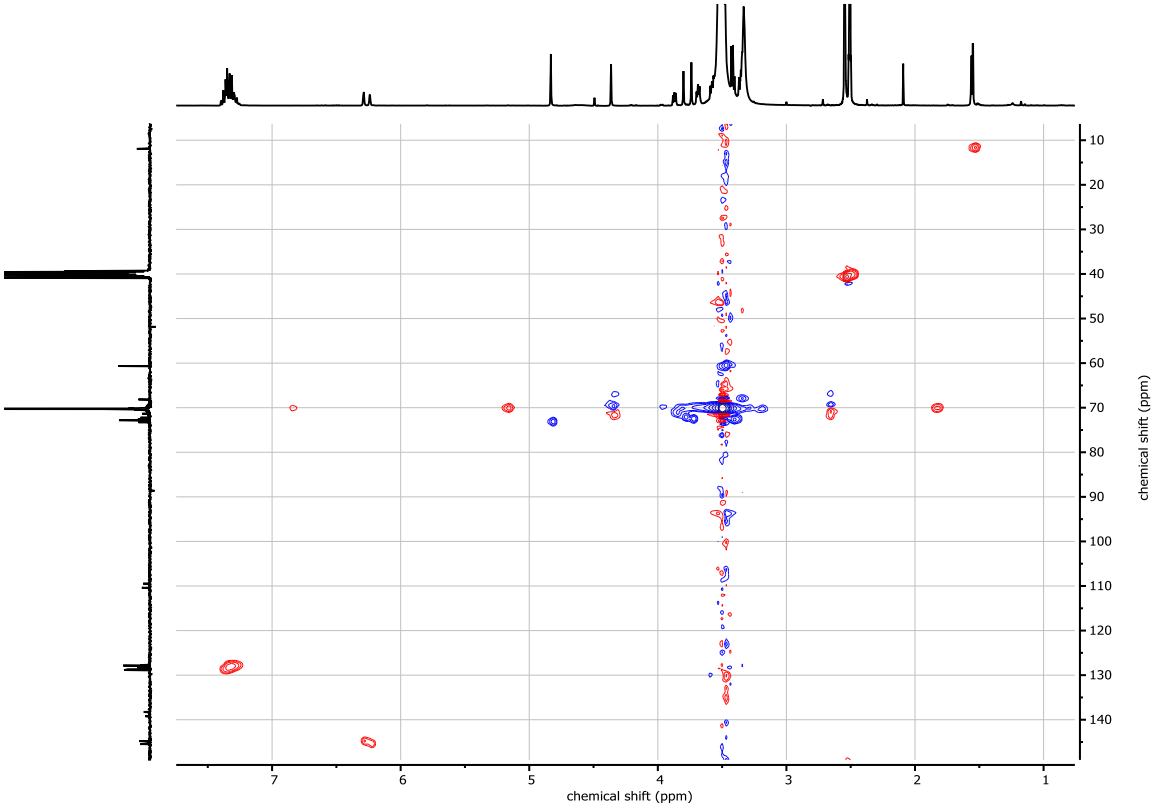

Figure S53: ^{1}H,^{13}C HSQC NMR spectrum (400 / 100 MHz, DMSO-d_6) of *iso*BMP-PEG$_{70}$.

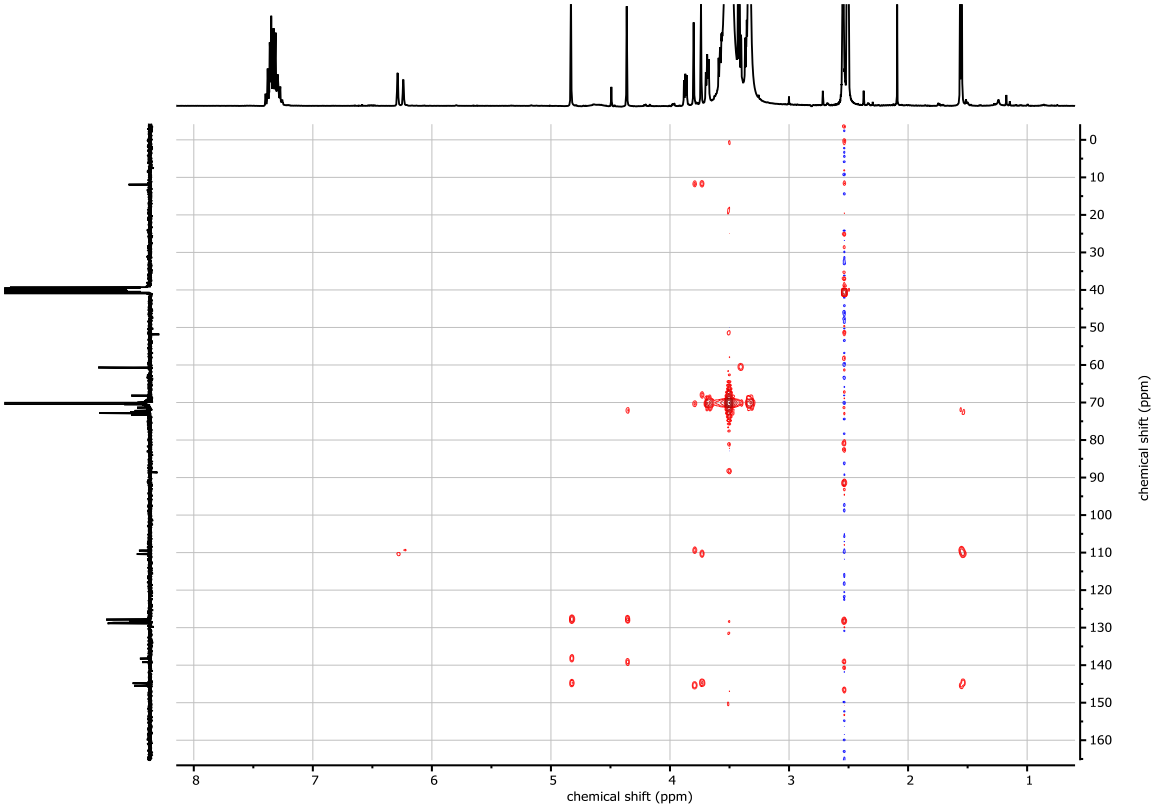

Figure S54: $^{1}H,^{13}C$ HMBC NMR spectrum (400 / 100 MHz, DMSO-d_6) of *iso*BMP-PEG$_{70}$.

4 APPENDIX

4.1 A non-conventional approach towards multi-hydroxy functional polystyrenes relying on a simple Grignard reagent

Philipp von Tiedemann,[a,b] Erik Kersten,[a] Johannes Ewald,[a] Torsten Linder,[a] Christian Fuchs,[a] Manfred Wagner,[c] Holger Frey,[a]*

[a] Institute of Organic Chemistry, Johannes Gutenberg University, Duesbergweg 10-14, 55128 Mainz (Germany)

[b] Graduate School Materials Science in Mainz, Staudingerweg 9, 55128, Mainz (Germany)

[c] Max-Planck Institute for Polymer Research, Ackermannweg 10, 55128, Mainz (Germany)

Published in Macromolecules (DOI: 10.1021/acs.macromol.0c00541)

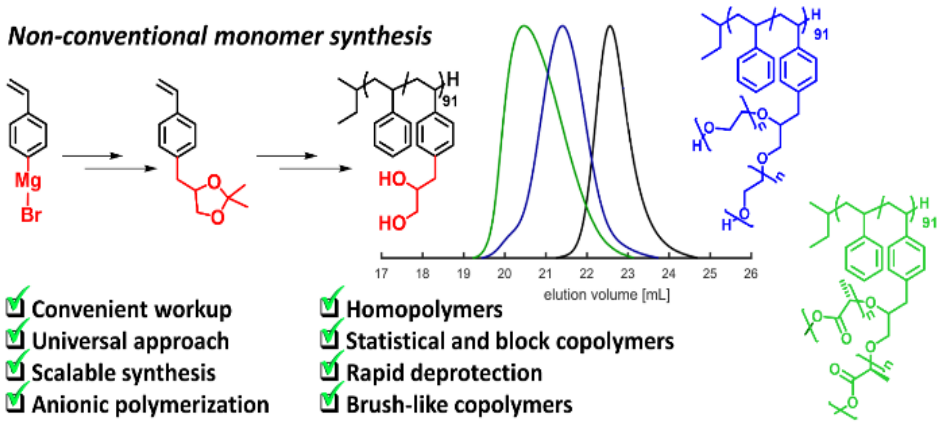

4.1.1 ABSTRACT

Capitalizing on the inertness of styrene towards Grignard-reagents, 4-vinylphenyl magnesium bromide was utilized for the rapid and convenient preparation of the protected monomer 2,2-dimethyl-4-(4-vinylbenzyl)-1,3-dioxolane (DMVBDO), avoiding the use of catalysts and painstaking purification protocols. Well-defined homopolymers, statistical copolymers, and block copolymers with styrene (S) as a comonomer were prepared in THF at -78 °C via carbanionic living polymerization. The overall molecular weights ranged from 4.5 to 68.9 kg mol^{-1} with low dispersities ($Đ$ 1.04 to 1.15). Copolymers were synthesized with styrene feed ratios (X_{feed}) from 15 to 95 mol% with glass transition temperatures (T_g) between 74 and 98 °C. Whereas polystyryllithium served as an excellent macroinitiator for the preparation of the block copolymer $PS_{0.5}$-*b*-$P(DMVBDO)_{0.5}$, the inverse block order, i.e. synthesis of $P(DMVBDO)_{0.5}$-*b*-$PS_{0.5}$ yielded a bimodal molecular weight distribution (MWD) with increased dispersity, which is ascribed to slow crossover. Rapid deprotection of both homo- and copolymers to release two hydroxyl groups per DMVBDO unit was achieved via acidic hydrolysis. The deprotected block copolymer $PS_{0.5}$-*b*-$P(VPPDO)_{0.5}$ showed phase separation, indicated by two T_g values (68 °C and 86 °C). Homogeneous brush copolymers of the type $P(S_{85}$-*co*-$VPPDO_5)$-*g*-PLLA and $P(S_{85}$-*co*-$VPPDO_6)$-*g*-PEO were demonstrated, using quantitative "grafting from" with L-lactide and ethylene oxide, respectively. The brush-like copolymers were obtained in quantitative yields, while maintaining monodisperse MWD.

4.1.2 INTRODUCTION

Substituted styrenes[1–8] are valuable monomers that are compatible with nearly all polymerization techniques, giving rise to an immense variety of functional polymers for many different applications. In the recent decades, controlled radical polymerization (CRP) techniques[9,10] have become key tools in academia, however, they are scarcely used in industry.[11] In contrast to all controlled polymerization techniques,[12] the truly living anionic polymerization,[13,14] initially described by Szwarc *et al.* in 1956,[15,16] is known to be the most reliable strategy for the preparation of well-defined and also complex macromolecular architectures. Anionic living polymerization enables the synthesis of polymers with very narrow molecular weight distributions (MWDs), while additionally benefitting from an extraordinary atom economy, short polymerization times, and convenient polymer isolation or purification protocols. In addition, specific material properties can be precisely engineered for almost any type of application.[17,18] The seemingly countless possibilities for variation in terms of functionality combined with their simplicity render substituted styrene monomers highly promising also for the future of polymer science.[19]

Among functional polymers, hydroxyl-functionalized polystyrenes like poly(4-hydroxy styrene) (PHS) serve as the key material for many interesting polymer topologies, e.g. as a macroinitiator for the synthesis of dendronized architectures.[20–22] However, in order to make use of the high precision of the carbanionic living polymerization, protective group chemistry is mandatory for functional monomers due to the high reactivity and basicity of carbanions. Whereas monomers like 4-*tert*-butoxystyrene (*t*BuOS)[23–25] or *p*-(1-ethoxy ethoxy) styrene (*p*EES)[26,27] are well established, protection of multi-hydroxy functional monomers represents a considerable challenge.

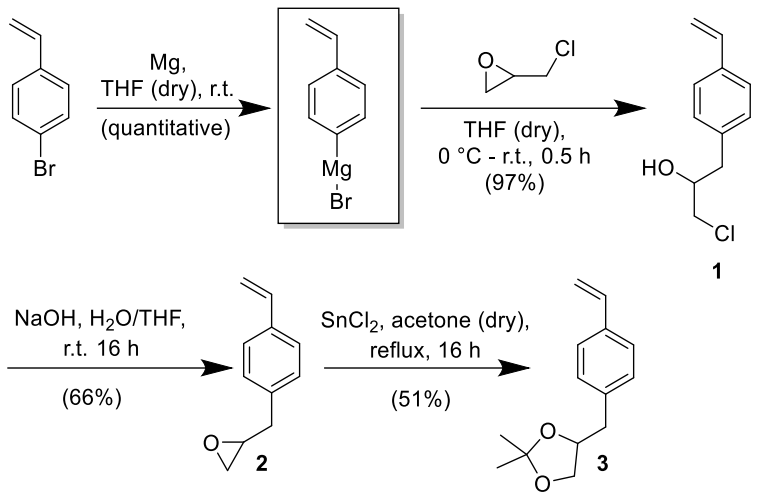

Scheme 1. Synthesis of DMVBDO from 4-bromostyrene.

Suitable protective chemistry for monomers with diol moieties has been introduced via 2,2-dimethyl-1,3-dioxolanes, e.g. for catechol derivatives. Catechol based monomers have been investigated for different applications ranging from metal ion complexation to surface binding.[28–32] However, catechols commonly exhibit low storage stability, as they are easily oxidized. Aliphatic diols represent a highly interesting structural motif, because they can be used for the rapid synthesis of complex macromolecular architectures as well as hydrophilic-hydrophobic block copolymers that undergo self-assembly with tuneable phase behavior.[33,34]

Aliphatic diols are less prone to oxidation, but can in principle be easily protected in a similar fashion. However, linkage of different 1,3-dioxolanes to styrene in order to produce functional monomers that can be subjected to carbanionic living polymerization was found to be challenging.[35,36] The monomer design has to be well planned due to the high basicity of the living carbanion present throughout the polymerization. For instance *para*-substituted styrene monomers bearing the benzyl ether moiety are known to undergo a 1,6-elimination once the anionic polymerization is initiated.[37] In pronounced contrast, the dioxolane moiety is known to be stable under the harsh conditions of the carbanionic living polymerization, and deprotection can readily be achieved via acidic hydrolysis.[35]

The development of novel functional monomers ideally should fulfil three criteria: (i) universality, (ii) scalability, and (iii) a convenient workup procedure that gives fast access to the monomer in good yields and high purity. We recently described a scalable synthesis procedure relying on an optimized Wittig reaction that enables the rapid preparation of *para* alkyl styrenes.[38] In the current work we demonstrate a rather simple synthesis approach based on the use of the simple Grignard reagent (4-vinylphenyl)magnesium bromide, which enables the versatile introduction of a broad variety of functional groups. To the best of our knowledge (4-vinylphenyl)magnesium bromide has rarely been utilized for the preparation of functional monomers for the carbanionic living polymerization.[39–41] As aryl Grignard reagents do not possess sufficient nucleophilicity to initiate the anionic polymerization of styrene monomers, they are attractive for the rapid attachment of electrophilic compounds. Due to the high reactivity and selectivity, functional monomers can thus be easily synthesized (**Scheme 1**). The present work aims at a general synthesis avenue for functional styrene monomers, avoiding expensive catalysts and tedious purification protocols. Relying on the established procedure, the monomer 2,2-dimethyl-4-(4-vinylbenzyl)-1,3-dioxolane (DMVBDO) was synthesized (Scheme 1) and subjected to carbanionic living polymerization, giving access to well-defined homo- as well as random and block copolymers. All polymers were investigated with respect to MWD, dispersity, and thermal properties (glass transition temperature). After acidic deprotection the aliphatic diol moieties were accessible at each repeating unit of the polymer. Subsequently, the deprotected copolymer was used as a macroinitiator for the synthesis of brush-like copolymers in a “grafting from” approach with l-lactide (LLA) and ethylene oxide (EO).

4.1.3 RESULTS AND DISCUSSION

4.1.3.1 MONOMER SYNTHESIS

The monomer 2,2-dimethyl-4-(4-vinylbenzyl)-1,3-dioxolane (DMVBDO) (3) was synthesized in three steps (**Scheme 1**), albeit the first two intermediates 1-chloro-3-(4-vinylphenyl)propan-2-ol (1) and 2-(4-vinylbenzyl)oxirane (2) were used without further purification for the subsequent steps. DMVBDO was synthesized on a multigram scale (typically 30 g of starting material) followed by purification via vacuum distillation. No column chromatography was required, which renders the synthesis sequence suitable for further scale-up.

4.1.3.2 POLYMERIZATION BEHAVIOR OF DMVBDO AND DEPROTECTION

The polymerization of DMVBDO was first investigated in non-polar media (cyclohexane and benzene) with *sec*-butyllithium (*s*-BuLi) as an initiator (**Scheme 2**). To our surprise, neither DMVBDO homopolymers nor DMVBDO copolymers with styrene (S) (X_{feed}(S) = 0.9, 0.5) could be obtained within 3 hours after initiation.

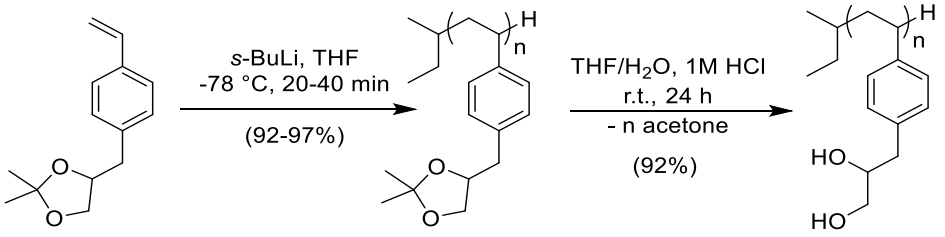

Scheme 2. Polymerization of DMVBDO in THF and subsequent deprotection to P(VPPDO).

Subsequently, THF/cyclohexane solvent mixtures were tested for the homopolymerization of DMVBDO at room temperature. A gradual increase of THF in the polymerization solvent mixture resulted in an increase of monomer conversion (measured after 3 h), which leveled off, when a THF/Li ratio exceeding 100 was reached. (**Figure 1**, **Figure S57**). The obtained MWDs (**Table S3**) are slightly broader than

commonly observed for the living anionic polymerization ($Đ$ > 1.1). Nonetheless, it was found that upon raising the amount of THF, the molecular weight of the obtained polymer (M_n by SEC) increased from 3.5 to 6.9 kg mol^{-1} and that the dispersity gradually decreased from 1.31 to 1.15 (see **Table S3**, **Figure S58**). To clarify whether side reactions occur in neat cyclohexane or benzene in the course of the reaction, polymerization aiming at an oligomer ($M_n^{targeted}$ = 1 kg mol^{-1}) of DMVBDO was initiated via *s*-BuLi and monitored over the course of 7 days.

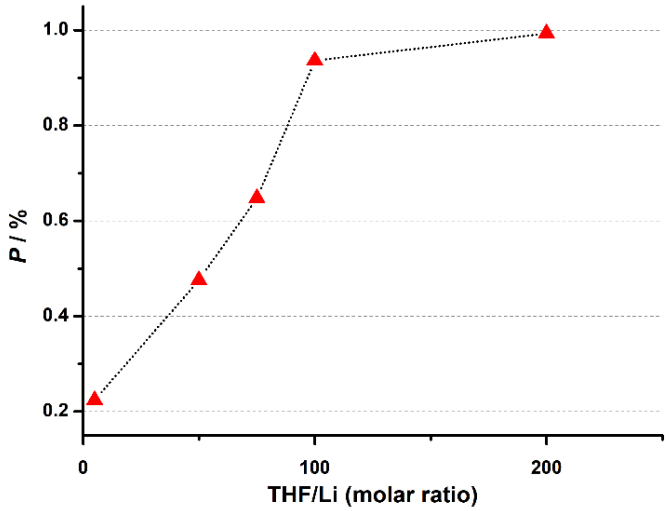

Figure 1. DMVBDO conversion as a function of THF/Li molar ratio (P(DMVBDO) $M_n^{targeted}$ = 5 kg mol^{-1}).

Finally, the (still colored, i.e. living) reaction mixture in pure apolar solvent was terminated with degassed methanol, and the solvent was removed under reduced pressure. The viscous residue was analyzed via ^{1}H NMR spectroscopy. The spectra indicated no side reactions over time, showing only additional signals of unreacted monomer (**Figure S59**). ^{1}H NMR characterization revealed that a tetramer was formed and a monomer conversion of 88% was reached.

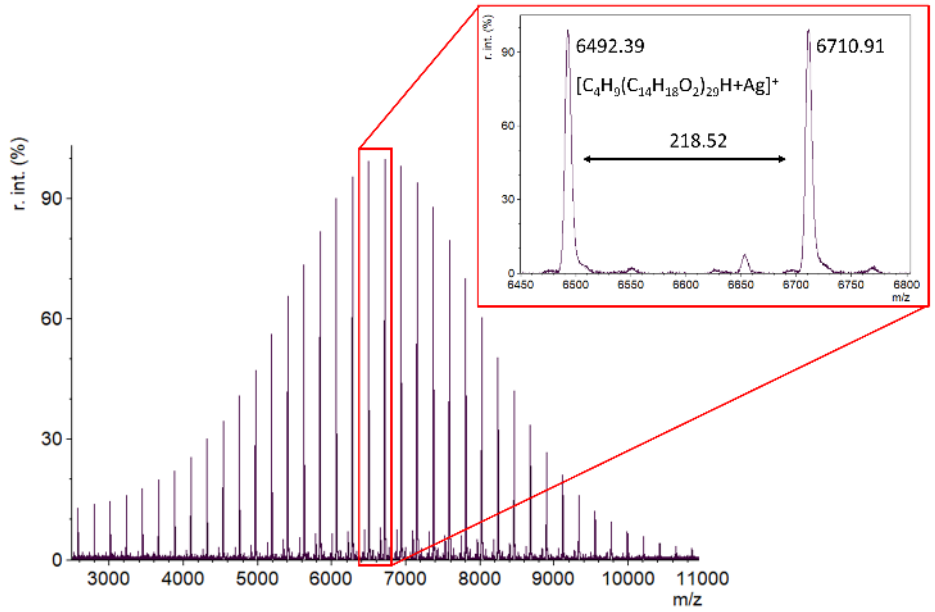

Figure 2. MALDI-ToF-MS analysis of P(DMVBDO) homopolymer.

Unlike the polymerization in non-polar media, the living polymerization of P(DMVBDO) was readily achieved in pure THF at -78 °C within 20 minutes with near quantitative yields (92%). After precipitation in cold methanol the homopolymer (white, glassy powder) was analyzed via SEC, NMR, and FT-IR spectroscopy (**Figures S14-19**).

^{1}H NMR spectroscopy revealed full monomer conversion and high purity of the polymer. SEC characterization showed a homogeneous distribution (**Figure 3**). The molecular weights (M_n) determined both by SEC and ^{1}H NMR spectroscopy were found to be in good agreement with the targeted M_n. SEC revealed that a polymerization time of 20 minutes was sufficient to reach full monomer conversion. The MALDI-ToF-MS analysis enabled a detailed understanding of the resulting homopolymer with respect to mass distribution. The mass of the repeating unit (218.52 g mol^{-1}) was found to agree well with the calculated value of DMVBDO (218.13 g mol^{-1} based on natural abundance) (**Figure 2**).

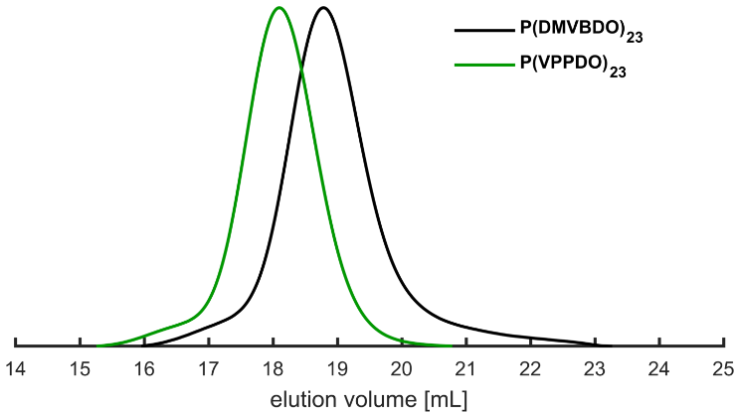

Figure 3. SEC traces (DMF, UV signal, PS standards) of P(DMVBDO)$_{23}$ and P(VPPDO)$_{23}$.

Quantitative deprotection of P(DMVBDO)$_{23}$ was readily achieved in a homogenous H_2O/THF mixture by the addition of 1 M HCl overnight (see Experimental Part for details). The clear shift of the SEC elution trace (**Figure 3**) after the completed deprotection confirm quantitative conversion. The deprotected homopolymer (P(VPPDO)$_{23}$) eluted at lower elution volume compared to P(DMVBDO)$_{23}$.

Table 1. Homopolymer deprotection results of P(DMVBDO).

Polymer	M_n[a] / kg mol^{-1}	M_n[b] / kg mol^{-1}	$Đ$[a]	Yield /%
P(DMVBDO)$_{23}$	5.4	5.1	1.06	92
P(VPPDO)$_{23}$	8.5	5.0	1.11	89

[a] Determined by SEC in DMF (UV signal, PS standard), [b] determined by ^{1}H NMR spectroscopy (pyridine-*d5*) by referencing to the methyl protons of the initiator.

According to the decrease in mass, this result is counterintuitive and thus tentatively attributed to a different hydrodynamic volume in DMF due to the highly polar 1,2-diol moieties at the deprotected repeating units. The NMR (**Figure S20-23**) and FT-IR (**Figure S24**) spectra verified the quantitative deprotection of P(DMVBDO)$_{23}$. The solubility of the deprotected homopolymer P(VPPDO)$_{23}$ was found to be completely altered in comparison to the protected polymer (**Table 2**).

Table 2. Solubility of P(DMVBDO) and P(VPPDO).

Polymer	THF	Acetone	MeOH	H_2O	$CDCl_3$	Pyridine	DMSO
P(DMVBDO)$_{23}$	+	+	(+)	-	+	+	+
P(VPPDO)$_{23}$	-	-	+	-	-	+	-

+ = soluble (at least 10 mg / mL), - = insoluble, (+) = partially soluble.

Due to the large number of hydroxyl groups P(VPPDO)$_{23}$ was difficult to analyse via MALDI-ToF MS. Nonetheless, the appropriate molecular weight of the monomer repeating unit ($[M]^+$: 178.10 calculated based on natural abundance, 178.06 found) was identified (**Figure S25**).

4.1.3.3 STATISTICAL AND BLOCK COPOLYMERS OF DMVBDO WITH STYRENE

Under the same conditions as for the homopolymerization, DMVBDO was statistically copolymerized with styrene ($M_n^{targeted}$ = 10 kg mol^{-1}). In the copolymerization the styrene feed ratio (Xfeed (S)) was probed as the independent variable by varying the styrene fraction in the feed from 15 to 95 mol%. The amount of initiator (s-BuLi) and the concentration of the polymerization solution (20 wt%) were kept constant over all reactions to maintain comparability. All statistical copolymerizations were carried out for 45 minutes at -78 °C to ensure full monomer conversion, terminated with degassed methanol and subsequently precipitated in cold methanol. For the precipitation of the copolymers with 45 and 55 mol% DMVBDO 5 vol% of water was added to methanol, as the precipitation in pure methanol resulted in lower yields due to the intermediate solubility. SEC elution traces are shown in the supporting information (**Figure S60**). Well-defined copolymers of the type P(S$_x$-*co*-DMVBDO$_{1-x}$) ($M_n^{targeted}$ = 10 kg mol^{-1}) were obtained with high yields (74 – 98%), monomodal and narrow ($Đ$ = 1.04 – 1.15) MWDs as well as molecular weights (M_n) close to those targeted (**Table 3**). For all copolymers the styrene content, determined by ^{1}H NMR spectroscopy, was found to be close to the targeted styrene feed (X_{feed}(S)).

Examples of typical NMR spectra are shown for P(S_{39}-*co*-DMVBDO$_{30}$) in the Supporting Information (**Figures S26-S30**). The DOSY analysis (**Figure S30**) showed only one diffusion trace and thereby confirmed that no homopolymers were formed over the course of the statistical copolymerization with styrene in THF at -78 °C. Furthermore, one copolymer (50/50 molar ratio of S and DMVBDO) with $M_n^{targeted}$ = 70 kg mol^{-1} was synthesized to prove that higher molecular weight copolymers can also be prepared. The MWD remained monomodal, but the dispersity increased slightly ($Đ$ = 1.13), and the SEC elution trace (UV signal) showed a small tailing towards higher elution volume (**Figure S61**). In addition, block copolymers of the type $PS_{0.5}$-*b*-P(DMVBDO)$_{0.5}$ and P(DMVBDO)$_{0.5}$-*b*-$PS_{0.5}$ with a targeted molecular weight of 20 kg mol^{-1} and a 50/50 molar block ratio were synthesized. It was found that polystyryllithium served as a good macroinitiator for DMVBDO, enabling the facile preparation of $PS_{0.5}$-*b*-P(DMVBDO)$_{0.5}$. A narrow and monomodal MWD was obtained (**Figure 4**, solid line), exhibiting low dispersity ($Đ$ = 1.14).

Table 3. Overall results from the statistical and block copolymerization of styrene with DMVBDO in THF (-78 °C), $M_n^{targeted}$ = 10 kg mol^{-1}, except for sample 10 ($M_n^{targeted}$ = 70 kg mol^{-1}) and sample 11, 12 ($M_n^{targeted}$ = 20 kg mol^{-1}).

No.	Polymer	X_{NMR}(S) / mol%	M_n^a / kg mol^{-1}	M_n^b / kg mol^{-1}	$Đ^a$	T_g / °C
1	P(S_7-*co*-DMVBDO$_{43}$)	14	10.1	10.2	1.15	46
2	P(S_{15}-*co*-DMVBDO$_{39}$)	27	13.6	10.2	1.13	58
3	P(S_{21}-*co*-DMVBDO$_{36}$)	37	10.6	10.0	1.04	59
4	P(S_{29}-*co*-DMVBDO$_{33}$)	47	11.2	10.3	1.10	66
5	P(S_{39}-*co*-DMVBDO$_{30}$)	57	11.3	10.8	1.05	72
6	P(S_{49}-*co*-DMVBDO$_{24}$)	67	11.1	10.3	1.15	75
7	P(S_{60}-*co*-DMVBDO$_{18}$)	76	8.2	9.6	1.04	78

8	P(S_{79}-*co*-DMVBDO$_{14}$)	85	11.6	11.4	1.05	78
9	P(S_{85}-*co*-DMVBDO$_{6}$)	94	8.8	10.0	1.08	91
10	P($S_{0.5}$-*co*-DMVBDO$_{0.5}$)	55	68.9	n.d.	1.13	69
11	$PS_{0.5}$-*b*-P(DMVBDO)$_{0.5}$	53	22.1	13.2	1.14	58
12	P(DMVBDO)$_{0.5}$-*b*-$PS_{0.5}$	69	40.2	22.2	1.19	70

[a] Determined by SEC in THF (UV signal), [b] determined by ^{1}H NMR spectroscopy (C*D*Cl$_3$) by referencing to the methyl protons of the initiator. Entry 10 was not evaluated due to increasing inaccuracy at high molecular weights.

The block copolymer composition (XNMR = 53 mol%) determined by 1H NMR spectroscopy was close to the targeted styrene feed content (Xfeed(S) = 50 mol%) and the molecular weight (Mn = 22.1 kg mol-1) determined by SEC in DMF (due to solubility) was found to agree well with the targeted molecular weight of 20 kg mol-1.

On the contrary, P(DMVBDO)lithium was found to be slow and not homogeneous as a macroinitiator for the sequential polymerization of styrene as the second block. SEC characterization revealed a bimodal MWD with an increased dispersity ($Đ$= 1.19) (**Figure 4**, dashed line). Strikingly, the molecular weight determined both by ^{1}H NMR spectroscopy and SEC was found to be significantly larger compared to the targeted value. This result hints at a rather slow crossover, resulting in a non-quantitative initiation step of the second block, when P(DMVBDO)lithium is utilized as a macroinitiator for the subsequent polymerization of styrene. Due to incomplete initiation of the polystyrene block, the monomer/initiator ratio ([M_0]/[I]) increases, which results in fewer growing polymer chains, resulting in higher molecular weight and an enriched average styrene content. Indeed, it was found that the glass transition (T_g) value for P(DMVBDO)$_{0.5}$-*b*-$PS_{0.5}$ (70 °C) was measured 12 °C higher compared to $PS_{0.5}$-*b*-P(DMVBDO)$_{0.5}$ (58 °C). The higher T_g value originates from the larger styrene content in the majority fraction of the former block copolymer. To sum up, the crossover

from PSLi to DMVBDO is quantitative and fast, whereas on the other hand the crossover from P(DMVBDO)lithium to styrene is rather slow and non-quantitative.

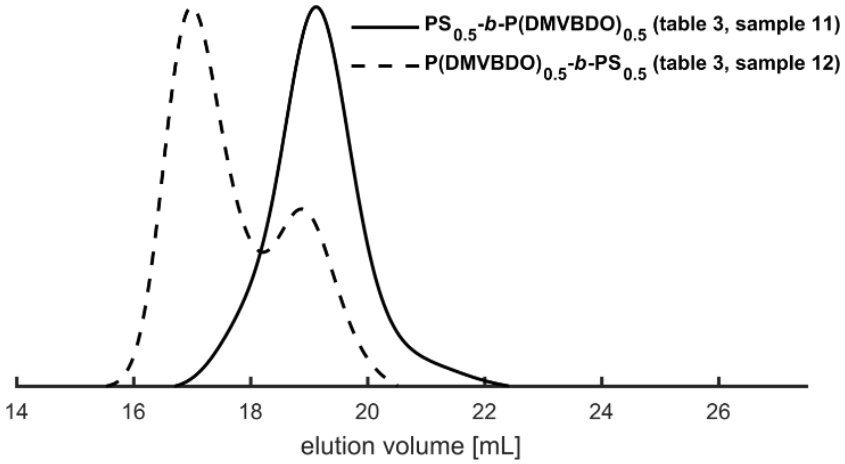

Figure 4. SEC traces (DMF, UV signals, PS standards) of $PS_{0.5}$-*b*-$P(DMVBDO)_{0.5}$ and $P(DMVBDO)_{0.5}$-b-$PS_{0.5}$ block copolymers, $M_n^{targeted}$ = 20 kg mol^{-1}.

In addition, the DOSY analysis of $PS_{0.5}$-*b*-$P(DMVBDO)_{0.5}$ revealed only one monomodal diffusion trace (**Figure S39**), whereas the synthesis of $P(DMVBDO)_{0.5}$-*b*-$PS_{0.5}$ showed a bimodal diffusion peak, originating from the presence of unreacted P(DMVBDO) macroinitiator (**Figure S49**).

4.1.3.4 DEPROTECTION AND THERMAL PROPERTIES

The glass transition (T_g) values of the protected copolymers $P(S_x$-*co*-$DMVBDO_{1-x})$ (**Table 3**) were found to be in between those of the two homopolymers PS and P(DMVBDO). DSC measurements revealed that the T_g value of the deprotected homopolymer $P(VPPDO)_{23}$ (48 °C) is approximately 50 K lower compared to polystyrene, which is a consequence of the flexible side chains. For the synthesized block copolymer $PS_{0.5}$-*b*-$P(DMVBDO)_{0.5}$ it was found that after the deprotection phase separation occurred, as indicated by the appearance of two T_gs (68 °C and 86 °C instead of 58 °C).

Deprotection of the copolymers was carried out in a similar fashion as the homopolymer deprotection. However, instead of 1 M HCl, 6 M HCl was used, as the 1 molar solution was found to be not sufficiently effective for complete copolymer deprotection, which is a consequence of the strongly apolar character of the copolymers with styrene. **Figure 5** shows the stacked ^{1}H NMR spectra of the protected (P(S_{85}-*co*-$DMVBDO_6$)) and deprotected (P(S_{85}-*co*-$VPPDO_6$)) copolymer.

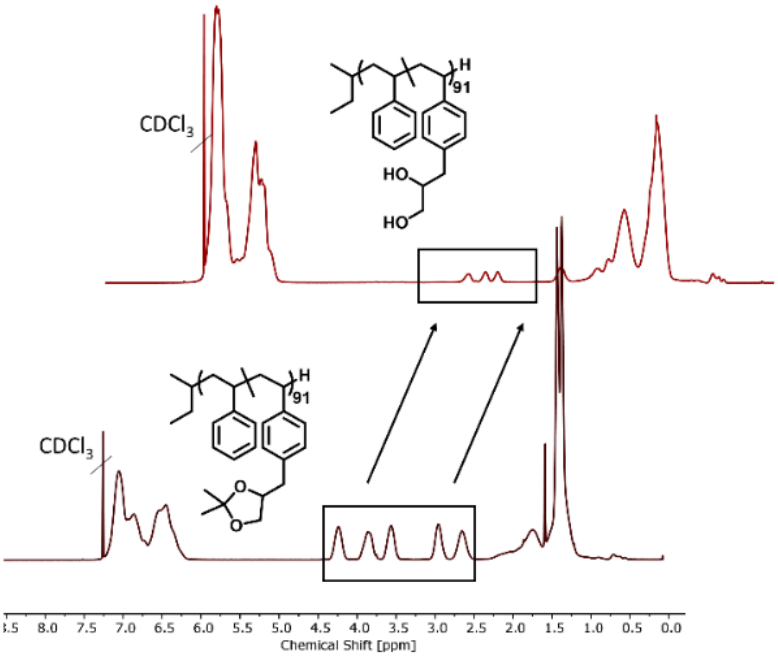

Figure 5. ^{1}H NMR spectra (stacked) of P(S_{85}-*co*-$DMVBDO_6$) (bottom) and P(S_{85}-*co*-$VPPDO_6$) (top) (400 MHz, C*D*Cl_3).

The signal changes in the region of 2.5 – 4.5 ppm clearly indicate quantitative deprotection of the copolymer within 24 h at room temperature. Nevertheless, it is noteworthy that at longer reaction times the solution and the precipitated product became slightly yellow in color. Whereas the SEC elution traces (**Figure S32**) did not change over time, ^{1}H NMR analysis revealed a decrease in molecular weight over time (**Table S2**). Further, additional signals in the region of 2.5 – 4.5 ppm (**Figure S33**) became visible. These signals most probably result from undesired elimination reactions at the hydroxyl groups.

4.1.3.5 SYNTHESIS OF BRUSH-LIKE COPOLYMERS

With the readily deprotected copolymer P(S_{85}-*co*-VPPDO$_6$) a large variety of well-defined brush-like copolymers is accessible. This is exemplified by using a "grafting from" approach with both L-lactide (LLA) and ethylene oxide (EO) (for details see Experimental Part). This procedure permitted rapid access to brush-like copolymers (Scheme 3).

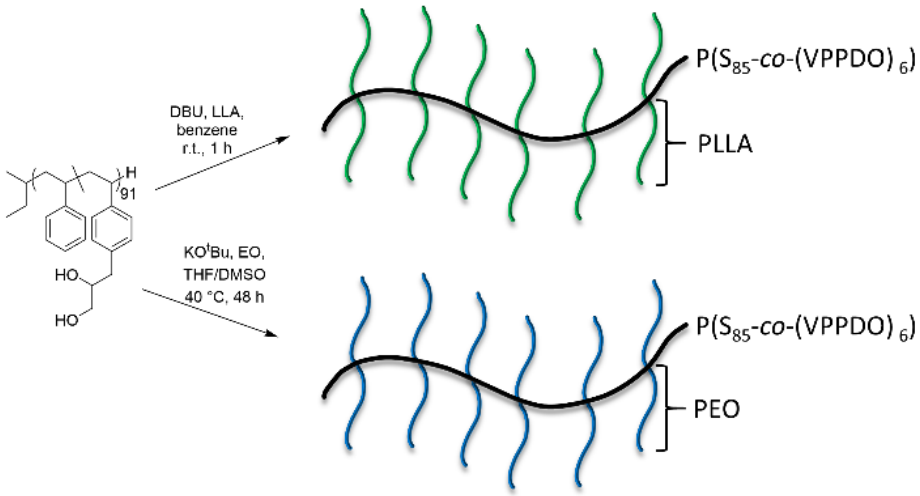

Scheme 3. Synthesis of P(S_{85}-co-VPPDO$_5$)-g-PLLA, and P(S_{85}-co-VPPDO$_5$)-g-PEO.

With the aliphatic hydroxyl groups of the propane-1,2-diol moiety at every comonomer unit rapid grafting of PLLA was achieved with DBU in benzene at room temperature within 1 h. As the target molecular weight of the grafted PLLA chains 20 kg mol^{-1} was chosen. The resulting MWD of the graft copolymer P(S_{85}-*co*-VPPDO$_5$)-*g*-PLLA remained monomodal with a slight increase in dispersity from $Đ$ 1.06 to 1.22 (**Table 5**). The respective SEC traces are shown in **Figure 6**. SEC results (M_n[a], **Table 5**) reveal that the M_n is close to the targeted value. Nevertheless, it is noteworthy that the given M_n values are based on PS standards and thus in principle represent only apparent molecular values. The complete disappearance of the propane-1,2-diol signals in the NMR spectra (**Figure S50-56**) along with the appearance of 2 pronounced signals in the region of 5 – 5.5 ppm (resulting from the methine proton of PLLA) and in the region of

1.4 – 1.6 ppm (resulting from the methyl group of PLLA) further confirm the successful synthesis of P(S_{85}-*co*-VPPDO_5)-*g*-PLLA.

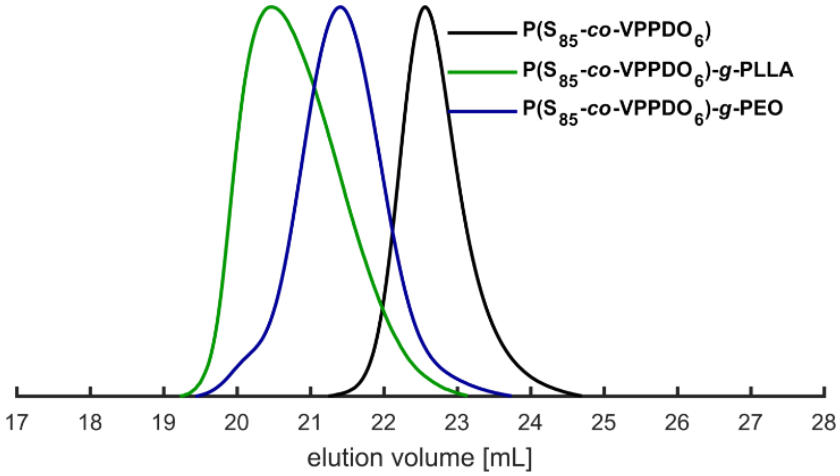

Figure 6. SEC traces (THF, UV signal, PS standards) of P(S_{85}-co-VPPDO_5), P(S_{85}-co-VPPDO_5)-g-PLLA, and P(S_{85}-co-VPPDO_5)-g-PEO.

The molecular weight based on ^{1}H NMR analysis (M_n^b, **Table 5**) was found to be lower than the targeted molecular weight ($M_n^{targeted}$, **Table 5**).

Table 5. Characteristics of the brush-like copolymers P(S_{85}-co-VPPDO_5)-*g*-PLLA, and P(S_{85}-co-VPPDO_5)-*g*-PEO.

Polymer	$M_n^{targeted}$ / kg mol^{-1}	M_n^a / kg mol^{-1}	M_n^b / kg mol^{-1}	$Đ^a$	T_g / °C	T_m / °C
P(S_{85}-*co*-VPPDO_6)	8.7	8.9	8.7	1.06	90	-
P(S_{85}-*co*-VPPDO_6)-*g*-PLLA	28.9	27.6	21.2	1.22	45	227
P(S_{85}-*co*-VPPDO_6)-*g*-PEO	23.9	18.8	n.d.	1.16	-12	45

[a] Determined by SEC in THF (UV signal, PS standards), [b] determined by ^{1}H NMR spectroscopy (C*D*Cl$_3$) by referencing to the methyl protons of the initiator. Entry 3 was not evaluated due to increasing inaccuracy at such high molecular weights.

However, the molecular weight by ^{1}H NMR analysis was determined by referencing to the methyl protons of the initiator *s*-BuLi. In this molecular weight range NMR is often found to be inaccurate due the low signal intensity. DOSY analysis further proved successful grafting with LLA, as only one diffusion coefficient was obtained (**Figure S55**).The complete disappearance of the propane-1,2-diol signals in the NMR spectra (**Figure S50-56**) along with the appearance of 2 pronounced signals in the region of 5 – 5.5 ppm (resulting from the methine proton of PLLA) and in the region of 1.4 – 1.6 ppm (resulting from the methyl group of PLLA) further confirm the successful synthesis of P(S_{85}-*co*-$VPPDO_5$)-*g*-PLLA.

DSC revealed a decrease of the T_g value (ΔT_g = 45 °C) from 90 °C to 45 °C, and a melting point of 227 °C was found. This is due to the fact that more than half (59% based on M_n^b) of the polymer now consists of PLLA. In a similar fashion P(S_{85}-*co*-$VPPDO_6$)-*g*-PEO was synthesized by anionic ring-opening polymerization based on partial deprotonation. This approach enables the synthesis of amphiphilic graft structures, since PEO is water soluble. A DMSO/THF solvent mixture was used to ensure a homogeneous reaction solution over the whole course of the ethylene oxide polymerization. After thorough solvent removal via freeze drying the yield was found to be quantitative. Characterization via SEC revealed a narrow and monomodal MWD of the synthesized graft copolymer P(S_{85}-*co*-$VPPDO_6$)-*g*-PEO with a slight increase in dispersity from $Đ$ 1.06 to 1.16 (**Table 5**) molecular weight (SEC) was determined to be 18.8 kg mol^{-1} (based on PS standards). In the ^{1}H NMR spectrum of the graft copolymer the signals of the methylene and methine protons (3.44–4.07 ppm) of the former 1,2-diol moieties disappeared, and at the same time a characteristic signal appeared for the polyether backbone at 3.96 – 3.25 ppm. The DOSY analysis (**Figure S67**) confirmed smooth "grafting from" synthesis, as only one diffusion trace was visible. The T_g value decreased from 90 °C to -12 °C (ΔT_g = 102 °C) whereas a melting point was detected for the graft copolymers was observed at 45 °C (resulting from the PEG side-chains).

4.1.4 CONCLUSIONS

We report a novel approach for the rapid access towards *para*-functional styrene monomers suitable for any kind of successive polymerization, demonstrated for living anionic polymerization. Relying on (4-vinylphenyl)magnesium bromide as a readily accessible Grignard reagent, the fast introduction of a base stable functionality becomes possible via a simple nucleophilic addition or substitution reaction. In this work this is exemplified using epichlorohydrine. In this manner, functional styrene monomers were conveniently be synthesized, avoiding the introduction of the reactive vinyl group only in the final step of the synthesis route, as it is usually performed. To the best of our knowledge this approach has hardly been studied to date. Relying on this method, 2,2-dimethyl-4-(4-vinylbenzyl)-1,3-dioxolane (DMVBDO), a valuable functional monomer with a protected 1,2-diol moiety was synthesized on a multi-gram scale and subsequently used for the carbanionic living polymerization, avoiding purification by chromatography. Whereas in nonpolar media DMVBDO did not homo- or copolymerize with styrene, well-defined homopolymers, statistical copolymers as well as block copolymers were prepared in THF at -78 °C. Molecular weights ranged from 4.5 to 68.9 kg mol^{-1} with low dispersity ($Đ$) in the range of 1.04 to 1.15. Statistical copolymers were accessible with any styrene feed ratio (X_{feed}) from 15 to 95 mol%. The copolymers´ thermal properties can be adjusted gradually, as the T_g values changed according to X_{feed} and ranged from 74 to 98 °C. Block copolymer synthesis worked well for the preparation of $PS_{0.5}$-*b*-$P(DMVBDO)_{0.5}$, whereas the reverse approach, i.e. synthesis of $P(DMVBDO)_{0.5}$-*b*-$PS_{0.5}$ yielded a bimodal MWD resulting from slow and non-quantitative (macro)initiation of the second block. All polymers could be rapidly deprotected overnight in slightly acidic solution and were found not to be prone to autoxidation like catechol polymers. The deprotected block copolymer $PS_{0.5}$-*b*-$P(VPPDO)_{0.5}$ showed two T_g values at 68 °C and 86 °C indicating phase separation. The aliphatic hydroxyl groups of VPPDO were used for "grafting from" of LLA and EO, respectively, which so far is not widely established for

monodisperse polystyrene derivatives. Thereby, homogeneous brush-like copolymers of the type P(S_{85}-*co*-VPPDO_5)-*g*-PLLA and P(S_{85}-*co*-VPPDO_6)-*g*-PEO were synthesized in quantitative yields.

We consider the present work an important steppingstone in the field of functional polymer synthesis. DMVBDO represents a versatile monomer with a protected functional group that remains stable under the harsh conditions of carbanionic living polymerization due to acetal protective chemistry. Furthermore, (4-vinylphenyl)magnesium bromide introduces a new aspect to the area of functional styrene monomers. The synthesis procedure is non-conventional due to the high reactivity of the Grignard moiety. It follows that a large variety of functional monomers can rapidly be synthesized with this method, suitable for anionic as well as for radical polymerization. As functional polymers play a key role for block copolymer architectures and in many commercial products and applications, this scalable synthesis procedure holds promise for future use.

4.1.5 EXPERIMENTAL PART

Terminology. Styrene and 2,2-dimethyl-4-(4-vinylbenzyl)-1,3-dioxolane are abbreviated as S and DMVBDO, respectively. 3-(4-vinylphenyl)propane-1,2-diol is abbreviated VPPDO.

Reagents. Chemicals and solvents were purchased from commercial suppliers (Acros, Sigma-Aldrich, Fisher Scientific, Alfa Aesar, TCI). Deuterated solvents were obtained from Deutero GmbH. Isopropyl alcohol and methanol were used as received without further purification. Cyclohexane was purified by stirring over diphenylhexyllithium (adduct of sec-butyllithium and 1,1-diphenylethylene), vacuum-transferred and degassed by four freeze-pump-thaw cycles prior to use. The monomers S and DMVBDO were purified by stirring over CaH_2 overnight, followed by distillation.

All monomers for the anionic polymerization were degassed by four freeze-pump-thaw cycles prior to use. L-Lactide (LLA) was kindly provided by BASF SE and was recrystallized three times from toluene and dried *in vacuo* prior to use.

Instrumentation. All NMR spectra (^{1}H, ^{13}C, ed. HSQC, HMBC, ^{1}H, ^{1}H-COSY and DOSY) were recorded on a Bruker Avance II 400 spectrometer equipped with a 5 mm BBFO-SmartProbe with z gradient and ATM, as well as a SampleXPress 60 sample changer. All spectra are referenced internally to residual proton signals of the deuterated solvent.

Size exclusion chromatography (SEC) measurements were performed using an Agilent 1100 Series, equipped with a SDV column set from PSS (SDV 103, SDV 105, SDV 106). Tetrahydrofuran (THF) or *N,N*-Dimethylformamide (DMF) was used as the mobile phase (flow rate 1 mL min^{-1}) and as the solvent. Poly(styrene) standards were provided by PSS for calibration. The measurements were carried out at 30 °C with an RI and UV (275 nm) detector. For analysis the PSS WinGPC® UniChrom (V 8.31, Build 8417) software provided by PSS Polymer Standards Service GmbH was used.

Glass transitions temperatures (T_g) as well as melting temperatures (T_m) were determined by evaluating differential scanning calorimetry (DSC) curves recorded on a Perkin Elmer 8500 differential scanning calorimeter. A temperature range from 0 °C to 250 °C was used. For the first cycle a heating rate of 10 °C min^{-1} and a cooling rate of 10 °C min^{-1} was employed. A second heating cycle (20 °C min^{-1}) was used to evaluate the thermal properties of the (co)polymers. All samples were measured three times, and the mean value was used for further analysis of the thermal properties.

MALDI-ToF MS measurements were performed on a Bruker Rapiflex. 2-(4-Hydroxyphenylazo)benzoic acid (HABA) was used as a matrix (1:1 in water) for P(VPPDO) and sodium trifluoroacetate was used as the cationization salt. The spectrum was measured in a linear positive mode with a laser wavelength of 337 nm. P(DMVBDO)

was measured with trans-2-[3-(4-*tert*-Butylphenyl)-2-methyl-2-propenylidene]malononitrile (DCTB) as the matrix and silver trifluoroacetate. An analyte:matrix:salt ratio of 10:10:1 in CH_2Cl_2 was used. The mass spectrum was recorded in a reflector positive mode with a 337 nm laser. For all polymers 1 mg analyte was dissolved in 1 mL solvent.

All FT-IR spectra were recorded using a Thermo Scientific iS10 FT-IR spectrometer, equipped with a diamond ATR unit.

Monomer synthesis. *1-chloro-3-(4-vinylphenyl)propan-2-ol (1).* According to a modified literature procedure from Farzaliev and coworkers,[42] a few drops of 4-bromostyrene were slowly added under vigorous stirring (large stirring bar, 700 rpm) to a solution of magnesium turnings (4.02 g, 166 mmol) in 150 mL of freshly distilled and dry THF in a 500 mL three-necked flask at room temperature under an argon atmosphere. After the exothermic reaction started, 4-bromostyrene (30 g, 166 mmol) was slowly added while keeping the solution at gentle reflux. After complete addition, the reaction mixture was left to stir for one hour before the reaction solution was cooled to 0 °C. A solution of epichlorohydrin (12.3 mL, 157 mmol) mixed with 150 mL of freshly distilled and dry THF was slowly added via a dropping funnel while keeping the temperature below 10 °C. After complete addition, the reaction mixture was stirred at room temperature for 30 minutes. The conversion was checked by TLC (15 vol% ethyl acetate, 85 vol% cyclohexane, R_f(product) = 0.29). When quantitative conversion had been reached, the reaction mixture was poured into a separating funnel containing 125 mL of saturated ammonium chloride solution and 500 mL of deionized water. The crude product was extracted three times with diethyl ether (total amount: 750 mL). The combined organic layers were washed with brine (250 mL), dried over sodium sulfate, filtered and concentrated under reduced pressure. The crude product was obtained as a clear yellow oil which was used for the next step without further purification. Yield 94%.

^{1}H NMR (400 MHz, chloroform-d_1): δ (ppm) = 7.36 (d, 2H), 7.19 (d, 2H), 6.69 (dd, J = 17.6, 10.8 Hz, 1H), 5.73 (dd, J = 17.6, 0.9 Hz, 1H), 5.23 (dd, J = 10.9, 0.9 Hz, 1H), 4.13 – 3.92 (m, 1H), 3.60 (dd, J = 11.1, 3.9 Hz, 1H), 3.48 (dd, J = 11.2, 6.1 Hz, 1H), 2.87 (d, J = 6.6 Hz, 2H), 2.60 (s, 1H). Figure S1. For 13C and 2D spectra see Figure S2-4.

2-(4-vinylbenzyl)oxirane (2). According to a modified literature procedure from Farzaliev and coworkers,[42] a solution of sodium hydroxide (50.15 g, 1.25 mol) in 120 mL of deionized water was slowly added to a solution of 1-chloro-3-(4-vinylphenyl)propane-2-ol (30 g, 153 mmol) in 104 mL of THF at 0 °C under vigorous stirring (large stirring bar, 700 rpm). After complete addition, the reaction mixture was warmed to room temperature and stirred overnight. The conversion was checked by TLC (20 vol% diethyl ether, 80 vol% cyclohexane, R_f (product) = 0.49) the following morning. Upon complete conversion, the reaction mixture was poured into a separation funnel with 350 mL of deionized water. The product was extracted three times with ethyl acetate (total amount: 530 mL). The combined organic layers were dried over sodium sulfate, filtered and concentrated under reduced pressure. The crude product was obtained as a clear, yellow oil which was used for the next reaction without further purification. Yield 89%.

^{1}H NMR (400 MHz, chloroform-d_1): δ (ppm) = 7.39 (d, J = 8.1 Hz, 2H), 7.24 (d, J = 8.2 Hz, 2H), 6.73 (dd, J = 17.6, 10.9 Hz, 1H), 5.76 (dd, J = 17.6, 1.0 Hz, 1H), 5.26 (dd, J = 10.9, 0.9 Hz, 1H), 3.16 (m, 1H), 2.96-273 (m, 3H), 2.56 (dd, J = 5.0, 2.7 Hz, 1H). Figure S5. For 13C and 2D spectra see Figure S6-8.

2,2-dimethyl-4-(4-vinylbenzyl)-1,3-dioxolane (3). According to a modified literature procedure from Meyer and coworkers,[43] a 1 L two-necked flask with a stirring bar was evacuated and backfilled with argon three times. Tin(II) chloride (234 mg, 1.23 mmol) and 450 mL of dry acetone were carefully added under argon counterflow. After the catalyst was dissolved, 2-(4-vinylbenzyl)oxirane (19.79 g, 124 mmol) was slowly added via syringe. After the addition was completed, the reaction mixture was heated

under reflux overnight. The next morning, the conversion was checked by ^{1}H NMR spectroscopy. Once full conversion was attained, the solvent was removed under reduced pressure. The crude product was distilled under reduced pressure to give a colorless oil. Yield 47%.

^{1}H NMR (400 MHz, chloroform-d_1): δ (ppm) = 7.38 (d, J = 8.1 Hz, 2H), 7.20 (d, J = 7.9 Hz, 2H), 6.72 (dd, J = 17.6, 10.9 Hz, 1H), 5.75 (d, J = 17.5 Hz, 1H), 5.24 (d, J = 10.9 Hz, 1H), 4.43 – 4.27 (m, 1H), 3.99 (dd, J = 8.2, 5.8 Hz, 1H), 3.67 (t, J = 7.5, 5.6 Hz, 1H), 3.03 (dd, J = 13.6, 6.2 Hz, 1H), 2.80 (dd, J = 13.7, 7.0 Hz, 1H), 1.43 (d, J = 33.4 Hz, 6H). Figure S9. For 13C and 2D spectra see Figure S10-13.

General (co)polymerization procedure in apolar media and cyclohexane/THF mixtures. All polymerizations were carried out in cyclohexane (or cyclohexane/THF mixtures, respectively) at room temperature in an argon-filled glovebox (MBraun UNILAB, <0.1 ppm of O_2 and <0.1 ppm of H_2O) in 40 mL glass vials equipped with a magnetic stir bar, screw caps and septa. The monomer/solvent (20 wt%) mixture was initiated with 0.1 mL of sec-butyllithium (1.3 M in cyclohexane/hexane 92/8) via 1 mL syringe. The polymerization was terminated by adding 0.5 mL of methanol (degassed with argon for 1 h prior to use) by a syringe after the appropriate time (see results and discussion). The polymers were precipitated in 30 mL of cold methanol, dried at reduced pressure (room temperature) and stored in the freezer (-20 °C).

General polymerization procedure for the (co)polymer and block copolymer synthesis in THF at -78 °C. All (co)polymerizations were carried out in 100 mL Schlenk flasks equipped with a magnetic stir bar and Teflon stopper in dry THF at room temperature under argon. THF was dried over sodium benzophenone ketyl, followed by distillation onto molecular sieves (3 Å, activated at 450 °C for 4 h) and vacuum transferred into the polymerization reactor after 72 h. For the statistical copolymerization S was dried together with DMVBDO in one flask by stirring over CaH_2

overnight, followed by distillation into the polymerization flask. The monomer/solvent (20 wt%) mixture was initiated with 0.1 mL of *sec*-butyllithium (1.3 M in cyclohexane/hexane 92/8) via 1 mL syringe. The solution was stirred for 20 or 40 min (see Results and Discussion) to ensure full monomer conversion. The polymerization was terminated by adding 0.5 mL of methanol (degassed with argon for 1 h prior to use) by a syringe. The polymers were precipitated in 30 mL cold methanol, dried under reduced pressure (room temperature) and stored in the freezer (-20 °C).

For the preparation of sequential block copolymers S (10 wt% solution in THF) (or DMVBDO, respectively) was initiated by *sec*-butyllithium (1.3 M in cyclohexane/hexane 92/8) in a first step. At full styrene conversion (usually after 20 min) DMVBDO was added via syringe (or vice versa).

P(DMVBDO)$_{23}$ ($M_n^{targeted}$ = 5 kg mol^{-1}). 93%, white solid. ^{1}H NMR (400 MHz, chloroform-d_1) δ (ppm) = δ 7.10 – 6.15 (m, 92H), 4.38 – 4.10 (m, 23H), 3.98 – 3.75 (m, 23H), 3.68 – 3.44 (m, 23H), 3.10 – 2.84 (m, 23H), 2.77 – 2.53 (m, 23H), 1.54 – 1.19 (m, 180H), 0.76 – 0.44 (m, 6H). Figure S14. For 13C and 2D spectra see Figure S15-19.

P(S$_{0.5}$-co-DMVBDO$_{0.5}$) ($M_n^{targeted}$ = 10 kg mol^{-1}). 74 – 98%, white solid. ^{1}H NMR (400 MHz, chloroform-d_1) δ (ppm) = 7.22 – 6.16 (m, 319H), 4.37 – 4.14 (m, 30H), 3.99 – 3.71 (m, 31H), 3.68 – 3.43 (m, 31H), 3.11 – 2.83 (m, 30H), 2.79 – 2.53 (m, 31H), 1.56 – 1.16 (m, 321H), 0.78 – 0.47 (m, 6H). Figure S26. For 13C and 2D spectra see Figure S27-30.

PS$_{0.5}$-*b*-P(DMVBDO)$_{0.5}$ ($M_n^{targeted}$ = 20 kg mol^{-1}). 75 – 76%, white solid. ^{1}H NMR (400 MHz, chloroform-d_1) δ (ppm) = 7.23 – 6.11 (m, 406H), 4.38 – 4.07 (m, 42H), 3.99 – 3.71 (m, 45H), 3.66 – 3.46 (m, 43H), 3.13 – 2.84 (m, 42H), 2.82 – 2.52 (m, 43H), 1.52 – 1.11 (m, 419H), 0.79 – 0.54 (m, 6H). Figure S34. For 13C and 2D spectra see Figure S35-39.

General procedure for the deprotection of DMVBDO (co)polymers and block copolymers at room temperature. The (co)polymer or block copolymer (typically 100 mg) was dissolved in THF (20 mL) and 5 mL 1M (6 M respectively) HCl solution was added dropwise under stirring. After completion of the addition, THF was added again until the THF/water mixture was no longer cloudy. The resulting mixture was let run for 24 h or longer (see results and discussion) before the deprotected polymer was precipitated in cold acetone (homopolymer) or in a mixture of cold MeOH/H_2O 95:5 (copolymer and block copolymer). The resulting suspension was centrifuged at 4500 rpm at -10 °C for 10 min. before being decanted and dried at 40 °C *in vacuo*.

P(VPPDO) ($M_n^{targeted}$ = 5 kg mol^{-1}). 92%, white solid. ^{1}H NMR (400 MHz, pyridine-d_1) δ (ppm) = 9.02 – 8.03 (m, 235H), 6.00 – 5.75 (m, 35H), 5.49 (s, 68H), 4.62 (s, 68H), 4.24 – 3.67 (m, 38H), 3.61 – 2.90 (m, 86H), 2.14 (d, J = 34.4 Hz, 6H). Figure S20. For 13C and 2D spectra see Figure S21-25.

P($S_{0.95}$-*co*-$VPPDO_{0.05}$) ($M_n^{targeted}$ = 10 kg mol^{-1}). quantitative yield, white solid. ^{1}H NMR (400 MHz, chloroform-d_1) δ (ppm) = 7.36 – 6.23 (m, 512H), 4.07 – 3.78 (m, 5H), 3.72 – 3.58 (m, 5H), 3.56 – 3.44 (m, 5H), 2.87 – 2.55 (m, 12H), 2.42 – 1.21 (m, 337H), 0.82 – 0.53 (m, 6H). Figure S31.

$PS_{0.5}$-*b*-$P(DVPPDO)_{0.5}$ ($M_n^{targeted}$ = 20 kg mol^{-1}). quantitative yield, white solid. ^{1}H NMR (400 MHz, pyridine-d_5) δ (ppm) = 7.52 – 6.56 (m, 472H), 4.55 – 4.22 (m, 39H), 4.13 – 3.90 (m, 73H), 3.37 – 2.93 (m, 73H), 2.77 – 1.46 (m, 257H), 0.81 – 0.54 (m, 6H). Figure S40. For ^{13}C and 2D spectra see Figure S41-45.

General procedure for the "grafting from" approach of P($S_{0.95}$-*co*-$VPPDO_{0.05}$) ($M_n^{targeted}$ = 29 kg mol^{-1}) with L-lactide. The polymerization of LLA using 1,8-diazabicyclo[5.4.0]undec-7-ene (DBU) as the catalyst was performed according to the work of Hedrick and Waymouth.[44] The macroinitiator P($S_{0.95}$-*co*-$VPPDO_{0.05}$) and LLA were dissolved in dry (molecular sieves 3Å) benzene and dried *in vacuo* overnight, prior

to use. DBU was stirred over CaH_2 and distilled into a Schlenk flask. The polymerization was performed in a glovebox (MBraun UNILAB, <0.1 ppm of O_2 and <0.1 ppm of H_2O). LLA (100 mg, 0.7 mmol, 139 eq) and the macroinitiator (55.5 mg, 0.01 mmol, 1 eq) were added to a screw cap vial and dissolved in 1 mL of dry chloroform. A stock solution of DBU was prepared by dissolving 8.0 mg of DBU in 1 mL of dry chloroform. Subsequently, 0.1 mL (0.8 mg, 0.01 mmol, 1 eq) of the stock solution was added to start the polymerization. After stirring at room temperature for 1 h the polymerization was quenched by adding 5 mg of benzoic acid. The polymer was precipitated in cold methanol, centrifuged and dried *in vacuo* at 40 °C. The polymer was obtained with quantitative yield as a colorless solid.

P($S_{0.5}$-*co*-VPPD$O_{0.5}$)-*g*-P(LLA) ($M_n^{targeted}$ = 26 kg mol^{-1}). quantitative yield, white solid. ^{1}H NMR (400 MHz, chloroform-d_1) δ (ppm) = 7.22 – 6.21 (m, 365H), 5.32 – 4.95 (m, 192H), 2.91 – 2.57 (m, 13H), 2.09 – 1.11 (m, 816H), 0.77 – 0.49 (m, 6H). Figure S50. For 13C and 2D spectra see Figure S51-56.

General procedure for the "grafting from" approach of P($S_{0.95}$-*co*-VPPD$O_{0.05}$) ($M_n^{targeted}$ = 24 kg mol^{-1}) with ethylene oxide. KO^{t}Bu (11 mg, 9.7 10^{-2} mmol) and P(S_{85}-*co*-VPPDO_6) (97 mg, 9.7 10^{-3} mmol) were placed in a flame-dried flask and dissolved in a mixture of dry benzene (10 mL) and dry (molecular sieves 3Å) DMSO (0.2 mL). The solution was stirred at 50 °C under slightly reduced pressure for 30 minutes and dried *in vacuo* for 16 h. After cooling to room temperature, dry DMSO (2.5 mL) was added via syringe and dry THF (1.5 mL) was vacuum transferred into the flask. EO (0.15 mL, 3.3 mmol, 341 eq) was vacuum transferred via a graduated ampule and the resulting solution was stirred at 40 °C for 48 hours. After quenching (1 mL MeOH), THF and MeOH were removed under reduced pressure. The residue was dissolved in DCM, extracted twice with brine, dried over $MgSO_4$ and lyophilized to remove DMSO.

P($S_{0.95}$-*co*-VPPDO$_{0.05}$)-*g*-PEO ($M_n^{targeted}$ = 24 kg mol^{-1}). quantitative yield, brownish solid. ^{1}H NMR (400 MHz, chloroform-d_1) δ (ppm) = 7.21 – 6.18 (m, 512H), 3.96 – 3.25 (m, 1863H), 2.17 – 1.17 (m, 438H), 0.94 – 0.43 (m, 6H). Figure S62. For 13C and 2D spectra see Figure S63-74.

4.1.6 REFERENCES

(1) Hirao, A.; Loykulnant, S.; Ishizone, T. Recent advance in living anionic polymerization of functionalized styrene derivatives. *Prog. Polym. Sci.* **2002**, *27*, 1399–1471.

(2) Hirao, A.; Kubota, S.; Sueyoshi, T.; Sugiyama, K. Living Anionic Polymerization of Functionalized Monomers, 2. Anionic Polymerization of p-Alkenylstyrene Derivatives. *Macromol. Chem. Phys.* **2001**, *202*, 1044–1052.

(3) Ishizone, T.; Hirao, A.; Nakahama, S. Anionic polymerization of monomers containing functional groups. 6. Anionic block copolymerization of styrene derivatives para-substituted with electron-withdrawing groups. *Macromolecules* **1993**, *26*, 6964–6975.

(4) Ishizone, T.; Uehara, G.; Hirao, A.; Nakahama, S.; Tsuda, K. Anionic Polymerization of Monomers Containing Functional Groups. 13. Anionic Polymerizations of 2-, 3-, and 4-(3,3-Dimethyl-1-butynyl)styrenes, 1 2-, 3-, and 4-(1-Hexynyl)styrenes, 2 and 4-(Phenylethynyl)styrene. *Macromolecules* **1998**, *31*, 3764–3774.

(5) Kawabe, M.; Murata, M. Syndiospecific Living Block Copolymerization of Styrenic Monomers Containing Functional Groups, and Preparation of Syndiotactic Poly{(4-hydroxystyrene)-block-[(4-methylstyrene)-co-(4-hydroxystyrene)]}. *Macromol. Chem. Phys.* **2002**, *203*, 24–30.

(6) Hirao, A.; Ishino, Y.; Nakahama, S. Synthesis of linear poly(4-vinylbenzaldehyde) by means of anionic living polymerization of 1,3-dimethyl-2-(4-vinylphenyl)imidazolidine and subsequent hydrolysis. *Makromol. Chem.* **1986**, *187*, 141–147.

(7) Hirao, A.; Nakahama, S. Protection and polymerization of functional monomers. 10. Synthesis of well-defined poly(4-vinylbenzaldehyde) by the anionic living polymerization of N-[(4-ethenylphenyl)methylene]cyclohexamine. *Macromolecules* **1987**, *20*, 2968–2972.

(8) Hirao, A.; Tanaka, S.; Goseki, R.; Ishizone, T. Living Anionic Polymerization of 1,4-Divinylbenzene. *Macromolecules* **2011**, *44*, 4579–4582.

(9) Kamigaito, M.; Ando, T.; Sawamoto, M. Metal-Catalyzed Living Radical Polymerization. *Chem. Rev.* **2001**, *101*, 3689–3746.

(10) Matyjaszewski, K.; Xia, J. Atom Transfer Radical Polymerization. *Chemical reviews* **2001**, *101*, 2921–2990.

(11) Destarac, M. Controlled Radical Polymerization: Industrial Stakes, Obstacles and Achievements. *Macromol. React. Eng.* **2010**, *4*, 165–179.

(12) Grubbs, R. B.; Grubbs, R. H. 50th Anniversary Perspective. *Macromolecules* **2017**, *50*, 6979–6997.

(13) Hadjichristidis, N.; Hirao, A. *Anionic Polymerization*; Springer Japan: Tokyo, 2015.

(14) Hirao, A.; Goseki, R.; Ishizone, T. Advances in Living Anionic Polymerization. *Macromolecules* **2014**, *47*, 1883–1905.

(15) Szwarc, M. 'Living' Polymers. *Nature* **1956**, *178*, 1168–1169.

(16) Szwarc, M. *Living Polymers and Mechanisms of Anionic Polymerization*; Advances in Polymer Science 49; Springer Berlin: Berlin, 2013.

(17) Kim, H.-C.; Park, S.-M.; Hinsberg, W. D. Block copolymer based nanostructures: materials, processes, and applications to electronics. *Chem. Rev.* **2010**, *110*, 146–177.

(18) Schacher, F. H.; Rupar, P. A.; Manners, I. Functional block copolymers: nanostructured materials with emerging applications. *Angewandte Chemie (International ed. in English)* **2012**, *51*, 7898–7921.

(19) Bates, C. M.; Bates, F. S. 50th Anniversary Perspective. *Macromolecules* **2017**, *50*, 3–22.

(20) Grayson, S. M.; Fréchet, J. M. J. Divergent Synthesis of Dendronized Poly(p -hydroxystyrene). *Macromolecules* **2001**, *34*, 6542–6544.

(21) Laurent, B. A.; Grayson, S. M. Synthesis of cyclic dendronized polymers via divergent "graft-from" and convergent click "graft-to" routes: preparation of modular toroidal macromolecules. *J. Am. Chem. Soc.* **2011**, *133*, 13421–13429.

(22) Bender, J. T.; Knauss, D. M. Dendritic Polystyrene with Hydroxyl-Functionalized Branch Points by Convergent Living Anionic Polymerization. *Macromolecules* **2009**, *42*, 2411–2418.

(23) Conlon, D. A.; Crivello, J. v.; Lee, J. L.; O'Brien, M. J. The synthesis, characterization, and deblocking of poly(4-tert-butoxystyrene) and poly(4-tert-butoxy-.alpha.-methylstyrene). *Macromolecules* **1989**, *22*, 509–516.

(24) Rahman, S. S. A.; Kawaguchi, D.; Matsushita, Y. Monomer sequence of partially hydrolyzed poly(4-tert-butoxystyrene) and morphology of diblock copolymers composing this polymer sequence as one block. *Polymer* **2011**, *52*, 164–171.

(25) Schüll, C.; Frey, H. Controlled Synthesis of Linear Polymers with Highly Branched Side Chains by "Hypergrafting": Poly(4-hydroxy styrene)- graft -hyperbranched Polyglycerol. *ACS Macro Lett.* **2012**, *1*, 461–464.

(26) Ishikawa, T.; Morino, K.; Sudo, A.; Endo, T. Synthesis of photo-scissible poly(p-hydroxystyrene) derivatives by radical copolymerization of p-hydroxystyrene derivatives and methyl vinyl ketone. *J. Polym. Sci. A Polym. Chem.* **2011**, *49*, 4714–4720.

(27) Natalello, A.; Tonhauser, C.; Frey, H. Anionic Polymerization of para -(1-Ethoxy ethoxy)styrene: Rapid Access to Poly(p -hydroxystyrene) Copolymer Architectures. *ACS Macro Lett.* **2013**, *2*, 409–413.

(28) Leibig, D.; Müller, A. H. E.; Frey, H. Anionic Polymerization of Vinylcatechol Derivatives. *Macromolecules* **2016**, *49*, 4792–4801.

(29) Leibig, D.; Lange, A.-K.; Birke, A.; Frey, H. Capitalizing on Protecting Groups to Influence Vinyl Catechol Monomer Reactivity and Monomer Gradient in Carbanionic Copolymerization. *Macromol. Chem. Phys.* **2017**, *218*, 1600553.

(30) Niederer, K.; Schüll, C.; Leibig, D.; Johann, T.; Frey, H. Catechol Acetonide Glycidyl Ether (CAGE): A Functional Epoxide Monomer for Linear and Hyperbranched Multi-Catechol Functional Polyether Architectures. *Macromolecules* **2016**, *49*, 1655–1665.

(31) Takeshima, H.; Satoh, K.; Kamigaito, M. Scalable Synthesis of Bio-Based Functional Styrene: Protected Vinyl Catechol from Caffeic Acid and Controlled Radical and Anionic Polymerizations Thereof. *ACS Sustainable Chem. Eng.* **2018**, *6*, 13681–13686.

(32) Wang, Z.; Zhao, S.; Song, R.; Zhang, W.; Zhang, S.; Li, J. The synergy between natural polyphenol-inspired catechol moieties and plant protein-derived bio-adhesive enhances the wet bonding strength. *Scientific reports* **2017**, *7*, 9664.

(33) Kanimozhi, C.; Kim, M.; Larson, S. R.; Choi, J. W.; Choo, Y.; Sweat, D. P.; Osuji, C. O.; Gopalan, P. Isomeric Effect Enabled Thermally Driven Self-Assembly of Hydroxystyrene-Based Block Copolymers. *ACS Macro Lett.* **2016**, *5*, 833–838.

(34) Sweat, D. P.; Kim, M.; Schmitt, A. K.; Perroni, D. V.; Fry, C. G.; Mahanthappa, M. K.; Gopalan, P. Phase Behavior of Poly(4-hydroxystyrene- block -styrene) Synthesized by Living Anionic Polymerization of an Acetal Protected Monomer. *Macromolecules* **2014**, *47*, 6302–6310.

(35) Ishizone, T.; Kato, R.; Ishino, Y.; Hirao, A.; Nakahama, S. Protection and polymerization of functional monomers. 15. Anionic living polymerizations of 2-(3-vinylphenyl)-1,3-dioxolane and related monomers. *Macromolecules* **1991**, *24*, 1449–1454.

(36) Ishizone, T.; Tominaga, T.; Kitamura, K.; Hirao, A.; Nakahama, S. Protection and Polymerization of Functional Monomers. 25. Synthesis of Well-Defined Polystyrene Bearing a Triol Functionality by Means of Anionic Living Polymerization of 4-[(4-(4-Vinylphenyl)butoxy)methyl]-1-methyl-2,6,7- trioxabicyclo[2.2.2]octane. *Macromolecules* **1995**, *28*, 4829–4836.

(37) Ishizone, T.; Okamoto, K.; Hirao, A.; Nakahama, S. Protection and Polymerization of Functional Monomers. 29. Syntheses of Well-Defined Poly[(4-vinylphenyl)acetic acid], Poly[3-(4-vinylphenyl)propionic acid], and Poly(3-vinylbenzoic acid) by Means of Anionic Living Polymerizations of Protected Monomers Bearing Bicyclic Ortho Ester Moieties. *Macromolecules* **1999**, *32*, 1453–1462.

(38) von Tiedemann, P.; Blankenburg, J.; Maciol, K.; Johann, T.; Müller, A. H. E.; Frey, H. Copolymerization of Isoprene with p -Alkylstyrene Monomers: Disparate Reactivity Ratios and the Shape of the Gradient. *Macromolecules* **2019**, *52*, 796–806.

(39) Kawakami, Y.; Hisada, H.; Yamashita, Y. Polystyrenes with p-oligo-siloxane, silane, germanosiloxane, germane, or stannane as p-substituents as materials for oxygen permeable membranes. *J. Polym. Sci. A Polym. Chem.* **1988**, *26*, 1307–1314.

(40) Avgeropoulos, A.; Z-H Chan, V.; Lee, V. Y.; Ngo, D.; Miller, R. D.; Hadjichristidis, N.; Thomas, E. L. Synthesis and Morphological Behavior of Silicon-Containing Triblock Copolymers for Nanostructure Applications. *Chemistry of materials : a publication of the American Chemical Society* **1998**, *10*, 2109–2115.

(41) Allakhverdiev, M. A.; Mustafaev, K. N.; Farzaliev, V. M. Synthesis and Structure of Some Aryl-substituted Thiiranes. *Russian Journal of Organic Chemistry* **2002**, *38*, 1620–1623.

(42) Vyvyan, J. R.; Meyer, J. A.; Meyer, K. D. Conversion of epoxides to 1,3-dioxolanes catalyzed by tin(II) chloride. *J. Org. Chem.* **2003**, *68*, 9144–9147.

(43) Bas G. G. Lohmeijer, Russell C. Prat, Frank Leibfarth, John W. Logan, David A. Long, Andrew P. Dove, Fredrik Nederberg, Jeongsoo Choi, Charles Wade, Robert M. Waymouth, and James L. Hedrick Guanidine and Amidine Organocatalysts for Ring-Opening Polymerization of Cyclic Esters. *Macromolecules* **2006**, *39*, 8574–8583.

5 Curriculum vitae